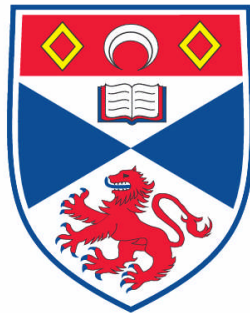


DESIGNING HYPERCYCLIC REPLICATING NETWORKS

Evan Alexander Wood

A Thesis Submitted for the Degree of PhD
at the
University of St Andrews



2007

Full metadata for this item is available in the St Andrews
Digital Research Repository
at:

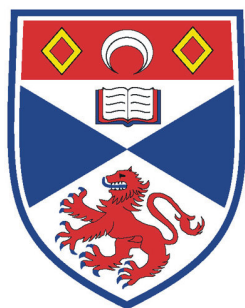
<https://research-repository.st-andrews.ac.uk/>

Please use this identifier to cite or link to this item:

<http://hdl.handle.net/10023/360>

This item is protected by original copyright

This item is licensed under a
Creative Commons License



University
of
St Andrews

Designing Hypercyclic Replicating Networks

By

Evan Alexander Wood

**A Thesis Presented for the Degree of
Doctor of Philosophy
in the
School of Chemistry
University of St Andrews**

St Andrews

April 2007

Synopsis

In the last 20 years there has been a number of synthetic and natural product based molecular replicators published in the literature. The majority of these systems have focused on the minimal model with only a few examples of cross-catalytic or reciprocal replication. Of the cross-catalytic systems investigated the majority focus around the use of natural products, oligonucleotides, peptides etc. This thesis will investigate the design, synthesis and kinetic analysis of both synthetic minimal and reciprocal replicating systems, and how these two forms of replication interact in a complex hypercyclic network.

Chapter 1 introduces key concepts such as molecular recognition, intramolecularity/ enzyme kinetic, bisubstrate systems and the work conducted into replication systems to date.

Chapter 2 describes the design, synthesis and kinetic analysis of a reciprocal replicating system, based on Diels-Alder and 1,3-dipolar cycloadditions, before going on to discuss what we have learned and how this system can be improved.

Chapter 3 focuses on the design, synthesis and kinetic analysis of a replicating network (minimal and reciprocal replication), based on 1,3-dipolar cycloadditions. Initial individual systems are examined in isolation to determine their behavior and nature. After which the systems are combined to observe how each species interacts in a potential complex hypercyclic network.

Chapter 4 investigates the redesign of the replicating network in Chapter 3 in order to overcome the problems identified from its kinetic analysis.

Chapter 5 introduces the shift in direction away from kinetically controlled replicating networks towards systems in thermodynamic equilibrium.

Acknowledgements

Firstly I would like to thank my supervisor Dr Douglas Philp for all the help, guidance he has given me over the course of the last 3.5 years, which has helped to make completion of this thesis possible.

Next I would like to thank all the members of the Philp group for their help and making the lab such an enjoyable place to work; Dr Simon Turega, (Dr) Jan Sadownik, (Dr) Annick Vidonne, Peter Donnelly, Dr Eleftherisos Kassianidis, Dr Mairead Minto, Dr Rosalyn Cowie and all the project students. Special thanks goes to Simon, Jan and Annick for an enjoyable last year and a half of my work, and an interesting conference trip to Budapest.

Special thanks go to the technical staff at the University of St Andrews, for making completion of my thesis possible. Thanks to Melanja Smith for NMR assistance, Caroline Horsburgh for mass Spectrometry, Prof A. Slawin for X-ray crystallography, Sylvia Williamson for Elemental Analysis. Special thanks must go to Oscar the 500 MHz NMR machine despite initial difficulties in the 1st year of my research in the end we managed to get along like old friends.

Finally I would like to thank my Mum, Dad, Brother and Gran for their constant support through out my time in St Andrews as well as the rest of my higher education. Without their help my time here would have been a lot more difficult and a lot less fun. And it is to my parents, that I dedicate this thesis.

List of abbreviations

AP	amidopyridine
br	broad
CA	carboxylic acid
d	doublet
CDI	carbodiimide
DCC	dynamic combinatorial chemistry
DCL	dynamic combinatorial library
dd	doublet of doublets
DMSO	dimethyl sulfoxide
DNA	deoxyribonucleic acid
EDC	<i>N</i> -ethyl- <i>N'</i> -(3-dimethylaminopropyl) carbodiimide
EM	effective molarity
eq	equivalent
ESI-MS	electrospray ionization mass spectrometry
Et	ethyl
EtOAc	ethyl acetate
h	hour(s)
HMTA	Hexamethylenetetramine
HOMO	highest occupied molecular orbital
IR	infra-red
<i>k</i>	rate constant
K_a	association constant
K_d	dissociation constant
kEM	kinetic effective molarity
LUMO	lowest unoccupied molecular orbital
<i>m</i>	meta
Me	methyl
NAC	near attack conformation
<i>o</i>	ortho

<i>p</i>	para
Ph	phenyl
PNP	<i>para</i> -nitrophenyl
Pyr	Pyridine
ppm	parts per million
q	quaternary
RNA	ribonucleic acid
rt	room temperature
s	singlet
R	Percent of mean absolute difference between theoretical concentrations with respect to the mean of experimental concentration
t	triplet
tEM	thermodynamic effective molarity
THF	tetrahydrofuran

Contents

Synopsis	3
Acknowledgements	4
List of Abbreviations	5
1. Introduction	12
1.1 Supramolecular and nanochemistry	12
1.2 Molecular Recognition	12
1.3 Hydrogen bonding molecular recognition	13
1.4 Recognition motifs containing one hydrogen bonding and the concept of cooperativity	15
1.5 Motifs containing two hydrogen bonds	17
1.6 Triply hydrogen bonded recognition motifs	18
1.7 Quadruply hydrogen bonded recognition motifs	19
1.8 Catalysis	23
1.9 Effective Molarities	24
1.10 Study of Intramolecularity	25
1.11 Templated Synthesis	32
1.12 Minimal model of replication	37
1.13 Potential Problems in a self-replicating system	39
1.14 Autocatalytic reactions vs. Self-replication	40
1.15 Reciprocal model of replication	41
1.16 Minimal self-replication incorporating natural products	43

1.17	Minimal synthetic replicating systems	47
1.18	Reciprocal replication incorporating natural products	62
1.19	Synthetic Reciprocal replication	69
1.20	Hypercyclic networks	77
1.21	Aims and Objectives	80
2.0	The design and synthesis of a reciprocal replicating system	81
2.1	Designing a reciprocal replicating system	81
2.2	The recognition motif	82
2.3	The reactive site	85
2.4	The spacer unit	89
2.5	The potential reciprocal replicating system	89
2.6	The synthesis of a reciprocal replicating system	93
2.7	Azide 103	93
2.8	Maleimide 73a	93
2.9	Maleimide 86	94
2.10	Furan 70	95
2.11	Synthesis of bis(amidopyridine) template 104	95
2.12	Synthesis of dicarboxylic acid template <i>exo</i> - 105	96
2.13	Results and Discussion	96
2.14	Kinetic analysis	96
2.15	Cross-catalytic formation of <i>exo</i> - dicarboxylic acid 105	98
2.16	Cross-catalytic formation of bis(amidopyridine) 104	113

2.17	Conclusions	115
2.18	Future work	115
3.	Design and Synthesis of a replicating network	117
3.1	Design of a replicating network	117
3.2	The synthesis of the potential replicating systems	123
3.3	Maleimide 116	124
3.4	Nitrone 115	124
3.5	Nitrone 117	125
3.6	Isoxazolidine 118a and 118b	126
3.7	Isoxazolidine 119	126
3.8	Isoxazolidine 120	127
3.9	Isoxazolidine 121	127
3.10	Results and discussion	128
3.11	Kinetic experiments	128
3.12	Potential minimal replicator isoxazolidine <i>trans</i> - 118	130
3.13	Potential minimal replicator isoxazolidine <i>trans</i> - 119	143
3.14	Potential reciprocal replicator isoxazolidine <i>trans</i> - 120	148
3.15	Potential reciprocal replicator isoxazolidine <i>trans</i> - 121	160
3.16	Hypercyclic Networks	168
3.17	Conclusions	180
3.18	Future work	181
4.	Redesign of a replicating network	183

4.1	Design of a replicating network	183
4.2	Synthesis of the potential replicating systems	188
4.3	Maleimide 132	188
4.4	Carboxylic acid nitron 133	189
4.5	Bis(amidopyridine) isoxazolidine <i>trans</i> - 135	190
4.6	Dicarboxylic acid isoxazolidine 136	190
4.7	Isoxazolidine 134 , 134b	191
4.8	Results and Discussion	191
4.9	Kinetic experiment	191
4.10	Minimal replicator <i>trans</i> - 118	192
4.11	Minimal replicator <i>cis</i> - 134	198
4.12	Reciprocal replicator <i>trans</i> - 135	206
4.13	Reciprocal replicator <i>cis</i> - 136	219
4.14	Hypercyclic Networks	225
4.15	Conclusions	240
4.16	Future work	242
5.	The future of small molecule synthetic replicating systems	243
5.1	Dynamic Combinatorial Chemistry	243
5.2	Synthetic artificial template system	247
5.3	Synthesis of synthetic artificial template systems	251
5.4	Synthesis of building block isoxazole 155 and 158	251
5.5	Synthesis of building block 156 and 159	254
5.6	Conclusions and Future work	255

5.7	Dynamic replicating templates, <i>via</i> reversible nitron exchange	256
5.8	Conclusions and Future work	263
6.	General Conclusions	265
7.	Experimental	267
8.	References	309
9.	Appendix	

1. Introduction

1.1 Supramolecular and nanochemistry

One of the most exciting and promising branches of chemistry is the recently emergent field of nanochemistry^[1]. Much of the development in this new field has arisen from advances in supramolecular chemistry. Over the past 20 years, there has been a dramatic increase^[1-2] in the number and complexity of so-called 'molecular machines' which are formed from complex supramolecular structures. The development of novel architectures like catenanes^[3-5], rotaxanes^[6-9] and knots^[4], has allowed the research groups of Stoddart and Leigh to develop functional assemblies like molecular shuttles^[7], valves^[1], elevators^[2] and memory^[6] to name just a few examples. Other structure with potential applications in the area of supramolecular and nanochemistry are dendrimers^[10-15]. Their branched structure can be utilized in molecular recognition, as a consequence of the presence of multiple surface groups which are able to amplify binding interactions by multivalency. Dendrimers can also bind at their core encapsulating the guest in a unique microenvironment, this mimics the three dimensional structure of complex peptide structures like the active site of an enzyme. The work of Smith has demonstrated^[11-15] examples of cation and anion binding at the dendrimer core in both organic and aqueous media. Other examples of their work include the controlled release of an ammonium template encapsulated by the dendrimer, through the addition of K⁺ ions. There are a large number of potential applications for dendrimer structures, and as a result of this the future of dendrimer chemistry looks very promising.

However, an often overlooked area of supramolecular chemistry and nanochemistry is synthetic organic molecular replicating systems. These replicating systems incorporate a wide scope of supramolecular chemistry such as molecular recognition, intramolecularity and catalysis and templated synthesis.

1.2 Molecular Recognition

Before discussing the different types of molecular recognition why do individual compounds associate and recognize each other? In solution before recognition between

two molecules **A** and **B** can occur molecules of solvent have to be replaced with specific intermolecular interactions. Molecular recognition occurs when more favorable interactions occur between two molecules **A**, **B** and the association of released solvent, than occurs when **A** and **B** are solvated, resulting in the formation of complex **A-B**. Before investigating molecular recognition it is important to introduce two key principles, complementarity and preorganization. Complementarity is the use of a host that has a binding cavity which resembles the guest structure. Preorganization is where the receptor is complementary before the binding event, which is energetically favorable. In 1967, Pedersen noted^[16-17, 21] that the cyclic polyether, 18-crown-6, formed (**Figure 1.1**) very tight complexes to potassium cations, K^+ .

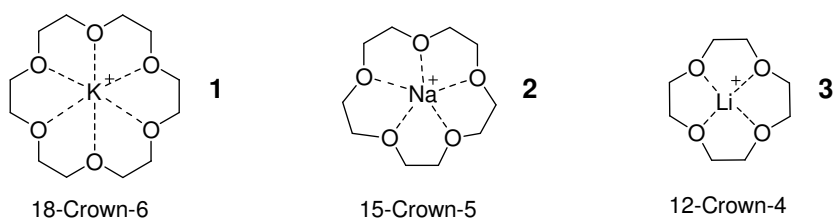


Figure 1.1 Variety of Crown ether of different ring sizes. The size of the ring cavity determines the preference for the cation.

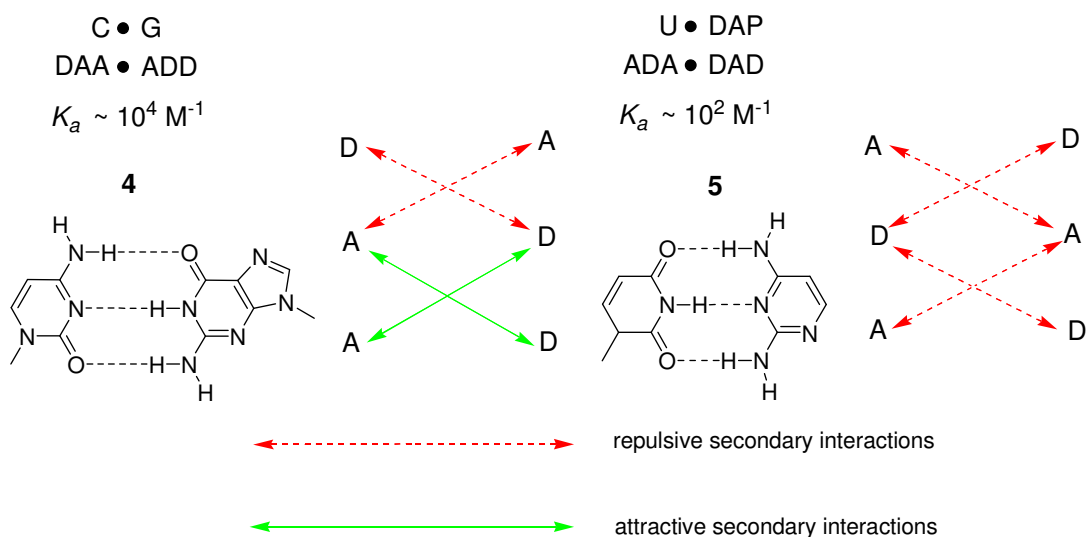
The crown nomenclature arises from the shape of these complexes. Pedersen's discovery was utilized by Cram^[14] and Lehn^[16-17] and all three received the Nobel prize for chemistry in 1987. After the discovery of crown ethers, a whole host of different molecular recognition processes were investigated, like the hydrophobic effect^[22] in cyclodextrins, π interactions *via* thermodynamic cycles^[23-24] and ion pairing to name but a few examples. A detailed analysis of molecular recognition is out with the scope of this thesis. Instead, a focused examination of only one form of recognition which is of the utmost relevance to work conducted in this investigation of replicating networks, namely hydrogen bonding.

1.3 Hydrogen bonding molecular recognition^[25]

A hydrogen bond occurs between molecules containing a polar X-H bond and nonbonding electrons pairs on atom Y. The X-H bond is referred to as a hydrogen bond donor (D) and the Y atom is referred to as the hydrogen bond acceptor (A). Hydrogen bonding strength is determined by the magnitude of the dipole moment of the X-H bond

and the lone pair on the Y atom. Therefore, the strongest hydrogen bonding occurs when N, O and F are the X and Y atoms.

The strength of a single hydrogen bond is not large enough to control the structure of macromolecules or encourage binding of guest molecules. However, the contribution of a number of hydrogen bonds acting together cooperatively can provide the necessary energy to allow binding between hosts and guest molecules. In 1967, Rich and co-workers discovered^[26] that different hydrogen bonding networks containing triply bonded dimeric complexes in CHCl_3 had very different stability constants (**Scheme 1.1**).



Scheme 1.1 Attractive secondary interactions account for the differences in thermodynamic stability of for the 1-methylcytosine, 9-methylguanine (C•G), **4** dimer and the 1-methyluracil, 2,6-diaminopyridine (U•DAP) dimer, **5**. A = hydrogen bond acceptor, D = hydrogen bond donor. K_a is used as a measure of the stability of binding. Adapted from reference 28

This result proved surprising, after all why should two structures comprising of identical hydrogen bonds arranged differently have such a large discrepancy in association. Clearly, the number of hydrogen bonds is not the sole determinant of binding stability between complementary molecules^[27]. After a period of more than 20 years, Jørgensen and co-workers determined^[28,29] that the difference in binding stabilities observed in **Scheme 1.1** corresponded to attractive and repulsive secondary interactions. Stabilization arises from electrostatic attraction between positive and negative polarized atoms in adjacent hydrogen bonds. However, destabilization will occur between two positively or negatively polarized atoms on adjacent hydrogen bonds. This model predicts the highest association for a triple hydrogen bonded dimeric complex containing the AAA•DDD recognition motif pattern. In this hydrogen bonding pattern, the maximum

number of attractive secondary interactions are occurring with no repulsive ones to reduce binding^[30]. Sartorius and Schneider derived^[31] an empirical rule in order to predict binding strength of a complex. They stated that the free energy of dimerization consists of only two increments; (i) a contribution of 1.88 kcal mol⁻¹ for each hydrogen bond and (ii) ± 0.7 kcal mol⁻¹ for each attractive or repulsive secondary interaction.

1.4 Recognition motifs containing one hydrogen bonding and the concept of cooperativity

There are a number of functionalities which can dimerize through one hydrogen bond, for example phenol, amines, amides etc. However, these have low stability and are of little use in molecular recognition in host guest chemistry. There are a few strategies employed to overcome this problem, but they all use the concept of cooperativity between a number of hydrogen bonding interactions to increase stability. A complex which makes two intermolecular hydrogen bonds may be associated with a binding which is more than twice as large as a similar complex that makes only one. This effect^[25, 32-36] is referred to as positive cooperativity when the Gibbs free energy of binding is more negative than the sum of all free energies for individual binding interactions. In the case of positive cooperativity, the formation of one hydrogen bond encourages the creation of another, but the formation of one interaction does not always enhance the formation of another. Sometimes the creation of one hydrogen bond weakens the formation of another and therefore, the overall binding is weaker than the sum of its parts, this effect is referred to as negative cooperativity. Stated in terms of free energy, negative cooperativity occurs when the Gibbs free energy of binding is more positive than the sum of the Gibbs free energy change for each individual binding interaction. The final type of cooperativity is non-cooperative where overall binding is the sum of individual binding or ΔG of binding is equal to the sum of the individual binding ΔG .

The binding energy of molecule A-B to the host consists of three parts (**Figure 1.3**), intrinsic Gibbs free energy of binding **A** (ΔG_A^i), Gibbs free energy of binding **B** (ΔG_B^i) and the connection Gibbs free energy (ΔG^s).

$$\Delta G_{AB}^{\circ} = \Delta G_A^i + \Delta G_B^i + \Delta G^s$$

Figure 1.3 Equation of free energy for binding guest molecule A-B to the host structure.

The connection Gibbs free energy is the extent to which through linking **A** and **B** together as **AB** differs in binding strength compared to the sum of individual binding of **A** and **B** to the host. It is claimed that the favorable portion of ΔG^s is mostly a consequence of entropic factors, however, enthalpy can be involved. In binding **AB** to the host, the loss in translational/rotational entropy is paid only once, but if **A** and **B** were bound separately to the host this cost would be paid twice. Therefore, binding of **AB** will be favored compared to the individual binding of **A** and **B** by the amount corresponding to a loss of translational and rotational entropy of a single molecule. This linking of molecules **A** and **B** together to obtain more favorable binding to the host than individually binding **A** and **B** is known as the chelate effect. The intrinsic binding energy of **A** (or **B**) is the additional energy this motif brings to the binding of the rest of the molecule, **B** (or **A**), if no difference in strain or entropy occurs when **A** (or **B**) interacts with the host molecule (**Figure 1.4**).

$$\Delta G_A^i = \Delta G_{BA}^{\circ} - \Delta G_B^{\circ} \qquad \Delta G_B^i = \Delta G_{AB}^{\circ} - \Delta G_A^{\circ}$$

Figure 1.4 Equations for intrinsic binding energy of motif **A** and **B**.

If **Figure 1.3** is rearranged to calculate free energy of connection and the equations for intrinsic energy of binding of **A** and **B** are then substituted into this calculation, the result is **Figure 1.5**.

$$\Delta G^s = \Delta G_B^{\circ} + \Delta G_A^{\circ} - \Delta G_{AB}^{\circ}$$

Figure 1.5 Equation for calculating Gibbs free energy of connection ΔG^s .

If a positive value for Gibbs free energy is calculated using the equation in **Figure 1.5** it represents a favorable positive cooperativity, the opposite is true for a negative value which indicates negative cooperativity. Normally, cooperativity is determined by multiplying individual binding values together for **A** and **B** and comparing the result to the actual value for associating **AB**, any difference is considered cooperativity. However, using **Figure 1.5** and substituting $\Delta G^{\circ} = -RT \ln K$ into this equation an empirical measurement (**Figure 1.6**) of cooperativity can be obtained.

$$\Delta G^s = RT \ln \left(\frac{K_{AB}}{K_A K_B} \right)$$

Figure 1.6 Equation for calculating free energy of connection, cooperativity, using association constants for binding of **A**, **B** and **AB**.

In **Figure 1.6** R is the gas constant, T temperature in Kelvin, K_A , K_B and K_{AB} is the binding constant for binding of moiety **A**, **B** and guest **AB** to the host.

1.5 Motifs containing two hydrogen bonds

There is a wide variety of polar functionalities which can dimerize through two hydrogen bonding recognition motifs, for example carboxylic acids, amides, oxalamides and heterodimers based on carboxylic acid 2-amidopyridine derivatives etc. Two hydrogen bonding complexes with the AD•DA (A = Hydrogen bond acceptor, D = Hydrogen bond donor) recognition pattern are only stable at relatively high ($> 10^{-2}$ M) concentrations (as a consequence of repulsive secondary interactions). A K_a value for these patterns of around 60 M^{-1} is predicted, which is too low to be useful in non-covalent synthesis. The stability of complexes with AA•DD recognition patterns is considerably higher than the previous self-complementary motifs. Zimmerman and Murray calculated^[37] values of association around 260 M^{-1} for these complexes, however, interestingly they recorded^[38-39] much greater binding constants for bifurcated (**Figure 1.7**) hydrogen bonding systems, AA•DDD.

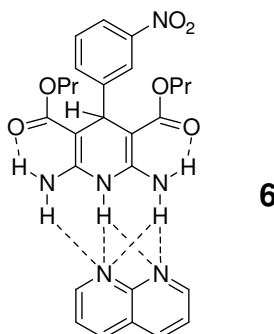


Figure 1.7 Zimmerman and Murray's two hydrogen bonded motif with bifurcated hydrogen bond.

In a bifurcated system the association is stabilized through an attractive secondary interaction between a free donor site and the adjacent hydrogen bonded acceptor atom.

Zimmerman and Murray in this work showed by adding a bifurcated hydrogen bond an increase in association to around 3000 M^{-1} could be obtained.

1.6 Triply hydrogen bonded recognition motifs

Complexes formed by three hydrogen bonding interactions demonstrate larger binding stability than their two hydrogen bonding counterparts as expected. Whereas, one and two hydrogen bonding recognition pattern could recognize themselves, homodimerization is impossible for these motifs. As mentioned previous Jørgensen predicted that the most stable triply hydrogen bonded complex would have the recognition pattern AAA•DDD. Zimmerman and co-workers investigated^[40, 209] similar complexes with the patterns ADA•DAD, AAD•DDA and AAA•DDD with 0, 2 and 4 favorable secondary hydrogen bonding interactions. The stability constants determined for these complexes matched Jørgensen's prediction with values of $10^2, 10^3$ to 10^4 and $>10^5 \text{ M}^{-1}$ in CHCl_3 . The AAA•DDD complex used by Zimmerman is illustrated in **Figure 1.8**.

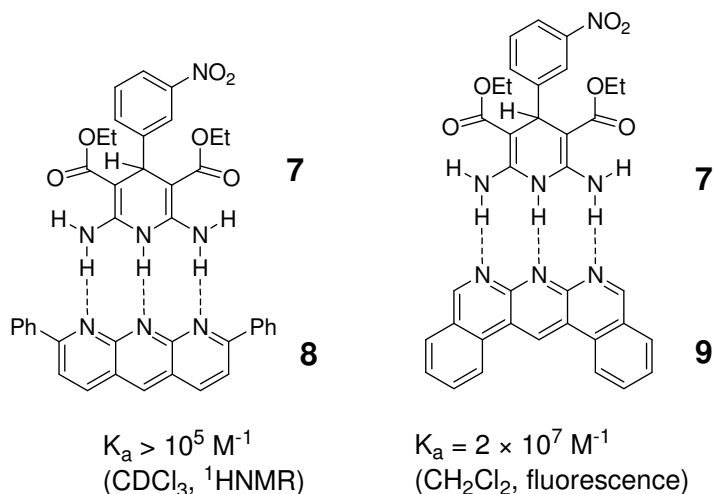


Figure 1.8 AAA•DDD triple hydrogen bonded complex [**7•8**], by Zimmerman and co-workers, and [**7•9**], by Leigh, McNab and Zerbetto.

Since the original work by Zimmerman and Murray into triple hydrogen bonded complexes there have been few advances in developing enhanced AAA•DDD systems. However, in 2007 a communication by Leigh, McNab and Zerbetto tried to address^[41] some of the problems associated with Zimmerman's system with the hope of providing a

better AAA•DDD complex. The two problems with the complex [7•8] in **Figure 1.8** are that the association constant is only an approximation, as a consequence of the limits of measuring K_a by ^1H NMR spectroscopy. The second problem is a result of the reactive nature (**Figure 1.9**) of the donor molecule, DDD.



Figure 1.9 7 can convert between two tautomeric forms; 1,4-dihydro, DDD, and its unwanted 3,4-dihydro state, 10.

The donor molecule DDD, 7, can convert (**Figure 1.9**) to its tautomeric form 10, which has a DAD configuration. In order to overcome this problem, Zimmerman used 1,8-bis(dimethylamino)naphthalene (proton sponge) to prevent hydride shift between the C-4 and C-10 position of 7. Leigh and co-workers in an attempt to stabilize the chemical stability of complex 7•8 extended the anthryridine aromatic framework of 8 to form 9, as shown in **Figure 1.8**. It was hoped that 9 would bind more strongly to 7 stabilizing the structure and preventing or reducing conversion to its tautomeric form 10. The end result was a complex with an association constant of $2 \times 10^7 \text{ M}^{-1}$ in CH_2Cl_2 measured by fluorescence. This increased binding strength results in a more chemically stable complex [7•9] compared to [7•8]. In Zimmerman's original system, 10 equivalents of 8 were required to fully convert 10 to its 1,4 dihydro-form, however, in this system only 0.5 equivalents of 9 are required to convert 10 to its 1,4 dihydro-form in > 98:2.

1.7 Quadruply hydrogen bonded recognition motifs^[25, 42, 46]

The final group of complexes investigated are those involved in quadruple hydrogen bonding arrays. As anticipated these form more stable complexes than their three hydrogen bonding counterparts, but like their two hydrogen bonding cousins can form homodimers. With four bonding arrays the number of possible complexes has increased to six which are demonstrated in **Figure 1.10**.

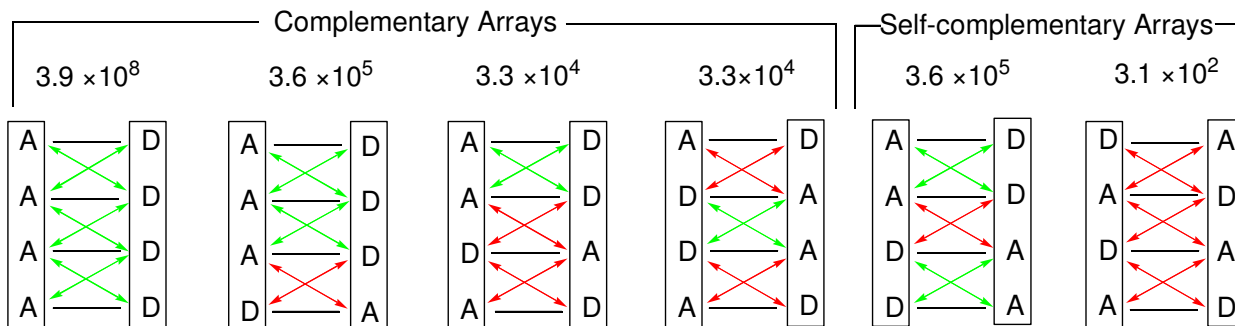


Figure 1.10 All the possible combinations of arrays formed by four hydrogen bonding sites and their predicted stability constants (in M^{-1}) in $CDCl_3$. Attractive and repulsive secondary interactions are indicated by green and red double headed arrows. Adapted from reference 42.

Conceptually, the simplest way of forming a quadruple hydrogen bonded array is to link together two doubly bonded arrays into one molecule. A good example, and one of the first examples of this approach utilised two pyridine units and was developed^[43-44] (**Figure 1.11**) by Ducharme and Weust. The self-complementary nature of **11** meant it could dimerize as the complex **[11•11]**, with a binding constant of $6 \times 10^4 M^{-1}$. **Figure 1.11** also demonstrates a non-self complementary bispyridone where dimerization *via* only two hydrogen bonds is possible, this complex has considerably weaker association of $10^2 M^{-1}$.

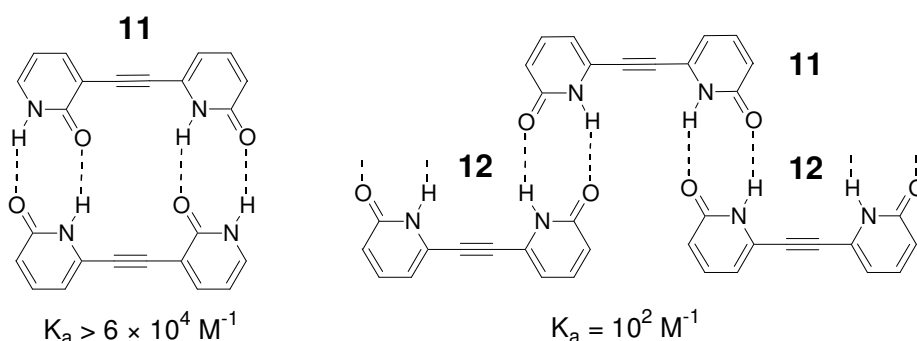


Figure 1.11 Self and non-self complementary dipyrindone quadruple hydrogen bonding arrays **11** and **12**.

Another method of forming quadruple hydrogen bonded arrays is to create entirely new recognition motifs. An example of such a recognition motif was created accidentally^[42] by Sijbesma and Meijer in their attempts to create a strong triple hydrogen bonded complex. In fact they had actually created a molecule capable of forming (**Figure 1.12**) five hydrogen bonds but could only dimerize *via* four intermolecular interactions.

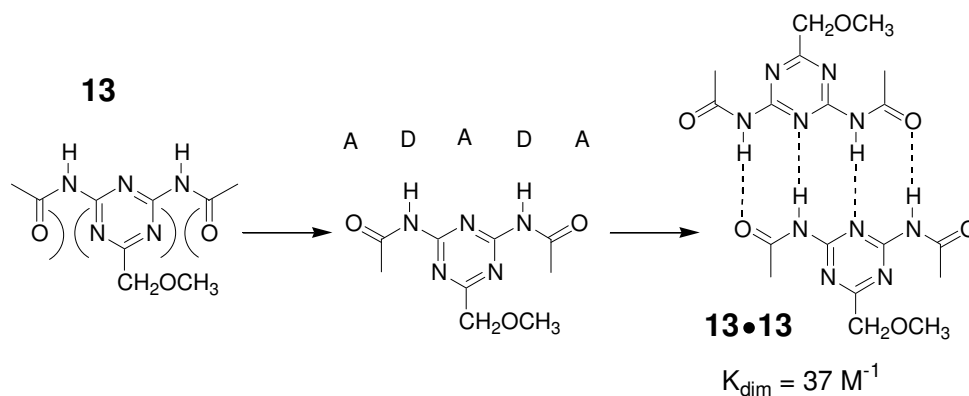


Figure 1.12 Weak ADADA hydrogen bonding molecule **13** capable of dimerizing in an ADAD•DADA complex,) (indicates spectator repulsions. Adapted from reference 42.

Unfortunately, however, the dimer complex in **Figure 1.12** demonstrated a much lower stability constant than predicted (**Figure 1.10**). The reason for this disappointingly low value was concluded to be the result of what Sijbesma coined as ‘spectator repulsions’ (**Figure 1.12**), between the carbonyl groups and nitrogen atoms on the triazine ring not involved in hydrogen bonding. Initial attempts at improving the stability of this recognition motif involved removing an acyl group, to prevent these spectator repulsions, this modification resulted in an increase in binding to 530 M^{-1} . A further increase in complex stability ($K_a = 2 \times 10^4 \text{ M}^{-1}$) was observed when an intramolecular hydrogen bond was used to preorganize the DADA array in a planar conformation. Finally, Sijbesma found the strongest bound DADA dimer complex was created^[42] when preorganization and a pyrimidine ring, in place of the triazine ring, were both utilized (**Figure 1.13**).

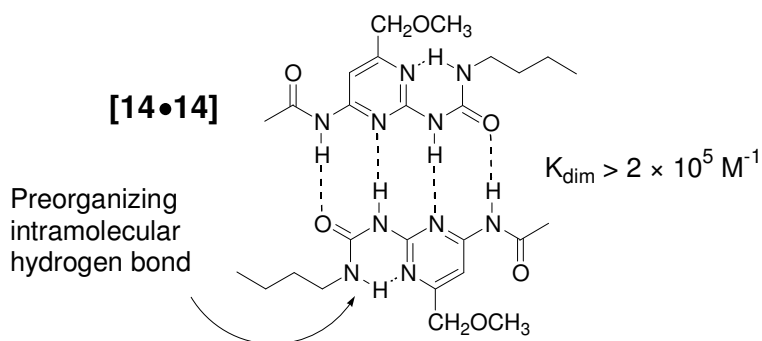


Figure 1.13 An extremely stable DADA array, as a result of an intramolecular preorganizing hydrogen bond.

The importance of this investigation is that it demonstrates the limits of using secondary interactions for predicting stability of hydrogen bonding arrays. According to Jørgensen’s model the stability of a DADA array should be in the order of $3 \times 10^2 \text{ M}^{-1}$. However,

Sijbesma has created a dimer complex with a considerably higher association constant. Sijbesma and co-workers claim this difference is a result of preorganization and other factors like overall charge distribution.

A number of other quadruple hydrogen bonding recognition motifs have been investigated utilizing an AADD self-complementary array. One example^[45] utilized the above concept of preorganization *via* an intramolecular hydrogen bond to form dimers which could undergo further self-assembly into “extended sheet like supramolecular structures”.

Although a vast amount of investigation has gone into the study of self-complementary quadruply hydrogen bonded arrays (**Figure 1.10**), hardly any examination of complementary arrays has occurred.

Despite these advances there is still a requirement for recognition units that form complexes with high stability and selectivity. The examples in this Section are mostly homocomplexes, there are few methods of forming heterocomplexes with high binding constants. However, recently Zimmerman and Meijer have conducted^[46-49, 210-211] detailed studies into the development of quadruply hydrogen bonded heterocomplexes which exhibit high fidelity. The major problem in developing such complexes is that a number of recognition motifs exhibit tautomeric forms which can result in self-association weakening the association between heterocomplexes. However, Zimmerman and co-workers have recently demonstrated examples of heterocomplexes with high stability and selectivity (**Figure 1.14**).

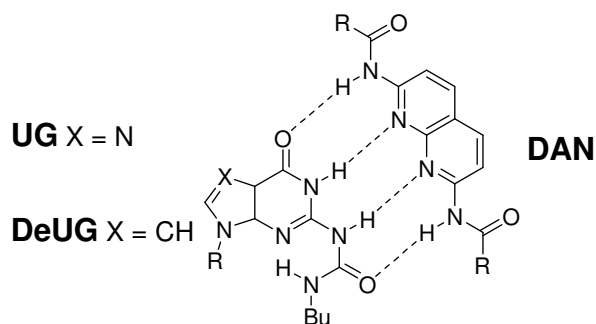


Figure 1.14 **UG** forms a stable quadruply hydrogen-bonded heterocomplex with **DAN**, but fidelity of complex is lower by Hoogsteen side oligomerization of **UG**. **DeUG** however lacks the Hoogsteen nitrogen atom and therefore forms a more stable complex with **DAN**.

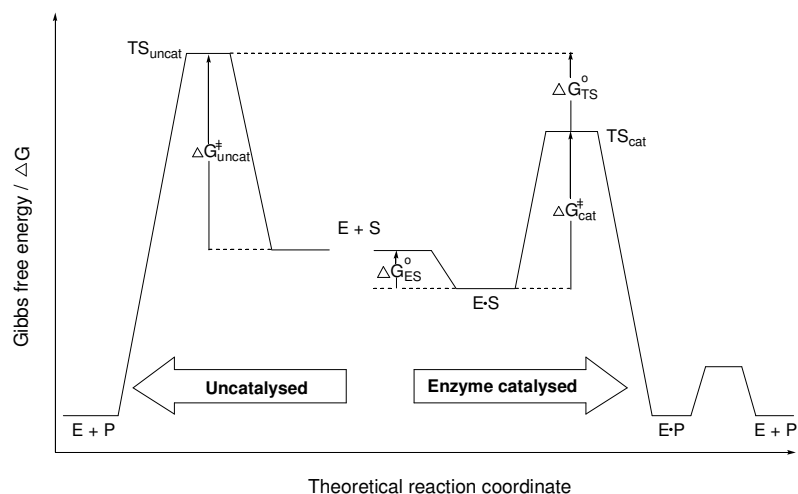
Zimmerman initially developed the **UG** motif which was found to bind **DAN** with a $K_a = 5 \times 10^7 \text{ M}^{-1}$, in CHCl_3 . However fidelity of **UG** for **DAN** is reduced as a consequence

of oligomerization of **UG** ($K_a \approx 230 \text{ M}^{-1}$) via the Hoogsteen nitrogen, therefore the author created **DeUG** to overcome this problem. **DeUG** lacks the Hoogsteen nitrogen, and therefore cannot oligomerize, this fact resulted in the formation of a much more stable complex with **DAN** (>10 fold higher K_a compared to **UG**). However **DeUG** was also found to dimerize reasonably strongly ($K_a = 880 \pm 40 \text{ M}^{-1}$) which reduces its fidelity. **DeUG** has a higher association constant for binding **DAN** and increased fidelity compared to **UG**, however, there is still scope for designing quadruply hydrogen-bonded heterocomplexes which exhibit improved fidelity recognition.

There are a few examples of hydrogen bonding arrays composed^[50] of greater than four intermolecular interactions, but these will not be discussed here.

1.8 Catalysis

The ability of enzymes to catalyze reactions^[51] with excellent regio- and stereoselectivity has intrigued chemists for decades. Enzymes are referred to as biological catalysts; however, there is a key feature which distinguishes enzymes from catalysts. This feature is the enzyme's ability to bind a substrate in close proximity to the catalytic group(s) on the enzyme. So how do enzymes accelerate a reaction? The basic principle of enzyme catalysis was first suggested by Pauling some 50 years ago. He stated that enzyme catalysis was achieved through the stabilization of the transition state. This stabilization of transition state can be achieved through either lowering the energy of the transition state or by raising the energy of the ground state. Therefore, ΔG_{cat} must be larger than ΔG_{ES} , when the transition state is stabilized more than the ground state of the substrate (**Scheme 1.2**).



Scheme 1.2 Energy profile for enzyme-catalyzed and uncatalyzed reaction of substrate S.

Chemists hope through understanding how enzymes^[52] work, that it will become possible to further the understanding of controlling and accelerating reactions.

From what has been observed of catalysis in nature, a number of key areas have been identified as important by chemists. The hope is that through improving our understanding of catalysis chemists will be able to develop systems capable of enzymatic like catalysis.

One area of study which has been identified as a large factor in the incredible acceleration observed by enzymes is that the reaction occurs in an [E·S] complex, this bringing of reactive sites close together renders the reaction *pseudo* intramolecular. This has lead chemists to study synthetic intramolecular reactions in an attempt to further the understanding of enzyme reactions.

1.9 Effective Molarities^[53]

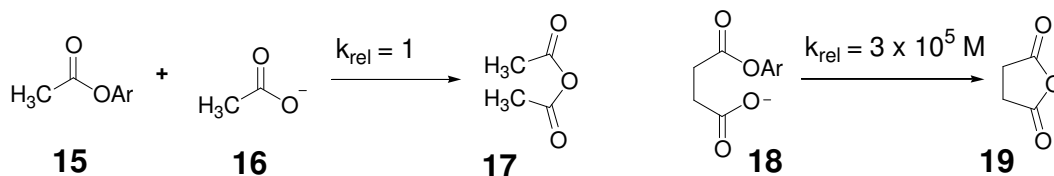
The study of intramolecular reactions has resulted in the invention of the term effective molarity (EM) as a way of measuring rate enhancement of intra over intermolecular reactions. The EM term is a hypothetical concentration of a reactant in an intermolecular reaction required to proceed at the same rate (or to the same extent) as its intramolecular equivalent. Effective molarity is measured through comparing the rate constant of the intramolecular (catalyzed in the case of enzymes) over that of the intermolecular (the uncatalyzed reaction) as shown in **Figure 1.15**.

$$EM (M) = \frac{k_{cat}}{k_{uncat}} = \frac{k_{intramolecular}}{k_{intermolecular}}$$

Figure 1.15 Calculation for determining effective molarity (EM), used to compare intra to intermolecular reactions.

Values of effective molarities ranging from 10^{-3} to 10^{16} M have been observed^[53].

These values have led to the question of why is there such a large variation in the effective molarities observed, and for what reason do intramolecular reactions proceed so much faster than their intermolecular counterparts? One of the simplest examples of the effect of intramolecularity is the comparison^[54] between the formation of succinic anhydride and acetic anhydride (**Scheme 1.3**). As this shows there is a dramatic increase in the observed rate on going from an inter to an intramolecular reaction.

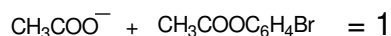


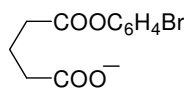
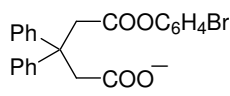
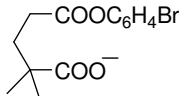
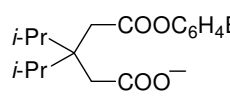
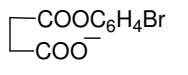
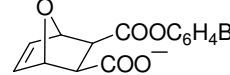
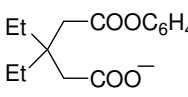
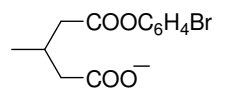
Scheme 1.3 Intermolecular vs. Intramolecularity.

1.10 Study of intramolecularity^[54-70]

In the 1950 and 1960's Bruice and Pandit conducted^[54-57] extensive studies into the effect of intramolecularity, through studying carboxylic group nucleophilic catalysis of the hydrolysis of various esters (**Table 1.1**). Their argument for the dramatic increase observed in an intramolecular reaction is that of a simple proximity effect, "Just as proximity of an electrophile and nucleophile in an intermolecular reaction increases rate, so is the juxtaposition of an enzyme substrate complex responsible for large portion of rate enhancement", Bruice referred to this as the 'proximity factor'.

Table 1.1 The relative rates of (I) to (VIII) for the intramolecular reaction between a carboxylate anion with a monophenyl ester to form the cyclic anhydride product compared to the standard intermolecular reaction.



	$k_{rel} (M)$		$k_{rel} (M)$
(I) 	$\sim 1 \times 10^3$	(V) 	$\sim 2.7 \times 10^5$
(II) 	$\sim 3.6 \times 10^3$	(VI) 	$\sim 1.3 \times 10^6$
(III) 	$\sim 1.8 \times 10^5$	(VII) 	$\sim 8 \times 10^7$
(IV) 	$\sim 2.3 \times 10^5$	(VIII) 	$\sim 4.4 \times 10^3$

Bruice and Pundit claimed the results they obtained showed the tremendous rate enhancement which enzymes can obtain through fixing their reactive sites in a steric conformation similar to that of the transition state of the reaction. They also concluded that bringing reactants close together resulted in considerable loss in translational entropy and these factors explain why enzymes can obtain high rate increases in the area of 10^8 M. Analysis of **Table 1.1** reveals the addition of a methyl group, comparison between (II) and (VIII) in **Table 1.1**, results in an increase in rate. The explanation for this effect is what is referred to as steric compression. The electrophile and nucleophile are pushed together forcing the structure towards that of the transition state. Another way of causing steric compression is through the use of gem di-alkyl groups, **Table 1.1** (III), (V), and (VI), in what is referred to as the Thorpe-Ingold effect^[67].

The proximity theory was not accepted by everyone though, and around the same time Koshland and Jencks suggested^[58-59] an alternative theory, that holding reactants in close proximity would only result in a rate enhancement of 55 M. Koshland's arguments revolve around the basis that reactant **A** and **B** are the size of water molecules, **A** is dissolved in neat **B** then the observed *pseudo*-first order rate constant (k_{obsd}) could only be 55.5 times greater than k_{obsd} when **B** is at 1 M. This argument did not, however, account for the large rate enhancements observed by Bruice, so Koshland came up^[66]

with the theory of 'orbital steering' to account for this. The argument behind this theory is that not only must reactants be in close proximity their orbitals must be optimally aligned. It is the latter which Koshland argues is the most important and even a small deviation of 10 degrees would result in a 10000 fold decrease in reaction rate (**Figure 1.16**).

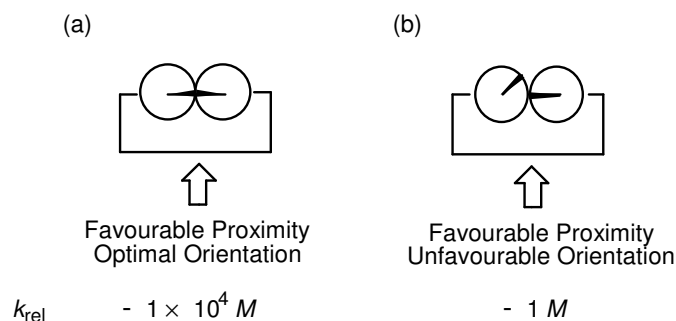


Figure 1.16 Koshland orbital steering theory (a) intramolecular reaction with close proximity and optimal orbital alignment (b) intramolecular reaction lacking optimal orbital alignment by more than 10 degrees.

Koshland also argued that this helped to explain the huge variations in values of EMs for intramolecular reactions.

Bruice attacked this theory on the argument that it required an unreasonably large force constant. However, the theory of orbital steering was upheld by two theoretical studies^[62] and a study by Menger^[63-64] pointed out that Bruice had overlooked the effect of solvent. Despite this, Menger also concluded that the effect of orbital steering was not as great as first believed.

In 1971, Jencks^[60-61] reversed his position and conceded that entropic contributions must have been larger than previously believed. Jencks, along with Page, went on to suggest that entropic factors account completely for large intramolecular rate acceleration. At this stage it is worth considering the different entropy contributions between bimolecular and intramolecular. There are different degrees of freedom lost in intramolecular and intermolecular reactions, which results in large differences in the entropy change between these two systems. A bimolecular reaction of a non-linear molecule containing n atoms has 3 degrees of translation, 3 degrees of rotation as well as $(3n-6)$ degrees of vibration. When the transition state forms or the product of bimolecular reaction forms there is an overall loss of three translational and three rotational degrees of freedom, however, there is a gain of 6 vibrational degrees of freedom (**Table 1.2**).

Table 1.2 The change in degrees of freedom during a bimolecular reaction.

	A	+	B	→	P
Translational	3		3		3
Rotation	3		3		3
Vibrational	3n-6		3n'-6		3n+3n'-6

In a unimolecular (intramolecular) reaction there is no net gain or loss in the number of degrees of freedom during a reaction (**Table 1.3**).

Table 1.3 The changes in molecular degrees of freedom during the course of a unimolecular reaction.

	A		B	→	P
	┌──────────┐				┌──────────┐
Translational	3		3		3
Rotation	3		3		3
Vibration	3n-6		3n-6		3n-6

These changes in degrees of freedom observed on passing from reactant to product can be quantified in terms of a change in entropy. It was observed that a loss of $190 \text{ J mol}^{-1} \text{ K}^{-1}$ could be estimated for a bimolecular reaction. The maximum rate acceleration obtained from rendering a reaction *pseudo*-unimolecular, can be estimated using the Eyring equation derived (**Figure 1.17**) from transition state theory.

If we assume there are no differences in ΔS^\ddagger between the inter- and intramolecular reactions ΔS^\ddagger , we can easily calculate the k_{uni} / k_{bi} value using the estimate of $190 \text{ J mol}^{-1} \text{ K}^{-1}$.

$$k = \frac{k_b T}{h} \exp\left(-\frac{\Delta G}{RT}\right) \quad \text{Rewritten in terms of } \Delta H \text{ and } \Delta S \quad k = \frac{k_b T}{h} \exp\left(-\frac{\Delta H^\ddagger}{RT}\right) \exp\left(-\frac{\Delta S^\ddagger}{R}\right)$$

Figure 1.17 Eyring equation transformed into its ΔG^\ddagger form, where R, k, k_b , h, and T are the gas constant, rate constant, Boltzmann constant, Planck's constant, vibrational frequency and absolute temperature. ΔG^\ddagger , ΔH^\ddagger and ΔS^\ddagger are the activation parameter free energy, enthalpy and entropy.

The value for k_{uni} / k_{bi} is calculated by dividing the Eyring equation for the unimolecular reaction, k_{uni} , by the Eyring equation for the bimolecular reaction, k_{bi} , which simplifies to give the equation in **Figure 1.18**.

$$\frac{k_{uni}}{k_{bi}} = \exp\left(\frac{\Delta(\Delta S^\circ)}{R}\right)$$

Figure 1.18 Equation for determining maximum rate acceleration.

Therefore, from the equation in **Figure 1.18** a value of 8×10^9 M for the maximum rate acceleration in an entropy only scenario can be calculated.

Menger argued^[62-64] however, that this does not account for differences between inter and intramolecularity, and this led him to develop his own approach to intramolecularity. The basis of this was that rate of reaction between functionalities A and B is proportional to the time that A and B reside at a critical distance. He suggested that reaction proceeds at intramolecular rates when the distance between reactants is at van der Waals contact distance (less than solvent distance), he referred to this as the 'spatiotemporal postulate'.

The conclusion drawn from the various studies into intramolecularity has lead to severally widely accepted concepts about the mechanics of enzyme reactions. In the 1990's, Bruice and Lightstone^[56-57,65] came up with another theory to explain intramolecularity- the theory of Near Attack Conformation (NAC). They claimed that changes in translational and rotational energies in the juxtaposing nucleophile and electrophile is not enough to explain large rate enhancements observed in intramolecular reactions. The large rate enhancement must be explained by the probability of formation of ground state conformers where the reacting groups are held in conformations to enter the transition state (NAC). The NAC is defined as the conformation required for the juxtaposed reactants to enter a transition state. The NAC is a genuine ground state where the reaction centres are properly aligned for reaction but are separated by 3 Å, where bond making and breaking has not yet been initiated (**Figure 1.19**).

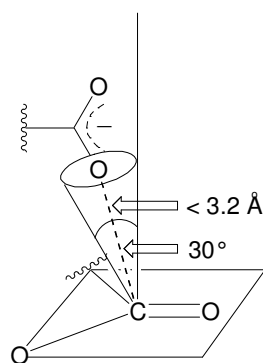


Figure 1.19 The geometry of a NAC for an intramolecular carboxylate anion interaction with a carbonyl ester. In which carbonyl is still sp^2 and the carboxylic acid is positioned above the carbonyl 3.2 Å away at a 30° angle from the perpendicular trajectory.

Bruice claims NAC calculations on esters highlight that the rate constant for the reaction is dependent on the mole fraction (P) of ground state of each ester present as a NAC, and that the values of P are related to the change in enthalpy for NAC formation rather than the change in entropy. He supported this claim by using the energies of the conformations of the mono-*p*-bromophenyl esters (**Table 1.1**) and a weighted Boltzmann distribution to calculate the P of the conformations present as NACs (**Figure 1.20** (a)). A plot of $\log P$ vs. experimental relative rate constants, $k_{(rel)}$, (**Figure 1.20** (b)) revealed a slope of 0.94 indicating a linear relationship between the log of the fraction of conformations present as NACs and ΔG^\ddagger . Therefore, Bruice stated that the rate constant for the reactions of the esters of **Table 1.1** are directly dependent upon the mole fraction of the ground state of each ester present as NACs. When the ground state consists of only NACs, the rate enhancement is 10^8 . **Figure 1.20** (c) shows the values of P are related to the change in ΔH° for NAC and not the variation in phase space entropy ($T\Delta S^\circ$). Therefore, the activation free energy (ΔG^\ddagger) is a function of the ground state enthalpy (ΔH°) for NAC formation. Mandolini^[204] stated intramolecular lactonizations, offered support for entropy of activation (ΔS^\ddagger) as the key feature of ΔG^\ddagger , but Bruice and Lightstone's work supports the idea that intramolecular lactone formation is driven by a favorable ΔH^\ddagger .

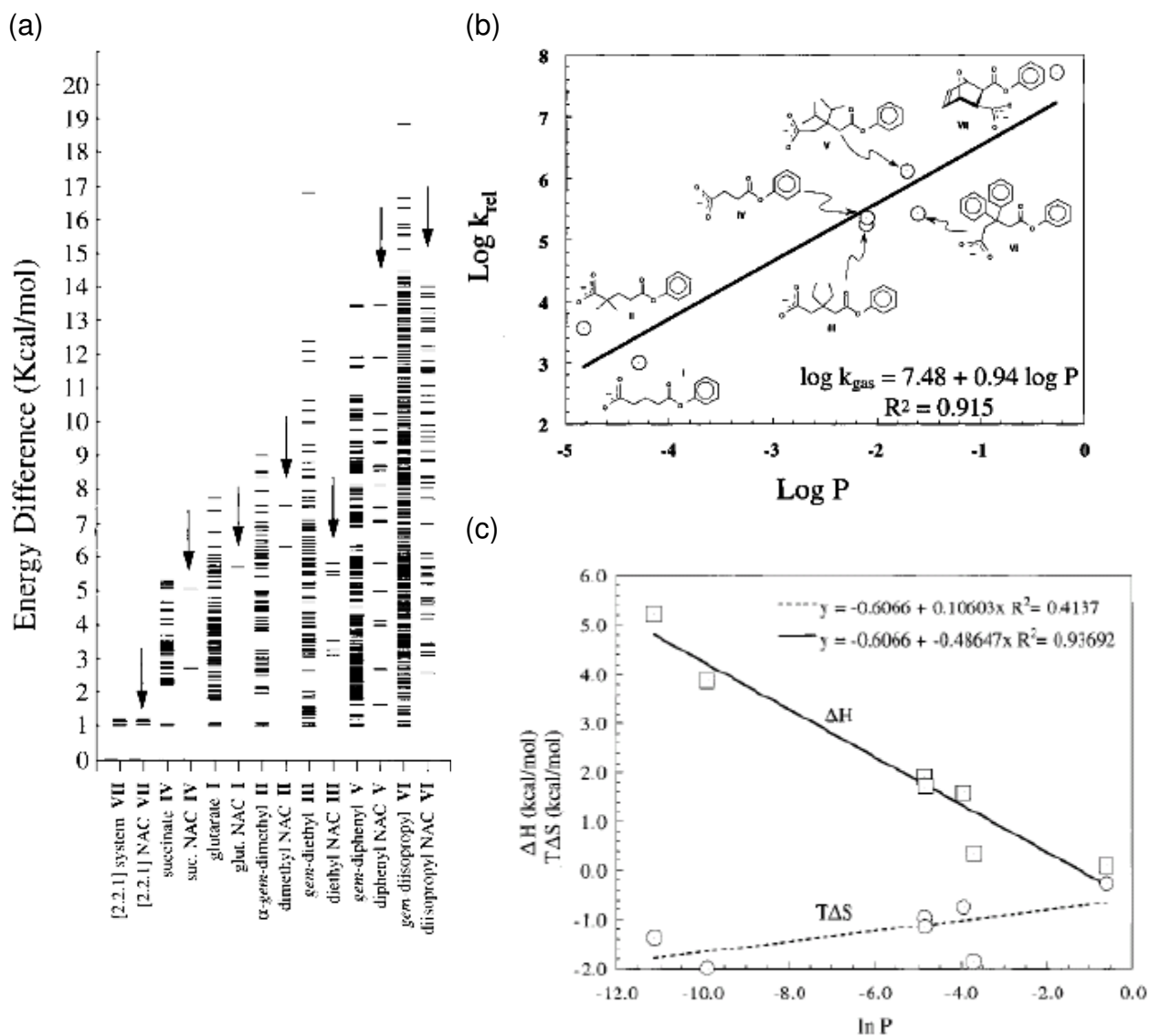


Figure 1.20 (a) Plot of differences of MM3 final energies of all local minimum conformations relative to the lowest energy ground state conformations for each ester in **Table 1.1**. (b) Log of the relative rate constants (k_{rel}) for formation of mono-p-bromophenyl esters vs. the log of the probability of (P) for the NAC formation of each monophenyl ester in **Table 1.1**. (c) Phase space calculated thermodynamic entropy change $T\Delta S$ and internal energy (ΔH) to attain a NAC vs. the natural log of the probability of being in a NAC. **Figure 1.18** taken from reference 65.

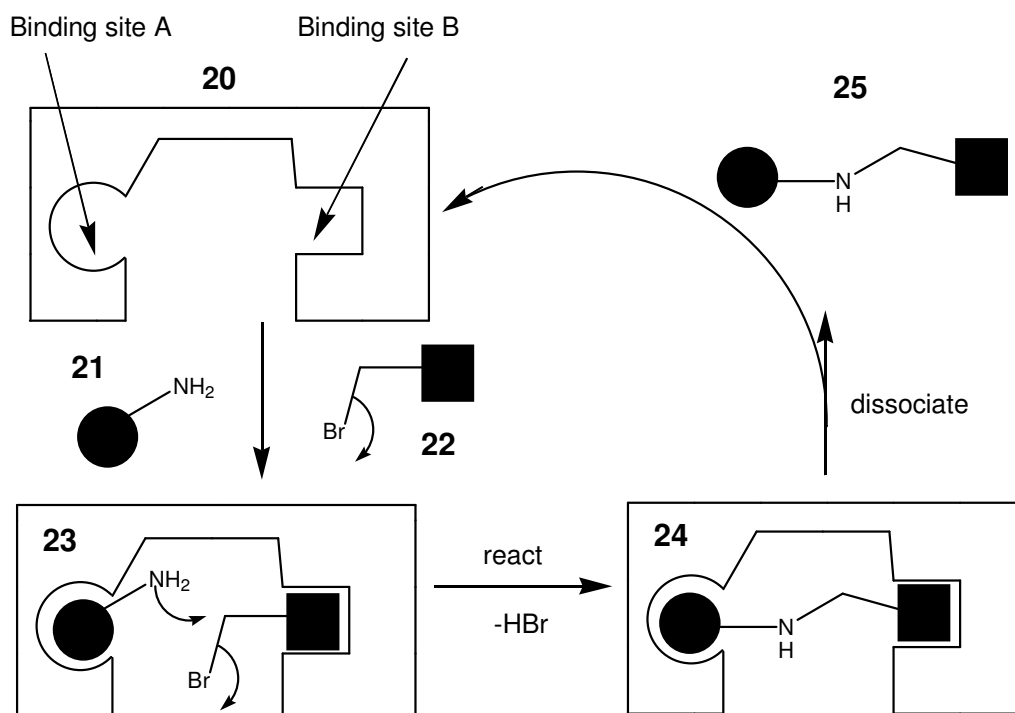
These NAC calculations agree with Menger's 'spatiotemporal' hypothesis that the "rate of reaction is directly proportional to the time **A** and **B** reside at a critical distance. Bruice restates this as the "rate of reaction between functionalities **A** and **B** is directly proportional to the mole fraction of **A** and **B** that reside at a critical distance, when $P = 1$ the ester is permanently fixed in the NAC". Although NACs are accepted as playing a part in enzyme catalysis some still question if they do indeed generate such large increases in rate.

These studies into intramolecularity have provided invaluable insight into reactions in enzymes^[68-70, 208] and have allowed chemistry to attempt to design and synthesize artificial enzymes and, ultimately self-replicating systems.

1.11 Templated Synthesis^[71-84]

The development of “artificial enzymes” capable of conducting reactions at rates normally not attainable in lab conditions, is of great interest to the synthetic chemist. As examined in the previous section (Section 1.10) enzymes exploit the kinetic advantage of turning what is normally an intermolecular reaction into an intramolecular process. However, until Kelly’s pioneering^[74-75] work the focus of artificial enzymes was exclusively^[79-84] on single substrates, which has limited applications to the synthetic chemist.

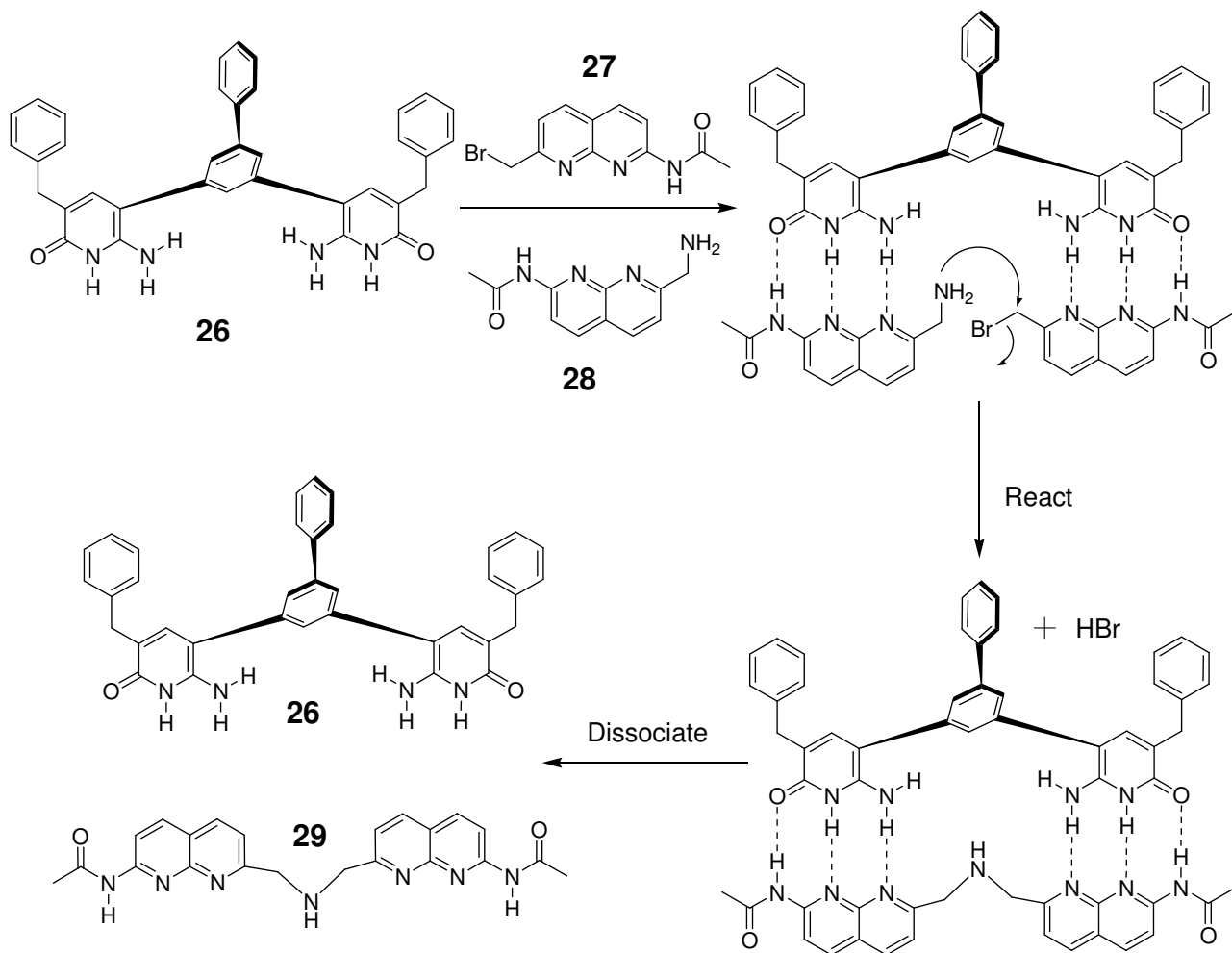
Kelly and co-workers were the first to examine a fully synthetic system where two substrates were bound to a template, in which a reaction between the substrates was accelerated because of transient intramolecularity. The reaction chosen to link the substrates together was a straightforward S_N2 alkylation of an amine to an alkyl halide. A cartoon model of the overall reaction process is illustrated in **Scheme 1.4**.



Scheme 1.4 Cartoon representation of the mechanism of amine alkylation by an artificial enzyme. Adapted from reference 75.

The ditopic receptor binds the two substrates, **21** and **22** *via* complementary recognition to form the ternary complex structure **23**, bringing the two reactive sites into close proximity. Bond formation then occurs to form a template-product duplex structure, **24** which then dissociates to complete the process.

The first system developed (**Scheme 1.5**) by Kelly utilized identical recognition motifs for simplicity. However, Kelly and co-workers would later go on to demonstrate the undesirable nature of this feature.



Scheme 1.5 Artificial enzyme system developed by Kelly and co-workers featuring identical binding sites on the template structure. Adapted from reference 75.

Kinetic measurements of the above system indicated a rate acceleration of six-fold for the alkylation of the amine when the reaction was conducted with template **26** compared to the simple bimolecular process. The authors also conducted a control experiment to demonstrate that the reaction was indeed accelerated *via* a ternary complex structure and not simple catalysis by a subunit of the template. Binding studies for the association

of the substrates to the template indicated that the ternary complex [26•27•28] is the primary constituent of a mixture of **26**, **27** and **28**. Although these results support the basic concepts involved in designing a bisubstrate template the rate enhancements are less than expected for an intramolecular reaction.

Kelly ascribed the poor rate enhancement to the identical recognition sites on the template. By having identical recognition sites the complex [26•27•28] will not be the only ternary complex structure formed. Non-productive ternary complex structures will occur where two molecules of the same substrate bind to the template as in **Figure 1.21**.

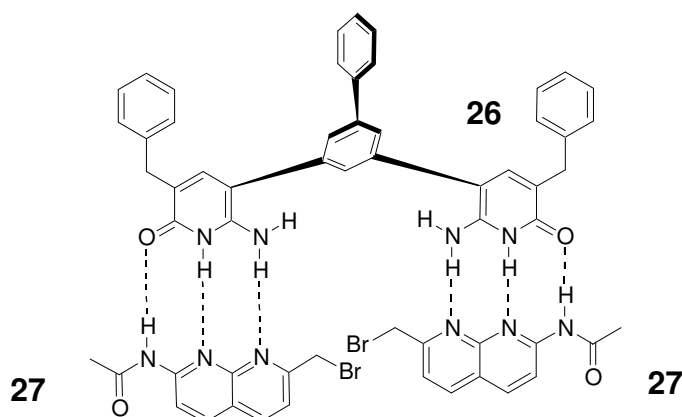


Figure 1.21 Example of one of the nonproductive ternary complex formed through the association of two identical molecules of substrate with the template.

These complexes will have the effect of reducing the rate of formation of **29**. Therefore, in order to circumvent this problem Kelly and co-worker designed a new system with non-identical recognition sites on the template. However, this modification is not as simple as it first sounds.

The binding sites in template **26** consists of a linear triad of two hydrogen bond donors and one acceptor, and therefore, can associate with a structure containing two hydrogen bond acceptors and one donor. This complex is represented as **D** in **Figure 1.22**, where crossed square represent hydrogen bond donors and white squares hydrogen bond acceptors. By rearranging hydrogen bond acceptors and donors a possible of seven other triads, along with their complementary substrate triads, are possible. Kelly decided to maintain the recognition on one of the template binding sites but alter the other. The original template binding site corresponds to **D**, therefore the other site must contain a recognition triad other than **D**. However, not all the remaining triads are acceptable.

Triad **H** is not acceptable as the two substrates would then have complementary binding and could associate with each other instead of the template, the same problem also applies to triad **F**. Another unsuitable triad is **B** as this arrangement is a mirror image of **H**, therefore, the same unproductive ternary complex formed in the system in **Scheme 1.5** would still occur. Therefore, only **A**, **C**, **E** and **G** are suitable triads for the other binding site on the template. Kelly decided to utilize hydrogen bonding pattern **C** and chose the recognition motifs in **Figure 1.23** for the substrate and other template binding site.

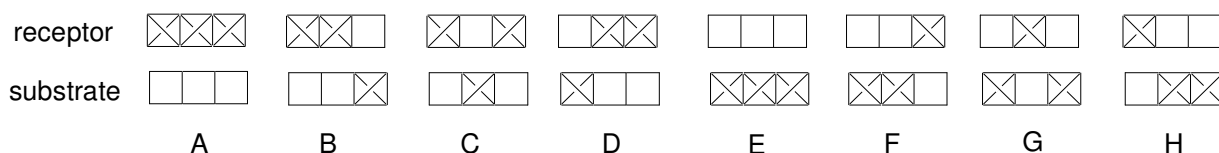


Figure 1.22 Representation of the eight possible linear arrangements of triads of hydrogen bonds involving receptor and substrate. Crossed boxes represent hydrogen bond donors; white box represents hydrogen bond acceptors. Adapted from reference 75.

However, this hydrogen bonding motif still contained a vertical axis of symmetry, with the substrate having the possibility of aligning itself in two possible orientations. One has the alkyl bromide pointing towards the amine ((A), **Figure 1.23**) in a productive complex, whereas the other has the alkyl bromide orientated away from the amine in a non-productive complex ((B), **Figure 1.23**).

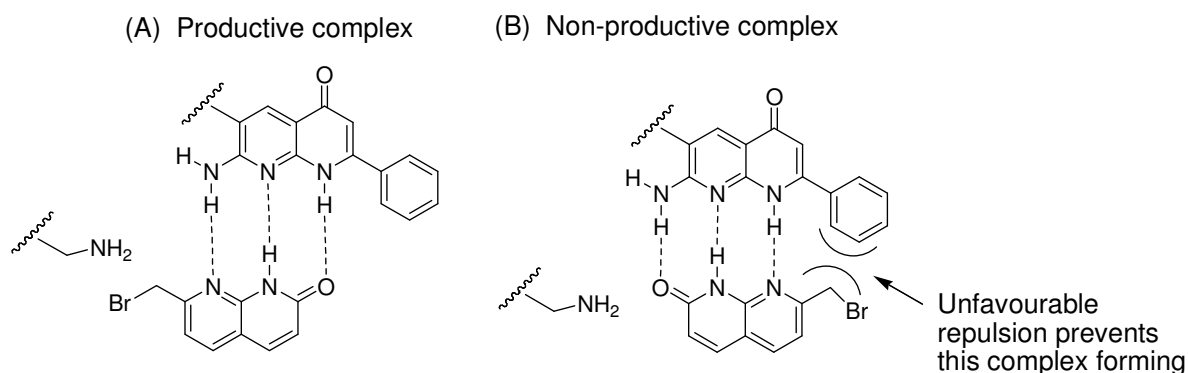


Figure 1.23 (A) Productive ternary complex with the alkyl bromide and amine in close proximity. (B) Unproductive ternary complex with alkyl bromide isolated from amine. Repulsive interaction between the phenyl group and alkyl bromide prevent the formation of this ternary complex.

In order to prevent the formation of this undesired arrangement a phenyl group was placed in the C-7 position of the template, which should provide suitable repulsion to

prevent the formation of this complex. The new template and substrates can now bind together and react through the ternary complex structure shown in **Figure 1.24**.

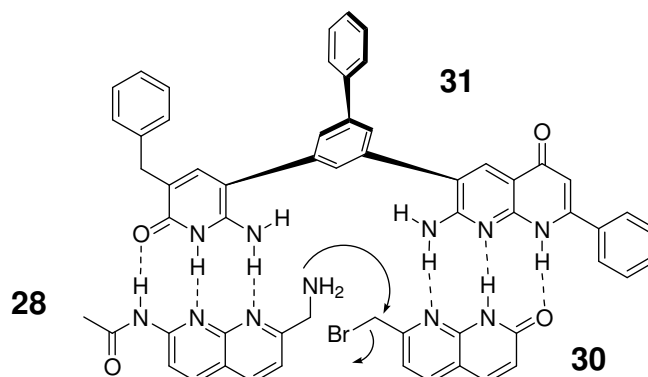


Figure 1.24 Kelly new ternary complex comprised of template with non identical binding sites and new alkyl bromide designed to fit new recognition motif.

Kelly predicted his new system should display a twelve-fold rate enhancement compared to the six fold enhancement observed by the system in **Scheme 1.5**. This doubling in rate arises from the difference in productive ternary complexes formed between the two systems. In the original system, containing two identical recognition sites on the template, a possible four ternary complexes could be formed (**Figure 1.25**), two productive and two non-productive complexes.

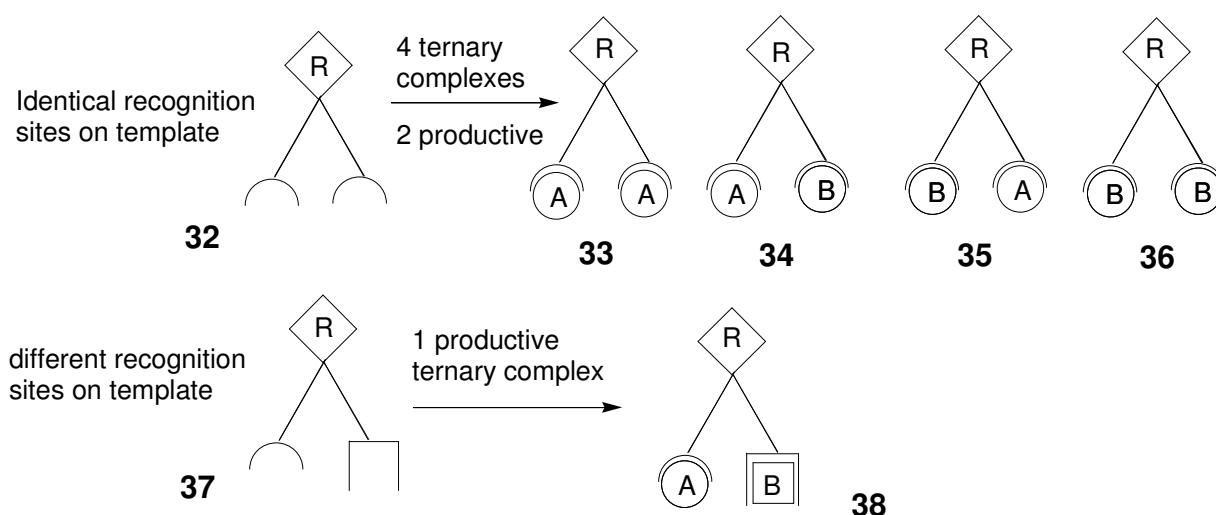


Figure 1.25 Possible ternary complex structures for template with identical recognition motifs, **33**, **34**, **35** and **36** and for template with different recognition groups, **38**. Adapted from reference 75.

In the diagrams in **Figure 1.25 A** represents the amine and **B** the alkyl bromide. However, in his new system only one productive ternary complex is possible. Therefore, in the original system 50 % of the ternary complexes formed will be productive, whereas in the new system 100 % of the ternary complexes are productive.

Indeed Kelly did observe a rate enhancement of twelve-fold compared to the bimolecular reaction for his new system, a doubling in rate of the six-fold enhancement observed in the original. However, the author noted the match of the predicted to the experimental is somewhat coincidental as a number of assumptions were made when comparing the two systems which happened to cancel each other out. One was the fraction of ternary complex present in the two systems. The new system has weaker binding than the original meaning a low fraction of the materials are present in the ternary complex yet increased rate acceleration is still observed. Indicating the new system is more efficient than the original, but this is partly offset by competitive inhibition, resulting in the twelve-fold enhancement observed by Kelly.

The work done by Kelly demonstrates how rational design can be utilized for the production and optimization of bisubstrate systems. Although Kelly's work focused on investigation of simple templated process his work is equally applicable to more complicated bisubstrate systems^[76-78, 212]. The concepts investigated by Kelly are also important in a special form of templated synthesis known as replication. As with the bisubstrated template reactions, replication occurs through the close proximity of two substrates bound to a template in a ternary complex structure. Therefore, the concepts developed by Kelly and co-workers on ternary complexes are essential to anyone who wishes to design, synthesize and analyze a replicating system. The work of Kelly provides a good link between templated synthesis and replication which will be examined in the next section.

1.12 Minimal model of replication^[85-92, 213-214]

The minimal model of replication is based on template directed synthesis and involves the production of identical versions of the same molecule. Utilizing the lessons learned by Kelly and co-workers the template molecule contains non-identical recognition units to avoid formation of unproductive complexes. In this system there are three possible channels available to the starting materials **A** and **B** (**Figure 1.26**).

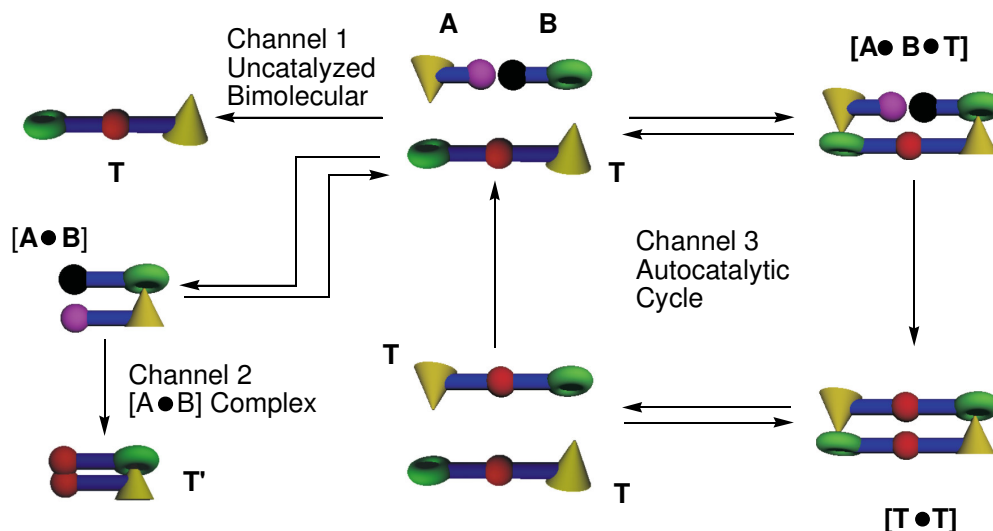


Figure 1.26 Schematic representation of minimal replicating system highlighting the three reaction channels available to building blocks **A** and **B**.

A and **B** contain a reactive site (Purple color sphere reacts with Black sphere) and complementary recognition (Green doughnut can associate with Yellow cones). The first of these channels is a simple bimolecular reaction between the template building blocks **A** and **B**, which results in the formation of a molecule of template (**T**), containing self-complementary recognition motifs. The second channel available is an autocatalytic cycle, in this channel **A** and **B** simultaneously associate to a molecule of **T**, via the self-complementary recognition to form a ternary complex **[A•B•T]**. The proximity of reactive sites and the correct orientation of the molecular orbitals in this ternary complex renders the reaction *pseudo*-unimolecular, facilitating bond formation between **A** and **B**. This reaction results in the formation of another molecule of **T** in a **[T•T]** duplex complex. The correct orientation and proximity are as a result of the specific interactions between the building blocks **A**, **B** and the molecule of **T** in the ternary complex, which has the effect of controlling the regio- and stereochemistry of the product **T**. At the **[T•T]** complex stage the system can be considered self-replicating as another molecule of **T** has been formed. However, it can not yet be considered autocatalytic, only when the **[T•T]** complex dissociates returning two molecules of **T** to the start of the cycle can the system be considered autocatalytic. Each turn of the cycle doubles the amount of template formed resulting in exponential growth, one makes two, two makes four, four makes eight and so until the source of building blocks is depleted. This exponential growth

results in the sigmoidal shape observed in the rate profile of an autocatalytic self-replicating system (**Figure 1.27**).

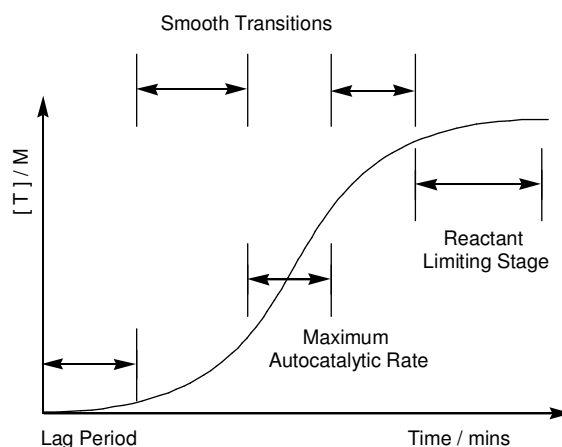


Figure 1.27 Rate profile for minimal self-replication consisting of three periods, a lag period, a maximum autocatalytic rate period and a reactant limiting period.

The final channel available to **A** and **B** is the AB channel. This channel arises because **A** and **B** have complementary recognition sites, these can associate leading to the reversible formation of an $[A \cdot B]$ complex. If the reactive sites of **A** and **B** are brought close enough together and in the correct orientation to each other, the reaction once again can be rendered *pseudo*-unimolecular. Through controlling the approach of the reactive sites the regio- and stereochemistry of the resulting product can be controlled. In the $[A \cdot B]$ channel the approach of the reactive sites can still be controlled and so an AB channel can still have regio- and stereochemical control. However, unlike the previous channel the reaction can not be considered autocatalytic as the product does not catalyze its own formation. This is because the complementary recognition sites are still associated in T' , in effect it is a closed template. Therefore T' is unable to associate with a molecule of **A** and **B** building blocks and so can not catalyze its own formation.

1.13 Potential problems in a self-replicating system

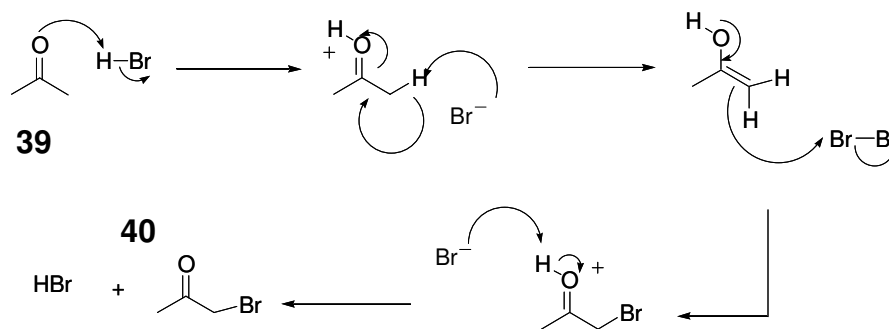
One of the potential problems that can occur in a minimal replicating system is if the AB channel is competing with the autocatalytic channel. The formation of the $[A \cdot B]$ complex is more favorable as this only requires one association between two molecules; whereas the ternary complex $[A \cdot B \cdot T]$ requires two associations between three molecules. The

result of this is that there is a much greater concentration of $[A \cdot B]$ complex than $[A \cdot B \cdot T]$. As previously mentioned, the $[A \cdot B]$ complex is not autocatalytic, therefore, the amount of T returned to the system is reduced, quenching the reaction. However, this problem can be reduced or eradicated through careful consideration and manipulation of the molecular structure.

In addition to the previous mentioned problem the stability of the product duplex $[T \cdot T]$ can also hinder autocatalytic replication. By its nature the product duplex $[T \cdot T]$ should be more stable than the ternary complex $[A \cdot B \cdot T]$ from which it was formed. This enhanced stability is a consequence of going from three molecules bound through two complementary recognition sites in the ternary complex, to only two molecules associated *via* two complementary recognition sites in the product duplex. A problem arises if the product duplex becomes too stable, if this occurs individual molecules of template are trapped in this complex structure, preventing them catalyzing the formation of more molecules of themselves. When this problem occurs the system can still be considered self-replicating but it cannot be thought of as autocatalytic.

1.14 Autocatalytic reactions vs. Self-replication

At this stage it is important to distinguish between self-replication and autocatalysis. In an autocatalytic reaction the product of the reaction is itself a catalyst for its own formation, returning more catalyst after each turn of the cycle. If it does not return catalyst to the reaction then it is not autocatalytic. A good example of an autocatalytic reaction is the bromination of acetone (**Scheme 1.6**).



Scheme 1.6 An example of autocatalysis showing the reaction between HBr and acetone, **39**, where the by-product of the reaction catalyzes the reaction.

The oxygen on the acetone is protonated under the acidic HBr conditions. This reaction leaves the bromonium ion free to attack the acidic α -proton on the acetone, reforming HBr and an enol. The enol can then attack a molecule of bromine to form the alkyl bromide and the bromonium ion, which deprotonates the oxygen to form 1-bromopropan-2-one and HBr as a by-product. This by-product can then catalyze the formation of more 1-bromopropan-2-one. The important factor in autocatalysis is that there is a total lack of specificity as any Brønsted acid would catalyze the reaction above, on top of this autocatalysis also catalyzes unwanted side reactions. It is this which distinguishes self-replication from autocatalysis, a self-replicating system will only catalyze its own formation (selfish catalyst). A simple autocatalyst cannot amplify 'information' (desired reaction) as it also amplifies the 'noise' (side reactions); however, a self-replicating system has the ability to only amplify the 'information' and not the 'noise'.

1.15 Reciprocal model of replication^[142-144]

A more complicated model of replication is that of reciprocal replication (cross-catalysis). The most famous example of a reciprocal replicating system is that of DNA^[151]. The complementary nature of DNA has interested scientists for a long time and has prompted interest into how a reciprocal system replicates.

The key difference between minimal and reciprocal replication is that template **T**, in a minimal system is self-complementary, however, **T** in a reciprocal system, is complementary to another non-identical molecule of template. This complementary nature opens up the possibility for the formation of a number of unproductive ternary complexes, like those discussed by Kelly in a previous section (Section 1.11).

The reciprocal replicating model starts with two templates **T**₁ and **T**₂ associating with their complementary fragments **A**, **B** and **C**, **D** (**Figure 1.28**).

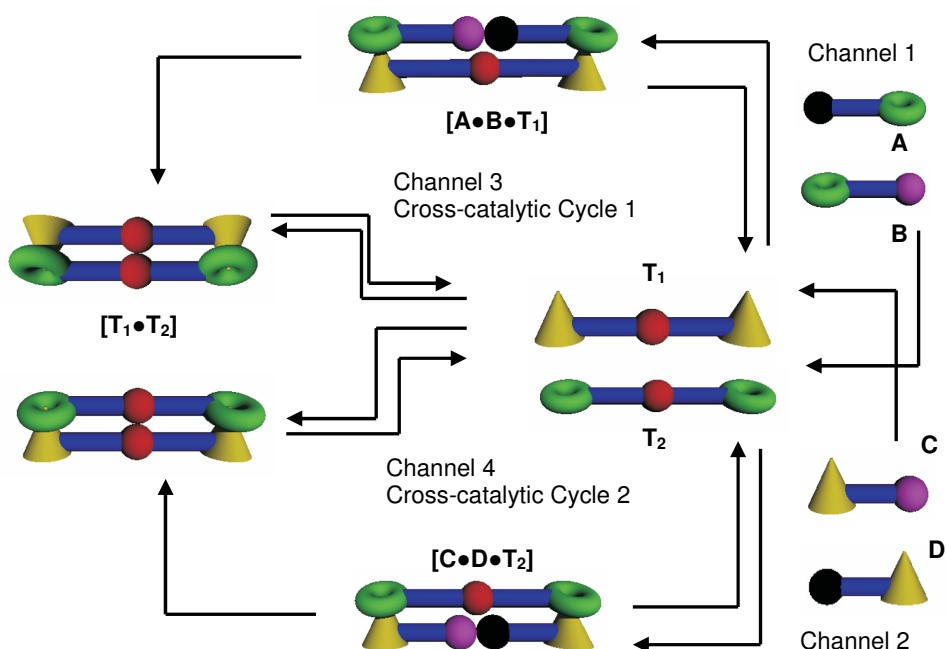
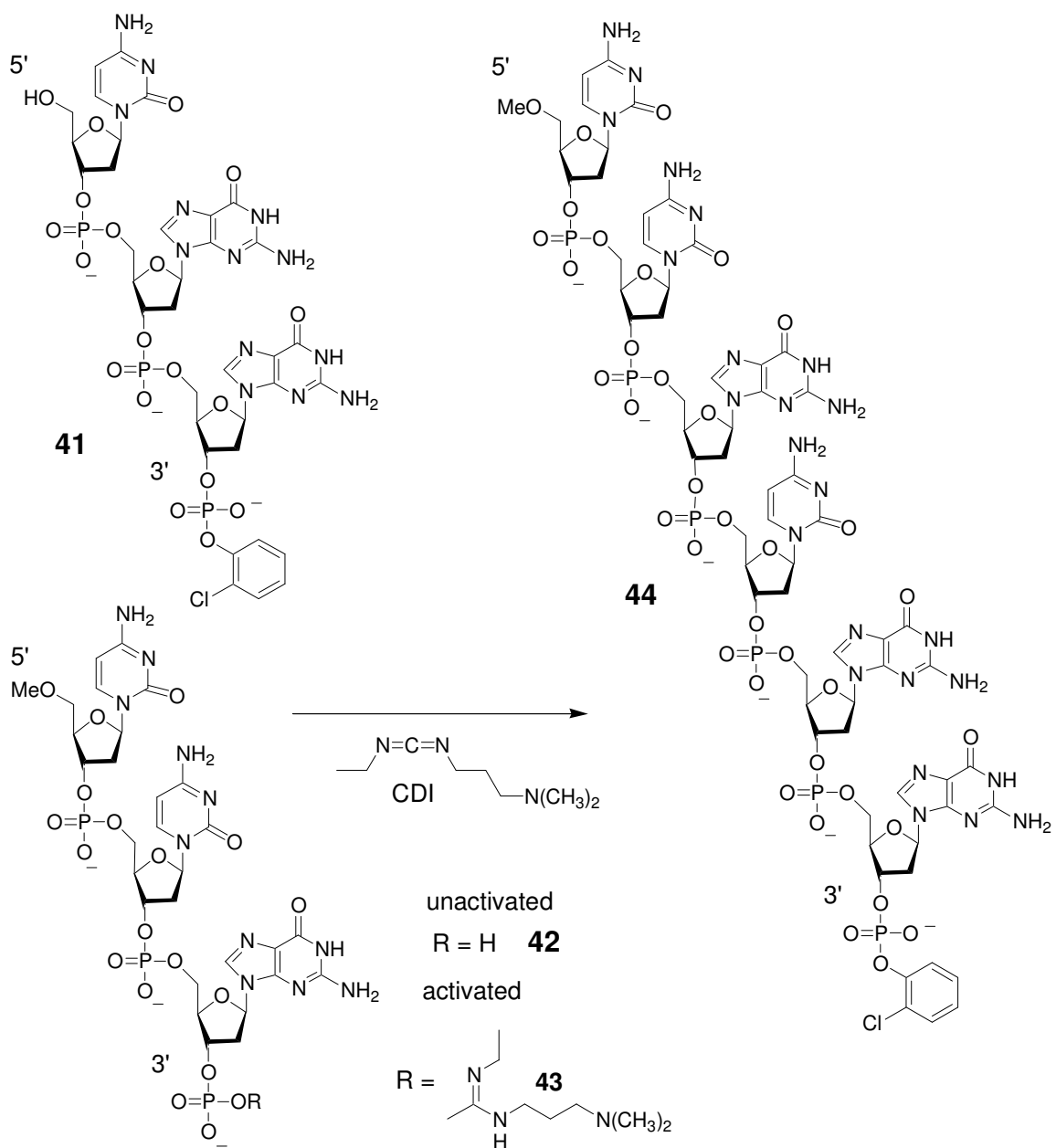


Figure 1.28 Schematic model of reciprocal replication consisting of two cross-catalytic channels.

As in the minimal model, the building blocks form a reversible ternary complex with their complementary template. This ternary complex brings the reactive sites close enough together to render the reaction *pseudo*-unimolecular, inducing covalent bond formation. Through controlling the approach of reactive sites in the ternary complex, regio- and stereochemical control of the product can be obtained, resulting in the formation of the $[T_1 \bullet T_2]$ duplex, which can then dissociate to form the complementary non identical template. This template is then available to associate with its complementary building blocks and repeat the whole cycle, whereas minimal replication involves replication through a single autocatalytic cycle; reciprocal replication involves replication through two cross-linked catalytic cycles in which each cycle provides the template for the other ones synthesis. One of the consequences of reciprocal replication can be observed in the rate profile. In a minimal model, a characteristic sigmoid shape is observed in the rate profile; whereas in the reciprocal model a parabolic graph (C-shaped) is observed. The loss of sigmoid shape is because the cycle is not autocatalytic but cross-catalytic.

1.16 Minimal self-replication incorporating natural products^[94-101]

Von Kiedrowski's^[94] first replicating system consisted of two trinucleotides, which could together undergo a condensation reaction to form a hexameric template with a palindromic sequence. The two trinucleotides were a trideoxyribonucleotide 3'-phosphate with its 5'-terminus protected as a methyl ester (d(MeC-C-Gp) and a complementary trideoxyribonucleotide-3-phosphate with its 3'-terminus protected as an *o*-chlorophenyl group (d(C-G-Gp) (**Scheme 1.7**).



Scheme 1.7 Von Kiedrowski's model for minimal self-replication based on hexadeoxynucleotides.

These two nucleotides can react together to form the self-complementary hexameric template d(MeC-C-G-C-G-Gp). For this reaction to occur, **42** had to be first activated with 1-(3-dimethylaminopropyl)-3-ethylcarbodiimide (CDI) to form **43**, before reacting with **41**. Two different products were observed in this reaction, the first was the desired hexameric template product **44**, the second was an unwanted 3'-3'-linked pyrophosphate (pp). The latter product was formed through the self condensation of **42** to form sequence d(MeCCGppGCCMe). The formation of the template should increase the rate of reaction as it should be able to associate with two molecules of the starting material to form a ternary complex due to its complementary nature. Starting molecules **41** and **43** can then react to form an identical molecule of template in a [**44**•**44**] duplex. This duplex can then dissociate allowing, the original and the new molecule of **44** to template further reactions, resulting in exponential growth. However, when von Kiedrowski monitored the reaction by HPLC, a non-sigmoidal rate graph was observed and only 12 % of combined product was observed (**Figure 1.29**).

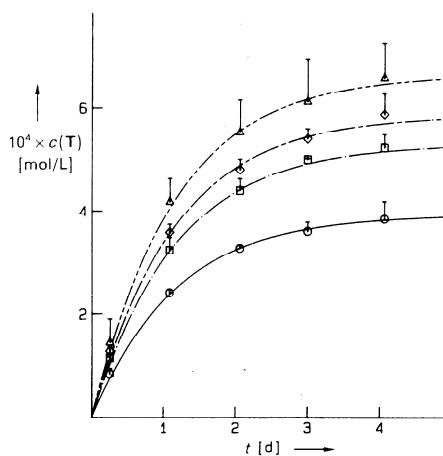


Figure 1.29 Time course of template **44** production in reaction mixtures containing different initial concentrations of template. Circles = 0 mM, squares = 0.2 mM (1 eq.), diamonds = 0.4 mM (2 eq.) and triangles = 0.8 mM (4 eq.). Figure taken from reference 95.

Von Kiedrowski explained that the low yield and lack of sigmoid shape in the rate profile graph was due to a number of reasons. The first of these was that the activated reactant **43** underwent rapid hydrolysis to the unreactive **42**; the second possibility was the formation of a number of unreactive binding events such as the binding of 3'-3'-linked pyrophosphate (pp) to building blocks **41** and **42** which would inhibit formation of the hexameric template.

Von Kiedrowski demonstrated that the kinetics of his system could be understood through the use of the following equation (**Figure 1.30**).

$$\{dc(T)\}_{initial} = k_a C_0(T)^p + k_b$$

Figure 1.30 The equation used by von Kiedrowski to describe the kinetics of his minimal replicating system.

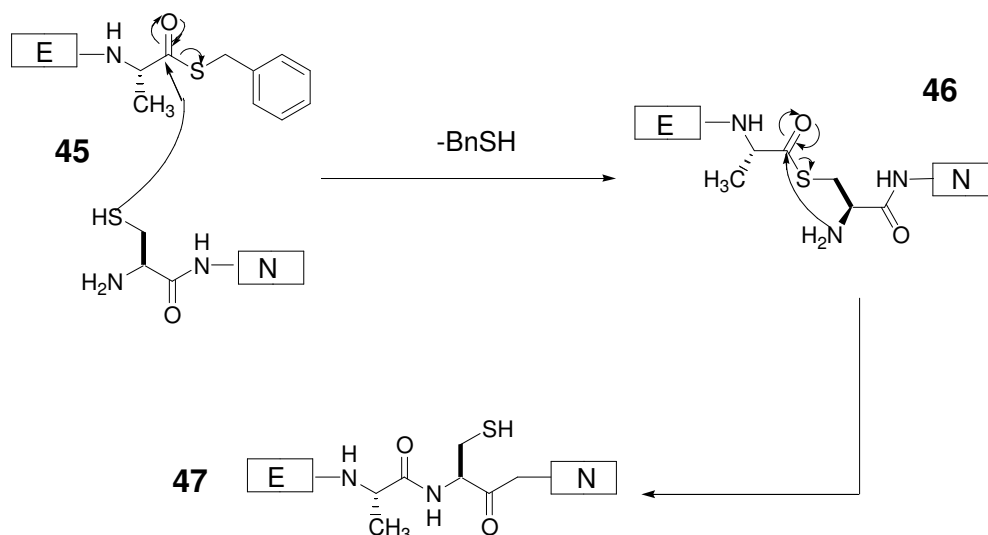
Where k_a is the rate constant of the catalytic process, $C_0(T)$ is the initial concentration of template, p is the reaction order with respect to T and k_b is the *pseudo* zero order constant of the uncatalyzed reaction. A value of 0.5 for p indicates that replication obeys square root law with stable $[T \bullet T]$ complex, indicating product inhibition, a value of 1 indicates unstable $[T \bullet T]$ complex and exponential growth with no inhibition.

Through the use of the least squares line fit, von Kiedrowski obtained a value of 0.48 for which he used to assume a reaction order of $\frac{1}{2}$ for initial stage of reaction. An efficient self-replicating system should exhibit a high k_a and a low k_b .

Later, von Kiedrowski developed^[95-96] a new oligonucleotide replicator with increased efficiency. From the values obtained for k_a von Kiedrowski showed his system was 75 times more effective than a system by Rebek^[104] and 130 times more efficient than a system designed by Orgel.

Minimal self-replicating systems based on natural products have interested other groups, which have come up with their own ideas of how to achieve this goal. Ghadiri came up with the first example of a self-replicating system based^[97] on peptide replication, which utilised a wide variety of non-covalent interactions. Unlike the nucleic acid example of replication developed by Orgel and Kiedrowski, polypeptides are not intrinsically self-complementary molecular structures. In peptides replication does not just involve the primary sequence, it also involves the secondary structure, when folded. Ghadiri based his system on a simple protein folding motif the α -helical coiled coil. Ghadiri postulated that a coiled-coiled peptide subunit may act as a template to organise two shorter subunits on to it to form an identical copy with higher coupling rates due to their close proximity and higher effective molarity. He based this assumption on the fact that monomeric peptide subunits of a coiled coil in aqueous solution are typically random coils, but almost all completely α -helical in the aggregated state, so coiled coil may be seen as a template for its own formation. Ghadiri's system consisted of a

nucleophilic peptide fragment **N** with a free cysteine residue at the N-terminal and an electrophilic peptide fragment **E** which is preactivated as a thiobenzyl ester. These peptides can undergo a condensation reaction in a strategy developed by Kent (**Scheme 1.7**).



Scheme 1.7 Mechanism of the condensation reaction. **E** represents an electrophilic peptide sequence and **N** represents the nucleophilic peptide sequence.

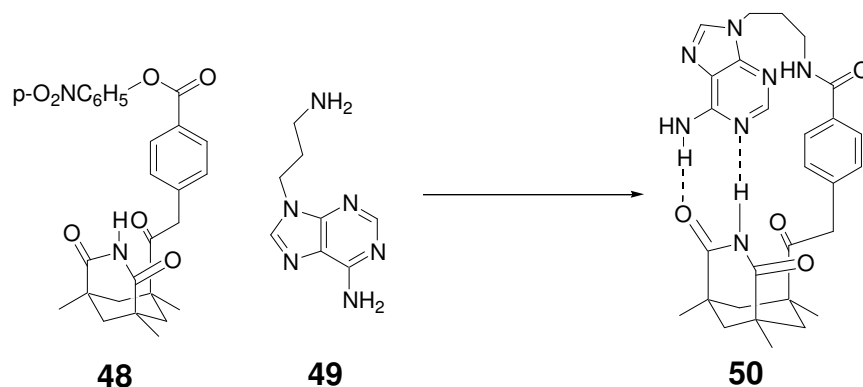
As a template for these peptide fragments a 32-residue polypeptide was chosen which was similar in sequence to a coiled coil α -helix of a yeast transcription factor GCN4. In a reaction with 30 % template added, there was a dramatic increase in rate of 540 %. It was also noted that there was reasonable regio- and chemoselectivity with less than 15 % side products observed. From the kinetic data a value for ρ of 0.63 was obtained which indicated that autocatalysis proceeded through the two stranded α -helix template. Later Chmielewski^[98] and co-workers showed through shortening chain length you could destabilise its coiled structure and hence improve its catalytic efficiency. They found that the resulting system was remarkably efficient compared to other self-replicating systems with a ρ value of 0.91. This was the first example of a self-replicating system that obtained a reaction order higher than the product inhibition order.

Another type of natural product based self-replication has been investigated by Joyce, that of self-replicating ligase ribozymes⁹⁹⁻¹⁰¹. This type of self-replicating system is based on a ribozyme that catalyzes additional copies of itself through RNA catalyzed RNA ligating reactions. The type of behavior in this system is unique when it is compared to other forms of self-replication; this is because the template substrate-dimer

is a ribozyme which adds more catalytic potential to the system with each template forming reaction. When the kinetic data were analysed a value of 1 was obtained for the reaction order, p , indicating the system was undergoing exponential growth, with no inhibition.

1.17 Minimal synthetic replicating systems^[103-130]

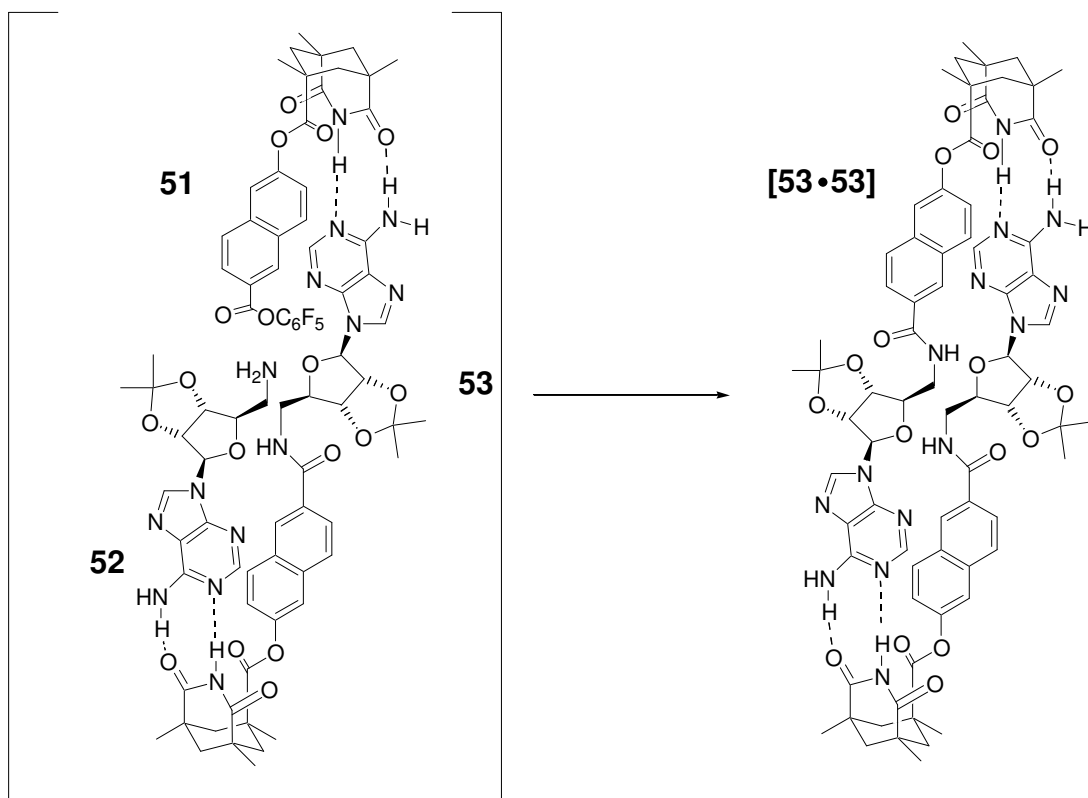
The first minimal synthetic self-replicating system was developed^[103-108] by Rebek. This system utilised the binding Rebek and co-workers had observed between Kemp's triacid^[102] and adenosine. This system comprised of two building block molecules a Kemp triacid imide with a phenyl spacer unit attached to it, and an adenine residue with an amino group attached (**Scheme 1.8**). The phenyl spacer had a *para* electrophilic acylating function associated with it and the 9-(3-aminopropyl)adenine had a nucleophilic amino group attached. Unfortunately however, this system was found to be unable to template its own formation. The reason for this Rebek claimed was due to the combination of a short spacer unit and the formation of the favored *trans* amide, which resulted in a reactive AB complex (**Scheme 1.8**). This complex can not template its own formation as it retains the intramolecular non-covalent interactions, meaning building blocks are unable to associate to this closed template.



Scheme 1.8 Rebek's first attempt at a synthetic replicating system resulted in an [A•B] complex.

As a result of this, Rebek redesigned^[106-109] his self-replicating system by increasing the size of the spacer unit. He achieved this through replacing the small phenyl spacer with a larger naphthalene spacer in compound **48**. Rebek also added a bulky ribose

derivative to the adenine component **49**; the reason for this was to help destabilise the [T•T] duplex by having two bulky groups in close proximity. By destabilising the [T•T] duplex this allows the templates to easily dissociate from one another, returning template to the autocatalytic cycle faster and so improving catalysis. These changes, resulted in the formation of 5'-aminoadenosine derivative which could couple to the imide bearing a 2,6-naphthalene ring (**Scheme 1.9**).



Scheme 1.9 Rebek's synthetic self-replicating system incorporating a naphthalene spacer in the template **53**. This template can associate with the two building blocks **51** and **52** as shown above to form the catalytic ternary complex and then the resultant product duplex **[53•53]**.

This system was shown to increase the rate of reaction by 43 % when 0.2 equivalents of template were added at the start of the reaction, and by 73 % when 0.5 equivalents were added. The rate profile for this reaction does not have the characteristic sigmoidal shape (**Figure 1.31**), a result of AB complex activity and 'systematic' errors, according to the author.

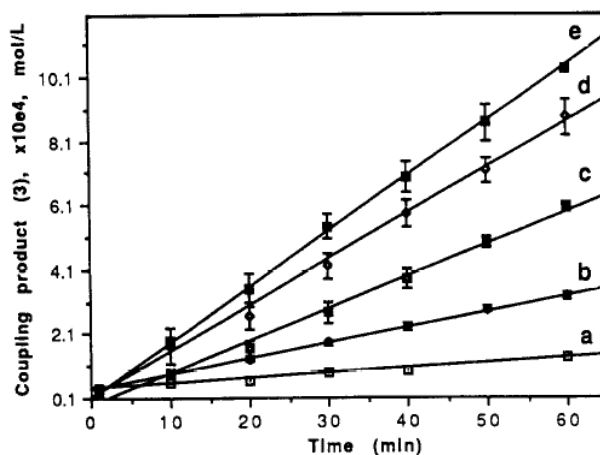
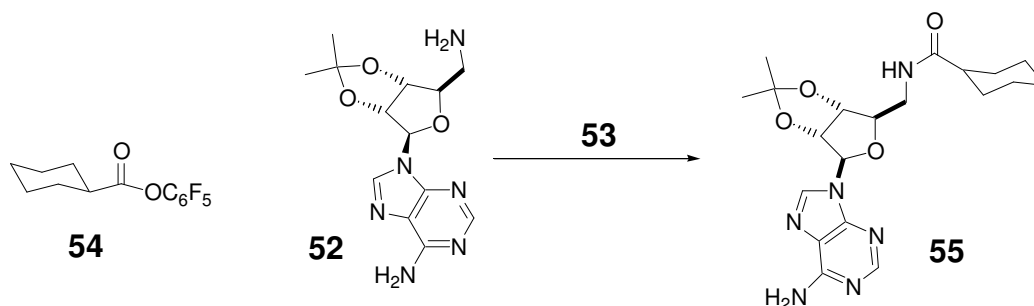


Figure 1.31 Rate of production of template **53**(a) using a non-binding control compound, (b) using a competitive binding compound, (c) with only the building blocks, (d) with 0.2 eq. of added template **53**, (e) with 0.5 eq. of added template **53**. Figure taken from reference 105.

In the AB complex, the *cis* amide isomer would be formed first, which could then undergo isomerisation to the *trans* isomer. At this stage the *trans* isomer can form a ternary complex with building blocks so is able to enter the autocatalytic cycle. An association constant was estimated for the ternary complex, this constant was in the area of 3600 M^{-2} . This value allowed Rebek to determine that 2 % of the building blocks are in the form of the ternary complex under autocatalytic conditions and 25 % are in the form of the AB complex. These values, Rebek concluded, showed how effective a catalyst the template was, as it was able to catalyze its own formation from such a small amount of catalytic complex.

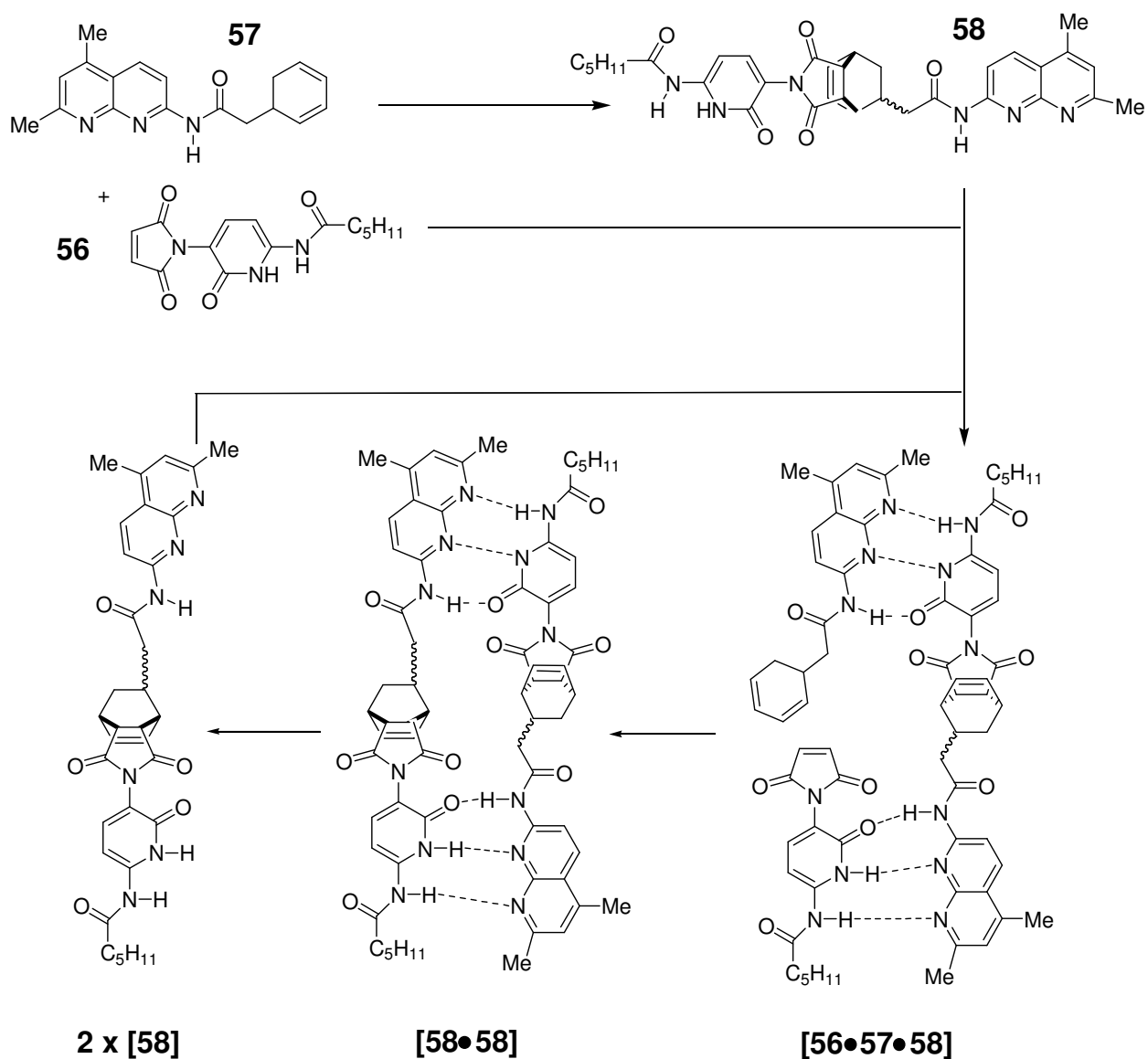
Rebek's claim that he had developed the first synthetic replicating system at the time was extremely controversial, and a number of people disputed Rebek's findings suggesting alternative mechanisms^[110-112] for the catalysis in Rebek's systems. Menger^[111-112] argued that the catalysis observed was nothing more than simple amide catalysis. Amides have been shown to accelerate aminolysis through stabilizing the tetrahedral zwitterionic intermediate through hydrogen bonding. In order to disprove this theory Rebek conducted^[103, 113-114] an experiment coupling the adenine ribose derivative **52** to **54** using template **53**, which is incapable of hydrogen bonding (**Scheme 1.10**). Template **53** did not act as a catalyst for formation of **55**, which would happen if simple amide catalysis was occurring, hence this proves that catalysis is as a result of template's ability to bind substrates through hydrogen bonding not simple amide catalysis.



Scheme 1.10 Rebek's experiment to disprove amide catalysis, the addition of **53** to the coupling reaction between **52** and **54** (which is incapable of forming hydrogen bonds) did not increase the rate of formation of **55**, showing simple amide catalysis was not the reason for the rate acceleration in Rebek's self replicating system.

All self-replicating systems so far discussed have been designed through consideration of prebiotic evolution, however, recently Wang and Sutherland^[121] described an alternative approach not based on natural recognition motifs. Their system revolved around a [4+2] cycloaddition between a 6-acrylamine-2-pyridine **56** derivative and a 2-acylaminonaphthyridine **57**. This system was decided upon after careful consideration of molecular modelling, solubility and ease of synthesis. In this system recognition between molecules does not involve binding between base pairs but instead hydrogen bonding between heterocycles (**Scheme 1.11**).

The addition of as little as 0.05 and 0.1 equivalents of template **58** produced initial catalysis resulting in the disappearance of the lag period (**Figure 1.32**). The kinetic data gave the catalyzed system a rate of $2.0 \times 10^{-3} \text{ s}^{-1}$ and the non-catalyzed reaction a rate of $2.8 \times 10^{-4} \text{ mol}^{-1} \text{ s}^{-1}$. From this it allowed the calculation of an effective molarity of 7 M, indicating efficient catalysis of the reaction as a result of the recognition mediated reaction.



Scheme 1.11 Wang and Sutherlands self replicating system using a Diels-Alder reaction at the reactive site.

Unfortunately, the authors were unable to determine whether only one or both of the diastereoisomers of **58** were involved in replication.

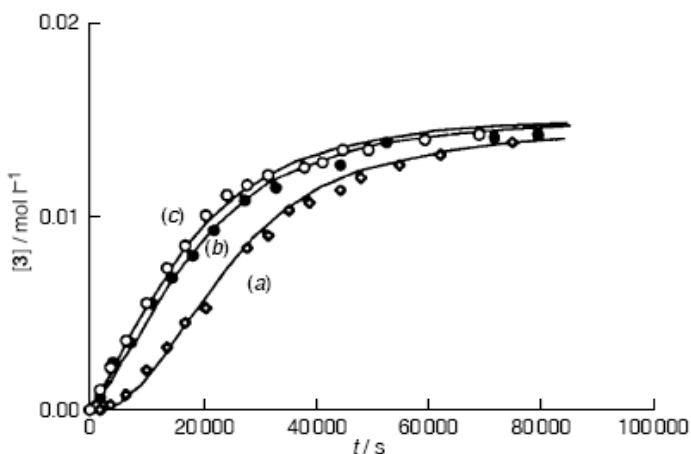
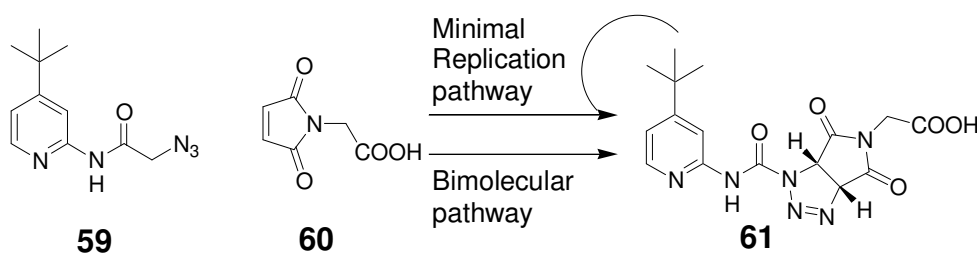


Figure 1.32 Rate profiles obtained for the reaction of **56** and **57** at 40°C in CD_2Cl_2 with (a) 0% added template **58** at $t = 0$ s, (b) 5% added template and (c) 10% added template. Figure taken from reference 121.

Although published after Wang and Sutherland's system Philp and co-workers were also investigating^[121-122] replication using synthetic chemistry at the same time. An example of one of their first systems involved^[122] the reaction between an azide (1, 3-dipole) and a maleimide (dipolarophile) (**Scheme 1.12**).

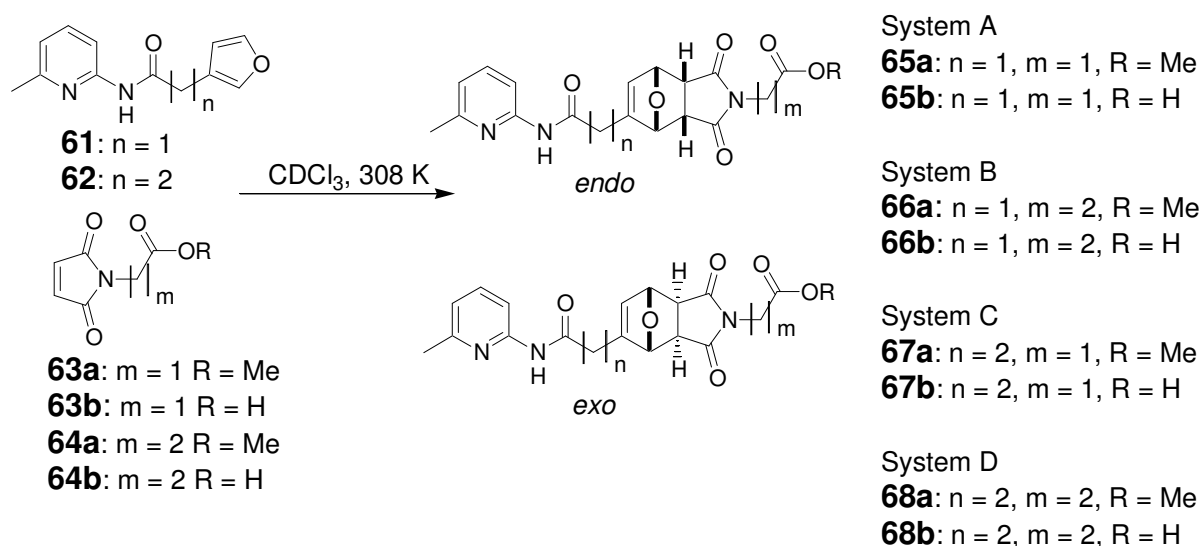


Scheme 1.12 The molecules used in Philp's replicating system, an azide **59** reacts with a maleimide **60** to form cycloadduct **61**, which is capable of acting as a template for its own formation.

Template **61** was found to undergo inefficient self-replication; a p value of 0.4 was calculated for this structure using the same equation von Kiedrowski used to analyze his oligonucleotide system (Section 1.16). This value indicated that the low autocatalytic effect was a consequence of a very stable product duplex [**61**•**61**], which limited turnover of catalyst reducing the rate of replication.

Interested by the difficulty in predicting the behavior of organic replicators, Philp and co-workers decided to try and establish a clear relationship^[123-128] between the relative orientation of the reactive and recognition sites in a particular system and its kinetic behavior.

In designing^[125-126] their new system they decided to utilize the amidopyridine/ carboxylic acid hydrogen bonding recognition motifs which they have extensively studied. The Diels-Alder reaction was chosen as the covalent bond forming step in order to link the building block molecules together to form the potential minimal template. This reaction is an excellent candidate as a consequence of its well understood mechanism and its strict stereoelectronic demands. In order to investigate the relationship between structure and function in minimal replicators four different building block molecules were designed and synthesized which could form four potential minimal replicating systems, Systems A- D (**Scheme 1.13**). As the Diels-Alder reaction can form both *exo*- and *endo*- product this feature means a total of eight template molecules are possible. These molecules were designed so that the effect of the number of methylene spacers between the recognition sites and the reactive sites (m and n in **Scheme 1.13**) could be investigated.



Scheme 1.13 Building blocks 1-4 can react to form four potential minimal replicating systems A-D with various spacer lengths between reactive sites and recognition moieties.

System A (**Scheme 1.13**) contains the shortest length tether (least methylene groups) between the recognition sites and the reactive sites, **61**. Detailed analysis of this system revealed both *exo*-**65b** and *endo*-**65b** were self-replicating molecules. With both templates showing signs of replication it opened the possibility that not only were *endo*-**65b** and *exo*-**65b** templating their own formation but cross-catalyzing the other's formation in a hypercyclic system. However, molecular mechanical calculation revealed that while both the [*endo*-**65b**•*endo*-**65b**] and [*exo*-**65b**•*exo*-**65b**] exhibit stable dimeric structures containing four hydrogen bonds, the heterodimer [*endo*-**65b**•*exo*-**65b**]

contains no low-energy structure with more than two hydrogen bonds. Because the transition state in the cycloaddition occurs relatively late these calculations of the product duplex resemble the ternary complex structure. Therefore, it seems unlikely that one diastereoisomeric template could support the transition state for the other. The selectivity in this system was found to favor *endo* to *exo* in a 5:3 ratio, compared to 3:1 if the reaction proceeds *via* only a bimolecular route. Selectivity has actually decreased; this decline is a consequence of the stronger recognition-mediated acceleration of the production of *exo-65b*.

System B (**Scheme 1.13**) introduces an additional methylene unit into the dienophile. Unfortunately, however, the insolubility of templates *endo-66b* and *exo-66b* prevented a detailed study of this system. From the data obtained and molecular modeling studies it appears though that any selectivity or rate enhancement in the system, would be the result of *endo-66b* proceeding *via* a binary complex route, with *exo-66b* at best replicating at such low rate as to make its effect insignificant.

System C (**Scheme 1.13**) introduces a CH₂CH₂ spacer between the recognition site and the diene, and a methylene group between the recognition site and the dienophile. Examination of this system revealed *endo-67b* was favored over *exo-67b* in a ratio of 5:1 compared to 1.6:1 in the comparative bimolecular reaction. Despite the four hydrogen bonding homoduplex solid state structure of *endo-67b*, as determined (**Figure 1.33**) by single X-ray diffraction, the kinetic data provided no evidence for formation *via* a minimal replicating pathway. Instead the kinetic data are consistent with a binary complex pathway.

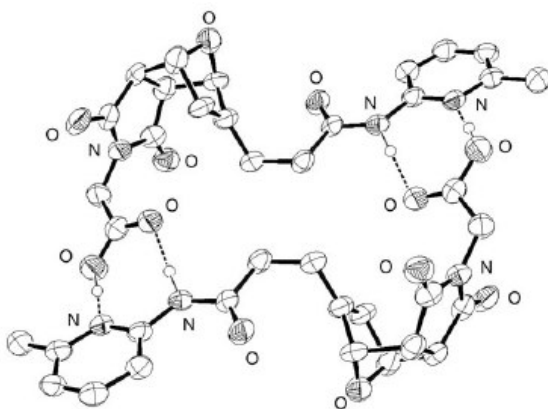


Figure 1.33 Ball and stick representation of the cycloadduct *endo-67b* in solid state determined by single crystal X-ray diffraction.

System D (**Scheme 1.13**) introduces a CH₂CH₂ spacer between the recognition site and the diene, and a CH₂CH₂ between the recognition site and the dienophile. This system again obtained its rate acceleration and selectivity by the formation of *endo*-**68b** occurring *via* a binary complex.

Examination of these four systems indicates that given enough conformational freedom the most likely recognition mediated pathway for reaction is that involving a binary complex. In order to generate an autocatalytic system the binary pathway must be prevented or at least reduced. This goal is obtainable if the shortest possible tether length is used one methylene group on the diene and one methylene group on the dienophile.

In a new series of potential replicators^[127] again utilizing Diels-Alder chemistry and amidopyridine/carboxylic acid recognition Philp and co-workers not only wanted to investigate the effect of spacer units between diene, dienophile and recognition motifs but also the location of the spacer on the diene. In order to study the influence of these factors four furan and two maleimide building block molecules were designed and synthesized. These molecules could form eight potential replicating templates as illustrated in **Figure 1.34**.

Systems 2, 3 and 4 were found to proceed through minimal replicating pathways, whereas the dominate recognition mediated process in other systems involves binary complexes. System 2 (**Figure 1.34**) contained a single methylene unit between the diene, **69**, and a CH₂CH₂ spacer between the recognition and the dienophile, **74a**. The formation of both *exo* and *endo* templates were found to proceed mainly *via* a self-replicating ternary complex pathway although evidence existed for minor formation of both diastereoisomers by binary complexes. As discussed in System A (**Scheme 1.13**) the presence of two minimal replicators in the same experiment opens up the possibility of cross-catalysis.

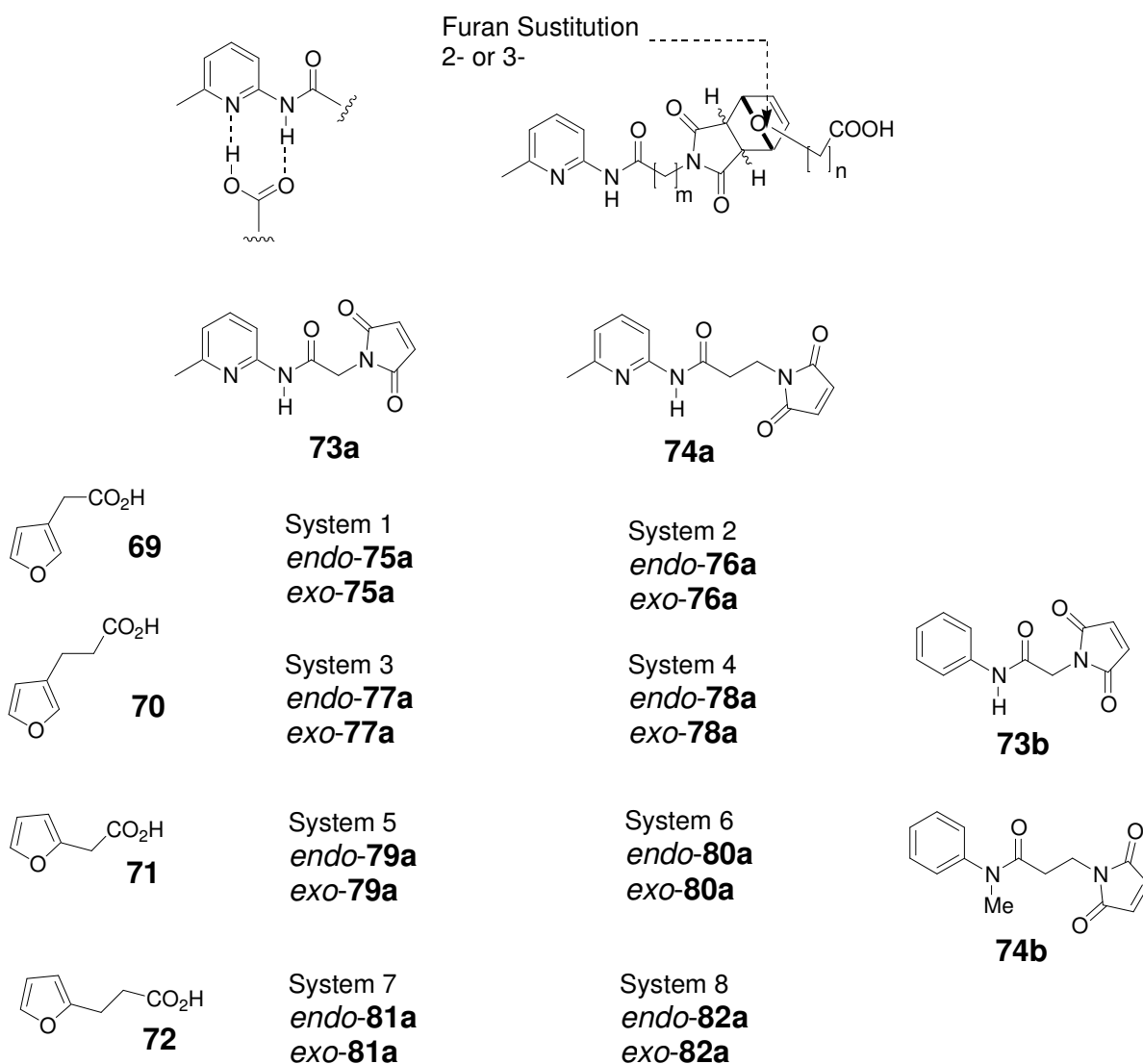


Figure 1.34 A possible 8 minimal replicating Systems can be formed from the reactions between furans **69-72** with maleimides **73a** and **74a**. Control compounds **74b** and **75b** were also produced.

However, using the same molecular mechanic calculations used in System A (**Scheme 1.13**); any cross-catalysis was ruled out. Kinetic and thermodynamic effective molarity values were calculated for this system (**Table 1.4**).

Table 1.4 Kinetic (kEM) and thermodynamic (tEM) effective molarities associated with formation of *endo-76a* and *exo-76a*.

Reaction pathway	kEM (<i>endo-76a</i>) [mM]	tEM (<i>endo-76a</i>) [mM]	kEM (<i>exo-76a</i>) [mM]	kEM(<i>exo-76a</i>) [mM]
Self-replication	663	289	1100	367
Binary reactive complex	70	31	96	37

Table 1.4 demonstrates that the efficiency of the binary complex channel is low compared to the autocatalytic pathway. The kEM of *exo-76a* is significantly higher than *endo-76a* indicating its better fit of transition state to template. However, the most interesting feature of this system is the fact that two independent autocatalytic cycles are operating in such a structurally simple system.

The diastereoisomeric pair *endo-77a/exo-77a* in System 3 are constitutional isomers of *endo-76a/exo-76a* in System 2. The length of spacer units are identical to System 2 but are on the opposite building block molecules (diene instead of dienophile). As a consequence of these similarities it comes as no surprise when both *endo-77a* and *exo-77a* are found to undergo minimal self-replication. Although this System appears similar to its constitutional isomer it in fact displays very different behavior. Comparisons of the kEM and tEM for System 2 (**Table 1.4**) and System 3 (**Table 1.5**) highlight this role of recognition is somewhat different. A $kEM(\textit{endo-76a}) > tEM(\textit{endo-76a})$ suggest the major role of recognition is transition state stabilization, but $kEM(\textit{endo-77a}) < tEM(\textit{endo-77a})$ indicates role of recognition is product ground state stabilization. *Exo-76a* and *exo-77a* both have a higher kEM than tEM , therefore, both appear to proceed through transition state stabilization with *exo-76a* being slightly more efficient.

Table 1.5 Kinetic (kEM) and thermodynamic (tEM) effective molarities associated with formation of *endo-77a* and *exo-77a*.

Reaction pathway	kEM (<i>endo-77a</i>) [mM]	tEM (<i>endo-77a</i>) [mM]	kEM (<i>exo-77a</i>) [mM]	kEM(<i>exo-77a</i>) [mM]
Self-replication	475	799	719	78
Binary reactive complex	46	216	65	16

System 4 (**Figure 1.34**) contains an additional methylene rotor compared to Systems 2 and 3. Therefore, from what was discussed in the previous series of potential minimal replicators (Systems 1-4) about increased conformation freedom favoring the binary pathway, it is expected this system will proceed *via* an $[A\bullet B]$ complex. However, surprisingly both diastereoisomers *endo-* and *exo-78a* proceed by a self-replicating autocatalytic pathway although at lower efficiency than systems 2 and 3, as indicated from analysis of effective molarities in **Table 1.6**.

Table 1.6 Kinetic (kEM) and thermodynamic (tEM) effective molarities associated with formation of *endo-78a* and *exo-78a*.

<i>Reaction pathway</i>	<i>kEM (endo-78a) [mM]</i>	<i>tEM (endo-78a) [mM]</i>	<i>kEM (exo-78a) [mM]</i>	<i>kEM(exo-78a) [mM]</i>
Self-replication	536	588	448	75
Binary reactive complex	36	43	65	63

System 2-4 have been shown to display self-replicating autocatalytic nature, but why not System 1? Philp and co-workers stated in their previous systems that the best replicator will contain the shortest spacer combination, therefore, System 1 should be the most efficient replicator. However, only minute rate enhancements were observed. The authors concluded that the limited conformational freedom in the system was actually inhibiting any recognition mediated process.

These studies by Philp and co-workers demonstrate the difficulties in trying to design new potential minimal replicators. Additional evidence of the difficulties in attempting to apply structure design principles to the production of replicating systems can be noted through comparisons of two similar but distinct systems. A recent minimal replicator developed^[148-149] by von Kiedrowski has almost identical structural features (**Figure 1.35**), with an identical spacer backbone, to a system developed by Philp and co-workers.

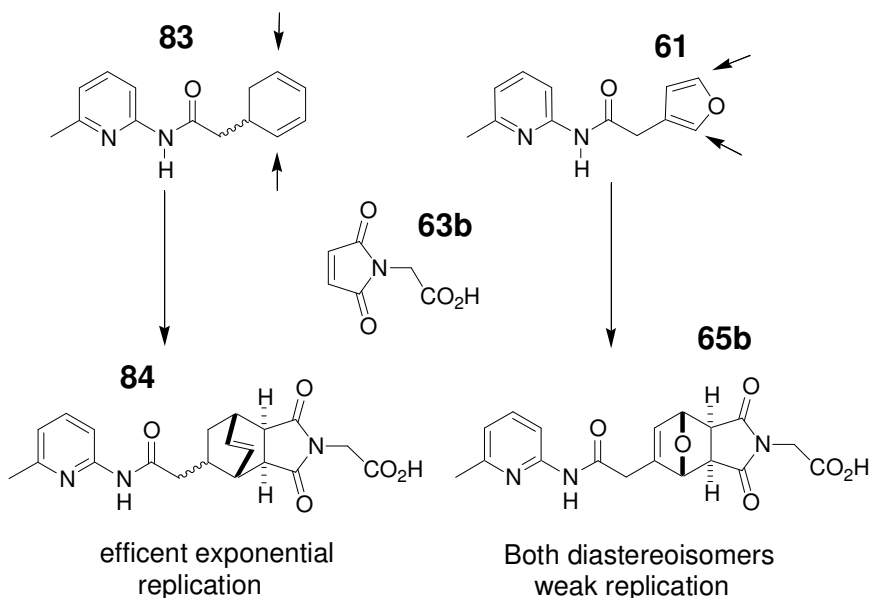


Figure 1.35 Two structurally similar systems with very different kinetic behavior.

This system developed by von Kiedrowski is a modified version of the one developed^[120] by Wang and Sutherland with the heterocyclic recognition replaced by amidopyridine and carboxylic acid interactions, in order to improve solubility. Analysis of **Figure 1.35** reveals the structural similarities between the two systems, with the only difference being the use of cyclohexadiene, **83**, instead of a furan-based Diels-Alder reaction to form the replicating template. However, this small difference is enough for the two systems to express very different behavior. As mentioned previously, this system by Philp and co-workers displays weak self-replication with the formation of *endo* and *exo* diastereoisomers occurring *via* two independent autocatalytic cycles. However, von Kiedrowski's template exhibited near exponential replication by proceeding through both autocatalytic and cross-catalytic channels. Presumably the discrepancy in behavior between the two replicators is because of the position of the diene termini (indicated by arrows in **Figure 1.35**) and the dissimilar reactivity of a furan diene to a cyclohexadiene. Disappointed with the relatively weak rate enhancements, the best system only obtained an acceleration of around half in the magnitude, and low selectivities, Philp and co-worker set about designing, synthesizing and analyzing a new more efficient system. In the latest minimal replicator developed^[128] by Philp and co-workers the same recognition motifs are utilized as previously, namely carboxylic acid and amidopyridine. However, there has been a change in the covalent bond formation reaction between building block molecules. Now the desired templates are formed (**Figure 1.36**) *via* the reaction of an *N*-aryl nitron with a maleimide. This reaction has the advantage of proceeding readily at room temperature and is resistant to a number of electronic substituent effects and catalysis by Brønsted acids. As in the previous system two different diastereoisomeric cycloadduct products were formed *exo*- and *endo*-**88** products. The *endo*-**88** cycloadduct product was determined, by electronic structure calculation, to have an open template structure making it a potential minimal replicating template. Whereas, *exo*-**88** was shown to have a closed structure making it unsuitable as a template for self-reproduction.

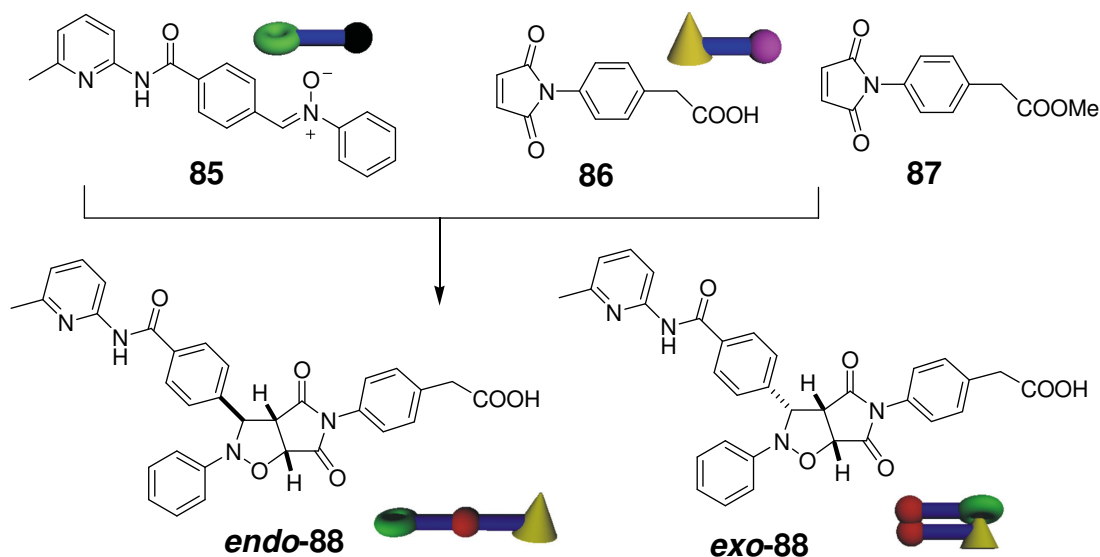


Figure 1.36 Nitrone **85** and maleimide **86** can react to form two diastereoisomeric cycloadducts *endo-88*, open template minimal replicator and *exo-88*, closed template non-replicator.

Analysis of this potential minimal system was achieved as in previous systems through a series of control, native (recognition mediated reaction between **85** and **86**) and templated experiments (between **85**, **86** and **88**). The maximum rate accelerations for these experiments are summarized in **Table 1.7**.

Table 1.7 Maximum observed rate or reaction^[a].

Entry	Conditions	Maximum rate [nMs^{-1}]	
		<i>endo-88</i>	<i>exo-88</i>
1	[85] = [87] = 25mM	39	13
2	[85] = [86] = 25mM	528	21
3	[85] = [86] = 25mM	105	17
4	[benzoic acid] = 50 mM [85] = [86] = 25 mM [<i>endo-88</i>] = 2.5 mM	561	<1

[a] Maximum rate accelerations measured in $CDCl_3$ at $-10^\circ C$ by 1H NMR spectroscopic analysis.

Examination of **Table 1.7** reveals the formation of *endo-88* in the native experiment (Entry 2) proceeds 13 times faster than its bimolecular counterpart (Entry 1). In the templated experiment (Entry 4) where *endo-88* is added to the reaction between maleimide **86** and nitrone **85** at the beginning of the experiment a 14 fold increase occurred compared to Entry 1. Analysis of **Table 1.7** also demonstrates that *exo-88* formation is not being accelerated and, therefore, is not undergoing self-replication.

As well as an increase in rate, the ratio of *endo-88* to *exo-88* has also increased in the native (115:1) and templated reaction (250:1) compared to the bimolecular (3:1).

Analysis of the concentration vs. time profile (**Figure 1.37**) for the formation of *endo-88* in the native experiment provides further evidence that autocatalytic self-replication is occurring.

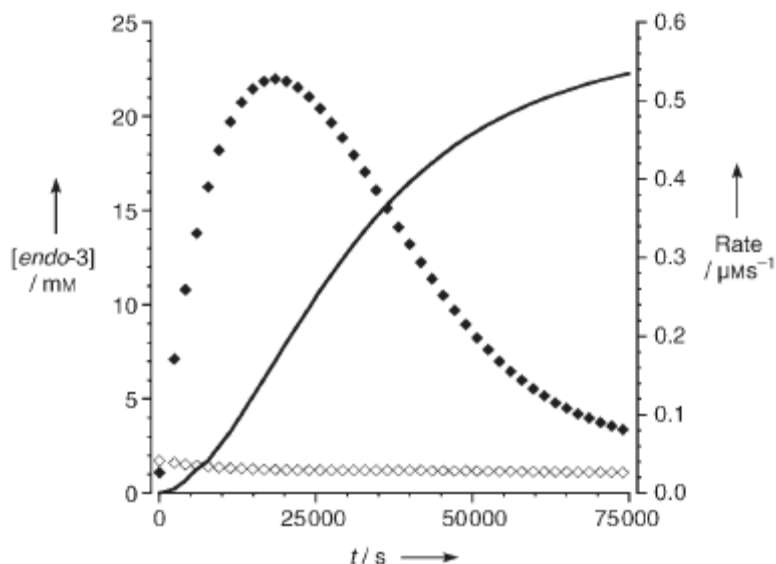


Figure 1.37 Experimental concentration vs. time data for *endo-88* (solid line, left axis) in the native experiment. Variation of reaction rate for the formation of *endo-88* (filled diamonds, right axis) vs. time in the native experiment.

The sigmoidal shape for the concentration vs. time curve demonstrates the presence of autocatalysis (Section 1.12), which is further supported by the reaction rate vs. time curve for the formation of *endo-88*. This curve displays an increase in rate reaching a maximum after 5 hours, at an *endo-88* concentration of ≈ 7 mM, before rate begins to decrease.

Philp and co-workers discovered that this system reached its autocatalytic limit upon addition of only 0.1 equivalents of *endo-88* template. The maximum autocatalytic rate occurs in the time region in which $0.1 < \rho = [C] / [\text{precursor}] < 1.0$, where ρ is the ratio of *endo-88* over total concentration of precursors **85** and **86**. This is when the concentration of *endo-88* is between 2.5 and 12.5 mM for this system. Upon the addition of 2.5 mM of *endo-88* the system is placed into this region in which the rate only increases by a further 6%. Therefore, the addition of greater concentrations of initial *endo-88* would be futile, as identical results to the templated experiment with 0.1

equivalents would be observed. Therefore the system operates at the limit of self-replicating capacity when $\rho_{\text{initial}} = [\text{C}]_{\text{initial}} / [\text{precursor}]_{\text{initial}} = 0.1$.

The [*endo-88*•*endo-88*] product duplex was determined to have a considerably higher stability constant of $4.7 \times 10^6 \text{ M}^{-1}$, which is greater than the additive individual binding interaction indicating that the system displays positive cooperativity. From optimized rate constants for the ternary complex, an effective molarity of greater than 20 M was calculated for this *pseudo*-unimolecular reaction compared to the bimolecular. This value for the effective molarity is considerably higher than previous minimal replicators developed by Philp and co-workers illustrating its enhanced efficiency. The efficiency of this system is also illustrated by the fact that the concentration of free *endo-88* is never greater than 5 μM . Philp and co-workers in this minimal replicator demonstrated that despite a high product duplex stability constant an efficient minimal replicator was still possible if the template had a high level of complementarity to the transition states.

This section has provided a summary of a selected few synthetic minimal self replicating systems from a variety of other systems that have been designed by Rebek, von Kiedrowski and Philp. Recently, von Kiedrowski introduced a novel system based on Troger's base analogue^[129], this system was unique in that it was undertaken in a stepwise manner. Another attempt at self replicating system by Crossley and co-workers focused^[130] on the self-replication of bis(capped porphyrins), however, these systems did not show signs of self-replication. Now the focus will change away from the simplest model of replication to the more complicated reciprocal or cross-catalysis model.

1.18 Reciprocal replication incorporating natural products^[131-141]

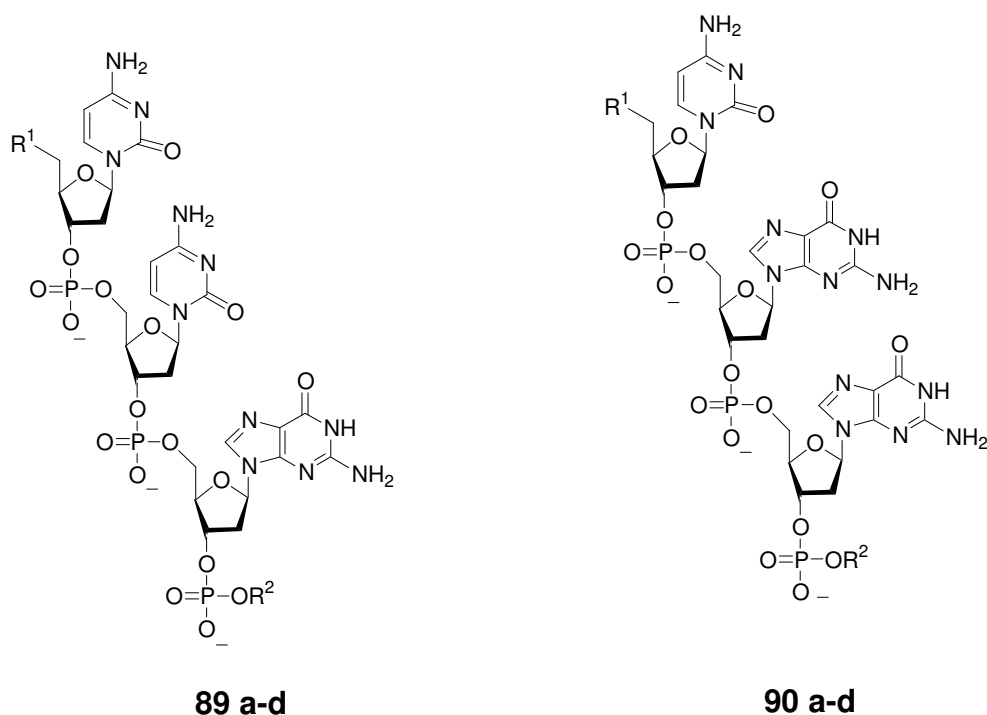
The first non-enzymatic catalyzed system was first reported^[131] in 1962 by Schramm and involved the synthesis of polynucleotides *in vitro*. In 1966, Gilham reported^[132] the first template directed organic synthesis which involved the condensation of two hexathymidylic acid residues on a polyadenylic (poly(A)) template using a carbodiimide as a coupling reagent. Later Orgel^[133] went on to link together adenosine derivatives to a poly uridylic acid (poly(U)) again using a carbodiimide as a coupling reagent. Orgel found that the condensation of adenylic acid with adenosine is greatly enhanced in the presence of poly(U). However, poly(U) had no influence in the condensation of adenylic acid with uridine, cytidine or guanosine. In a parallel series of experiments Orgel also

showed that polycytidylic acid (poly(C)) greatly enhanced the condensation of guanylic acid with guanosine but no effect in combinations of guanylic acid with uridine, cytidine or adenosine. These experiments help to establish that Watson-Crick^[151] rules applied to nonenzymatic template-catalyzed condensation reactions.

These experiments set the ground work for Orgel in 1984 to demonstrate^[134] that nonenzymatic synthesis of oligonucleotides by using template was indeed possible. This template directed synthesis of oligonucleotides was achieved through starting with a mixture of two activated mononucleotides guanosine 5'-phospho-2-methylimidazole and cytidine 5'-phospho-2-methylimidazole and a pentanucleotide C-C-G-C-C template. From this Orgel achieved a 17 % yield of the complementary sequence pG-G-C-G-G. Orgel had managed to use a template with a specific sequence to catalyze the formation of the complementary strand without the use of an enzyme. Later Orgel went on to synthesize^[135-137] the sequence 5'-CCCGCCCGCCCGCC-3' in 2 % yield which, at the time, was the longest oligomer copied.

In 1994 Li and Nicolaou^[138] reported the self-replication of a palindromic (identical) duplex DNA-like oligonucleotide 24 monomers in length in the absence of enzymes. Although described for a palindromic DNA sequence it could be potentially capable of replicating non-symmetrical sequences. Replication in this system proceeds through the well know principles of triple strand (Watson-Crick-Hoogsteen) and double strand (Watson-Crick). The weaker Hoogsteen binding involved in the triple helix helps to allow the release of the newly formed strand from the triple helix. Li and Nicolaou showed that DNA-like double stranded molecules could be replicated without the requirement of catalysis from an enzyme. This finding has important implications on how replicating systems might have first appeared on primitive earth.

After studying the minimal self-replication of oligonucleotides von Kiedrowski turned his attention to comparing the autocatalytic self replication of hexadeoxynucleotides to cross-catalytic replication of hexadeoxynucleotides^[139-141]. His study revolved around the use of monoterminal trideoxynucleotides. Von Kiedrowski started with two nucleotide sequences the sequence CCG and the complementary sequence GGC. He chooses a variety of different reactive site (R^1 and R^2) which as before could be coupled using a carbodiimide (EDC) (**Figure 1.38**).



89, 90	R ¹	R ²	Ap	Bp	nA	nB
a	N ₃	H	89a	90a	89c	90c
b	CH ₃ SCH ₂ O	H				
c	NH ₂					
d	NH ₂					

Figure 1.38 Von Kiedrowski's reciprocal replicating system based on deoxynucleotides.

In the first experiment, von Kiedrowski conducted a series of individual experiments, one single 5'-protected trideoxynucleotide 3'-phosphate, ^{N3}CCGp (**Ap**) or ^{N3}GGCp (**Bp**) was reacted with one single 5'-amino-trideoxynucleotide 3'-(2-phenylthioethyl)-phosphate, nCCGp^{PTE} (**nA**) or nCGGp^{PTE} (**nB**) both in absence and presence of one of the four hexadeoxynucleotide templates CCGCCG (**ApA**), CCGCGG (**ApB**), CGGCCG (**BpA**) and CGGCGG (**BpB**). Only the two reciprocal cross-catalytic templates **ApA** and **BpB** will be examined here, the two minimal replicating templates **ApB** and **BpA** will not be discussed. These reactions were monitored by HPLC and the results can be seen in the table below (**Table 1.8**).

Table 1.8 Yields of **ApnB**, **BpnA**, **ApnA** and **BpnB** in absence (-) and presence of one of the templates **ApA**, **BpB**, **ApB** and **BpA**.

	—	+ ApA	+ BpB	+ ApB	+ BpA
ApnB	23 %	23 %	23 %	32 %	23 %
BpnA	21 %	21 %	21 %	21 %	29 %
ApnA	4 %	4 %	15 %	4 %	4 %
BpnB	4 %	15 %	4 %	4 %	4 %

These results indicate that the formation of a specific template is only catalyzed by its complementary template, for example **ApnA** is only catalyzed by its complementary template **BpB** (15 % yield) and not by itself (4 % yield no different than without additional **ApnA** added). Complementary results are observed for the formation of the **BpnB** template, where the formation of **BpnB** is only accelerated by its complementary template **ApA**. When **ApnA** was synthesized in various concentrations of **BpB** template the graph shows (**Figure 20**) that both the concentration of product and the rate at which it is formed increases, an almost identical graph (**Figure 1.39**) can be seen for the formation of **BpnB** in various concentrations of **ApA**.

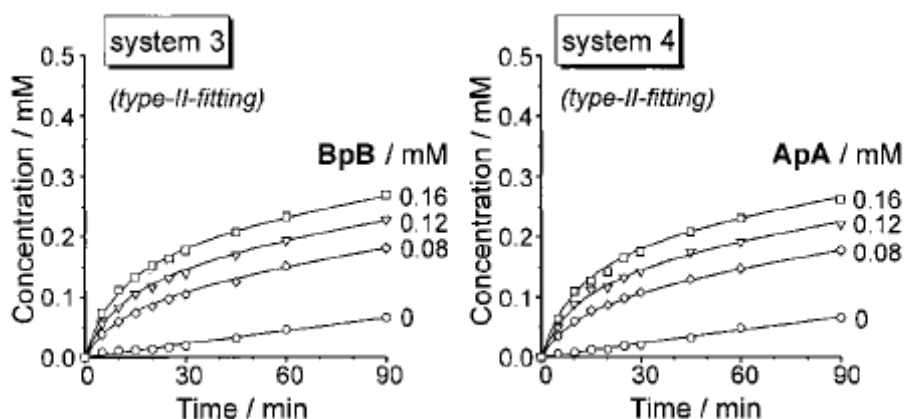
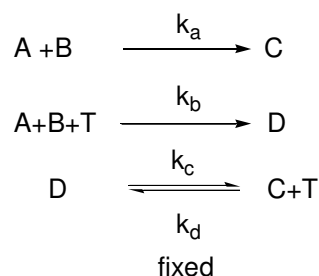


Figure 1.39 Increase in rate of **ApA** (System 3) and **BpB** (System 4) on addition of various concentration of complementary template. Taken from reference 140.

Von Kiedrowski employed a different type of fitting using his *Simfit* computer model (**Scheme 1.14**), than is used for minimal models.



Scheme 1.14 Type II fitting

Where k_a describes template independent synthesis of the phosphoramidates, k_b is the value from the reversible formation of termolecular complex and the irreversible template-directed reaction, k_c is the rate constant for the reversible dissociation of the hexamer to a single-stranded hexadeoxynucleotide, and k_d is the rate constant for duplex association which can be chosen arbitrarily. This model allowed the rate constants of the template directed reaction k_2 to be determined using the following equation (**Figure 1.40**).

$$k_2 \approx k_b \times (k_d / k_c)^{-1/2}$$

Figure 1.40 The equation von Kiedrowski used to determine the value of the rate constant for the template directed reaction k_2 .

The rate constants for the formation of the **ApA** from **BpB** were $4.91 \text{ M}^{-3/2} \text{ s}^{-1}$ compared to the template independent rate constant of $1.31 \times 10^{-2} \text{ M}^{-1} \text{ s}^{-1}$. Whereas, the rate constant for the formation of **BpB** from **ApA** was $4.43 \text{ M}^{-3/2} \text{ s}^{-1}$ compared to the template independent rate constant of $1.31 \times 10^{-2} \text{ M}^{-1} \text{ s}^{-1}$. Therefore, von Kiedrowski's system showed that two non-identical complementary hexadeoxynucleotide analogue templates could template the formation of their complementary partner but not their own formation. Chmielewski and co-workers recently developed^[145] a peptide replicating system capable of autocatalysis and cross-catalysis. This system consisted of four different building block peptide fragments E1, E2, K1 and K2, which could form four different template products E1E2, K1K2, E1K2 and K1E2. Where it was hoped E1E2 could undergo self-replication or cross-catalyze the formation of complementary template K1K2 and vice versa. It was also hoped E1K2 could self-replicate and cross-catalyze the formation of complementary template K1E2 and vice versa. The system was designed so that binding strength between the templates would vary with pH, with the templates either undergoing self-replication, *via* homomeric coiled coil (eg. [E1E2•E1E2]), or cross-

catalysis, *via* heteromeric coiled coil (eg. [E1E2•K1K2]), indicated by **Table 1.9**. The aim of the study was to investigate whether the system could be biased towards formation and amplification of one of the four templates.

Table 1.9 The potential autocatalytic and cross-catalytic templated reactions possible under various pH conditions.

	Autocatalysis				Cross-Catalysis			
	pH 7.5				pH 7.5			
	2M	pH 4.0	pH 7.5		pH 7.5			
	NaClO ₄							
Template	K1K2	E1E2	K1E2	E1K2	K1K2	E1E2	K1E2	E1K2
Fragments	K1,K2	E1, E2	K1, E2	E1,K2	E1, E2	K1, K2	E1, K2	K1, E2
	↓	↓	↓	↓	↓	↓	↓	↓
Product	K1K2	E1E2	K1E2	E1K2	E1E2	K1, K2	E1K2	K1E2

Initial experiments containing only two peptide fragments were run at varying pH values, in the absence or presence of template. These experiments revealed the E1E2 and K1K2 peptides to be the most efficient catalysts in the autocatalytic and cross-catalytic reactions. Templates E1K2 and K1E2 were suspected to undergo cross-catalysis as a 1:1 mixture of each displayed a high level of helical character at pH 7.5. However, the individual building block peptides have a random coil appearance under the same conditions. Despite this fact though E1K2 and K1E2 were found only to undergo minimal replication, indicating homeric complexes were favored, which was demonstrated by circular dichroism.

Following analysis of the previous experiments, a series of four component studies were conducted with equimolar concentrations of E1, E2, K1 and K2, in the absence and presence of one of the four template peptides. The experiment conduct in the absence of templated resulted in the production of equal concentrations of all four peptide templates. It was anticipated that addition of a prefabricated peptide template at the beginning of the reaction between E1, E2, K1 and K2 would result in the experiment being biased towards one product. However, the results of these experiments did not support this hypothesis. Instead a series of unpredictable binding modes between the different templates and building block peptide units altered the expected distribution of

products. Chmielewski's peptide replicators were reproducing (**Figure 1.41**) through a complex series of interlinked minimal and cross-catalytic cycles referred to as a hypercyclic network. Hypercyclic networks will be discussed in detail in future Section **1.20**, but the diagram in **Figure 1.41** demonstrates the interactions originally suspected (Blue lines) by Chmielewski and co-workers and the additional (Red lines) replicating pathways not initially anticipated.

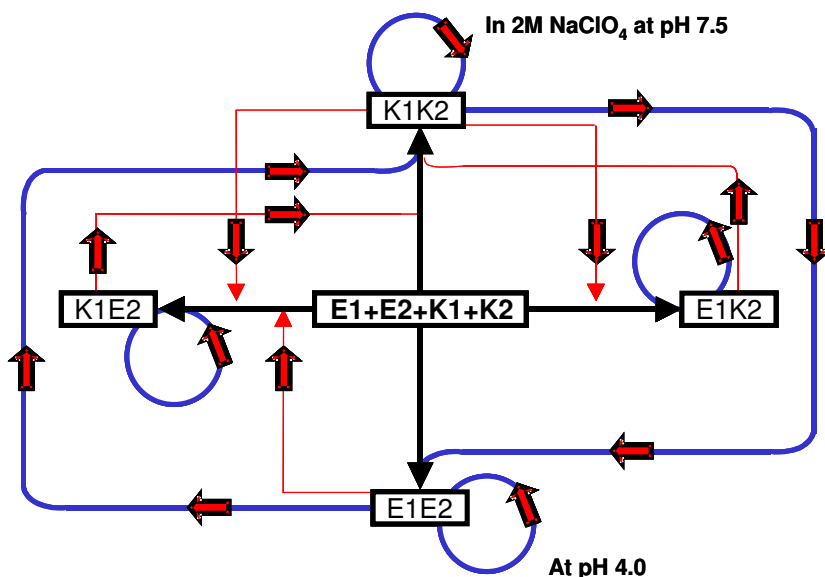


Figure 1.41 Diagram illustrating the initially anticipated replicating pathways (Blue lines) available in Chmielewski's system, and the additionally discovered (Red lines) pathways available resulting in the formation of a hypercyclic network.

The Blue lines in **Figure 1.41** demonstrate the reactions Chmielewski and co-workers initially anticipated would occur. Fragments E1, E2, K1 and K2 were expected to react together and form the four template molecules K1K2, E1E2, K1E2 and E1K2 (Black line). Each of these templates has the ability to replicate themselves autocatalytically as indicated through the blue loops on **Figure 1.41**. As discussed earlier it was expected only complementary templates E1E2 and K1K2 could replicate cross-catalytically which is illustrated in **Figure 1.41** (by the solid blue line linking K1K2 to E1E2 and the complementary blue line linking E1E2 to K1K2). The Red lines in **Figure 1.41** illustrate the additional interactions observed by Chmielewski when he conducted his four component experiments. These lines indicate cross-catalysis is occurring between more than just the E1E2 and K1K2 templates. For example a red line can be observed linking E1E2 to K1E2 indicating that the E1E2 template can cross-catalyze the formation of

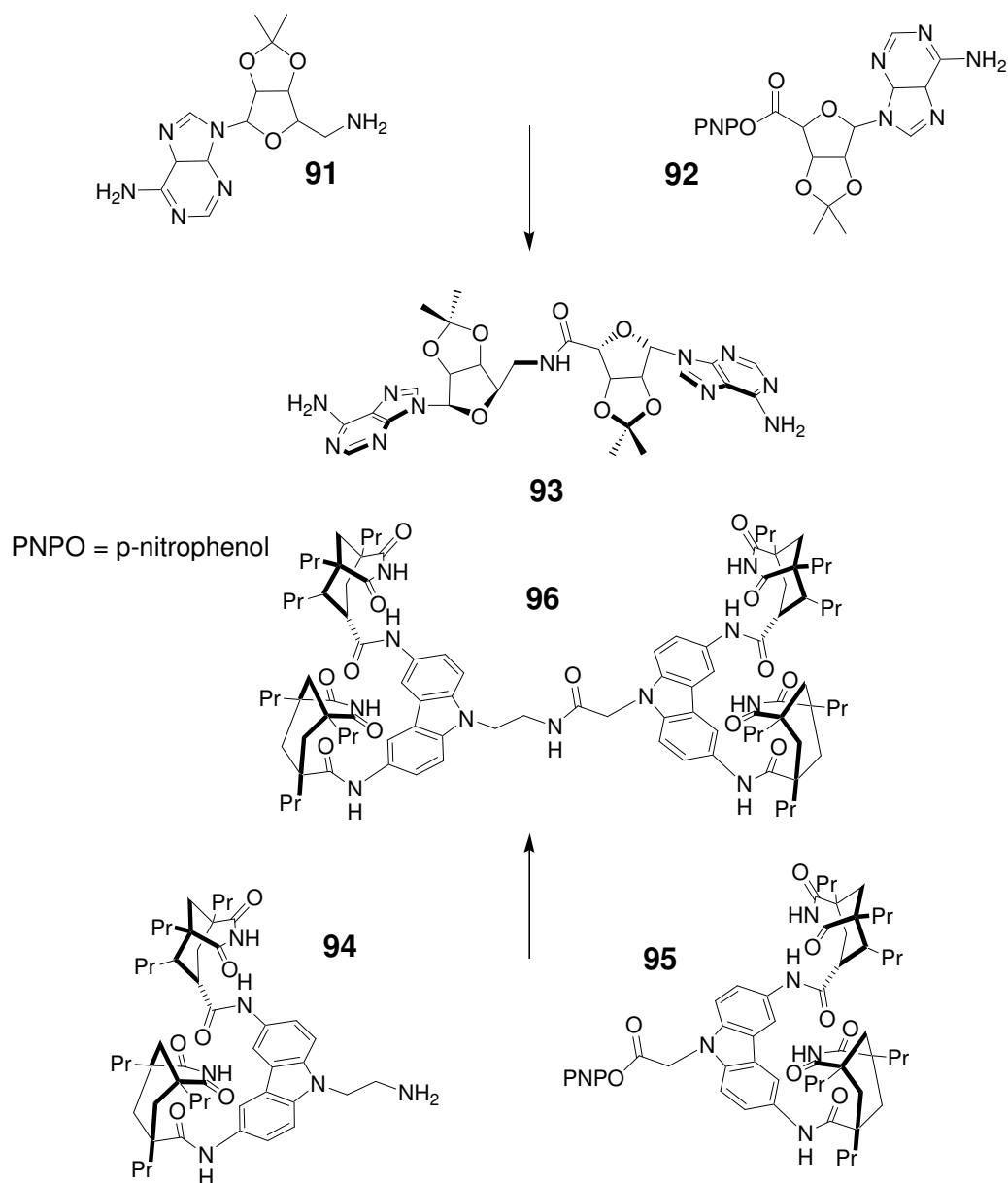
K1E2. However the solid red arrow indicates this occurs only one way, as K1E2 does not cross-catalyze the formation of E1E2.

Detailed analysis of this hypercycle was prevented as a consequence of its complexity but general trends could be observed. The species with the weakest association constants display lowest catalytic rate constants; however, conversely the species with large association constants do not have the highest catalytic rate either. These trends can be easily rationalized. The rate of catalysis depends on the concentration of ternary complex, the weaker the association the lower the concentration of ternary complex. Conversely in the second case, if there is too large a stability constant between two templates in a product duplex catalytic turnover will not occur, resulting in a reduced rate.

1.19 Synthetic Reciprocal Replication^[142-144]

The first synthetic reciprocal replication was first designed^[142-143] by Rebek and was based around the binding of adenine to a scorpion shaped molecule. Association of these two molecules involved the chelation of the purine nucleus to the adenine through two imides which were attached through a carbozole surface. These two imides allow for simultaneous Watson-Crick and Hoogsteen base pairing, while carbozole stacks to the purine. Rebek utilized this recognition to design the reciprocal replicating system in **Scheme 1.15**.

Template **93** is formed from the reaction between **91** and **92**, it can associate molecules **94** and **95**, via the adenine/imide recognition motifs, cross-catalyzing the formation of template **96**. Molecule **96** can reciprocal replicate the bisubstrated receptor **93** in a complementary cross-catalytic cycle.



Scheme 1.15 Complementary templates **93** and **96** formed from building blocks **91**, **92**, **94** and **95**.

In order to investigate the behavior of the two reciprocal templates Rebek conducted a series of kinetic experiments. The bimolecular reactions between compounds **91** and **92** proceeded at an initial rate of $1.5 \times 10^{-8} \text{ M min}^{-1}$. When the reaction between **91** and **92** was carried out in the presence of 1 equivalent of complementary template **96**, formed from **94** and **95**, the reaction proceeded ten times faster when in CDCl_3 . Rebek noted that the reaction increased thirteen-fold in the presence of CCl_4 , but in the presence of a more polar solvent like tetrahydrofuran, no rate enhancement was observed. This effect on rate enhancement was attributed to the fact that a more polar solvent disturbs

recognition between the reactants and the template, by competing for hydrogen bonding sites. The rate of reaction between **91** and **92** increases up until two equivalents of template **96** are added (**Figure 1.42**), after this, additional initial equivalents of template **96** decreases coupling rate.

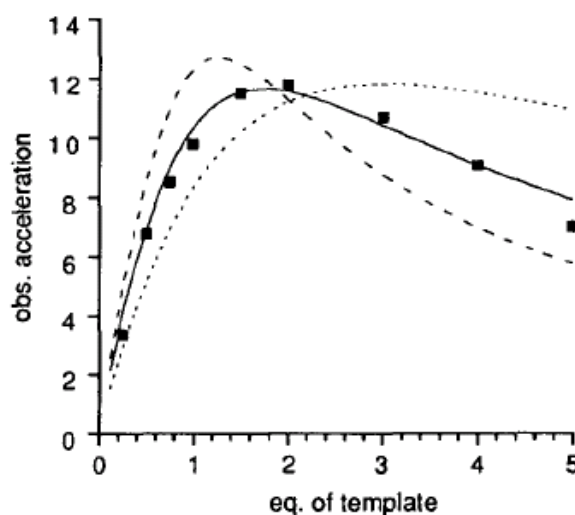


Figure 1.42 Observed acceleration vs. equivalents of template, black squares represent observed acceleration, black solid line calculated acceleration. Taken from reference 143.

The solid line in the graph in **Figure 1.42** corresponds to an independent binding site model^[143-144]. This model assumes that rate acceleration observed for the production of template **93** is directly proportionally to the concentration of active ternary complex, **[91•92•96]**. If it is assumed that each starting material, **91** and **92**, binds to the complementary template **96** independently with the same association constant, then it becomes possible to calculate the concentration of these complexes, using the parameter in **Figure 1.43**.

$[B]$ = Concentration of free binding site
 $[BR]$ = Concentration of binding sites occupied by reagent
 $[T]_{tot}$ = Total concentration of template
 $[R]$ = Concentration of free reagent
 $[R]_{tot}$ = Total concentration of reagent

$$[B] + [BR] = 2[T]_{tot} \quad [R] + [BR] = [R]_{tot} \quad \text{and} \quad K = \frac{[BR]}{[B][R]}$$

$$\text{Solving for } [R]: [R]^2 + \left(2[T]_{tot} - [R]_{tot} + \frac{1}{K}\right)[R] - \frac{[R]_{tot}}{K} = 0$$

Figure 1.43 Equations for solving the concentration of free reagent [R] Part one.

This equation for solving [R] is in the form $ax^2 + bx + c = 0$, and therefore, the standard quadratic solution (**Figure 1.44**) can be used for x, [R].

$$x = \frac{b \pm \sqrt{b^2 - 4ac}}{2a}$$

$$\text{In this case, } a = 1, b = \left(2[T]_{tot} - [R]_{tot} + \frac{1}{K}\right); c = -\frac{[R]_{tot}}{K}$$

$$[R] = \frac{\left(2[T]_{tot} - [R]_{tot} + \frac{1}{K}\right) \pm \sqrt{\left(2[T]_{tot} - [R]_{tot} + \frac{1}{K}\right)^2 - 4 \times 1 \times -\frac{[R]_{tot}}{K}}}{2 \times 1}$$

Figure 1.44 Equations for solving the concentration of free reagent [R] Part two.

Once [R] is calculated we can now determine the fraction of template sites occupied by reagent (**Figure 1.45**)

$$\frac{[BR]}{2[T]_{tot}} = \frac{K[R]}{1 + K[R]}$$

Figure 1.45 Equation for determining fraction of occupied template sites by reagents

Hence, we can calculate the concentration of catalytic ternary complex using equation in **Figure 1.46** and the appropriate substitution for [R] derived earlier in **Figure 1.44**.

$$[TR_2] = [T]_{tot} \left(\frac{K[R]}{1 + K[R]} \right)^2$$

Figure 1.46 Equation for calculating the concentration of ternary complex.

Through varying the value of K in the quadratic equation in **Figure 1.44**, then calculating the concentration of ternary complex, a set of theoretical accelerations can be determined through the use of a scaling factor. The value of K , which gives the optimal fit to the experimental data represents the individual associations in the ternary complex. Therefore, multiplying the individual binding associations a value for the template duplex complex stability constant (K^2) can be determined.

Rebek claimed the optimal fit of the experimental data to this model supports his proposed reciprocal replicating mechanism. The best fit for this system was obtained when a value of 14000 M^{-1} was used for the association constant of the ternary complex. When the complementary reaction between **94** and **95** with template **93** was conducted, a maximum rate enhancement of five fold was observed with one equivalent of template, compared to the bimolecular reaction, with an initial rate of $4.3 \times 10^{-9} \text{ M min}^{-1}$. Rebek noted that rate acceleration in his reciprocal system was larger than similar self-complementary systems, but whether generally these systems are more efficient than minimal self-complementary replication requires more research.

More recently, Philp and co-workers published^[144] a reciprocal replicating system using non-nucleotide base recognition. Utilizing their knowledge and understanding of recognition between amidopyridines and carboxylic acids, obtained from their studies of minimal self-replicators, Philp and co-workers developed a new synthetic reciprocal replicating system (**Figure 1.47**). This system comprised of four building blocks molecules, which can react together to form four potential reciprocal templates.

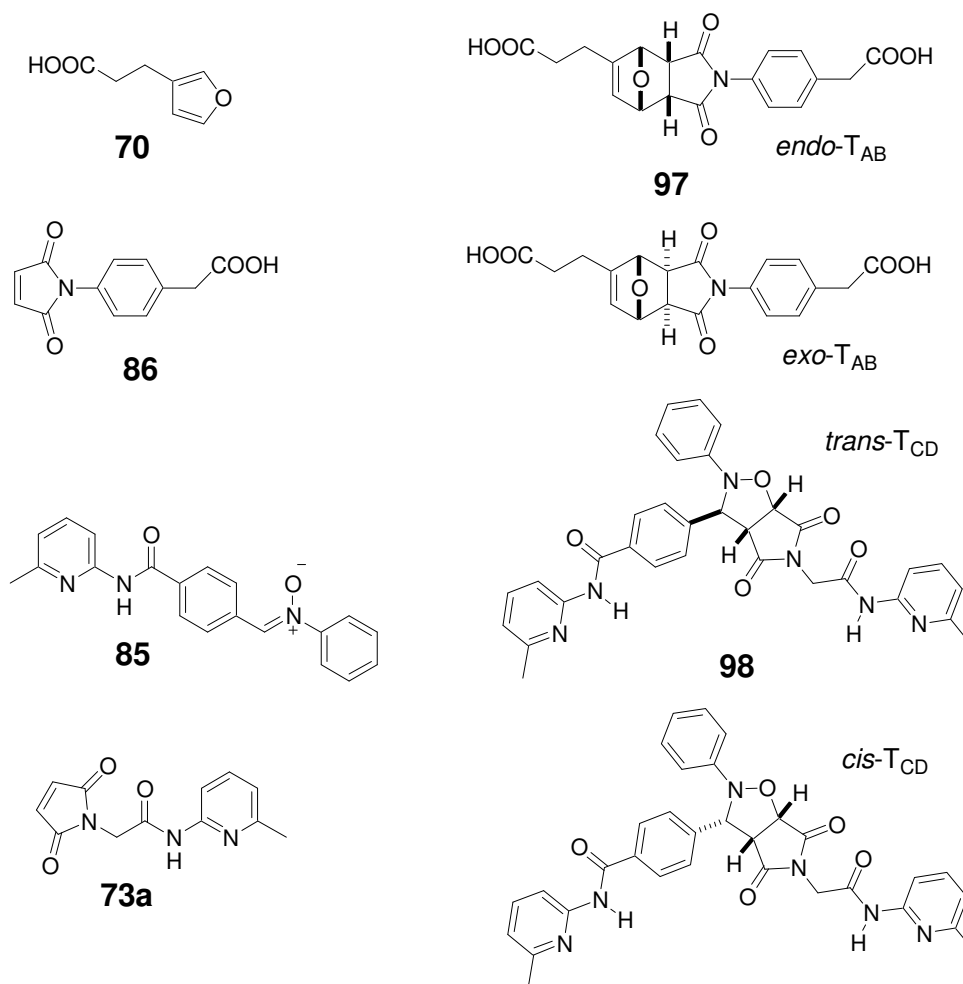


Figure 1.47 Building block molecules **70**, **85** and **86**, **73a** can react together to form potential reciprocal templates dicarboxylic acid *endo*-, *exo*-T_{AB}, **97**, and bis(amidopyridine) *trans*-, *cis*-T_{CD}, **98**. Adapted from reference 144.

Exploiting their experience with furan Diels-Alder and *N*-aryl nitronium cycloaddition reactions, these processes were chosen to link the building blocks together to form the resultant potential replicator molecules. Furan **70** can react with phenyl maleimide **86** to form a diastereoisomeric pair of dicarboxylic acid molecules *exo*-T_{AB} and *endo*-T_{AB}. Nitronium **85** and maleimide **73a** can react to form a diastereoisomeric pair of bis(amidopyridine) molecules *trans*-T_{CD} and *cis*-T_{CD}. Electronic structure calculations (**Figure 1.48**) of these two dicarboxylic acid and bis(amidopyridine) molecules suggest that the principle reciprocal template effect should occur between *exo*-T_{AB} and *trans*-T_{CD}.

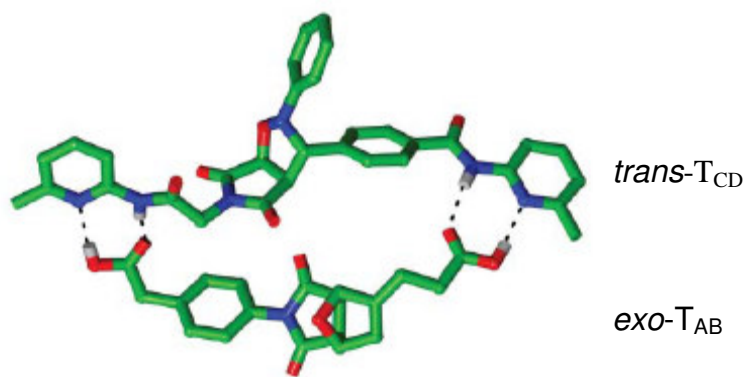


Figure 1.48 Stick representation of calculated (HF/6-31(d)) structure of the $[\text{exo-T}_{\text{AB}} \bullet \text{trans-T}_{\text{CD}}]$ complex. Carbon atoms Green, nitrogen atoms blue, oxygen atoms red and hydrogen white. Dashed black lines show hydrogen bonds.

Analysis of **Figure 1.48** shows that these two templates form a reasonably well matched duplex.

Before analyzing this potential reciprocal system, bimolecular reaction between molecules **70** and **86** and then **85** and **73a** were conducted. The results of these reactions can be examined in the concentration-time profiles (a) and (b) in **Figure 1.49**.

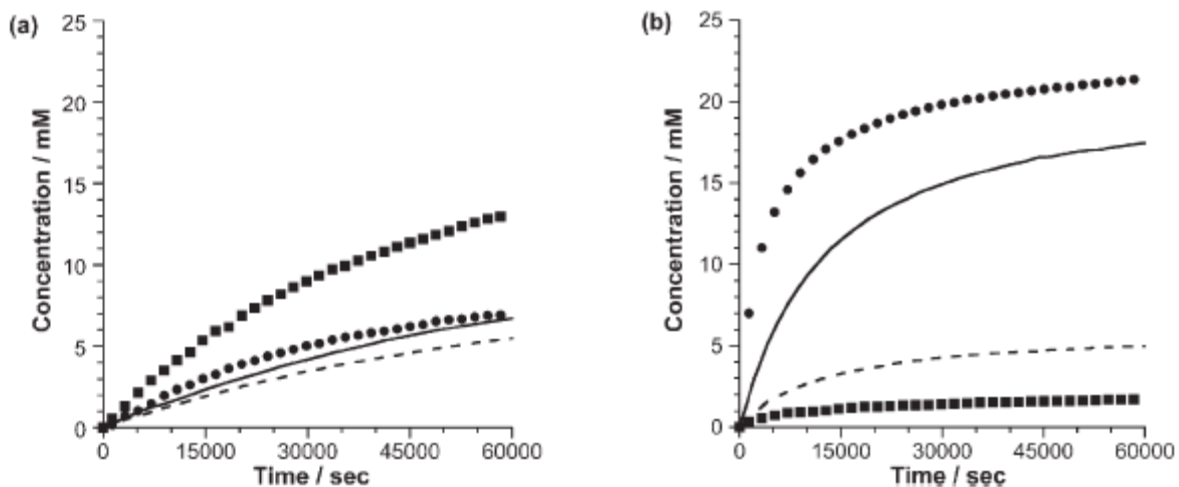


Figure 1.49 Concentration-time profiles for the formation of (a) *exo*- (solid line) and *endo*- T_{AB} (dashed line) from **70** and **86**; (b) *trans*- (solid line) and *cis*- T_{CD} (dashed line) from **85** and **73a**. Filled circles (*endo*- T_{AB} and *trans*- T_{CD}) and filled squares (*exo*- T_{AB} and *cis*- T_{CD}) represent the reaction where (a) 60 mol % *trans*- T_{CD} or (b) 35 mol % *exo*- T_{AB} where added at start of appropriate reaction.

Once the bimolecular experiments were analyzed, the effect of adding reciprocal template to these reactions could be investigated. Accordingly, 60 mol % of template *trans*- T_{CD} was added at the start of the reaction between **70** and **86**. The result of this addition was an increase in the rate of formation of *exo*- T_{AB} by 2.3 fold and *endo*- T_{AB} by

1.5 fold compared to the bimolecular reaction. Overall conversion increased from 50 % in the bimolecular reaction between **70** and **86** to 81 % in the reciprocal templated experiment. Selectivity for the reaction also increased from an *exo* to *endo* ratio of 1.3:1 to 2:1 in the experiment with bis(amidopyridine) *trans*-T_{CD}.

In the complementary cross-catalytic cycle, the rate of reaction between **85** and **73a** was also increased when 35 mol % of dicarboxylic acid *exo*-T_{AB} was added at the start of the experiment. The addition of complementary template was found to increase the rate of formation of *trans*-T_{CD} by 3.6 fold and reduce the formation of *cis*-T_{CD} by 2 fold compared to the bimolecular experiment. As a consequence of this increase and decrease in rate, diastereoselectivity was enhanced from a ratio of *trans* to *cis* of 3:1 in the bimolecular experiment to 14:1. The results of these two templated experiments illustrate that *exo*-T_{AB} has the ability to cross-catalyze the formation of *trans*-T_{CD} from building block molecules **85** and **73a**. While *trans*-T_{CD} can template the production of *exo*-T_{AB} from building block molecules **70** and **86**.

In order to probe the nature of this reciprocal system further, Philp and co-workers performed a series of experiments, where the concentration of templated added was increased from 0.1 equivalents to 2 equivalents. These experiments could only be done for the addition of *trans*-T_{CD} to molecules **85** and **73a**, as a consequence of the insolubility of *exo*-T_{AB} at concentrations above 40 mol %. The initial rate and rate accelerations for each of these templated experiments were calculated. Then rate acceleration was plotted (**Figure 1.50**) against equivalent of added template *trans*-T_{CD}.

Examination of the graph in **Figure 1.50** demonstrates an increase in rate acceleration for the formation of *exo*-T_{AB} from 1.2 at 0.2 equivalents of added *trans*-T_{CD} to ≈ 3 between 1.2 and 1.5 equivalents. The experimentally determined rate acceleration values were then fitted (dashed line, **Figure 1.50**) to the independent binding site model developed by Rebek for his reciprocal system. Philp and co-workers found the model provided a good fit to the experimental values for rate acceleration when a K_a value of 4500 M^{-1} for the [*exo*-T_{AB}•*trans*-T_{CD}] complex was used. This calculation was not too dissimilar to the value ($5000 \pm 600 \text{ M}^{-1}$) they determined for this complex by ¹H NMR dilution studies. The individual binding of an amidopyridine to a carboxylic acid moiety at 35 °C is 200 M^{-1} suggesting that interaction in the [*exo*-T_{AB}•*trans*-T_{CD}] complex display negative cooperativity. Indicating that *trans*-T_{CD} and *exo*-T_{AB} are not perfect complementary fits for each other.

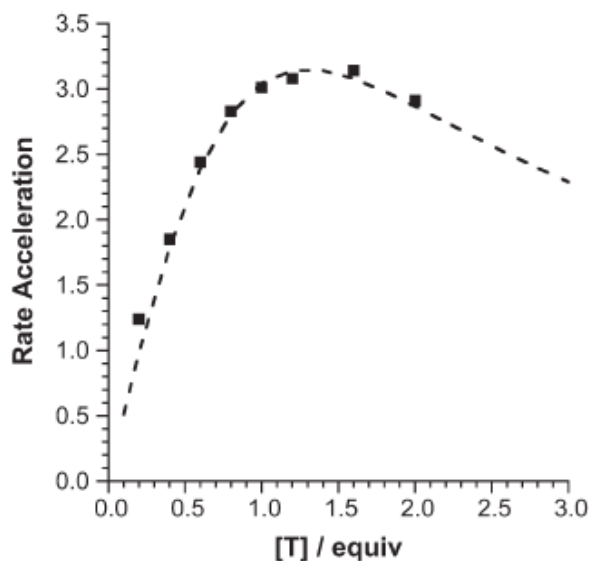


Figure 1.50 Rate acceleration observed in the formation of *exo*-T_{AB} as a function of the equivalents of complementary template *trans*-T_{CD}. Experimental points are filled squares and the dashed line is a fit of the experimental data to an independent binding model.

Philp and co-workers managed to create a reciprocal replicating system exhibiting moderate rate accelerations, although the rate accelerations of their system were lower than those observed in Rebek's. However, this comparison is unfair as in Rebek's system the system was linked together by formation of an amide bond. Whereas, the system developed by Philp required the simultaneous formation of two bonds in the Diels-Alder and 1,3-dipolar cycloaddition reactions. Also, Rebek's system had no concerns over the formation of different diastereoisomers. Nevertheless the reciprocal system developed by Philp and co-workers is far from perfect, as demonstrated by the negative cooperativity between the templates. This system leaves plenty of scope for the development of more efficient reciprocal replicating systems with enhanced rate accelerations, selectivity and optimum fit between the two reciprocal templates.

1.20 Hypercyclic networks^[145-147]

As discussed in previous sections the two main modes of replication are minimal and cross-catalytic systems. The examples of replication mentioned so far treat these two models as independent processes, with a template either reproducing itself by autocatalysis or cross-catalysis. However, there are examples of systems which exhibit both self and reciprocal behavior in a series of complex interlinked cycles. These

systems are referred to as hypercyclic networks in which a template can reproduce itself or template the formation of a non-identical complementary template, and *vice versa*. A hypercyclic network can arise where sub-exponential growth of minimal replicating system, as a consequence of autocatalyst saturation, occurs and where an alternative cross-catalytic pathway is available.

Recently Ghadiri and co-workers published^[146-147] an example of a hypercyclic network formed (**Figure 1.51**) from two self-replicating peptide molecules **T1** and **T2**, comprised of a shared electrophilic section **E** and nucleophilic fragments **N1** and **N2**.

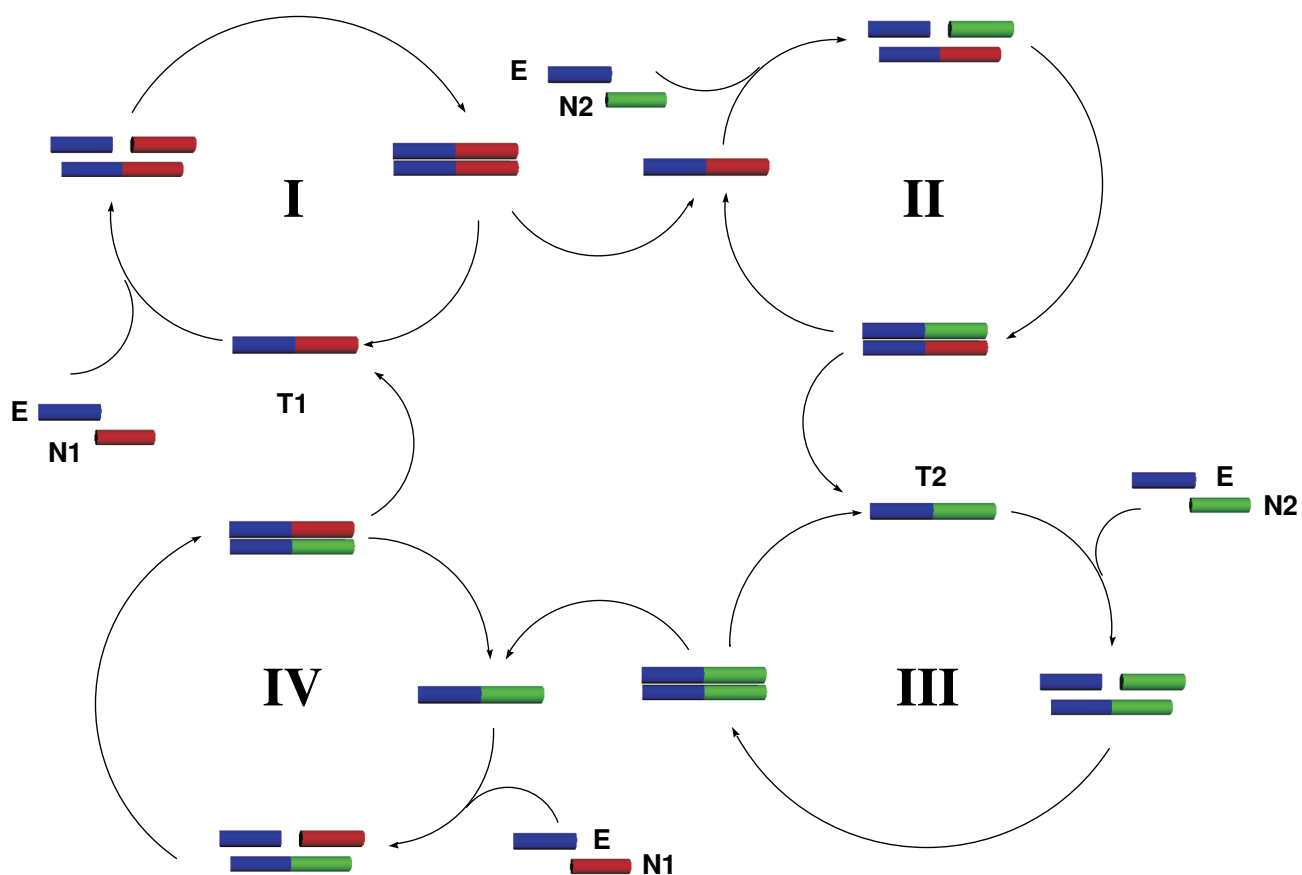


Figure 1.51 Diagram of a hypercyclic network consisting of four catalytic cycles. The four cycles are composed of two self-replicating templates (**T1** and **T2**), which are formed from a common electrophilic fragment **E**, and two nucleophilic peptides **N1** and **N2**. Self-replicating cycles I and III are linked together through two cross-catalytic cycles II and IV. Each template can either replicate itself or template the formation of the other in a mutually rewarding process.

Instead of the expected more efficient replicator commandeering vital resources and out-competing the weaker counterpart a mutually beneficial interaction occurs. This interaction involves **T1** cross-catalyzing the formation of **T2** in cycle II and **T2** reciprocally

templates the formation of **T1** in cycle IV. These two cross-catalytic channels are linked to the minimal replicating cycles forming the hypercyclic network. Therefore, **T1** can not only template the formation of itself but also **T2**, with **T2** also not only reproducing itself but also **T1**. The two cross-catalytic channels were demonstrated to exhibit higher efficiencies than minimal cycles I and III which aided in ensuring the stability of the hypercycle.

In 2005 Kiedrowski published^[148-149] a synthetic minimal replicating system in which its templates displayed not only self-reproducing behavior but also a cross-catalytic nature. This system was based on the work of Wang and Sutherland^[120] (Section 1.17) but utilizing amidopyridine/ carboxylic acid recognition developed by the research groups of Hamilton and Philp in place of the heterocyclic recognition motifs. The work by Wang and Sutherland indicated (Section 1.17) only the *endo*-template for their system demonstrated exponential growth, but they could not identify which one of the two *endo*-diastereoisomers exhibited this behavior. The aim of Kiedrowski system was to try and resolve this question. The author conducted an extensive investigation of the system illustrated in **Figure 1.52**.

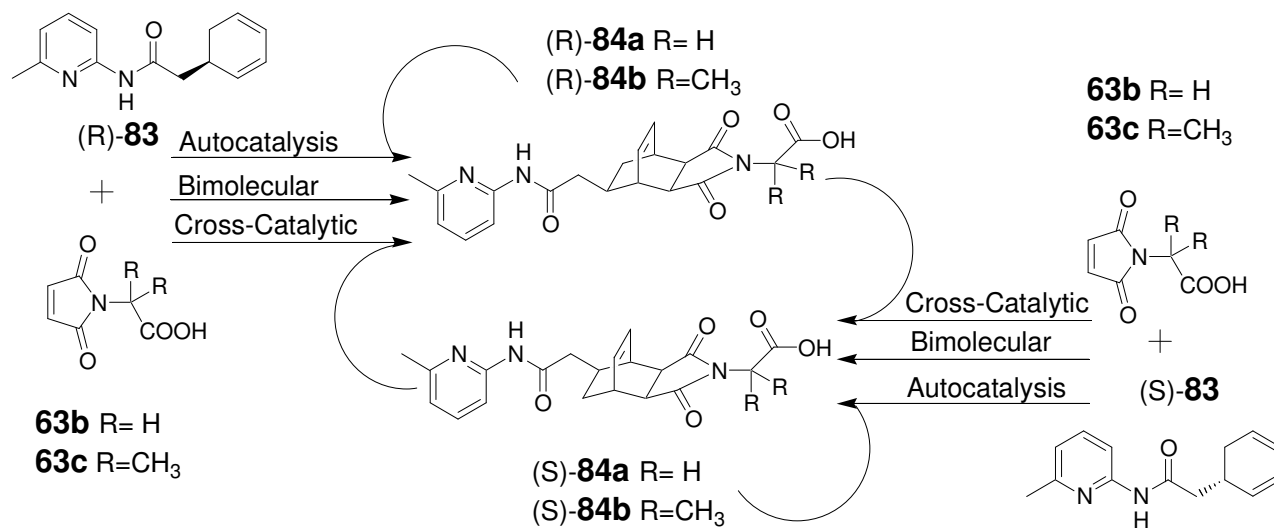


Figure 1.52 Synthetic replicating system developed by von Kiedrowski and co-workers, templates **(R)-84a**, **(R)-84b**, **(S)-84a** and **(S)-84b** are capable of self-replication and cross-catalysis.

In **Figure 1.52** diene **(R)-83** can react with maleimide **63b** (or **63c**) if forming template **(R)-84b**, **(S)-84b**, to form template **(R)-84a**, or maleimide **63b** can react with diene **(S)-83** to form diastereoisomer **(S)-84a**. Kiedrowski conducted a series of experiment in

order to investigate the behavior of this system. In the first experiment the author demonstrated that the addition of 10 mol % (R)-**84a** at the beginning of the reaction between diene (R)-**83** and maleimide **63b** resulted in increased product of (R)-**84a** compared to the bimolecular experiment. This experiment indicated the self-replicating nature of template (R)-**84a**. In the second experiment 10 mol % of (R)-**84a** was added to the reaction of maleimide **63b** with (S)-**83**, this resulted in the increased formation of template (S)-**84a** compared to bimolecular experiment. This experiment demonstrated that not only could (R)-**84a** template its own production, but it could also cross-catalyze the formation of (S)-**84a**. Analysis of the system in **Figure 1.52** indicates that not only can the diastereoisomers (R)-**84a** and (S)-**84a** self-replicate but they can also cross-catalyze the formation of the other. The exponential growth observed in the reaction between racemic diene ((R)-**83** and (S)-**83**) and **63b** for the production of templates (R)-**84a** and (S)-**84a** is a result of the occurrence of both autocatalytic and cross-catalytic cycles in a hypercyclic network. However, von Kiedrowski's system is confusing as he states at the beginning of the investigation only the formation of one diastereoisomer is observed in the range of his detection limits. But demonstrates that the system exhibits exponential growth through minimal and cross-catalytic interactions between the two template diastereoisomers ((R)-**84a** and (S)-**84a**).

1.21 Aims and Objectives.

In this Chapter, recent progress in the field of synthetic and artificial replicators has been outlined. The initial aim of this research project is to investigate the area of synthetic reciprocal replicators, with the goal of producing systems with greater efficiency than the ones developed by Rebek and Philp previously.

Once an efficient pair of cross-catalytic templates have been constructed and their behavior characterized, the aim of this research project will shift towards the investigation of the interactions between reciprocal and minimal replicating templates in a potential hypercyclic network.

In both cases a detailed examination will focus on the design, synthesis and kinetic analysis of these replicating templates, with the goal of determining the key requirements necessary for the design of an efficient replicating network.

2 The design and synthesis of a reciprocal replicating system

2.1 Designing a reciprocal replicating system

When designing a reciprocal replicating system, or for that matter a minimal replicating system, there are three essential features required a;

- (I) suitable recognition motif
- (II) suitable reactive site
- (III) suitable spacer unit

A suitable recognition motif is required for a replicating system in order to allow the molecules to associate together in the correct manner. The successful reciprocal replicating system must have complementary recognition between the templates, but at the same time not be self-complementary with itself or its own building blocks (**Figure 2.1**).

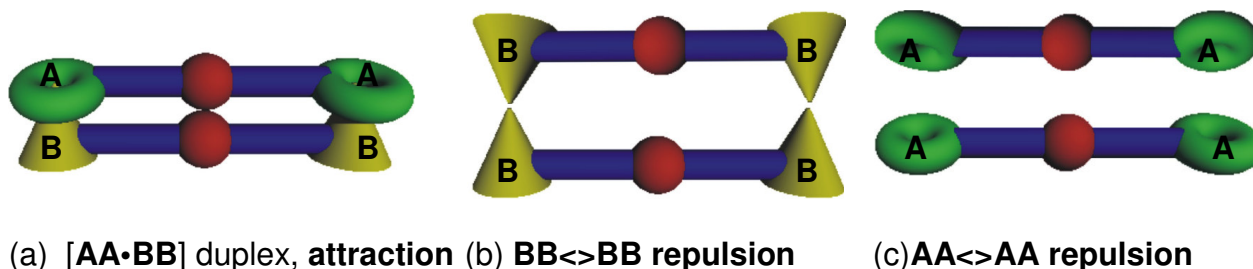


Figure 2.1 Schematic demonstration showing advantage of complementary association (a) complementary recognition to form a [AA•BB] duplex. (b) BB<->BB identical recognition repulses two templates, therefore, no formation of duplex (c) AA<->AA identical recognition repulses two templates, therefore, no formation of duplex.

In **Figure 2.1(a)** a cartoon model represents the association between a template containing two identical recognition sites **A** (green doughnut), with another molecule of template containing two complementary recognition sites **B**. However, the cartoon models in **Figure 2.1 (b)** and **(c)** illustrate that the two templates containing identical recognition are non-complementary and will not be able to associate into a duplex structure. In other words recognition site **A** will only recognize **B** and *vice versa*, therefore, a template containing **AA** recognition is only complementary to **BB**, with the same applying in reverse. The end result of this complementarity is a template containing **AA** recognition can only be formed using the complementary **BB** structure and the reverse is also true, with self-replication impossible.

Another important design feature of a replicating system is that the association between the two templates in the [AA•BB] duplex is relatively weak (**Figure 2.1**). The weakness of this association is important because, if the two templates are strongly associated in the [AA•BB] duplex, it will not be easy for them to dissociate. Hence the turnover of catalyst will be inhibited resulting in a decrease in catalytic efficiency. The recognition motif also affects the practical conditions required for the system, such as temperature and solvent.

A second important feature of a replicating system is the reactive sites, which form the covalent bonds, which connect the building blocks together to form the templates. A suitable coupling reaction between the building blocks must be utilized that is kinetically simple and does not require a catalyst or co-factor. Such reactions include substitutions and cycloadditions. One of the advantages of cycloaddition reactions is that they can form a variety of isomers with different regio- and stereochemistries providing a potential source of variation.

A final key requirement for a reproducing replicating system is a suitable spacer unit between the reactive sites and the recognition motif.

These features are essential for an efficient replicating system and careful contemplation is required in choosing each component.

2.2 The recognition motif

Important consideration has to be taken when deciding upon a suitable recognition motif for a self-replicating system. In Rebek's systems^[102] the association between a Kemp's triacid imide and an adenosine derivative was chosen, whereas von Kiedrowski used^[94] the recognition between nucleic acid base pairs. However, both these systems utilize natural recognition motifs, instead we are interested in novel synthetic recognition units. Previous work in our group focused^[201] on the recognition between crown ethers and ammonium ions, but this motif proved troublesome as a consequence of unknown salt effects and complicated synthetic procedures. Therefore, attention instead turned towards hydrogen bonding between aminopyridine units and carboxylic acids^[150] derivatives, after the work conducted by Hamilton in this area. Hamilton has described^[152-153] extensive studies of the binding between carboxylic acids and aminopyridine substrate derivatives. In one study he compared the association between

dicarboxylic acids **100**, **101**, **102** and the rigid diamide receptor **99**, which through molecular modelling studies Hamilton determined was particularly suitable for the complexation of dicarboxylic groups separated by three or four methylene groups (**Figure 2.2**).

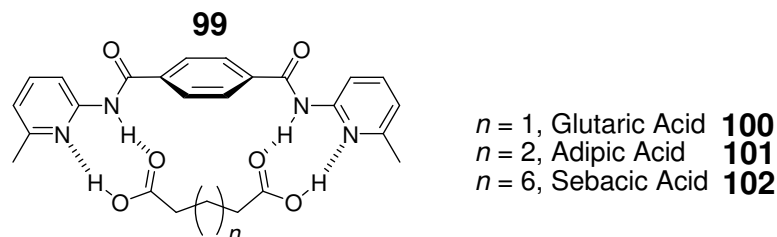


Figure 2.2 A diamide receptor **99** capable of binding with dicarboxylic acids **100**, **101**, and **102** through hydrogen bonding.

When Hamilton analyzed^[154-155] the ¹H NMR spectra of these complexes he established the strongest association was between glutaric acid and adipic acid with the receptor in a 1:1 complex. Hamilton attributed this finding to the fact that these two dicarboxylic acid's length and steric features best corresponded to the interior cavity of the template. The binding constant for adipic acid was determined to be $>10^5 \text{ M}^{-1}$ compared to $5.9 \times 10^4 \text{ M}^{-1}$ for glutaric acid and $3.3 \times 10^3 \text{ M}^{-1}$ for sebacic acid. The substantially larger association constants observed for adipic and glutaric acid were associated with positive cooperative binding effects. Other groups have conducted studies in to the association of dicarboxylic acids with aminopyridine residues. Goswami measured^[156] the coupling between a derivative of Tröger's base and dicarboxylic acid and also observed strong cooperative binding effects. As a result of the study conducted by Hamilton and Goswami it was decided to choose a similar recognition pattern for the system in this report, with one template containing two dicarboxylic acid motif and the other template containing two aminopyridine units.

The amidopyridine/carboxylic acid recognition motif has been extensively investigated in our group. Therefore, a range of association constants have been calculated over a range of temperatures. The result of this work means we can use already calculated association constants in a van't Hoff plot (**Figure 2.3**) to determine^[165] non-experimentally obtained values.

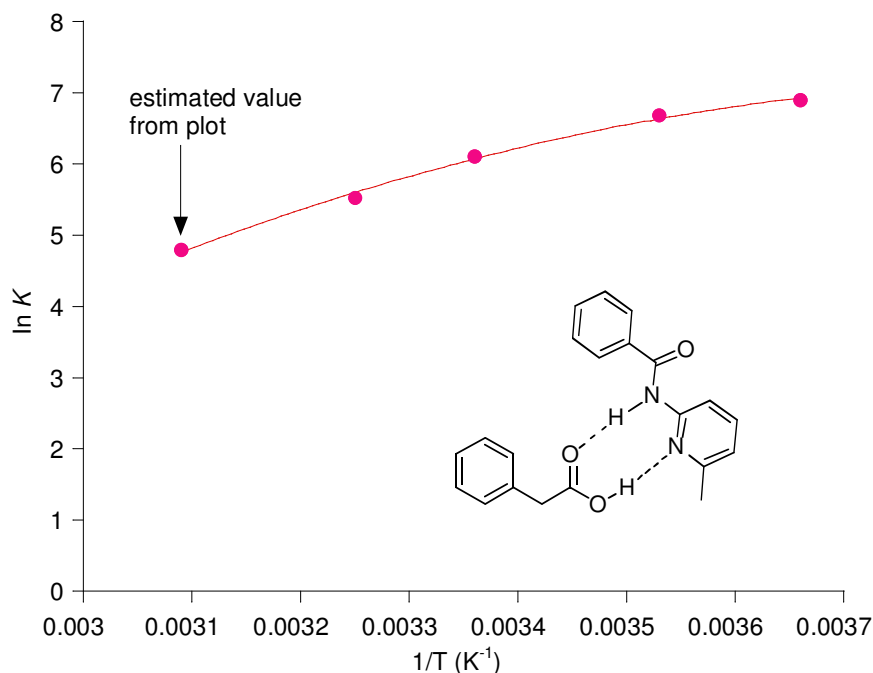


Figure 2.3 van't Hoff plot of experimentally determined association constants for the hydrogen bonding between a amidopyridine and a carboxylic acid derivative.

The graph in **Figure 2.3** displays a series of points which demonstrate a non-linear relationship, indicating $\Delta C_p^\circ \neq 0$. All experiments in this potential replicating system will be conducted at 50 °C, or 323 K, as a consequence of the slow reaction rate between starting materials. Therefore, by examining the graph in **Figure 2.3** it is possible to calculate the association constant for the hydrogen bonding of a carboxylic acid group to an amidopyridine derivative by fitting the equation in **Figure 2.4** to the experimental obtained values. A value of 120 M⁻¹ was calculated for this binding interaction at 323 K.

$$R \ln K_a = -\Delta H^\circ \frac{1}{T} + \Delta C_p^\circ \ln T + (\Delta S^\circ - \Delta C_p^\circ)$$

Figure 2.4 Equation used to fit non-linear van't Hoff plot. Where R is the gas constant, K_a equilibrium constant, T is temperature, ΔH° , ΔC_p° and ΔS° are change in enthalpy, heat capacity and entropy respectively.

2.3 The reactive site

Having decided upon a suitable recognition motif the focus turned to the reactive sites. As already mentioned there is a variety of reactions which are suitable for this role, one such reaction is the Diels-Alder cycloaddition. The Diels-Alder reaction is a concerted

reaction between a diene and a dienophile. The diene and dienophile react in parallel planes in which the orbitals reacting are those on the top of the alkene at both ends and at the bottom of the diene at both ends (**Figure 2.5**). For this [4+2] cycloaddition the HOMO of the ethylene is of the same symmetry as the LUMO of the butadiene.

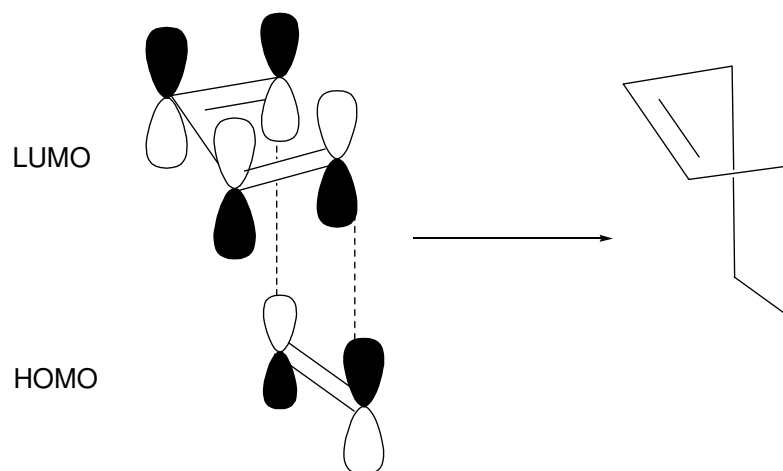


Figure 2.5 [4n+2] Diels-Alder reaction in which there is parallel approach of the diene and alkene, orbitals on top of diene react with orbital at the bottom of the diene in a concerted process.

Reactions that are from the same face at each end of the conjugated system are called suprafacial reaction. As a result of the concerted nature of the reaction it is stereospecific with respect to diene and alkene. For a Diels-Alder reaction to occur the diene must be in the 's-cis' conformation and not in the 's-trans' conformation. Dienes and dienophiles can approach each other in several ways giving rise to diastereomers. These two diastereomers are referred to as *exo* and *endo* (**Figure 2.6**).

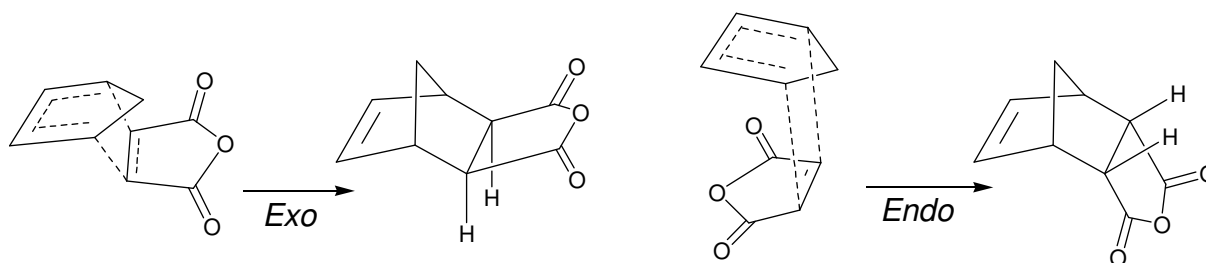


Figure 2.6 *Exo* and *endo* products from a Diels-Alder reaction between a diene and a dienophile, different diastereomers arise from the way the two reactants approach each other.

A feature^[157] of the Diels-Alder stereochemistry is what is referred to as the *endo* effect. In this stereochemical effect an acceptor group on the dienophile ends up on the *endo*

position of the product (**Figure 2.6**). This effect is rationalized through the use of secondary orbital effects, these are molecular orbital interactions not involved in determining whether a reaction is allowed or forbidden (**Figure 2.7**).

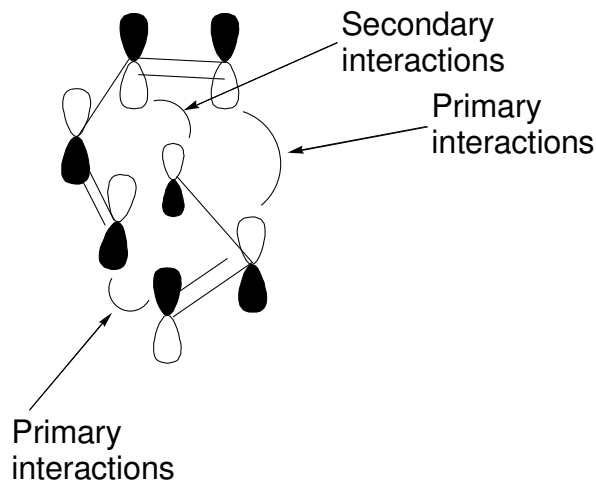
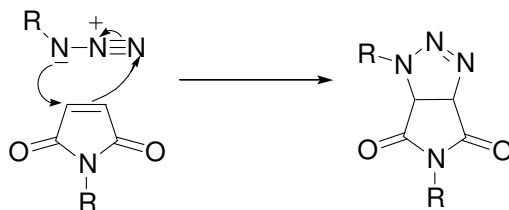


Figure 2.7 Secondary orbital interactions between an alkene and a diene.

In **Figure 2.7** the primary interactions mean this is an allowed reaction, however, the molecular orbital acceptor group on the dienophile can interact with an orbital in the diene in a secondary orbital interaction. This interaction means the *endo*- product is stabilized compared to the *exo*- product, therefore, this explains why the *endo*- product is favored in **Figure 2.6**.

Previous work by our group^[158] has focused on a [3+2] cycloaddition^[159-160] between an azide and a maleimide (**Scheme 2.1**).



Scheme 2.1 1,3-dipolar cycloaddition between an azide and a maleimide, concerted reaction involving 5 atoms, 6 electrons.

Extensive work has been carried out onto the mechanism of 1,3-dipolar cycloaddition reactions. A 1,3-dipolar cycloaddition is a five atom, six electron cycloaddition between a

1,3-dipole (azide) and a dipolarophile (maleimide). Huisgen^[160-162] proposed that the mechanism for 1,3-dipolar cycloadditions involves a concerted bond forming step between the 4π electron system of the dipole and 2π electron system of the alkene. Why do 1,3-dipoles react so easily with most types of dipolarophiles? The reason for this comes from the orbital energies associated with a 1,3-dipole. A 1,3-dipole generally has a fairly high energy HOMO (highest occupied molecular orbital) and a fairly low energy LUMO (lowest unoccupied molecular orbital). This high HOMO and low LUMO energy means there is only a relatively small energy difference between the LUMO of the dipolarophile and the HOMO of the dipole or the HOMO of the dipolarophile and the LUMO of the dipole. Therefore they can readily react.

The regiochemistry of 1,3-dipolar cycloadditions is now considered to be controlled by the magnitude of frontier orbital coefficients. The frontier orbital coefficients of the dipole and the dipolarophile allow the regiochemistry of a 1,3-dipolar cycloaddition reaction to be predicted. When considering frontier orbital coefficients one must also consider the groups attached to the dipole and the dipolarophile. If an electron withdrawing group (Z) is attached to one of the reactive partners it will usually have the effect of lowering the energy of both the LUMO and the HOMO, whereas an electron donating group (X) usually has the effect of raising both the energies of the HOMO and LUMO. If a conjugated group (C) is attached to a reactive partner, it has the effect of bringing the energies of HOMO and LUMO closer together. All reactions between 1,3-dipoles and dipolarophiles containing electron donating groups should be successful according to LUMO-dipole and HOMO dipolarophile control. However, if an electron withdrawing group or conjugation is attached to the dipolarophile the matter is complicated and the reaction becomes dependent on specific frontier orbital interactions. The frontier molecular orbital energies have been estimated for the 1,3-dipolar cycloaddition reaction between a phenyl azide and a dipolarophile with an electron donating (X), electron withdrawing (Z) and a conjugated (C) substituent by Houk (**Figure 2.8**)^[163-164].

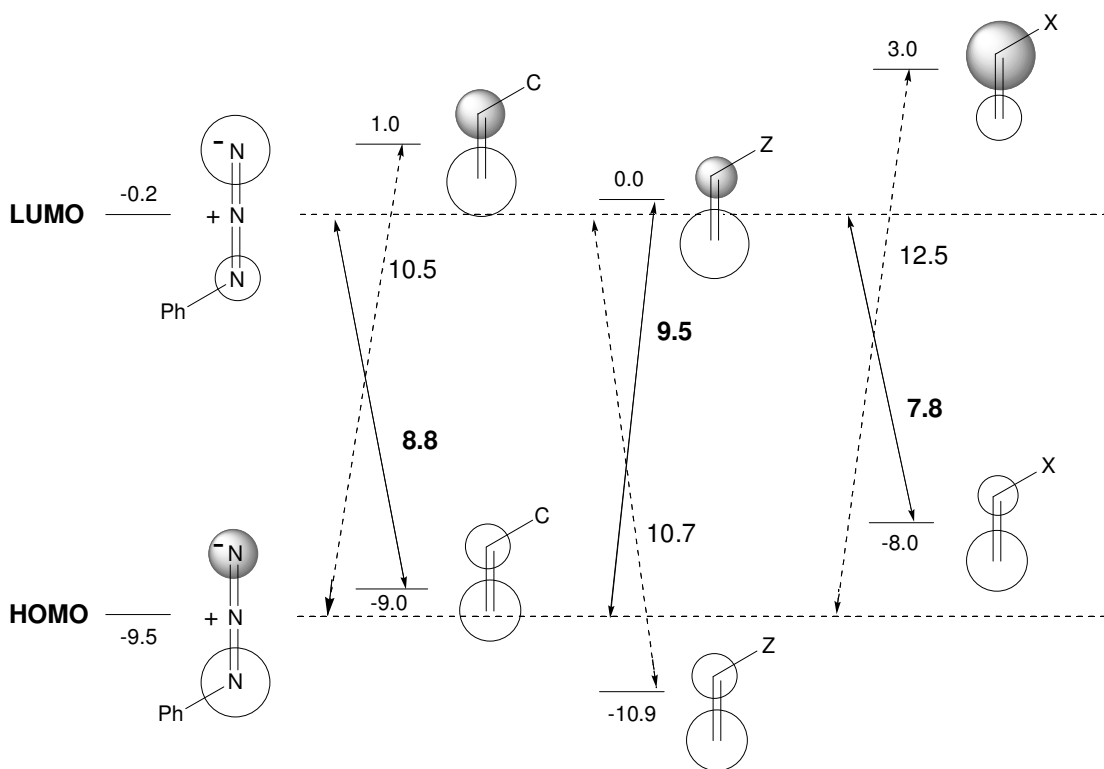


Figure 2.8 Frontier molecular orbital energies for a 1,3-dipolar cycloaddition between phenyl azide and various substituted alkenes. Taken from reference 164.

Houk found the smallest difference in energy was between a phenyl azide and styrene bearing an electron donating substituent (X) (7.8 eV). Therefore, this reaction is a result of dipole-LUMO and dipolarophile HOMO interaction resulting in a 1,5-product (**Figure 2.9**). The same 1,5-product is observed for a styrene bearing a conjugated group with an energy gap of 8.8 eV, however, for an electron withdrawing group a 1,4-product is observed as this reaction is controlled by HOMO of the dipolar and LUMO of the dipolarophile (**Figure 2.9**).



Figure 2.9 1,5- and 1,4-products from a [3+2] cycloaddition, where X is an electron donating group, C is a conjugated group and Z is an electron withdrawing group.

Regiochemistry only has to be considered if both of the products are unsymmetrical, if one or more of the reactants are symmetrical then regiochemistry is not a concern. However, frontier molecular orbitals are still of importance, as previously mentioned the effect of electron donating, electron withdrawing and conjugated substituents can decrease the energy gap between HOMO and LUMO interactions between dipoles and dipolarphiles increasing the reactivity of the cycloaddition.

2.4 The spacer unit

The spacer unit acts as a scaffold for the recognition sites and the reactive sites. Its job is more than just connecting the recognition sites to the reactive site. The spacer unit must be reasonably rigid so as to hold the reactive sites at the correct distance to induce covalent bond formation. If the spacer unit is too flexible then the reactive sites will not be as close in space in the ternary complex, decreasing the reaction rate. Rebek also showed that a bulky spacer unit can help in the dissociation of the resultant duplex. Therefore, careful consideration must be taken when choosing a suitable spacer unit.

2.5 The potential reciprocal replicating system

Having identified how best to satisfy the key requirements of a potential reciprocal replicating system, four compounds were identified as initial building blocks for this system (**Figure 2.10**).

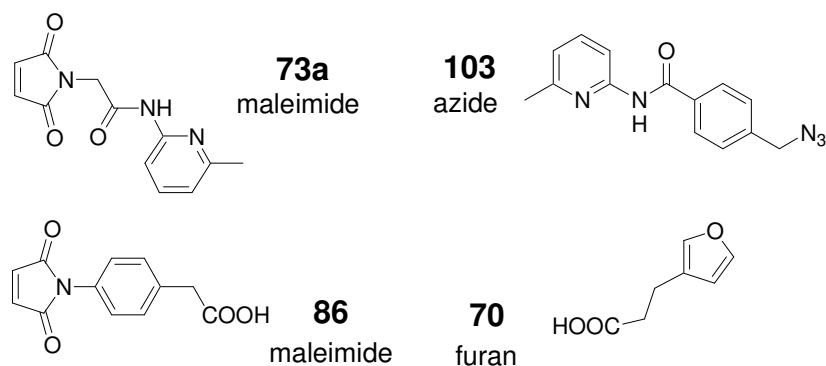
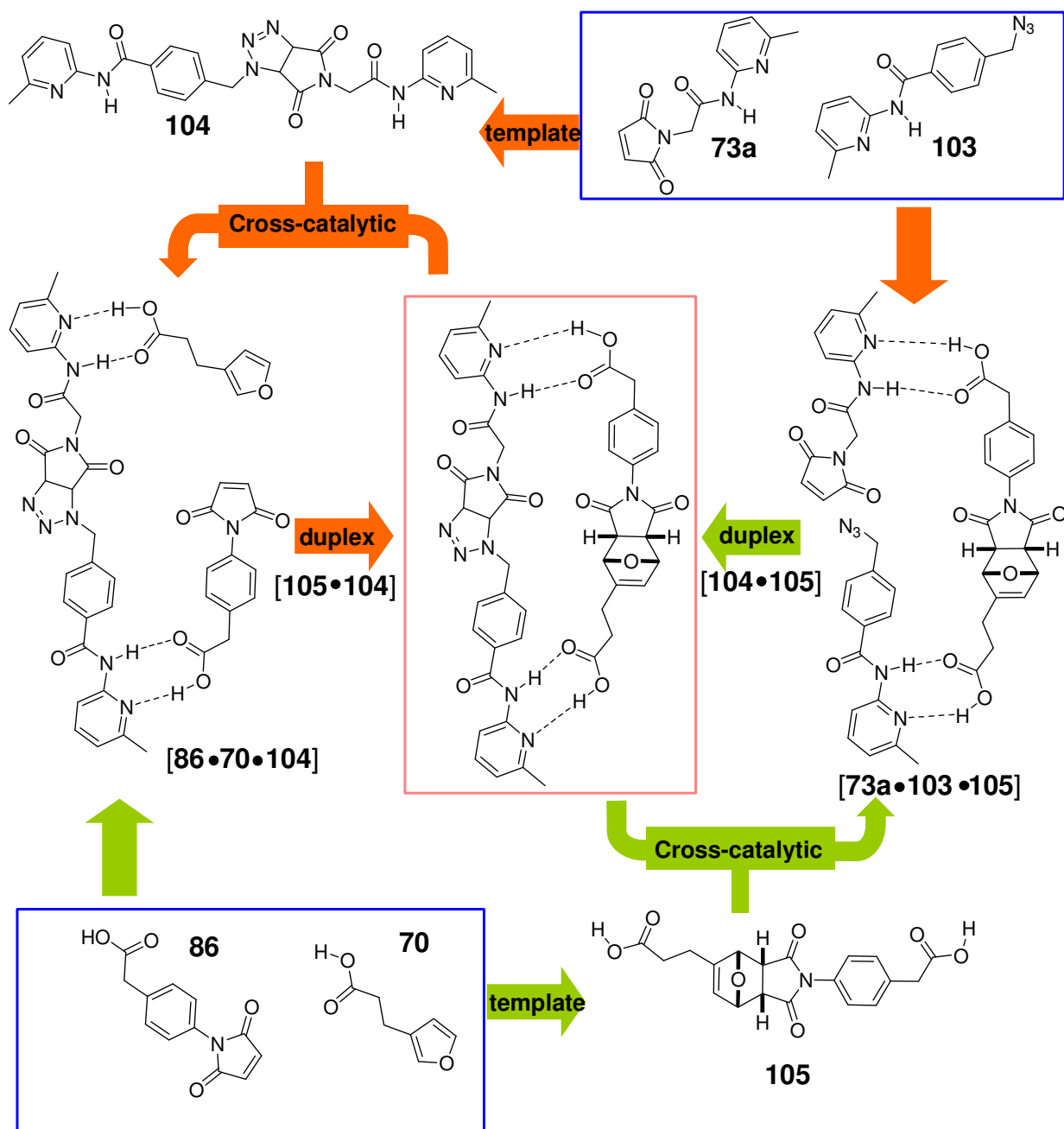


Figure 2.10 Four initial template building blocks maleimide **73a**, **86**, furan **70** and azide **103**.

The first template for this reciprocal system is synthesised through the bimolecular reaction between maleimide **73a** and azide **103** (blue square, **Scheme 2.2**) to form template **104**. Bis(amidopyridine) **104** can associate starting material furan **70** and maleimide **86** in a ternary complex structure [**70•86•104**].



Scheme 2.2 Proposed cross-catalytic cycle for formation of cycloadduct **104** from **73a** and **103** using the reciprocal template **105**, and for the template's formation of *exo*-cycloadduct **105** using bis(amidopyridine) **104** from furan **70** and maleimide **86**.

This ternary complex renders the reaction *pseudo*-unimolecular, bringing the reactive sites close enough together to accelerate the reaction between furan **70** and maleimide **86** in a regio-chemical control fashioned, it is hoped. The result of this reaction is the formation of the duplex structure [104•*exo*-105] (pink square, **Scheme 2.2**). The reason that *exo*-105 is predicted and not *endo*-105 can be explained through analysis (**Figure 2.11**) of the transition state diagrams for the reaction between a furan derivative and a maleimide derivative.

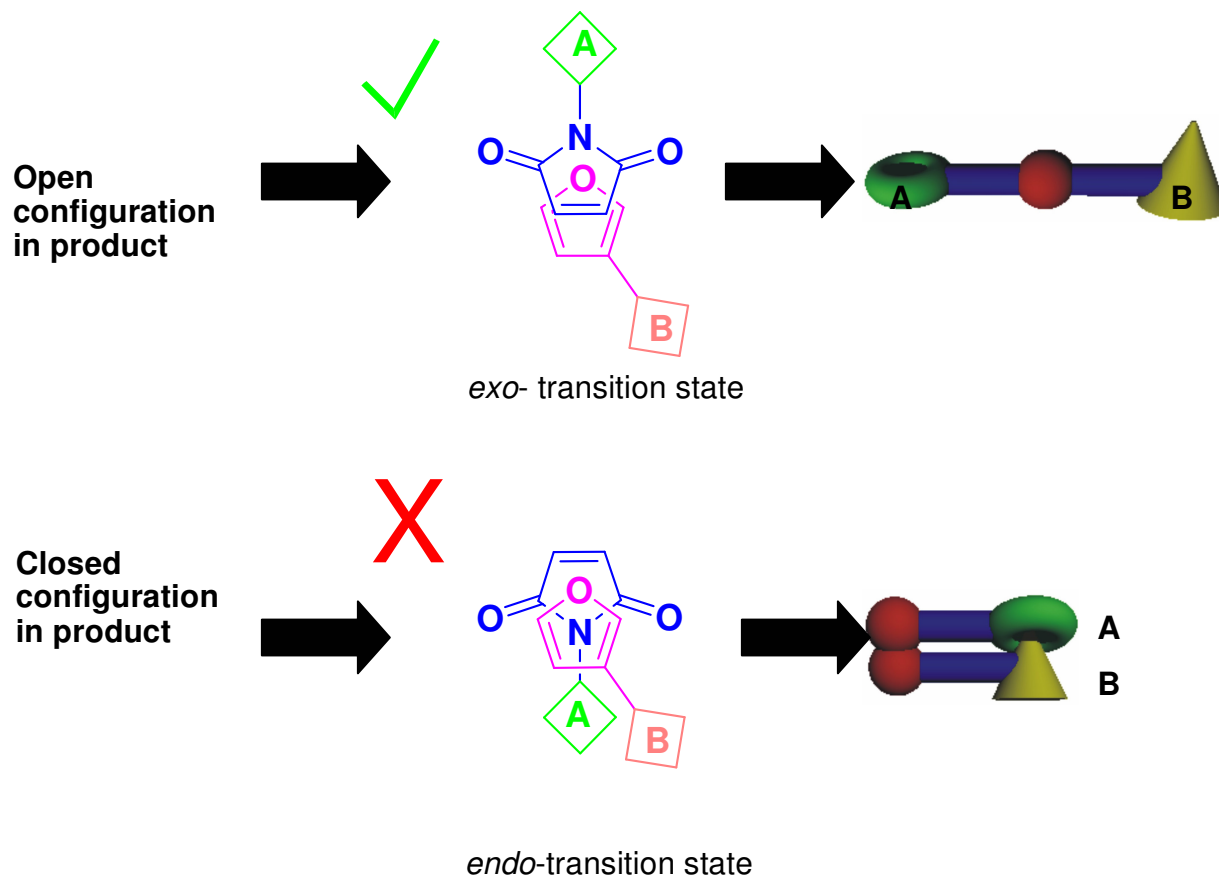


Figure 2.11 Transition state diagrams of Diels-Alder reaction between a maleimide containing recognition site **A** and furan containing recognition site **B**. The *exo* transition state has recognition site **A** and **B** held wide apart in an open conformation resulting in the open template (green tick), demonstrated by the 3D cartoon with yellow and green recognition site. The *endo* transition state has **A** and **B** overlapping in a closed conformation resulting in a closed template (red cross), demonstrated in the cartoon with overlapping recognition sites green and yellow.

The cartoon diagrams in **Figure 2.11** demonstrate how the *exo* transition state for the reaction between a maleimide and a furan holds recognition sites **A** (green block, **Figure 2.11**) and **B** (yellow block, **Figure 2.11**) wide apart in an open configuration. This open configuration is translated onto the product template, shown by the cartoon model (**Figure 2.11**) containing green recognition site **A** and yellow recognition site **B**.

However, the *endo* transition state (**Figure 2.11**) has recognition **A** and **B** overlapping in a closed structure and therefore, the resultant product is expected to have a closed structure, with recognition sites unavailable, as shown in the cartoon model of the *endo*-product.

If the association between **104** and *exo*-**105** is weak enough both template structures can dissociate. This dissociation returns the bis(amidopyridine) **104** to the start of Cycle one, leaving dicarboxylic acid **105** free to enter Cycle two where it can template the formation of bis(amidopyridine) **104** from azide **103** and maleimide **73a**, utilizing the same principles described in Cycle one.

In order to demonstrate the template complementarity between bis(amidopyridine) **104** and dicarboxylic acid *exo*-**105** the lowest energy structure for this product duplex was calculated using molecular mechanics. A series of Monte Carlo conformational searches were performed, starting from individually minimized conformations of the two templates on their own and associated with the complementary partners, utilizing MMFFs forcefields and the GB/SA solvation model for CDCl₃. The results of these calculations demonstrate (**Figure 2.12**) that both templates provide a complementary fit to one another. Cartesian coordinates for this duplex structure can be examined in Appendix 8.

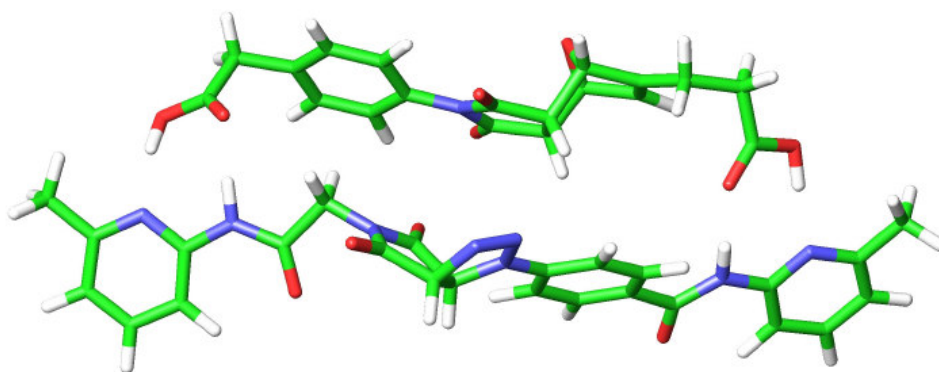
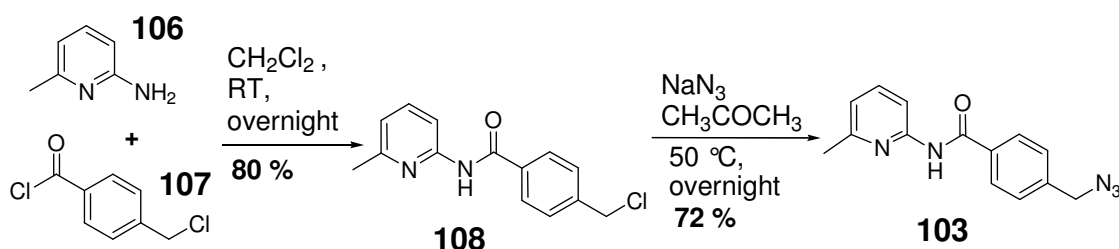


Figure 2.12 Molecular mechanics model of [**104**-*exo*-**105**] duplex. Carbon atoms are Green, Nitrogen atoms are blue, oxygen atoms red and hydrogen atoms are white.

2.6 Synthesis of a reciprocal replicating system

2.7 Azide 103

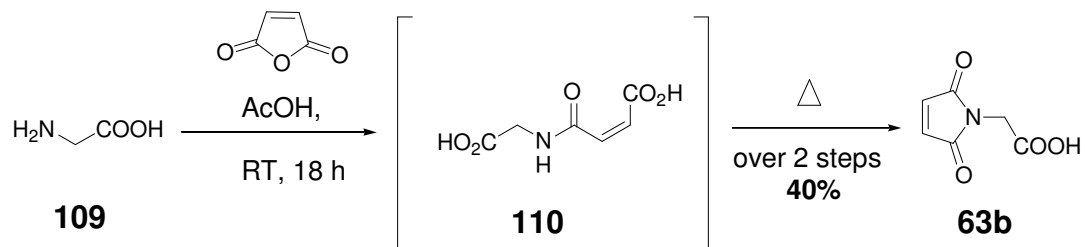
The synthesis of azide **103** was achieved in two separate steps. The first step involved nucleophilic attack of aminopyridine **106** on 4-(chloromethyl)benzoyl chloride, **107**. Reaction of **106** and **107** in CH_2Cl_2 at room temperature, afforded alkyl chloride **108** in 80 % yield, after chromatography. The second step involved the nucleophilic substitution of the chloride for an azide moiety. This substitution was achieved by reacting **108** with sodium azide in acetone overnight, to afford azide **103** in 72 % yield (**Scheme 2.3**).



Scheme 2.3 The synthetic route for the preparation of dipole **103**.

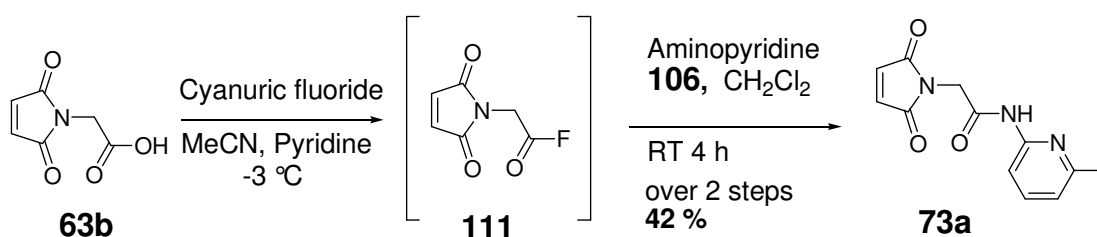
2.8 Maleimide 73a

Three reactions were required for the formation of the maleimide **73a**. The first reaction involved the formation of maleimide **63b**. This maleimide was formed by mixing glycine **109** and maleic anhydride in acetic acid, this solution was left to stir overnight at room temperature to form the intermediate maleic acid **110**. This maleic acid intermediate was cyclized to the maleimide by heating under reflux until the solution turned clear. The crude product was then purified using column chromatography on silica gel and recrystallized to afford **63b** in 40 % yield (**Scheme 2.4**).



Scheme 2.4 The synthetic route for the preparation of maleimide **63b**.

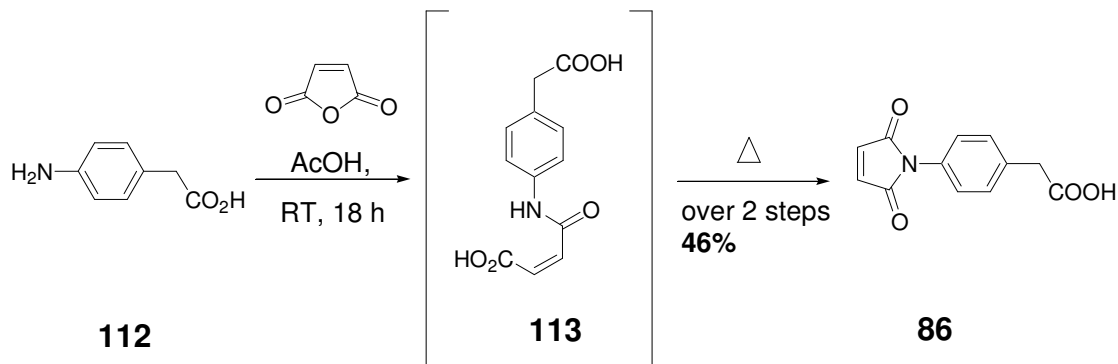
The maleimide **63b** could not react directly with aminopyridine **106** as a result of its poor nucleophilicity and the poor nature of the hydroxyl group on the maleimide as a leaving group. Therefore, maleimide **63b** first had to be converted to the acid fluoride **111**, which has a far better leaving group in the fluoride ion. An ideal reagent for this is cyanuric fluoride^[207] as a result of its highly reactive nature. The acid fluoride intermediate was not isolated as a consequence of its reactivity (although a small sample was taken for ¹⁹F NMR spectroscopy, which indicated the presence of an acyl fluoride compound). Instead it was reacted immediately with aminopyridine **106** in CH₂Cl₂ at room temperature for 4 hours, to afford maleimide **73b** in 42 % yield (**Scheme 2.5**), after column chromatography.



Scheme 2.5 The synthetic route for the preparation of maleimide **73a**.

2.9 Maleimide **86**

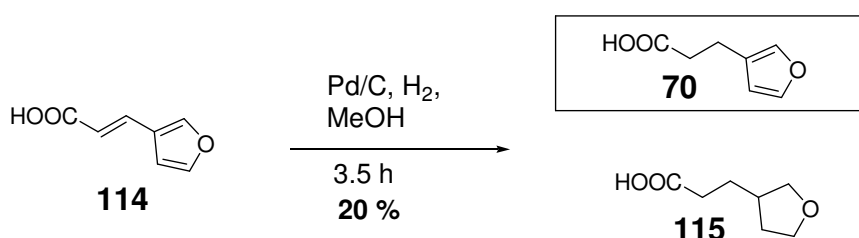
Maleimide dienophile **86** was synthesized in the same manner as the previous maleimide using a mixture of 4-aminophenylacetic acid **112** and maleic anhydride in acetic acid resulting in the formation of **86** in 46 % yield (**Scheme 2.6**), after recrystallization.



Scheme 2.6 The synthetic route for the preparation of the dienophile maleimide **86**.

2.10 Furan 70

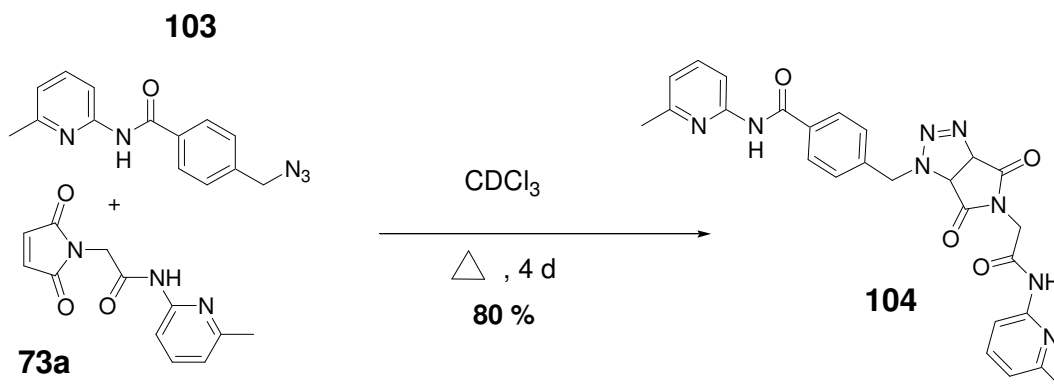
The synthesis of furan **70** was achieved through the reduction of 3-furan-3-yl-acrylic acid **114**. A round bottom flask containing 3-furan-3-yl-acrylic acid and Pd/C was flushed with nitrogen for 30 minutes before methanol was carefully syringed into the flask. The flask was then flushed with hydrogen gas and a hydrogen filled balloon attached and the reaction mixture was monitored using thin layer chromatography (TLC). However, the trouble with monitoring this reaction through TLC was that no change in the R_f value was observed only a change in intensity of the spot so as a result a high amount of the unwanted fully reduced product was obtained **115**. Furan **70** was afforded in 20 % yield (**Scheme 2.7**), after purification by Kugelrohr distillation and then recrystallization.



Scheme 2.7 The synthetic route for the preparation of furan **70** and fully reduced by-product **115**.

2.11 Synthesis of bis(amidopyridine) template 104.

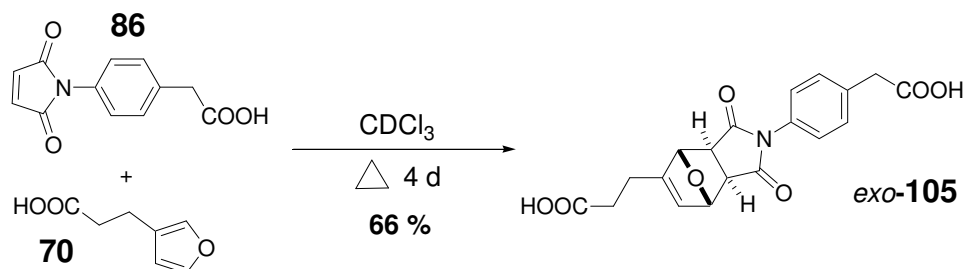
The 1,3-dipolar cycloaddition reaction between azide **103** and maleimide **73a** was performed in the dark at 50 °C in CHCl₃ for four days, affording bis(amidopyridine) **103** in 80 % yield (**Scheme 2.8**), after purification by column chromatography.



Scheme 2.8 The synthetic route for the preparation of template **104**.

2.12 Synthesis of dicarboxylic acid template *exo*-105

Dicarboxylic acid template *exo*-105 was synthesized through the Diels-Alder reaction between furan **70** and dienophile **86** in the dark in CHCl_3 for four days at 50 °C. This procedure led to the formation of template *exo*-105 in 66 % yield (**Scheme 2.9**). Template **105** was isolated only as the *exo*-diastereoisomer.



Scheme 2.9 The synthetic route for the preparation of template *exo*-105

2.13 Results and Discussion

2.14 Kinetic analysis

All kinetic experiments were conducted in CDCl_3 , with an initial concentration of 25 mM for all template starting materials. All experiments in this Chapter were conducted at 50 °C for over 14 hours. Samples for kinetic analysis were prepared in the manner described in the general experimental (Section 7.4).

The different reactions were monitored by 500 MHz ^1H NMR spectroscopy and the product and remaining starting material concentrations were extracted from the individual spectra using the deconvolution 1 tool of 1D WINNMR 6.0 NMR post-processing tool. A more detailed discussion of this procedure is again given in the general experimental (Section 7.5).

Product concentrations were extracted through monitoring the growth of the H_a and H_b ^1H NMR peaks on the cycloadducts and the disappearance of the H_c peaks of the starting material (**Figure 2.13**, see also General experimental, Section 7.5). Appendix One shows the ^1H NMR spectrum for the bimolecular and templated reaction between maleimide **86** and Furan **70**, after 5.5 and 4.5×10^4 s. The maleimide starting material and cycloadduct proton peaks, which are deconvoluted, are highlighted.

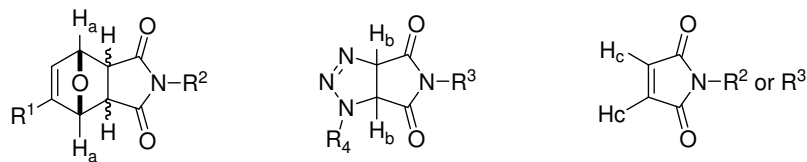
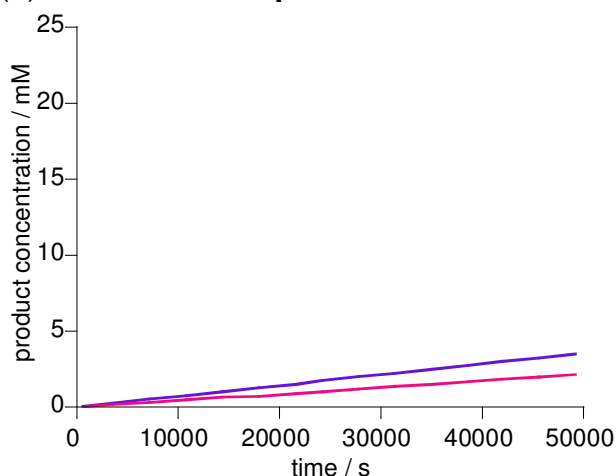


Figure 2.13 Deconvolution of ^1H NMR signal H_a , H_b and H_c used to determine product concentrations of template cycloadducts.

Two different sets of kinetic experiments were conducted in order to determine the behavior of these potential reciprocal replicating templates. The first experiment conducted is a bimolecular control. In this reaction the two starting material molecules at equimolar concentrations are allowed to react in the absence of template. This experiment provides details of the rate, selection and conversion when no cross-catalysis is possible. A bimolecular rate profile like the one in **Figure 2.14** (a) is expected for this process. Once the behavior of the bimolecular reactions is characterized we can then go on to examine the templated experiments. In these experiments, reciprocal template is added at the start of the reaction between equimolar concentrations of the two complementary starting materials. If cross-catalysis is occurring we would expect to see an increase in rate and potentially selectivity resulting in a parabolic appearance to the rate profile, as demonstrated in the example in **Figure 2.14** (b).

(a) Bimolecular experiment



(b) Templated experiment

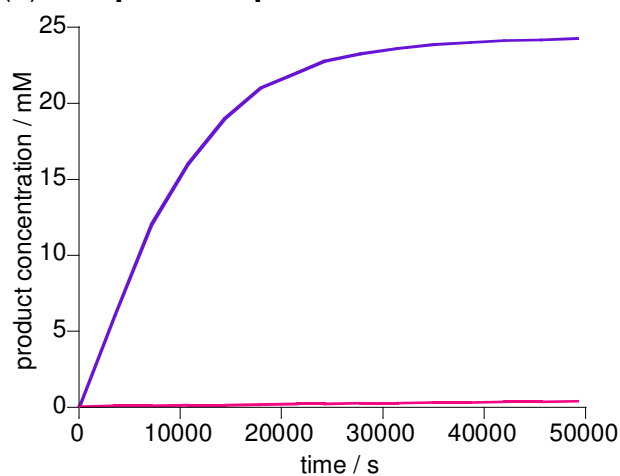
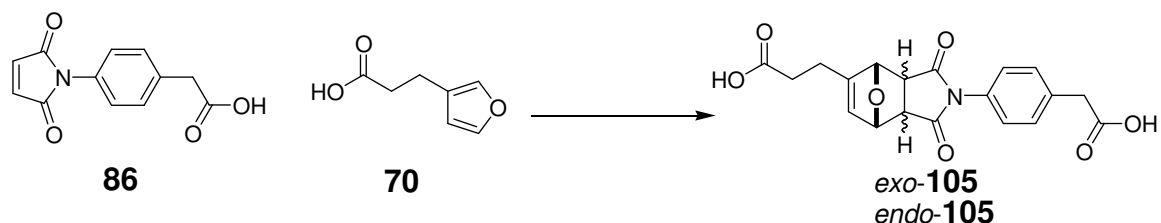


Figure 2.14 Examples of expected product concentration vs. time graphs (rate profiles) for the two different types of experiment conducted to determine behavior of system. (a) Typical bimolecular profile. (b) Templated experiment demonstrating parabolic curve with increase rate and selectivity compared to the bimolecular counterpart.

2.15 Cross-catalytic formation of *exo*-dicarboxylic acid **105**

The cross-catalytic template dicarboxylic acid **105** is formed from the Diels-Alder reaction (**Scheme 2.10**) between furan **70** and maleimide **70**, where the formation of *exo*-**105** has the potential to be templated by bis(amidopyridine) **104**.



Scheme 2.10 Diels-Alder reaction between **86** and **70** for the formation of reciprocal template *exo*-**105**.

The bimolecular experiment between maleimide **86** and furan **70** was conducted and monitored using the conditions and techniques described in Section 2.14. Product concentrations were extracted, *via* deconvolution of individual spectra, from the control experiment and plotted (**Figure 2.15** (a)) against time.

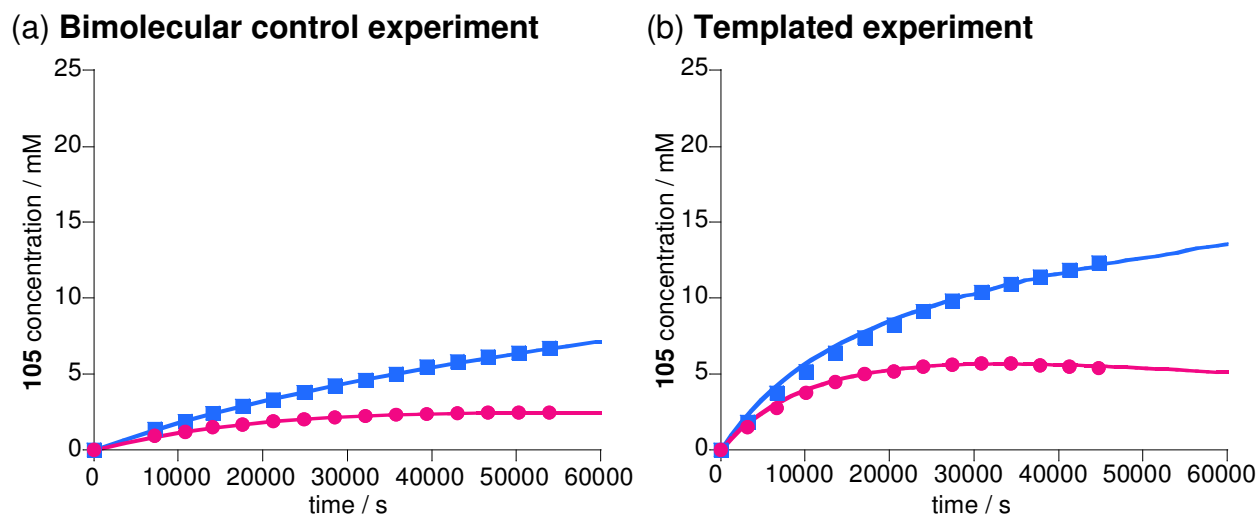
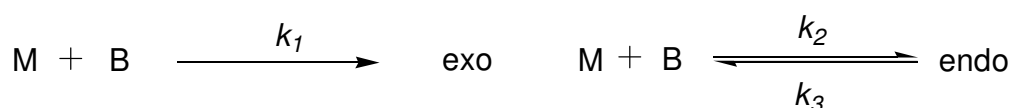


Figure 2.15 Product concentration vs. time graphs. (a) Bimolecular reactions between equimolar concentrations of furan **70** and maleimide **86** ($[\mathbf{70}] = [\mathbf{86}] = 25$ mM, at 50 °C in CDCl_3). (b) Templated experiment between equimolar concentrations of furan **70**, maleimide **86** and 2 equivalents of complementary bis(amidopyridine) **104** (50 mM) in CDCl_3 at 50 °C. *Exo*-**105** is indicated by blue squares, *endo*-**105** as pink circles on both graphs. Solid line indicates optimal fit curves. Error in concentration values is ± 4 %.

Investigation (**Figure 2.15** (a)) of the control experiment graph demonstrates the expected bimolecular profile with an *exo* to *endo* ratio of 2.7:1, after 14 hours, with an overall conversion of 37 %. An error of ± 4 % is anticipated in calculated concentration values in **Figure 2.15** as a result of deconvolution errors and errors in the accurate measurement of mass and volume of starting materials. Analysis of the *endo*- product curve reveals what appears to be a decrease in rate of production after the first 10000 seconds. This decrease in formation is actually a result of the reversible nature of the Diels-Alder reaction for the production of *endo*-**105**. The decrease in concentration of starting materials maleimide **86** and furan **70** as the reaction proceeds pushes the equilibrium in favor of the reactants. Resulting in a retro Diels-Alder reaction of *endo*-**105**, back to the initial building block molecules. In order to extract rate data, rate constants k_1 , k_2 and k_3 , from the concentration vs. time graph a kinetic model was computationally fitted to these curves (**Scheme 2.11**) using the SimFit program. This program transforms the reaction model into a series of rate equations which it then integrates to determine the concentration of a reactant or product species at a specific time. It can vary one or a more parameters to obtained value/s for an unknown constant through fitting a theoretical product concentration curve to an experimentally obtained curve, with an R error value. The model in **Scheme 2.11** describes the bimolecular reaction between maleimide **86** (M) and furan **70** (B) to form (*exo* and *endo*) products **105**. The percentage of the mean absolute difference between the experimental and theoretical concentrations with respect to the mean of experimental concentration, R, was 1.3 %. This value is an indication of how well the experimental data is described by the theoretical model, 0-3 % is a good fit, 3-5 % is an average fit and above 10 % no fit.



Rate Constant / $\times 10^{-4} \text{ M}^{-1}\text{s}^{-1}$ $k_1 = 3.33 \pm 0.01$

$k_2 = 2.45 \pm 0.03$

$k_3 = 0.24 \pm 0.07$

Scheme 2.11 Kinetic model computationally fitted to the experimental data in **Figure 2.15**(a) for the bimolecular 1,3-dipolar cycloaddition reaction between maleimide **86** (M) and furan **70** (B) and the optimized rate constants k_1 and k_2 .

Only the *endo*- product is shown to be reversible in **Scheme 2.15**. When the model was modified to allow for the *exo* reaction to be reversible a poorer fit is observed, with an R

value equal to 2.3 %. In addition the rate of the reverse reaction was very slow, $k = 5.00 \times 10^{-8} \text{ M}^{-1} \text{ s}^{-1}$. As a consequence of these two factors the formation of *exo*-**105** is considered to be irreversible.

The calculated rate constant determined in **Scheme 2.11** will prove useful in the analysis of the templated experiment. **Figure 2.15** (b) demonstrates the results of the templated reaction between two equivalents (50 mM) of bis(amidopyridine) **104**, furan **70** and maleimide **86**. Comparisons to the bimolecular experiment instantaneously reveal the presence of a template effect. Overall conversion has increased from 37 % to 71 % by doping the reaction between furan **70** and maleimide **86** with two equivalents of complementary template. However, the selectivity of the reaction is relatively unchanged going from an *exo* to *endo* ratio of 2.7:1 in the bimolecular control to 2.3:1 in the templated experiment. Individual analysis of the *exo* and *endo* curves in **Figure 2.15** (a) and (b) indicates there has been an increase in production of both diastereoisomers on going from the bimolecular to the templated experiment. This increase demonstrates that the formation of both diastereoisomers of dicarboxylic acid template **105** are cross-catalyzed by bis(amidopyridine) **104**. Analysis of the beginning of the templated experiment reveals almost identical rates of formation for both diastereomeric products, with the production of *endo*-**105** decreasing after 10000 seconds. The reason for this decline is the same as in the bimolecular experiment. If the reaction was to continue beyond 14 hours the ratio between *exo* and *endo* would increase, with more *exo* formed and *endo*- product converted to starting materials.

In order to investigate the efficiency of the ternary complex reaction, a kinetic model was used to extract values for the rate and association constants of the *pseudo*-unimolecular reaction. Experimentally obtained data for the ternary complex reaction using model compounds would be difficult, as a compound would have to be designed which precisely mimicked the *pseudo*-intramolecular reaction occurring in the ternary complex, in order to determine an accurate value for the rate constant. In addition ^1H NMR spectroscopy titration studies to determine the association constant [**104**•**105**] were unsuccessful. Therefore, the only way to determine values for these two parameters was through the use of the SimFit program to computationally fit a theoretical model to our experimental data. Details of this procedure are discussed in the general experimental Section **7.8**. The model used is illustrated in **Scheme 2.12** and will be the general model used in the investigation of future reciprocal replicators. This kinetic model made a

number of assumptions about the possible reactions and interactions which could occur. The first assumptions were as a consequence of the identical recognition motifs on the template molecule. In the work conducted by Kelly examined in Chapter One Section 1.11, identical recognition resulted in the formation of more than one ternary complex, some were productive others were unproductive. In the system examined in this Chapter the result of this was the possible formation of four ternary complexes illustrated in Figure 2.16.

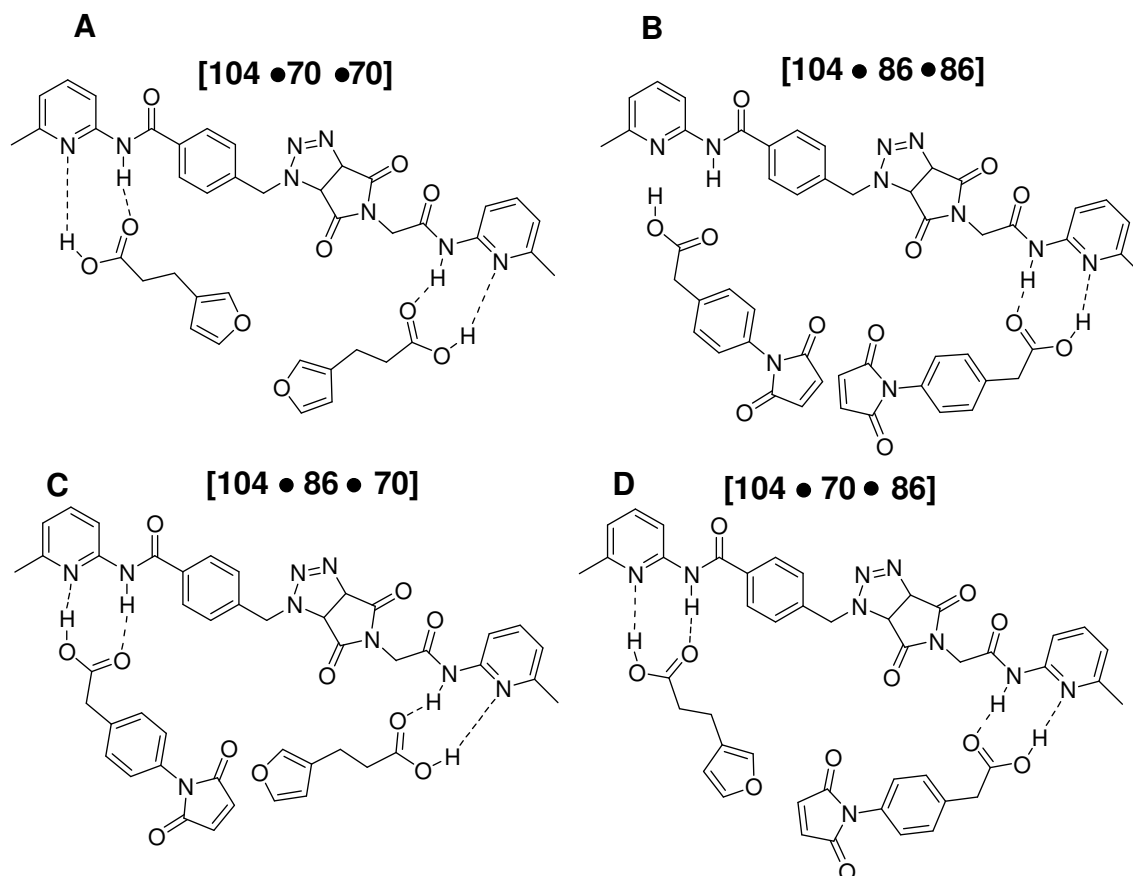


Figure 2.16 A possible four ternary complexes can be formed, **A**, **B**, **C** and **D**. **A** and **B** are unproductive whereas **C** and **D** are productive.

Ternary complexes **A** and **B** are unproductive with identical building block molecules **70** or **86** attached at both end of the bis(amidopyridine) template **104**, whereas complexes **C** and **D** are productive successfully resulting in the formation of **105**. An interesting feature of having identical recognition sites on both sides of template **104** is that building block molecules **86** and **70** can arrange themselves in two possible ways. This feature also applies to binary complexes between template **104** and **70** or **86**, with **70** or **86** associating with **104** in two possible ways. All these possible interactions are considered

in the kinetic model (**Scheme 2.12**) doubling the number of interactions possible. Although a large number of binding interactions can occur each individual association between an amidopyridine derivative and a carboxylic acid group is considered to have an association constant $K_1 = 120 \text{ M}^{-1}$, as calculated from the van't Hoff plot previously in **Figure 2.3**.

The reciprocal kinetic model is complex involving a number of different reactions and interactions. In order to clarify the model's appearance building block molecules, templates, complexes and product names have been simplified; M = maleimide **86**, B = furan **70**, T = bis(amidopyridine) template **104**, *exo* = dicarboxylic acid template *exo-105* and *endo* = dicarboxylic acid template *endo-105*. Examination of the kinetic model demonstrates there are three different ways of producing dicarboxylic acid **105** (*exo* and *endo*). The first is a simple pair of bimolecular reactions (utilizing rate constants k_1 , k_2 and k_3 calculated previously), where **86** and **70** react to form *exo*- and *endo-105*. These reactions use the rate constants k_1 , k_2 and k_3 that were calculated in **Scheme 2.11**. The second is the *pseudo*-unimolecular ternary complex reaction, as described previously this occurs through two ternary complex structures. The rate constant k_4 is unknown for these reactions and is one of the parameters optimized by the kinetic program SimFit. The final way of forming *exo*- and *endo-105* is through bimolecular reactions of complexes. This pathway involves for example **70** associating with template **104** to form a binary complex which then reacts with **86** to form **105**. This reaction does not involve a ternary complex and therefore is not *pseudo*-unimolecular, it is just a bimolecular reaction with one building block molecule associated to the template. As this reaction type is bimolecular it is assumed to have the same rate constants (k_1 , k_2 and k_3) for the normal bimolecular reactions mentioned above.

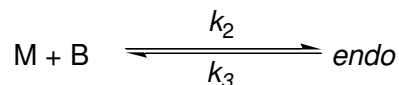
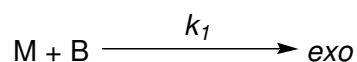
The one remaining part of the kinetic model in **Scheme 2.12** left to explain is the duplex association section. As a consequence of solubility issues it was not possible to directly measure the association constant K_2 and K_3 between bis(amidopyridine) template **104** and dicarboxylic acid templates *exo* or *endo-105*. Therefore this parameter, along with k_4 , would have to be optimized in this kinetic model through the SimFit program, although a very inaccurate estimation can be obtained through squaring K_1 .

Through placing parameters for the bimolecular reactions (k_1 , k_2 and k_3), calculated previously, and the association between amidopyridine and carboxylic acid recognition groups into the kinetic model ($K_1 = 120 \text{ M}^{-1}$), optimized values for ternary complex rate

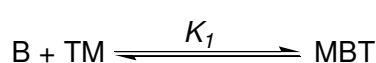
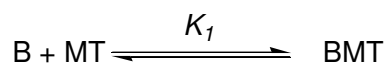
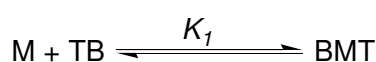
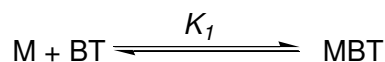
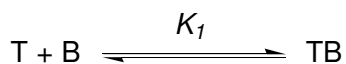
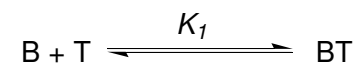
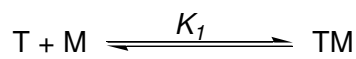
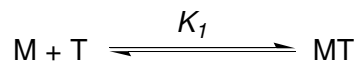
constants (k_4 and k_5) and duplex stability (K_2 and K_3) could be determined. The Simfit input file used for this reciprocal kinetic model can be examined in Appendix Seven. Values for the rate constants in the ternary complex are examined in the **Table 2.1** and compared to the bimolecular rate constants. The theoretical model fits the experimental data in **Figure 2.15** (b) with an R value = 1.6 %. The optimized values in **Table 2.1** contain calculated errors from fitting this specific data set (Experimental determined product concentration vs. time curve in **Figure 2.15** (b)). However, when this kinetic model is used to fit other data sets (reactions conducted at different equivalents of template **104**), the optimized parameters are found to be within $\approx \pm 10$ % between each data set.

The kinetic effective molarities (kEM) of the ternary complex reactions were measured as a way of determining the efficiency of the cross-catalytic process. In order to measure the kEM the rate constant for the catalyzed ternary complex, $k_{catalyzed}$, reaction is divided by the value for the bimolecular reaction, $k_{bimolecular}$. When the kEM for the cross-catalyzed formation of *exo-105* is compared to that of *endo-105* similar values are observed (**Table 2.1**), indicating both diastereoisomers are equally enhanced by template bis(amidopyridine) **104**. Analysis of the kEM for the retro Diels-Alder reaction in *endo-105* also indicates an increase in rate caused by the ternary complex. The thermodynamic effective molarity, (tEM = $(k_3 \times k_5) / (k_2 \times k_6)$), was also calculated for the cross-catalytic formation of *endo-105*, 0.85 M. This value is higher than the kEM, 0.71 M, indicating ground state stabilization of *endo-105* through the product duplex. The diastereoisomer *exo-105*, however, is under kinetic control and the increase in rate is as a consequence of transition state stabilization in the ternary complex structure.

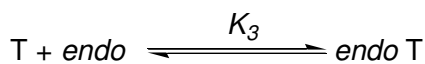
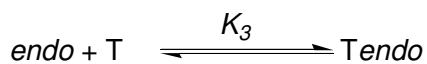
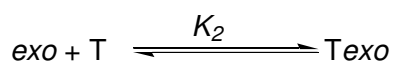
BIMOLECULAR REACTIONS



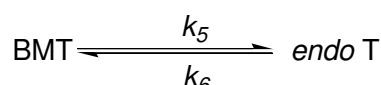
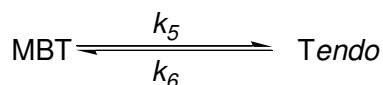
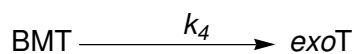
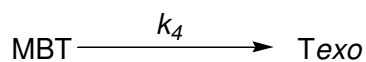
ROUTES FOR THE FORMATION OF BINARY AND TERNARY COMPLEXES



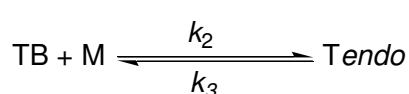
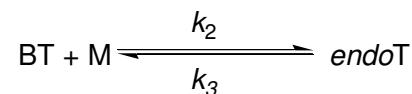
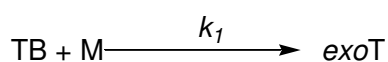
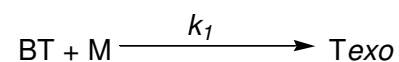
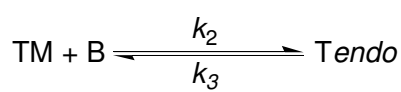
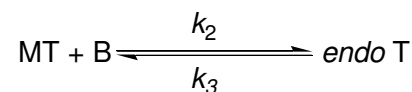
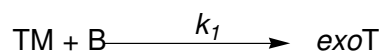
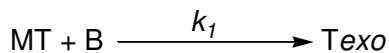
DUPLEX ASSOCIATION



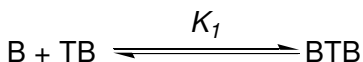
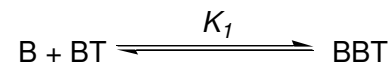
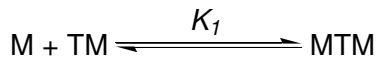
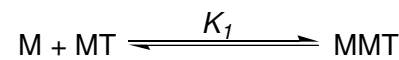
TERNARY COMPLEX REACTION



BIMOLECULAR REACTIONS OF COMPLEXES



UNPRODUCTIVE COMPLEXES



Scheme 2.12 Kinetic model used to computationally fit theoretical curves to the experimental observed results for the templated experiment in **Figure 2.15** (b), in order to extract data about the catalyzed ternary complex reactions. **M** = maleimide **86**, **B** = furan **70** **T** = bis(amidopyridine) template **104**, *exo* = dicarboxylic acid template *exo*-**105** and *endo* = dicarboxylic acid template *endo*-**105**.

Table 2.1 Table of calculated rate constants from the optimal fit curves of theoretical to experimental product concentrations vs. time curves and the kinetic effective molarities of the ternary complex reactions.

Bimolecular Reactions^a Rate Constant / $\times 10^{-4} \text{ M}^{-1} \text{ s}^{-1}$	Recognition Mediated^a Rate Constant / $\times 10^{-4} \text{ s}^{-1}$	kEM^b
$k_1 = 3.33 \pm 0.01$	$k_4 = 2.13 \pm 0.04$	$0.64 \pm 0.06 \text{ M}$
$k_2 = 2.45 \pm 0.03$	$k_5 = 1.74 \pm 0.03$	$0.71 \pm 0.07 \text{ M}$
$k_3 = 0.24 \pm 0.07$	$k_6 = 0.20 \pm 0.01$	$0.83 \pm 0.08 \text{ M}$

^a Rate constant relate directly to **Scheme 2.12**. ^b kEM is calculated by dividing the recognition mediated rate constant by the bimolecular rate constant, $kEM = k_4/k_1$ or k_5/k_2 or k_6/k_3 .

A reasonable estimation for the association constant for [104•105] product duplex can be determined by multiplying the values for individual binding between carboxylic acid and amidopyridine moieties. This value was calculated as $120 \times 120 = 1.44 \times 10^4 \text{ M}^{-1}$. The optimized values for the product duplex were $1.5 \times 10^3 \text{ M}^{-1}$ for the *exo*-105 and $2.4 \times 10^3 \text{ M}^{-1}$ for the *endo*-105. A value higher than the estimated $1.44 \times 10^4 \text{ M}^{-1}$ suggests positive cooperativity, whereas, a value below is indicative of negative cooperativity. A more empirical measurement of cooperativity can be obtained by calculating the Gibbs free energy of connection, using the equation in **Figure 2.17**.

$$\Delta G^s = \Delta G_B^0 + \Delta G_A^0 - \Delta G_{AB}^0$$

Substitute $\Delta G^0 = -RT \ln K$ into above equations results in the equation below;

$$\Delta G^s = RT \ln \left(\frac{K_{AB}}{K_A K_B} \right)$$

Figure 2.17 Equation of Gibbs free energy of connection, ΔG^s . Where ΔG_A^0 is Gibbs free energy of binding molecule A to the host, ΔG_B^0 is Gibbs free energy of binding molecule B to the host and ΔG_{AB}^0 is Gibbs free energy of binding molecule A joined to B to the host. K_{AB} is the binding constant for A joined to B with the host and K_A and K_B is the association constant for the individual binding of molecules A and B to the host.

Modifying the second equation in **Figure 2.17** for this system; K_{AB} is equal to K_2 or K_3 and K_A and K_B are equivalent to K_1 in **Scheme 2.12**. These changes result in the equations illustrated in **Figure 2.18**, for the Gibbs free energy of connection for the *exo*- and the *endo*- products.

$$\text{Exo } \Delta G^{\text{s}} = RT \ln \frac{K_2}{K_1 K_1} \qquad \text{Endo } \Delta G^{\text{s}} = RT \ln \frac{K_3}{K_1 K_1}$$

Figure 2.18 Equation of Gibbs free energy of connection.

The Gibbs free energy of connection was discussed in Chapter One Section **1.4**, it utilizes the gas constant R, temperature T, the individual binding association, K_1 (120 M^{-1}), and the calculated product duplex association constant, K_2 or K_3 (1.5 and $2.4 \times 10^3 \text{ M}^{-1}$). A positive Gibbs free energy of connection suggests positive cooperativity and a negative value indicates negative cooperativity. A value of -6.1 kJ mol^{-1} was calculated for the *exo*- product duplex whereas a value of -4.8 kJ mol^{-1} was determined for the *endo*- product duplex. The calculated values for ΔG^{s} implies that template *endo-105*, rather than *exo-105*, is a better fit for the bis(amidopyridine) **104** template.

Bis(amidopyridine) **104** was very soluble over a wide range of concentrations (in excess of 100 mM). This fact allowed the templated experiment to be conducted a number of times, each occasion with a different initial concentration of prefabricated cycloadduct **104**. The graphs in **Figure 2.19** (a) and (b) demonstrate the product concentrations of *exo*- and *endo-105* at different concentrations of bis(amidopyridine) **104** after 13 hours. Analysis of **Figure 2.19** reveals two similar graphs with each point on the *exo* graph approximately double the concentration of the equivalent data point on the *endo* graph. This fact indicates that with increasing concentration of template bis(amidopyridine), the cross-catalytic formation of *exo*- and *endo-105* is accelerated by the same extent. The maximum concentration of product in both cases occurs between the range of one and three equivalents of template **104**, indicating somewhere in this range exists the optimal concentration of added template.

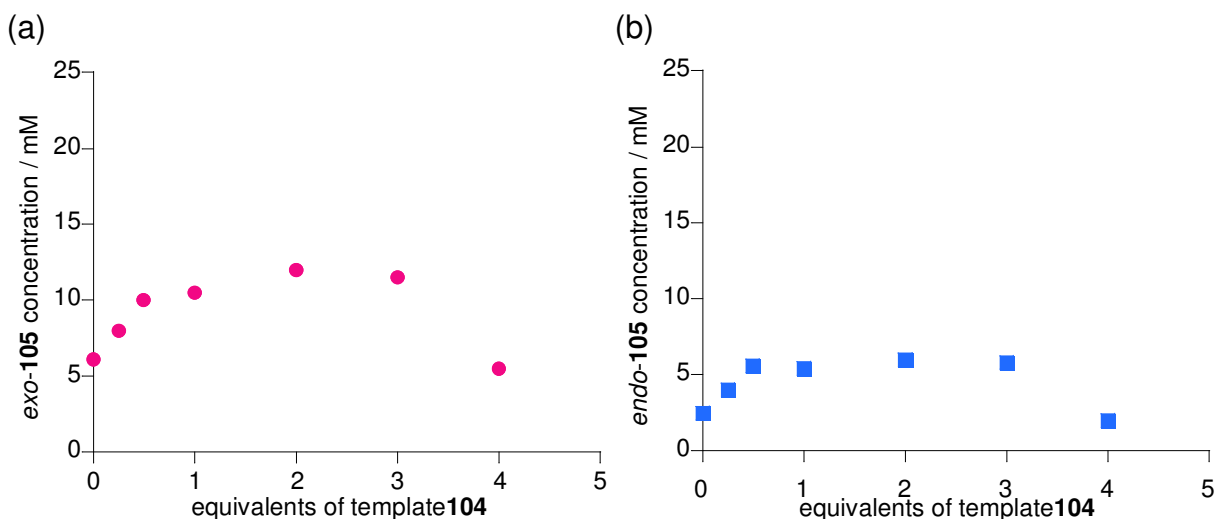


Figure 2.19 Concentration of *exo*-105 (a) and *endo*-105 (b) for the reaction between **86** and **70** after 13 hours under a range of different initial concentrations of bis(amidopyridine) **104**. Error in concentration values is $\pm 4\%$.

The advantage of repeating the experiment over a range of template equivalents is that it allows us to calculate rate acceleration at a specific concentration of added **104**. In order to measure rate acceleration, the initial rate (ideally in the first 10 % conversion of the reaction) must first be measured. The initial rate can be determined through measuring the initial gradient of the product concentration vs. time curve (**Figure 2.15** (a) and (b)); when the reaction is less than 10 % complete. Measuring the rate so early in the reaction gives a more accurate estimation of the rate, before the reduction in starting material concentration causes the initially straight line to become a curve. As the product curve at the beginning of the reaction can be approximated by a straight line, the initial rate can be calculated (**Figure 2.20**) using the gradient of this line.

$$\text{approximately 10 \% conversion} = \frac{d[105]}{dt} \approx \frac{\Delta[105]}{\Delta t} = \text{Gradient of line}$$

Figure 2.20 Equation for measuring initial rate of reaction, as a consequence of initial rate being approximately equal to the gradient of the line.

Table 2.2 shows the calculated initial rates for the formation of *exo*-105 over a range of equivalents of bis(amidopyridine) **104**.

Table 2.2 Table of experimentally measured initial rates for the formation of *exo-105* at various concentration of added template **104**. The table also displays calculated rate acceleration values for each of the templated reactions

Equivalents of template-104	0	0.25	0.5	1.0	2.0	3.0	4.0
Initial rate/ $\times 10^{-4} \text{ mM s}^{-1}$	1.4	2.8	4.8	5.2	5.7	5.3	3.1
Error $\approx \pm 5 \times 10^{-6} \text{ mM s}^{-1}$							
Rate acceleration^a	1.0	2.0	3.4	3.7	4.1	3.8	2.2

^a Rate acceleration is calculated by the dividing initial rate of the templated experiment over that of the bimolecular, 0 equivalents of added **104**. Plotted in graph in **Figure 2.22** (a).

Table 2.3 displays the calculated initial rates for the formation of *endo-105* over a range of equivalents of bis(amidopyridine) **104**.

Table 2.3 Table of experimentally measured initial rates for the formation of *endo-105* at various concentration of added template **104**. The table also displays calculated rate acceleration values for each of the templated reactions

Equivalents of template-104	0	0.25	0.5	1.0	2.0	3.0	4.0
Initial rate/ $\times 10^{-4} \text{ mM s}^{-1}$	1.3	1.9	3.6	4.1	4.6	4.0	2.5
Error $\approx \pm 5 \times 10^{-6} \text{ mM s}^{-1}$							
Rate acceleration^a	1	1.5	2.8	3.2	3.6	3.1	1.9

^a Rate acceleration is calculated by the dividing initial rate of the templated experiment over that of the bimolecular, 0 equivalents of added **104**. Plotted in graph in **Figure 2.22** (b).

Table 2.2 and **2.3** also display calculated rate accelerations for the formation of *exo-* and *endo-105*, which are obtained through measuring the initial rate of all the templated reactions and individually dividing them by the initial rate of the bimolecular reaction. These rate accelerations can then be plotted against equivalents of bis(amidopyridine) **104** (**Figure 2.22**).

The solid lines in graphs (a) and (b) in **Figure 2.22** correspond to an independent binding site model. This model was discussed in detail in Chapter One Section **1.19**, it assumes that rate acceleration observed for the production of *exo-* and *endo-105* is directly proportional to the concentration of active ternary complex, **[86•70•105]**. The two equations in **Figure 2.21** and a scaling factor are used to calculate the association constant for the ternary complex, and a best fit curve for the theoretical rate accelerations to experimental determined values. The more optimal the fit the more accurate the value of ternary complex stability constant.

$$\text{Solving for } [R]: [R]^2 + \left(2[T]_{tot} - [R]_{tot} + \frac{1}{K} \right) [R] - \frac{[R]_{tot}}{K} = 0$$

$$ax^2 + bx + c = 0$$

$$[TR_2] = [T]_{tot} \left(\frac{K[R]}{1 + K[R]} \right)^2$$

Figure 2.21 Equations for solving the concentration of free reagent $[R]$ and ternary complex $[TR_2]$.

Figure 2.22 illustrates the rate accelerations observed for the *exo*- (a) and *endo*- (b) product at various concentrations of prefabricated template.

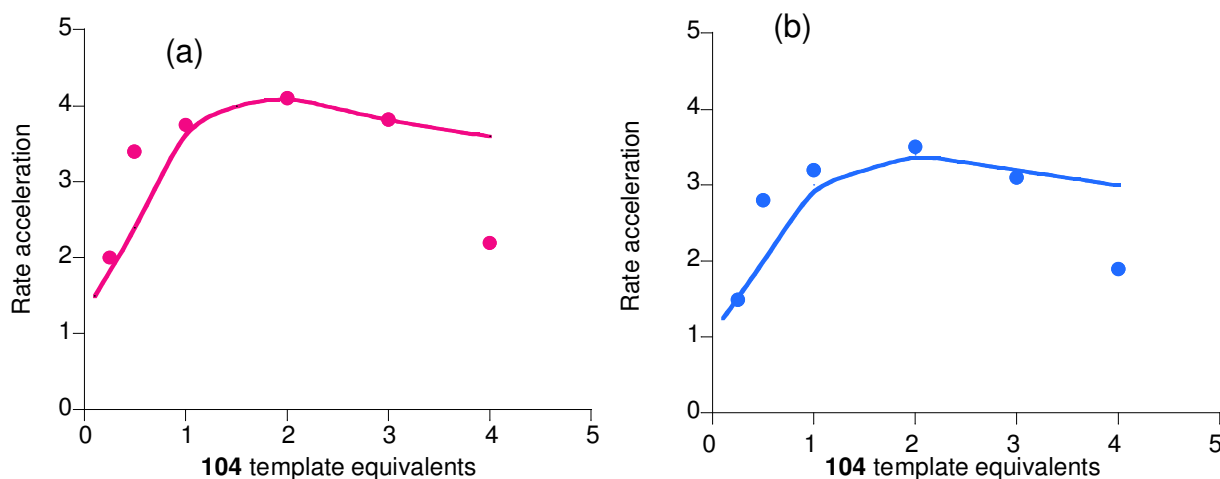


Figure 2.22 Rate acceleration vs. equivalents of bis(amidopyridine) **104** added to the reaction between maleimide **86** and furan **70**; (a) Cross-catalyzed formation of *exo*-**105**, (b) Cross-catalyzed formation of *endo*-**105**. Measured rate acceleration are shown as circles and squares, the solid line represents a fitted curve optimized for the product duplex association constant.

The two graphs are very similar with identical shapes, although the rate accelerations observed for the *endo*-product are slightly lower. Both graphs indicate that the maximum rate acceleration occurs at around two equivalents of template, after which a decline in rate is observed. At below two equivalents of bis(amidopyridine) **104** the greatest possible concentration of ternary complex is not achieved, therefore, starting materials, maleimide **86** and furan **70**, are present unassociated in the free solution. When greater than two equivalents of template are added the starting materials become isolated on different molecules of template, therefore, they have to dissociate and then associate on

the same template molecule before they can react. The result of this process is a decrease in rate acceleration demonstrated in the graphs in **Figure 2.22** (a) and (b).

Through varying the value of K in the quadratic equation in **Figure 2.21**, then calculating the concentration of catalytic ternary complex, a set of theoretical rate accelerations are determined through the use of a scaling factor, which optimally fits the experimental data. The association constant value K which gives the best fit, represents the individual associations in the ternary complex. Therefore, by multiplying the individual binding associations a value for the duplex [105•104] stability constant, $(K)^2$, can be determined. Using the independent binding site model to fit a theoretical line to the *exo* and *endo* rate acceleration vs. template equivalents curves a $(K)^2$ value of approximately 500 M^{-1} was obtained for both graphs. The model does not provide a good fit to the experimentally determined rate constants. The value for the stability constant of the ternary complex structures is also substantial different from the calculated product duplex association constants for the [*endo*-105•104] and [*exo*-105•104].

In order to investigate the discrepancies between the experimentally determined rate accelerations, in **Figure 2.22**, and the theoretical fit from the independent binding model the isosim program in SimFit was utilized. This program was used to simulate product concentration vs. time curves for this system under various concentrations of bis(amidopyridine) **104**, using the kinetic model in **Scheme 2.12** and the rate and equilibrium constants determined previously, $k_1 - k_6$ and $K_1 - K_3$. The result of these simulations is examined in the graphs in **Figure 2.23**.

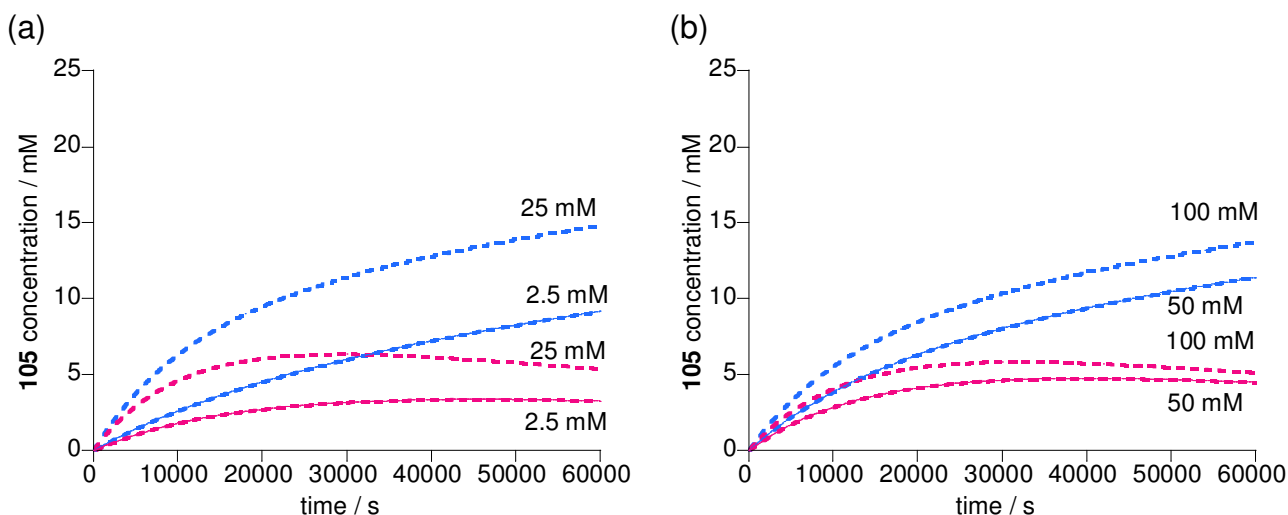


Figure 2.23 (a) Simulation for 2.5 and 25 mM for reaction between maleimide **86** and Furan **70** with various equivalents of added template, *exo-105* (blue dashed line), *endo-105* (pink dashed line). (b) Simulation for 50 and 100 mM for reaction between maleimide **86** and Furan **70** with various equivalents of added template, *exo-105*(blue dashed line), *endo-105* (pink dashed line).

The initial rates for a range of different template equivalent were extracted from these simulation and rate accelerations calculated. **Table 2.4** examines the calculated initial rates and rate accelerations for the formation of *exo-105* under a range of template equivalents.

Table 2.4 Table of simulated initial rates for the formation of *exo-105* at various concentrations of added template **104**. The table also displays calculated simulated rate acceleration values for each of the templated reactions

Equivalents of template-104	0	0.1	0.5	1.0	1.5	2.0	3.0	4.0
Initial rate/ $\times 10^{-4} \text{ mM s}^{-1}$	2.1	3.1	6.9	9.3	9.3	8.0	6.5	5.1
Error $\approx \pm 1 \times 10^{-5} \text{ mM s}^{-1}$								
Rate acceleration^a	1	1.5	3.3	4.4	4.4	3.8	3.1	2.4

^a Simulated rate acceleration is calculated by dividing initial rate of the templated experiment over that of the bimolecular, 0 equivalents of added **104**. Plotted in graph in **Figure 2.24** (a).

Table 2.5 examines the calculated initial rates and rate accelerations for the formation of *endo-105* under a range of template equivalents.

Table 2.5 Table of simulated initial rates for the formation of *endo*-105 at various concentrations of added template 104. The table also displays calculated simulated rate acceleration values for each of the templated reactions.

Equivalents of template-104	0	0.1	0.5	1.0	1.5	2.0	3.0	4.0
Initial rate/ $\times 10^{-4} \text{ mM s}^{-1}$	1.5	2.4	6.6	7.6	7.6	6.6	5.1	4.2
Error $\approx \pm 1 \times 10^{-5} \text{ mM s}^{-1}$								
Rate acceleration^a	1	1.5	3.3	4.4	4.4	3.8	3.1	2.4

^a Simulated rate acceleration is calculated by dividing initial rate of the templated experiment over that of the bimolecular, 0 equivalents of added 104. Plotted in graph in **Figure 2.24** (b)

Rate accelerations from **Table 2.4** and **2.5** were plotted in two different graphs against template equivalents (**Figure 2.24**).

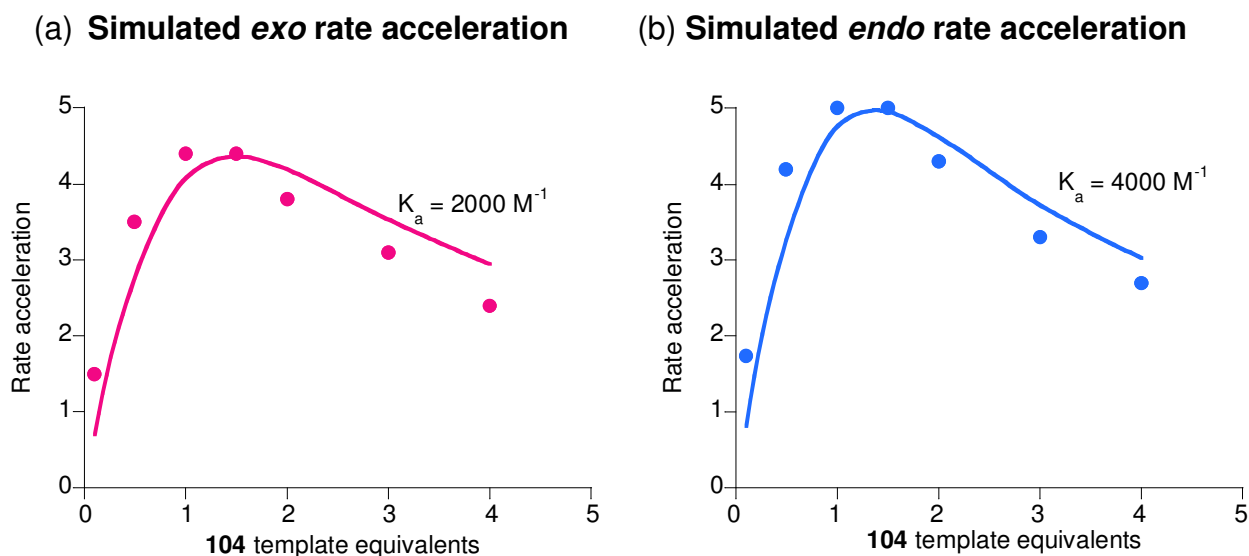


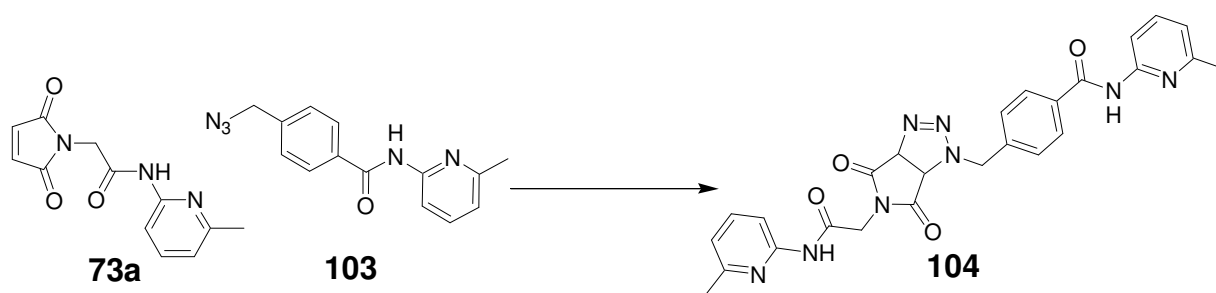
Figure 2.24 Graphs of simulated rate accelerations vs. template equivalents. (a) Simulated rate accelerations (purple circles) for formation of *exo*- (a) and *endo*-products (b) fitted to the independent binding model (solid line).

The first graph demonstrates the simulated rate accelerations for the formation of *exo*-105 (pink circles) fitted to the independent binding model (solid line) and second graph does the same for the *endo*-105 product. If you compare these graphs to the experimental obtained plots in **Figure 2.22**, discrepancies in shape and rate acceleration can be observed. The simulated rate accelerations suggest a maximum between 1 and 1.5 equivalents instead of around 2 equivalents (as in **Figure 2.22**). The fit of the independent binding model to the simulated rate accelerations provides values for the ternary complex stability which are significantly closer to the duplex association constants determined from the kinetic model. Kinetic model values of 1.5×10^3 and

$2.4 \times 10^3 \text{ M}^{-1}$ were determined which are similar in magnitude to the values, 2×10^3 and $4 \times 10^3 \text{ M}^{-1}$ determined from independent binding model in **Figure 2.24**. The improved fit of the simulated rate accelerations to the independent binding model, compared to the experimental obtained rate accelerations, indicates that one or more of the experimental measured initial rates are inaccurate. However, inaccuracies in experimental initial rates can be resolved by fitting the overall product concentration vs. time curve for templated experiments to a kinetic model and extracting the initial rates from the resultant simulations. This section has demonstrated one of the problems with the independent binding site model is that an accurate fit is dependent on precisely measured initial rates. When low rate accelerations are observed these errors are small and their effects marginal. However, as rate accelerations become larger it becomes more difficult to measure initial rates accurately, with small errors in measurement resulting in larger differences in rate accelerations. Therefore, the fitting of a kinetic model and kinetic simulations, as utilized in this section, can result in a more accurate measurement of initial rates, which in turn corresponds to an improved fit to the independent binding model. The experimentally measured initial rates and rate accelerations conducted in this Section were only performed once, ideally these experiments should be repeated several times in order to build up a more precise set of values which could then be compared to the simulated values. This would allow for an improved comparison between the simulated and experimentally obtained values.

2.16 Cross-catalytic formation of bis(amidopyridine) **104**.

The cross-catalytic template bis(amidopyridine) **104** is formed from the 1,3-dipolar cycloaddition reaction (**Scheme 2.16**) between maleimide **73a** and azide **103**, where the formation of **104** has the potential to be templated by dicarboxylic acid **105**.



Scheme 2.16 1,3-dipolar cycloaddition reaction between maleimide **73a** and azide **103** to form bis(amidopyridine) **104**.

In order to provide a reference point to which the cross-catalytic formation of bis(amidopyridine) **104** can be compared the first experiment investigated in this section was the bimolecular reaction between maleimide **73a** and azide **103**. The product concentration was deconvoluted from the individual spectra and plotted against time (Figure 2.25).

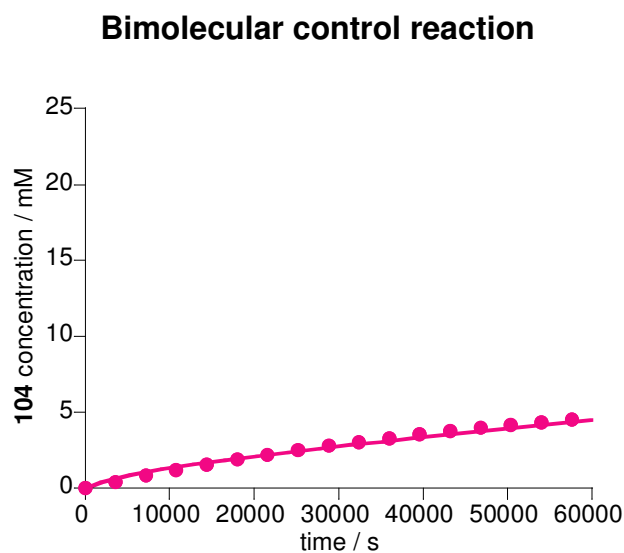


Figure 2.25 Product concentration vs. time graph for the bimolecular equimolar ($[73a] = [103] = 25$ mM) in $CDCl_3$ at 50 °C. The templated experiment could not be conducted as a consequence of the complete insolubility of dicarboxylic acid **105**. Error in concentration values is ± 4 %.

Analysis of the graph in **Figure 2.25** reveals the typical bimolecular profile, with low conversion (≈ 20 %), after 16 hours in $CDCl_3$. Unlike in the previous section only one product is formed, so there are no *exo*- or *endo*- isomers. Normally we would now go on to analyze the bimolecular experiment extracting rate constants, which we could compare to the templated experiment. However, this procedure is pointless as analysis of the cross-catalytic formation of bis(amidopyridine) **104** by dicarboxylic acid **105** proved impossible. The reason for this was the complete insolubility of dicarboxylic acid **105** in $CDCl_3$. Although the dicarboxylic acid template **105** was soluble when it was formed in Section 2.15, once out of solution all attempts to re-dissolve it proved unsuccessful. Therefore, the reaction between azide **103** and maleimide **73a** could not be cross-catalyzed. A more polar solvent could be used to dissolve the dicarboxylic acid template **105** but this weakened hydrogen bonding, destroying the template's ability to associate starting materials and hence preventing replication. The insolubility of the

dicarboxylic acid template may come as a surprise as the same molecule was used in the reciprocal replicator developed by Philp and co-workers examined in Section 1.19, using the same solvent. However, the dicarboxylic acid template was only soluble in CDCl_3 in the presence of the starting materials of the complementary template. This fact indicates that the dicarboxylic acid template is a poorer fit to the bis(amidopyridine) template discussed in this Chapter than to the one investigated in the Introduction. That is why cycloadduct **105** was insoluble in this system but not the other.

2.17 Conclusions

At the start of the Chapter our aim was to design two cross-catalytic templates utilizing the Diels-Alder and azide maleimide 1,3-dipolar cycloaddition reactions and amidopyridine/carboxylic acid recognition. The first system investigated was the cross-catalytic formation of dicarboxylic acid **105**, using complementary template **104**. From the transition state diagrams (**Figure 2.11**) and molecular modeling (**Figure 2.12**) it was expected that bis(amidopyridine) **104** would cross-catalyze the formation of the *endo*-product only. However, the experimental results revealed (**Figure 2.15**) that both *exo* and *endo* were cross-catalyzed to approximately the same extent.

Unfortunately, analysis of the complementary cross-catalytic formation of bis(amidopyridine) **104** by dicarboxylic acid template **105** proved impossible. This failure was a consequence of the insoluble nature of the dicarboxylic acid template.

Table 2.6 Overview of the results for replicating systems examined in this Chapter

System	Cross-catalyzed formation	Mechanism	Kinetic effective molarity
2.15	<i>exo</i> - 105	Reciprocal replicator	0.64 M
	<i>endo</i> - 105	Reciprocal replicator	0.68 M
2.16	104	unknown	Template insoluble

2.18 Future work

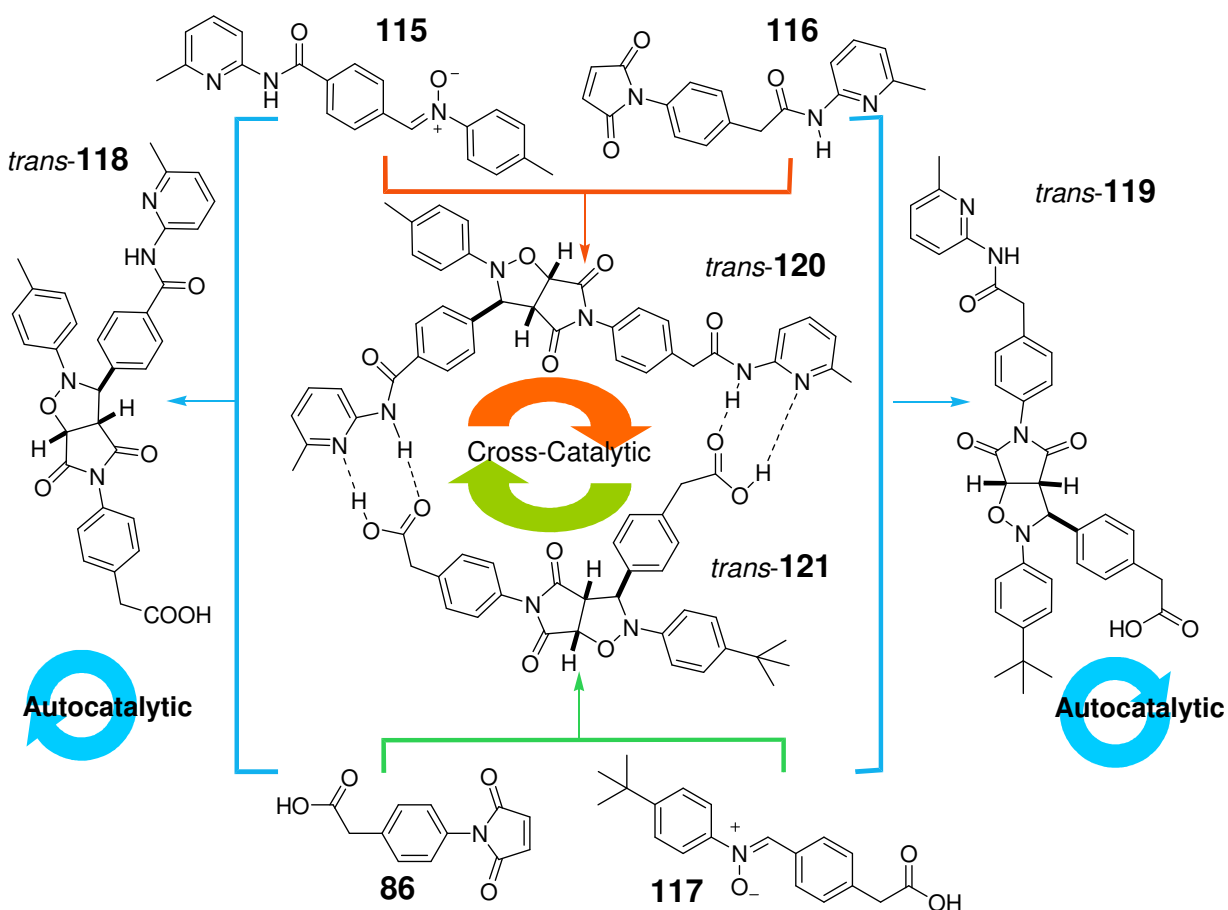
The investigation of the reciprocal replicating network in this Chapter revealed a series of problems in the design of our systems. Although this Chapter has demonstrated that

reciprocal replication is possible the results are not very impressive, with non-selective cross-catalysis and template solubility both a problem. The low efficiency of the replicating system could be a result of the high temperature employed. A high temperature had to be used because of the low reactivity of the Diels-Alder and azide dipolar cycloaddition reactions. A consequence of this high temperature was the low strength of binding in hydrogen bonding complexes, like the ternary complex. This weak association would decrease the efficiency of the cross-catalytic reaction. An additional problem with this reciprocal system is that we are comparing the cross-catalysis of two different types of reaction, a Diels-Alder and a cycloaddition. This comparison is inherently unfair as both occur at different rates.

Therefore, when designing the next reciprocal replicating network all these factors were taken into account. The 1,3-dipole nitron maleimide cycloaddition reaction was chosen to link our starting materials together to form the reciprocal templates. Using a singular reaction type means that a fairer comparison between the cross-catalysis of different templates is now possible. The reason for choosing this 1,3-dipolar cycloaddition reaction is its increased reactivity at lower temperature compared to the Diels-Alder and azide 1,3-dipolar cycloaddition. This lower temperature will increase the hydrogen bonding strength and hopefully the efficiency of the ternary complex reaction. The reason for the increased reactivity of the nitron-maleimide reaction is a consequence of the higher energy HOMO than their 1,3-dipole counterparts the azides. The result is that the energy gap between nitron HOMO and the maleimide LUMO is less and, therefore, the reaction will proceed faster compared to that of the azide maleimide reaction.

Chapter 3 Design and synthesis of a replicating network

3.1 Design of a replicating network

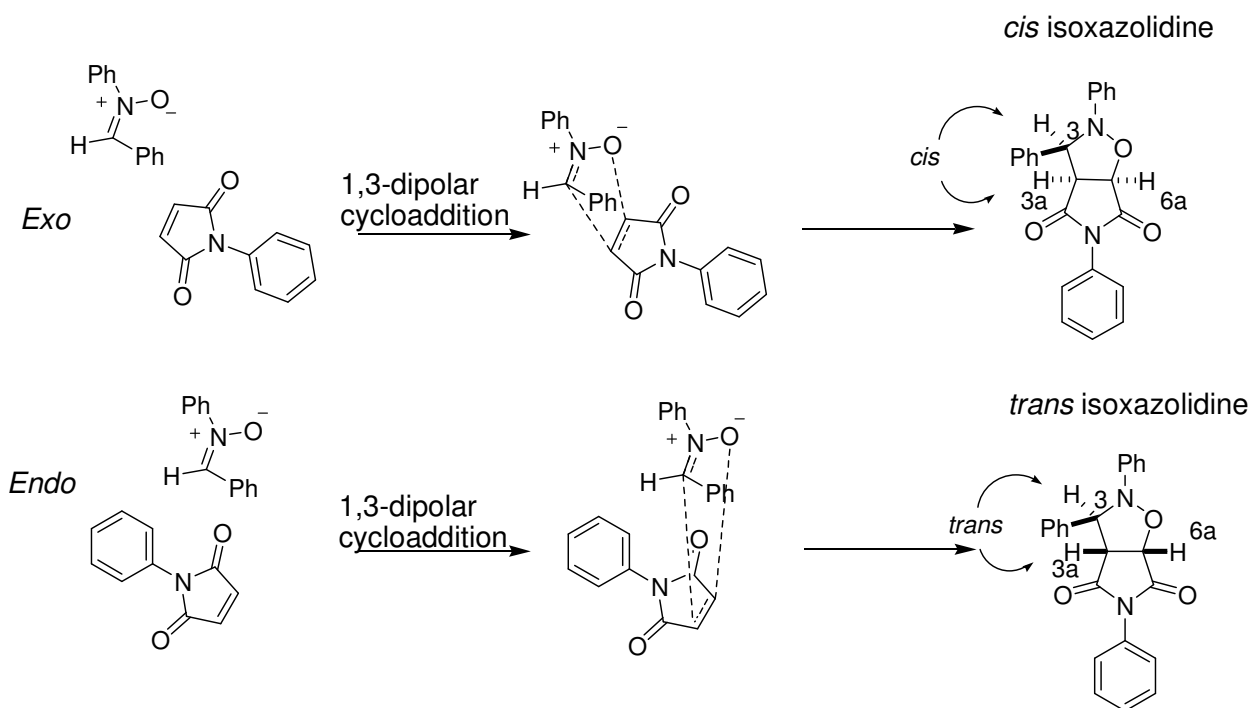


Scheme 3.1 Building block molecules maleimide **116**, **86** and nitron **115**, **117** can react to form potential minimal replicators *trans*-**118**, **-119** or cross-catalytic templates *trans*-**120**, **-121**.

The requirement for extensive redesign of the reciprocal replicating system was explained at the end of Chapter Two. These modifications have resulted in the design and synthesis of building block molecules maleimide **116**, nitrones **115** and **117**. The only unchanged feature of this newly designed system is maleimide **86**. The emphasis until now has only been on investigating reciprocal replication, but in this Chapter we will also study (**Scheme 3.1**) in detail two potential minimal replicators. **Scheme 3.1** demonstrates the two minimal templates *trans*-**118**, **-119** and the reciprocal replicator *trans*-**120**, **-121**, which can be formed from the four building block molecules. Each template is formed from the 1,3-dipolar cycloaddition reaction between a nitron and a maleimide. This feature allows for a fairer comparison between the different replicators,

overcoming one of the problems of the systems investigated in Chapter Two. The bis(amidopyridine) template *trans*-**120** is formed from the reaction between maleimide **116** and nitron **115**, its complementary partner dicarboxylic acid *trans*-**121** is formed from the reaction of maleimide **86** and nitron **117**. The potential minimal template *trans*-**118** is formed from the reaction of maleimide **86** and nitron **115**, whereas self-replicating template *trans*-**119** is formed from the reaction of maleimide **116** with nitron **117**.

In each case, the cycloaddition reaction of a maleimide with a nitron results in the formation of two diastereoisomeric products namely *cis* and *trans*. Usually, this reaction affords these two products in a 3:1 ratio in favor of the *trans*-diastereoisomer. This outcome can be rationalized in a manner similar to that discussed in Chapter Two in connection with the Diels-Alder reaction. In isoxazolidine formation, there are two possible modes of attack (**Scheme 3.2**) of the dipole on the maleimide, *exo* ('extended' transition state) and *endo* ('compressed' transition state).



Scheme 3.2 *Exo* and *endo* modes of attack, of a nitron on a maleimide to form *cis*- and *trans*-isoxazolidines. Positions on the isoxazolidine skeleton are represented by heterocyclic numbering system, only the relevant positions are numbered.

Exo attack of the nitron on the maleimide leads to the formation of the *cis*-product (protons in the 3 and 3a positions are on the same face of the fused bicyclic ring

system), whereas *endo* attack results in the formation of the *trans*-product (protons in the 3 and 3a positions are on opposite faces of the bicyclic system). Throughout this thesis the *cis* and *trans* nomenclature will be used to identify isoxazolidine products. In the early 1970's the substituent effect of the dipole and dipolarophile on the reaction of nitrones with *N*-(substituted phenyl) maleimides was investigated^[166] by Iwakura and co-workers. They investigated (**Figure 3.1**) several reactions in which the R¹, R² and R³ substituents were varied.

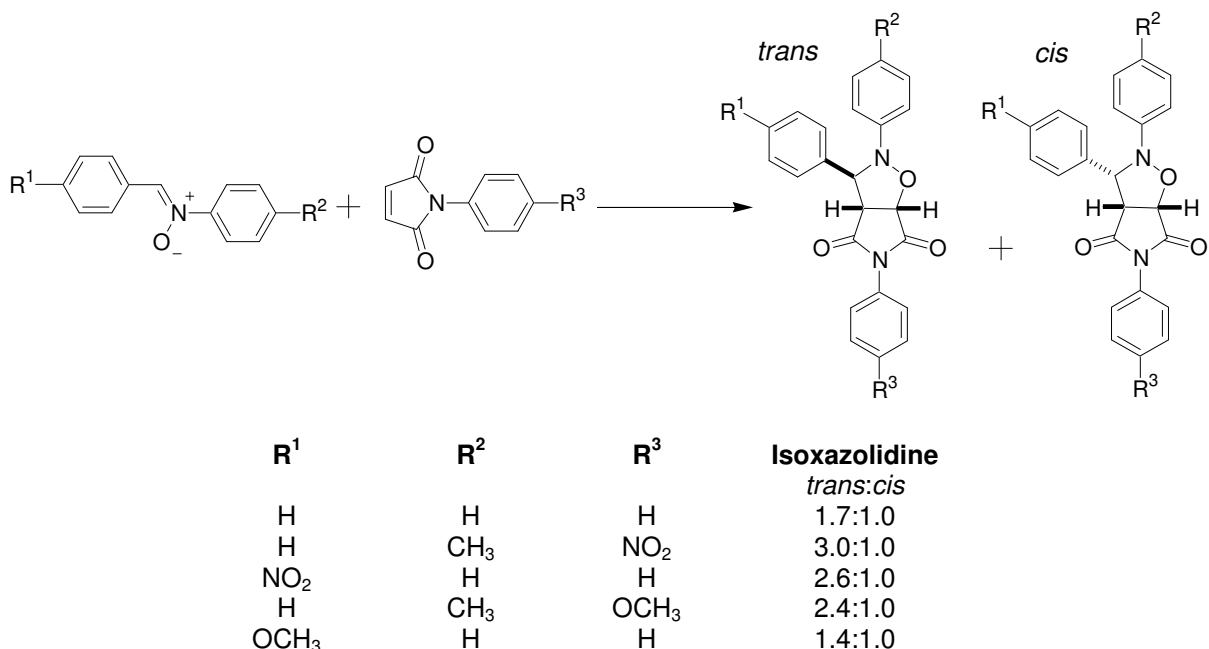


Figure 3.1 Table of substituent effect in the reaction of nitrones with *N*-(substituted phenyl) maleimides, for different substituents R¹, R² and R³.

A selected set of results from this investigation are displayed in the above **Figure 3.1**. From examination of these results it was concluded that dipole orientation of the dipole and dipolarophile, and π stacking between the *N*-phenyl group on nitron and *N*-phenylmaleimide influence the *cis* to *trans* ratios. The ratio of *trans*- to *cis*-products varied from a minimum of 1.4:1 to a maximum of 3.9:1 depending on the substituent present on R¹, R² and R³. However, in our experience the range of *trans* to *cis* ratios is somewhat narrower 2.7 to 3.6:1^[86-87, 128, 148]. Therefore, in our system, we should expect to see a similar ratio for the bimolecular reaction between the nitrones and maleimides investigated in this thesis.

Analysis of **Scheme 3.1** reveals only the *trans*- diastereoisomers are highlighted as the replicating templates, with the *cis* conspicuous in its absence. Why are only the *trans*-configurations shown as the replicating templates? The reason for this is explained by analyzing (**Figure 3.2**) the transition state diagrams for a 1,3-dipolar cycloaddition reaction between a recognition containing maleimide and nitrene.

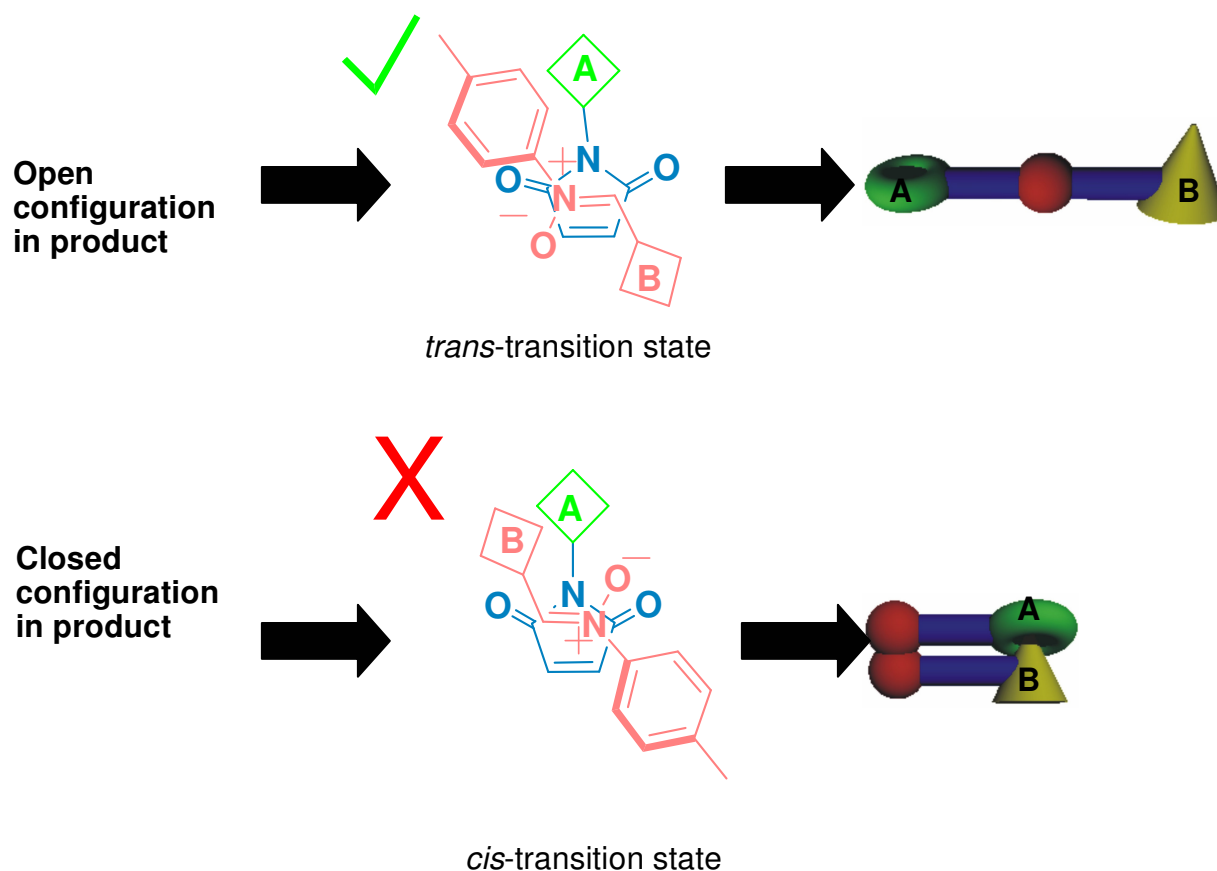


Figure 3.2 Transition state diagrams of 1, 3-dipolar cycloaddition reaction between a maleimide containing recognition site **A** and nitrene containing recognition site **B**. The *trans* transition state has recognition site **A** and **B** held wide apart in an open conformation resulting in the open template (green tick), demonstrated by the 3D cartoon with yellow and green recognition site. The *cis* transition state has **A** and **B** overlapping in a closed conformation resulting in a closed template (red cross), demonstrated in the cartoon with overlapping recognition sites green and yellow.

The diagrams in **Figure 3.2** show the transition states which result in the formation of the *trans*- and *cis*-isoxazolidine. In the *trans* transition state the recognition sites **A**, on the maleimide, and **B**, on the nitrene, are held far apart in an open conformation. This conformation is transferred to the configuration of the resultant *trans*-isoxazolidine product. Therefore, the *trans*-product will have an open configuration with its recognition sites **A** and **B** held wide apart, and available to associate with complementary

molecules, and hence, available to act as a template. The *cis* transition state however, has recognition sites **A** and **B** overlapping in a closed conformation, with recognition sites **A** and **B** unavailable to associate with complementary molecules. This conformation will result in a closed configuration in the *cis*-product and hence a closed template structure. Therefore, only the *trans*- products are suitable to act as templates in each of the replicating systems mention in **Scheme 3.1**.

In order to further demonstrate that the *trans*-configuration had the desired open template structure, the lowest energy structures of both *cis*- and *trans*- diastereoisomers were calculated using molecular mechanics. A series of Monte Carlo conformational searches were performed, starting from individually minimized conformations of the *trans*- and *cis*-templates on their own and associated with their complementary *trans*- and *cis*-isoxazolidine partners, utilizing the MMFFs forcefield and the GB/SA solvation model for CHCl₃. This procedure was conducted for all four replicating systems, the two minimal and two cross-catalytic templates, the results for the minimal replicator *trans*-**118** are examined in **Figure 3.3**. This figure shows the global minimum conformations for each of the *cis*-isomer, *trans*-isomer, [*trans*-**118**•*trans*-**118**] and the [*trans*-**118**•*cis*-**118**] product duplexes. The open structure of *trans*-**118** and the closed structure of *cis*-**118** can be observed in **Figure 3.3** (a) and (b). **Figure 3.3** (c) demonstrates that the association between two *trans*-**118** results in an excellent fit in the product duplex, [*trans*-**118**•*trans*-**118**] with four hydrogen bonds (dashed lines), although two are obscured in the diagram. The *cis*-**118** isoxazole has a closed structure and therefore, can not associate building block materials in order to self-replicate. However, can the *cis*-**118** product be formed through a [*trans*-**118**•**115**•**86**] ternary complex? The structure for the product duplex [*trans*-**118**•*cis*-**118**] only has two hydrogen bonds formed between the two molecules. Because the transition state for 1,3-dipolar cycloadditions is late then the ternary complex structure resembles the product duplex. Therefore, *trans*-**118** is not able to template the formation of *cis*-**118**.

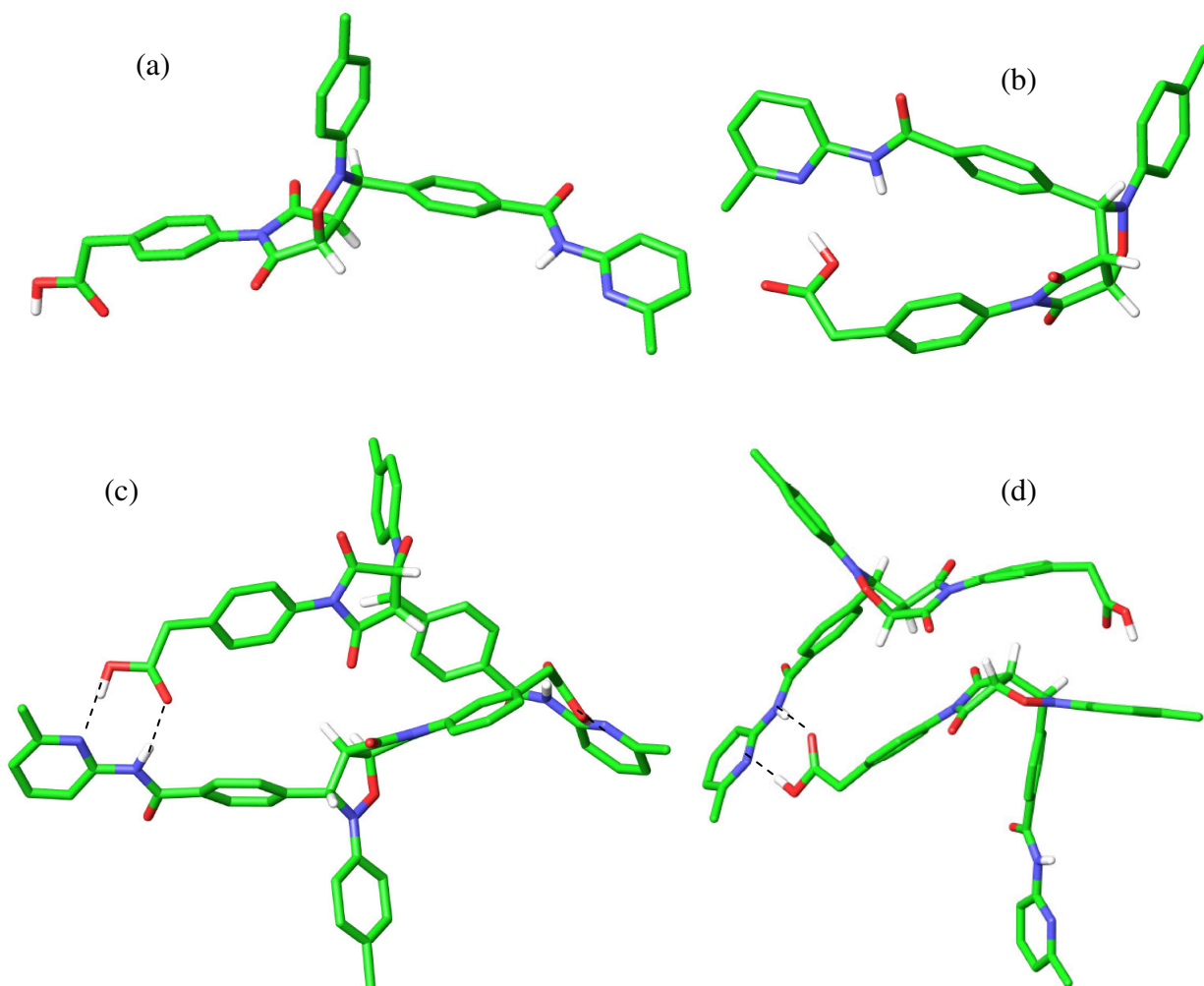


Figure 3.3 Molecular mechanics models for different structures and complexes of the minimal replicating system **118**. Green atoms are carbon, blue atoms are nitrogen, red atoms are oxygen and white atoms are hydrogen. Most hydrogen atoms have been removed for clarity. (a) *trans*-**118**, (b) *cis*-**118**, (c) [*trans*-**118**•*trans*-**118**] and (d) [*trans*-**118**•*cis*-**118**]. Dashed lines represent hydrogen bonds. Cartesian Coordinates for (c) can be found in Appendix Nine.

Further evidence for the open conformation of the *trans*-isoxazolidine templates comes from the solid state structure of dicarboxylic acid *trans*-**120** determined (**Figure 3.4**) by single-crystal X-ray crystallography. Very small crystals of *trans*-**120** were obtained from the slow evaporation of this isoxazolidine from a CDCl₃/acetone mixture.

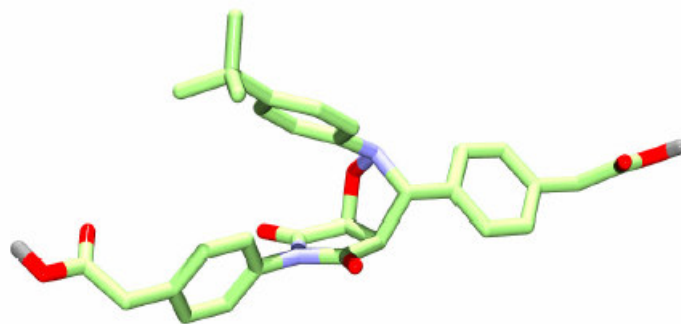
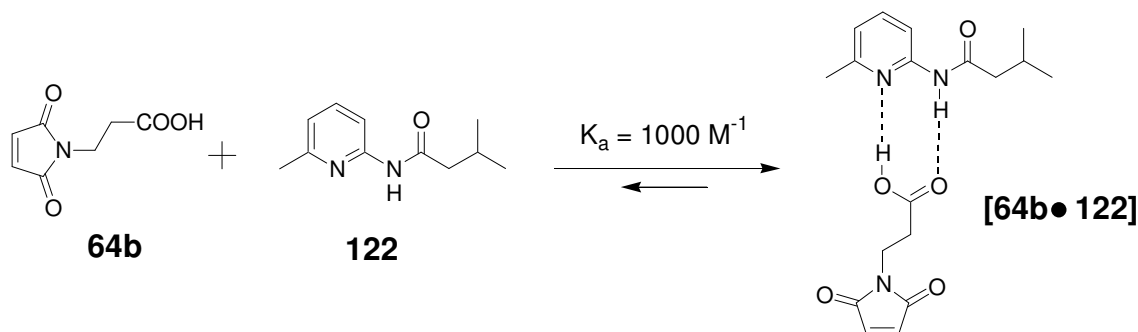


Figure 3.4 Single crystal X-ray structure obtained for *trans*-**120**. Carbon atoms are green, oxygen atoms are red, nitrogen atoms are blue, and hydrogen atoms are grey. Only carboxylic acid hydrogen's are shown for clarity

Although identical recognition motifs are used to those described in Chapter Two, the more reactive nature of nitrones with maleimides compared with azides or furan derivatives means the reaction can be carried out at a lower temperature, 0 °C. As a result of this decrease in temperature the association constant, K_a , for the binding between amidopyridine and carboxylic acid derivative will be different from the value used in Chapter Two. This value was determined in previous work conducted within our laboratory^[87] through NMR titration studies utilizing maleimide **64b** and amidopyridine derivative **122** to be 1000 M^{-1} .



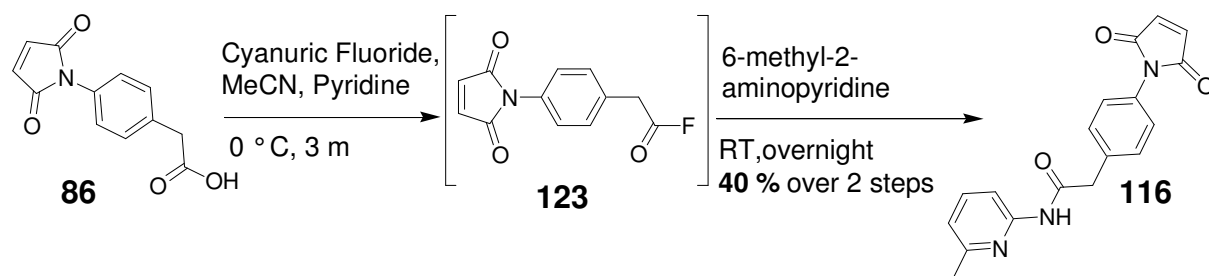
Scheme 3.3 The association between maleimide **64b** and amidopyridine derivative **122** in CDCl_3 at 0 °C.

3.2 The synthesis of the potential replicating systems

3.3 Maleimide **116**^[207]

Target maleimide **116** was prepared (**Scheme 3.4**) in two steps from pre-synthesized maleimide **86** (Chapter Two) *via* acid fluoride **123**. The reaction of maleimide **86** in MeCN and pyridine at 0 °C afforded intermediate **123**. As a result of the sensitive nature

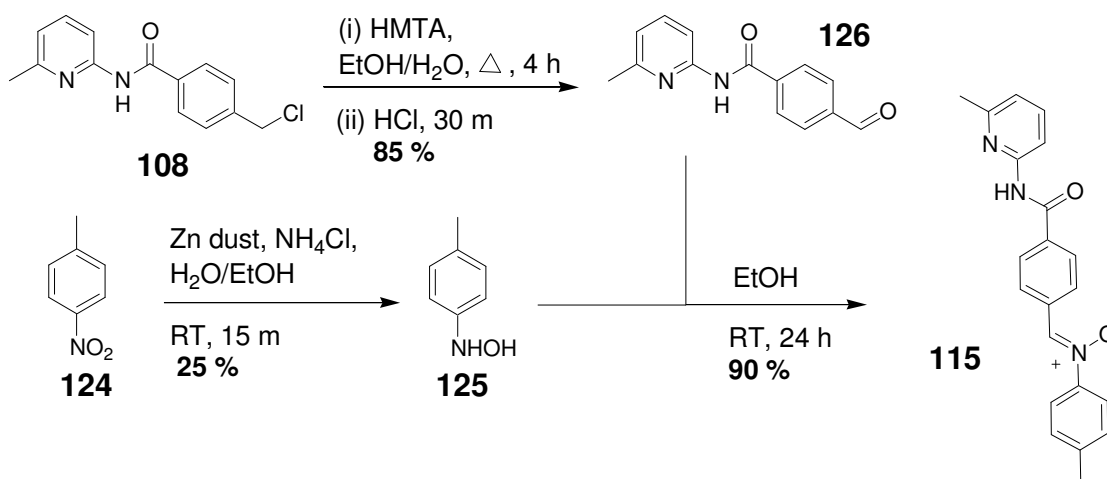
of the acid fluoride **123** it was not isolated but immediately used in its crude form, although a solution was taken assayed by ^{19}F NMR spectroscopy (δ_{F} **123** = + 44.8 ppm). This ^{19}F NMR spectrum demonstrated that we had indeed formed the acid fluoride compound. The acid fluoride **123** was reacted with 6-methyl-2-aminopyridine at room temperature overnight to afford maleimide **116**, in a 40% yield over two reaction steps.



Scheme 3.4 Synthetic route for the formation of maleimide **116** *via* acid fluoride intermediate **123**.

3.4 Nitron 115

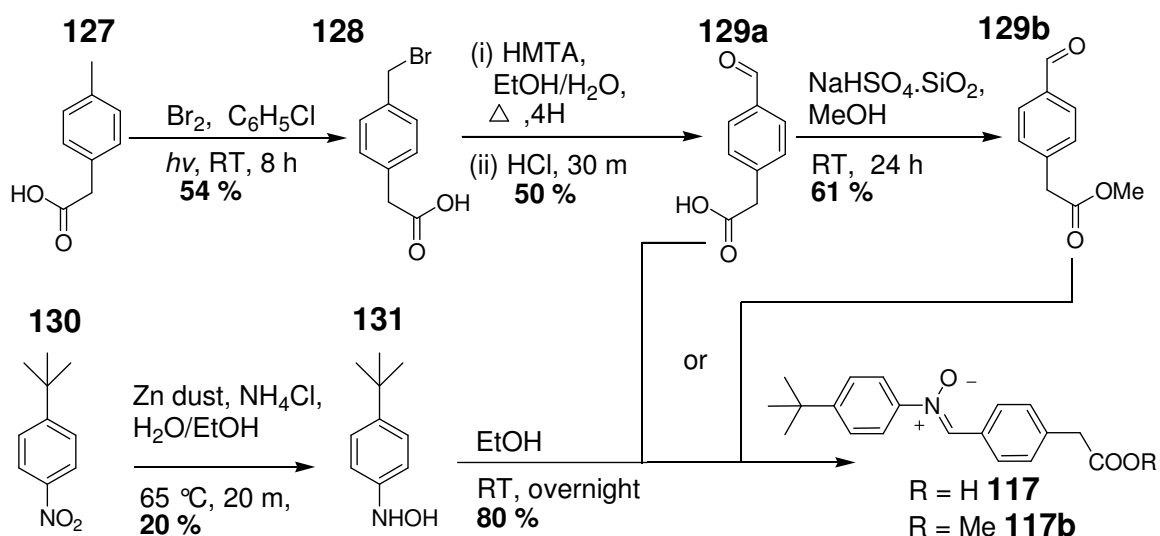
The synthesis of nitron **115**, bearing an amidopyridine recognition site, was accomplished in three steps. Benzylic chloride **108** was converted to aldehyde **126**, by adding hexamethylenetetramine^[168] (HMTA) to a solution of **108** in EtOH/ water and heating under reflux. The imine formed was hydrolyzed to the aldehyde through the addition of HCl, to afford **126** in 85% yield. The second step involved the reduction of **124** to hydroxylamine **125** by the careful addition of zinc dust to the solution of **124**, NH_4Cl , in EtOH/ H_2O , stirring at ambient temperature. This reaction afforded hydroxylamine in 25% yield, after recrystallization. The final step involved the addition of hydroxylamine **125** to a solution of aldehyde **126** in EtOH at room temperature. This reaction afforded nitron **115** in a 90% yield



Scheme 3.5 Synthetic route for the synthesis of nitrone **115**.

3.5 Nitrone **117**

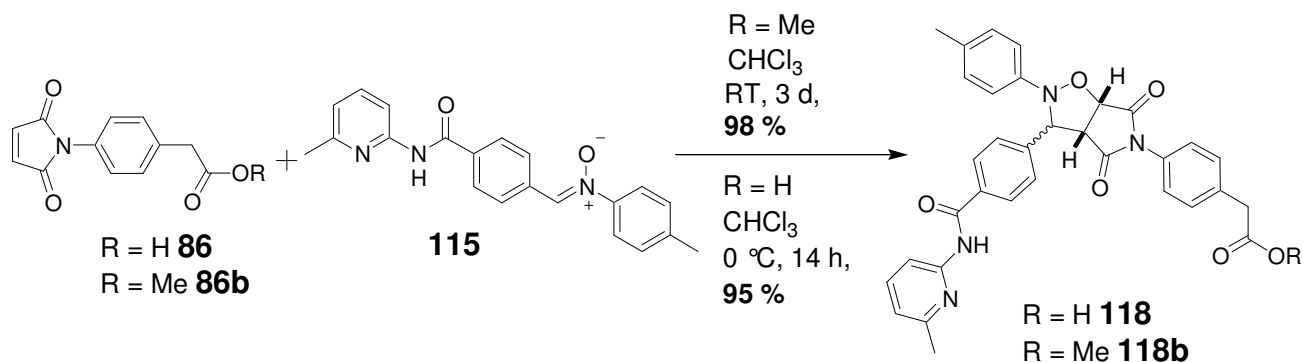
The target nitrone **117** or **117b**, bearing a carboxylic acid recognition site, was prepared in four, or five steps. The alkyl bromide **128** was formed^[167] through the addition of bromine to a solution of **127** in chlorobenzene illuminated by tungsten 60 watt lamp in 54% yield, after recrystallization. Aldehyde **129a** was formed by adding HMTA to a solution of **128** in EtOH/H₂O and heating under reflux. This reaction afforded an imine which was hydrolyzed to the aldehyde through the addition of HCl to afford **129a** in 50% yield. The third step involved the reduction of nitro **130** to the hydroxylamine **131** by the careful addition of zinc dust to the solution of **130**, NH₄Cl, in EtOH/H₂O, stirring at 65 °C. This reaction afforded hydroxylamine **131** in 20% yield, after recrystallization. The next step was only performed in the formation of ester **129b**. Aldehyde **129a** was dissolved in methanol, and NaHSO₄·SiO₂ was added^[169]. The resulting suspension was stirred at room temperature to afford the carboxylate ester **129b** in 61%. In the final step, hydroxylamine **131** was added to aldehyde **129a** or the carboxylate ester **129b** in ethanol at room temperature. This reaction afforded nitrone **117** or **117b** in approximately 80% yield.



Scheme 3.6 Synthetic route for the synthesis of nitron **117**, **117b**.

3.6 Isoxazolidine **118a** and **118b**

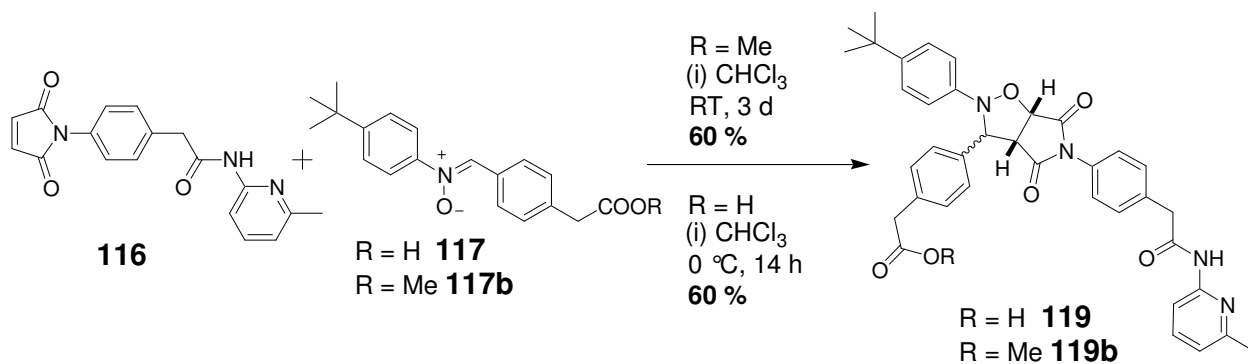
The 1,3-dipolar cycloaddition reaction between maleimide **86b** and nitron **115** was performed (**Scheme 3.7**) in the dark at room temperature for 3 days, affording a 3:1 *trans* to *cis* diastereoisomeric mixture of **118b** in 98% yield. The recognition mediated reaction between **86** and **115** was conducted in the dark at 0 °C for 14 hours, affording *trans*-**118** in 95% yield.



Scheme 3.7 Synthetic route for the formation of **118** and **118b**.

3.7 Isoxazolidine **119**

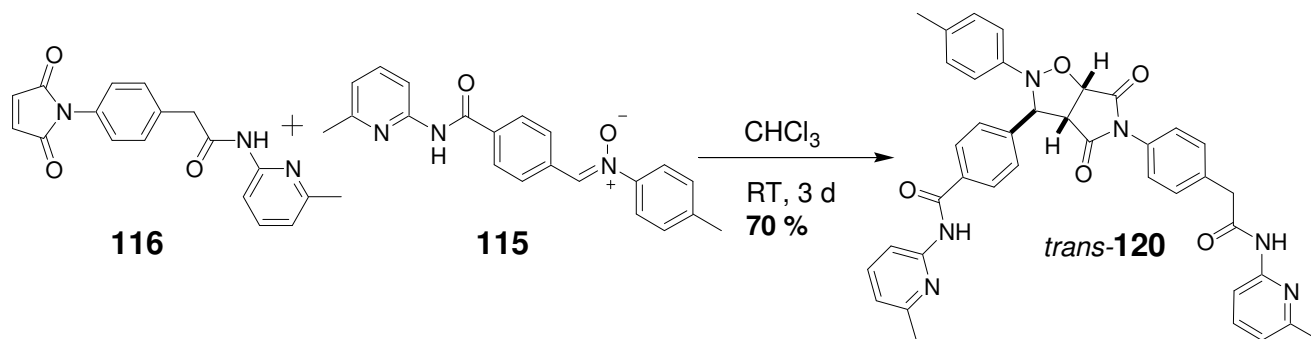
Identical conditions to the ones used for isoxazolidine **118** and **118b** were used for the formation (**Scheme 3.8**) of ester **119b**, in 60% yield, and *cis*-**119**, in 60% yield, after diastereoisomers separated by column chromatography.



Scheme 3.8 Synthetic route for the formation of **119** and **119b**.

3.8 Isoxazolidine **120**

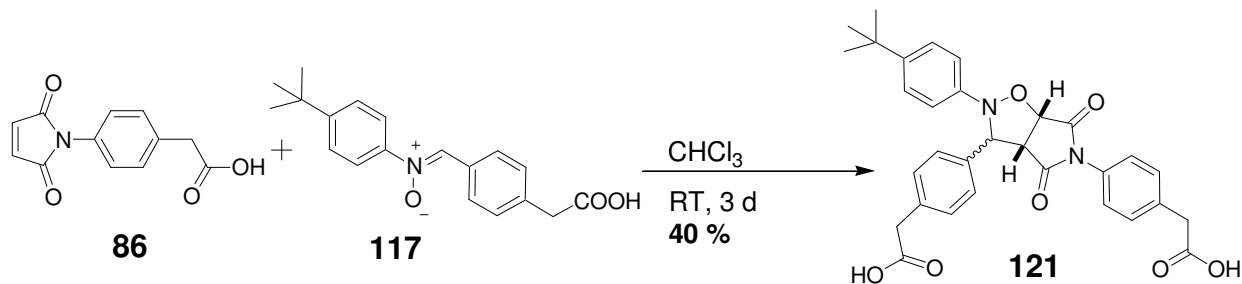
The 1,3-dipolar cycloaddition reaction between maleimide **116** and nitron **115** was performed (**Scheme 3.9**) in the dark at room temperature for 3 days, affording *trans*-**120** in 70% yield, after separation of diastereoisomers by column chromatography.



Scheme 3.9 Synthetic route for the synthesis of *trans*-**120**.

3.9 Isoxazolidine **121**

The 1,3-dipolar cycloaddition reaction between **86** and **117** was performed (**Scheme 3.10**) in the dark at room temperature for 3 days, affording a diastereomeric mixture of *cis* and *trans*-**121** in 40% yield.



Scheme 3.10 Synthetic route for the synthesis of *trans/cis*-**121**.

3.10 Results and discussion

3.11 Kinetic experiments

All reactions in this Chapter were conducted at 0 °C in CDCl₃, with initial concentrations of 25 mM for each of the building block molecules over a period of approximately 14 hours. Product concentrations were determined using a similar method as described in Chapter Two Section 2.14 (detailed discussion Section 7.5). However, as a different type of cycloadduct is formed the product ¹H NMR spectroscopy peaks H_a or H_{b1} and H_{b2} are compared (**Figure 3.5**) to the starting material maleimide H_c peaks, when calculated concentrations of species in reaction mixture. Appendix Two and Three shows the maleimide peaks and cycloadduct peaks in ¹H NMR spectra deconvoluted in the bimolecular and native reactions for systems 3.12 and 3.13.

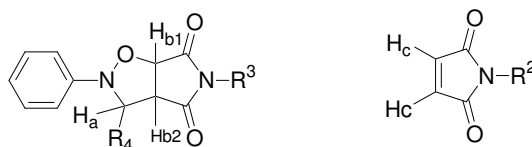
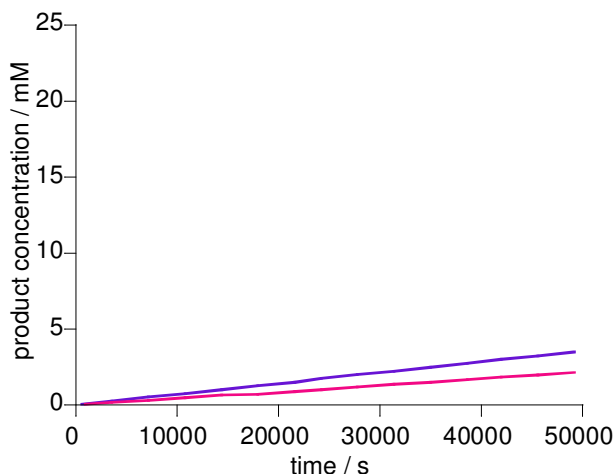


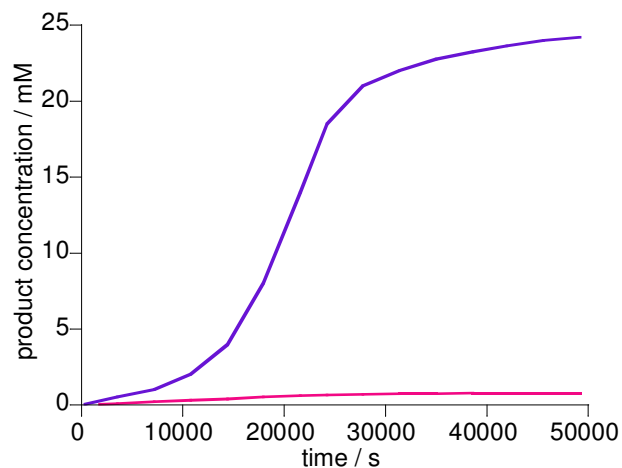
Figure 3.5 Deconvolution of ¹H NMR signal H_a, H_b and H_c used to determine product concentrations of template cycloadducts.

When analyzing the minimal replicators, four reactions were conducted; an ester control, competitive inhibition control, native and a templated reaction. The bimolecular control reaction blocks or removes the recognition site on the phenyl acetic acid building block derivative preventing the reaction from proceeding *via* the recognition mediated channels in the minimal model. This control provides data (**Figure 3.6** (a)) on the bimolecular pathway in the minimal model, which occurs in the lag period of autocatalytic process. The native reaction is the experiment in which the resultant isoxazolidine formed, from the maleimide and nitrone, has the potential to replicate autocatalytically through the association of the amidopyridine and carboxylic recognition sites. If autocatalysis is occurring in the native experiment the resultant graph should have a sigmoidal shape (**Figure 3.6** (b)), as described in Chapter One Section 1.12. Results from the native experiment demonstrate only that autocatalysis is occurring.

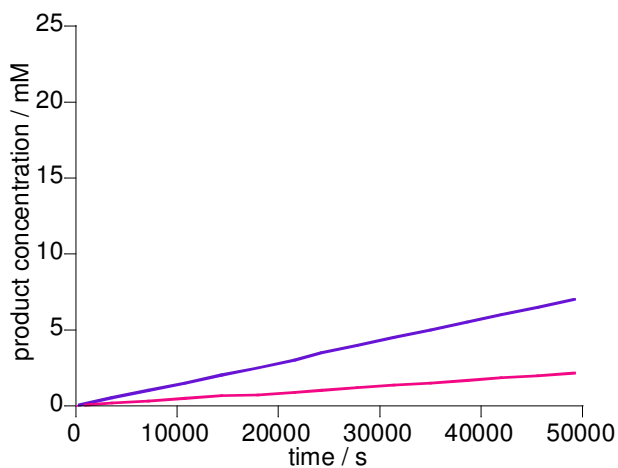
(a) **Bimolecular experiment**



(b) **Native experiment**



(c) **Competitive inhibition experiment**



(d) **Templated experiment**

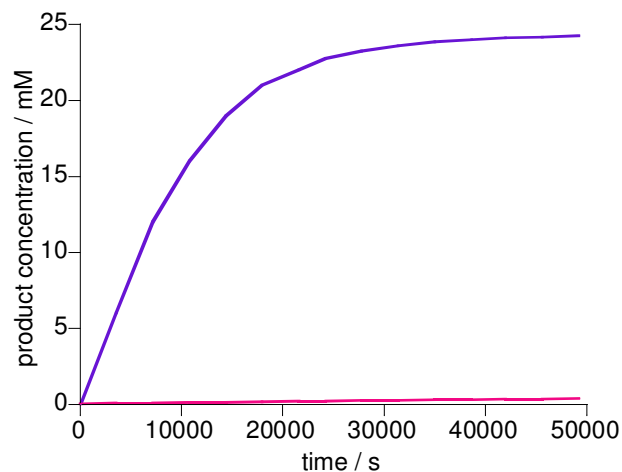


Figure 3.6

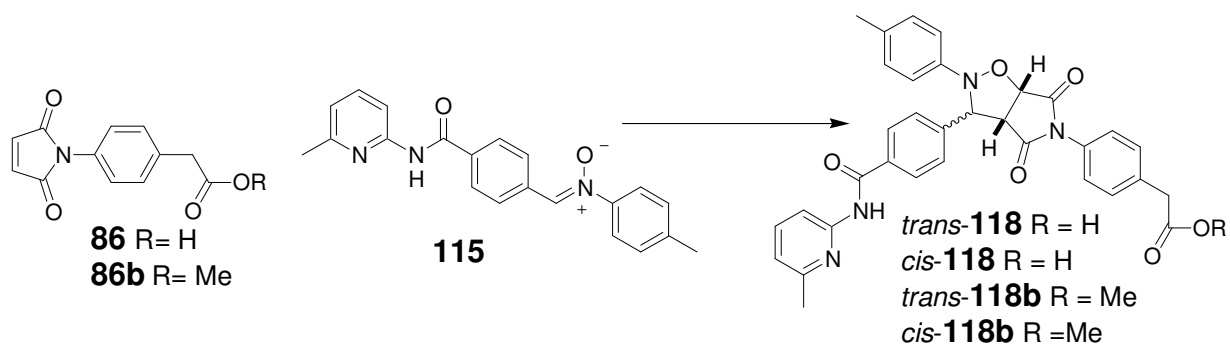
Examples of product concentration vs. time graphs expected for the four different experiments, blue line represents replicating isoxazolidine or equivalent ester, pink line unwanted non-replicating isoxazolidine or equivalent ester. (a) Typical bimolecular profile. (b) Characteristic sigmoidal shaped graph for the replicating isoxazolidine, containing a lag, autocatalytic and reactant limiting period, indicative of an autocatalytic system limited by finite resources. (c) Competitive inhibition or benzoic acid control, depending on level of inhibition the replicating isoxazolidine product curve may be similar or faster in rate to the bimolecular control. (d) In the templated experiment, addition of template has removed the initial lag period in the replicating isoxazolidine as a result of exponential growth from the start of the reaction.

The competitive inhibition reaction (**Figure 3.6** (c)) like the bimolecular experiment also obstructs association, but this time by adding a molecule which can directly compete for hydrogen bonding sites. Depending on the effectiveness of the inhibition, either the rate will be similar to the bimolecular experiment or reduced from the native experiment, with evidence remaining of the recognition mediated processes. The effectiveness of inhibition will depend on binding strength (K) between complexes of building blocks with each other and with molecules of formed template compared to association with the competitive inhibitor. If the association of building blocks with molecules of template, formed in the experiment, is substantially greater than the binding strength of the building blocks with the competitive inhibitor, reaction inhibition will be decreased and the rate will be greater than the bimolecular reaction. Results of this control reaction provide information as to whether the reaction is proceeding *via* a recognition mediated pathway. The final experiment is the templated reaction (**Figure 3.6** (d)). This experiment is conducted in a similar fashion to the native, but prefabricated template is added at the beginning of the reaction to promote autocatalysis by removing the lag period. The removal of the lag period turns the product curve for the replicating template from sigmoidal in the native to parabolic in the templated experiment (**Figure 3.6** (b) and (d)). Analysis of the results of the templated experiments informs the investigator if the reaction is indeed proceeding *via* a minimally replicating pathway. In conclusion all four experiments have to be studied in order to determine if the reaction is first autocatalytic, second recognition mediated and thirdly, and most importantly, whether the reaction mechanism is *via* self-replication.

Studies into the cross-catalytic systems, as a result of the complementary nature of the building blocks in a molecule of template, only require two types of reaction a bimolecular control and a templated reaction. These two experiments types were discussed in Chapter Two Section **2.14**.

3.12 Potential minimal replicator isoxazolidine *trans*-118

The first system investigated was the potential self-replicator *trans*-**118** formed from the 1,3-dipolar cycloaddition reaction between **86** and **115** (**Scheme 3.11**).

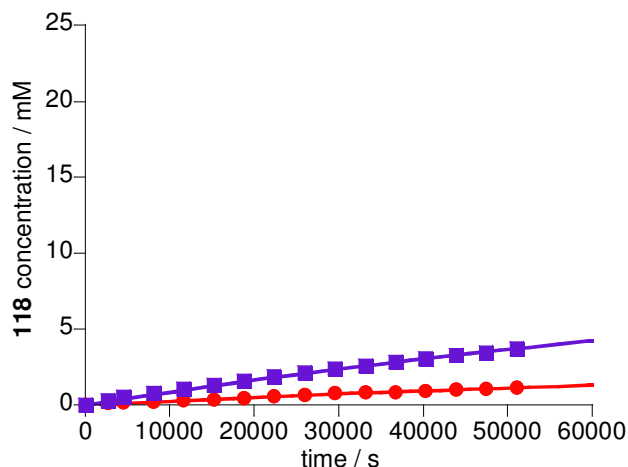


Scheme 3.11 1,3-dipolar cycloaddition between maleimide **86**, **86b** and nitron **115** to form isoxazolidine **118**, **118b**.

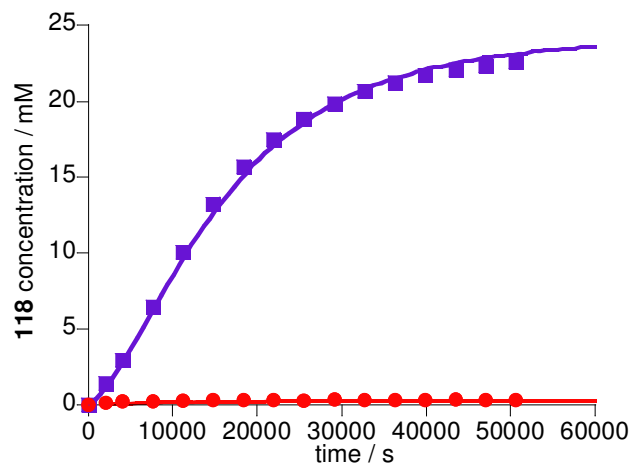
As discussed, at the start of Chapter Three, it is the *trans*-diastereoisomer which is expected to be capable of self reproduction. The *cis*-diastereoisomer is expected to be formed *via* the bimolecular or [A•B] pathways but not the autocatalytic minimal replicating cycle. This potential minimal replicator was studied in detail by conducting a series of kinetic experiments, mentioned earlier Section 3.11, in order to provide important information into the mechanism of replication.

Before investigation of this potential self-replicating system can start, a bimolecular control experiment must be conducted to provide a reference to which the results of the replicating experiments can be compared. An ester control building block **86b** was used in the reaction with amidopyridine nitron **115** to ensure any possible recognition mediated process was eliminated from the experiment. The bimolecular experiment (**Figure 3.7** (a)), between nitron **115** and maleimide **86b**, precedes slowly forming a 3:1 ratio of *trans*- and *cis*-diastereoisomers (Appendix Two), this diastereomeric ratio is indicative (**Figure 3.6** (a)) of a non-recognition mediated 1,3-dipolar cycloaddition reaction between a maleimide and a nitron. Overall conversion after 14 hours in CDCl₃ at 0 °C is approximately 11%.

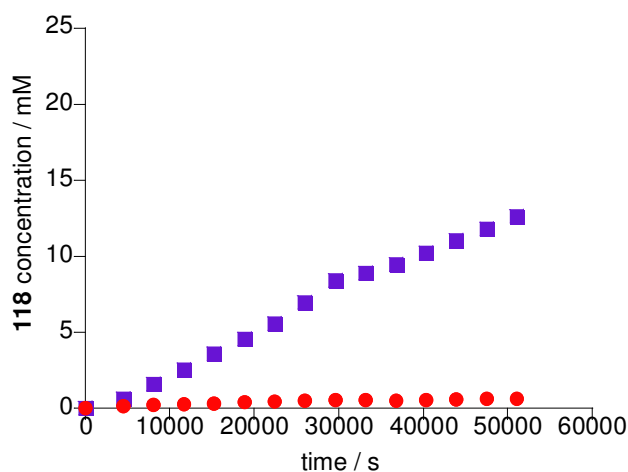
(a) Bimolecular reaction



(b) Native reaction



(c) Benzoic acid control



(d) Templated reaction

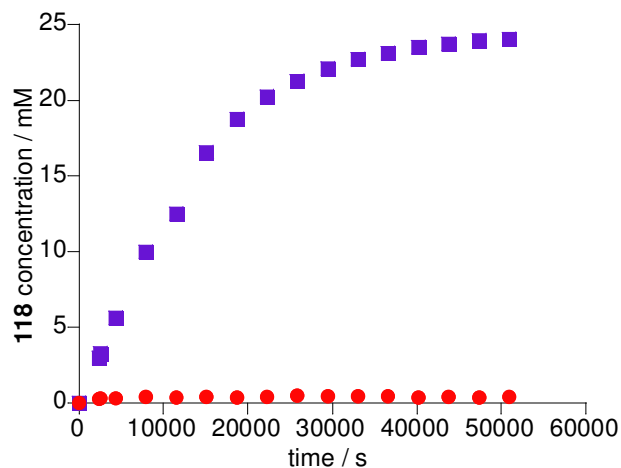


Figure 3.7 Product concentration vs. time profile, solid lines indicate optimal fit curves. (a) Bimolecular reaction between equimolar concentrations of nitrone **115** and maleimide **86b** ($[115] = [86b] = 25 \text{ mM}$) at $0 \text{ }^\circ\text{C}$ in CDCl_3 , for the formation of *trans*-**118b** (purple squares) and *cis*-**118b** (red circles). (b) Native reaction between equimolar concentrations (25 mM) of nitrone **115** and maleimide **86** at $0 \text{ }^\circ\text{C}$ in CDCl_3 , for formation of *trans*-**118** (purple squares) and *cis*-**118** (red circles). (c) Benzoic acid control reaction, between an equimolar concentration (25 mM) of nitrone-**115** and maleimide **86** inhibited competitively with 100 mM of benzoic acid at $0 \text{ }^\circ\text{C}$ in CDCl_3 . (d) Template reaction, with the addition of 2.5 mM (0.1 equivalents) of prefabricated *trans*- template **118** to the reaction between nitrone **115** and maleimide **86** in CDCl_3 at $0 \text{ }^\circ\text{C}$. Errors in concentration values is $\pm 4\%$.

These data points indicate that when no recognition is present, no autocatalysis is occurring and no self-replication, as there is no increase in rate or selectivity of either diastereomeric product as the experiment proceeds. The product concentration vs. time curve was fitted computationally to a kinetic model (as in Chapter Two section 2.15), which only optimized (Scheme 3.12) two parameters the rate constant, k_1 and k_2 , for the formation of the *trans*- and *cis*-isoxazolidine products. This procedure is discussed in

more detailed in Section 7.8, but involves the optimal fit of theoretical to experimental product concentration vs. time curves. The percentage of the mean absolute difference between the experimental and theoretical concentrations with respect to the mean of experimental concentration (R) was 3.60%. This value indicates a reasonable fit of the experimental data to the theoretical model. The R value is for both curves in **Figure 3.7** (a) and therefore is for the overall data individual curves may have an error greater than 3.6% fit (**Scheme 3.12**).



Rate constant / $\times 10^{-4} \text{ M}^{-1} \text{ s}^{-1}$ $k_1 = 0.47 \pm 0.06$ $k_2 = 1.49 \pm 0.01$

Scheme 3.12 Kinetic model for the bimolecular 1,3-dipolar cycloaddition reaction between maleimide **86** and nitrone **115** and optimized rate constants k_1 and k_2 . Error values are rounded up to three decimal points.

An initial examination of the product concentration vs. time curve for the native reaction (**Figure 3.7** (b)), between nitrone **115** and maleimide **86**, reveals the dramatic affect recognition has had on the reaction. Comparison between the bimolecular and native experiments reveal an approximate 25-fold increase in the *trans* to *cis* ratio, from 3:1 in the bimolecular to 75:1 in the native experiment (Appendix Two). Scrutiny of **Figure 3.7** (a) and (b) reveals the increase in selectivity for formation of the *trans*- product is result of two factors. The first factor is the increased rate of formation of the *trans*-product, the second is a decrease in rate of formation of the *cis*-product. This increase in rate of formation of the *trans*- isoxazolidine selectively, indicates the *cis*-product is not undergoing autocatalysis, as we would expect to see an increase in *cis* formation as the reaction progress if it was autocatalytic. Also the rate of *cis* formation shows no sign of exponential growth, indicative of autocatalysis. The rate of formation of *cis*-**118** does not only show no increase in rate, it actually demonstrates a decreased rate compared to the bimolecular experiment. A reduced rate of formation of the *cis*-isoxazolidine in the native reaction compared to the bimolecular is a result of a decreased availability of starting materials maleimide **86** and nitrone **115**. These building block molecules are being consumed in synthesizing the *trans*-product meaning less are available to form *cis*-**118**.

Overall conversion in CDCl_3 after 14 hours at $0\text{ }^\circ\text{C}$ is approximately 90%, a large increase compared to the bimolecular control experiment. The increase in conversion and selectivity are not the most characteristic feature of the graph in **Figure 3.7 (b)**, it is the sigmoidal shape of the *trans* product curve. In Chapter One Section 1.12 the characteristic feature of an autocatalytic system is the resultant sigmoidal shaped curve in the concentration vs. time profile. The graph in **Figure 3.5** clearly displays such a curve demonstrating that autocatalysis is present in the reaction mechanism. A superior way of demonstrating the presence of autocatalysis in this experiment is to analyze the velocity time curve over the reaction timescale. In order to plot this graph, first a sixth order polynomial was fitted (**Figure 3.8**) to the product concentration vs. time graph in **Figure 3.7 (b)**.

$$[C]_t = a + bt + ct^2 + dt^3 + et^4 + ft^5 + gt^6$$

Figure 3.8 Sixth order polynomial fitted to the native product concentration vs. time curve, where $[C]_t$ is total concentration in mM at a particular time, t is time in seconds and $a-g$ represent constant values.

The values for the constants in **Figure 3.8** are $a = 4.5653 \times 10^{-2}$, $b = 1.813 \times 10^{-4}$, $c = 4.7836 \times 10^{-8}$, $d = -1.6076 \times 10^{-12}$, $e = 7.6889 \times 10^{-18}$, $f = 3.2809 \times 10^{-22}$ and $g = -3.6967 \times 10^{-27}$. The variables $C(t)$ and t represent total concentration (mM) of *trans*-118 at a particular time and time (seconds) respectively. The polynomial fitted the experimentally observed curve with an R value of 1.00. Next the first derivative was taken (**Figure 3.9**) of the fitted function, to provided a measure of velocity.

$$\frac{d[C]_t}{dt} = b + 2ct + 3dt^2 + 4et^3 + 5ft^4 + 6gt^5$$

Figure 3.9 First derivative of the sixth order polynomial fitted to the native product concentration vs. time curve, where $[C]_t$ is total concentration in mM at a particular time, t is time in seconds and $a-g$ represent constant values.

Now that the velocity over the reaction timescale has been calculated it can be plotted against time to produce the graph in **Figure 3.10**.

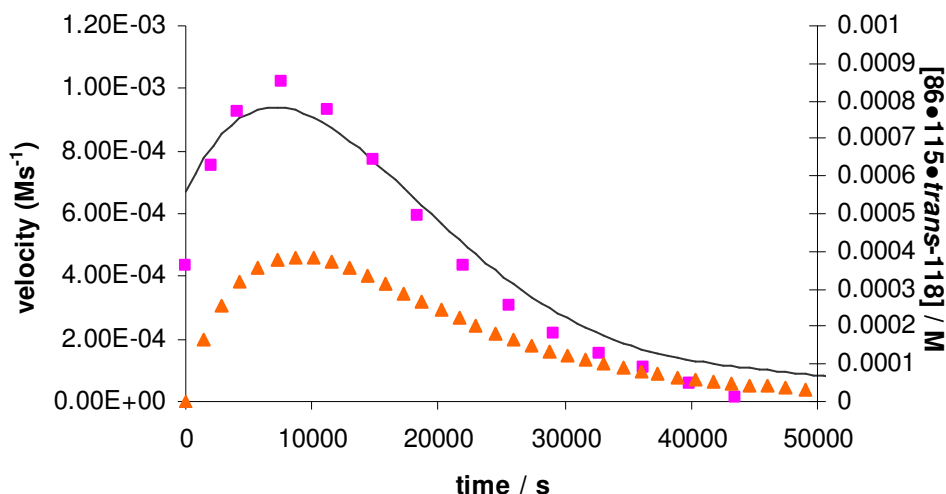
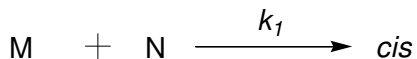


Figure 3.10 Velocity (Purple squares) or $[86\bullet115\bullet trans-118]$ (orange triangles) vs. time graph of native experiment. The velocity vs. time graph is from the first derivative of a sixth order polynomial fitted to the *trans* curve of the product concentration vs. time graph. Purple squares are experimentally determined values, the solid black line is a theoretical optimally fit line using the kinetic model in **Scheme 3.13**. The $[86\bullet115\bullet trans-118]$ vs. time plot (orange triangles) is the concentration of ternary complex present at anyone time over the reaction time course. Errors in velocity and concentration values is $\pm 4\%$.

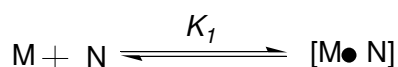
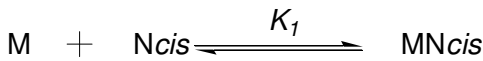
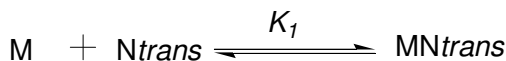
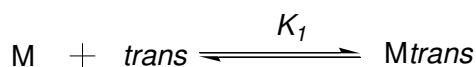
This graph demonstrates an increase in reaction velocity reaching a maximum approximately between 5000-12500 seconds (1.5-3.5 hours), after which there is a gradual decline. The data points in this graph highlight the key features which occur in any autocatalytic system, an initial lag period, where velocity is slow, an exponential growth period, where velocity increases to a maximum, and final a reactant limiting stage, where a decline in reactant concentration results in a decline in velocity.

Additional kinetic data for the native reaction were obtained by computationally fitting the product concentration vs. time curve to a kinetic model (**Scheme 3.13**), which optimized two parameters only, the rate constant for the ternary complex and the stability constant for the product duplex $[trans-118\bullet trans-118]$.

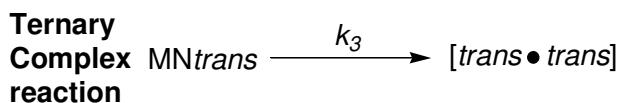
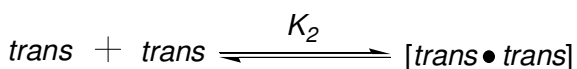
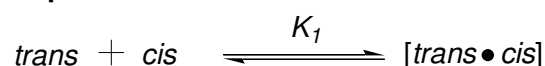
Bimolecular Reactions



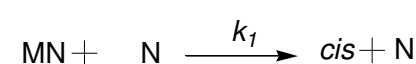
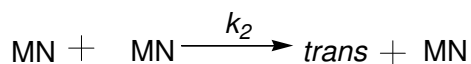
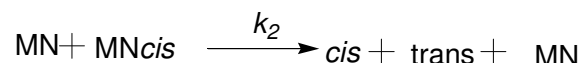
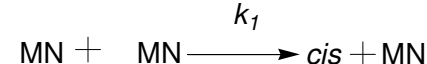
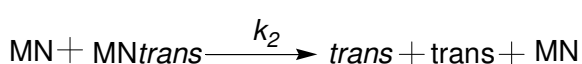
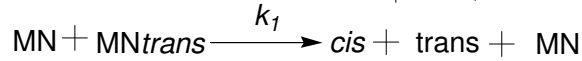
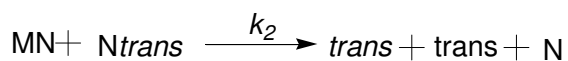
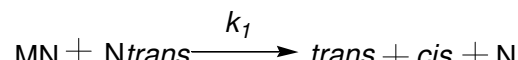
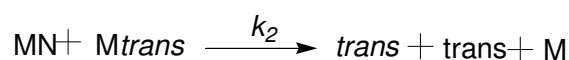
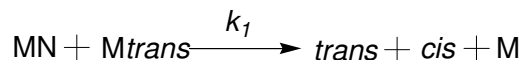
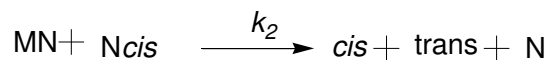
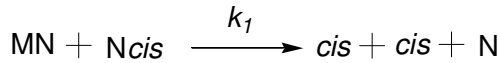
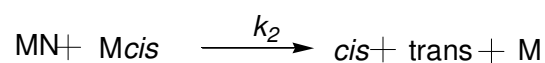
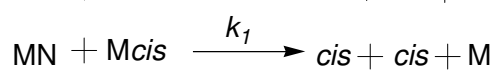
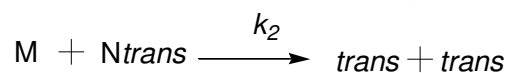
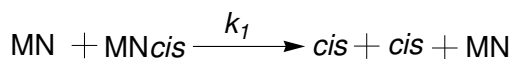
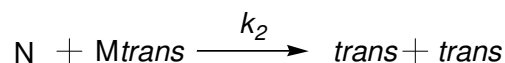
Routes towards formation of binary and ternary complexes



Duplex association



Bimolecular reactions of complexes



Scheme 3.13 Kinetic model used to computationally fit theoretical curves to the experimentally observed results for the native experiment in **Figure 3.7** (b), in order to extract data about the catalyzed ternary complex reaction. Where M = maleimide **86**, N = nitrone **115**, *trans* = *trans*-**118** and *cis* = *cis*-**118**.

The kinetic model comprises of 5 sections which link together to provide a comprehensive and realistic set of reactions for this system. The first section describes the reactions for the formation of the isoxazolides *via* the normal bimolecular routes utilizing rate constants k_1 and k_2 , determined theoretically through the optimal fit of the *trans*- and *cis*-product *vs.* time curves in **Figure 3.7** (a). Next is the section which describes the associations resulting in the formation of binary and ternary complexes. In these complexes a stability constant is used for the mono association between an amidopyridine and carboxylic acid residue K_1 ($K_1 = 1000 \text{ M}^{-1}$). The third section describes the formation of duplex structures between the different isoxazolidine diastereoisomers. There are two different types of association present for the formation of these duplexes. The first is a mono-association containing two hydrogen bonds between one amidopyridine and one carboxylic acid unit, the second is a di-association. This association contains a possible four hydrogen bonds between two amidopyridine and two carboxylic acid moieties. For the mono-association the K_1 equilibrium constant is used. However, in the case of the di-association constant, K_2 , where experimental determination is not possible, a theoretical value can be estimated through optimal fit of the kinetic model to the product concentration *vs.* time curve. If the isoxazolidine diastereoisomers are not of similar shape and in the open configuration only mono association can occur. However, if their structures meet these two criteria di-association is possible as in the case of the [*trans*•*trans*]. The next section contains the ternary complex reaction of the experiment. Determination of the rate constant, k_3 , is the main reason for fitting this kinetic model to the product concentration *vs.* time curve present in **Figure 3.7** (b). Experimental measurement of k_3 would be almost impossible as a model compound would have to be designed to represent the *pseudo*-unimolecular reaction in the ternary complex and this reaction would have to be easily monitored. Therefore, the only possible way of determining k_3 is to calculate a theoretical value, by varying an estimated value through the computational optimal fit of a kinetic model. The final section in the kinetic model in **Scheme 3.13** contains other possible bimolecular reactions for the formation of *cis*- and *trans*-products. Unlike the simple interactions described in the first section of the kinetic model these reactions involve binary and ternary complexes reacting bimolecularly to form the *cis*- and *trans*-isoxazolidines. As these reactions proceed in a bimolecular fashion rate constants k_1 and k_2 can be used depending on which diastereoisomer is formed. The combination of all these reactions

and associations produces a comprehensive and accurate model for this system. Only an accurate model will provide an optimal fit to the experimental data.

Utilizing the kinetic model in **Scheme 3.13** a theoretical curve was optimally fitted (R = 2.6%) to the product concentration vs. time curves in **Figure 3.7** (b), which optimized two parameters only the rate constant for the ternary complex (**Scheme 3.13**), k_3 , and the stability constant for the product duplex [*trans*-118•*trans*-118], K_2 . The duplex association constant K_2 was determined as $8.8 \pm 0.08 \times 10^6 \text{ M}^{-1}$, and values for the rate constant of the ternary complex as well as the bimolecular reaction are displayed in **Table 3.1**.

Table 3.1 Table of computationally determined rate constants from optimal fit curves of theoretical to experiment product concentration vs. time curves and the kinetic effective molarity of the recognition mediated reaction.

Bimolecular Reactions^a Rate constant / $\times 10^{-4} \text{ M}^{-1} \text{ s}^{-1}$	Recognition Mediated^a Rate constant / $\times 10^{-4} \text{ s}^{-1}$	kEM^b
$k_1 = 0.47 \pm 0.01$	Reaction not catalyzed by ternary complex	Reaction not catalyzed by ternary complex
$k_2 = 1.49 \pm 0.01$	$k_3 = 31.3 \pm 0.1$	$21 \pm 2.1 \text{ M}$

^a Rate constants relate directly to **Scheme 3.13**. ^b kEM, kinetic effective molarity is calculated by dividing the recognition mediated reaction over the bimolecular, $kEM = k_1$ or k_2 / k_3 or k_4 .

Examination of **Table 3.1** reveals that the formation of *trans*-isoxazolidine is greatly accelerated in the catalytic ternary complex compared to the control reaction, $4.18 \times 10^{-3} \text{ s}^{-1}$ compared to $7.41 \times 10^{-5} \text{ M}^{-1} \text{ s}^{-1}$ in the bimolecular reaction. By dividing the rate of the ternary complex over that of the bimolecular, $kEM = k_3/k_2$, it is possible to determine the kinetic effective molarity for the *pseudo*-unimolecular reaction. When this calculation is carried out an effective molarity of 21 M is found. As discussed earlier the formation of the *cis*-isoxazolidine product does not undergo autocatalysis and, therefore, is not catalyzed in the ternary complex structure.

An additional advantage of using the SimFit program to fit a kinetic model to the experimental data is that it allows you to calculate the concentration of different species through out the reaction timescale. In **Figure 3.10** we demonstrated autocatalysis through a velocity vs. time curve; however, this graph also has a second y-axis scale. This axis is a measure of ternary complex concentration throughout the experiment. Therefore, using the SimFit program and the kinetic model, values for the concentration

of ternary complex were extracted and plotted against time to produce the curve (orange triangles) in **Figure 3.10**. The velocity vs. time curve displays a maximum autocatalytic velocity at around 8000 seconds. As the increase in velocity is caused by the ternary complex structure there should be a direct relationship between ternary complex concentration and reaction velocity. Analysis of the graph in **Figure 3.10** reveals the presence of this direct relationship. At 8000 seconds the velocity vs. time curves (blue diamonds) shows a maximum and so does the [86•115•*trans*-118] vs. time curve (orange triangles), proving reaction velocity is directly proportional to the concentration of the catalytic ternary complex structure.

The product concentration vs. time graph for the native experiment provides unequivocal proof that autocatalysis is present in this system, however, it does not conclusively prove the reaction is recognition mediated or self-replicating. In order to prove these facts two further experiments are required, a competitive inhibition and a templated experiment.

The competitive inhibition reaction involves the addition, at the beginning of the reaction, of four equivalents of benzoic acid to the reaction of nitron **115** and maleimide **86**. Product concentrations were extracted and plotted against time to produce the graph in **Figure 3.7** (c). As discussed at the beginning of this section the benzoic acid will interfere with any recognition present, decreasing the reaction rate. Inspection of **Figure 3.7** (b) revealed that addition of benzoic acid has reduced the reaction rate, producing a graph with a bimolecular appearance. The selectivity has fallen sharply from the native reaction with a ratio of *trans* to *cis* of around 20:1. Overall conversion in CDCl₃ at 0 °C, after 14 hours, has fallen from 90% in the native to 52% in this competitive inhibition experiment.

A decreased selectivity, conversion and rate in this control experiment all combine to prove that the reaction between nitron **115** and maleimide **86** is recognition mediated. The addition of benzoic acid has blocked the recognition moieties on the nitron, maleimide and resultant isoxazolidines.

The three experiments so far have proven that this system is autocatalytic and recognition mediated for the formation of the *trans*-isoxazolidine **118**. However, in order to final prove this system is replicating in a minimal fashion one final experiment has to be conducted. If replication is occurring, the addition of prefabricated template *trans*-**118** at the start of the reaction between maleimide **86** and nitron **115** should remove the lag period from product concentration vs. time curve. The addition of

template should cause autocatalysis to occur immediately with no need for a lag period to form catalytic *trans*-**118**. The templated reaction is the ultimate test of any potential replicating system. Therefore, the experiment between maleimide **86** and nitroene **115** was conducted with the addition of 2.5 mM (maximum solubility) of isoxazolidine *trans*-**118** at the start of the reaction. The resultant product concentrations were extracted *via* deconvolution from individual spectra and plotted (**Figure 3.7** (d)) against time. As anticipated the resultant graph displays a parabolic graph, the addition of template has removed the lag period and hence the sigmoidal shape. The selectivity for the *trans*-product remains identical to the native reaction with a *trans* to *cis* ratio of 75:1. Overall conversion for the templated reaction in CDCl₃ at 0 °C after 14 hours is close to 100%. These two facts demonstrate that a template effect is present and hence minimal replication is occurring in this system. The final piece of evidence which demonstrates the minimal nature of this system can be observed by comparing (**Figure 3.11**) the velocity vs. time for the templated reaction to that of the native reaction. The templated line on this velocity vs. time curve was produced by fitting a sixth order polynomial to the *trans* curve on **Figure 3.7** (d) and taking the first derivative of the resultant function.

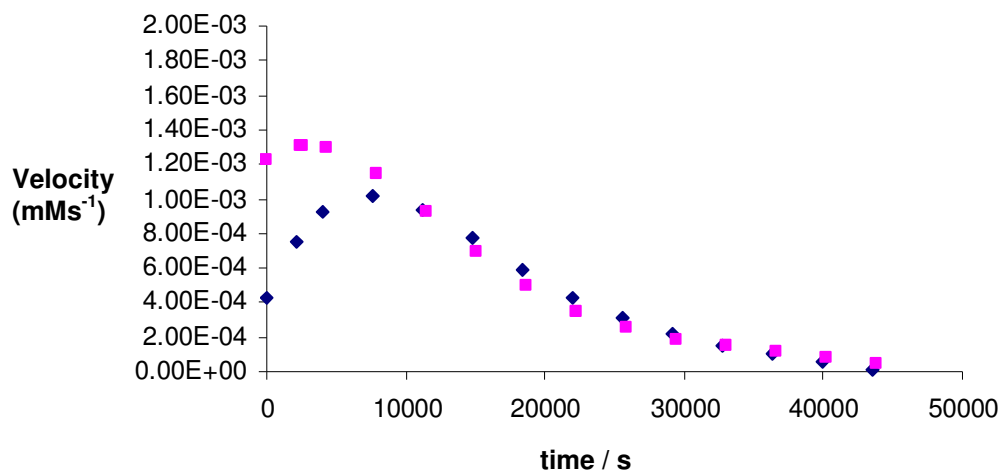


Figure 3.11 Velocity vs. time graph of native experiment (blue diamonds) and templated experiment (purple squares), from first derivative of sixth order polynomial fitted to the *trans* curves in the product concentration vs. time graphs. Errors in velocity are $\pm 4\%$.

Investigation of **Figure 3.11** demonstrates almost the complete elimination of the lag period with the maximum autocatalytic rate occurring nearly immediately. The maximum autocatalytic rate for the templated reaction is also very similar to that of the native reaction, only occurring earlier in the reaction timescale. Congruous maximal velocities

demonstrate that the same mechanistic processes are occurring in the templated and native experiments. The maximum autocatalytic velocity occurs in the time region where $0.1 < \rho < 1.0$, $\rho = [\text{template}]/[\text{precursor}]$. Examination of the native curve in **Figure 3.11** indicates this is in the region between 5000 and 20000 seconds, which corresponds to a concentration of *trans*-**118** between 2 and 10 mM approximately. In the templated reaction the maximum solubility of *trans*-**118** limited studying the addition of concentrations above 2.5 mM (where $\rho = [\text{template}]/[\text{precursor}] \approx 0.1$) of prefabricated template. However, examination of the velocity time curve indicates that this would have been irrelevant, as addition of a larger concentration of *trans*-**118** would only have resulted in a maximum 8-10% increase in rate, from approximately 6.50 to $7.10 \times 10^{-4} \text{ Ms}^{-1}$. Therefore, in the template experiment, where $\rho = [\text{template}]/[\text{precursor}] \approx 0.1$, the system is operating effectively at the limits of its self-replicating capacity, with autocatalysis commencing at $t = 0$.

The analysis of this system clearly demonstrates the main pathway for formation of the *cis*-isoxazolidine **118** is through the bimolecular pathway whereas the formation of *trans*-**118** template is *via* a reaction in the ternary complex structure. A maximum autocatalytic rate was observed (**Figure 3.11**) at around 9000 sec when the concentration of ternary complex was approximately 400 μM . The resultant product duplex was calculated to have an association constant of around $8.8 \times 10^6 \text{ M}^{-1}$. This value is higher than might be anticipated from the classical chelate effect, which states the additive effect of energies of individual non-covalent interactions. Therefore, dimerization constant K_2 is expected to have a magnitude of around $K_1^2 = 1000^2 = 1 \times 10^6 \text{ M}^{-1}$. The fact that the actually determined value is higher than $1 \times 10^6 \text{ M}^{-1}$ means positive cooperativity is present in this system. A more empirical measurement of cooperativity can be obtained by using (**Figure 3.12**) the equation for Gibbs free energy of connection, for a detailed discussion see Chapter One Section **1.4**.

$$\Delta G^S = \Delta G_B^0 + \Delta G_A^0 - \Delta G_{AB}^0$$

Substitute $\Delta G^0 = -RT \ln K$ into above equations results in the equation below;

$$\Delta G^S = RT \ln \frac{K_{AB}}{K_A K_B}$$

Figure 3.12 Equation of Gibbs free energy of connection, ΔG^S . Where ΔG_A^0 is Gibbs free energy of binding molecule A, ΔG_B^0 is Gibbs free energy of binding molecule B and ΔG_{AB}^0 is Gibbs free energy of binding molecule A joined to B. K_{AB} is the binding constant for A joined to B with the host and K_A and K_B is the association constant for the individual binding of molecules A and B to the host.

Modifying the second equation in **Figure 3.12** for this system; K_{AB} is equal to K_2 and K_A and K_B are equivalent to K_1 in **Scheme 3.13**. These changes result in the equation illustrated in **Figure 3.13**.

$$\Delta G^S = RT \ln \frac{K_2}{K_1 K_1}$$

Figure 3.13 Equation of Gibbs free energy of connection, modified for the system in this section. K_2 is the association constant for the duplex [*trans*-118•*trans*-118]. K_1 is the binding constant for the individual association of an amidopyridine moiety to a carboxylic acid recognition group.

Utilizing the individual binding constants for the binary association K_1 (1000 M^{-1}) and K_2 (1000 M^{-1}) and the calculated product duplex stability constant K_2 ($8.8 \times 10^6 \text{ M}^{-1}$) a value of 4.94 kJ mol^{-1} is calculated for the Gibbs free energy of connection, ΔG^S . The fact that the value is positive indicates positive cooperativity. This positive cooperativity indicates the fit between the two *trans*-templates is optimal, where the association of one hydrogen bond predisposes the formation of the other. Interestingly, the high duplex association constant must mean very low concentrations of the free template are present in solution. The concentration of free *trans*-template **118** was calculated, using the SimFit program, from the kinetic model (**Scheme 3.13**) to be never any higher than $5.5 \text{ }\mu\text{M}$. This value demonstrates the efficiency of this minimal replicating system, even with such small concentrations of free template present throughout the reaction dramatic autocatalysis is observed.

This minimal system is almost identical to the system developed previously in our laboratory, and discussed in Chapter One Section **1.17**. The only difference is an

addition methyl group present on the phenyl ring (**Figure 3.14**) attached to the nitrogen of the isoxazolidine ring. Therefore, we would expect the results to be similar between these two systems and indeed they are. Both exhibit very high selectivity 115:1 (R = H) compared to 75:1 (R = Me). The maximum autocatalytic rate in the native experiments for each of these two systems occurs at a C \approx 7.0 mM. In addition both systems have a similar kinetic molarity of around 20 M.

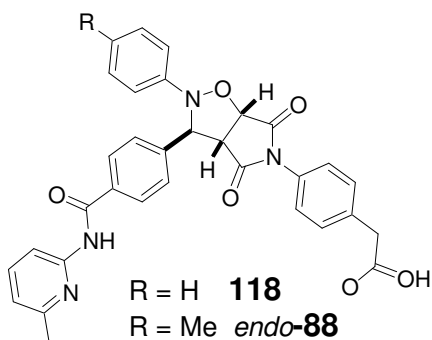
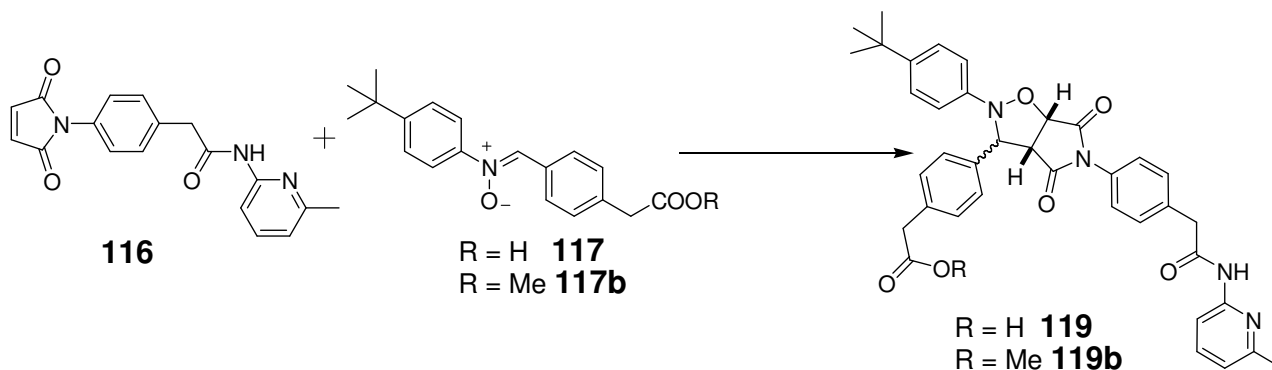


Figure 3.14 Minimal replicator *trans*-**118** or *endo*-**88**.

3.13 Potential minimal replicator isoxazolidine *trans*-**119**

The next system studied is the minimal replicator *trans*-**119** formed (**Scheme 3.14**) from the 1,3-dipolar cycloaddition between nitron **117** and maleimide **116**.



Scheme 3.14 1,3-dipolar cycloaddition between maleimide **116** and nitron **117** and **117b** to form isoxazolidine **119**, **119b**.

As with the previous minimal replicators a series of reactions were conducted to determine the mechanism of reaction. The first experiment studied as with the previous system was a bimolecular control reaction and as before this is to provide a set of

reference data points to which the catalyzed reactions can be compared. Similar to the previous system, an ester control building block **117b** was used in the bimolecular reaction to exclude any recognition mediated process from the experiment. Product concentrations were deconvoluted from the individual spectra of the reaction between nitrene **117b** and maleimide **116** and plotted (**Figure 3.15** (a)) in a graph against time.

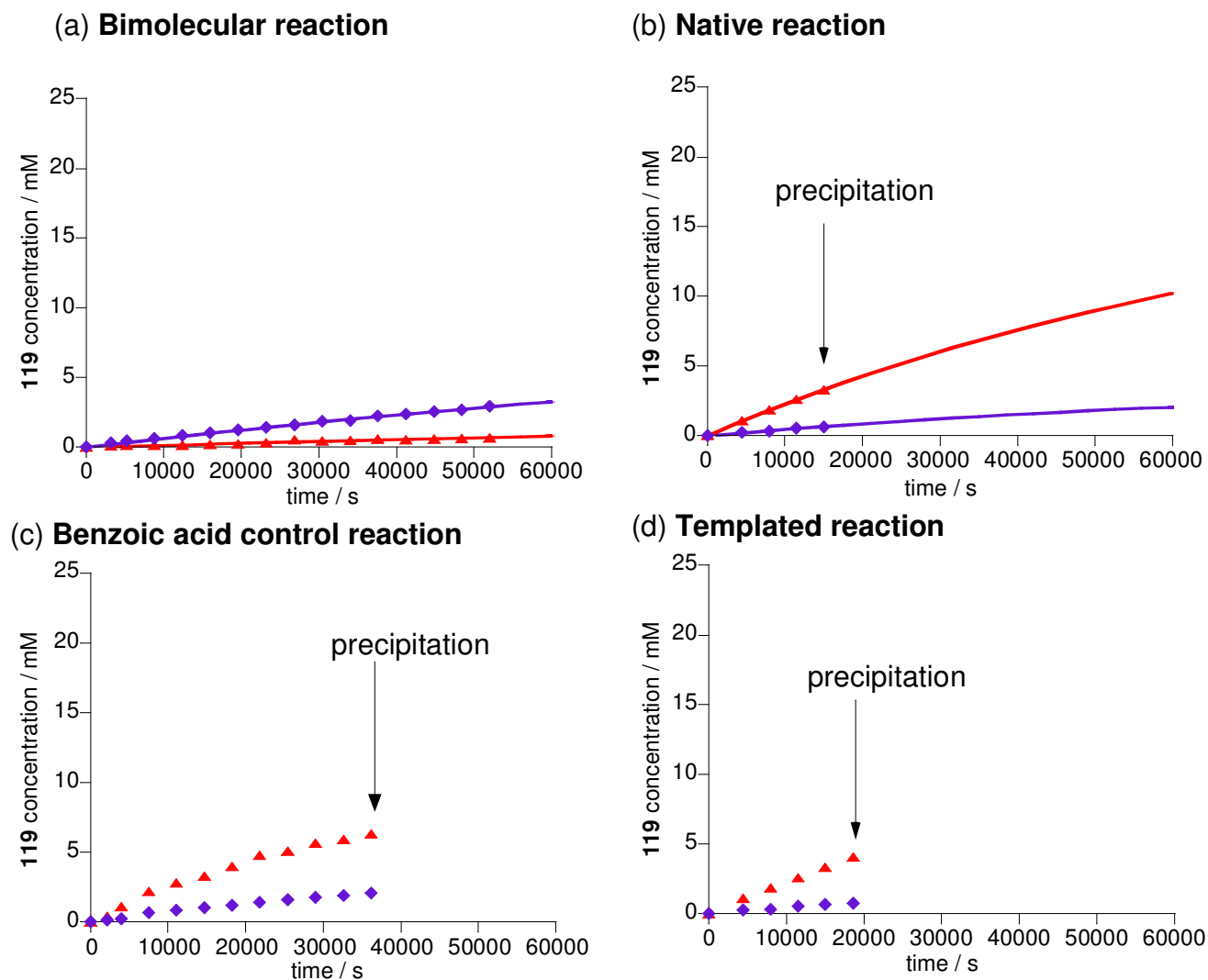


Figure 3.15 Product concentration vs. time profile, solid lines indicate optimal fit curves. (a) bimolecular reaction between equimolar concentrations of nitrene **117b** and maleimide **116** ($[117b] = [116] = 25 \text{ mM}$) at $0 \text{ }^\circ\text{C}$ in CDCl_3 , for the formation of *trans*-**119** (purple diamonds) and *cis*-**119** (red triangles). (b) native reaction between equimolar concentrations (25 mM) of nitrene **117** and maleimide **116** at $0 \text{ }^\circ\text{C}$ in CDCl_3 , for formation of *trans*-**119** (purple diamonds) and *cis*-**119** (red triangles). (c) Benzoic acid control reaction, between an equimolar concentration (25 mM) of nitrene **117** and maleimide **116** inhibited competitively with 100 mM of benzoic acid at $0 \text{ }^\circ\text{C}$ in CDCl_3 . (d) Template reaction, with the addition of 2.5 mM (0.1 equivalents) of prefabricated *trans*-template **119** to the reaction between nitrene **117** and maleimide **119** in CDCl_3 at $0 \text{ }^\circ\text{C}$. Errors in concentration are $\pm 4\%$.

Inspection of the product concentration vs. time for the bimolecular reaction revealed the formation of **119** in a 4:1 *trans* to *cis* ratio (Appendix Three). Overall conversion for the experiment in CDCl₃ at 0 °C after 14 hours is approximately 15%. A kinetic model was computationally fitted to the curves in **Figure 3.15** (a) with an R value of 5.6% to calculate (**Scheme 3.15**) rate constant, k_1 and k_2 , for the bimolecular formation of *trans*- and *cis*-isoxazolidine products.



Rate Constant/ $\times 10^{-5} \text{ M}^{-1}\text{s}^{-1}$ $k_1 = 2.61 \pm 0.07$ $k_2 = 10.6 \pm 0.01$

Scheme 3.15 Kinetic model for the bimolecular 1,3-dipolar cycloaddition reaction between maleimide **116** and nitrone **117b** and optimized rate constant k_1 and k_2 .

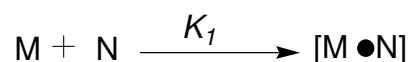
The next experiment studied was the native reaction between nitrone **117** and maleimide **116** with both recognition sites free, allowing recognition mediated processes to occur. Product concentrations were determined from the individual spectra in the standard fashion and plotted against time to produce the graph in **Figure 3.15(b)**. The graph demonstrates an overall conversion of 18% with a selectivity, for the *cis*-product over *trans*-isoxazolidine (Appendix Three), in a 5:1 ratio after 16000 seconds (4.5 hours). Initial inspection of the graph immediately reveals a number of concerns about the mechanistic nature of this potential minimal replicator. Perhaps the most obvious but least worrying of the concerns is the lack of any data points above 16000 seconds, as a result of the insolubility of the *cis*-product after this time. The *cis*-product was observed to precipitate out of solution as a gel like structure after this period of time, meaning any deconvoluted product concentrations above 4.5 hours would be inaccurate. However, this is a relatively minor problem the main trouble with the native experiment, demonstrated in **Figure 3.15** (b), is the favoring of the *cis* over the *trans*-diastereoisomer. As discussed earlier in **Figure 3.2** in the transition state diagrams, only the resultant *trans*-isoxazolidine will have the desired open structure with free recognition sites necessary for the structure to act as a template. The *cis*-transition state for the reaction between nitrone **117** and maleimide **116** has a folded over structure with overlapping recognition motifs. This structure suggests that the favoring of the *cis*-isoxazolidine could be the result of nitrone **117** and maleimide **116** reacting *via* an [A•B] binary complex. The resulting *cis*-product will maintain the closed template structure

present in the [A•B] complex and, therefore, will not be able to replicate itself in an autocatalytic fashion. Examination of the product concentration vs. time graph supports this fact as no exponential growth of the *cis*-product is observed. The [A•B] complex catalyzes the formation of the *cis*-product but the resulting product cannot catalyze its own formation, autocatalytically. Therefore, the curve for *cis*-118 in **Figure 3.15** (b) displays an increased rate of formation compared to the bimolecular *cis*-117 curve in **Figure 3.15** (a). However, this increased rate is a constant value displaying no sign of exponential growth. Additional evidence that this system is proceeding *via* an [A•B] mechanism came from the fitting of a kinetic model to the experimental data of the native reaction to determine rate constants for the catalyzed reaction. As discussed earlier only an accurate model will fit the experimental data. Therefore, when an [A•B] complex model is used to describe the native reaction a good fit of the theoretical to experimental data is observed (**Scheme 3.16**), R = 2.21%, by optimizing two parameters only, the catalytic binary complex rates k_3 and k_4 .

Bimolecular Pathways



Complex Formation



Catalytic binary complex



Scheme 3.16 Kinetic model for the native experiment between nitrone **117** (M) and maleimide **116** (N).

The first section in **Scheme 3.16** describes the bimolecular reactions which form the *cis*- and *trans*-isoxazolidines. Values for the rate constants k_1 and k_2 were calculated earlier from the optimal fit of theoretical values to the product concentration vs. time curves in **Figure 3.15** (a). The second section depicts the binary association, K_1 , which results in the formation of the [A•B] complex. Finally, the last section describes the *pseudo* unimolecular reaction between nitrone **117** and maleimide **116** in the binary complex. Analysis of the calculated rate constants for the bimolecular reactions, k_1 and k_2 , and the

binary complex reactions, k_3 and k_4 , allowed for the determination (**Table 3.2**) of the kinetic effective molarities.

Table 3.2 Table of calculated rate constants from optimal fit curves of theoretical to experimental product concentrations vs. time curves and the kinetic effective molarity of the recognition mediated reaction.

Bimolecular Reactions^a Rate constant / $\times 10^{-5} M^{-1} s^{-1}$	Recognition Mediated^a Rate constant / $\times 10^{-5} s^{-1}$	kEM^b
$k_1 = 2.61 \pm 0.01$	$k_3 = 1.20 \pm 0.01$	460 ± 46.0 mM
$k_2 = 10.6 \pm 0.07$	$k_4 = 0.23 \pm 0.01$	22 ± 2.2 mM

^a Rate constants relate directly to **Scheme 3.16**. ^b kEM, kinetic effective molarity is calculated by dividing the recognition mediated reaction over the bimolecular, $kEM = k_3 / k_1$ or k_4 / k_2 .

Analysis of the kinetic effective molarities in **Table 3.2** demonstrates the inefficiency of the two [A•B] complexes. The kEM for the formation of the *trans*- product is close to the starting concentrations of the starting materials nitron **117** and maleimide **116** (25 mM) and, therefore, is not increasing the rate above the bimolecular level. For the formation of the *cis*-isoxazolidine *via* the [A•B] complex pathway a higher effective molarity is calculated, however, it is still a relatively low value for *pseudo*-unimolecular [A•B] binary complex reaction^[123]. The low kinetic values for the two binary complexes suggest reactive sites are poorly preorganized in the [A•B] complex, which will increase entropic costs in entering the resultant transition state for the formation of the isoxazolidine.

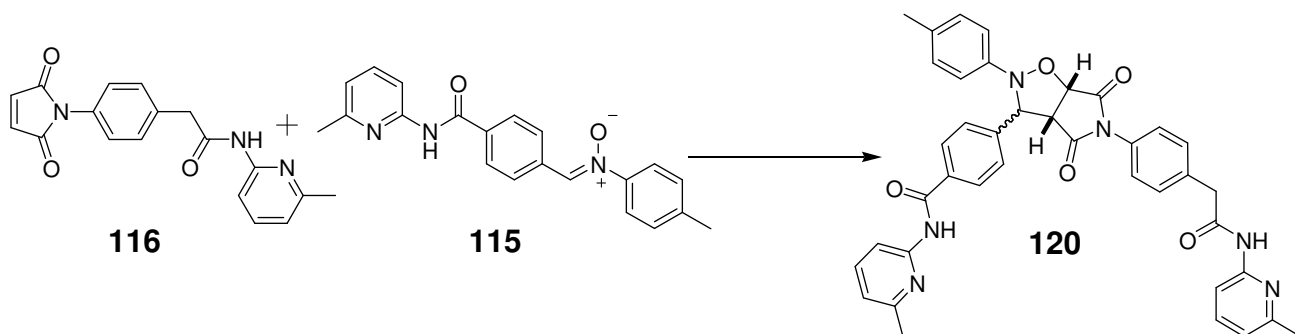
If this system is proceeding *via* a binary complex route and not an autocatalytic pathway it should still be adversely affected by a competitive inhibitor like benzoic acid. Therefore, the native reaction was repeated, but this time with the addition of 100 mM of benzoic acid at the start of the reaction. The inhibitor should block recognition sites preventing the formation of the catalytic [A•B] complex. Product concentrations for this reaction were plotted against time, to produce the graph in **Figure 3.15** (c). Inspection of this graph immediately suggests an interference in the recognition mediated processes. The *cis*-isoxazolidine remains selectively favored over the *trans*-product, but to a lesser extent than in the native experiment, in a 3:1 ratio. Also there has been a slight decrease in conversion compared to the native, from 18% to 16% after 16000 seconds in CDCl₃ at 0 °C. The fact that the *cis*-product is still favored, however, means that the recognition mediated process is still occurring, but to a lesser extent. If complete disruption of

recognition was to occur, the graph in **Figure 3.15** (c) should mirror that of the bimolecular experiment.

The information so far suggests that this system proceeds *via* an [A•B] recognition mediated *pseudo*-unimolecular complex and not the desired minimal replicating reaction mechanism. However, in order to be absolutely sure of this one last experiment has to be conducted. The addition of prefabricated *trans*-template at the start of the experiment should have no effect on the reaction if it is indeed proceeding *via* an [A•B] complex pathway. However, if the *trans*-isoxazolidine is able to minimal replicate its own formation we should observe an increase in production. Therefore, the reaction between nitron **117** and maleimide **118** was conducted with the addition of 1 mM of *trans*-**119** at the start of the reaction. The results of this experiment can be analyzed on the graph in **Figure 3.15** (d). Inspection of the native and templated experiments, **Figure 3.15** (b) and (d), reveals no significant difference, proving once and for all this system is catalyzed by a binary [A•B] complex and not an autocatalytic minimal replicator.

3.14 Potential reciprocal replicator isoxazolidine *trans*-**120**

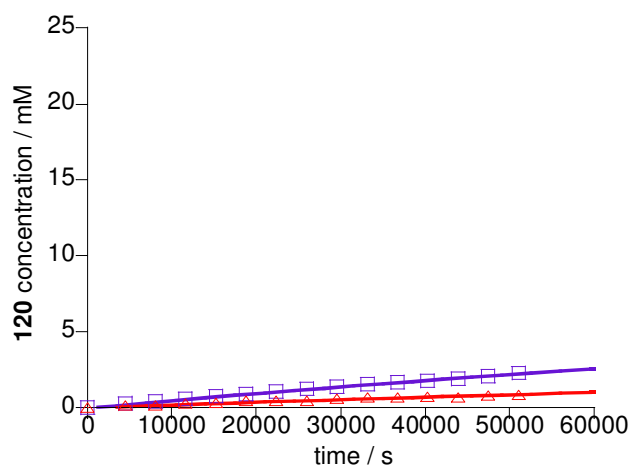
The two systems so far studied have been the two potential minimal replicators *trans*-**116** and binary complex *cis*-**119**, but now the focus of the investigation will shift to the detailed examination of the two reciprocal systems. This study will begin with the cross-catalytic formation of bis(amidopyridine) **120**, from its building block molecules, maleimide **116** and nitron **115** (**Scheme 3.17**), using dicarboxylic acid template *trans*-**121**.



Scheme 3.17 1,3-dipolar cycloaddition between maleimide **116** and nitron **115** to form isoxazolidine **120**.

As a result of the identical amidopyridine recognition motifs on starting material molecules, nitrone **115** and maleimide **116**, fewer types of experiments have to be conducted. The non-self complementary nature of the starting materials means no ester control reactions or competitive inhibition experiments are required, only two types of experiments are necessary, a bimolecular and a templated one. As usual the first experiment investigated is the bimolecular reaction. The product concentrations of the reaction between maleimide **116** and nitrone **115** were deconvoluted from the individual spectra and plotted (**Figure 3.16** (a)) against the reaction timescale.

(a) **Bimolecular reaction**



(b) **Templated reaction**

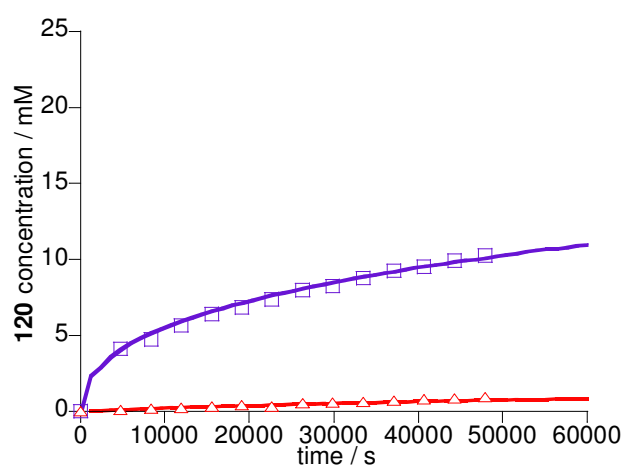


Figure 3.16 Product concentration vs. time profile for (a) bimolecular reaction between equimolar concentrations of **116** and **115** ($[\mathbf{116}] = [\mathbf{115}] = 25 \text{ mM}$) at $0 \text{ }^\circ\text{C}$ in CDCl_3 , for the formation of *trans*-**120** (blue squares) and *cis*-**120** (red triangle) and (b) templated reaction with mixture of diastereoisomers ≈ 0.1 equivalents (2.5 mM) of *trans*-dicarboxylic acid, and 0.03eq (0.8 mM) of *cis*-dicarboxylic acid template **121** ($[\mathbf{116}] = [\mathbf{115}] = 25 \text{ mM}$), for the formation of *trans*-**120** (blue squares) and *cis*-**120** (red triangles). Optimal fit curves are represented as solid lines. Errors in concentration are $\pm 4\%$.

Analysis of **Figure 3.16** (a) revealed the typical set of results for a bimolecular 1,3-dipolar cycloaddition reaction at $0 \text{ }^\circ\text{C}$ in CDCl_3 , a slow reaction with selectivity for the *trans*-isoxazolidine over its *cis* counterpart, in the ratio of approximately 3:1. Overall conversion for the experiment after 14 hours was 13%. From the product concentration vs. time curves, just like with the minimal systems, rate constants were calculated from computational fitting of a reaction model to the experimental bimolecular data (**Scheme 3.18**).



Rate Constant / $\times 10^{-5} \text{ M}^{-1}\text{s}^{-1}$ $k_1 = 0.17 \pm 0.05$ $k_2 = 0.40 \pm 0.05$

Scheme 3.18 Kinetic model for the bimolecular 1,3-dipolar cycloaddition reaction between maleimide **116** and nitrene **115**. M = **116**, N = **115**, *cis* = *cis*-**120** and *trans* = *trans*-**120**.

Values k_1 and k_2 were calculated, with an R value of 4.93%, these values will provide a reference point to which the potential cross-catalytic experiment can be compared. The R value is slightly higher than desired as a result of the difficulties of accurately measuring concentrations below 2 mM.

Examination of the templated cross-catalytic reaction was conducted through the addition of 2.5 mM of *trans*- and 0.8 mM of *cis*-isoxazolidine **121** (mixture of diastereoisomers, 3:1 *trans* to *cis*) at the beginning of the reaction between maleimide **116** and nitrene **115**. A mixture of diastereoisomers was added, as attempts to separate the *trans*- and *cis*-products proved unsuccessful. However, molecular mechanics models (**Figure 3.3**) showed the *cis*-product to have a closed structure and therefore, it will not contribute any cross-catalytic influence to the experiment. Product concentrations from the templated experiment were deconvoluted and the data plotted in a graph against time (**Figure 3.16** (b)).

Comparisons of the bimolecular and templated reaction profiles for this system immediately indicate the presence of a cross-catalytic effect. The overall conversion for the templated experiment at 0 °C in CDCl₃, after 14 hours is approximately 30%, a rise of around 20% from the bimolecular experiment. However, the most important result of the templated experiment is the amplification of the *trans*-isoxazolidine product, with an increase in *trans* to *cis* ratio from 3:1 to 12:1. When the term amplification is used it does not just mean an increase in rate, but a selective increase in rate for the formation of a specific product over any undesired products. Investigation of **Figure 3.16** (b) highlights this point, the rate for formation of the *trans*-product has increased but this is not the case for the *cis*-isoxazolidine. Examination of the *cis*-product curve for the templated experiment demonstrates a decrease in formation compared to the bimolecular reactions. This inhibitor effect is because of an increase in the concentration of starting materials, maleimide **116** and nitrene **115**, being commandeered for the formation of the *trans*-product.

Utilizing a kinetic model (**Scheme 3.19**) a theoretical curve was fitted to the product concentration vs. time curves for the templated experiment. A similar model was used to the one discussed in Chapter Two, with a few alterations, although the assumption made in Chapter two are equally applicable to the system in this Chapter. In Chapter Two the terminology *exo* and *endo* was used to describe the product cycloadducts, but from here on the terms *cis* and *trans* will be used in their place. The next important difference is as a result of the non-reversible nature of the 1,3-dipolar cycloaddition reactions between nitrones and a maleimides, in Chapter Two the Diels-Alder reactions are reversible. This difference means that all the reactions between the starting material molecules must be non-reversible in order to provide an accurate model for the system. Apart from these differences the same basic model is used as in Chapter Two.

The kinetic model utilized the values calculated for the bimolecular rate constants and the association constant K_1 , between an amidopyridine and carboxylic acid recognition motif, for bimolecular reactions and formation of binary and ternary complexes. Therefore, only two variables were optimized to achieve the best fit (with an R value equal to 2.9%), the rate constant for the catalytic ternary complex k_3 (**Table 3.3**) and the association constant K_2 ($1.60 \pm 0.01 \times 10^5 \text{ M}^{-1}$) for the product duplex [*trans*-**120**•*trans*-**121**]. Assumptions of the magnitude of the association constant K_2 can be determined utilizing the classical chelate theory, which discusses the additivity of energies of individual non-covalent interactions. An assumed value for K_2 of around K_1^2 ($1 \times 10^6 \text{ M}^{-1}$), therefore, is logical. However, the calculated value determined from fitting of the kinetic model is $K_2 = 1.6 \times 10^5 \text{ M}^{-1}$. The fact that this value is lower than K_1^2 indicates the presence of negative cooperativity, meaning that the dicarboxylic acid and bis(amidopyridine) templates in the duplex structure are not an optimal fit. An empirical value of $-4.16 \text{ kJ mol}^{-1}$ for this negative cooperativity is obtained using the equation of Gibbs free energy of connection (**Figure 3.13**).

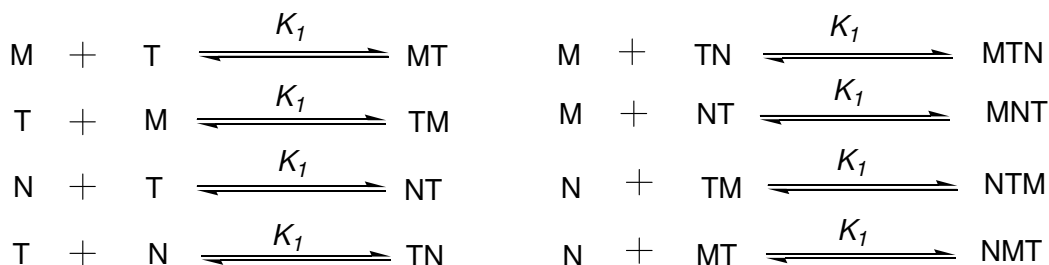
The kinetic effective molarity for the cross-catalytic formation of isoxazolidine *trans*-**120** was determined (**Table 3.3**) to be 25 M. Unfortunately, experimental attempts at determining the duplex association constant, K_2 proved unsuccessful. The insolubility of the template *trans*-**121** meant templated experiments with concentrations greater than 1.2 mM were not possible. Therefore, the fitting of a number of experiments of varying template concentration to the kinetic model to determine the accuracy of the effective molarity and duplex association constant was not possible. However, the use of the

calculated equilibrium constant can be used when investigating the complementary cross-catalytic formation of dicarboxylic acid *trans*-**121**.

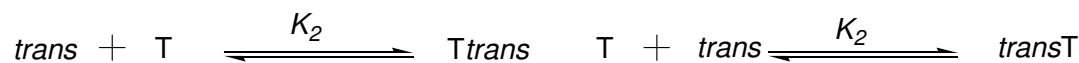
Bimolecular Reactions



Routes towards formation of binary and ternary complexes



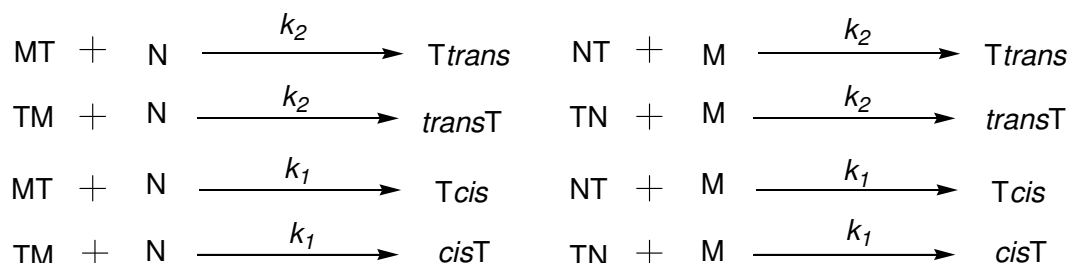
Duplex association



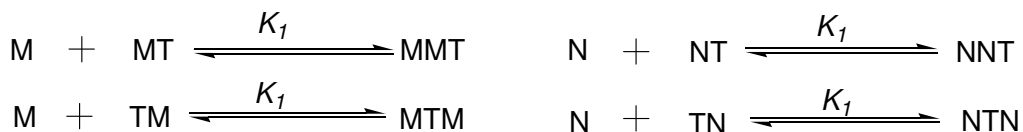
Ternary Complex reaction



Bimolecular reactions of complexes



Unproductive complexes



Scheme 3.19 Comprehensive kinetic model used in the theoretical fitting of the templated reaction between **115** and **116** for the determination of reaction rate constants. Where N = nitrone **115**, M = maleimide **116**, *trans* = *trans*-**120**, *cis* = *cis*-**120** and T = Dicarboxylic acid *trans*-**121** for System **3.14**. For System **3.15** N = nitrone **117**, M = maleimide **86** *trans* = *trans*-**121**, *cis* = *cis*-**121** and T = Bis(amidopyridine) *trans*-**120**.

Table 3.3 Table of calculated rate constants from the optimal fit curves of theoretical to experimental product concentrations vs. time curves and the kinetic effective molarity of the ternary complex reaction.

Bimolecular reactions^a Rate constants / $\times 10^{-4} M^{-1} s^{-1}$	Recognition Mediated^a Rate constant / $\times 10^{-4} s^{-1}$	kEM^b
$k_1 = 0.17 \pm 0.03$	Not recognition mediated	Not recognition mediated
$k_2 = 0.40 \pm 0.01$	$k_3 = 10.1 \pm 0.1$	$25 \pm 2.5 M$

^a Rate constants relate directly to **Scheme 3.19**. ^b kEM, kinetic effective molarity is calculated by dividing the recognition mediated reaction over the bimolecular, $kEM = k_2 / k_3$

Analysis of the concentration curve for the formation of *trans*-120 in **Figure 3.16** (b) indicates an initial acceleration in production compared to the bimolecular reaction. However, as the reaction proceeds there is a gradual decline in rate. This decrease in rate is easier to observe through plotting (**Figure 3.17**) a velocity vs. time graph of the templated experiment. The graph in **Figure 3.17** was produced from taking the first derivative of the 6th order polynomial fitted to the *trans*-120 concentration curve on **Figure 3.16** (b).

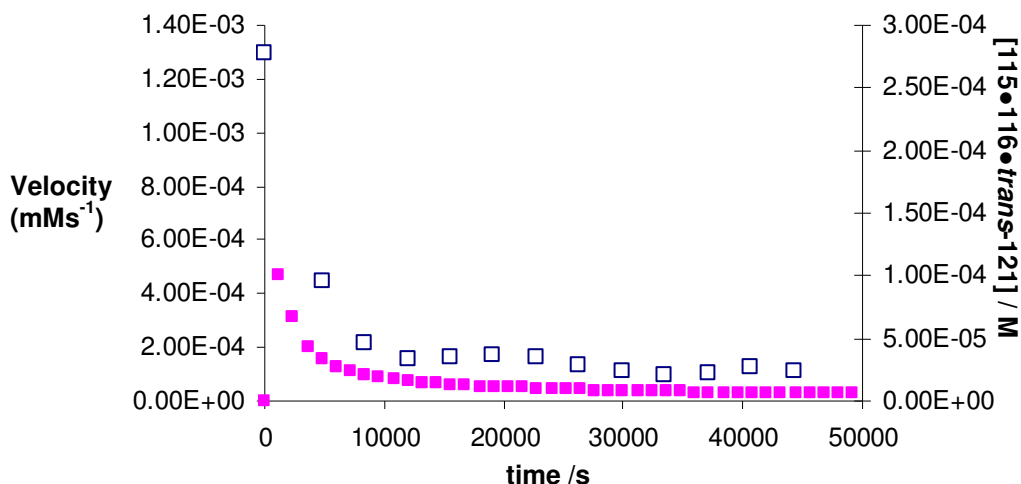


Figure 3.17 Double y-axis plot of velocity (open blue squares) or ternary complex concentration, $[115\bullet 116\bullet trans-121]$, (purple squares) vs. time (seconds). Errors in velocity and concentration are $\pm 4\%$.

Analysis of the graph in **Figure 3.17** demonstrates an initial maximum velocity (open blue squares), of approximately $1.40 \times 10^{-3} mMs^{-1}$, which decreases rapidly as the experiment progresses. The decrease in rate is supported by the curve of ternary

complex concentration vs. time in **Figure 3.17**, purple squares. This curve displays a maximum of around 1.25×10^{-4} M at 1200 seconds which decreases to 5.00×10^{-6} M after 50000 seconds. As the concentration of ternary complex is directly responsible for the increased reaction velocity, the [116•115•*trans*-121] curve mirrors the velocity vs. time curve in **Figure 3.17**. One possible explanation for this trend could be as a result of saturation of the catalyst, dicarboxylic acid *trans*-121. This saturation of the catalyst would occur if there was a large value for the stability constant, K_2 , for the duplex [*trans*-120• *trans*-121]. This would reduce the amount of free dicarboxylic acid template *trans*-121 and so inhibit the cross-catalytic formation of *trans*-bis(amidopyridine) 120. Unfortunately, as discussed previously in this section all attempts to determine a value for K_2 through experimental means proved unsuccessful. However, a theoretical value ($K_2 = 1.6 \times 10^5 \text{ M}^{-1}$) was determined through a computational fit of a kinetic model to the experimental data. In order to demonstrate the influence of K_2 , on cross-catalysis a series of simulations were run varying this association constant. These simulations utilized the previously calculated rate constants, the kinetic model in **Scheme 3.19** and the simulation package available within SimFit (isosim) to predict the outcome of the template experiment under a range of K_2 values. This program was used to predict the development of reacting species over a specified period of time, the result of these simulations is examined in **Figure 3.18**.

The graphs in **Figure 3.18** display the expected product concentration curves for the template experiment if the duplex association constant was larger or smaller than the calculated value. On the graph are also displayed the experimentally obtained product concentrations for comparison. When the value for K_2 is larger than $1.6 \times 10^5 \text{ M}^{-1}$ as in **Figure 3.18** (a) the formation the *trans*-product is initially accelerated. However, after 2 mM the reaction rate declines to that of the bimolecular rate with the dicarboxylic acid template trapped in the product duplex. Therefore, it is unable to template the formation of more *trans*-bis(amidopyridine) 120, leaving only the bimolecular pathway available for its formation. At the saturation point, although not obvious from the graph, an increase in rate of formation of the *cis*-product is simulated to occur as the ternary complex structure is no longer available to siphon off starting material.

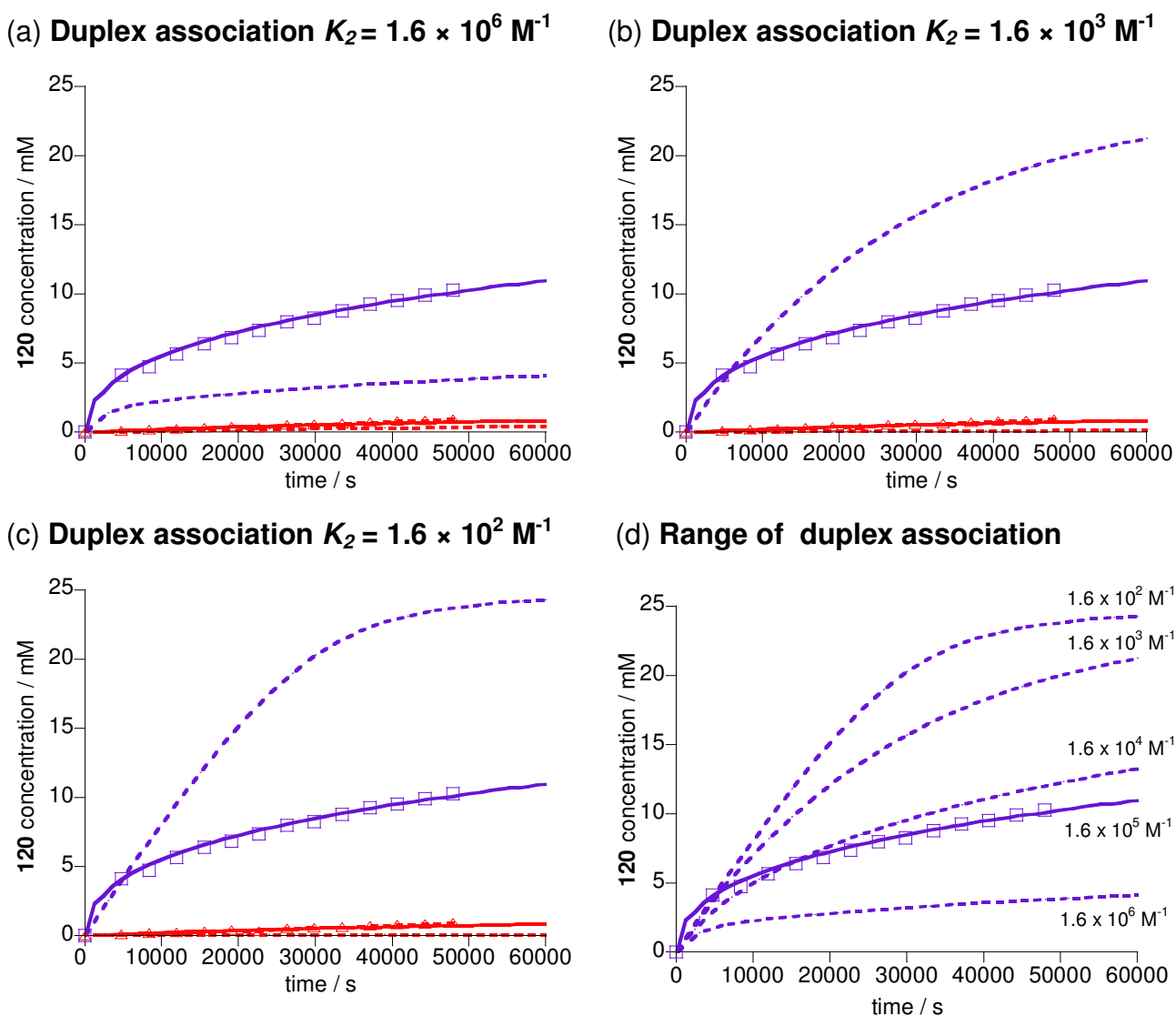


Figure 3.18 Simulated product vs. time graphs for different values of duplex, $[trans\text{-}120 \bullet trans\text{-}121]$, association constant K_2 . Between the reaction of maleimide **116** with nitron **115** cross-catalyzed with 0.1 equivalents of dicarboxylic acid template *trans*-**121**. Purple squares with solid purple line through them and red triangles demonstrate the experimentally obtained values for *trans*- and *cis*-**120** fitted to a duplex stability constant of $K_2 = 1.6 \times 10^5 \text{ M}^{-1}$. The purple and red dashed lines demonstrate simulated values for *trans*- and *cis*-**120** if an alternative value for K_2 is utilized.

When the association constant for the $[trans\text{-}120 \bullet trans\text{-}121]$ is lower than $1.6 \times 10^5 \text{ M}^{-1}$ as in the case demonstrated in **Figure 3.18** (b)-(c) the reaction displays less template saturation. The simulated *trans*-**120** product curve for a $K_2 = 1.6 \times 10^3 \text{ M}^{-1}$ demonstrates a rate maximum at the start of the reaction, but as the reaction continues catalytic turnover is reduced resulting in a decline in rate. However, as the stability constant for the product duplex is lower than in **Figure 3.18** (a), this decrease in production is to a much smaller extent than the previous simulation. The graph in **Figure 3.18** (c) shows the simulated results for an association constant $K_2 = 1.6 \times 10^2 \text{ M}^{-1}$. At

this value the binding in the product duplex is low and, therefore, the two complementary templates readily dissociate. Therefore, there is rapid turnover of catalyst and so no decrease in rate as a result of template saturation. The final graph in **Figure 3.18** (d) demonstrates the simulated product curve for the formation of *trans*-**120** over a range of different association constant values.

In addition to the isosim program in SimFit allowing for the theoretical varying of the product duplex, it also allows us to demonstrate the template experiments at high equivalents of added dicarboxylic acid *trans*-**121**. The dicarboxylic acid template was only soluble at a maximum concentration of around 2.5 mM (0.1 equivalents). Therefore, conducting templated experiments at concentrations above this proved impossible. However, the isosim program allows us to simulate the experiments over a range of template concentrations using the same kinetic model (**Scheme 3.19**) if the template was more soluble. **Figure 3.19** (a) and (b) examines the simulated templated experiment at equivalents of added isoxazolidine *trans*-**121** for the calculated [*trans*-**120**•*trans*-**121**] product duplex association constant, $K_2 = 1.6 \times 10^5 \text{ M}^{-1}$.

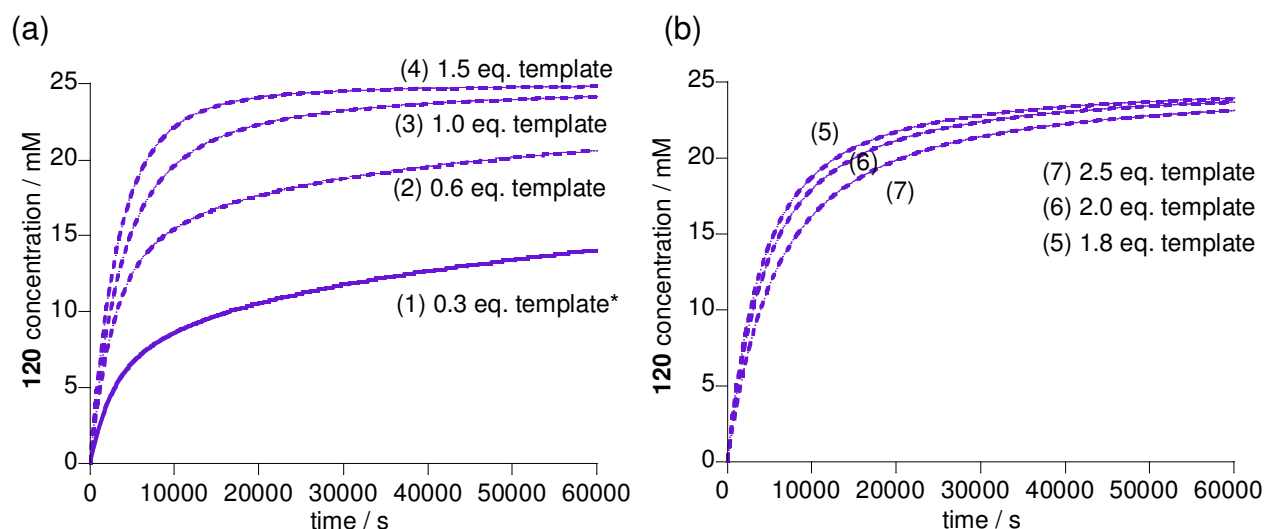


Figure 3.19 Simulated *trans*-**120** concentration vs. time graphs for a range of added dicarboxylic acid *trans*-**121**. Graph (a) simulates the templated experiment for template equivalents of (1) 0.3*, (2) 0.6, (3) 1.0 and (4) 1.5. Graph (b) simulates the templated experiment for template equivalents of (5) 1.8, (6) 2.0 and (7) 2.5. The resultant product concentration for *trans*-bis(amidopyridine) **120** are plotted as a dashed purple line, product concentration curves for *cis*-bis(amidopyridine) are excluded to clarify the graphs appearance. * Demonstrates the experimentally obtained data from the conducted experiment with 0.3 equivalents of added template. Errors are estimated to be $\pm 10\%$.

As stated earlier the large stability constant for the product duplex results in template saturation. Therefore, in the templated experiment we observed a decrease in rate after the production of 2.5 mM of bis(amidopyridine) *trans*-120, equal to concentration of added template. However, if more template is added initially, we should observe that the concentration of template saturation also increases. After more than one equivalents of template is added complete saturation of template is impossible and, therefore, no decline in rate should be observed. The simulated graphs in **Figure 3.19** support this hypothesis below one equivalents of added dicarboxylic acid template saturation is still observed (**Figure 3.19** (a)). However, in the simulations, above one equivalent of template there is no evidence of template saturation, with all the experiments proceeding to almost 100% conversion after 17 hours.

An additional advantage of conducting these templated experiment simulations is it allows us to compare the initial rate for the reaction over a range of concentrations. This goal would be impossible to achieve experimentally as a consequence of the low solubility of template *trans*-121. Because these simulations utilize parameters derived from the fitted kinetic model results of the experimental templated reaction they provide realistic values for the theoretical initial rates. Therefore, theoretical initial rates were extracted, using the same technique examined in Chapter Two, for the bimolecular and templated experiments, as well as for a range of templated simulated reactions. The values of these initial rates can be compared in **Table 3.4**.

Table 3.4 Table of initial rate for the formation of *trans*-120 at various concentration of added *trans*-121 template. The table also displays calculated rate acceleration values for each of the templated reactions.

Equivalents of <i>trans</i>-121	0 ^b	0.1 ^b	0.3 ^c	0.6 ^c	1.0 ^c	1.5 ^c	1.8 ^c	2.0 ^c	2.5 ^c
Initial rate × 10⁻³ mM s⁻¹	0.04	0.86	2.41	4.85	6.72	5.68	5.20	4.70	3.80
Rate acceleration^a	0	20	60	120	170	140	130	120	95

^a Rate acceleration is calculated by dividing initial rate of the templated experiment over that of the bimolecular, 0 equivalents of added *trans*-121. ^b Experimental conducted values. ^c Denotes simulated experiment. Errors are estimated to be ± 10% for simulated initial rates and rate accelerations.

These values are what we might expect to observe if the *cis*-**121** template was soluble above 0.1 equivalents. Examination of the **Table 3.4** indicates an increase in initial rate up until one equivalent of added template, above one equivalent there is a slow decline in the initial rate. This fact would seem to indicate an optimal template equivalent of between 1.0 and 1.5. By dividing the initial rate of a templated reaction over that of the bimolecular, it is possible to calculate the rate acceleration (**Table 3.4**). This rate acceleration can be plotted against equivalents of template to produce the graph in **Figure 3.20**.

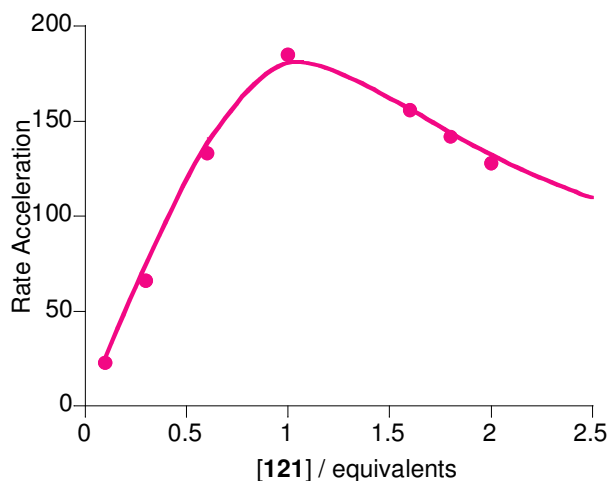


Figure 3.20 Rate acceleration vs. equivalents of dicarboxylic acid template *trans*-**121** added to the reaction between nitrones **115** and maleimide **116**. Measure rate accelerations are represented as red diamonds, the solid purple line represents a fitted curve optimized for the product duplex association.

Examination of this graph indicates that maximum rate acceleration occurs at around the addition of one equivalent (25 mM) of dicarboxylic acid *trans*-**121**, with an approximate 180 fold increase in rate compared to the bimolecular experiment. Therefore, at approximately one equivalent of *trans*-isoxazolidine **121** the greatest concentration of ternary complex possible must be present. The justification of this statement comes from the fact that rate acceleration is directly a consequence of the ternary complex reaction. Therefore, the maximum rate acceleration will occur when the concentration of ternary complex is at its greatest. At concentrations below 25 mM of complementary template excess starting material molecules, nitrone **115** and maleimide **116**, are present unassociated in the free solution. When the number of equivalents of dicarboxylic acid *trans*-**121** is above one, the building block molecules nitrones **115** and maleimide **116** become separated on different molecules of complementary template. This isolation

means they then have to dissociate and then associate on the same template molecule before they can react. This process cause the decrease in initial rate observed in **Figure 3.20**.

The solid purple line in **Figure 3.20** corresponds to an independent binding site model. This model utilizes the previously discussed principle that rate acceleration is directly proportional to the concentration of active ternary complex. For a detailed discussion of this model see Chapter One Section **1.19**. In this model a function is utilized, which describes the variation in the concentration of ternary complex with added template, to fit the observed rate acceleration. This function uses only the binding constant for the individual association, K_1 and a scaling factor as variable parameters (**Figure 3.21**).

$$\text{Solving for } [R]: [R]^2 + \left(2[T]_{tot} - [R]_{tot} + \frac{1}{K}\right)[R] - \frac{[R]_{tot}}{K} = 0$$

$$ax^2 + bx + c = 0$$

$$[TR_2] = [T]_{tot} \left(\frac{K[R]}{1 + K[R]} \right)^2$$

Figure 3.21 Equations for solving the concentration of free reagent $[R]$ and ternary complex $[TR_2]$.

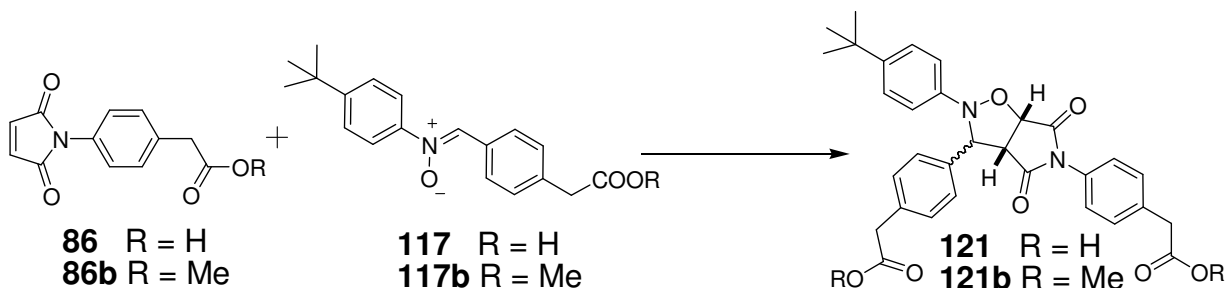
Utilizing this function the best fit for theoretical to the experimental data was obtained when an association constant of $3.50 \times 10^5 \text{ M}^{-1}$ was used for the ternary complex structure. This value is in the same order of magnitude as the theoretical determined association constant K_2 ($1.6 \times 10^5 \text{ M}^{-1}$) for the product duplex from the optimized kinetic model.

In conclusion the association between the dicarboxylic acid template *trans*-**121** and the product template bis(amidopyridine) *trans*-**120** is larger enough to observe template saturation. The experimentally obtained product concentrations for the templated reaction with 0.1 equivalents of complementary template were fitted to a stability constant value of $K_2 = 1.6 \times 10^5 \text{ M}^{-1}$. A value of this magnitude results in a decrease in production of isoxazolidine *trans*-**120** after the formation of 2.5 mM. This decline is substantial, however, the stability constant still allows a small degree of template turnover. The result of this turnover, is that reaction rate does not fall to the level of the

bimolecular reaction. If the calculated association constant value for product duplex [*trans*-**121**•*trans*-**120**] is correct similar effects should be observed in the investigation of the complementary cross-catalytic pathway.

3.15 Potential reciprocal replicator isoxazolidine *trans*-**121**

Reciprocal replicator **121** was formed from the 1,3-dipolar cycloaddition reaction between maleimide **86** and nitron **117** (Scheme 3.20)

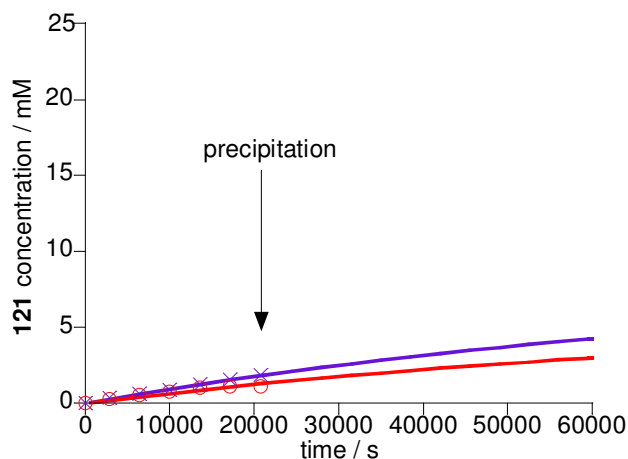


Scheme 3.20 1,3-dipolar cycloaddition between maleimide **86** and nitron **117** to form isoxazolidine **121**.

The behavior of the reciprocal replicator was investigated in identical manner to previous cross-catalytic systems. Two different types of experiment were conducted. A bimolecular experiment between maleimide **86** and nitron **117** and a templated reaction, where the formation of dicarboxylic acid **121** is potential cross-catalyzed by complementary bis(amidopyridine) *trans*-**120**. The product concentrations for these two experiments were extracted *via* deconvolution of individual spectra and plotted in two different graphs against time (**Figure 3.22** (a) and (b)).

Analysis (**Figure 3.22** (a)) of the control experiment graph reveals the expected bimolecular profile with a *trans* to *cis* selectivity of 1.5:1. Unfortunately, as a result of the low solubility, dicarboxylic acid product **121** precipitated out of solution after 20000 seconds (5.5 hours).

(a) **Bimolecular control experiment**



(b) **Templated experiment**

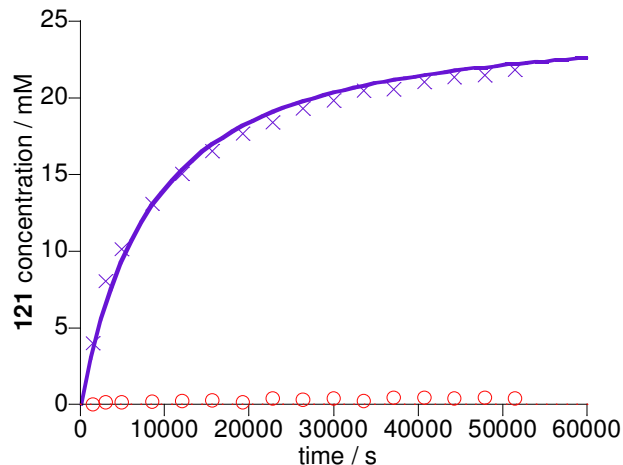


Figure 3.22 Product concentration vs. time curves. (a) Bimolecular reaction between nitrone **117** and maleimide **86** (equimolar, 25 mM) in CDCl_3 at 0 °C. Forming *trans*- (purple crosses) and *cis*- (red circles) dicarboxylic isoxazolidines **121**. (b) Templated reaction between nitrone **117** and maleimide **86** with the addition of 50 mM (2 equivalents) complementary *trans*-bis(amidopyridine) **120** at the start of the experiment. Forming *trans*- (purple crosses) and *cis*- (red circles) dicarboxylic isoxazolidines **121**. Solid lines represent computational optimal fit curves from theoretical kinetic model. Errors in concentration are $\pm 4\%$.

Overall conversion at 5.5 hours was approximately 10% in CDCl_3 at 0 °C. A bimolecular model was computationally fitted to the experiment product concentration vs. time curves in **Figure 3.22** (a) to calculate (**Scheme 3.21**) theoretically the rate constants, k_1 and k_2 , with $R = 3.50\%$.



Rate Constant / $\times 10^{-4} \text{ M}^{-1} \text{ s}^{-1}$ $k_1 = 1.15 \pm 0.02$

$k_2 = 1.64 \pm 0.02$

Scheme 3.21 Kinetic model for the bimolecular 1,3-dipolar cycloaddition reaction between maleimide **86** and nitrone **117** and optimized rate constants k_1 and k_2 .

Analysis of the fitted curves allowed a theoretical determination for the concentrations of *trans*-**121** and *cis*-**121** after 14 hours. The overall conversion after 14 hours was calculated as 25%, which will be used in the comparisons with the templated reaction.

The templated reaction could be conducted in a greater concentration of complementary template than in the reciprocal system examined in Section 3.14. This was a result of the increased solubility of the bis(amidopyridine) template *trans*-**120** compared to the dicarboxylic acid *trans*-**121**. Therefore, it was possible to conduct the template reaction several times, each time varying the concentration of isoxazolidine *trans*-**121** initially

added. The graph obtained in **Figure 3.22** (b) was the concentrations vs. time curve for the formation of dicarboxylic acid **121**, from the addition of 50 mM (2 equivalents) of bis(amidopyridine) *trans*-**120** at the beginning of the reaction. Analysis, of this templated concentration vs. time graph clearly demonstrated that the addition of isoxazolidine *trans*-**120** has accelerated the formation of dicarboxylic acid *trans*-**121**. Overall conversion after 14 hours has increased from the calculated 25% in the bimolecular reaction to approximately 90% in the templated reaction conducted at 0 °C in CDCl₃. The diastereoisomeric ratio in this templated reaction has also increased with selectivity now favoring the *trans*-product in a 50:1 ratio, compared to 1.5:1 in the bimolecular control experiment. Therefore, the addition of template has not only increased the reaction rate but has selectively favored one product over another, i.e. amplification. As investigated (**Figure 3.2**) through transition state diagrams and through molecular mechanical modeling at the start of this Chapter, the [*trans*•*cis*] duplex structure was found not to be a complementary fit. Suggesting bis(amidopyridine) *trans*-**120** would not templated the formation of dicarboxylic acid *cis*-**121**. This hypothesis is supported through examination of the templated graph in **Figure 3.22** (b). **Figure 3.22** (b) displays no evidence of the cross-catalytic formation of *cis*-isoxazolidine, in fact it actually shows inhibition compared to the bimolecular experiment. Amplification of the *trans*-product results in a lower concentration of free building block molecules, nitrone **117** and maleimide **86**, available to form the *cis*-isoxazolidine. This results in the inhibitor effect observed in the *cis* product concentration vs. time curve in the templated experiment.

In order to provide a measure of the rate acceleration observed in this cross-catalytic reaction the rate constant for the ternary complex reaction, k_3 , was calculated. This was achieved using the same technique described in previously studied replicators, through the computational fit of a theoretical model to experimentally observed data. The same model used in Section **3.14** (**Scheme 3.19**) is utilized to provide an optimal fit for the experimental data. The conditions are identical to ones used in Section **3.14**. Therefore, the same value for the binary complex association is used, $K_1 = 1000 \text{ M}^{-1}$, and the calculated stability constant for the [*trans*-**120**•*trans*-**121**] duplex, $K_2 = 1.60 \pm 0.01 \times 10^5 \text{ M}^{-1}$. The previously calculated rate constant, k_1 and k_2 , for the bimolecular reaction between nitrone **117** and maleimide **86** were also utilized, but k_1 had to be optimized to provide an optimal fit to the *cis* product curve. Therefore, using these parameters and simplex optimization of the rate constant for the ternary complex

[**86•117•trans-120**] a good fit of the experimental data to the model was obtained (**Figure 3.22 (b)**), $R = 3.0\%$.

The solubility of the added template allowed for the optimal fit of this kinetic model to a range of templated (2.5 mM, 7.5 mM, 25 mM, 40 mM and 62.5 mM) experiments at different concentrations, providing a more accurate measure (**Table 3.5**) of the rate constant k_3 .

Table 3.5 Table of calculated rate constants from the optimal fit curves of theoretical to experimental product concentrations vs. time curves and the kinetic effective molarity of the ternary complex reaction.

Bimolecular Reaction^a Rate Constant / $\times 10^{-4} M^{-1} s^{-1}$	Recognition Mediated^a Rate Constant / $\times 10^{-4} s^{-1}$	kEM^b
$k_1 = 1.15 \pm 0.01$	Not recognition mediated	Not recognition mediated
$k_2 = 1.64 \pm 0.02^c$	$k_3 = 4.70 \pm 0.15^d$	2.8 M ^d
	$k_3 = 4.01 \pm 0.40^e$	2.5 \pm 0.25 M ^e

^a Rate constants relate directly to **Scheme 3.19**. ^b kEM, kinetic effective molarity is calculated by dividing the recognition mediated reaction over the bimolecular, $kEM = k_2 / k_3$. ^c Optimized using reciprocal kinetic model. ^d Calculated from 50 mM templated experiment. ^e Calculated from simultaneous fitting of three optimal fit curves to three different templated experiments.

The kinetic effective molarity of the ternary complex reaction was calculated as 2.8 M for the templated experiment in **Table 3.5**. Through the simultaneous fitting of a series of optimal fit curves to three different templated reactions (40 mM, 50 mM and 62.5 mM of added *trans-135* a potentially more accurate measurement of k_3 could be obtained, which resulted in the calculation (**Table 3.1**) of an kinetic effective molarity of 2.5 ± 0.25 M.

When this value is compared to the kEM of the complementary ternary complex reaction [**115•116•trans-121**], in Section **3.14**, a large difference is observed. The kEM for the *pseudo*-unimolecular formation of bis(amidopyridine) *trans-120* by the dicarboxylic acid template *trans-121* was calculated as 25 M. This is considerably higher than the 2.8 M calculated for the system discussed in this section. Therefore, this implies that the *trans*-dicarboxylic acid isoxazolidine **121** pre-arranges the reactive sites of maleimide **86** and nitrene **117** in a more optimal conformation than the complementary reaction examined in this section. This enhanced pre-arrangement will result in a lower entropy cost in the

resultant *pseudo*-unimolecular reaction which will correspond to the increased the rate of formation and hence kinetic effective molarity.

In addition to allowing a more accurate determination of the catalytic ternary complex rate constant, conducting the templated experiments over a range of added template concentrations allows for individual rate accelerations to be compared against template concentrations. The templated reactions were conducted under six different initial template concentrations 2.5, 10, 25, 40, 50 and 62.5 mM (0.1 to 2.5 equivalents).

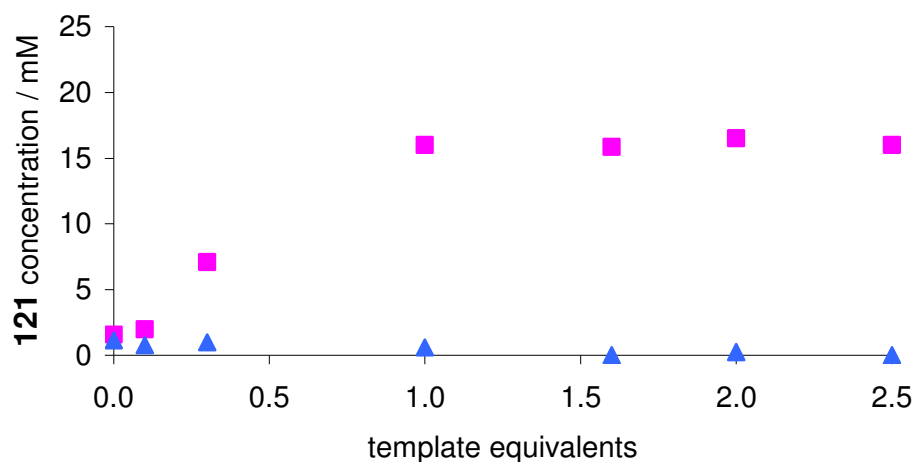


Figure 3.23 Graph of **121** concentration vs. template **120** equivalents at approximately 16000 seconds. Purple squares *trans*- template **121**. Blue triangles *cis*-isoxazolidine **121**.

The graph in **Figure 3.23** displays the product concentration of *trans*- and *cis*-**121** formed at approximately 16000 seconds. Unfortunately, after this period in some of the lower template equivalent experiments precipitation was observed to occur, meaning accurate measurement of product concentration was impossible. However, the graph in **Figure 3.23** demonstrates that the highest concentration of *trans*-product formed over this time is between one and two equivalents (25-50 mM) of added template. Analysis of the graph would indicate the ideal amount of doped template is between one and two equivalents. The *cis*-product as expected is formed in the highest concentration when no template is added, but as template equivalents increase the concentration of *cis*-isoxazolidine produced decreases.

An additional advantage of conducting the reaction over a range of template concentrations is it becomes possible to measure (**Table 3.6**) and compare initial rates for each templated reaction.

Table 3.6 Table of initial rates for the formation of *trans*-**121** at various concentrations of added *trans*-**120** template. The table also displays calculated rate acceleration values for each of the templated reactions.

Equivalents of <i>trans</i>-120	0	0.1	0.3	1.0	1.6	2.0	2.5
Initial rate/ $\times 10^{-3} \text{ mM s}^{-1}$	0.07	0.15	0.73	1.82	2.32	2.68	1.96
Errors $\pm 10^{-5} \text{ mM s}^{-1}$							
Rate acceleration^a	0	2	10	25	32	37	27

^a Rate acceleration is calculated by dividing initial rate of the templated experiment over that of the bimolecular, 0 equivalents of added *trans*-**120**. Errors in initial rate and rate accelerations are assumed to be $\approx 4\%$.

Through the comparison of initial rates of templated to that of the bimolecular experiments it is possible to calculate a value of rate acceleration, which can be plotted against time to produce the graph in **Figure 3.24**.

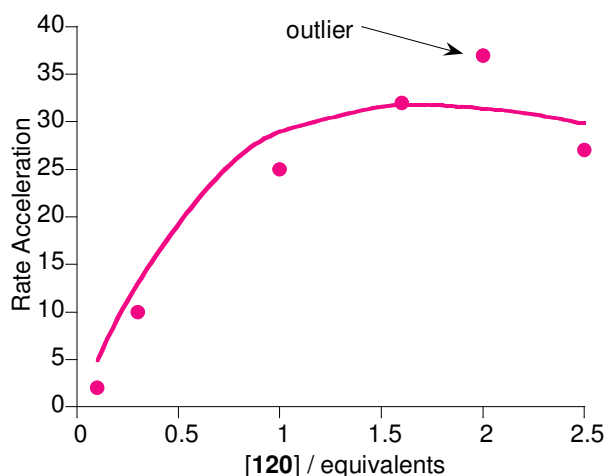


Figure 3.24 Rate acceleration vs. equivalents of bis(amidopyridine) template *trans*-**120** added to the reaction between nitrones **117** and maleimide **86**. Measure rate accelerations are represented as red diamonds, the solid line represents the best fit from independent binding model.

The circles in **Figure 3.24** indicate the experimentally measured rate accelerations calculated from dividing the initial rate of the templated reaction at a specific concentration over that of the initial rate of the bimolecular reaction ($r_{\text{catalyzed}}/r_{\text{bimolecular}}$). Examination of the plot reveals that a maximum rate acceleration of approximately 40 fold is obtained when 1.5-2.0 equivalents of bis(amidopyridine) **120** is added. The maximum rate acceleration logically must occur at the greatest concentration of catalytic ternary complex. Therefore, at around 1.8 equivalents of *trans*-**120**, the uncomplexed

concentration of maleimide **86** and nitroene **117** must be at a minimum, with the majority of these starting materials present in the [**86**•**117**•*trans*-**120**] complex. In template experiments below 1.8 equivalents the maximum possible concentration of ternary complex is unattainable as a result of building block molecules existing uncomplexed in the free solution. Whereas, in template experiments above 1.8 equivalents the starting material molecules nitroene **117** and maleimide **86** become isolated on different molecules of the bis(amidopyridine) template. Therefore, starting materials have to dissociate and then associate on the same molecule of template, causing the decline in rate observed in **Figure 3.24**.

The solid purple line in **Figure 3.24** corresponds to an independent binding site model. This model utilizes the previously discussed principle that rate acceleration is directly proportional to the concentration of active ternary complex. In this model a function is utilized, which describes the variation in the concentration of ternary complex with added template, to fit the observed rate acceleration. This function uses only the binding constant for the product duplex, K_2 and a scaling factor as variable parameters (**Figure 3.21**). Unfortunately, the fit was very poor, suggesting a ternary complex association constant of 1000 M^{-1} , which is considerably less than the calculated product duplex [*trans*-**120**•*trans*-**121**] stability constant of $1.6 \times 10^5 \text{ M}^{-1}$. The fact that the experimentally obtained curve does not fit the theoretical one could be a result of measured errors. At high equivalents of template the reaction proceeds too fast for the product concentration to be measured in the ideal first 5-10% overall conversion. This problem could result in inaccurate initial rates, which could explain the reason why the theoretical curve does not fit the experimentally observed curve. In order to try and circumvent this problem initial rates were determined through using the isosim program in SimFit. This program utilizes the kinetic model in **Scheme 3.19** and the calculated and experimental determined association constants (K_1 , K_2) and rate constants (k_1 , k_2 and k_3) to simulate the product concentration vs. time curves over a range of bis(amidopyridine) template concentrations. The initial rates can be extracted (**Table 3.7**) from these simulations and used to determine rate accelerations.

Table 3.7 Table of simulated initial rates for the formation of *trans*-**121** at various concentration of added *trans*-**120** template. The table also displays calculated simulated rate acceleration values for each of the templated reactions.

Equivalents of <i>trans</i>-120	0	0.1	0.3	1.0	1.6	2.0	2.5
Initial rate/ $\times 10^3 \text{ mM s}^{-1}$	0.10	0.40	1.00	2.63	2.09	1.76	1.49
Errors $\approx \pm 10^{-4} \text{ mM s}^{-1}$							
Rate acceleration^a	1	4	10	27	21	18	15

^a Rate acceleration is calculated by dividing initial rate of the templated experiment over that of the bimolecular, 0 equivalents of added *trans*-**120**. Errors in initial rate and rate accelerations are assumed to be $\approx 10\%$.

These rate accelerations could then be plotted against the equivalents of added template *trans*-**120** to produce the graph in **Figure 3.25**.

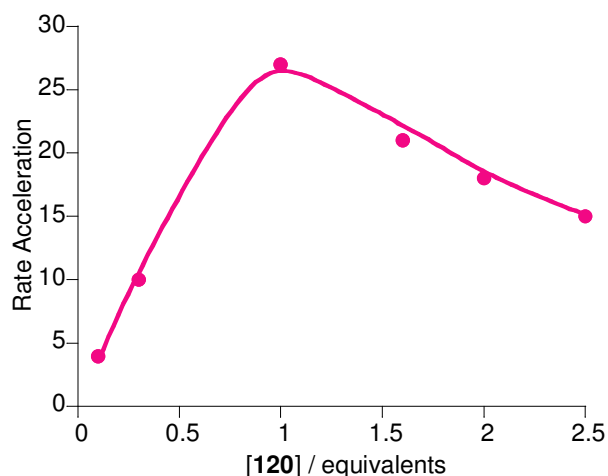


Figure 3.25 Simulated rate acceleration vs. equivalents of bis(amidopyridine) template *trans*-**120** added to the reaction between nitrones **117** and maleimide **86**. Measure rate accelerations are represented as red circles, the solid line represents the best fit from independent binding model.

The theoretical rate accelerations points display a different trend to the experimentally determined values in **Figure 3.24**. A maximum acceleration is observed at around 1.0 equivalents of added bis(amidopyridine) *trans*-**120**, instead of between 1.5-2.0 equivalents as indicated from the experimentally obtained values. As before the independent binding site model was fitted to the determined rate accelerations. However, unlike in **Figure 3.24** a much better fit is observed for these simulated values. This model calculated a ternary complex association constant of $K = 2.7 \times 10^5 \text{ M}^{-1}$, which is much closer in magnitude to the value for the product duplex

[*trans-120•trans-121*], $1.6 \times 10^5 \text{ M}^{-1}$. Interesting in Chapter Two it was claimed errors were greater at larger rate accelerations. However, when the rate accelerations for the simulated are compared to the experimentally obtained values in this Chapter the errors at very high rate accelerations, 1.6-2.5 equivalents are lower than at lower rate accelerations, 0.1-1 equivalents. One possible explanation is at lower equivalents of bis(amidopyridine) template rate acceleration is still too fast to be measure accurately by ^1H NMR spectroscopy and when the first data point is recorded the rate has already started to decrease as a result of inhibition caused by the stability of the [*trans-120•trans-121*] duplex. With the result being that a lower initial rate is measured. However, at template concentrations above one equivalent of *trans-120* product inhibition by duplex stability is not an issue and there is along time available to measure the rate before the curve starts to level off. The experimentally measured rate acceleration were obtained from a series of single templated reactions, ideally these reaction should be repeated in order to provide more accurate measurements.

As in Chapter Two we have demonstrated that difficulties in determining the initial rate experimental can be overcome through using detailed kinetic modeling and simulation to provide values with improved accuracy and decreased errors.

3.16 Hypercyclic networks^[146-148]

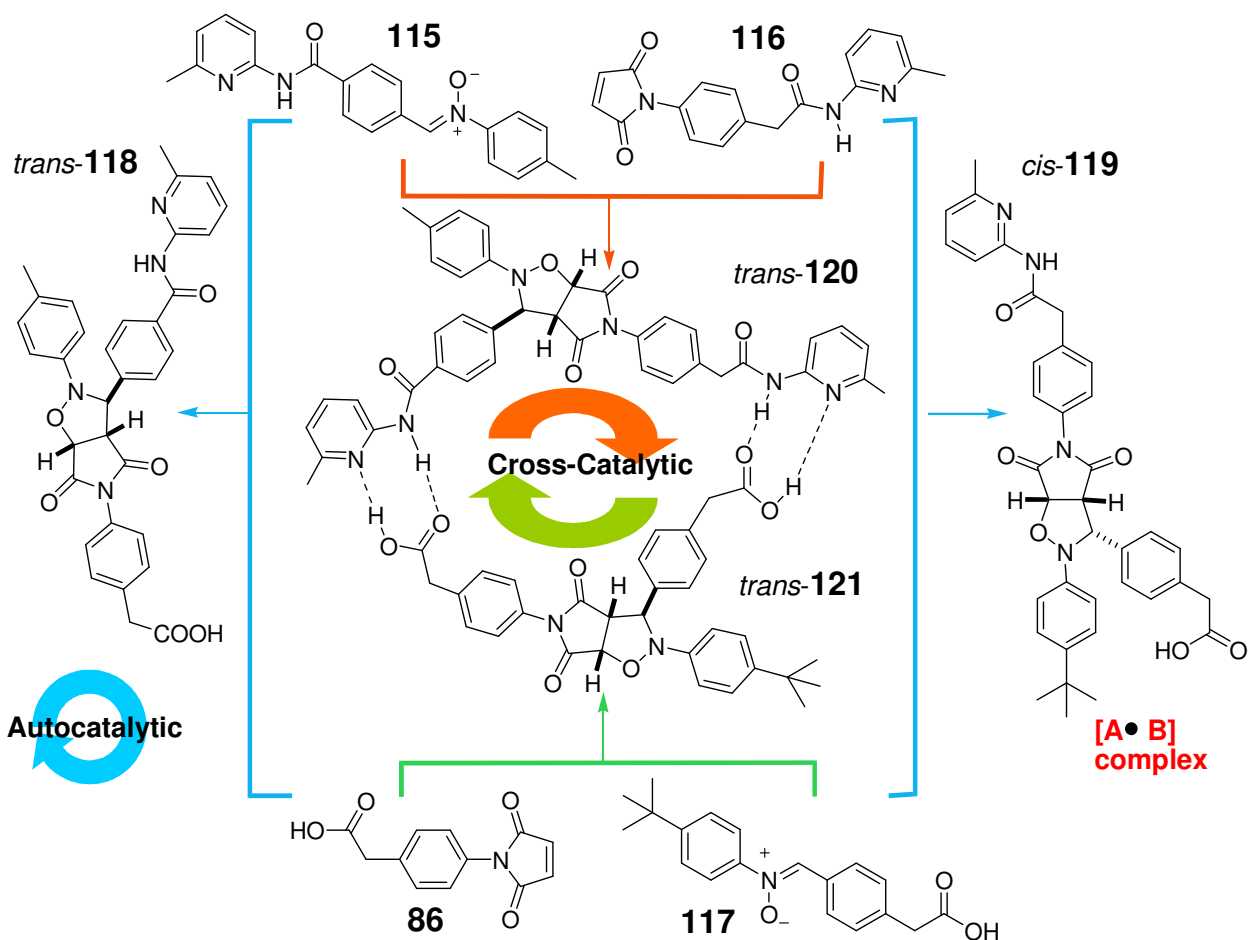
The investigation of hypercycles is expected to reveal important information into the nature of intricate evolving biochemical networks and macroscopic ecosystems^[172-176]. However, we are only interested in investigating the different mechanisms of replication involved in these networks.

Hypercyclic networks were discussed in detail in Chapter One Section 1.20, therefore, only a brief reminder will be given at this point. A hypercyclic network arises from a replicating network of minimal replicators exhibiting weak autocatalysis. In non-enzymatic conditions sub-exponential growth, as a consequence of template saturation, results in the arrangement of self-replicating systems into a cross-catalytic partnership. This collaboration inevitably results in co-existence with the increased production of one replicator causing a rise in formation of its partner. This process is demonstrated by the diagram in **Figure 1.51**.

Now if a self-replicating network is combined with a reciprocal replicating network the possibility of creating a series of different cross-catalytic processes occurs. In such a complex network not only would the two complementary reciprocal systems cross-catalyze each others formation, but the two minimal replicators might also cross-catalyze one another's formation. If such a thing occurred the result would be a complex hypercyclic network.

The goal at the start of this Chapter was to endeavor to design a series of replicating templates, this objective, however, was unsuccessful. Unfortunately the potential minimal replicator examined in Section 3.13 was proven to proceed *via* an [A•B] complex pathway instead of the desired minimal reproducing route. As a consequence of this fact our replicating network consists (**Scheme 3.22**) of an [A•B] binary complex, two reciprocal and one minimal replicating system.

The reason for developing a series of replicating templates was so that we could investigate a potentially complex hypercyclic network. As discussed previously a hypercyclic network consists of a series of different replicators, composed of common starting materials, which can cross-catalyze one another's formation. When these replicating templates are forced to co-exist, one of two things can happen. The first is a Darwinian evolution^[177-183] survival of the fittest situation, where only the most efficient templates will survive commandeering starting materials from their inefficient counterparts. Another possibility is that instead of competing, each replicating system aids its counterparts by cross-catalyzing the formation of the other in a hypercyclic network, which in turn ensures its own survival.



Scheme 3.22 Building block molecules maleimide **116**, **86** and nitron **117**, **115** can react to form minimal replicators *trans*-**118**, cross-catalytic templates *trans*-**120**, *trans*-**121** and closed template structure *cis*-**119**, formed via [A•B] complex.

Regrettably, the presence of an binary [A•B] complex system instead of the desired minimal replicators means that it will be impossible to study the interactions which might occur in a complex hypercyclic network, using the systems designed in this Chapter.

However, we decided to carry on with investigating the replicating and binary complex systems which make up the network demonstrated in **Scheme 3.22**.

In order to study such a network a series of four component experiments (nitron **115**, **117** and maleimide **86**, **116**) were conducted. The investigation of this network is conducted in a similar manner to how the replicators were studied in isolation, with bimolecular control, recognition mediated native and templated reactions. The goals of each type of reaction are also identical to before. The aim of the bimolecular reaction control is to provide data on the non-catalyzed reactions between the different nitrones and maleimides to provide a reference point to which all recognition mediated and template experiments can be compared. As with bimolecular reaction controls in the

minimal system and [A•B] binary complex system (Section 3.12 and 3.13) ester equivalents of **117b** and **86b** were used in this control experiment. The native reaction was designed to allow for the recognition mediated interactions necessary for replication, therefore, all recognition sites on building block molecules **115-117** and **86** were readily available. The purpose of the templated reactions was to selectively enhance the formation of a desired product by addition of the complementary template at the start of the experiment. All experiments were conducted with an initial concentration of 25 mM for the four starting material molecules nitrones **115,117** and maleimides **116, 86**. As when the systems were studied in isolation these starting materials were monitored in CDCl₃ at 0 °C overnight. The product and starting material peaks deconvoluted in the ¹H NMR spectra for these experiments, in order to determine species concentrations, can be examined in Appendix Six.

The ester control reaction between maleimide **86b, 116** and nitrone **115, 117b** proceeded very slowly at 0 °C in CDCl₃, as is evident from the analysis (**Figure 3.26 (a)**) of the bar chart of product concentration after 6.5 hours. Overall conversion (for all possible isoxazolidines) after 6.5 hours was approximately 3%. This low conversion clearly demonstrates that no amplification and hence no replication is occurring in this control experiment. The conversion is so low that there is no point in comparing the selectivity between the different diastereoisomers or isoxazolidines.

The native reaction was conducted using maleimide **116, 86** and nitrone **115, 117** at 0 °C in CDCl₃ overnight. Unfortunately, precipitation occurred after 6.5 hours and so product concentrations were extracted after this timeframe and plotted in a graph (**Figure 3.26 (b)**). Examination of **Figure 3.26 (b)** immediately reveals evidence of catalysis and replication. Overall conversion for the reaction after 6.5 hours is approximately 45%, compared to 3% after 16 hours for the ester control experiment. The ratio between *trans*- and *cis*-diastereoisomers has also dramatically changed as demonstrated in **Table 3.8**.

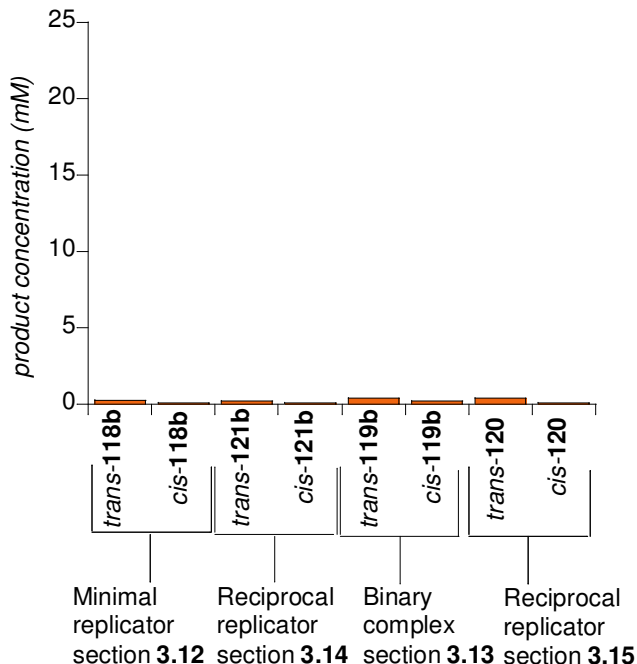
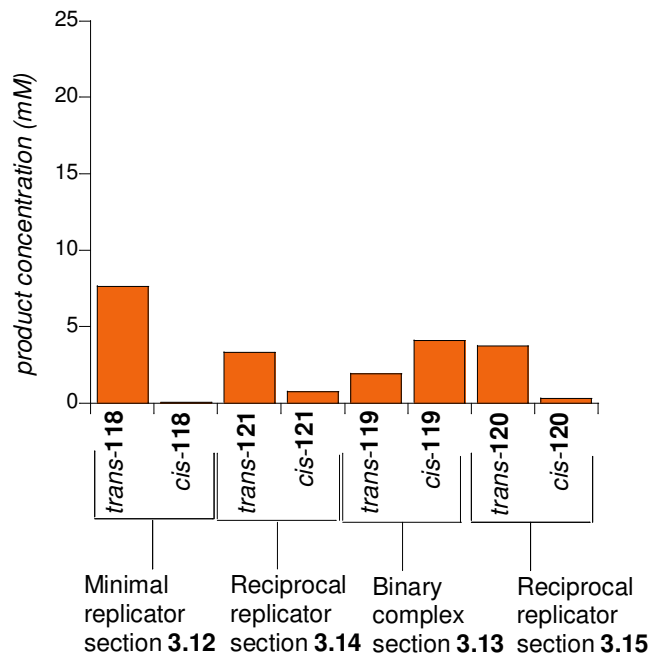
(a) **Bimolecular ester control reaction**(b) **Recognition mediated Cycle 1 (native)**

Figure 3.26 (a) Results of ester control reaction between equimolar concentration (25 mM) of maleimide **86b**, **116** and nitrone **115**, **117b** in CDCl_3 after 16 hours. (b) Results of recognition mediated reaction equimolar concentrations (25 mM) of maleimide **86**, **116** and nitrone **117**, **115** in CDCl_3 after 20000 seconds.

The largest increase in selectivity is observed for the minimal replicating and [A•B] complex pathway reactions. The selectivity for the minimal replicator *trans*-**118** in the native reaction has increased approximately 18 folds, 75:1 (7.50:0.10 mM) compared to the bimolecular experiment, 4:1 (4.10:1.90 mM). For the production of isoxazolidine **119**, selectivity has been reversed from favoring the *trans*-product in the bimolecular control to the closed template structure in *cis*-**119**. An increase in production and selectivity can be observed for the formation of reciprocal templates *trans*-**121** and *trans*-**120**. The selectivity for *trans*-**121** over *cis*-**121** has increased from 3:1 (0.37:0.12 mM) in the bimolecular control to 5:1 (3.30:0.70 mM) in native reaction. For the complementary template *trans*-**120** there has been a greater increase in selectivity between the bimolecular and native experiments. The selectivity for **120** has increase from 4:1 (0.40:0.10 mM) in the bimolecular to 13:1 (3.75:0.30 mM) in the native experiment. The increase in selectivity in the native reaction for *trans*-**120** and *trans*-**121** isoxazolidine is a consequence of the cross-catalysis occurring between these two complementary templates. To sum up the native reaction demonstrates the presence of

both forms of replication (minimal and cross-catalytic), as well as the recognition mediated [A•B] complex process. The most efficient complexes in this replicating network appear to be the minimal replicating and [A•B] binary systems with both these products formed in the greatest concentration.

Table 3.8 Table of *trans* to *cis* ratio of non-associative isoxazolidines **86b**, **117b**, **116** and **115**, and associative isoxazolidines **86**, **117**, **115** and **116**, for bimolecular and native four component experiments

	<i>trans:cis-118/b</i>	<i>trans:cis-121/b</i>	<i>trans:cis-119/b</i>	<i>trans:cis-120</i>
Bimolecular experiment	4:1	3:1	2:1	4:1
Native experiment	75:1	≈5:1	1:2	≈13:1

After investigation of the native system, the next logical test of the replicating network is to investigate the mechanism of selectively favoring one particular system. In order to achieve this goal the experiment was designed similar to the native reaction, by reacting maleimide **86**, **116** and nitron, **115**, **117** together in CDCl₃ at 0 °C, but with the addition of prefabricated template at the beginning of the reaction. This type of experiment was carried out for one minimal and one reciprocal replicating template. The resulting product concentration for each of these reactions after 6.5 hours was recorded. Although precipitation did not occur after 6.5 hours for comparison with the native experiment product concentrations were recorded after this time period. Each reaction was compared to the native experiment and the difference in individual product concentrations between the templated and native experiments (Δ) was plotted (**Figure 3.28** (a) and (b)) on a graph of Δ concentration vs. product diastereoisomer. A second graph of the natural logarithm (ln) of the ratio of the templated to native product concentration ($[T_{\text{product}}]:[N_{\text{product}}]$) was also plotted (**Figure 3.28** (b)). However, the resultant graph was unclear, as when the concentration was low even a small difference in concentration produced a large value. As mentioned previously at low concentrations below 0.1 mM accurate measurement by deconvolution of ¹H NMR spectra was impossible. Therefore, we decided produce a new graph but link it to concentration of product formed, which should provide a more accurate comparison (**Figure 3.28**) and provide an enhancement factor (**Figure 3.27**).

$$\text{Enhancement Factor} = \ln\left(\frac{[\text{Template}]}{[\text{Native}]}\right) \times C_T$$

[Template] = concentration of product in the template experiment after 6.5 hours

[Native] = concentration of same product in the native experiment after 6.5 hours

C_T = Product concentration in templated experiment

Figure 3.27 Equation for determination of enhancement factor.

The Enhancement factor was obtained by multiplying the natural logarithm utilized in **Figure 3.28** (b) by the concentration of the particular isoxazolidine examined, produced in the templated experiment. The result of this calculation was the plot in **Figure 3.28** (c). A positive enhancement factor value indicates increased formation in the templated experiment compared to the native. A negative value indicates decreased production compared to the native experiment. The charts in **Figure 3.28** (a)-(c) excludes the addition of the prefabricated template from the concentration values, therefore only product formed in the reaction are taken into consideration.

The graph in **Figure 3.28** examines the results of the templated experiment between the four components, nitrones **115**, **117** and maleimide **86**, **116**, templated with 0.1 equivalents (2.5 mM) of dicarboxylic acid *trans*-**121** isoxazolidine. The experiment was conducted overnight with an overall conversion of 46% after this time period, equal to the native experiment.

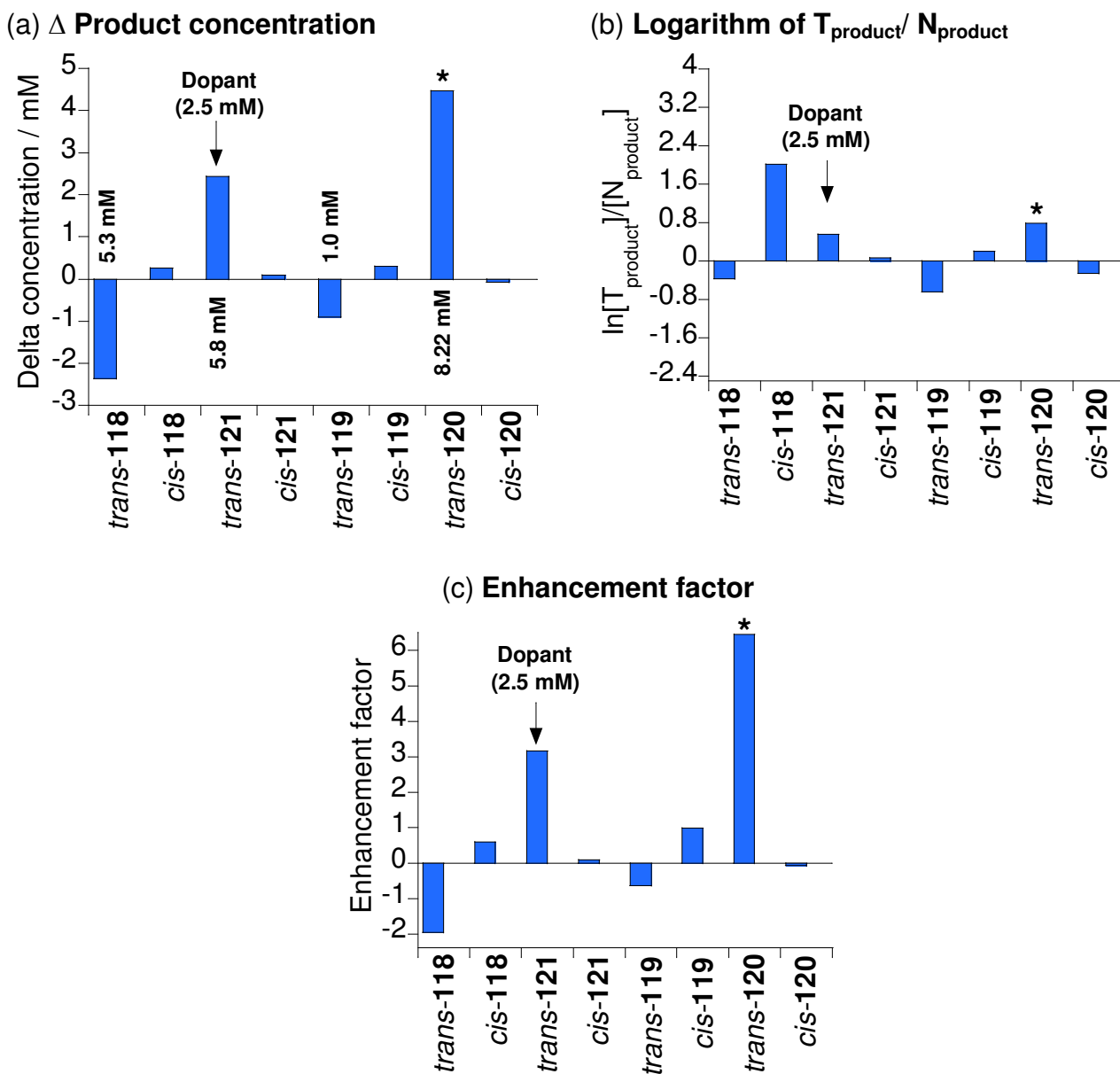


Figure 3.28 Dicarboxylic acid *trans*-121 templated (≈ 2.5 mM) equimolar four component reaction (maleimide [86], [116] and nitrones [115], [117] equals 25 mM). (a) Δ product concentration, templated subtracted from negative isoxazolidine concentration vs. diastereoisomers. Actual product concentrations of major products for this four component reaction are include on the graph above or below bar (b) Natural log of ratio $[T_{\text{product}}]/[N_{\text{product}}]$. (c) Graph of enhancement factor for each individual isoxazolidine product. *Expected enhanced products. Errors in concentration are $\pm 4\%$.

Although, overall conversion of this templated experiment is the same as the native, **Figure 3.28** (a) demonstrates that the distribution of individual products is not. The largest increase in concentration is for the complementary partner of the dicarboxylic acid template, bis(amidopyridine) *trans*-120. There has been an increase in the formation of *trans*-120 isoxazolidine by 5 mM compared to the native experiment. This increase in the production of isoxazolidine **120** has been specifically for the *trans*-

diastereoisomer with no increase in formation of the *cis*-product. Actually examination of **Figure 3.28** (a) and (c) indicates there has been a slight decrease in the production of *cis*-**120** isoxazolidine. This selective increase in the synthesis of *trans*-**120** has resulted in an increase in the *trans* to *cis* ratio from 13:1 in the native reaction to 36:1 in the dicarboxylic acid templated experiment. This increase in formation of the *trans*-**120** template has itself resulted in an increase in production of the added dicarboxylic isoxazolidine *trans*-**121**, by ≈ 2.5 mM. The cross-catalytic nature of *trans*-**121** and **120** means the increased production of one should result in an increase in formation of the other. This fact is demonstrated by the graphs in **Figure 3.28** (a) and (c). Again this increase is selective for the *trans*-diastereoisomer only, resulting in a rise in the *trans* to *cis* ratio from 5:1 in the native to 9:1 in the templated experiment. The increased production of the two reciprocal templates has not been matched by the minimal replicating system *trans*-**118**. This is not unsurprising as an increase in production of *trans*-isoxazolidines **120** and **121** means there is less starting materials nitrones **115**, **117** and maleimide **86**, **116** available. The expected consequence of this should be a decline in the production of *trans*-**118** and *cis*-**119** isoxazolidine. While this hypothesis is indeed the case for the minimal template *trans*-**118** the *cis*-**119** template is relatively unaffected. Actually examination of the enhancement factor indicates there has actually been a slight increase in production of the *cis*-**119** isomer. The reason for this rise is not known. However, as mentioned earlier there has been a decrease in production in minimal replicator *trans*-**118**, which has been accompanied by a small increase in production of its diastereoisomer *cis*-**119**. This effect has resulted in a decrease in the *trans* to *cis* ratio from 75:1 in the native to 18:1 in this templated reaction. The reason for the rise in production of *cis*-**118** is a consequence of fall in formation of *trans*-**118**. With less of the minimal template around there is more chance of nitron **115** and maleimide **86** reacting *via* a bimolecular route to form the closed structure *cis*-**118** product. In conclusion the dicarboxylic acid templated experiment has selectively favored the formation of the reciprocal *trans*-templates **120** and **121** over their minimal replicating and [A•B] complex system competitors.

Having studied the four component experiment with the addition of reciprocal template at the beginning, the next logical experiment is to try doping the four component reaction with prefabricated minimal template. This experiment was conducted under the standard conditions with 2.5 mM of *trans*-**118** isoxazolidine added at the start of the reaction. The

resultant product concentration for this experiment were extracted and compared with the native experiment (**Figure 3.26**) to afford the two graphs in **Figure 3.29**.

(a) Δ product concentration

(b) Enhancement factor

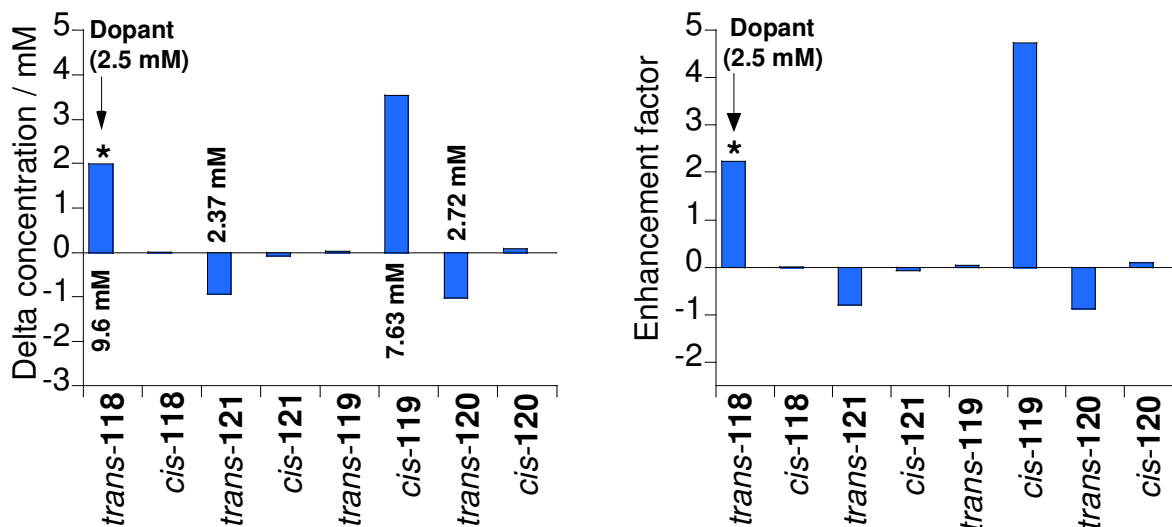


Figure 3.29 Minimal replicator *trans*-118 templated (≈ 2.5 mM) equimolar four component reaction (maleimide [86], [116] and nitrones [115], [117] equals 25 mM). (a) Δ product concentration, templated subtracted from negative isoxazolidine concentration vs. diastereoisomers. Actual product concentrations of major products for this four component reaction are include on the graph above or below bar. (b) Natural log of ratio $[\text{Template}_{\text{product}}] / [\text{Native}_{\text{product}}] \times C_T$, enhancement factor, vs. diastereoisomers. *Expected enhanced product. Errors in concentration values are $\pm 4\%$.

Examination of the two graphs in **Figure 3.29** immediately reveals an increase in the synthesis of *trans*-118 and *cis*-119 isoxazolidines. Through doping the experiment with *trans*-118 template, it has increased its own formation *via* self-replication by 2 mM. Although an increase of 2 mM is substantial the enhancement factor is decreased, as a large concentration of *trans*-118 is formed in the native experiment. As anticipated the minimal template is selective for the production of the *trans*-diastereoisomer only with no increase in production of the *cis* product. This effect has increased the *trans* to *cis* ratio from 75:1 in the native to 96:1 in this templated experiment. The increase in *trans*-118 in this experiment is accompanied by a large increase, 4 mM, in concentration of the [A•B] binary complex product *cis*-119. This large increase in concentration compared to the native has resulted in a high enhancement factor of approximately 5. This increase has arisen from the fact that by forming a greater concentration of *trans*-118, less nitrone 115 and maleimide 86 are available to form the isoxazolidines 120 and 121. The result of this is more maleimide 116 and nitrones 117 are available to form closed template

structure *cis*-119. The increased production of *cis*-119 has raised the selectivity from 1:2 in the native to 1:4 in the *trans*-118 templated experiment. For the reasons discussed earlier, the increased production of *cis*-119 and *trans*-118 has indirectly inhibited the formation of reciprocal replicators *trans*-120, 121 as demonstrated through analysis of the Δ concentration and enhancement factor graphs.

In order to conclude our investigation of this replicating network one final experiment remained. This experiment involved conducting another cycle of the native reaction, Cycle two, but with the addition of a 20 mol% solution of the original native experiments left to run to competition. The goal of this experiment was to investigate the effect of repeating the native reaction but with quantities of all replicating templates added at the start of the reactions. It was hoped that this addition would result in the selective production of all the replicating isoxazolidines at the expense of the unwanted products. This experiment was conducted in an identical fashion to before and the resultant product concentrations were extracted from deconvolution of the ^1H NMR spectra after 6.5 hours. These isoxazolidine concentrations were compared to the original native experiment and plotted (**Figure 3.30** (a) and (b)) in the two graphs below, using the procedure described earlier.

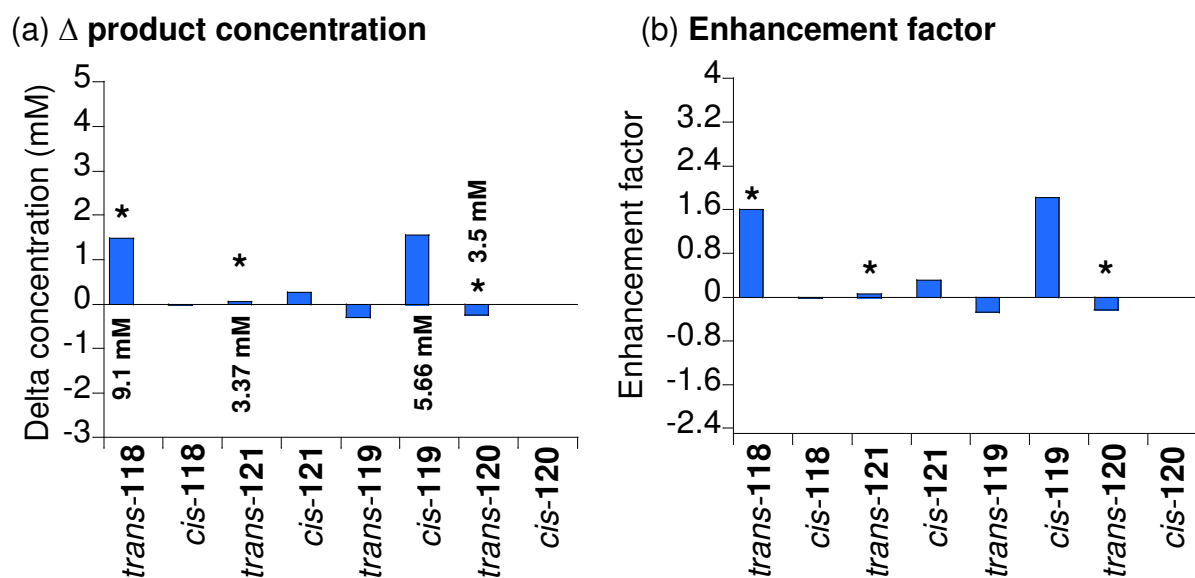


Figure 3.30 20 mol% native templated Cycle Two experiment, equimolar four component reaction (maleimide [86], [116] and nitrones [115], [117] equals 25 mM). (a) Δ product concentration, templated subtracted from negative isoxazolidine concentration vs. diastereoisomers. Actual product concentrations of major products for this four component reaction are include on the graph above or below bar. (b) Natural log of ratio $[\text{Template}_{\text{product}}] / [\text{Native}_{\text{product}}] \times C_T$, enhancement factor, vs. diastereoisomers. *Expected enhanced product. Errors in concentration values are $\pm 4\%$.

Scrutiny of Cycle Two in **Figure 3.30** (a) and (b) reveals our initial hypothesis was incorrect, not only has the minimal replicator *trans*-**118** increased but the binary complex product *cis*-**119** has also increased. However, the remaining two reciprocal templates display no noteworthy change. The formation of *trans*-**118** and *cis*-**119** isoxazolidines has increased by around 1.5 mM compared to the native reaction. Although template *trans*-**118** is still the major product (9 mM) the largest enhancement factor is in the formation of *cis*-**119**, which has increased in concentration from 4.1 to 5.5 mM. This enhanced formation of the closed structure is an indirect effect of the increased production of template *trans*-**118**. An increase in formation of *trans*-**118** removes starting materials necessary for the formation of reciprocal **120** and **121** products. The result of this eradication means there is an increased concentration of nitrones **117** and maleimide **116** allowing more of *cis*-**119** to be formed at an increased rate. The reason why there is no observable increase in production of reciprocal *trans*-**120**, -**121** is a direct effect of the efficiency of the self-replicating *trans*-**118** isoxazolidine and saturation. As demonstrated in Section **3.12** the additional of even small quantities of minimal template to the reaction of nitrones **115** and maleimide **86** resulted in an immediate exponential growth in isoxazolidine *trans*-**118** production. From investigation of this self-replicator a high association constant, $K_a = 8.8 \times 10^6 \text{ M}^{-1}$, for the product duplex was determined. However, despite the resultant low turnover of catalyst the reaction still displayed exponential growth. Therefore, when investigating the minimal system in the above Cycle Two, despite all the possible inhibitor interactions *trans*-**118** isoxazolidine was still able to replicate itself. This achievement occurs even though only very small concentrations of free *trans*-**118** are present in solution at any one time. The reciprocal replicators *trans*-**120** and -**121**, however, as demonstrated from their study in isolation, experience template saturation when less than 1 equivalent of complementary partner is added. This effect is a result of the high stability constant, $K_a = 1.6 \times 10^5 \text{ M}^{-1}$, for the [*trans*-**121**•*trans*-**120**] product duplex. The ratio of *trans*-bis(amidopyridine) **120** to dicarboxylic acid **121** in the added 20 mol% native experiment solution was 1:1. This ratio meant *trans*-**120**, **121** isoxazolidine were present almost completely in the duplex structure, meaning they were unable to template the formation of each other when added to the new cycle (Cycle Two). These small quantities of free reciprocal templates were probably associated in unproductive complexes. As discussed in Kelly's templated

synthesis Chapter One (Section 1.11), unproductive complexes inhibit catalysis preventing any noticeable template effect.

Investigation of the replicating network in **Scheme 3.22** has demonstrated a number of interesting features. The native experiment illustrated that all four recognition mediated processes (minimal, reciprocal replication and binary [A•B] complex) occurred to some extent. However, the minimal replicator *trans-118* was the most efficient under these competitive circumstances. This efficiency was again highlighted in the Cycle Two experiment. The final interesting feature from these four component experiments was the ability to selectively enhance either a minimal or reciprocal replicator through the addition of one or the other at the beginning of the experiment.

3.17 Conclusions

At the beginning of the Chapter we wanted to design a series of replicators formed from the 1,3-dipolar cycloaddition reactions between a maleimide and a nitron. The reason for this aim was to allow for a fairer comparison between the different replicating systems, one of the problems with the system examined in Chapter Two. An additional advantage was that the reactions could be conducted at lower temperatures, allowing for stronger association between recognition sites, another problem with the system in Chapter Two. Although we were successful in developing two reciprocal and one minimal replicating system, one of our systems turned out to be non-reproducing, instead progressing through an [A•B] binary complex (**Table 3.9**). The result of this was that we were unable to investigate complex hypercyclic networks through combining the replicators in one experiment.

Table 3.9 Overview of the results for replicating systems examined in this Chapter.

System	isoxazolidine	Mechanism	kEM
3.12	<i>trans-118</i>	Minimal Replicator	21 M
3.13	<i>trans-119</i>	Binary complex	22 mM
	<i>cis-119</i>	Binary complex	460 mM
3.14	<i>trans-121</i>	Reciprocal replicator	25 M
3.15	<i>trans-120</i>	Reciprocal replicator	2.5 M

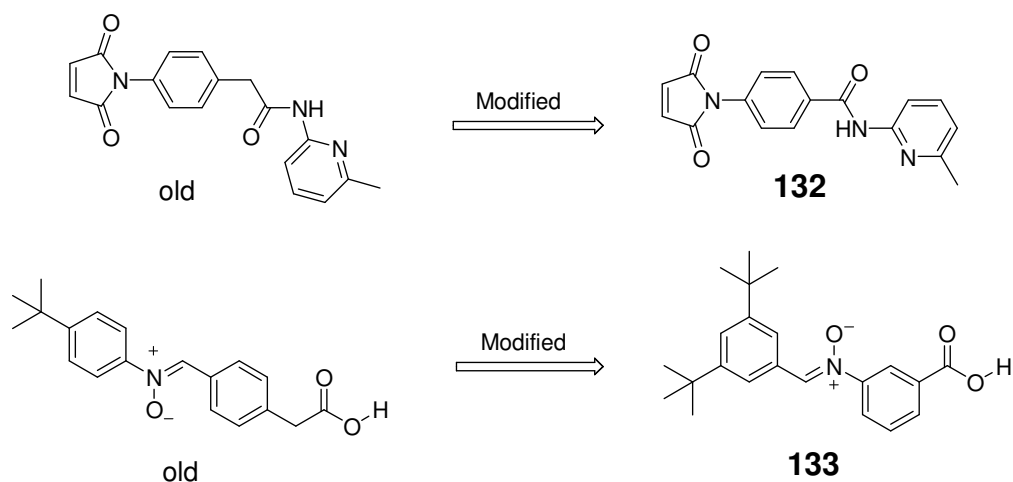
Investigation of the replicating network (**Scheme 3.22**) revealed that the most efficient system appeared to be the minimal replicator *trans*-**118**. In addition investigation of the four component experiments revealed it was possible to selectively enhance the formation of a particular replicator through doping the reaction with its complementary template.

3.18 Future Work

In this Chapter we examined three replicating systems and an [A•B] binary complex. It was this binary complex which was the major limitation. This complex prevented the analysis of a potentially complex hypercyclic network. Therefore, our goal in designing and synthesizing a new replicating network should be to replace this binary complex with a minimal replicating system. In this Chapter we successfully designed, synthesized and analyzed a minimal and two cross-catalytic templates. Therefore, we wanted to try and avoid too much structural change to these replicators when designing the new minimal replicator. In fact, no changes have to be made to the self-replicator in Section **3.12**, but changes will have to be made to reciprocal templates as a consequence of redesigning the binary complex system.

It was hypothesized that the reason for the potential minimal replicator in Section **3.13** turning out to be a binary complex was a consequence of over flexibility in the starting material structures. This structural flexibility of nitrones **117** and maleimide **116** molecules must allow the approach of reactive sites in the [A•B] complex which induces covalent bond formation resulting in the formation of closed template structure *cis*-**119**. In order to circumvent this problem we decided to redesign these nitron and maleimide molecules. The rigidity of these starting materials was increased by removing (**Scheme 3.23**) a CH₂ spacer fragment in the molecule's backbone, directly linking the recognition motifs to a rigid phenyl ring.

Another modification was carried out to the newly designed nitron through reversal of the C=N double bond. In the nitrones used in this system the recognition motif has always been attached to the C side of the C=N bond, however, in this new nitron the recognition group is attached to N side.



Scheme 3.23 New maleimide **132** and nitron **131** starting materials.

This change will alter the configuration of the expected isoxazolidine replicator. Instead of the *trans*-configuration being the replicating template it will actually be the *cis*-replicator, for reasons discussed in Chapter Four. We will therefore, be able to investigate the first *cis*-replicators. The lowest energy conformations of both *cis*- and *trans*-diastereoisomers form the reaction between nitrones **133** and maleimide **132** were calculated using molecular mechanics. A series of Monte Carlo conformational searches were performed, starting from minimized conformations of *trans*-**134** and *cis*-**134** utilizing the MMFFs forcefield and the GB/SA solvation model for CHCl_3 . **Figure 3.31** shows the global minimal conformations for the *trans*-**134** and *cis*-**134** and product duplex structures. Notice the *cis*-**134** has an open recognition structure whereas *trans*-**134** has a more folded over structure.

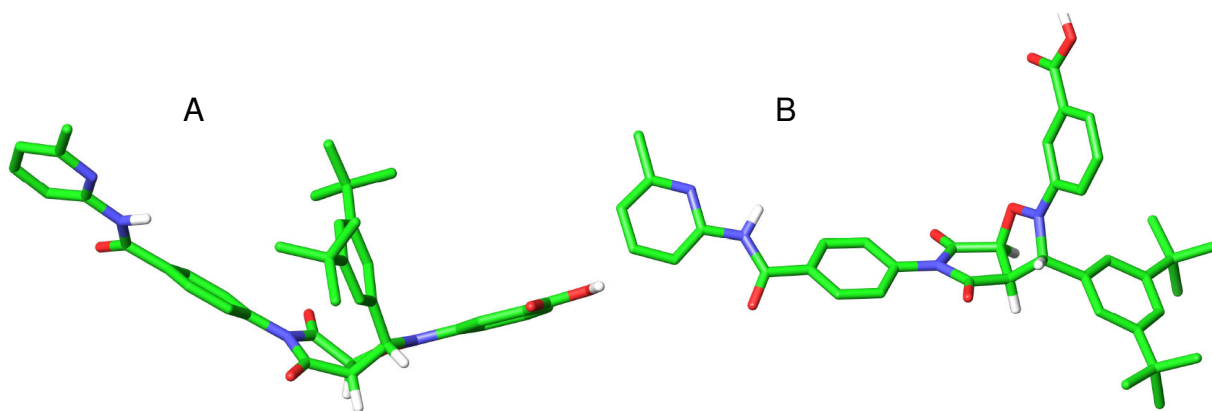


Figure 3.31 Molecular mechanics structures; (a) *cis*-**134** and (b) *trans*-**134**. Carbon atoms are green, nitrogen atoms are blue, oxygen atoms are red and hydrogen atoms are blue. Majority of hydrogen atoms removed for clarity.

Chapter 4 Redesign of a replicating network

4.1 Design of a replicating network

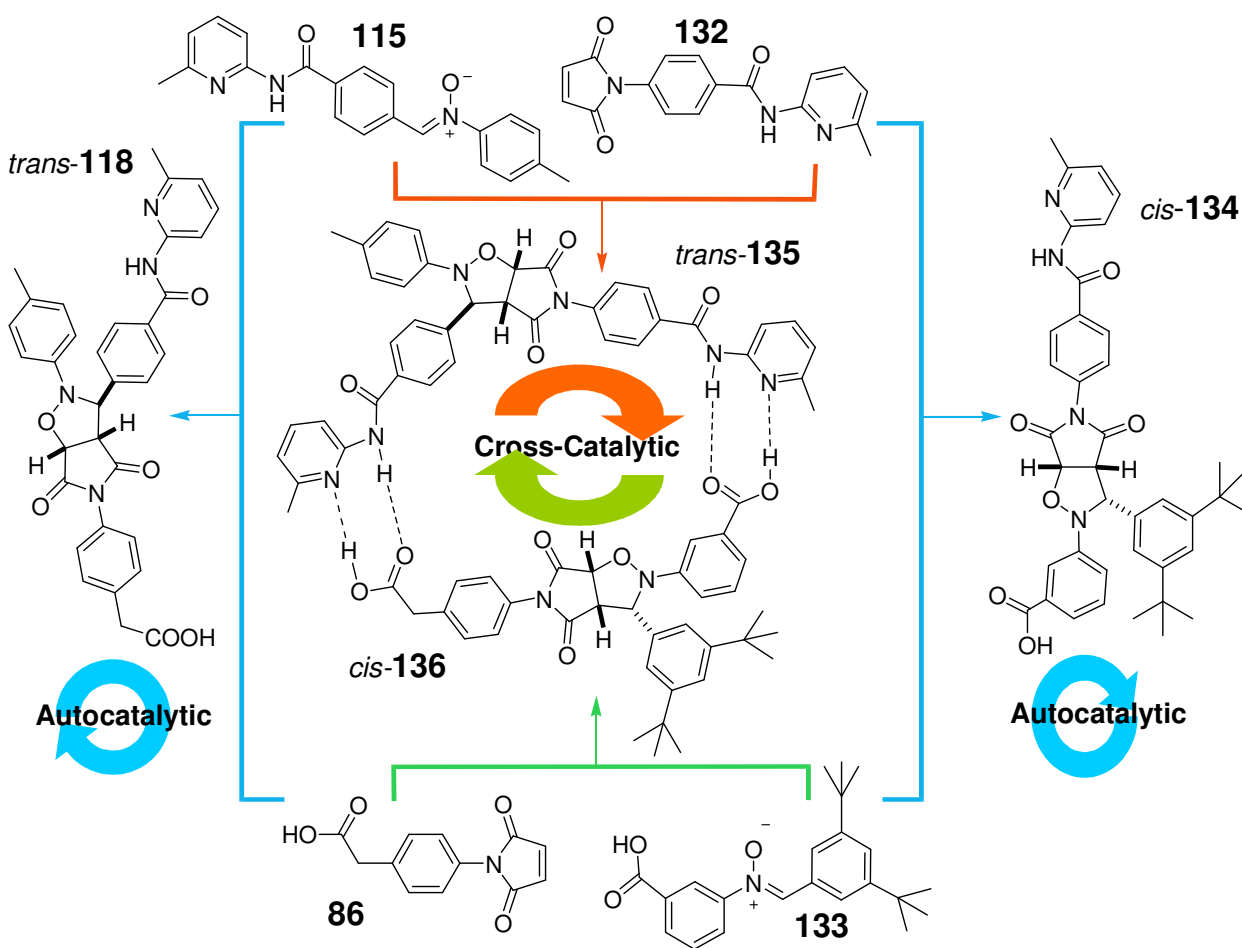
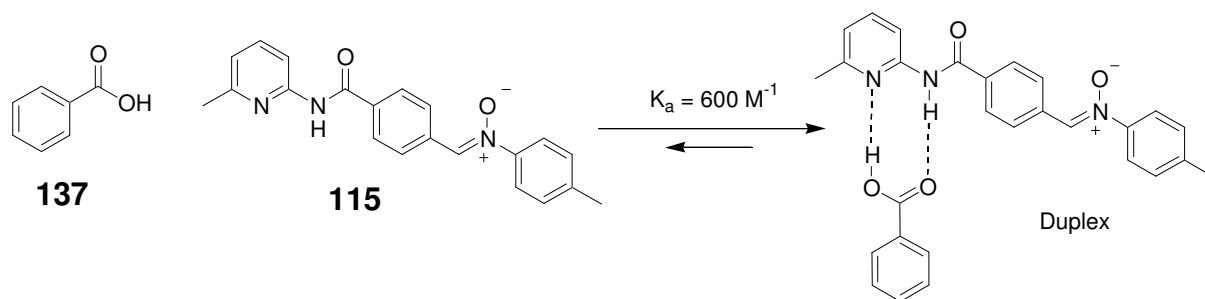


Figure 4.1 Building block molecules maleimide **132**, **86** and nitron **115**, **133** can react to form minimal replicators *trans*-**118**, *cis*-**134** or cross-catalytic templates *trans*-**135**, *cis*-**136**.

The need for a significant redesign of two of the building blocks, **116** and **117**, required by our minimal and reciprocal replicating systems was discussed at the end of the preceding chapter. In order to investigate a potentially hypercyclic network properly, systems containing two minimal and two reciprocal templates are required. Nitron **133** and maleimide **132** will undergo a 1,3-dipolar cycloaddition to form the *cis*-isoxazolidine **134**, which as a consequence of the self-complementary nature of the template has the potential to replicate itself autocatalytically. However, **Figure 4.1** also demonstrates that by modifying the two aforementioned starting material molecules, the two resultant potential cross-catalytic templates are altered. The two reciprocal systems are transmuted to varying extents, with the bis(amidopyridine) template *trans*-**118** being the

less effected. As it has only reduced in size by one CH₂ spacer compared to its counterpart in Chapter Three. However, this change will affect the molecule's overall size and flexibility, which in turn will influence its potential catalytic properties. Comparing the dicarboxylic acid recognition template **136** to its counterpart in Chapter Three **121**, a much more substantial series of changes have been made. As with the bis(amidopyridine) template **135**, the carbon skeleton of the molecule has been reduced in size by removing a single CH₂ fragment, which in turn has indirectly affected the recognition site. In the previous chapters the recognition site on the dicarboxylic acid templates has been a derivative of phenylacetic acid, by abstracting the CH₂ spacer, one of the carboxylic acids has been converted to a benzoic acid derivative. This modification to the recognition site could influence the magnitude to which it can associate with its complementary partner, bis(amidopyridine) **135**. As a result of this new recognition motif a new association constant value, K_a , had to be determined for the association between benzoic acid and amidopyridine recognition group. This value was determined through the dilution of a 100 mM 1:1 solution of the complex, between benzoic acid **137** and nitrone **115** (Scheme 4.1), utilizing 500 MHz ¹H NMR spectroscopy at 0 °C in CDCl₃ (For a detailed discussion and data see Section 7.5).



Scheme 4.1 The association between **137** and **115** in CDCl₃ at 0 °C.

The concentration of the 1:1, 100 mM solution, of nitrone **115** and **137** was diluted from 100 mM to 1 mM and in a manner identical to previously conducted K_a dilution studies, the chemical shifts arising from the proton resonances of the pyridine ring were recorded as the sample was diluted. Fitting of the chemical shift data to the appropriate isotherm afforded a $K_a = 600 \pm 60 \text{ M}^{-1}$. This value is lower than the association constant for the phenyl acetic acid counterpart bound to nitrone **115** ($1000 \pm 100 \text{ M}^{-1}$). The lower K_a value could have detrimental or beneficial consequences to the effectiveness of the

resultant templates bearing this recognition group. This association constant could decrease the catalytic efficiency of the template as a result of the poor association of complementary recognition partners. Conversely it could also improve catalysis, the resultant product duplex may have a weaker association constant K_a resulting in greater turnover of the catalyst and hence an increased rate of replication.

Another difference in the dicarboxylic acid template is the *cis* stereochemistry of the isoxazolidine ring, which is also present in the 'new' minimal template **134**. All the previous replicators have had a *trans* configuration, the reason for this change in product stereochemistry can be explained by examining the starting material nitrone **133** from which the reciprocal and minimal templates **134** and **136** are constructed. This 'new' nitrone has a different relationship between the 1,3-dipole and the recognition site to nitrones discussed in earlier chapters. In previous nitrones the recognition containing fragment has always been placed on the carbon side of the C=N double bond. However, in the new nitrone **133** the recognition is on the nitrogen side of the C=N double bond, the effect of this change can be seen by examining the transition state diagrams of the resultant 1,3-dipolar cycloaddition between the 'new' nitrone **133** and a recognition bearing maleimide and the previous nitrones with the same maleimide (**Figure 4.2**).

Figure 4.2 shows the different conformations which occur in the transition state between a 1,3-dipolar cycloaddition reaction, between the previous and 'new' nitrones (with recognition sites **B**, **Figure 4.2**) with a maleimide (with complementary recognition site **A**, **Figure 4.2**). For the previous nitrones, the left column in **Figure 4.2**, the *trans* transition state has the nitrone and maleimide with an open conformation in which the recognition sites **A** and **B** are held far apart. This conformation translates into an open configuration in the product template, with the recognition sites still in an open position, free to associate with their complementary partners. The *cis* transition state for these nitrones, however, results in an unwanted closed template structure, in which **A** and **B** recognition sites are folded over on each other with the recognition loci blocked from associating with their complementary partners. Therefore, for the previous nitrones, it is the *trans*-product form the cycloaddition reaction that is used as template for replication, however this situation is reversed for the 'new' nitrone.

In the case of the 'new' nitrone it can be demonstrated from **Figure 4.2** that the *cis*-configuration in the transition state results in the recognition sites **A** and **B** being held at opposite ends and not the *trans* conformation. This conformation translates into the

product template having an open configuration with the recognition loci available to associate with partners containing complementary recognition.

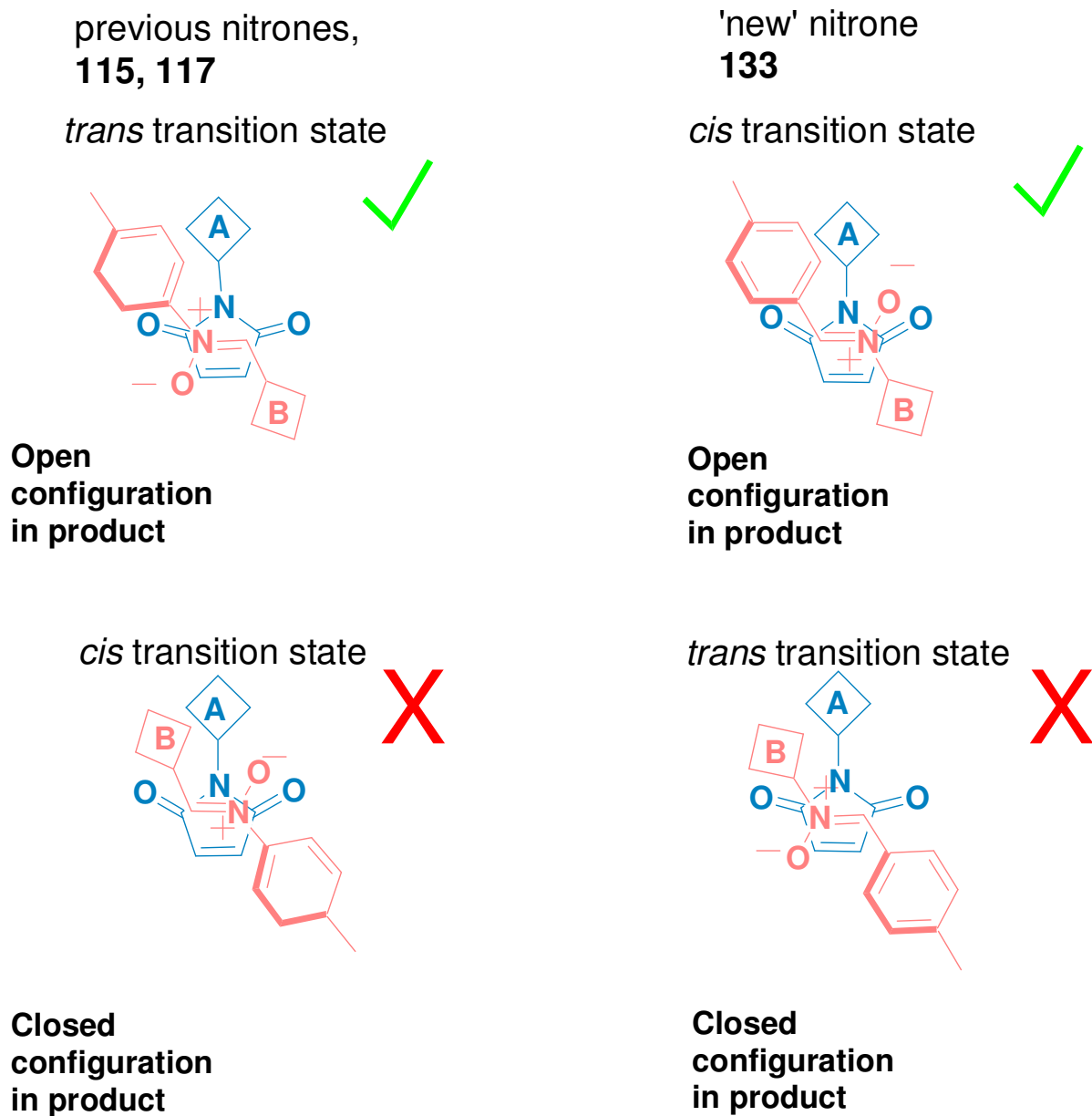


Figure 4.2 Diagram of open and closed conformations in product template, with recognition sites **A** and **B**. Top row shows the conformations which lead to the open template structure (replicating) for the 'normal' nitrone (top left column) and the new nitrone (top right column), highlighted with green ticks. The bottom row shows the conformations which leads to the unwanted closed template structure (AB pathway) for the normal nitrone (bottom left) and the new nitrone (bottom right), highlighted with a red cross.

The *trans* conformation of the transition state for this 'new' nitrone in the 1,3-dipolar cycloaddition reaction however, has the recognition sites overlapping, resulting in a closed structure for the resultant configuration of the template product. Therefore, in the

case of the 'new' nitron the *cis*-product, from the reaction between the nitron and the maleimide, is the product diastereoisomer which is used as a template in replication. In order to further prove the effect of this 'new' nitron **133** on the resultant configuration of the potential template product, the lowest energy structures of both *cis*- and *trans*-diastereoisomers were calculated using molecular mechanics. A series of Monte Carlo conformational searches were performed, starting from individually minimized conformations of *trans*-**134**, *cis*-**134**, [*cis*-**134**•*cis*-**134**], and [*trans*-**134**•*cis*-**134**] and utilizing the MMFFs forcefield and the GB/SA solvation model for CHCl₃. **Figure 4.3** shows the global minimal conformation for the two product duplexes [*cis*-**134**•*cis*-**134**], and [*trans*-**134**•*cis*-**134**]. **Figure 4.3** (a) shows the lowest energy conformation for [*cis*-**134**•*cis*-**134**] product duplex, consisting of four hydrogen bonds (dashed lines) indicating that the *cis*-transition state can form in the ternary complex. However, **Figure 4.3** (b) demonstrates the lowest energy conformation for the [*trans*-**134**•*cis*-**134**], notice that only two hydrogen bonds are formed at one end of the complex, suggesting the *trans* transition state is not supported by the *cis*-template in the ternary complex.

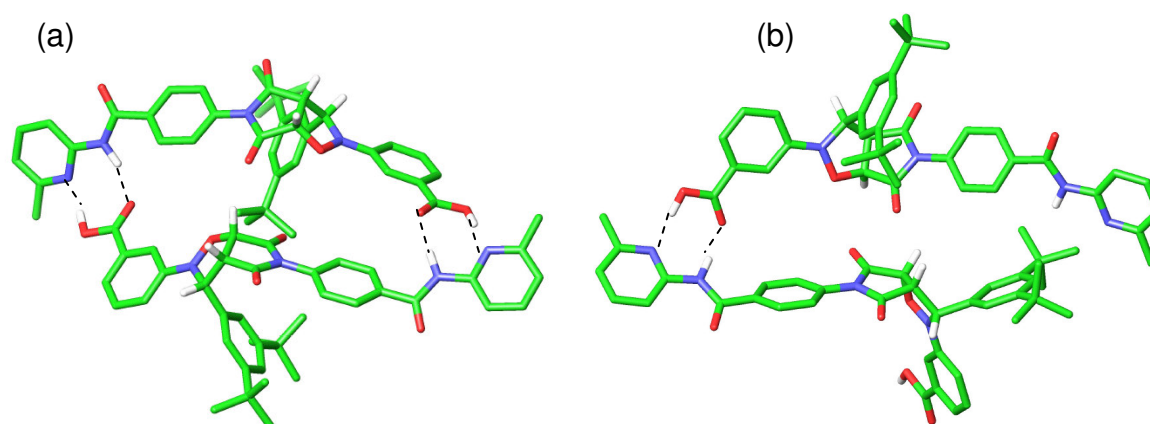


Figure 4.3 Molecular mechanics models for different (a) [*cis*-**134**•*cis*-**134**] duplex, (b) [*trans*-**134**•*cis*-**134**]. Carbon atoms are green, nitrogen atoms are blue, oxygen atoms are red and hydrogen atoms are white. The majority of hydrogen atoms have been removed for clarity. Dashed lines represent hydrogen bonds. Cartesian Coordinates for (a) can be found in Appendix Ten.

Evidence for the open conformation of the *trans*-isoxazolidine templates **135** and **118** comes from the solid state structure of bis(amidopyridine) *trans*-**135** determined (**Figure 4.4**) by single-crystal X-ray crystallography. Very small crystals of *trans*-**135**

were obtained from the slow evaporation of this isoxazolidine from an ethyl acetate/hexane mixture.

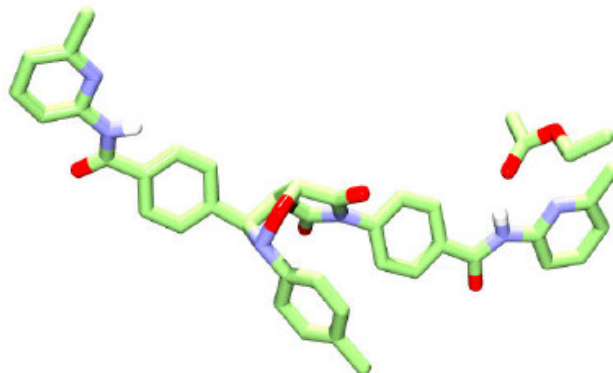


Figure 4.4 Single crystal X-ray structure obtained for *trans*-**135** bound to solvent ethyl acetate. Carbon atoms are green, oxygen atoms are red, nitrogen atoms are blue, and hydrogen atoms are grey. Majority of hydrogen atoms have been removed for clarity.

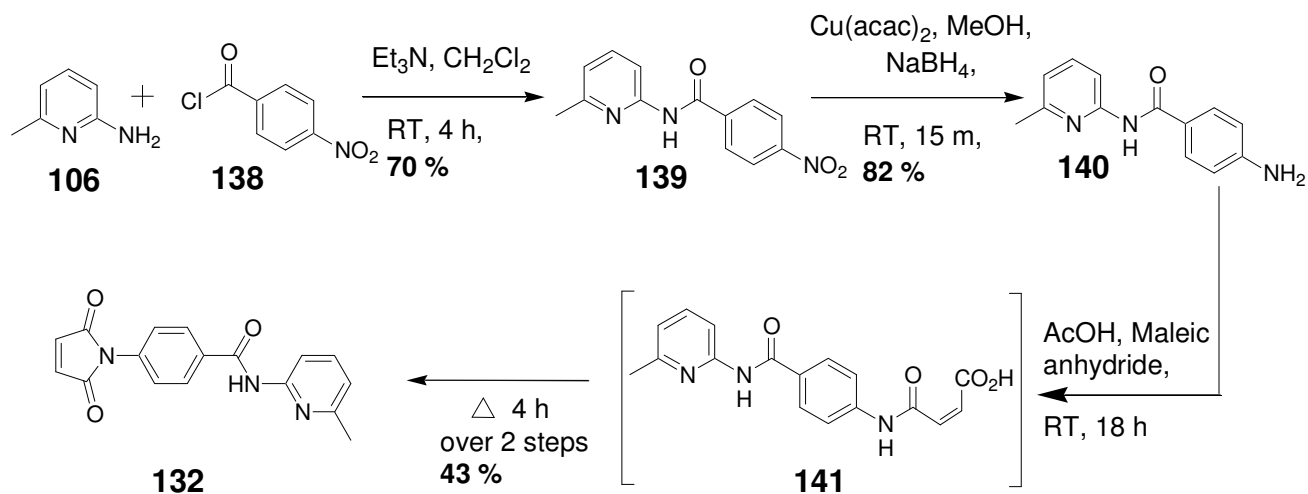
With the design principles of each of the new potential replicating systems proven all that remained was to synthesis each of the new building block molecules and the resultant templates. Once synthesized each of the individual replicators were first studied in isolation under identical conditions. When the individual studies were complete, more complicated interactive investigation could begin. If each of the replicating systems in **Figure 4.1** are combined together, they may interact with one another resulting in the formation of complex hypercyclic network. These hypercyclic systems were mentioned at the end of Chapter Three and involve complex cross-catalytic interactions between the different templates.

4.2 Synthesis of the potential replicating systems

4.3 Maleimide **132**

Target maleimide **132** was prepared in four steps (**Scheme 4.2**) from commercially available 2-amino-6-methylpyridine **106** and 4-nitrobenzyl chloride **138**. Reaction of **106** and **138** in CH₂Cl₂ at room temperature, in the presence of triethylamine, afforded amide **139** in 70% yield, after column chromatography. Selective reduction of the nitro group in the presence of the amide was achieved using Cu(acac)₂ and NaBH₄ in MeOH. Even though the exact mechanism^[170] of this reaction is somewhat obscure, an intermediate transition-metal boride is suspected to be responsible for the reduction affording **140** in 82% yield. Finally, reaction of amine **140** with maleic anhydride in glacial acetic acid

forms the intermediate acid **141** which in turn was converted to the target maleimide **132** in 43% yield.

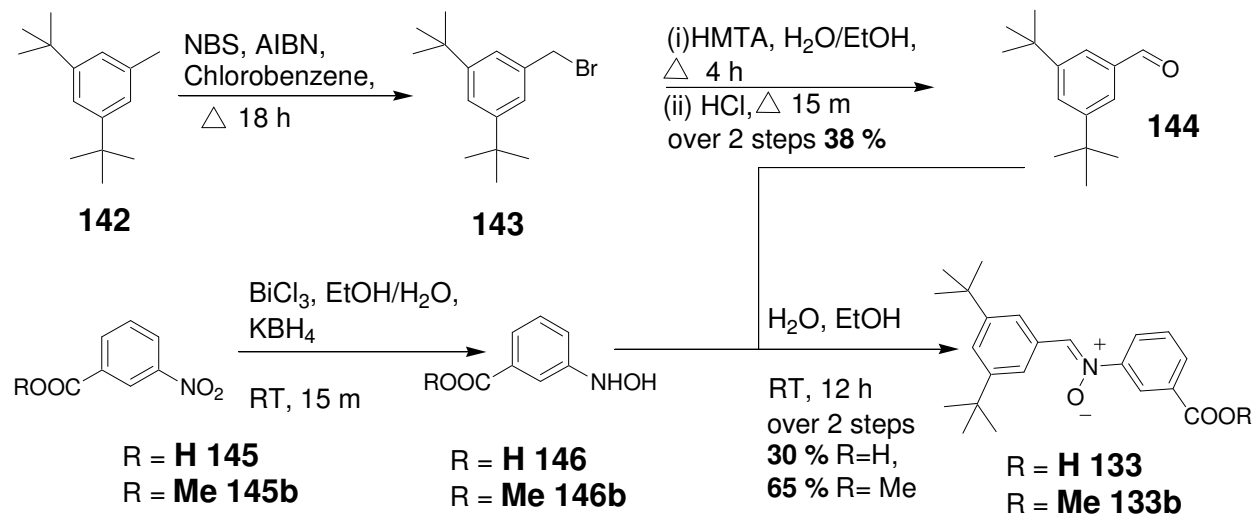


Scheme 4.2 Synthetic route for the preparation of **132**.

4.4 Carboxylic acid nitron 133

The synthesis of nitron **133**, bearing a carboxylic acid recognition site, was accomplished in four steps. Radical bromination of 3,5-di-*tert*-butyltoluene occurred using *N*-bromosuccinimide (NBS) and a radical initiator α -azo-iso-butyronitrile (AIBN) in a solution of 3,5 di-*tert*-butyltoluene and chlorobenzene, which was heated under reflux for 15 hours to afford a mixture of 3,5-di-*tert*-butylbenzyl dibromide and 3,5-di-*tert*-butylbenzyl bromide. This mixture was then converted to 3,5-di-*tert*-butylbenzaldehyde by adding hexamethylenetetramine (HMTA) to a solution of 3,5-di-*tert*-butylbenzyl dibromide and 3,5-di-*tert*-butylbenzyl bromide in EtOH/H₂O and heating under reflux. The imine formed was hydrolyzed to the aldehyde through the addition of concentrated HCl to afford **144** in 38% yield after purification by Kugelrohr distillation and recrystallization. The third step involved the reduction of **145** (ester **145b**) to the hydroxylamine **146** (ester **146b**) by the careful addition of potassium borohydride to the suspension of BiCl₃, *meta*-nitro benzoic acid (or *meta*-nitro benzoic methyl ester) in EtOH/H₂O, stirring at room temperature. Although the precise mechanism^[171] is unknown, an intermediate metal boride is a postulated intermediate. In the final step the aldehyde **144** was added to reaction mixture of the hydroxylamine and left in the dark at

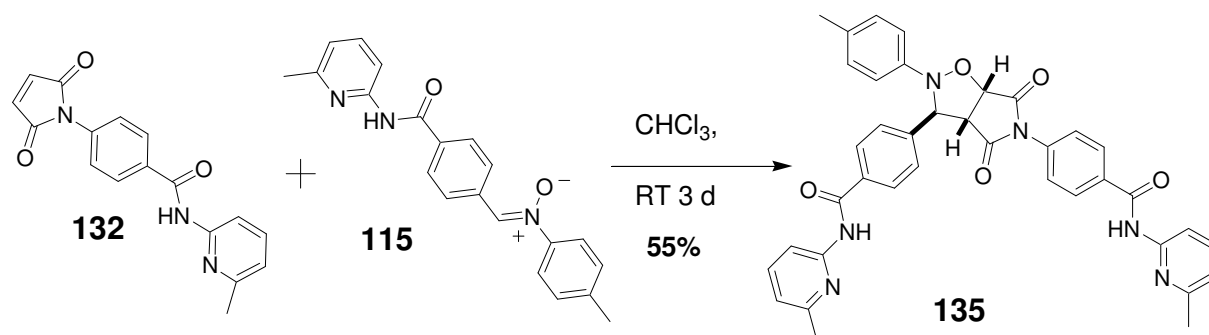
room temperature. This reaction afforded **133** in 30% yield or ester **133b** in 65% yield after recrystallization.



Scheme 4.3 Synthetic route for the preparation of **133** and **133b**.

4.5 Bis(amidopyridine) isoxazolidine *trans*-135

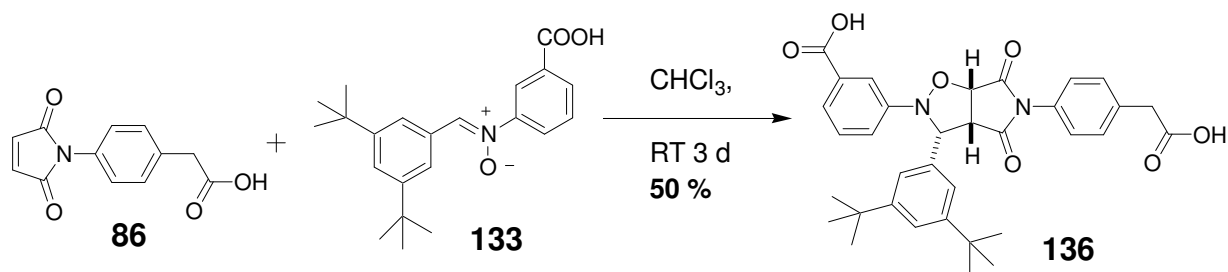
The 1,3-dipolar cycloaddition reaction between **132** and **115** was performed in the dark at room temperature for 3 days (**Scheme 4.4**), affording *trans*-**135** in 55% yield, after the diastereoisomers were separated by column chromatography.



Scheme 4.4 Synthetic route for the preparation of **135**.

4.6 Dicarboxylic acid Isoxazolidine **136**

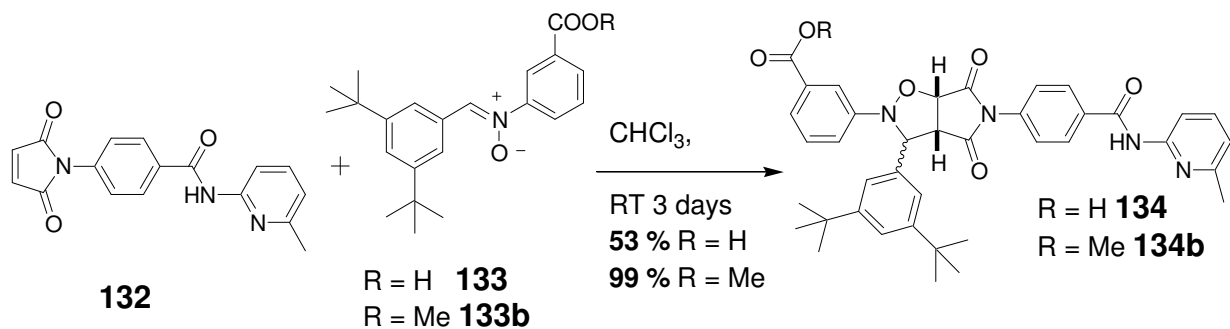
The 1,3-dipolar cycloaddition reaction between **86** and **133** was conducted under identical conditions to above affording *cis*-**136** in 50% yield, after the diastereoisomers were separated by column chromatography (**Scheme 4.5**).



Scheme 4.5 Synthetic route for the preparation of **136**.

4.7 Isoxazolidine **134**, **134b**

The 1,3-dipolar cycloaddition reaction between **132** and **133** (or **133b**) was performed in the dark at room temperature for 3 days (**Scheme 4.6**). This reaction afforded **134** in 53% (*cis*-diastereoisomer only), after the diastereoisomers were separated by column chromatography, and ester **134b** (both diastereoisomers) in 99% yield.



Scheme 4.6 Synthetic route for the preparation of **134** and **134b**.

4.8 Results and discussion

4.9 Kinetic experiment

All reactions in this chapter were conducted at 0 °C in CDCl_3 , with initial concentrations of 10 mM for each building block molecule. For the minimal replicators four reactions were conducted; an ester control, competitive inhibition control, native and a templated reaction, unless otherwise stated. The bimolecular control, blocks or removes the recognition site on the phenylacetic acid building block derivative preventing the reaction from proceeding *via* the recognition mediated channels in the minimal model. This control provides data on the bimolecular pathway in the minimal model, which occurs in

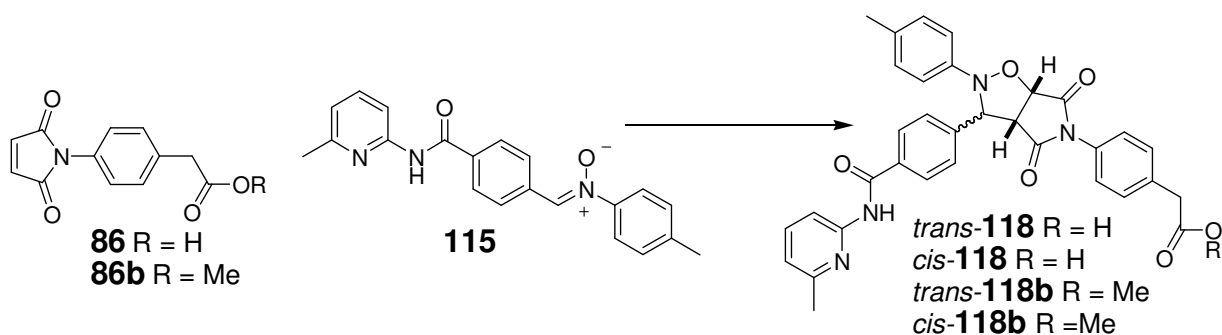
the lag period of autocatalytic process. The competitive inhibition reaction also obstructs association by adding a benzoic acid, which can directly compete for hydrogen bonding sites, preventing self-replication. The native reaction is the experiment in which the resultant isoxazolidine, formed from maleimide and nitron, have the potential to replicate autocatalytically through the association of the amidopridine and carboxylic acid recognition sites. The final experiment is the templated reaction. This reaction is similar to the native, but prefabricated template is added at the beginning of the reaction to promote autocatalysis by removing the lag period, proving the reaction is template directed

Studies into the cross-catalytic systems, as a consequence of the complementary nature of the building blocks in a molecule of template, only require two types of experiment, a bimolecular control and a templated experiment. The bimolecular reaction does not require the recognition sites to be blocked or inhibited, as both building block molecules contain identical recognition sites which are not able to associate with each other and hence self-replicate. Instead replication is only possible indirectly through the addition of a non-identical template containing complementary recognition sites. This occurs in the templated reaction, where the template is added at the start of the reaction to selectively cross-catalyze the 1,3-dipolar cycloaddition between the nitron and maleimide molecules.

4.10 Minimal replicator *trans*-118

Although the minimal replicator *trans*-118 (**Scheme 4.7**) was studied and its behavior described in detail in Chapter Three, those experiments were conducted at a concentration of 25 mM.

In order to compare accurately the efficiency of this template to its counterparts in this new replicating network, the same kinetic experiments in Chapter Three were repeated, Section **3.12**, at a concentration of 10 mM. This system was described in detail in the previous chapter, and will, therefore, only be discussed here briefly.



Scheme 4.7 1,3-dipolar cycloaddition between **86** or (**86b**) and **115** to form minimal-replicating template **118** or **118b**.

The bimolecular reaction (**Figure 4.5** (a)) between maleimide **86b** and nitron **115** at 0 °C proceeds slowly, as expected from the previous chapter, forming an 3:1 ratio of the *cis*- and *trans*-diastereoisomers. Overall conversion after 16 hours in CDCl₃ at 0 °C is < 10%. These data points indicated that when the recognition site is blocked, no autocatalysis was occurring and no self-replication. A kinetic model was computationally fitted to the product concentration vs. time curve to calculate (**Scheme 4.8**) rate constants for the formations of the *trans*- and *cis*-isoxazolidines, with an R value of 4.3%.



Rate constant / $\times 10^{-4} \text{ M}^{-1}\text{s}^{-1}$ $k_1 = 0.40 \pm 0.06$ $k_2 = 1.26 \pm 0.01$

Scheme 4.8 Kinetic model for the bimolecular 1,3-dipolar cycloaddition reaction between maleimide **86** and nitron **115** and optimized rate constants k_1 and k_2 . M = maleimide **86**, N = nitron **115** and *cis* and *trans* = *cis* or *trans* isoxazolidine **118**.

When the reaction between maleimide **86** and nitron **115**, with available recognition sites, is conducted in the native experiment, a very different result is obtained (**Figure 4.5** (b)). The product concentration vs. time plot now has the diagnostic sigmoidal shape for the formation of *trans*-product **118** (consisting of a lag, autocatalytic growth and starting material limiting phase), evidence of an autocatalytic process. Compared to the bimolecular reaction conversion has increased from < 10% to 85% after approximately 17 hours (overnight). However, an increase in conversion is not the only change, the selectivity for *trans*-isoxazolidine is also enhanced. The *trans* to *cis* ratio for the bimolecular reaction are 3:1, but for this recognition-mediated experiment, it is now 50:1. The plot in **Figure 4.5** (b) indicates that not only is catalysis not occurring

for the *cis*-isoxazolidine but this product is actually inhibited, with the starting material necessary for its formation being 'siphoned off' to form the *trans*-template. The product **118** concentration vs. time curve in **Figure 4.5** (b) was fitted computationally to a kinetic model (**Scheme 4.9**).

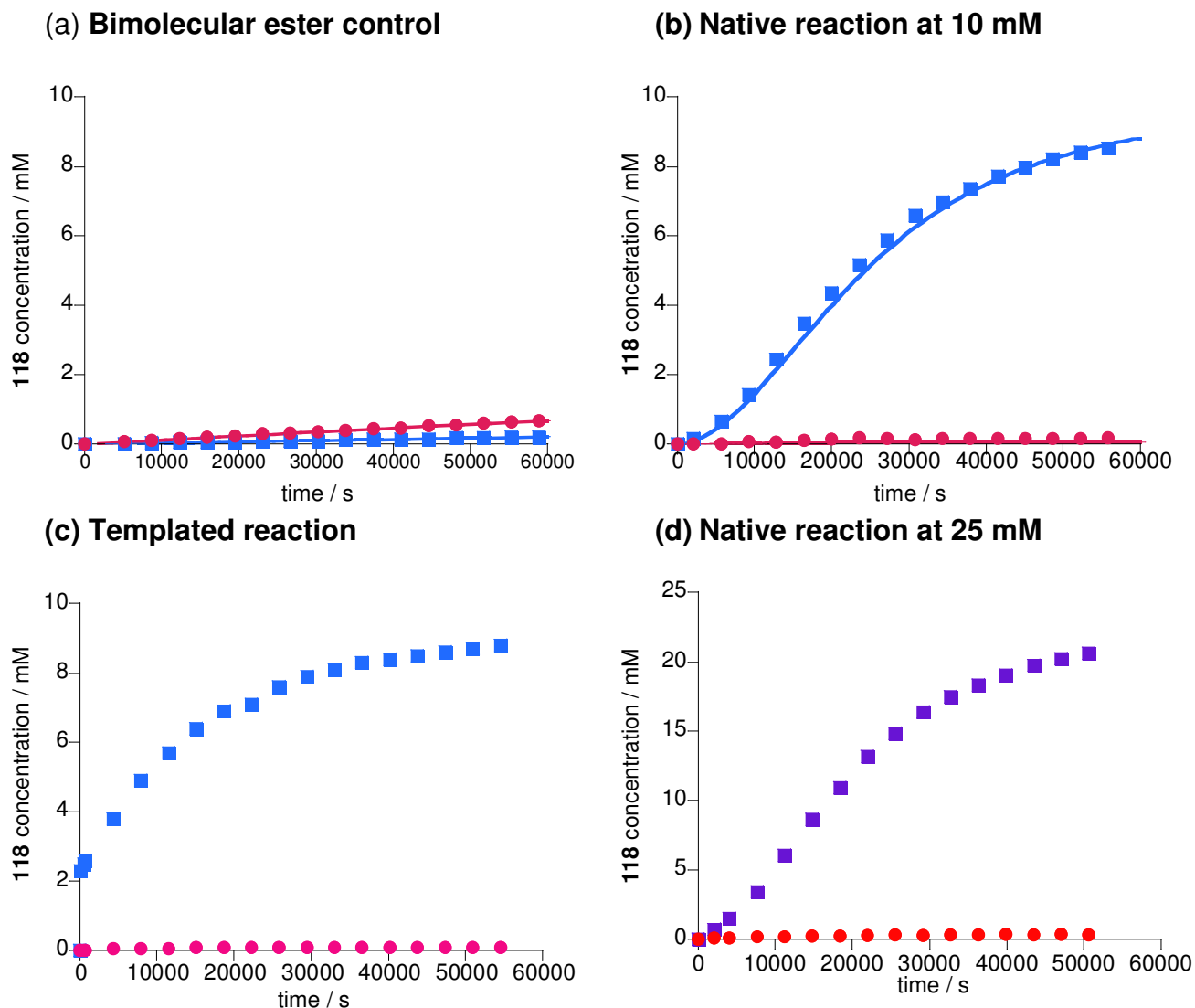
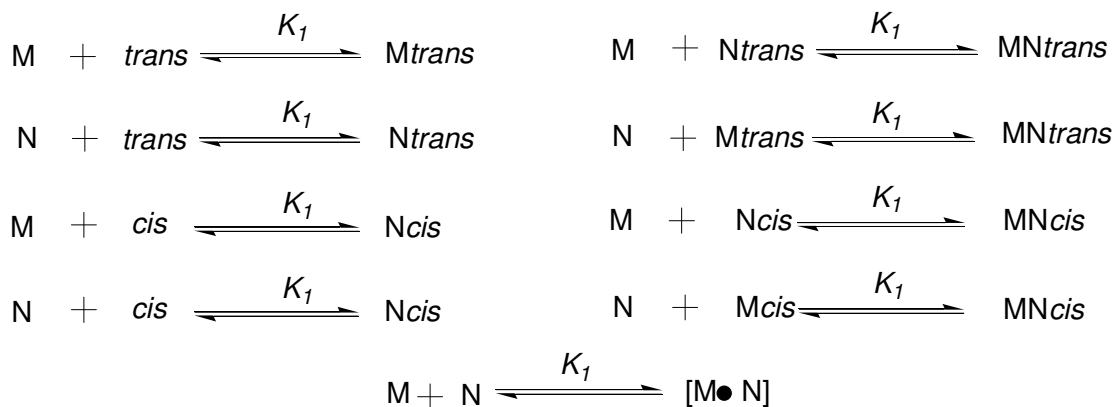


Figure 4.5 **118** concentration vs. time profile for (a) bimolecular reaction between equimolar concentrations of **86b** and **115** ($[\mathbf{86b}] = [\mathbf{115}] = 10 \text{ mM}$) at $0 \text{ }^\circ\text{C}$ in CDCl_3 , for the formation of *trans*-**118** (blue squares) and *cis*-**118** (pink circles), (b) native reaction between equimolar concentrations of **86** and **115** ($[\mathbf{86}] = [\mathbf{115}] = 10 \text{ mM}$) at $0 \text{ }^\circ\text{C}$ in CDCl_3 , for the formation of *trans*-**118** (blue squares) and *cis*-**118** (pink circles), (c) templated reaction with 0.1 equivalents of prefabricated template *trans*-**118** ($[\mathbf{115}] = [\mathbf{86}] = 10 \text{ mM}$), for the formation of *trans*-**118** (blue squares) and *cis*-**118** (pink circles) and (d) native reaction between equimolar concentrations of **86** and **115** ($[\mathbf{86}] = [\mathbf{115}] = 25 \text{ mM}$) at $0 \text{ }^\circ\text{C}$ in CDCl_3 , for the formation of *trans*-**118** (purple squares) and *cis*-**118** (red circles). Optimal fit curves are represented as solid lines. Errors in concentrations are $\pm 4\%$.

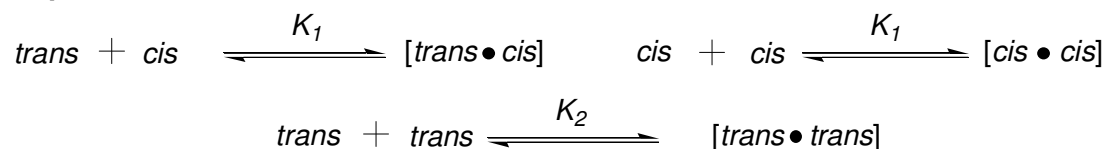
Bimolecular Reactions



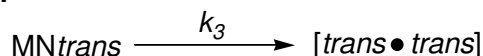
Routes towards formation of binary and ternary complexes



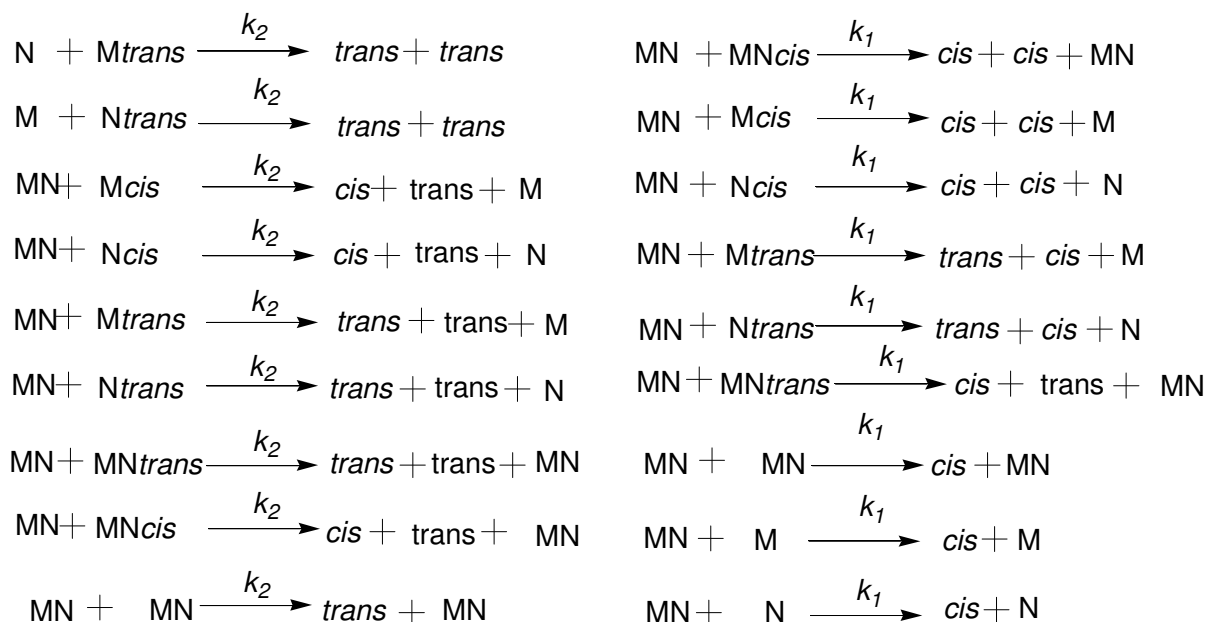
Duplex association



Ternary Complex reaction



Bimolecular reactions of complexes



Scheme 4.9 Comprehensive kinetic model used in theoretical simulations of the native reaction between **86** and **115** for the determination of reaction rate constants. M = maleimide **86**, N = nitrone **115** and *cis* and *trans* = *cis*- or *trans*- isoxazolidine **118**.

This model optimized two parameters the rate constant for the ternary complex reaction ($k_3 = 2.96 \pm 0.13 \times 10^{-3} \text{ s}^{-1}$) and stability constant ($K_a = 4 \times 10^6 \text{ M}^{-1}$) for the product duplex [*trans*•*trans*]. The optimal fit was achieved with an R value of 2.84%. For a detailed explanation of this kinetic model refer to Chapter Three Section 3.12. A $kEM = 23.5 \pm 2.8 \text{ M}$ was calculated for this system, which as expected is almost identical to the value calculated at 25 mM in Section 3.12. Through multiplying the individual binding interactions an association constant of $K_2 = 1000 \times 1000 = 1 \times 10^6 \text{ M}^{-1}$, might be expected. The larger calculated ($4 \times 10^6 \text{ M}^{-1}$) value is indicative of positive cooperativity. A more empirical measurement of this positive cooperativity can be calculated through the Gibbs free energy of connection (Figure 4.6), which was discussed in Chapter One.

$$\Delta G^s = \Delta G_B^0 + \Delta G_A^0 - \Delta G_{AB}^0$$

Substitute $\Delta G^0 = -RT \ln K$ into above equations results in the equation below;

$$\Delta G^s = RT \ln \left(\frac{K_{AB}}{K_A K_B} \right)$$

Figure 4.6 Equation of Gibbs free energy of connection, ΔG^s . Where ΔG_A^0 is Gibbs free energy of binding molecule A, ΔG_B^0 is Gibbs free energy of binding molecule B and ΔG_{AB}^0 is Gibbs free energy of binding molecule A joined to B. K_{AB} is the binding constant for A joined to B with the host and K_A and K_B is the association constant for the individual binding of molecules A and B to the host.

Modifying the second equation in Figure 4.6 for this system; K_{AB} is equal to K_2 and K_A and K_B are equivalent to K_1 in Scheme 4.9. These changes result in the equation illustrated in Figure 4.7.

$$\Delta G^s = RT \ln \frac{K_2}{K_1 K_1}$$

Figure 4.7 Equation of Gibbs free energy of connection, modified for the system in this section. K_2 is the association constant for the duplex [*trans*-118•*trans*-118]. K_1 is the binding constant for the individual association of an amidopyridine moiety to a carboxylic acid recognition group.

Using the individual binding constants for the binary complex K_1 (1000 M^{-1}) and calculated product duplex stability constant K_2 ($4 \times 10^6 \text{ M}^{-1}$), a value of 3.14 kJ mol^{-1} was obtained. This positive value is evidence of positive cooperativity.

The amplification of *trans*-**118** is good evidence of autocatalysis, but the test of any potential minimal replicator is the affect addition of prefabricated template has on the reaction. If *trans*-**118** is indeed a self-replicator then the addition of prefabricated *trans*-**118** should produce a template effect removing the lag period, resulting in exponential growth from the start of the reaction. Therefore, the reaction between **115** and **86** was repeated, but with the addition of 0.1 equivalents (1 mM) of pre-synthesized *trans*-**118** template (**Figure 4.5 (c)**). As expected from the discussion in Chapter Three, this experiment produced the desired template effect. With an increased initial rate compared to the native reaction, resulting in the disappearance of the lag period and sigmoidal shape in the concentration vs. time profile for the *trans*-isoxazolidine. The addition of template has enhanced selectivity in favor of the *trans*-isoxazolidine to the extent where the reaction could be considered completely *trans* selective (100:1 *trans*:*cis*).

The velocity vs. time curve (**Figure 4.8**, pink squares) for the native reaction was constructed using the same method described in the previous chapter, mainly through fitting a 6th order polynomial to the concentration vs. time curve in **Figure 4.5 (b)** then taking the first derivative of this function. Through plotting the first derivative against time a measure of reaction velocity can be obtained for the reaction time course.

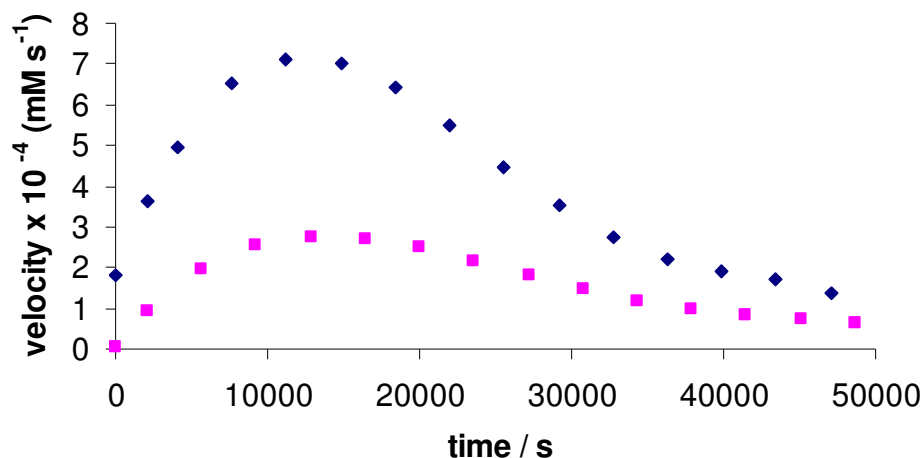


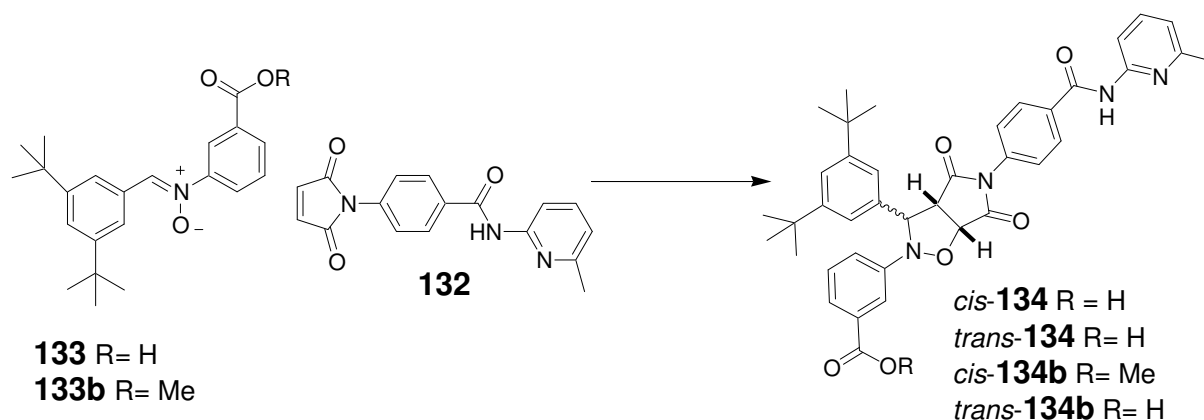
Figure 4.8 Velocity vs. time graph for reaction at 25 mM (blue circles) and at 10 mM (pink squares). Errors in concentration $\approx \pm 4\%$.

The velocity vs. time graph (**Figure 4.8**, pink squares) demonstrates the characteristic hill shaped curve for an autocatalytic system, with an initial increase in velocity until reaching a maximum and then a gradually decrease as reactants become limited. The

maximum autocatalytic rate for the reaction occurs at around 2.5 mM of template concentration. Comparisons of the velocity vs. time curve for the reaction at 10 mM and 25 mM (**Figure 4.8**, blue squares) reveals the maximum rate at approximately the same time, around 13000 seconds (3.5 hours). The maximum autocatalytic velocity occurs in the time region where $0.1 < \rho < 1.0$, $\rho = [\text{template}]/[\text{precursor}]$. In this system this occurs between 5×10^3 s and 2×10^4 s seconds, which corresponds to a concentration of *trans*-**118** between 1 and 5 mM. In the templated reaction the maximum solubility of *trans*-**118** limited studying the addition of concentrations larger than 1 mM of prefabricated template. However, the velocity vs. time curve demonstrates this would have been some what futile as addition of a larger concentration of *trans*-**118** would only have resulted in a maximum 7% increase in rate, increase in velocity from 2.54 to $2.71 \times 10^{-4} \text{ mM s}^{-1}$, before velocity is diminished at $\rho = 1.0$ and beyond. The curve at 25 mM is almost identical to the curve at 10 mM apart from the fact of the greater velocity values, corresponding to the increased concentration. The congruous velocity time curve maximums also explain why the selectivity of the reaction at 10 mM and 25 mM is similar 50:1 compared to 45:1.

4.11 Minimal replicator *cis*-**134**

A potential minimal replicator (*cis*-**134**) is formed from the 1,3-dipolar cycloaddition reaction between maleimide **132** and nitron **133** (**Scheme 4.10**).



Scheme 4.10 1,3-dipolar cycloaddition between maleimide **132** and nitron **133** (or **133b**) to form **134** or **134b**.

For reasons discussed at the beginning of this chapter, the minimal template **134** is the first potential replicator studied in which the *cis*-isoxazolidine is predicted to be the

autocatalytic template. As a result of this difference in configuration, it will be interesting to note how this molecule compares to its *trans* minimal replicating counterpart (Section 4.10). As with previous potential minimal replicators, a series of reactions were conducted to determine its ability to replicate starting with a bimolecular control reaction (Figure 4.9).

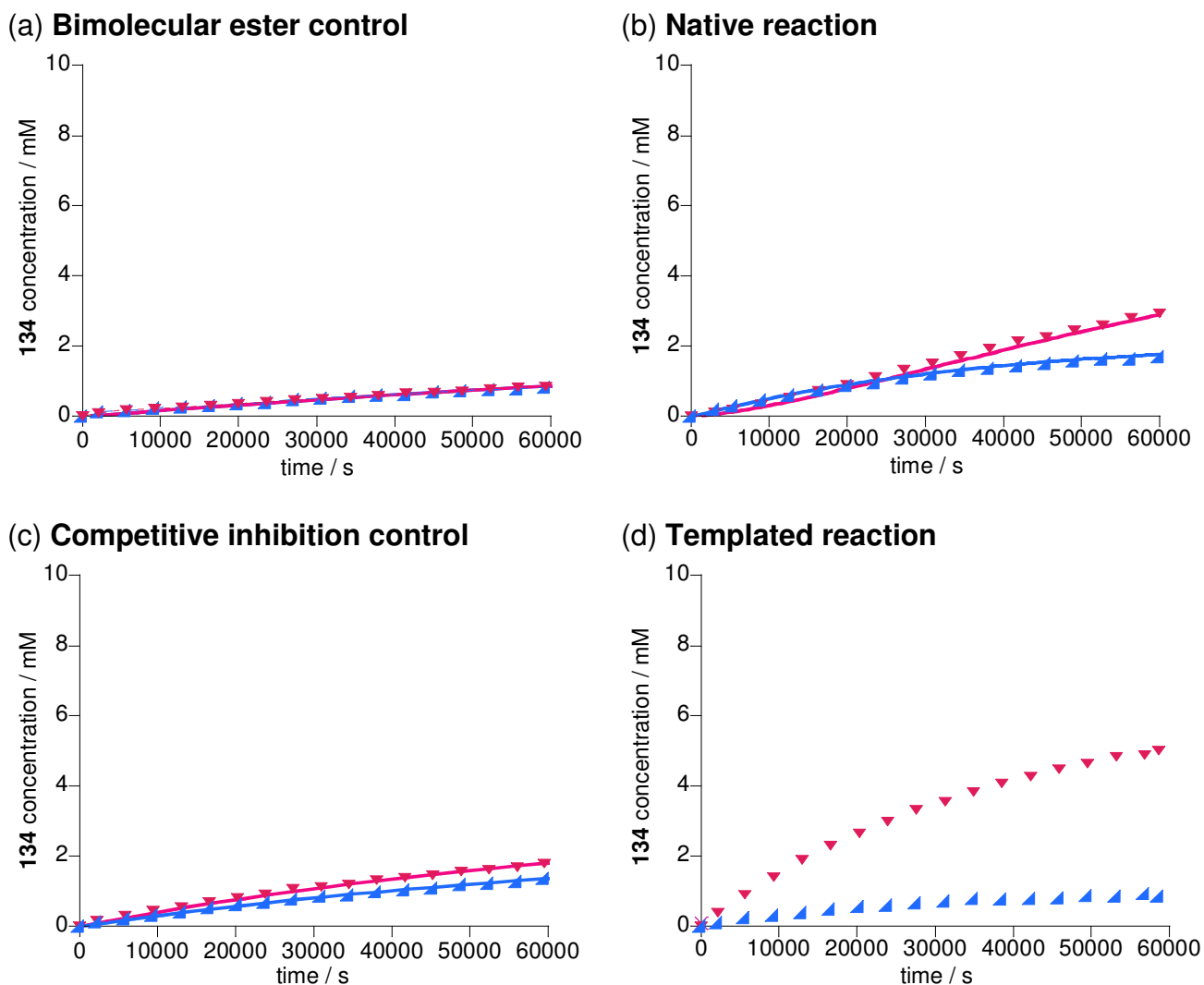


Figure 4.9 Product concentration vs. time profile for (a) bimolecular reaction between equimolar concentrations of **132** and **133** ($[\mathbf{132}] = [\mathbf{133b}] = 10 \text{ mM}$) at $0 \text{ }^\circ\text{C}$ in CDCl_3 , for the formation of *trans*-**134b** (blue triangles) and *cis*-**134b** (pink triangles) and (b) native reaction between equimolar concentrations of **132** and **134** ($[\mathbf{132}] = [\mathbf{133}] = 10 \text{ mM}$) at $0 \text{ }^\circ\text{C}$ in CDCl_3 , for the formation of *trans*-**134** (blue triangles) and *cis*-**134** (pink triangles) (c) Competitive inhibition reaction between equimolar concentrations of **132** and **133** ($[\mathbf{132}] = [\mathbf{133}] = 10 \text{ mM}$) with 4 equivalents of benzoic acid in CDCl_3 at $0 \text{ }^\circ\text{C}$, for the formation of *trans*-**134** (blue triangles) and *cis*-**134** (pink triangles) (d) templated reaction with 0.3 equivalents of prefabricated template *cis*-**134** ($[\mathbf{132}] = [\mathbf{133}] = 10 \text{ mM}$), for the formation of *trans*-**134** (blue triangles) and *cis*-**134** (pink triangles). Optimal fit curves are represented as solid lines. Errors in concentration values are $\pm 4\%$.

The control reaction between maleimide **132** and nitrone **133b** afforded the typical bimolecular reaction profile, with low conversion < 20% after 6×10^4 s, as a result of the slow rate constant value (**Scheme 4.11**) for k_1 and k_2 , and no selectivity (1:1 ratio of *cis* to *trans*).



Rate Constant / $\times 10^{-4} \text{ M}^{-1}\text{s}^{-1}$ $k_1 = 1.80 \pm 0.02$ $k_2 = 1.80 \pm 0.02$

Scheme 4.11 Kinetic model used to determine the magnitude of rate constants k_1 and k_2 for the bimolecular reaction between **132** and **133b** to form *cis*-**134b** and *trans*-**134b**. M = maleimide **132**, N = nitrone **133b** and *cis* and *trans* = *cis*- or *trans*-isoxazolidine **134b**.

Values for the k_1 and k_2 were determined (**Scheme 4.11**) from the optimal fit of theoretical (solid line in **Figure 4.9** (a)) to experimental product concentration vs. time curves using the method described in Section 7.8. The percentage of the mean absolute difference between the experimental and theoretical concentrations with respect to the mean of experimental concentrations (R) was 7.5%. This value is slightly higher than normal as a consequence of the low conversion and errors in determining low concentration (< 2 mM) of product.

An initial examination of the recognition-mediated native reaction (**Figure 4.9** (b)) between nitrone **133** and maleimide **132** indicates little evidence of replication. However, a more detailed inspection of the product concentration vs. time plot provides subtle evidence of a catalytic effect. Initially, the native reaction is not dissimilar to the bimolecular control reaction with both *cis*- and *trans*-isoxazolidine formed at identical rates, however, after 3×10^4 s the rate vs. time curve for the *cis*-product begins to diverge from that for the *trans*-product, whose rate appears to level out as the reaction progresses. After 6×10^4 s, reaction has progressed to 45% conversion, compared to < 20% for the bimolecular control, with a *cis* to *trans* ratio of 1.7:1. In order to investigate the autocatalytic nature of this system a velocity vs. time curve was plotted (**Figure 4.10**) using the same method described in Section 3.12, mainly fitting a 6th order polynomial to the product concentration vs. time curve and taking the first derivative of the resultant function.

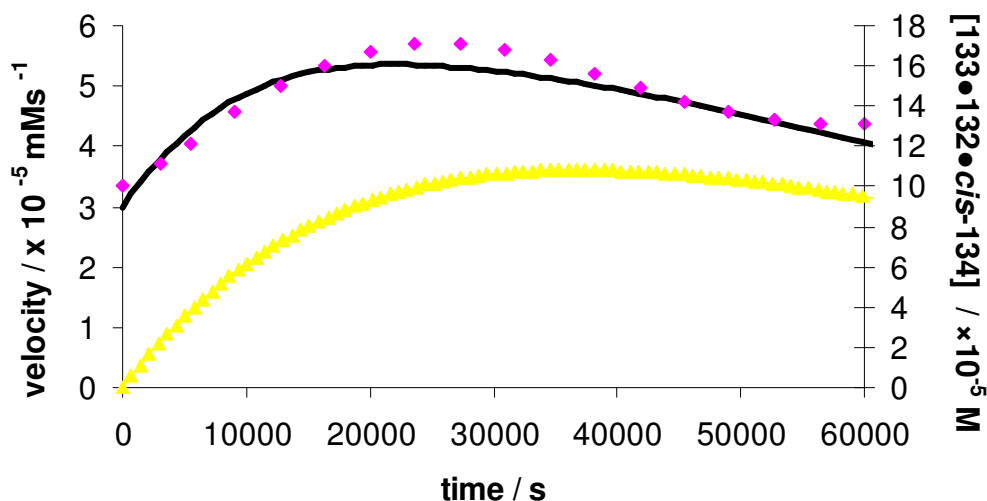
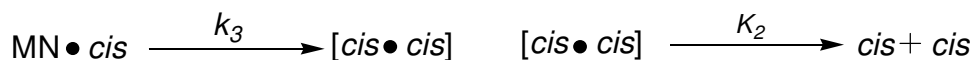


Figure 4.10 Velocity vs. time curve for the native reaction between maleimide **132** and nitrone **133** at 10 mM in CDCl_3 at 0 °C. Purple squares represent experimental calculated velocity curve, whereas the solid line demonstrates the velocity curve calculated from the kinetic model optimal fit. The yellow triangles are the concentration of ternary complex $[\mathbf{132}\bullet\mathbf{133}\bullet\text{cis-}\mathbf{134}]$ present at any one time over the reaction time course. Errors in velocity $\approx \pm 10\%$, concentration $\pm 4\%$.

The velocity time curve demonstrates that there is an increase in rate reaching a maximum at around 2.5×10^4 s after which a decline occurs. This information indicates that this system could be exhibiting some signs of autocatalysis, although this evidence is far from conclusive. Further investigation is warranted to provide definitive proof of the true nature of this potential minimal replicator.

The product concentration vs. time curve in **Figure 4.9** (b) was fitted computationally to a kinetic model similar to **Scheme 4.9**, with *cis*-product catalyzed in ternary complex instead of the *trans*-product, forming a $[\text{cis}\bullet\text{cis}]$ duplex (**Scheme 4.12**).



Scheme 4.12 Parameters optimized using the kinetic model in **Scheme 4.9**, but with the *cis*-products formation catalyzed in the ternary complex in place of the *trans* indicated in **Scheme 4.9**. M = maleimide **132**, N = nitrone **133** and *cis* and *trans* = *cis* and *trans* isoxazolidine **134**.

This model optimized two parameters the rate constant for the ternary complex reaction, k_3 , and stability constant for the product duplex $[\text{cis-}\mathbf{134}\bullet\text{cis-}\mathbf{134}]$, K_2 , with an R value equal to 3.4%. The general method for this is explained in detail in Section 7.8. As stated earlier the value of the association constant, K_2 , for the product duplex was surmised to be larger, unfortunately it could not be measured. However, through fitting

the product concentration vs. time curve to the kinetic model a theoretical value of $K_2 = 2.5 \times 10^6 \text{ M}^{-1}$ was calculated. This value for K_2 is higher than the anticipated $600 \times 600 \text{ M}^{-1} = 3.6 \times 10^5 \text{ M}^{-1}$ value indicating positive cooperativity, which is supported with the positive Gibbs free energy of connection of $+ 4.4 \text{ kJ mol}^{-1}$.

The theoretical rate constant for the catalytic ternary complex is compared to the bimolecular values in **Table 4.1**. By dividing the catalytic rate constant over the bimolecular, $kEM = k_3/k_1$, it is possible to determine the kinetic effective molarity for the *pseudo*-unimolecular reaction. When this calculation is carried out a kEM of 6.0 M is found.

Table 4.1 Table of computationally determined rate constant from optimal fit curves of theoretical to experiment product concentration vs. time curves and the kinetic effective molarity of the recognition mediated reaction.

Bimolecular Reactions^a Rate constant / $\times 10^{-4} \text{ M}^{-1} \text{ s}^{-1}$	Recognition Mediated^a Rate constant / $\times 10^{-4} \text{ s}^{-1}$	kEM^b
$k_1 = 1.8 \pm 0.02$	$k_3 = 10.0 \pm 0.01$	$6 \pm 0.6 \text{ M}$
$k_2 = 1.8 \pm 0.02$	Not applicable	Not applicable

^a Rate constants relate directly to **Scheme 4.9**. ^b kEM, kinetic effective molarity is calculated by dividing the recognition mediated reaction over the bimolecular, $kEM = k_3 / k_1$.

As discussed in Chapter Three Section **3.12**, one advantage of fitting the experimental data to a kinetic model is it allows the calculation of the concentrations of a range of reactant species over the time course of the experiment. In **Figure 4.10** we prove the presence of autocatalysis through a velocity vs. time curve; however, this graph also had a secondary y-axis. This secondary y-axis measures the concentration of ternary complex present [**132•133•cis-134**], which is displayed on the graph as the curve of yellow triangles. As the increase in velocity exhibited in **Figure 4.10**, is caused by the ternary complex structure, there should be a direct relationship between ternary complex concentration and reaction velocity. Evidence of this relationship can be observed in **Figure 4.10**. A maximum velocity occurs in the native experiment at around 25000 seconds, which is around the point where the concentration of ternary complex reaches its maximum concentration of 100 μM . Once the concentration of ternary complex has reached a maximum it starts to decline, a similar trend is observed in the velocity vs. time curve. Therefore, examination of the graph in **Figure 4.10** has demonstrated the

direct relationship between reaction velocity and concentration of catalytic ternary complex.

In order to determine if this system has the ability to template its own formation, we first have to resolve if the native reaction is recognition-mediated. Therefore, the experiment between **132** and **133** was repeated with the addition of 4 equivalents of a competitive inhibitor, benzoic acid, at the start of the reaction, in order to disrupt association between **132** and **133**. The effect of this competitive control can be examined through analysis of the plot in **Figure 4.9** (c). Comparing the data for the control to the native reaction, the conversion has fallen to below 30% with *cis*, *trans* selectivity also decreasing to a ratio of 1.3:1. The lower conversion, rate and selectivity in this competitive control demonstrated that the native reaction is recognition-mediated. Although the addition of a competitive inhibitor does weaken the recognition-mediated reaction, it is not completely eradicated. This fact can be illustrated by comparing the competitive and bimolecular control plots (**Figure 4.9** (a) and (c)); if recognition was completely inhibited by the benzoic acid then the two reactions should mirror each other. However, the competitive inhibition reaction has a higher rate constant for the formation of both *cis*- and *trans*-isoxazolidine than that of the bimolecular experiment, which results in the increased conversion and selectivity observed for this control.

Now, that the reaction has been proven to be recognition-mediated, all that remains is to demonstrate that the *cis*-**134** isoxazolidine can template its own formation. This goal was achieved by adding 0.3 equivalents (3 mM) of prefabricated template at the start of the reaction between **132** and **133**. The effect of this addition is immediately apparent when you compare the product concentration vs. time plot for the templated experiment (**Figure 4.9** (d)) to that of the native (**Figure 4.9** (b)). At this point it should be mentioned that the data for the product concentration vs. time graph for the templated experiment excludes the initial prefabricated template, therefore, the plot only contains isoxazolidines produced in the reaction. Analysis of these two graphs clearly demonstrates an increase in selectivity and initial rate for the formation of the open structure *cis*-template. Compared to the native reaction conversion has increased to 60% and selectivity has increased from a *cis* to *trans* ratio of 1.7:1 to 5:1. This amplification of the *cis*-product is a result of two factors. The first of these is an increase in the rate of formation of the *cis*-product and the second is an inhibition in the formation of the *trans*-product. Examination of the data for the *trans*-isoxazolidine reveals that the

rate of formation in the templated reaction is almost identical to that in the bimolecular control reaction (**Figure 4.9** (a)), but not the native reaction (**Figure 4.9** (b)). This information implies that the *trans*-isomer is involved in some type of recognition mediated reaction, possibly an [A•B] binary complex, in the native reaction. However, as starting material is consumed, forming the *cis*-product in the template reaction less is available to form the *trans*-product. Although, the evidence clearly supports the conclusion that the *cis*-product is templating its own formation, it does not support the idea that this is an efficient minimal replicator. The analysis of **Figure 4.9** (d) revealed that the reaction rate decreases after 2×10^4 s when the *cis*-product concentration is close to 3 mM. This value is identical to the concentration of prefabricated *cis*-134 added to the templated reaction. The explanation of this fact is self evident; it implies that catalytic turnover is low. A substantial concentration of the template is present in the duplex form leaving only a low concentration of free *cis*-isoxazolidine available to replicate its own formation. This high concentration of template in the duplex form implies a large value for the association constant, K_2 , between the two molecules, a common problem in many potential minimal replicating systems. Unfortunately *cis*-134 was insoluble in concentration above 3 mM, meaning the duplex binding constant could not be directly measured *via* ^1H NMR spectroscopy titration or dilution studies. Examination of the velocity time curve in **Figure 4.11** for the templated reaction supports the idea of a low catalytic turnover and a high K_a value, for the [*cis*-134•*cis*-134] duplex.

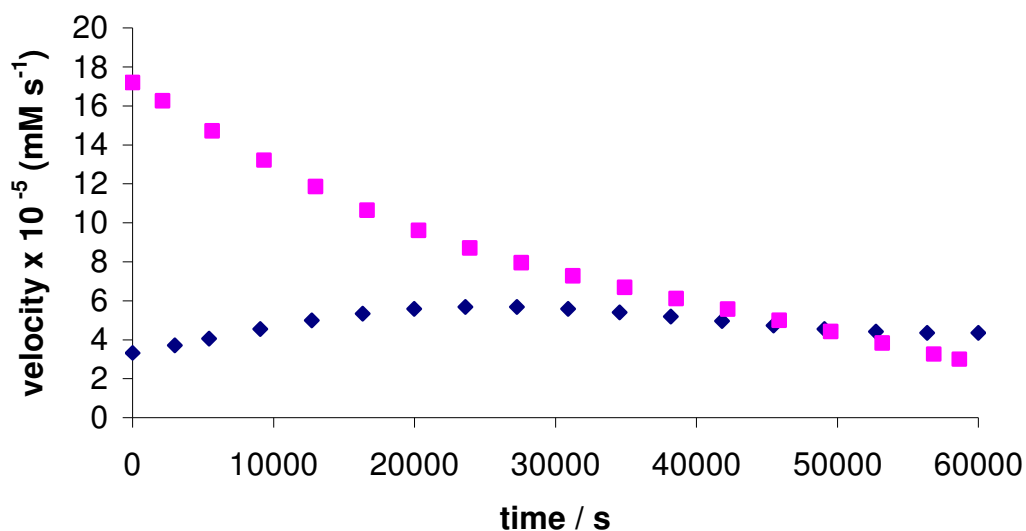


Figure 4.11 Velocity vs. time curves for the templated reaction (pink squares) and the native reaction (blue circles) for minimal replicating system *cis*-134. Errors in velocity are $\approx \pm 4\%$.

The velocity vs. time curve displays an initial high value for the templated reaction decreasing gradually over the time course of the reaction to the same value as the beginning of the native reaction. The maximum autocatalytic rate in the templated reaction should be identical to that in the native reaction. However, the graph in **Figure 4.11** demonstrates this is not the case, the templated reaction has a considerably higher maximum velocity than the native experiment. This difference in velocity supports the hypothesis of a large association constant, K_2 , for the [*cis*-**134**•*cis*-**134**] duplex. In the native reaction only a slight increase in velocity is observed corresponding to the fact that as soon as any template is formed and catalyzes its own formation, it is trapped in the duplex structure. Which has the effect of limiting any increase in velocity. In the template reaction at the start of the reaction a large concentration of free *cis*-**134** is present, allowing for a much greater reaction velocity, in the free form, but as it catalyzes its own formation more and more is trapped in the duplex structure resulting in the decline in velocity recorded. In order to demonstrate the influence that the high association constant K_2 , has on the system a series of simulations were conducted in which the only parameter varied was the stability of the product duplex [*cis*-**134**•*cis*-**134**]. These simulations used the same kinetic model as was fitted to the experimental native product curves, as well as the calculated ternary complex and bimolecular rate constants and the binary association constant K_1 (600 M^{-1}). The concentrations of isoxazolidines-**134** were extracted from the simulations and plotted against time to give the hypothetical product curves in **Figure 4.12**.

Graph (a) in **Figure 4.12** illustrates the experimentally fitted product curve for *cis*- and *trans*-**134** and the simulated curves for a K_2 value of $2.5 \times 10^4 \text{ M}^{-1}$. Comparison between the experimentally fitted and simulated curves reveals that if the stability constant was 100 times weaker we would expect to see a sigmoidal curve, with $\approx 90\%$ conversion. The weaker product duplex allows greater turnover of *cis*-**134**, which autocatalytically templates its own formation resulting in exponential growth, which gives the curve its sigmoidal appearance and increased conversion. A lower K_2 value also results in a decline in formation of the *trans*-isoxazolidine **134**. This effect arises because *cis*-**134** template is sequestering starting materials nitrene **133** and maleimide **132** in its exponential self-replication leaving less building blocks for formation of *trans*-**134**. The increased production of *cis*-template **134** and the decreased formation of *trans*

isoxazolidine **134** combine to increase selectivity, from the 1.7:1 observed for the experiment data to 12:1 *cis* to *trans*. Graph (b) in **Figure 4.12** demonstrates the simulated *cis*-product curve over a range of product duplex stability constant values ($2.5 \times 10^2 - 10^6 \text{ M}^{-1}$), the *trans*-product curve has been removed for convenience.

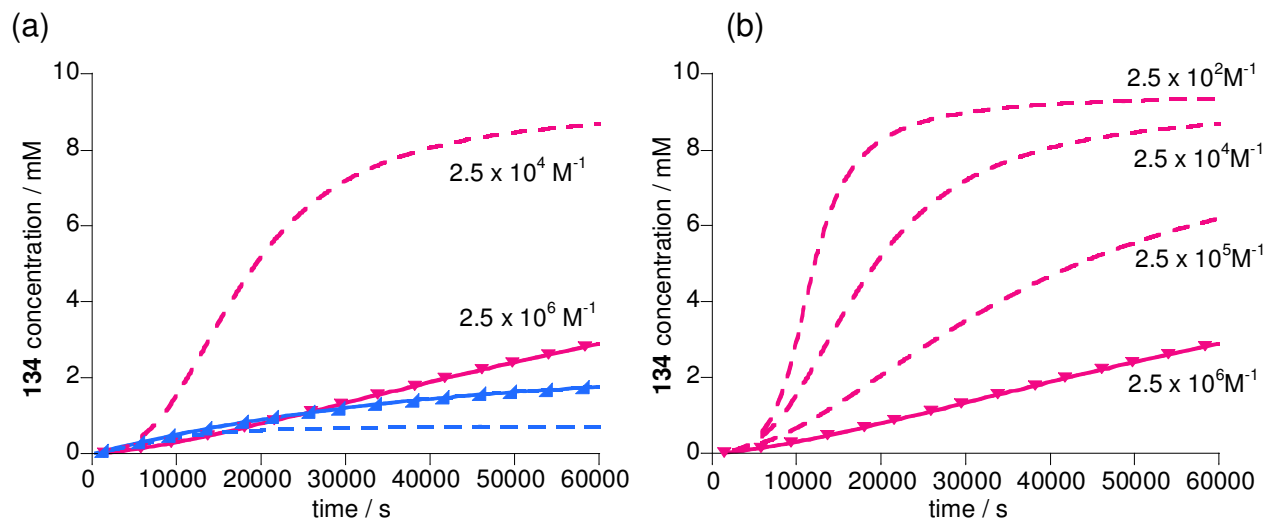
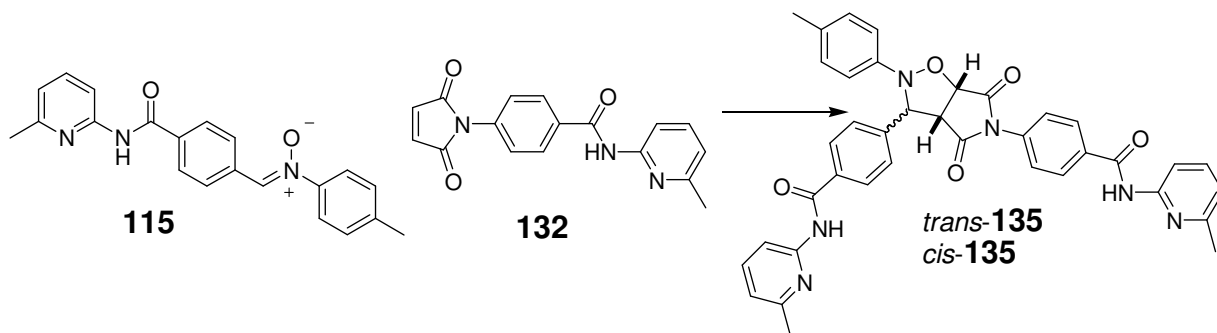


Figure 4.12 Simulated graphs of the **134** concentration vs. time for the reactions between nitrones **133** and maleimide **132**, using different values for the product duplex association constant K_2 . Each graph also contains the experimental fitted data to a $K_2 = 2.5 \times 10^6 \text{ M}^{-1}$, solid lines with triangles. (a) Graph shows experiment *trans*, *cis*-product curves (triangles with solid lines through them) and simulated curves (dashed line). (b) demonstrates the product curves for the replicating *cis*-**134** template only under various product duplex association constant values. Error in simulated data are $\approx 12\%$.

4.12 Reciprocal replicator *trans*-**135**

Reciprocal replicator **135** was formed from the 1,3-dipolar cycloaddition reaction between maleimide **132** and nitron **115** (**Scheme 4.13**)



Scheme 4.13 1,3-dipolar cycloaddition between **115** and **132** to form cross-catalytic template *trans*-**135** and *cis*-**135**.

As discussed in previous chapters a reciprocal or cross-catalytic template contains identical non-self complementary recognition sites. This recognition motif, therefore, means reciprocal systems are unable to template their own formation directly, instead only a complementary partner containing compatible recognition sites can cross-catalyze their formation. The non-associative nature of *trans*-**135** means no ester control or competitive inhibition reactions are necessary. Only a simple bimolecular reaction is necessary to confirm no minimal replication is occurring and to provide data for the non-catalyzed reaction. The results for the bimolecular reaction are displayed in the product concentration vs. time plot in **Figure 4.13 (a)**.

(a) **Bimolecular reaction**

(b) **Templated reaction**

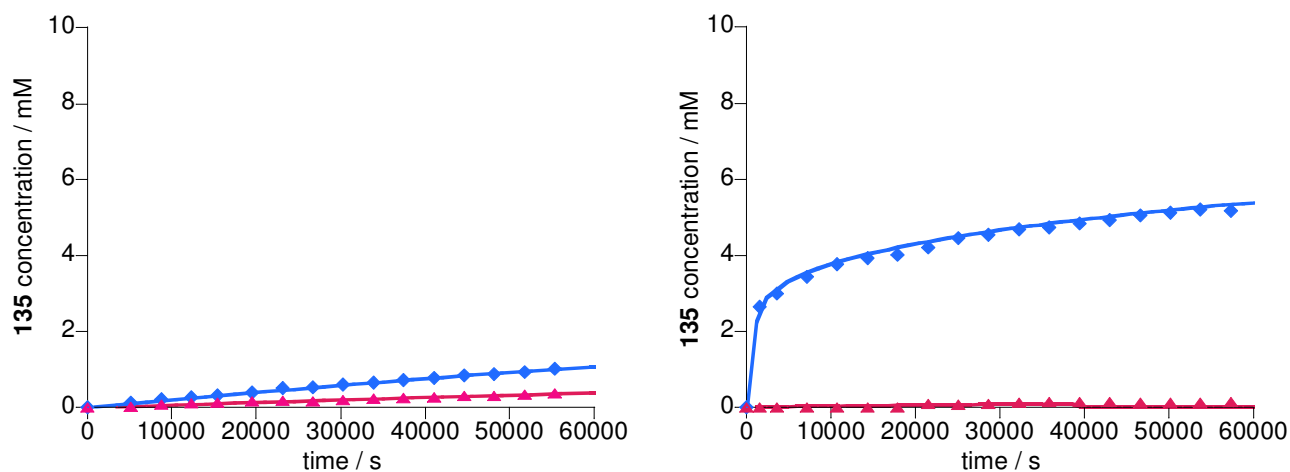


Figure 4.13 Product concentration vs. time profile for (a) bimolecular reaction between equimolar concentrations of **115** and **132** ($[\mathbf{115}] = [\mathbf{132}] = 10$ mM) at 0 °C in CDCl_3 , for the formation of *trans*-**135** (blue diamonds) and *cis*-**135** (purple triangles) and (b) templated reaction with 0.3 equivalents (3 mM) of dicarboxylic acid template *cis*-**136** ($[\mathbf{132}] = [\mathbf{115}] = 10$ mM), for the formation of *trans*-**135** (blue diamonds) and *cis*-**135** (purple triangles). Optimal fit curves are represented as solid lines. Errors in concentration values are $\pm 4\%$.

The results for this reaction are as expected, with no evidence of any recognition mediated process. As expected the reaction precedes slowly in a bimolecular fashion, with conversion less than 20% after 6×10^4 s. Selectivity for this 1,3-dipolar cycloaddition affords the expected ratio of *trans* (blue diamonds) to *cis* (purple triangles) of 3:1 for nitron, maleimide reaction (Appendix Five). The rate constants for the formation of both diastereoisomers (k_1 and k_2) of the isoxazolidines were determined using the method described in Section 7.8, through the optimal fit of theoretical to experimental concentration vs. time curves using the kinetic model in **Scheme 4.14**



Rate constant / $\times 10^{-4} \text{ M}^{-1} \text{ s}^{-1}$ $k_1 = 0.77 \pm 0.01$ $k_2 = 2.15 \pm 0.01$

Scheme 4.14 Kinetic model used to determine the magnitude of rate constants k_1 and k_2 for the bimolecular reaction between **132** and **115** to form *cis*-**135** and *trans*-**135**. M = maleimide **132**, N = nitrone **115** and *cis* and *trans* = *cis* or *trans* isoxazolidine **135**.

Values for k_1 and k_2 were calculated, with an R value of 4.2%, these values will aid in the study of the templated cross-catalytic reaction.

The templated reaction was conducted in the presence of 3 mM of complementary *cis*-**136** dicarboxylic acid template. The reason for this concentration is that the maximum solubility of the carboxylic template is only 3 mM. The results of this experiment can be examined in the product concentration vs. time plot in **Figure 4.13** (b). It is immediately evident from comparing this plot to the bimolecular graph that a 'template effect' is present, conversion has increased to approximately 60% after a period of 6×10^4 s. This increased conversion is as a result of amplification of the *trans*-isoxazolidine, selectivity has increased from 3:1 *trans* to *cis* in the bimolecular to 37:1 in the templated reaction (Appendix Five). This amplification is a result of two factors the first is an increase in rate of formation of the *trans*-product, as a result of the complementary template selectively catalyzing its production, the second is the decline in rate for the synthesis of the *cis*-isoxazolidine. The dicarboxylic acid template is such an effective catalyst for the formation of the *trans*-product, that hardly any of the starting material is available to produce the *cis*-isoxazolidine. Although the complementary template is a very effective catalyst for the selective formation of the *trans*-product, the turnover of catalyst is not as effective. The analysis of the plot in **Figure 4.13** (b) revealed a decline in rate of *trans* formation after the production of 3 mM of **135**, what is the reason for this leveling off in rate? A velocity vs. time graph demonstrates (**Figure 4.14**) the fall off in rate better. This graph was prepared use the same technique described in earlier sections.

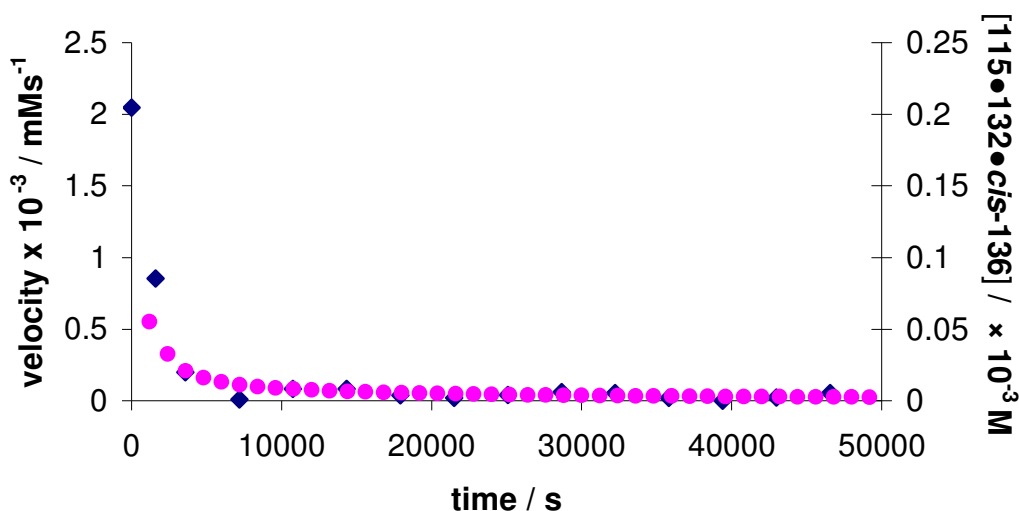


Figure 4.14 Double y axis plot of velocity (blue diamonds) or [115•132•cis-136] (pink squares) vs. time (sec). Errors in velocity are $\approx \pm 4\%$.

The graph in **Figure 4.14** illustrates an initial maximum velocity of approximately $2 \times 10^{-3} \text{ mM s}^{-1}$ which immediately declines reaching a minimum after 2 hours of $1 \times 10^{-5} \text{ mM s}^{-1}$. A similar trend is observed in the concentration of ternary complex [115•132•cis-136]. The concentration of ternary complex at the beginning of the reaction is around $200 \mu\text{M}$, but as the reaction proceeds this decreases until after 2 hours less than $10 \mu\text{M}$ is present. As stated previously the reaction velocity is directly related to the concentration of ternary complex and this fact is highlighted again in **Figure 4.14**. The graph in **Figure 4.14** indicates the decrease in rate corresponds to a fall in the ternary complex concentration, but what is the cause of this decline? This problem is similar to the one examined in Section 4.11 for the minimal replicator. At the start of the templated reaction 3 mM of complementary template was added to the reaction mixture, which will associate **115** and **132** in a ternary complex. These two molecules will react to form the *trans*-product in a duplex structure with the complementary dicarboxylic template. The duplex then dissociates releasing both molecules, however, this depends on the stability of the duplex. If the association constant K_3 is large, then turnover of the catalyst will be slow or non-existent. Therefore, this reciprocal replicating system would appear to have a high association constant for the duplex structure.

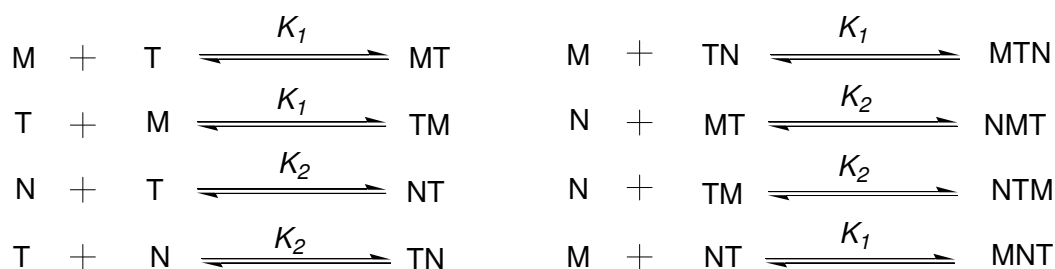
In order to determine a K_3 value for the product duplex and a rate constant (k_3) for the ternary complex a comprehensive kinetic algorithm was designed (**Scheme 4.15**), to

account for all plausible reactions and interactions in this replicating system, and to computational provide values for these parameters. A detailed discussion of this reciprocal kinetic model was provided in Chapter Three. This model uses the bimolecular rate constants determined (**Scheme 4.14**) earlier and the experimental measured association constants between binary complexes of amidopyridine derivatives with, phenyl acetic acid ($K_2 = 1000 \text{ M}^{-1}$) and benzoic acid ($K_1 = 600 \text{ M}^{-1}$).

Bimolecular Reactions



Routes towards formation of binary and ternary complexes



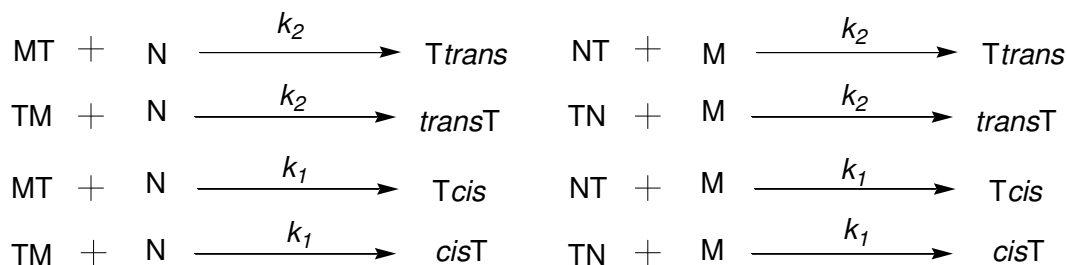
Duplex association



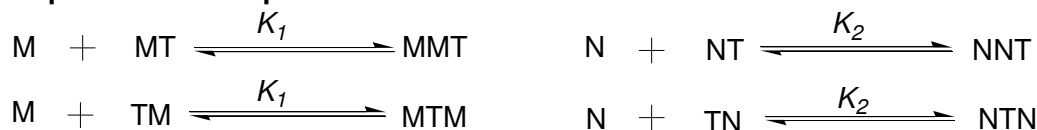
Ternary Complex reaction



Bimolecular reactions of complexes



Unproductive complexes



Scheme 4.15 Comprehensive kinetic model used in theoretical simulations of the templated reaction between **132** and **115** for the determination of reaction rate constants. M = maleimide **132**, N = nitrone **115** and *cis* and *trans* = *cis*- or *trans*- isoxazolidine **135**, T = dicarboxylic acid *cis*-**136**.

These values were used to determine a product duplex association constant, K_3 , of $6 \times 10^6 \text{ M}^{-1}$ and a rate constant value of $k_3 = 58.8 \times 10^{-4} \text{ s}^{-1}$. Through dividing the rate of the ternary complex over that of the bimolecular reaction (**Table 4.2**) a kinetic effective molarity (kEM) of $27.0 \pm 2.0 \text{ M}$ was obtained.

Table 4.2 Table of computationally determined rate constants from optimal fit curves of theoretical to experiment product concentration vs. time curves and the kinetic effective molarity of the ternary complex reaction.

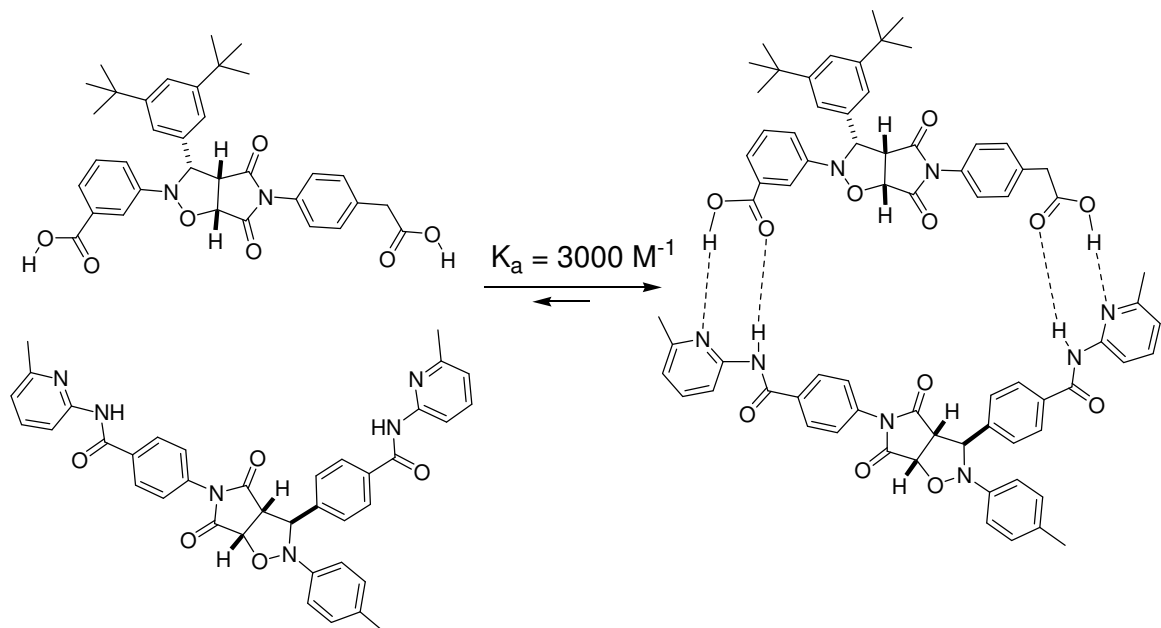
Bimolecular Reactions^a Rate Constant / $\times 10^{-4} \text{ M}^{-1} \text{ s}^{-1}$	Recognition Mediated^a Rate Constant / $\times 10^{-4} \text{ s}^{-1}$	kEM^b
$k_1 = 0.77 \pm 0.11$	Not applicable	Not applicable
$k_2 = 2.15 \pm 0.01$	$k_3 = 58.8 \pm 0.01$	$27.0 \pm 2.0 \text{ M}$

^a Rate constants relate directly to **Scheme 4.15**. ^b kEM, kinetic effective molarity is calculated by dividing the recognition mediated reaction over the bimolecular, $\text{kEM} = k_3 / k_2$.

The graph in **Figure 4.13** (b) indicated, that the duplex dissociation must have a high stability constant to explain the sudden decrease in rate as the reaction proceeds. The results from the kinetic model support this hypothesis with a high K_3 value of $6 \times 10^6 \text{ M}^{-1}$. By multiplying the individual values for the binding of phenyl acetic acid (1000 M^{-1}) and benzoic acid (600 M^{-1}) derivative to an amidopyridine derivative it is possible to estimate the binding constant for the product duplex [*trans*-**135**•*cis*-**136**]. When K_1 is multiplied by K_2 an estimated value for the product duplex can be calculated as $K_3 = 6 \times 10^5 \text{ M}^{-1}$. The fact that the value extracted from the kinetic model is higher than the estimated value indicates the presence of positive cooperativity in the binding of *trans*-**135** to *cis*-**136** isoxazolidine. A value of 5.22 kJ mol^{-1} for the Gibbs free energy of connection supports this claim of positive cooperativity.

In an attempt to provide experimental evidence for the value of the product duplex stability constant an ^1H NMR spectroscopy dilution study was conducted. A concentrated solution of the duplex in CDCl_3 was gradually diluted and monitored by 500 MHz ^1H NMR spectroscopy at 0°C . A 100 mM solution of a 1:1 mixture of **135** and **136** isoxazolidine was prepared, this solution was gradually diluted to a concentration of 1 mM. Usually the change in chemical shifts of a series of proton resonances is recorded

and compared and an average taken to determine a K_3 value, unfortunately, however, only one proton resonance on one of the pyridine ring proved suitable (**Scheme 4.16**).



Scheme 4.16 The measured association constant (K_3) for the stability of the duplex structure [*trans*-135•*cis*-136] in CDCl_3 at 0 °C.

An association constant of 3000 M^{-1} ($K_d = 3.3 \times 10^{-4} \text{ M}$) was calculated, from fitting of the experimentally determined data to the appropriate isotherm, for the binding of the dicarboxylic acid to the *trans*-bis(amidopyridine), however, as this was calculated from the chemical shift of only one proton the accuracy is questionable. This K_3 value is considerably smaller than expected judging from the theoretically determined constant from the kinetic model. To verify if this was a possible value for the association constant of the product duplex, the kinetic model in **Scheme 4.14** was used to optimally fit a theoretical curve to the product concentration vs. time plot in **Figure 4.13** (b). Previously both the duplex association and ternary complex constants were optimized to provide a suitable fit to the plot, R value = 1.6%, however, in this case the K_3 was fixed at the experimentally determined value of 3000 M^{-1} and only the ternary rate constant was optimized. However, this failed to provide a suitable fit to the product concentration vs. time curve, R value of > 30%, supporting the theory that the experimental determined product duplex constant was too low and that the theoretical value was more realistic.

In order to illustrate the influence of the product duplex [*cis*-136•*trans*-135] a series of simulations were run to provide hypothetical results for the experimental templated

reaction (**Figure 4.15**). These simulations used a range of association constants (K_3) for the product duplex above and below the calculated $6 \times 10^6 \text{ M}^{-1}$. The simulations were run using the isosim feature on the kinetic modeling package Simfit. Each simulation utilized the kinetic model in **Scheme 4.15**, the calculated bimolecular and ternary rate constants (k_1 , k_2 and k_3), and the binary association between amidopyridine and carboxylic acid or benzoic acid derivatives (1000 and 600 M^{-1}). The results of the simulated reaction between nitrones **115**, maleimide **132** and 0.3 equivalents of dicarboxylic acid *cis*-**136** are demonstrated in the product concentration vs. time graph in **Figure 4.15**. For comparisons reasons each graph contains the experimentally obtained results, with a calculated product duplex stability constant of $6 \times 10^6 \text{ M}^{-1}$.

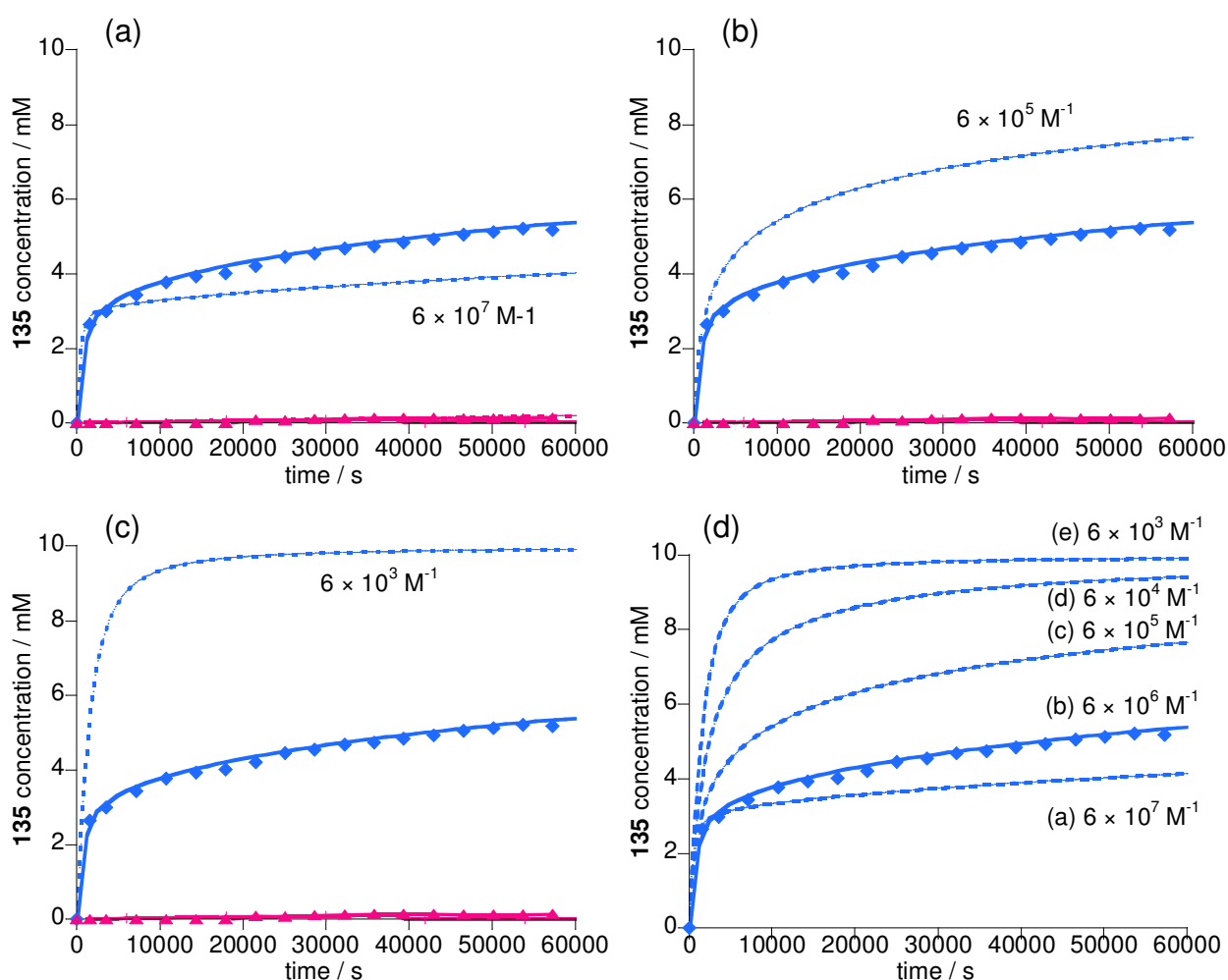


Figure 4.15 Simulated product vs. time graphs for different values of duplex, [*cis*-**136**•*trans*-**135**], association constant K_3 . Between the reaction of maleimide **115** with nitron **132** cross-catalyzed with 0.3 equivalents of dicarboxylic acid template *cis*-**136**. Blue diamonds and purple triangles with solid line through them demonstrate the experimentally obtained values for *cis*- and *trans*-**135** fitted to a duplex stability constant of $K_3 = 6 \times 10^6 \text{ M}^{-1}$. The blue and red dashed lines demonstrate simulated values for *cis*- and *trans*-**135** if an alternative value for K_3 is utilized. Errors in simulated concentrated values are $\approx \pm 6\%$.

The first graph (a) in **Figure 4.15** displays the expected product curve for a product duplex with an association constant of $6 \times 10^7 \text{ M}^{-1}$. The simulated curve displays an initially fast rate of formation for the *trans*-**135** product. However, after the formation of 3 mM of product a dramatic decrease is observed in the formation of the *trans*-bis(amidopyridine) **135**. This decline is a result of the saturation of the dicarboxylic acid *cis*-**136** template. At the start of the experiment there are 0.3 equivalents (3 mM) of free unbound template in solution. However, as a consequence of the high association constant in the product duplex, after the production of 3 mM *trans*-isoxazolidine **135** all the template is bound to its complementary partner in the [*trans*-**135**•*cis*-**136**] complex. Therefore, there is no free template available to catalyze the formation of isoxazolidine *trans*-**135** and the rate for its formation falls to the bimolecular level. Although, unclear in the first graph in **Figure 4.15** after the saturation point there is an increase in rate of production of *cis*-bis(amidopyridine) product. This increase is a result of the removal of the indirect inhibition caused by the cross-catalyzed formation of *trans*-bis(amidopyridine) **135**. The dicarboxylic acid template consumed starting material for the production of its complementary partner leaving less available for the formation of the unproductive *cis*-diastereoisomer. This effect meant the rate of formation of *cis*-**135** was less than in the bimolecular experiment (**Figure 4.13** (a)). However, when this inhibition is removed the rate can return to the normal bimolecular level, causing the slight increase in formation of the *cis*-product observed after the saturation point in **Figure 4.15** (a). The second graph (**Figure 4.15** (b)) simulates the experiment if the product duplex was less than the calculated value. When a K_a value of $6 \times 10^5 \text{ M}^{-1}$ is used in the simulation, template saturation is reduced. Although, the rate can still be observed to decrease after the production of 3 mM of *trans*-**135** isoxazolidine, the stability constant for the product duplex is low enough to allow some turnover of catalyst. Therefore, the rate of formation of the *trans*-**135** product never falls to the bimolecular level, but is still reduced. In the simulation in **Figure 4.15** (c) a lower product duplex association constant, $K_a = 6 \times 10^3 \text{ M}^{-1}$, is used than in **Figure 4.15** (b). This smaller value as we expect results in even less evidence of template saturation and reduces it enough to allow the experiment to go to almost complete conversion in 17 hours. A goal not achieved with higher values of product duplex association constants.

The high stability constant for the [*trans*-**135**•*cis*-**136**] duplex structure explains the template saturation observed in the templated experiment (**Figure 4.13** (b)). Ideally the templated reaction would be conducted over a range of dicarboxylic *cis*-**136** equivalents. Unfortunately, the solubility of template *cis*-**136** prevented cross-catalyzed experiments above 0.3 equivalents (3 mM). If such experiments were possible at concentrations above one equivalent of *cis*-isoxazolidine **136** there should be no evidence of template saturation, as there would always be more template around than produced bis(amidopyridine) *trans*-**135**. Although it is impossible to test this hypothesis experimentally, it is possible to simulate the templated experiment over a range of concentrations of added *cis*-dicarboxylic acid **136**. These simulations were conducted using the same techniques and parameters used for the K_3 simulations, except the K_3 value was kept constant and only the equivalents of template were varied. A series of simulations were run for a range of concentrations of dicarboxylic acid *cis*-**136** between 0.6 and 2.5 equivalents. The results of these hypothetical experiment simulations were plotted (**Figure 4.16**) against time to produce a series of product curves. For comparison the results of the conducted templated experiment were also plotted on the graphs.

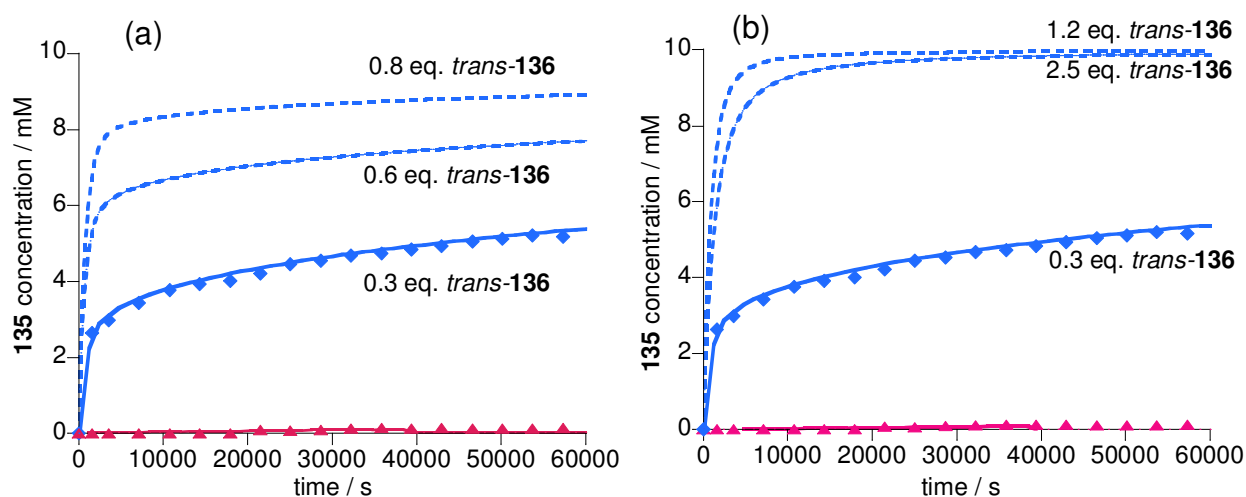


Figure 4.16 Simulated graphs of the product concentration **135** vs. time for the reactions between nitrones **115** and maleimide **132** under various equivalents of dicarboxylic acid *cis*-**136**. Purple triangles and blue diamonds with solid line through them illustrates the conducted experiment at 0.3 eq. of added dicarboxylic acid *cis*-**136**. Blue dashed line demonstrate simulated experiments at different equivalents of added template *cis*-**136**. Errors in concentration values are $\approx \pm 6\%$.

Figure 4.16 (a) examines the simulated results of the templated experiment at 0.6 and 0.8 equivalents of isoxazolidine *cis*-**136**. Both these simulations still display signs of template saturation as expected, but they also illustrate that inhibition is not occurring

until a greater *trans*-**135** concentration than in the experimental templated reaction. When the templated experiment is simulated with 1.2 equivalents of complementary template (**Figure 4.16** (b)) no saturation is observed and the reaction goes approximately to completion. In the case of the 1.2 equivalent simulation, there is always some remaining uncomplexed dicarboxylic acid *cis*-**136** to cross-catalyze the reaction between nitrones **115** and maleimide **132**, so no decrease in rate is observed. However, as the number of equivalents increases above 1.2 another inhibitor effect comes into play. In **Figure 4.16** (b) a simulated curve displays the results of the theoretical templated experiment with 2.5 equivalents of initially added template. Compared to the simulation conducted with 1.2 equivalents, this theoretical experiment demonstrates a decreased rate and level of conversion. The reason for this inhibition is a consequence of building block molecules nitrones **115** and maleimide **132** becoming isolated on different molecules of template *cis*-**136**. The bis(amidopyridine) *trans*-**135** starting materials, therefore, have to dissociate and then associate on the same molecule of template before they can react, which has the effect of decreasing the overall rate of reaction.

One of the advantages of simulating the templated experiments over a range of equivalents of complementary template is that it allows for the comparison of individual initial rates for the formation of bis(amidopyridine) *trans*-**135**. Since each simulation uses parameters derived (**Figure 4.13** (b)) from the templated experimental results, they provide realistic and accurate theoretical values for the theoretical experiments if template *cis*-**136** was more soluble. Therefore, it is fair to compare the initial rates extracted from these simulations and conducted experiments. This allows us to calculate theoretical initial rates for the template reaction if the template was soluble at concentrations greater than 0.3 equivalents. The initial rates were calculated (**Table 4.3**) using the same method discussed in Chapter Two Section **2.15**.

Table 4.3 Table of initial rate for the formation of *trans*-**135** at various concentration of added *cis*-**136** template. The table also displays calculated rate acceleration values for each of the templated reactions.

Equivalents of <i>cis</i>-136	0 ^b	0.3 ^b	0.6 ^c	0.8 ^c	1.0 ^c	1.2 ^c	1.6 ^c	2.0 ^c	2.5 ^c
Initial rate / $\times 10^{-3} \text{ mM s}^{-1}$	0.025	4.16	7.86	9.66	10.45	10.40	9.25	8.10	7.00
Rate Acceleration^a	1	173	314	386	418	416	370	325	280

^a Rate acceleration is calculated by dividing initial rate of the templated experiment over that of the bimolecular, 0 equivalents of added *cis*-**136**. ^b Experimental conducted experiments. ^c Denotes simulated experiment. Errors in initial rates and rate accelerations are calculated as $\approx \pm 6\%$.

Examination of **Table 4.3** indicates that the optimal concentration of added complementary template is between 1.0 and 1.6 equivalents, as this is the region with the greatest initial rate values (10.45 to $9.25 \times 10^{-3} \text{ mM s}^{-1}$). The initial rate increases reaching a maximum in this region before starting to fall off at concentrations above 1.6 equivalents of dicarboxylic acid *cis*-**136**. By dividing the initial rate of the templated reaction over the bimolecular initial rate, 0 equivalents of *cis*-**136** in **Table 4.3**, it is possible to derive the rate acceleration (**Table 4.3**). This rate acceleration can be plotted against the complementary template equivalents to produce the graph in **Figure 4.17**.

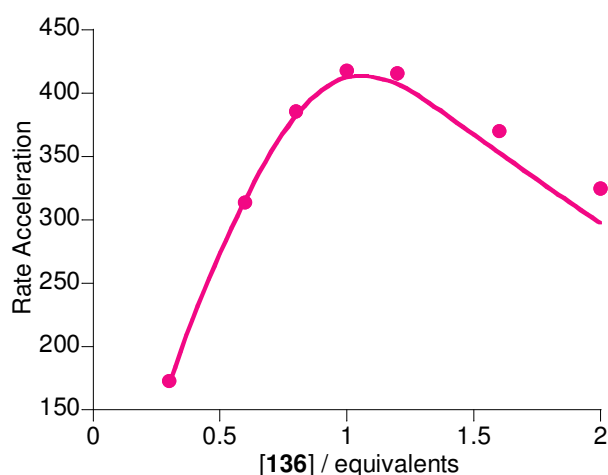


Figure 4.17 Rate acceleration vs. equivalents of dicarboxylic acid template *cis*-**136** added to the reaction between nitrones **115** and maleimide **132**. Measure rate accelerations are represented as pink circles, the solid pink line represents a fitted curve optimized for the product duplex association.

Analysis of the graph in **Figure 4.17** indicates that the maximum rate acceleration occurs at around 1.0 equivalents (10 mM) of template, with close to a 400 fold rate

enhancement over the bimolecular reaction for the formation of bis(amidopyridine) *trans*-**135**. Therefore, when ≈ 10 mM of dicarboxylic acid *cis*-**136** is added at the beginning of the reaction the greatest possible concentration of ternary complex possible must be formed. Since the ternary complex is responsible for the rate acceleration. At concentrations below 10 mM of added complementary template excess starting materials maleimide **132** and nitrone **115** are present unbound in the free solution. Therefore, the concentration of ternary complex is not at its optimal value. For reasons mentioned previous in this section, at concentrations greater than 1.2 equivalents the rate accelerations decreases.

The solid pink line in **Figure 4.17** corresponds to an independent binding site model. This model uses the previously discussed principle that rate acceleration is directly proportional to the concentration of active ternary complex. A detailed discussion of this model was conducted in Chapter One Section **1.19**. In this model a function is utilized, which describes the variation in the concentration of ternary complex with added template, to fit the observed experimental rate acceleration curve. This function utilizes only the binding constant for the product duplex, K_a and a scaling factor as variable parameters (**Figure 4.18**).

$$\text{Solving for } [R]: [R]^2 + \left(2[T]_{tot} - [R]_{tot} + \frac{1}{K}\right)[R] - \frac{[R]_{tot}}{K} = 0$$

$$ax^2 + bx + c = 0$$

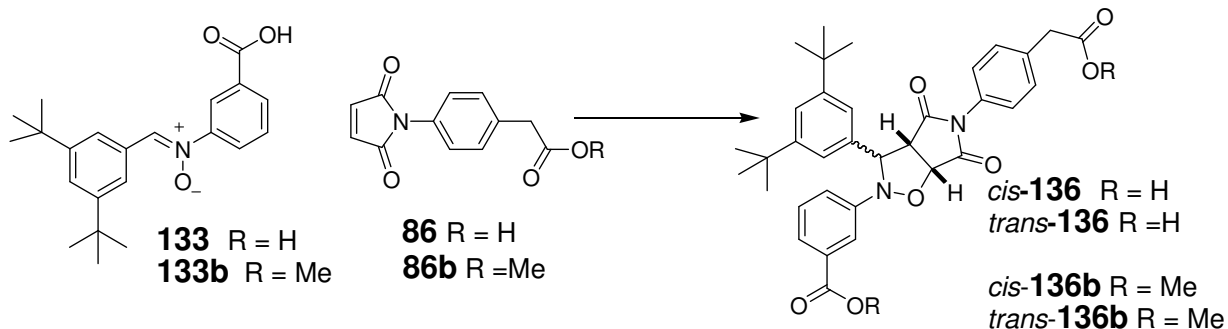
$$[TR_2] = [T]_{tot} \left(\frac{K[R]}{1 + K[R]} \right)^2$$

Figure 4.18 Equations for solving the concentration of free reagent $[R]$ and ternary complex $[TR_2]$.

Utilizing this function the best fit for theoretical to the experimental data was obtained when an association constant of $1.10 \times 10^6 \text{ M}^{-1}$ was used for the product duplex. This value is in the same order of magnitude as the theoretically determined association constant K_2 ($6 \times 10^6 \text{ M}^{-1}$) from the optimized kinetic model.

4.13 Reciprocal Replicator *cis*-136

The cross-catalytic template *cis*-136 is formed from the 1,3-dipolar cycloaddition reaction (Scheme 4.16) between nitron **133** and maleimide **86**.



Scheme 4.16 1,3-dipolar cycloaddition reaction between **133** and **86** for the formation of reciprocal template *cis*-136 and *trans*-136.

The behavior of this reciprocal replicator was investigated in an identical manner to previous cross-catalytic systems with two types of experiment conducted, a bimolecular control and a templated reaction. The results of these two reactions can be examined in

Figure 4.19

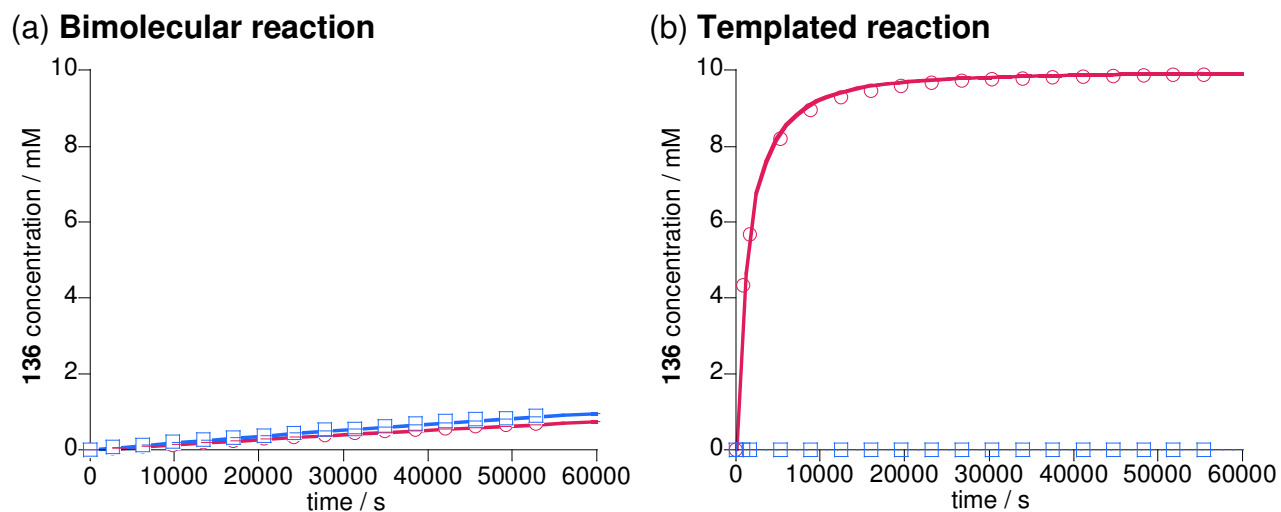


Figure 4.19 Product concentration vs. time profile for (a) bimolecular reaction between equimolar concentrations of **133** and **86** ($[\mathbf{133}] = [\mathbf{86}] = 10$ mM) at 0 °C in CDCl_3 , for the formation of *trans*-136 (blue squares) and *cis*-136 (pink circles) and (b) templated reaction with 1.5 equivalents (15 mM) of bis(amidopyridine) template **135** ($[\mathbf{86}] = [\mathbf{133}] = 10$ mM), for the formation of *trans*-136 (blue squares) and *cis*-136 (pink circles). Optimal fit curves are represented as solid lines. Errors in concentration values are $\approx \pm 4$ %

The bimolecular reaction (**Figure 4.19** (b)) proceeded slowly at 0 °C, forming a 1:1 ratio of *cis*- and *trans*-diastereoisomers (Appendix Four). Overall conversion of the reaction after 16 hours in CDCl₃ is <20%. Optimal fit of a theoretical curve to the product concentration vs. time plot in **Figure 4.19** (b), using the method described in Section 7.8, was used to obtain rate constants (k_1 and k_2) for the formation of both *cis*- and *trans*-isoxazolidines (R = 3.86%).



Rate Constant / $\times 10^{-4} \text{ M}^{-1}\text{s}^{-1}$ $k_1 = 1.49 \pm 0.01$ $k_2 = 1.96 \pm 0.01$

Scheme 4.17 Kinetic model used to computationally determine rate constants k_1 and k_2 for the formation of *cis*- and *trans*-**136** and optimized values. M = maleimide **86**, N = nitrone **115** and *cis* and *trans* = *cis*- or *trans*-isoxazolidine **136**.

The templated reaction could be conducted in greater concentrations of complementary template than in the reciprocal system examined in Section 4.12. This was a result of the increased solubility of the complementary bis(amidopyridine) partner which was soluble in concentrations greater than 20 mM. Therefore, the template reaction was conducted with a variety of different concentrations of *trans*-bis(amidopyridine) **135** added at the beginning of the reaction. The plot in **Figure 4.19** (b) was the result of the addition of 1.5 equivalents (15 mM) of bis(amidopyridine) template at the start of the experiment. Examination of the templated reaction plot indicated the occurrence of a large ‘template effect’, with the *cis*-product formed at a much faster rate than in the bimolecular reaction (**Figure 4.19** (a) and (b)). The increased formation of the *cis*-product is accompanied by a decline in production of the *trans*-isoxazolidine to almost non-existent concentrations. The diastereoisomeric ratio in the bimolecular reaction was around 1:1 where as in the templated reaction in **Figure 4.19** (b) it can be considered to be completely *cis* selective (around 100:1 in favor of the *cis*- isoxazolidine). With the increased rate of formation of the *cis*-product in the complementary templated reaction comes an inevitable rise in conversion. In the bimolecular reaction conversion was less than <20% after 16 hours, but in the cross-catalytic experiment the conversion is close to 100% (Appendix Four). These data prove that the *cis*- isoxazolidine is the replicating template supporting the hypothesis discussed in the transition state diagrams (**Figure 4.2**).

The amplification in formation of the *cis*-dicarboxylic acid template is highly efficient from examination of the curve in the product concentration vs. time plot (**Figure 4.19** (b)), with

high conversion and selectivity. To help provide a measure of the efficiency of this system a rate constant value, k_3 , was determined for the cross-catalytic reaction in the ternary complex. These values were determined computationally using the kinetic model (**Scheme 4.18**), using the method discussed in detail in Section 7.8, to fit a theoretical optimal curve to the experimental product vs. concentration plot. However, instead of optimizing the curve to fit one experiment it was used to fit three templated reactions (9 mM, 12 mM and 15 mM) with a different initial concentration of bis(amidopyridine) **135**. Solubility of the dicarboxylic acid template **136** limited this investigation in the previous section, but here that is not an issue. Through fitting a series of optimal curves to three different templated reactions a more accurate measure of the rate constant for the ternary complex reaction (k_3) could be calculated. This kinetic model is almost identical to the one used in the previous reciprocal system, Section 4.12, apart from the fact that the *cis*-isoxazolidine reaction is the cross-catalyzed (**Scheme 4.18**) product and, therefore, is formed in the ternary complex reaction, replacing the *trans*- isomer in previous models.

The same binary association constants between the amidopyridine with, phenylacetic acid ($K_1 = 1000 \text{ M}^{-1}$) and benzoic acid ($K_2 = 600 \text{ M}^{-1}$) were used as well as the product duplex association constant ($K_3 = 6 \times 10^6 \text{ M}^{-1}$) which was determined for the kinetic model in the complementary reciprocal system (Section 4.12). The value for the rate constant of the ternary complex is stated in the **Table 4.4**, after an R value of 3.3% was obtained from the fit of the kinetic model.

Table 4.4 Table of computationally determined rate constants from optimal fit curves of theoretical to experiment product concentration vs. time curves and the kinetic effective molarity of the ternary complex reaction.

<i>Bimolecular Reactions</i> Rate constant / $\times 10^{-4} \text{ M}^{-1} \text{ s}^{-1}$	<i>Recognition Mediated</i> Rate constant / $\times 10^{-4} \text{ s}^{-1}$	<i>kEM</i>
$k_1 = 1.49 \pm 0.01$	$k_3 = 20.9 \pm 0.70$	$14.0 \pm 1.7 \text{ M}$
$K_2 = 1.96 \pm 0.01$	Not applicable	Not applicable

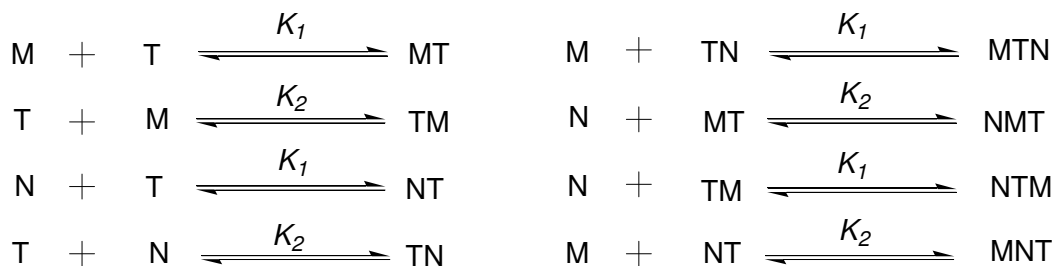
^a Rate constants relate directly to **Scheme 4.18**. ^b kEM, kinetic effective molarity is calculated by dividing the recognition mediated reaction over the bimolecular, $kEM = k_3 / k_1$.

The kEM of the *pseudo*-unimolecular ternary complex reaction was determined by dividing the catalyzed rate constant by the bimolecular reaction to get an effective molarity of $14.0 \pm 1.7 \text{ M}$.

Bimolecular Reactions



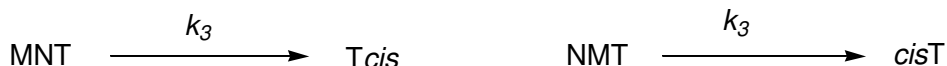
Routes towards formation of binary and ternary complexes



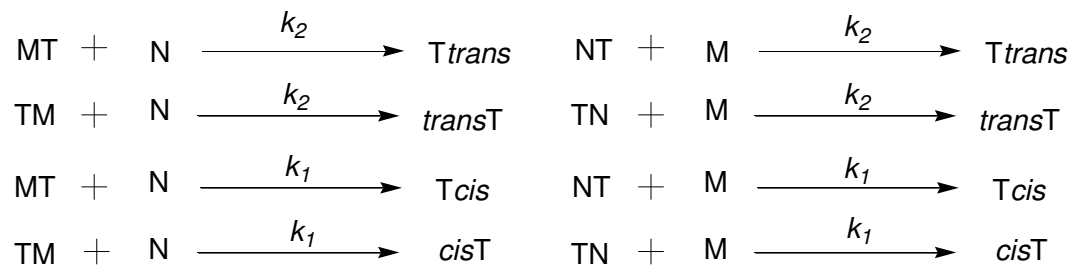
Duplex association



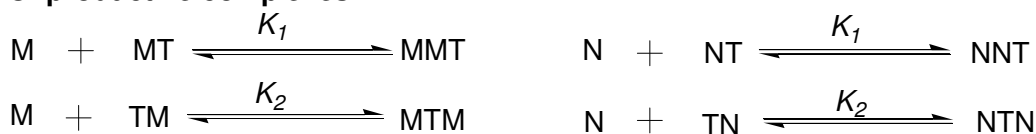
Ternary Complex reaction



Bimolecular reactions of complexes



Unproductive complexes



Scheme 4.18 Comprehensive kinetic model used in theoretical simulations of the templated reaction between **86** and **133** for the determination of reaction rate constants. M = maleimide **86**, N = nitrone **133** and *cis* and *trans* = *cis*- or *trans*- isoxazolidine **136**, T = bis(amidopyridine) **135**.

In addition to allowing a more accurate determination of the rate constant value for the ternary complex, conducting the templated reactions over a range of added template concentrations allows for individual rate acceleration to be compared against template equivalents. The templated reactions were conducted under seven different concentrations of added template, 1 mM, 4.5 mM, 6.5 mM, 9 mM, 12 mM, 15 mM and 20 mM (0.1 to 2.0 equivalents).

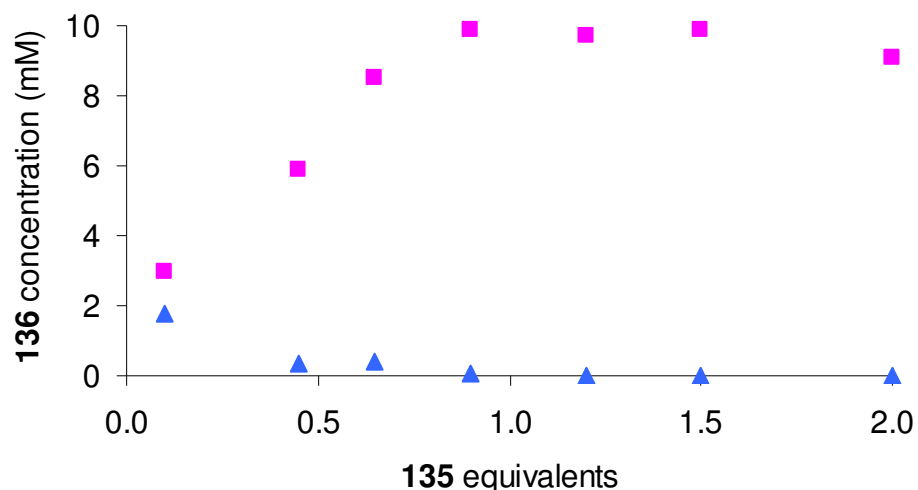
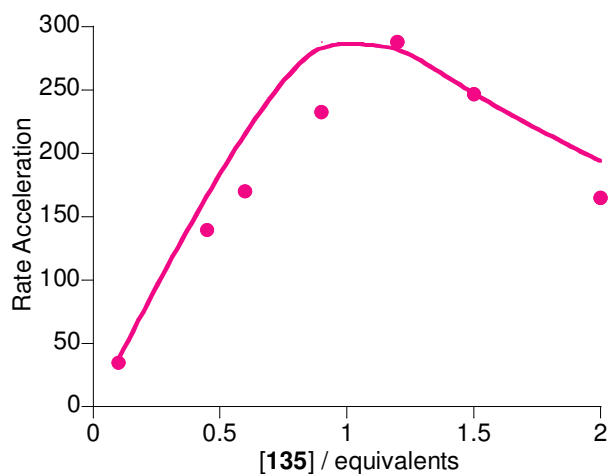


Figure 4.20 Chart of *cis*- (pink) and *trans*- (blue) product concentration vs. equivalents of bis(amidopyridine) template after 60000 seconds. Errors in concentration values $\approx \pm 4\%$.

The graph in **Figure 4.20** shows an increase in conversion from 0.1 to 0.9 equivalents, after this conversion is constant until 1.5 equivalents. Above 1.5 equivalents a slight drop in conversion is observed, probably as a result of building block molecules for the dicarboxylic acid template **136** being isolated on different molecules of the complementary bis(amidopyridine) replicator **135**. This graph demonstrates that the optimal concentration of template is between 9 mM and 15 mM (0.9-1.5 equivalents) for the cross-catalytic formation of dicarboxylic acid *cis*-**136**.

As was discussed in Chapter Two and Chapter Three by conducting the templated reaction under a range of template concentrations it was possible to measure the initial rate for each reaction. In addition by comparing this to the initial rate of the bimolecular reaction a measure of rate acceleration vs. template equivalents could be plotted (**Figure 4.21**).



Equivalents of <i>trans</i>-135	0	0.1	0.45	0.65	0.9	1.2	1.5	2.0
Initial rate / $\times 10^{-3} \text{ mM s}^{-1}$	0.02	0.59	2.36	2.85	3.90	4.83	4.15	2.27
Rate Acceleration^a	1	35	140	170	233	288	247	165

Figure 4.21 (a) Rate acceleration vs. equivalents of bis(amidopyridine) template **136** added to the reaction between **133** and **86**. Solid pink line represents the fit of the independent binding site model. (b) Table of initial rates for each templated reaction and rate acceleration of templated reaction compared to bimolecular. ^a Rate acceleration is calculated by dividing initial rate of the templated experiment over that of the bimolecular, 0 equivalents of added *cis*-**136**. Errors in concentration are assumed to be $\approx \pm 4\%$

The pink circles in **Figure 4.21** (a) indicate the experimentally measured rate accelerations determined from dividing the initial rate of the templated reaction at a specific concentration over that of the initial rate of the bimolecular reaction, 0 equivalents of *trans*-**135** in **Figure 4.21** (b). Examination of the plot reveals that a maximum rate acceleration for the reaction between nitron **133** and maleimide **86** is observed at around 1.2 equivalent of bis(amidopyridine) template **135**. This rate acceleration is in the order of around 290 folds greater than that of the bimolecular reaction. Therefore, at 1.2 equivalents of template the maximum concentration of ternary complex possible must be present, as it is this structure which is directly responsible for catalysis. Even at low concentrations of template, 1 mM and 4.5 mM (0.1 and 0.45 equivalents), a substantial rate acceleration is achieved. At concentrations below 12 mM of bis(amidopyridine) **135** a substantial amount of building block molecules **133** and **86** is present in the free solution. Whereas at higher equivalents (above 1.5 equivalents)

building block molecules are isolated on different molecules of template, and have to dissociate and then re-associate to react.

The pink line on **Figure 4.21** (a) corresponds to the independent binding site model (**Figure 4.18**). This provides the best model for this replicating system when the K_3 for the [*cis*-**136**•*trans*-**135**] complex is $2.5 \times 10^6 \text{ M}^{-1}$, which is similar in magnitude to the value determined for the product duplex, $6 \times 10^6 \text{ M}^{-1}$, previously (Section **4.12**) from fitting of the kinetic model. Although the fit of the independent binding site model to the experimentally obtained rate acceleration values is far from perfect, the value obtained for the product duplex is similar in magnitude to the one obtained using the kinetic model (**Scheme 4.18**). Therefore it was decided not to carry out simulated experiments, similar to the ones conducted in Chapter Three. The individual association constants between amidopyridine with phenylacetic acid and with benzoic acid are 1000 M^{-1} and 600 M^{-1} at $0 \text{ }^\circ\text{C}$ in CDCl_3 . Using the equation in **Figure 4.7** an empirical value for cooperativity of $+5.22 \text{ kJ mol}^{-1}$ was calculated indicating that the [*cis*-**136**•*trans*-**135**] complex exhibits positive cooperativity, implying that *cis*-**136** and *trans*-**135** are excellent fits for one another.

4.14 Hypercyclic Networks

The ultimate goal of this replicating network was to produce a series of replicators. Achieving this goal meant it was, therefore, possible to investigate the complex interactions which occur when each of the two minimal and reciprocal systems are forced to compete against each other in a potential hypercyclic network. In a hypercyclic network, each of the four different replicating templates compete (**Figure 4.1**) for the same building block molecules maleimide **132**, **86** and nitrone **115**, **133**. An example of this competition is the fact that maleimide **86** can react with nitrone **115** to form the minimal template *trans*-**118** or it can react with nitrone **133** to form reciprocal replicator *cis*-**136**. The results of all these possible reactions is that a total of eight different products can be formed, four pairs of diastereoisomers. As a described in Chapter Three, this competition for resources can result in a survival of the fittest situation with reciprocal and minimal systems battling for dominance. Another possibility is that each replicating system cross-catalyzes its neighbor resulting in a negative feedback loop,

where a decline in one system is corrected by an increase in formation of the others, which in turn increases the formation of the first system.

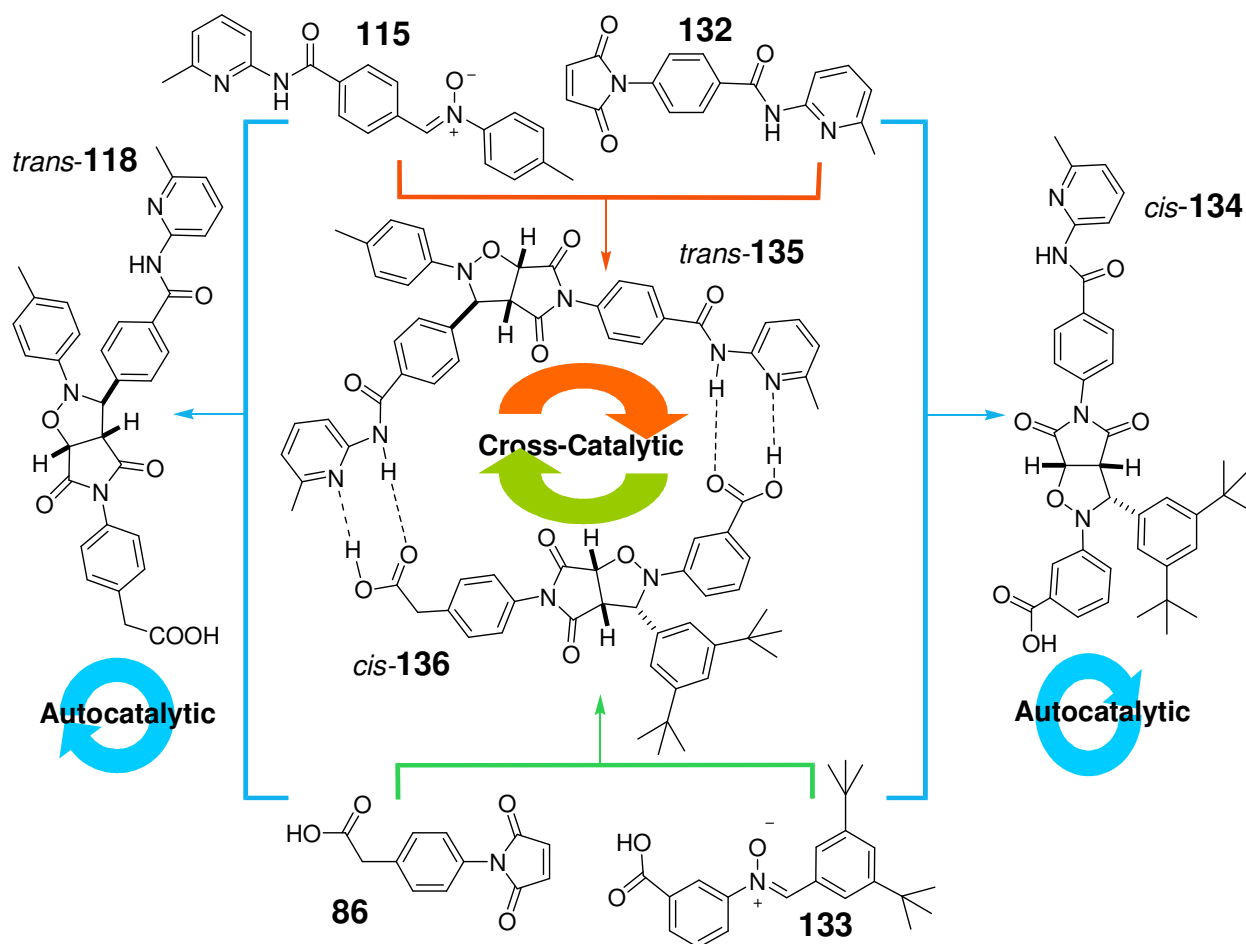


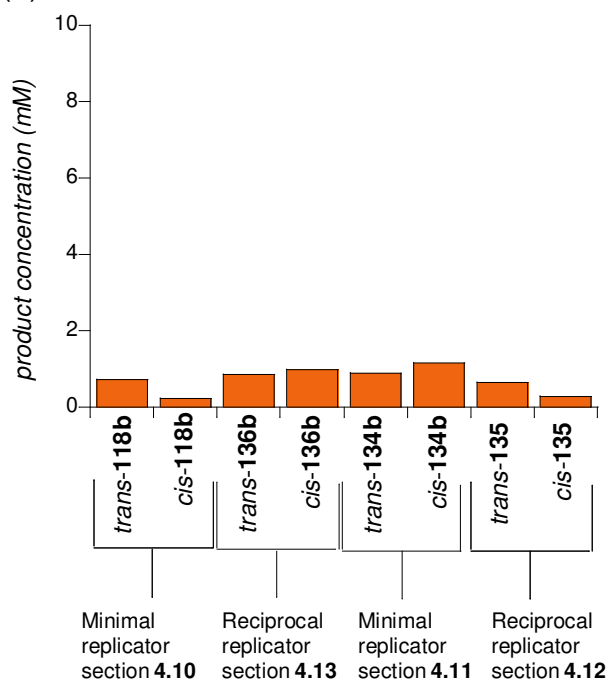
Figure 4.1 Building block molecules maleimide **132**, **86** and nitron **115**, **133** can react to form minimal replicators *trans*-**118**, *cis*-**134** or cross-catalytic templates *trans*-**135**, *cis*-**136**.

In order to study such a complex system a series of four component experiments (nitron **115**, **133** and maleimide **86**, **132**) were conducted. The investigation of this hypercyclic network is conducted in a similar manner to how the replicators were studied in isolation, with bimolecular control, recognition mediated native and templated reactions. The goals of each type of reaction are also identical to before. The aim of the bimolecular reaction control is to provide data on the non-catalyzed reactions between the different nitrones and maleimides to provide a reference point to which all recognition mediated and template experiments can be compared. As with bimolecular reaction controls in the minimal systems Section 4.10 and 4.11, ester equivalents of **86** and **133** were used in this control experiment. The native reaction was designed to allow

for the recognition mediated interactions necessary for replication, therefore, all recognition sites on building block molecules **86**, **115**, **132** and **133** were readily available. The purpose of the templated reactions was to selectively enhance the formation of a desired product by addition of the complementary template at the start of the experiment. The product and starting material peaks deconvoluted in the ^1H NMR spectra for these experiments, in order to determine species concentrations can be examined in Appendix Six.

The ester control reaction between nitrones **115**, **133b** and maleimide **86b**, **132** proceeded slowly at 0 °C in CDCl_3 , with conversion after 16 hours (overnight) < 25%. The overall concentrations after 16 hours can be examined in **Figure 4.21** (a).

(a) Ester control reaction



(b) Recognition mediated Cycle 1

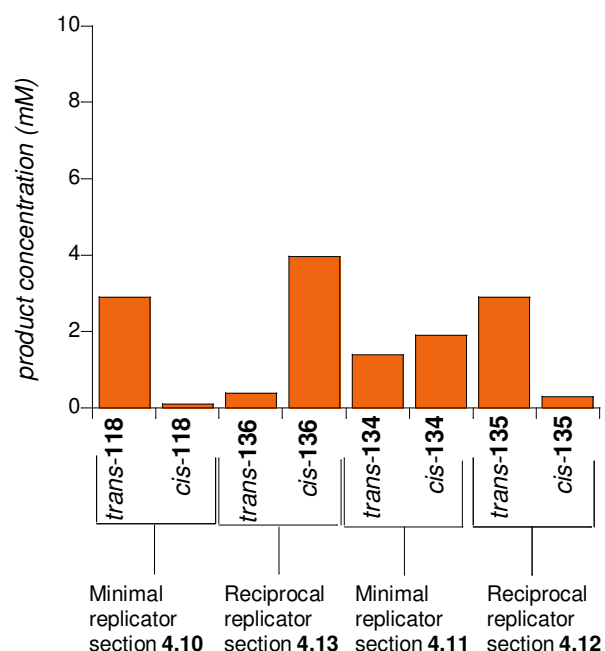


Figure 4.21 (a) Results of ester control reaction between equimolar concentrations (10 mM) of maleimide **86**, nitrone **115**, maleimide **132** and nitrone **133** in CDCl_3 after 16 hours. (b) Results of recognition mediated reaction between equimolar concentrations (10 mM) of maleimide **86**, nitrone **115**, maleimide **132** and nitrone **133** in CDCl_3 after 16 hours. Errors in concentration values are $\approx \pm 4\%$

This bar chart demonstrates that no amplification and hence no replication is occurring of the templates *trans*-**118**, **135** and *cis*-**136**, **134**. The *cis:trans* selectivity of each of the diastereoisomers for the different non associative templates is approximately identical to the ratios in the isolated bimolecular reactions. Having now determined reference values for the non-catalyzed reaction the native reaction could now be investigated in detail.

The native reaction was conducted using maleimide **86**, **132** and nitron **115**, **133** at 0 °C in CDCl₃ overnight. The different resultant product concentrations of this reaction were plotted on the graph in **Figure 4.21** (b). Examination of the graph reveals immediate differences between the native reaction and the bimolecular control. The overall conversion for the reaction after 16 hours has increased to approximately 70%, which is a result of an increase in formation of the replicating templates *cis*-**134**, **-136** and *trans*-**118**,**-135**. Conversely the overall concentration of the non-reproducing products *trans*-**134**,**-136** and *cis*-**118** ,**-135** has declined. Therefore, not only has there been an increase in conversion, but this increase has been selective (amplification), this fact is demonstrated in **Table 4.5**.

Table 4.5 Table of *cis* to *trans* ratio of non-replicating isoxazoles, **118**(b), **135**, **136**(b) and **134**(b) and replicating templates, *trans*-**118**, **-135** and *cis*-**134**,**-136**, for bimolecular and native four component experiments.

	<i>trans</i> : <i>cis</i> 118 / b	<i>trans</i> : <i>cis</i> 136 / b	<i>trans</i> : <i>cis</i> 134 / b	<i>trans</i> : <i>cis</i> 135
Bimolecular reaction	3:1	≈ 1:1	≈ 1:1	3:1
Native reaction	≈ 30:1	≈ 1:10	≈ 1:1.3	≈ 10:1

The largest increase in selectivity was recorded for the minimal system **118**, with a 10 fold rise in selectivity in favor of the replicating *trans*-isoxazolidine. Both the reciprocal systems experienced an increase in selectivity, with a 10:1 ratio in favor of the cross-catalytic template. The least affected replicator is the *cis*-minimal replicator **134**, this is not a major surprise as only a small autocatalytic effect was present in the isolated native reaction, with a slight increase in favor of the *cis*-replicator. Comparisons between the minimal and the reciprocal systems reveal that the cross-catalytic templates are marginally favored over their self-replicating counterparts, 6.85 mM to 4.80 mM. The results of the native reaction demonstrate the efficiency of each of the individual replicators, despite the competition and potential inhibition from an increased number of unproductive complexes evidence of replication is still present for each system.

After investigation of the native system, the next logical test of the replicating network is to investigate the mechanism of selectively favoring one particular system. In order to achieve this goal the experiment was designed similar to the native reaction, by reacting

maleimide **86**, **132** and nitrone, **115**, **133** together in CDCl_3 at 0°C , but with the addition of prefabricated template at the beginning of the reaction. This type of experiment was carried out for all four replicating templates. The resulting product concentrations for each of these reactions after 16 hours were recorded. Each reaction was compared to the native experiment and the difference in individual product concentrations between the templated and native experiments (Δ) was plotted (**Figure 4.22-4.25**) on a graph of Δ concentration vs. product diastereoisomer. A second graph of the natural logarithm (\ln) of the ratio of the templated to native product concentration ($[\text{T}_{\text{product}}]:[\text{N}_{\text{product}}]$) multiplied by individual isoxazolidine product concentration for the templated reaction C_T , enhancement factor, was also plotted (**Figure 4.22-4.25**). The charts in **Figure 4.22-4.25** exclude the addition of the prefabricated template from the concentration values, therefore, only products formed in the reaction are taken into consideration.

(a) Δ product concentration

(b) Enhancement factor

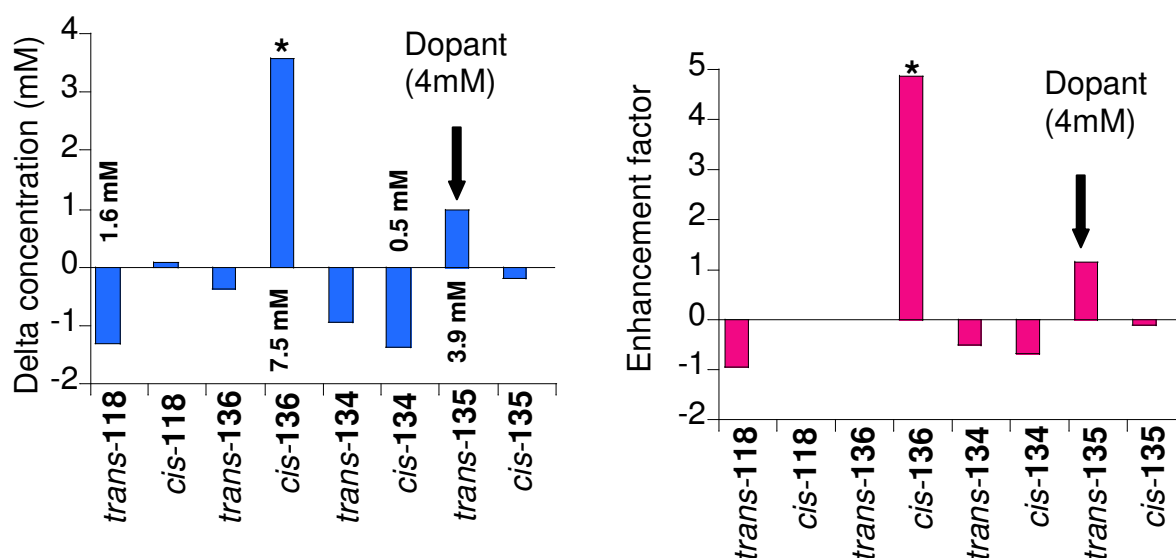


Figure 4.22 Bis(amidopyridine) *trans*-135 templated (4 mM) equimolar four component reaction (maleimide [**86**], [**132**] and nitrone [**133**], [**115**] equals 10 mM). (a) Δ product concentration, templated subtracted from native reaction isoxazolidine concentrations, vs. diastereoisomer (blue bars). Actual concentrations for the four major products are given above and below the bars for this four component experiment. (b) Natural log of ratio $[\text{Template}_{\text{product}}]/[\text{Native}_{\text{product}}] \times C_T$, enhancement factor, (pink bars) vs. diastereoisomer. * Denotes expected enhanced product. Errors in concentration values are $\approx \pm 4\%$.

The graph in **Figure 4.22** (a) displays the results of the four component experiment, templated with 0.4 equivalents (4 mM) of bis(amidopyridine) **135** template. The reaction was conducted overnight and the overall conversion was around 70%, similar to the native reaction. The chart demonstrates that the largest increase in concentration is of the complementary partner, *cis*-dicarboxylic acid **136**, of the *trans*-isoxazolidine **135**. The *cis*-**136** product has increased by 4 mM compared to the native reaction, whereas the *trans*-diastereoisomer **136** has declined very slightly, making it the leading isoxazolidine formed in the 4 component reaction, at 7.5 mM. The enhancement factor for the *cis*-dicarboxylic acid demonstrates the greatest rise, a factor of 5, of all the possible products as shown in **Figure 4.22** (b). This enhancement factor demonstrates that as well as the *cis*-isoxazolidine being formed at the greatest concentration, it is also synthesized at the fastest rate.

The only other product which exhibits any significant increase in formation, in this templated experiment, is the bis(amidopyridine) **135** product itself. This increased formation is a result of the indirect relationship inherent in reciprocal replication. As discussed above the addition of bis(amidopyridine) resulted in an increased formation of the complementary *cis*-dicarboxylic template **136**. However, by forming the *cis*-isoxazolidine **136** you, therefore, can cross-catalyze the formation of bis(amidopyridine) from nitrene **115** and maleimide **132**. Therefore, any increase in formation of one cross-catalytic template will inevitably result in an increase in formation of the complementary partner. The Δ concentration values in **Figure 4.22** (a) demonstrated that *trans*-**135** has increased in concentration by 1 mM compared to the native reaction over the same period of time. This increase in formation also means there must have been an increase in the enhancement factor.

Both minimal replicator's *trans*-**118** and *cis*-**134** are formed in a decreased amount than in the native reaction. This decline is a result of a diminished stock of building block molecules, which are being consumed in the production of the reciprocal templates.

Having studied the effects of adding the bis(amidopyridine) template to the four component reaction, the next reasonable experiment was to conduct the four component reaction with the addition of prefabricated *cis*-dicarboxylic acid **136**. After studying *trans*-isoxazolidine **135**, it will be interesting to investigate the affect of the complementary partner *cis*-**136** on the four component reaction. The templated reaction was conducted with 0.1 equivalents (1 mM) of dicarboxylic acid **136**, unfortunately

insolubility issues with the template prevent studies with greater concentrations. Conversion for this templated reaction after 16 hours was approximately 65%, slightly lower than that of the native reaction. However, analysis (**Figure 4.23** (a)) of the individual change in product concentration for each isoxazolidine and the enhancement factor indicates the incremented formation of *trans*-**135** of the products.

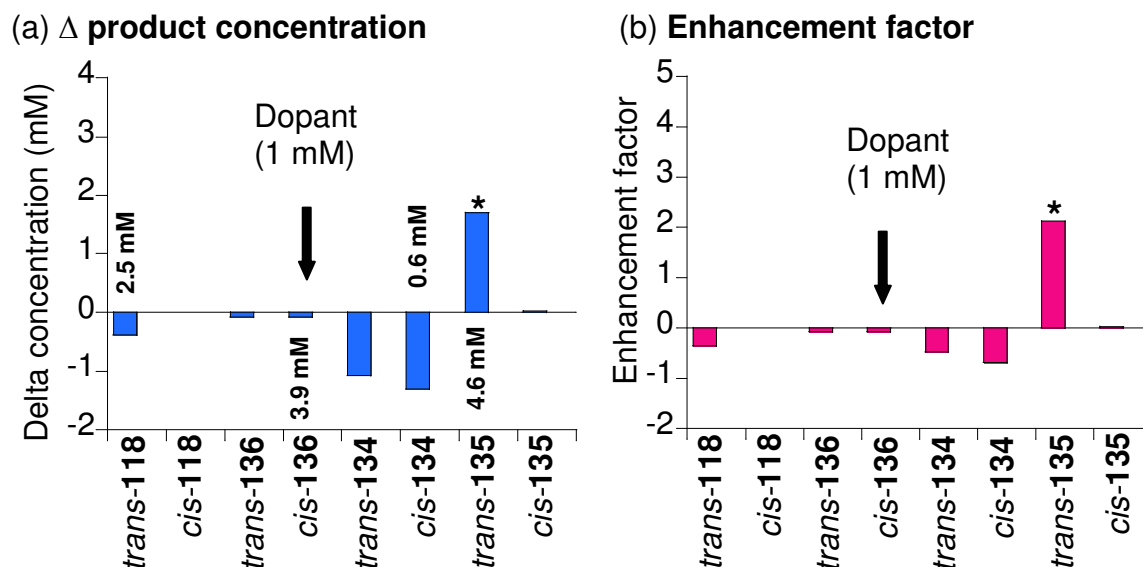


Figure 4.23 Dicarboxylic acid *cis*-**136**, templated (1 mM) equimolar four component reaction (maleimide [**86**], [**132**] and nitrone [**115**], [**133**] equals 10 mM). (a) Δ product concentration, templated subtracted from native reaction isoxazolidine concentrations, vs. diastereoisomer (blue bars). Actual concentrations for the four major products are given above and below the bars for this four component experiment. (b) Natural log of ratio $[\text{Template}_{\text{product}}]/[\text{Native}_{\text{product}}] \times C_T$, enhancement factor, (pink bars) vs. diastereoisomer. * Denotes expected enhanced product. Errors in concentration values are $\approx \pm 4\%$

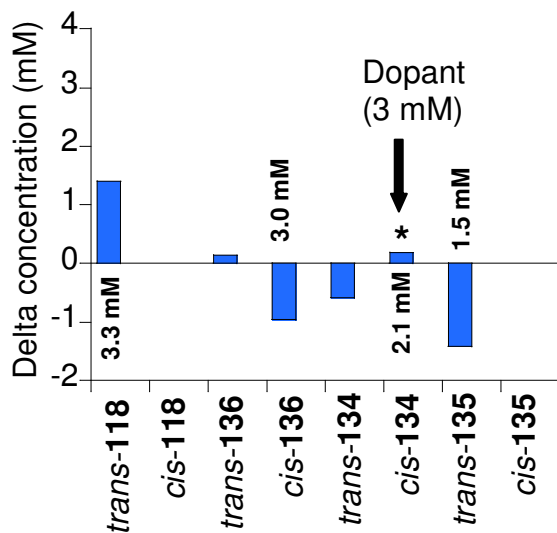
From the analysis of the graph in **Figure 4.23** (a) it is immediately apparent that the only significant increase in isoxazolidine formation is for the dicarboxylic acid complementary partner *trans*-**135**. This replicator has increased by a concentration of 2 mM compared to the native reaction and the enhancement factor values demonstrate that this product is replicating more rapidly than its counterparts. In the previous bis(amidopyridine), templated reaction an indirect catalysis of the added prefabricated template was observed due to the cross-catalytic nature of the reciprocal system. However, in the current reaction no increased formation of the *cis*-dicarboxylic acid template was observed, with the concentration almost equivalent to that in the native reaction. This fact would tend to imply that although *cis*-**136** is an excellent catalyst for the formation of *trans*-**135**, the *trans*-isoxazolidine **135** is not as good a catalyst for the formation of

dicarboxylic acid template **136**. If a greater concentration of bis(amidopyridine) **135** was produced in this four component reaction then cross-catalysis of the dicarboxylic acid template would be observed.

In a similar fashion to the bis(amidopyridine) template reaction, the dicarboxylic acid catalyzed reaction results in decreased formation of the minimal replicating isoxazolidines and their non-associative diastereoisomers. It can be observed that the self-replicator **134** is the most effected, with a larger difference in concentration between templated and native reactions and a large negative value for the enhancement factor. The minimal replicator **118** experiences only a smaller decrease of around 0.4 mM, this information demonstrates the increased efficiency of *trans*- **118** compared to *cis*-**134**.

In both these two templated reactions we have demonstrated the efficiency of the reciprocal systems, the addition of reciprocal template has resulted in cross-catalysis of the complementary partner. These reactions have proven that reciprocal replication can be templated and selected in complicated four component experiments. Having studied the effect of the cross-catalytic templates on the four component experiments, we decided to investigate the effect of adding prefabricated minimal template at the beginning of a four component reaction.

The first minimal replicator doped into the four component reaction was *cis*-isoxazolidine **134**. The reaction was conducted with the addition of 3 mM of *cis* minimal template **134** at the beginning of the experiment. After 16 hours, the experiment was found to have gone to approximately 65% conversion. However, as in the previous templated reaction increases and decreases were observed when individual product concentrations were analyzed. The changes in concentration between the templated and native reactions, Δ , and the enhancement factors were recorded and the data plotted in the graphs in **Figure 4.24**.

(a) Δ Product concentration

(b) Enhancement factor

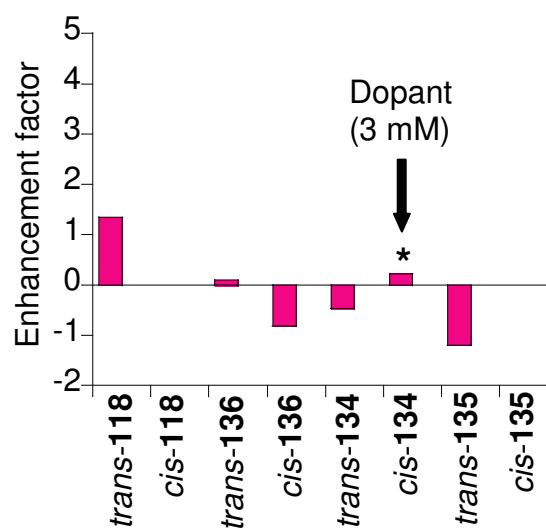


Figure 4.24 Minimal replicator *cis*-134, templated (3 mM) equimolar four component reaction (maleimide [86], [132] and nitrone [115], [133] equals 10 mM). (a) Δ product concentration, templated subtracted from native reaction isoxazolidine concentrations, vs. diastereoisomer (blue bars). Actual concentrations for the four major products are given above and below the bars for this four component experiment. (b) Natural log of ratio $[\text{Template}_{\text{product}}]/[\text{Native}_{\text{product}}] \times C_T$, enhancement factor, (pink bars) vs. diastereoisomer. * Denotes expected enhanced product. Errors in concentration values are $\approx \pm 4\%$

The analysis of the graph in **Figure 4.24** (a) reveals only a slight increase in formation of the minimal template *cis*-134 with the largest increase in formation occurring for the other minimal template *trans*-118. As there is only a small increase in formation of *cis* self-replicator it is unlikely, but not impossible, its is siphoning off enough maleimide 132 and nitrone 133 to explain the indirect increase in formation of *trans*-118. Another possibility is that *cis* minimal template 134 is cross-catalyzing the formation of *trans*-self-replicator 118. Not only is *trans*-118 formed at the greatest amount it formation also exhibits the greatest acceleration, demonstrated by analyzing the enhancement factor. These factors could indicate that *cis*-134 is better at cross-catalyzing the formation of *trans*-118 than replicating itself.

While addition of the minimal template has enhanced the production of the two minimal systems it has caused a decline in the formation of the reciprocal templates. This decrease in concentration of *trans*-135 and *cis*-136 in the templated reaction compared to the native reaction is an indirect result of increased formation of the minimal templates. This effect was discussed before in which a reduction in starting material

molecules, as a result of their use in other reactions, causes a decline in formation of the non-templated isoxazolidine products. Although overall there is a reduction in the formation of the reciprocal templates, analyzing the data after 16 hours fails to reveal the full reaction mechanism of the replicating network. If we compare (**Table 4.6**) the concentration of minimal replicator **118** to reciprocal replicator **136** as the reaction proceeds we observe an interesting trend.

Table 4.6 Table of ratios of concentrations of minimal replicator *trans*-**118** to reciprocal replicator *cis*-**136** at certain time intervals.

Time (hours)	≈ 4.5	≈ 8.5	≈ 13.5	≈ 18
[<i>trans</i>-118]:[<i>cis</i>-136]	1.6:1	1.4:1	1.3:1	1.2:1

The **Table 4.6** displays the calculated ratio of the concentration of minimal replicator **118** to reciprocal replicator **136**. As the reaction proceeds the ratio between the self replicating and cross-catalytic templates decreases. This decline indicates the minimal template is replicating faster at the start of the reaction, but towards the end cross-catalysis of the reciprocal template is quicker. Analysis of the reciprocal and minimal models of replication can explain this trend. In the minimal model as soon as one molecule of template is formed, it can autocatalytically catalyze the formation of another and so on in an exponential fashion. However, in the reciprocal model once one molecule of template is formed it first has to catalyze the formation of a complementary partner, which in turn can cross-catalyze the formation of the original molecule of template. This fact therefore implies, at the start of the reaction autocatalysis will occur more rapidly than cross-catalysis, which is what we observe in this template four component experiment. Judging from the **Table 4.6**, if the reaction was allowed to continue, eventually reciprocal replication would overtake minimal replication in this reaction.

The final templated reaction investigated involved the addition of 1.5 mM of minimal template-**118** to the four component reaction between maleimide **86**, **132** and nitron **115**, **133**. This reaction was run overnight with an overall conversion of approximately 65%. Individual concentrations for each product were extracted and compared to the native reaction and the results plotted (**Figure 4.25** (a)) in a graph of Δ product concentration vs. time. On a second graph the natural logarithm of the ratio of product

concentrations in the template reaction was compared (**Figure 4.25** (b)) to that of the native reaction, multiplied by C_T , enhancement factor. The initial concentration of added prefabricated template was excluded from the data plotted in **Figure 4.25** (a) and (b).

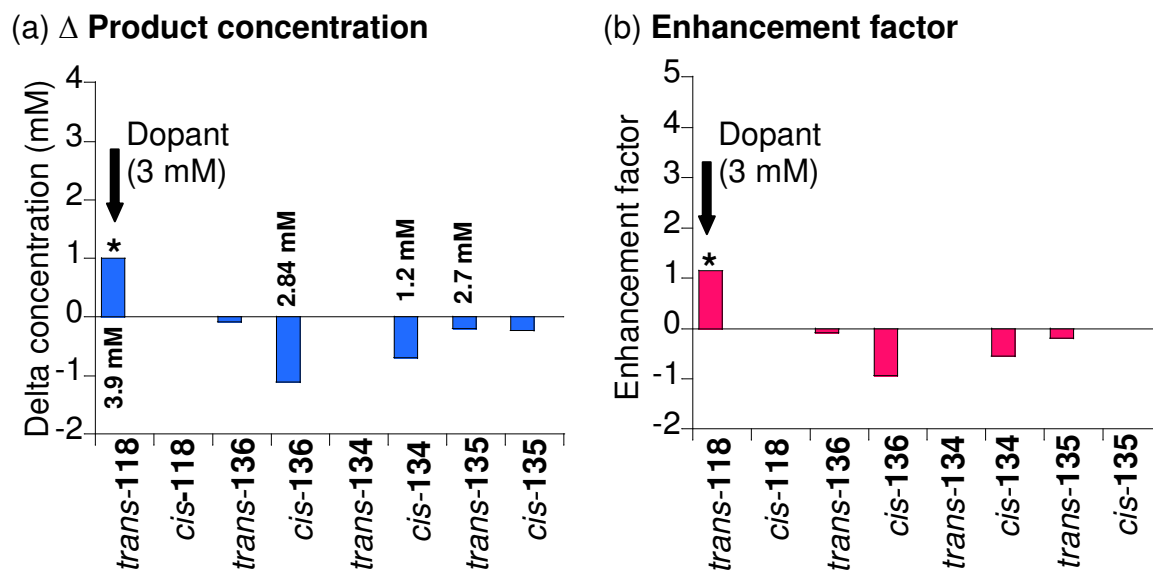


Figure 4.25 Minimal replicator *trans*-118, templated (1.5 mM) equimolar four component reaction (maleimide [86], [132] and nitrone [115], [133] equals 10 mM). (a) Δ product concentration, templated subtracted from native reaction isoxazolidine concentrations, vs. diastereoisomer (blue bars). Actual concentrations for the four major products are given above and below the bars for this four component experiment. (b) Natural log of ratio $[\text{Template}_{\text{product}}]/[\text{Native}_{\text{product}}] \times C_T$, enhancement factor, (pink bars) vs. diastereoisomer. * Denotes expected enhanced product. Errors in concentration values are $\approx \pm 4\%$.

The data plotted in **Figure 4.25** reveal that only an increase in concentration of the minimal template **118** itself is present, no other reaction is cross-catalyzed or accelerated indirectly. Addition of *trans*-118 at the start of the reactions has resulted in an increase of 1 mM over that of the native reaction. Whereas, the minimal template **134** potential cross-catalyzed the formation of *trans*-118 the reverse is not true, with minimal template **118** catalytic only towards its own reproduction. The growth of minimal template **118** utilizes building block molecules maleimide **86** and nitrone **115**, meaning the formation of reciprocal templates **135** and **136** are indirectly inhibited with less starting materials available for their production.

The templated four component experiments have demonstrated that it is possible to selectively enhance the formation of a replicating system, minimal or reciprocal, through the addition of a complementary partner at the beginning of the reaction. This increase in concentration is despite all the possible destructive and non-productive binding complexes and unwanted reactions possible in the four component experiment.

These templated reactions have demonstrated the efficiency of the two reciprocal systems. In the two reciprocal doped four component experiments addition of the cross-catalytic isoxazolidines resulted in a larger increase in the formation of their complementary partners, than was seen for the increase in minimal template in the self-replicator doped four component experiments. As well as this, although minimal templates were enhanced in the self-replicator doped four component experiments there is evidence of the reciprocal templates becoming increasingly more favored in these experiments as the reaction proceeds. These two facts would lead one to conclude that the reciprocal systems are more efficient than their two minimal counterparts.

In order to conclude our investigation into this potential hypercyclic network one set of reactions still remain. The final group of experiments involved conducting several cycles of the four component experiment, each time doping the next cycle with a percentage of the last cycle. For example the 1st Cycle of the four component reaction is simply the native reaction. The 2nd Cycle is a new four component experiment doped at the start with a molar percentage of the 1st Cycle. Through conducting such a set of cyclic experiments it is hypothesized that each cycle should observe a template effect with less of the non-associative templates formed and the more efficient replicating systems, reciprocal or minimal, being selectively enhanced over its competitors. A series of four experiments were designed, the first was simply the native experiment described at the start of this section. The second reaction was known as Cycle 2 and was the four component experiment between maleimide **86**, **132** and nitron **115**, **133** doped with 20 mol% of Cycle 1. Two different Cycle 3 were designed the first was simple the four component experiment doped at the beginning with 100 mol% of Cycle 2. The alternative Cycle 3 was the four component experiment doped at the beginning, with 20 mol% of the bis(amidopyridine) templated four component reaction. The results of these four reactions were plotted (**Figure 4.26**) on bar charts of product concentration vs. product diastereoisomer.

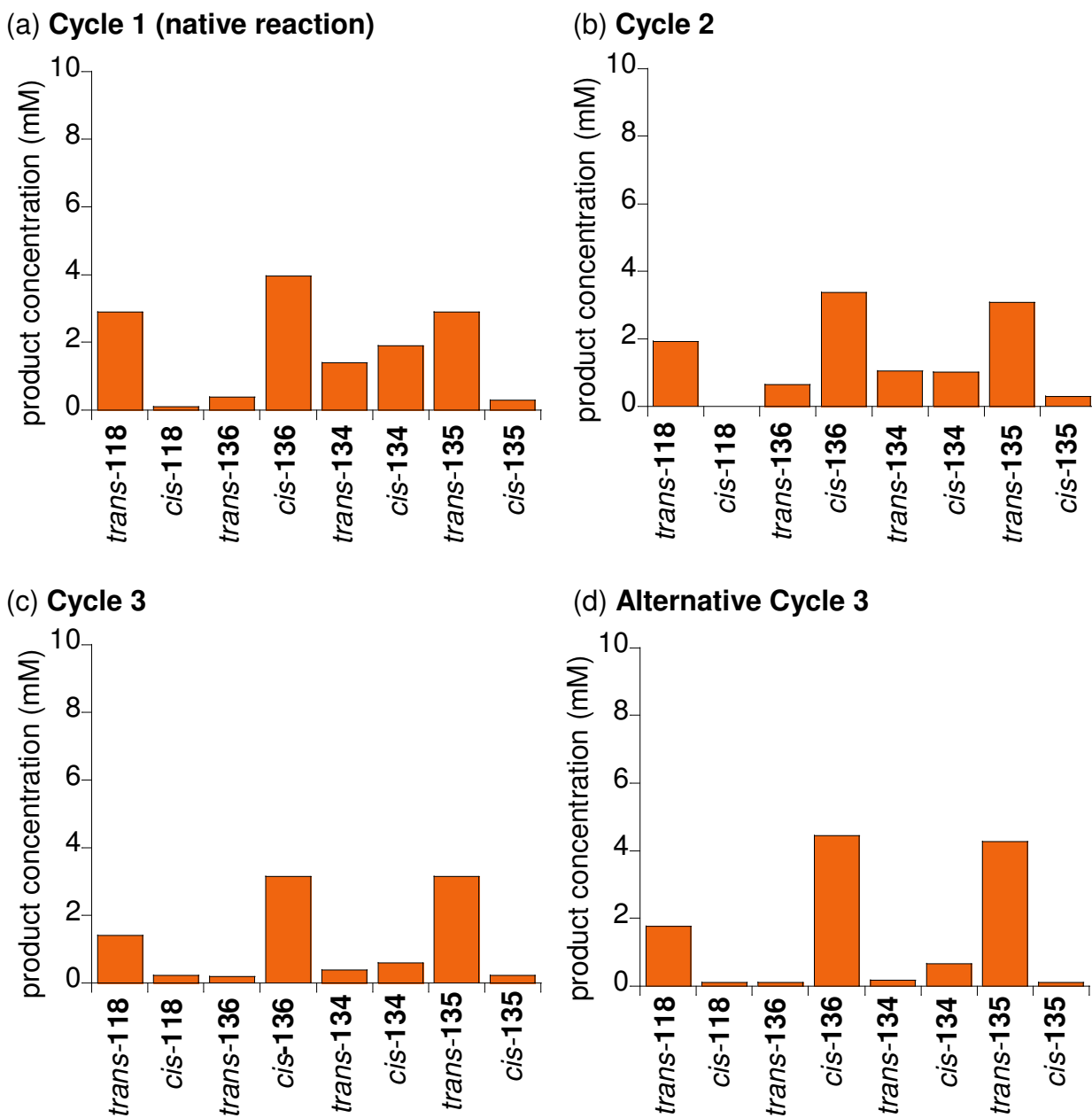


Figure 4.26 Cyclic reactions bar charts. (a) Cycle 1 or native four component reaction between equimolar concentrations (10 mM) of maleimide **86**, **132** and nitrone **115**, **133** in CDCl_3 at 0°C after 16 hours. (b) Cycle 2 four component reaction between equimolar concentrations (10 mM) of maleimide **86**, **132** and nitrone **115**, **133** doped with 20 mol% of Cycle 1, in CDCl_3 at 0°C after 16 hours. (c) Cycle 3 four component reaction between equimolar concentrations (10 mM) of maleimide **86**, **132** and nitrone **115**, **133** doped with 100 mol% of Cycle 2 in CDCl_3 at 0°C after 16 hours. (d) Alternative Cycle 3 four component reaction between equimolar concentrations (10 mM) of maleimide **86**, **132** and nitrone **115**, **133** doped with 20 mol% of bis(amidopyridine) four component experiment, in CDCl_3 at 0°C after 16 hours. Errors in concentration values are $\approx \pm 4\%$.

The product concentration graph for the native reactions was described at the start of this section, and is used here to provide a reference to which to compare the template

effects in Cycle 2 and Cycle 3. In Cycle 1 the graph shows a favoring in concentration for the reciprocal templates over that of the minimal templates of 2 mM. In the Cycle 2 four component reaction the product concentration vs. diastereoisomer graph indicates an overall decrease in conversion from Cycle 1, 60% compared to 70% for the native experiment. The individual conversion for each isoxazolidine product either exhibits no change or a decrease in concentration. This result, however, does not mean there is no template effect although conversion may have decrease there is still an enhancement in selectivity. The two reciprocal templates although at an overall lower concentration, are present in a greater ratio to the minimal replicating counterparts than in the native reaction, 2.2:1 (6.5:3.0 mM) compared to 1.4:1 (6.8:4.8 mM). The explanation for this effect could be a result of the slower nature of the cross-catalytic system with replication only occurring after two cycles compared to one for the minimal model. The overall concentrations for the reciprocal templates *trans*-**135** and *cis*-**136** are similar to those in the native reaction, 6.5 compared to 6.8, therefore, the small concentration of reciprocal templates added from Cycle 1 might selectively favor the cross-catalytic templates without enhancing rate. Therefore, in the final cycle it was decided to add a 100 mol% of Cycle 2 to a new four component experiment (Cycle 3). This experiment will include a larger concentration of reciprocal template than was added to Cycle 2 and it was, therefore, hoped that not only would an increase in selectivity be observed but also an increase in conversion. However, examination of Cycle 3 demonstrated that this was not the case. The selectivity towards the reciprocal templates has increased in Cycle 3, 3.2:1 compared to 2.2:1 in Cycle 2, but no increase in concentration of either *cis*-**136** or *trans*-**135** was observed. Despite adding a more concentrated solution of reciprocal templates no increase in conversion has occurred. A possible explanation for this lack of growth could be the high association constant, $K_a = 6 \times 10^6 \text{ M}^{-1}$ for the reciprocal duplex discussed earlier in Section 4.12-13. Despite the addition of an increased concentration of cross-catalytic templates only minute quantities of these isoxazolidines are present in the free form, with the majority present in the [*cis*-**136**•*trans*-**135**] duplex. In Cycle 2 a 20 mol% of Cycle 1 was added to the four component experiment, the total concentration of added *cis*-**136** added was 0.8 mM, of this concentration 1.3×10^{-7} mM was present in the free form at the start of the reaction. Therefore, even adding 100 mol% of Cycle 2 to a new four component reaction in Cycle 3 is not increasing the amount of free template

significantly enough, 6.3×10^{-7} mM of *cis*-**136**, to observe a major increase in conversion.

The final reaction studied was an alternative experiment to the previously investigated Cycle 3. The concentration data for each of the isoxazolidines produced in this experiment were extracted and the results plotted in a graph of product concentration vs. diastereoisomer. Examination of the graph indicated not only an increase in selectivity of cross-catalytic to self-replicating templates when compared to Cycle 3, but also an increase in conversion of *cis*-**136** and *trans*-**135**, 4.45 and 4.30 mM compared to 3.15 and 3.10 mM in Cycle 3. This result appears to contradict the explanation of why no increase in conversion is present in Cycles 2 and 3. In alternative Cycle 3, a 20 mol% solution of a four component experiment templated with 4 mM of bis(amdiopyridine) and left to react overnight, which produced a reaction mixture containing large concentration of cross-catalytic template *trans*-**135** and *cis*-**136**, was added as doping reagent. The cross-catalytic templates in this doping reagent are still in the ratio of 1:1. Therefore, the majority of template will exist in the duplex form, and for the reason discussed earlier in this section the high K_a value will mean marginal quantities of free template are available. Therefore, why is there an increase in conversion in this cycle but not in Cycles 2 and 3? An answer could lie in the isoxazolidine selectivity of the doping reagents. In Cycle 1 and Cycle 2 although the reciprocal templates are formed in the largest concentrations reasonable quantities of the minimal templates and some non-associative products are formed. These reaction mixtures are then used to dope Cycles 2 and 3 and it is possible that the non cross-catalytic isoxazolidine could be associating with the recognition sites on *trans*-**135** and *cis*-**136** forming non-productive complexes. These complexes would inhibit the reciprocal template's ability to associate complementary building block molecules. As mentioned earlier the K_a value for the reciprocal duplex means low concentrations of free *cis*-**136** and *trans*-**135** in solution. Therefore, even though the concentration of non cross-catalytic isoxazolidines is not large, it is still considerably larger than the concentration of free *cis*-**136** and *trans*-**135**. However, in alternative Cycle 3 the doping reagent is a solution mainly containing reciprocal template, with smaller quantities of minimal replicators **118** and **134** and non-associative complexes than the doping reagents in Cycles 2 and 3, meaning the free cross-catalytic template is less inhibited resulting in the increase in conversion observed in **Figure 4.26** (d).

4.15 Conclusions

At the start of this chapter the main goal was to design, synthesize and analyze a replicating network containing two minimal and two reciprocal replicating systems. In order to ensure this objective had been successfully achieved each replicator was studied in isolation. The first system examined was the self-replication of template *trans*-**118**. This minimal system was studied in Chapter Three at 25 mM but had to be repeated for an initial concentration of 10 mM for building block molecules nitrone **115** and maleimide **86**. This investigation produced comparable results to the examination at 25 mM concentration.

The second system studied was the redesigned minimal replicator *cis*-**134**. This replicator was unique as a result of it being the first *cis* replicator studied, for reasons discussed at the beginning of this chapter. Investigation of isoxazolidine *cis*-**134** revealed evidence of autocatalysis and self-replication. However, as a result of a high association constant, $K_a = 2.6 \times 10^6 \text{ M}^{-1}$, between the product duplex, replication was partially inhibited. Interestingly, all previously replicator enhanced the formation of the diastereoisomer already favoured in the bimolecular reaction, but in this system there was no selectivity to enhance. The bimolecular reaction between maleimide **132** and nitrone **133** afforded a 1:1 mixture of *cis*- and *trans*-isoxazolidine. Comparing this minimal replicator to *trans*-**118** is, therefore, difficult because although the selectivity and rate are much greater it is starting from a more favored position.

Investigation of two reciprocal networks revealed a pair of very efficient cross-catalytic templates. However, as in Chapter Three solubility of the dicarboxylic acid template limited the study of the cross-catalytic formation of the bis(amidopyridine) partner. Fortunately *trans*-**135** had no such problems with solubility, allowing a detailed examination of the cross-catalytic formation of the complementary partner *cis*-**136**. Reciprocal system **4.13** was demonstrated to be most efficient when ≈ 1.2 equivalents of bis(amidopyridine) **135** were added at the start of the reaction. Investigation of this system also supported the conclusion of a large association constant for the product duplex [*cis*-**136**•*trans*-**135**] reasoned in the study of reciprocal system **4.12**.

After demonstrating the ability of each of these systems to replicate in isolation, we now moved on to study our true goal, of how these systems will interact in a complex

potential hypercyclic replicating network. A series of four component reactions were designed to test the efficiency of each replicating system when it is forced to compete for the same starting materials. The templated four component experiments disclosed that it was possible to selectively favor a particular replicating template through addition of its complementary partner. The foremost results were obtained when the four component experiment was doped with reciprocal templates *trans*-**135** and *cis*-**136**. Although, addition of minimal template resulted in a favoring of the self-replicating systems after 16 hours, the rate of formation of the reciprocal replicating isoxazolidines was increasing as the reaction proceeded. This augmentation meant eventually even in these minimal doped reactions reciprocal replication would overtake self-replication. The final set of experiments conducted, were the cyclic four component reactions. By running a series of different cycles of the four component experiment it was hoped an increase in rate of formation and in selectivity of the most efficient replicators would be observed. However, although an increase in selectivity was observed from Cycles 1-3 no increase in concentration was observed for the major products. The examination of Cycles 1-3 and alternative Cycle 3, indicated that this could be the result of a combination of inhibition due to non-associative product, other replicating templates in doped solution and the high association constant between the [*cis*-**136**•*trans*-**135**] complex. These cyclic reactions again demonstrated that in this replicating network the most efficacious templates were the cross-catalytic isoxazolidines, with the selectivity increasing with each cycle at the expense of their minimal counterparts. These templated four component experiments have proven that it is possible to selectively favor the cross-catalytic products, by addition of reciprocal template at the beginning of the reaction. The four component experiments have demonstrated that the reciprocal templates are more efficient than the minimal templates in this replicating network. This fact is somewhat surprising when you consider the autocatalytic nature of minimal replicators. However, the experiments conducted in this Chapter have demonstrated the increased performance of reciprocal replicators *cis*-**136** and *trans*-**135**.

4.16 Future work

In Chapter Five the focus of this thesis will steer to future applications and advancements in the field of replication. Every replicating system discussed up until now has been under kinetic control, with the product formed at the fastest rate being the selected product. However, if a reversible reaction is used to form templates in a replicating system it should be possible to develop a system under thermodynamic control. In kinetic controlled reactions the dominate product is the one with the fastest rate. However, in a thermodynamic controlled reaction, as a result of the reversible nature of the bond forming step, the reaction is free to explore all possible products with the dominate product eventually being the one with the lowest energy. In the next Chapter, two different potentially thermodynamically controlled replicating systems will be investigated.

5. The future of small molecule synthetic replicating systems

5.1 Dynamic Combinatorial Chemistry

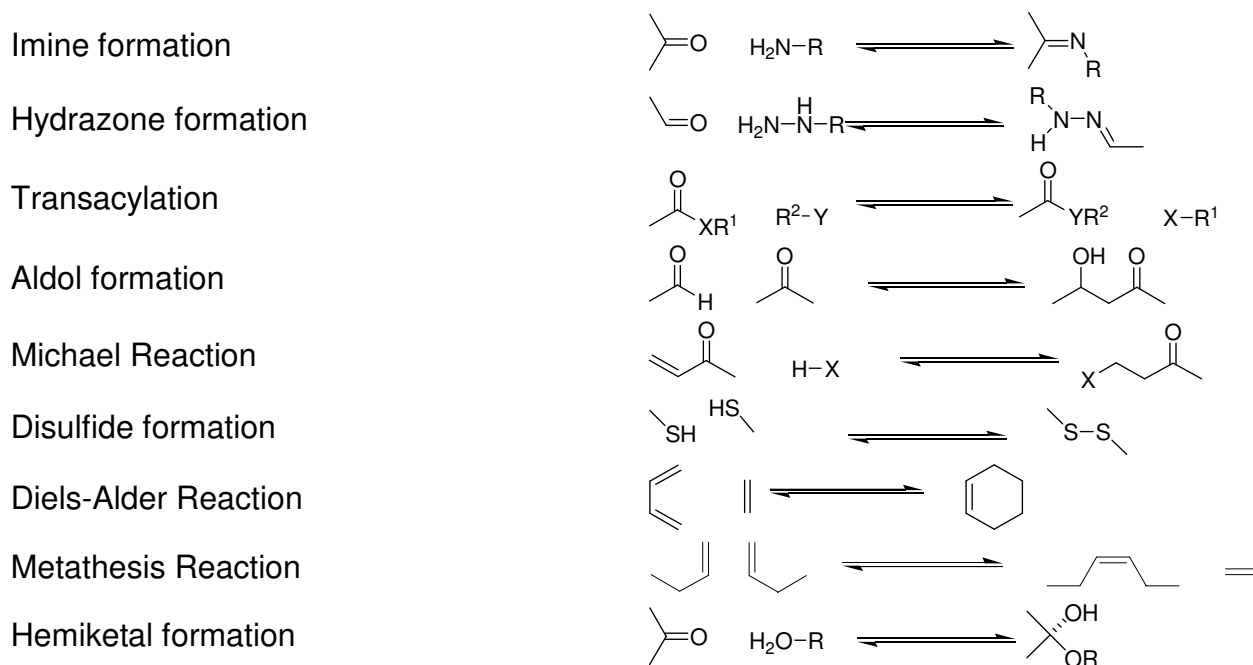
There are a number of possible applications for synthetic replicating system but one application which is under examination by research in the Philp group is their application in dynamic combinatorial chemistry^[187-188].

The term dynamic combinatorial chemistry (DCC) first arose in 1996 when Lehn^[189-191] used it to describe the result of varying the features of a metal salt on the type of helicate species generated^[189]. Since then DCC has been defined as combinatorial chemistry under thermodynamic control. In DCC all the different constituents interact with each other to form a dynamic combinatorial library (DCL) of molecules. All the species in DCL are in thermodynamic equilibrium, with the dominant components of the library in theory being the most thermodynamically stable and it is this feature which makes DCC unique. Since the whole system is under thermodynamic control, the stability of the members in the library can be affected through changing the experimental conditions, by varying the temperature, pressure or addition of a template to name a few examples. A change in stability of the library members will shift the equilibrium amplifying the formation of certain members while reducing others.

In order for a DCL to be under thermodynamic control a reversible chemical process is required to allow the interconversion between different library members. There are a number of possibilities for the nature of this chemical process like noncovalent (hydrogen bonds), coordinative and covalent bonds. However, whether it is covalent or noncovalent, the reversible reaction needs to meet six fundamental requirements. The first prerequisite is that the reversible reaction has to be reversible over a reasonable time-scale. A second key precondition is that equilibrium and selection should occur simultaneously. Therefore, the conditions for the reversible reaction need to be compatible with the experimental conditions of selection; this includes functional groups, solvent, pH etc. The third requirement is that the reaction conditions are mild in order to prevent disruption of the delicate non-covalent interactions often utilized as molecular recognition in DCL's. Another essential feature of the reversible bond is that library members at equilibrium are soluble. Otherwise an insoluble library member could act as a thermodynamic or kinetic trap. The reversible chemical process should also have the

potential to be stopped at any time kinetically halting the exchange of library members, allowing for them to be isolated and handled. Finally, the last requirement of the reversible exchange reactions is that all library species are isoenergetic, in order to stop formation of mixtures which are strongly biased toward certain products. This feature means it is therefore, not energetically costly to shift the equilibrium in any direction. However, this final prerequisite is not often met as a consequence of entropic factors. As discussed previously, a number of different bonding processes are possible for the reversible chemical process, but only a brief investigation of reversible covalent bonds utilized in DCC will be given here. A few examples of the different covalent bond formations utilized in DCC can be examined in **Table 5.1**.

Table 5.1 A selection of potentially reversible covalent bond forming reactions utilized in dynamic combinatorial chemistry. A more comprehensive list can be found in reference 187



Imine exchange^[193-195] is a common reversible reaction used in DCC and has been used to form cyclic ligands for transition metals for a long time; imines are prepared through the acid catalysis of ketones and aldehydes with amine derivatives. This reaction was originally discovered^[192] by Schiff and, therefore, imines are often referred to as Schiff bases. The imine condensation reaction is acid catalyzed, therefore, only aldehydes and ketones which do not aldolize easily in acidic media can be condensed efficiently with amines in strong acid catalysts. As a consequence of this feature, DCL's utilizing imine

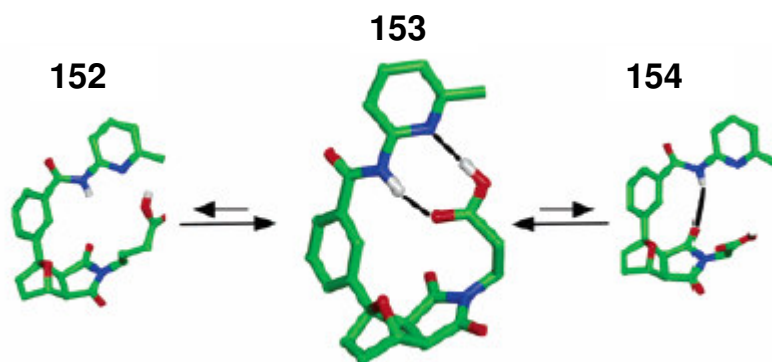


Figure 5.1 Three structures formed through binary complexes, **152**, **153** and **154**. Carbon atoms shown as green, oxygen atoms as red, nitrogen atoms as blue and hydrogen atoms as white.

The other two structures were formed *via* binary complexes, but the resultant products were not stabilized through two hydrogen bonds meaning they were less stable and, therefore, will undergo a retro Diels-Alder reaction at an increased rate to molecule **153**. All replicating systems and networks investigated in this thesis have been under kinetic control, a small combinatorial library of molecules has been created and their function analyzed. The bond forming step to link starting materials together to form replicating templates has been a non reversible reaction step. The *endo* Diels-Alder replicator in Chapter Two was reversible; however, the favored product was both the kinetic and thermodynamic product, which was the irreversible *exo*-**105** product.

The aim of this Chapter is to investigate a new type of replicating network, one which is under thermodynamic control, a dynamic replicating network capable of either minimal or reciprocal replication depending on the external conditions. If the experiment is under thermodynamic control, starting from a library of building blocks capable of forming either minimal or cross-catalytic replicators, the most stable type of replicator should have an advantage. Addition of template should also effect the composition of the dynamic replicating network.

In order to achieve this goal, the first objective must be the use of a suitable reversible bond forming reactions to allow our building blocks to be link together to form the desired template. Next, a suitable recognition motif must be used, which is compatible with the building block linking strategy. Finally, the design of the building blocks and the templates themselves must incorporate a suitable rigid structure to prevent the formation of undesired binary complexes.

5.2 Synthetic artificial template system

The goal of this section is to investigate a replicating network, which is under thermodynamic control, capable of reproducing *via* minimal or reciprocal replication. As our inspiration we have loosely based our replicating network on the structure of deoxyribonucleic acid (DNA) as demonstrated in **Figure 5.2**.

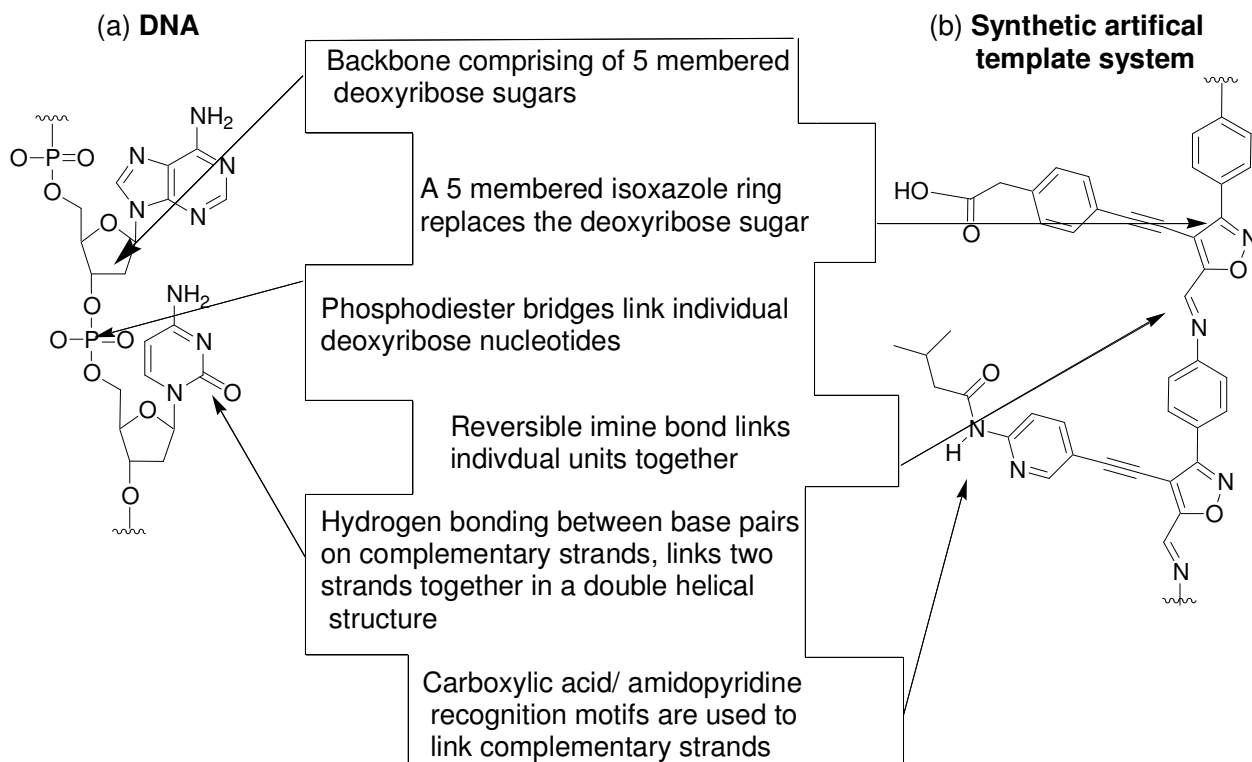


Figure 5.2 Similarities and differences between DNA and our synthetic artificial DNA mimic.

Figure 5.2 illustrates the key features in the structure of DNA and how we have mimicked these features in our design. In order to provide a rigid backbone for our replicating template, we have chosen an isoxazole ring in place of the ribose sugar. Instead of purine/pyrimidine base pairing used in DNA we have chosen a recognition motif studied extensively in our group amidopyridine/carboxylic acid. In order to link individual units together in a reversible fashion a suitable covalent bond forming step is necessary. Therefore, the imine formation reaction was decided upon, as imine exchange in dynamic combinatorial chemistry has been widely investigated^[192-195].

The reversible nature of the bond used to link individual units together to form replicating templates, allows template building block to interchange between a reciprocal and a minimal replicator. It is hoped this interchange will be under thermodynamic control with

the result being the formation of the most stable type of replicator. Why should one form of replication be preferred over another? One possible reason is as a consequence of secondary hydrogen bonding interactions. In Chapter One we examined Jorgensens model which predicted the most stable triply hydrogen bonded array would be [AAA•DDD] as a result of attractive secondary interactions with no repulsive interactions present. Therefore, in a reciprocal replicating system the number of repulsive secondary hydrogen bonding interactions will be weakened potential increasing its stability compared to its minimal counterparts.

The four building block molecules designed to form the artificial synthetic DNA are displayed in **Figure 5.3**. Building block **155**, **157**, **158** and **160** are designed to only be linkable at one end to allow for termination of strand growth.

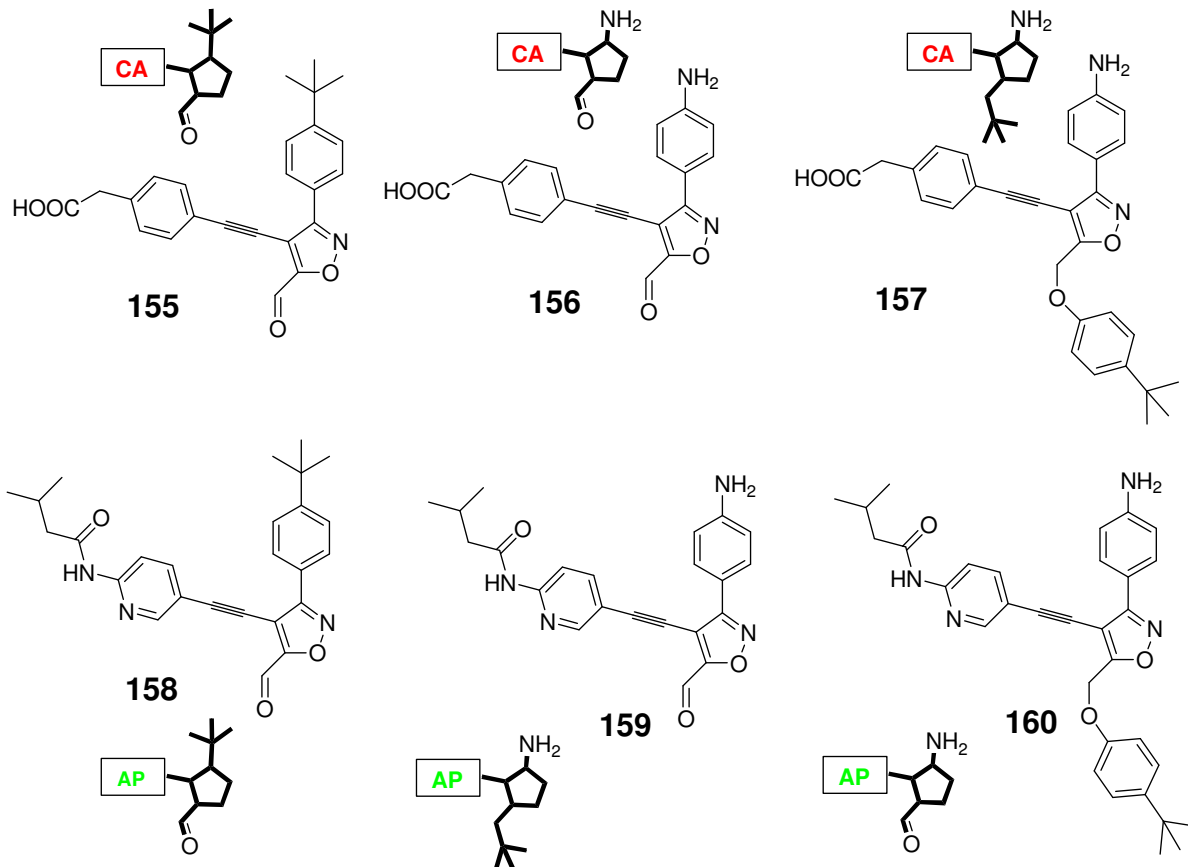
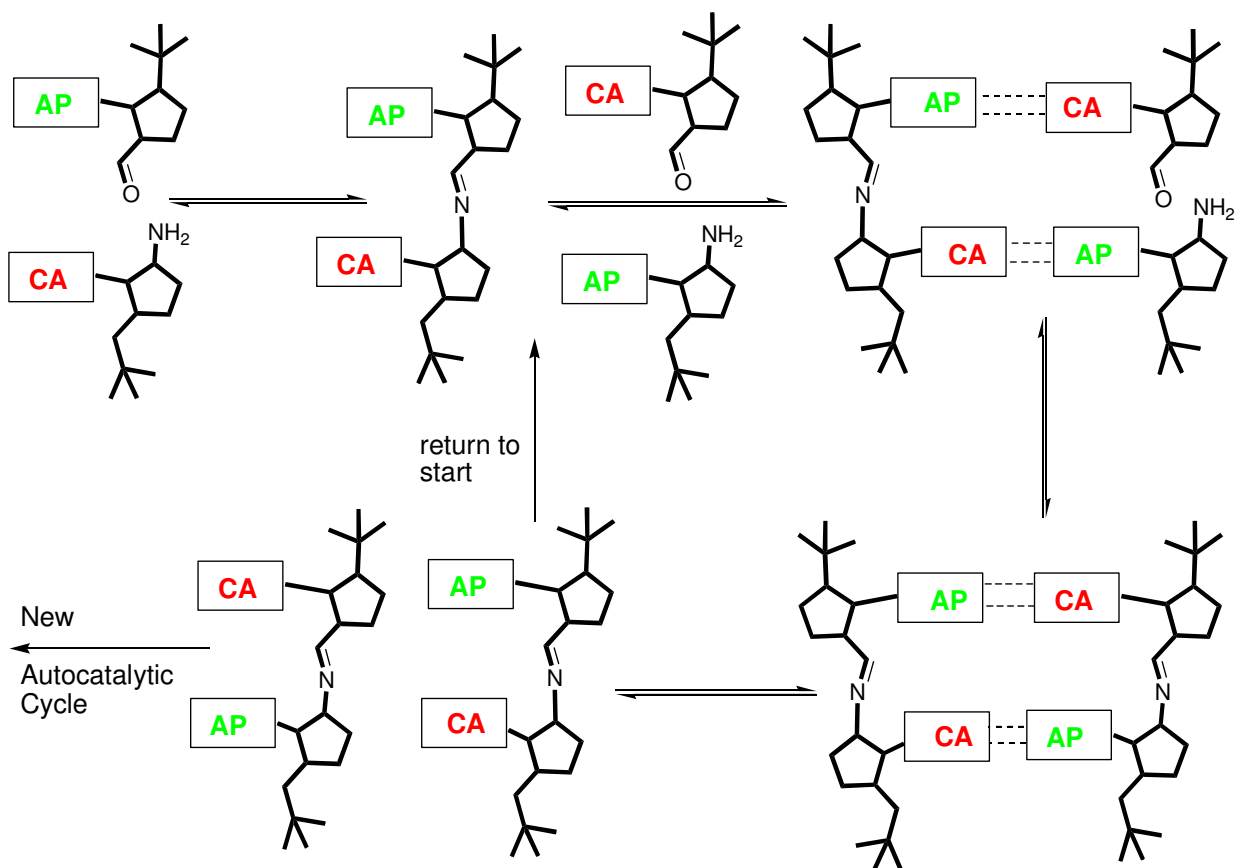


Figure 5.3 Six building blocks designed to form replicating templates, which are reversible in nature as a consequence of the imine bond used to link individual units. A cartoon representation of each building block is also illustrated with AP standing for amidopyridine and CA standing for carboxylic acid recognition motifs.

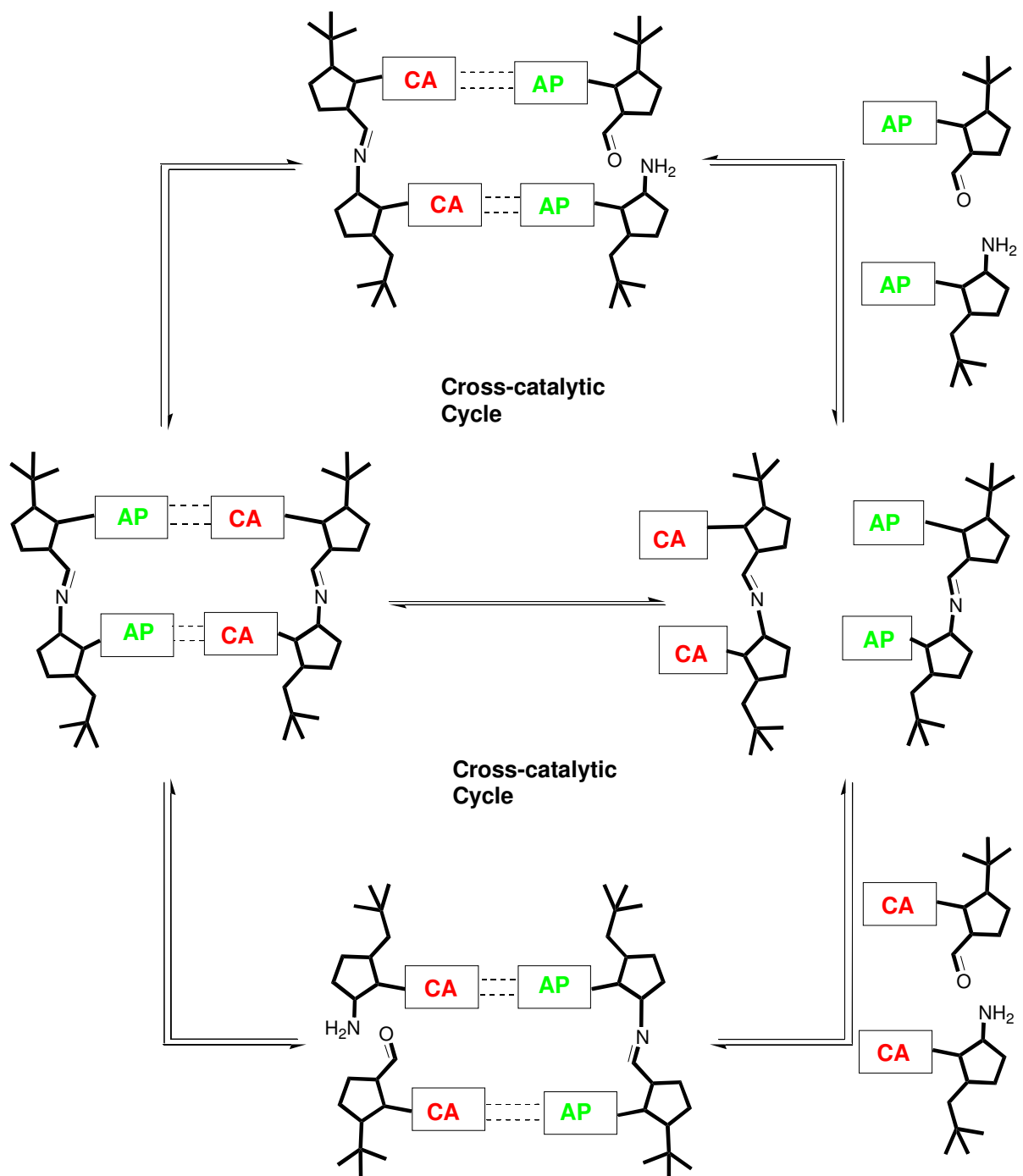
The six molecules in **Figure 5.3** can link together to form two different types of template, a palindromic self-replicator or a complementary reciprocal replicator. Each building block contains a cartoon representation illustrating the backbone, reactive sites and recognition moiety (AP = amidopyridine, CA = carboxylic acid). The simplest example of how these molecules can align themselves into a self-complementary minimal or reciprocal replicating system is illustrated in **Scheme 5.2**.



Scheme 5.2 Cartoon representation of minimal replicator utilizing building block molecules **155**, **157**, **158** and **159**.

In **Scheme 5.2** cartoon representations of building block **158**, **157**, **155** and **159** demonstrate how these molecules can react and associate to form two palindromic self-complementary strands, *via* an autocatalytic cycle. These two templates can then go on to self-replicate in two new autocatalytic cycles. These same building blocks, however, could react and associate to form two complementary strands (**Scheme 5.3**). The cartoon demonstrates how the formation of a dicarboxylic acid template can cross-catalyze the formation of a bis(amidopyridine) template. This bis(amidopyridine)

molecule could then go on to cross-catalyze the formation of a dicarboxylic acid strand. The two examples illustrated in **Scheme 5.2** And **5.3** are the simplest possible combinations, much larger strands could be formed, therefore, a series of minimal and reciprocal templates are possible composing of various numbers of building block units.



Scheme 5.3 Building block molecules **155**, **157**, **158** and **159** can react and associate to form a complementary reciprocal replicator duplex.

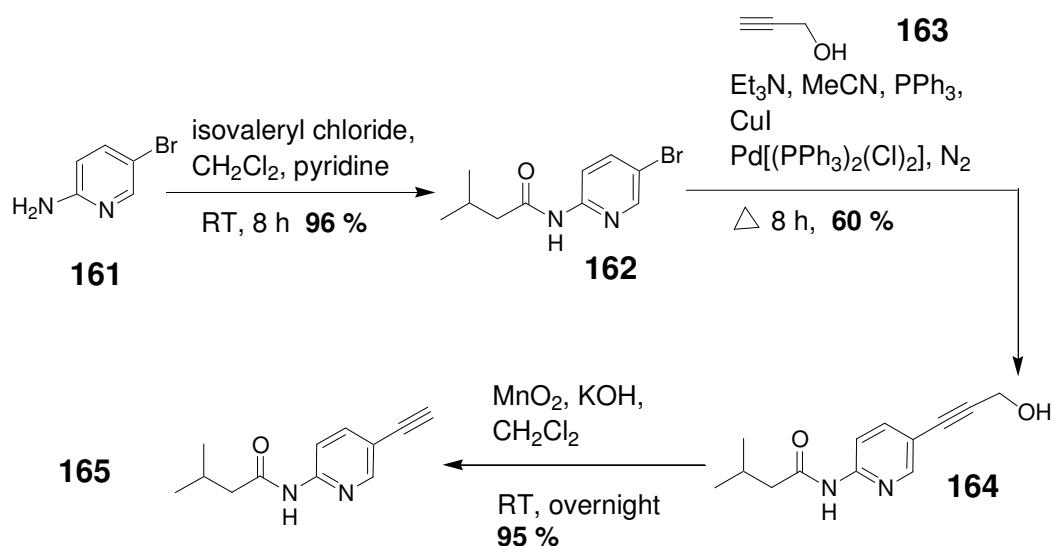
Therefore, this project has a number of questions that we wish to address. These include the obvious is replication occurring, either minimal or reciprocal? If replication is occurring which form is preferred, if either, self- or cross-catalysis? Which sequence is the most thermodynamically stable and will chains of more than two building blocks be formed?

5.3 Synthesis of synthetic artificial template system

5.4 Synthesis of building block isoxazole 155 and 158.

The synthesis of isoxazole building blocks **155** and **158** consists of three distinct stages formation of recognition containing molecule, backbone structure and finally the linking of these two molecules to form the complete building block.

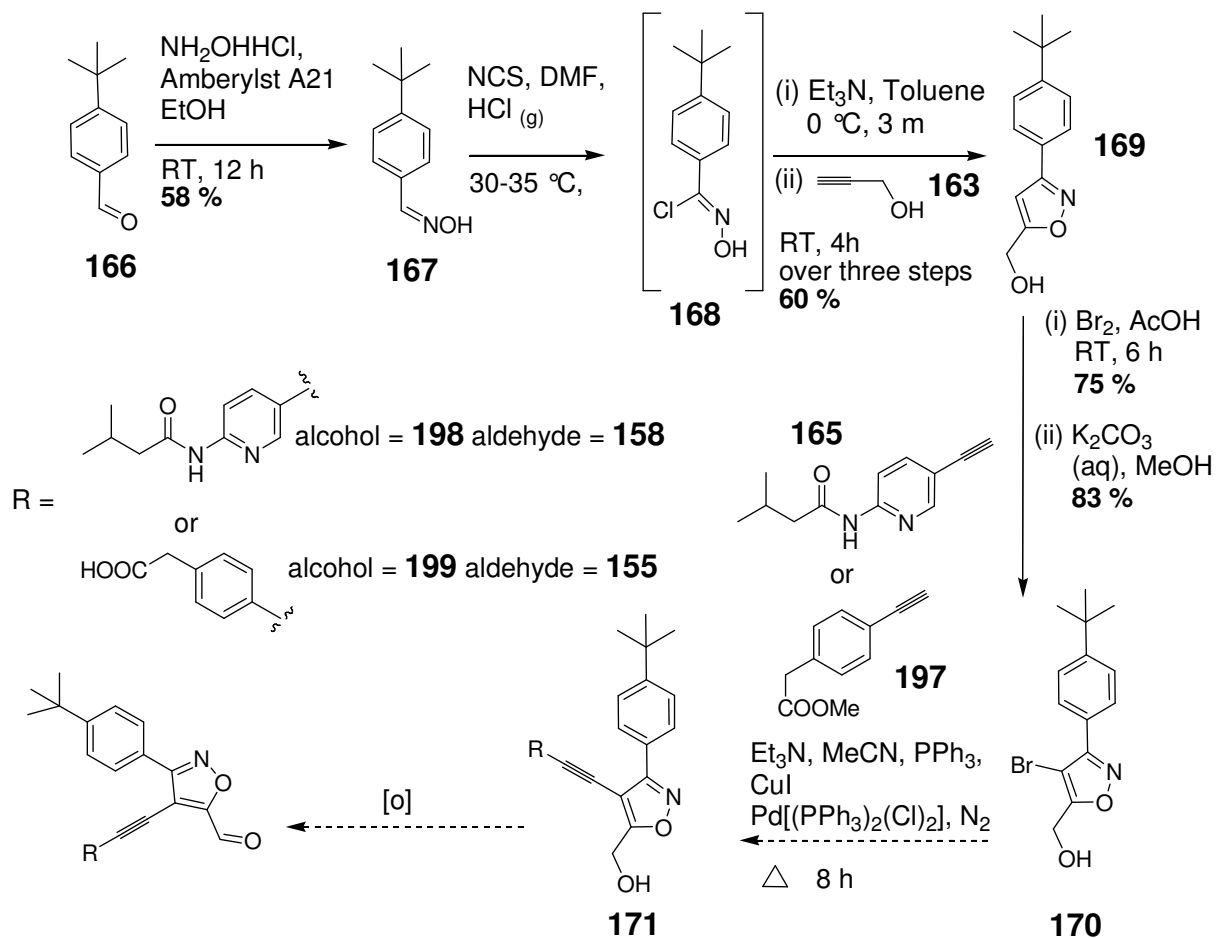
Amidopyridine derivative **162** was formed (**Scheme 5.4**) in three stages starting from commercially available 2-amino-5-bromopyridine. Isovaleryl chloride was added to a stirred solution of **161** in CH_2Cl_2 and pyridine at room temperature. After 8 hours alkyl bromide **162** was formed in 96% yield, following column chromatography. In order to convert this alkyl bromide to alcohol **164** a Sonogashira reaction^[184] between **163** and propargyl alcohol was conducted. As a consequence of the sensitive nature of this reaction all chemicals were dried and the experiment was conducted under a nitrogen atmosphere at all times, to exclude oxygen. A degassed suspension of **163** in dry $\text{Et}_3\text{N}/\text{MeCN}$, together with PPh_3 , $\text{Pd}[(\text{PPh}_3)_2(\text{Cl})_2]$, and CuI was stirred and heated until reflux. While stirring the suspension was left to cool to room temperature for 10 minutes, after which time a degassed solution of propargyl alcohol in triethylamine / acetonitrile was added. The resultant solution was then heated under reflux for 8 hour to form **164**. MnO_2 was then added to a suspension of alcohol **164**, KOH and CH_2Cl_2 . This mixture was left to stir overnight at room temperature, affording amidopyridine **165** in 95 % yield.



Scheme 5.4 Synthetic route for the preparation of amidopyridine **165**.

The synthetic route towards building block **172** and **173** involves a number of steps, starting from commercially available 4-*tert*-butylbenzaldehyde. Aldehyde **166** is converted^[185] to oxime **167** by adding hydroxylamine hydrochloride to a stirred mixture of 4-*tert*-butylbenzaldehyde, EtOH and Amberlyst A21 at room temperature. After 12 hours oxime **167** was formed in 83 % yield. Oxime **167** was converted^[186] to **168** by mixing *N*-chlorosuccinimide (NCS) with a stirred solution of **167** in DMF at 30 °C. A small volume of HCl gas was then added to this mixture to initiate the reaction. Intermediate chloro-oxime **168** was not isolated but instead dissolved in toluene and cooled to 5 °C. Triethylamine was then added and the reaction stirred vigorously. The resultant solution was filtered and mixed with propargyl alcohol and left to stir at room temperature for 4 hours in the dark, affording isoxazole **169** in 60 % over the three steps. Isoxazole **169** was then converted to the alkyl bromide *via* radical bromination. Bromine was added to a stirred solution of **169** dissolved in acetic acid, the resultant brown solution was left to stir at room temperature for 6 hours. This reaction resulted in the desired electrophilic substitution, however, the alcohol group was now protected as a methyl ester. In order to deprotect the alcohol the product of the bromination was dissolved in methanol and mixed with a stirred aqueous solution of potassium carbonate. The suspension was left to stir overnight at room temperature, affording **170** in 83 % yield. In order to link recognition containing group **165** to the alkyl bromide **170**, a Sonogashira cross-coupling was conducted. A degassed suspension of **165** in dry Et₃N/MeCN, PPh₃, Pd[(PPh₃)₂(Cl)₂], and CuI was stirred and heated until reflux, under a nitrogen

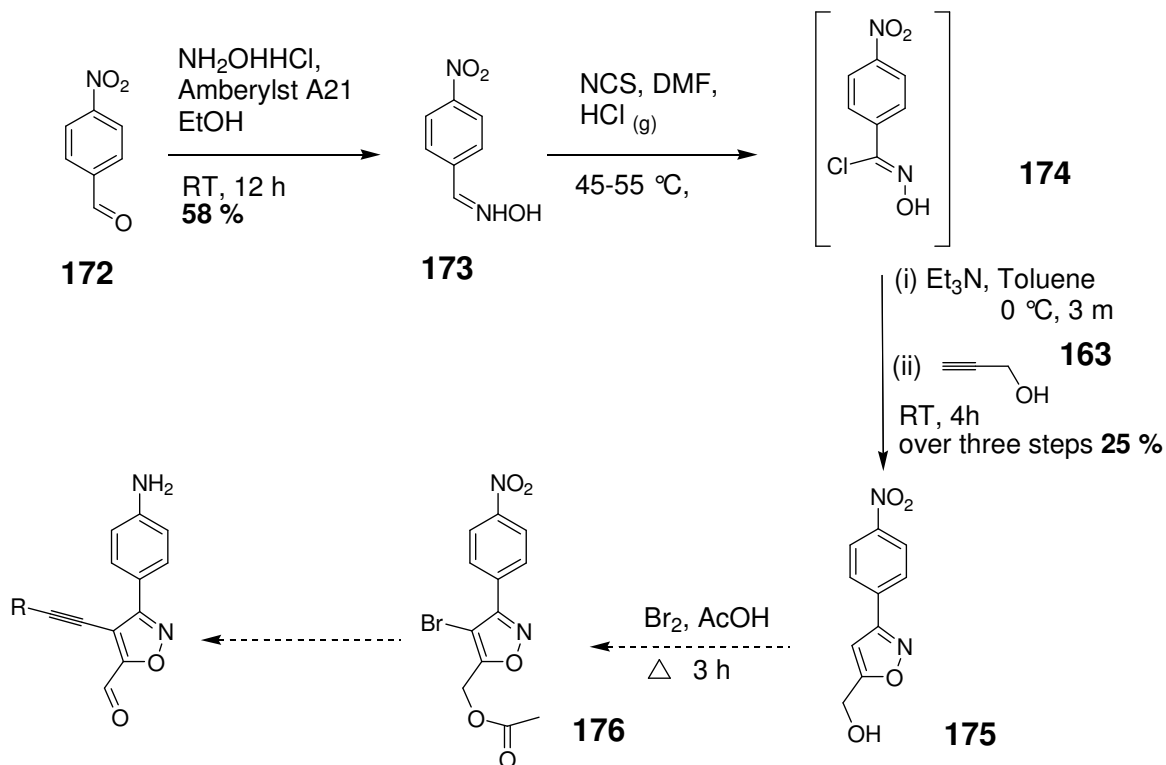
atmosphere. While stirring, the suspension was left to cool to room temperature for 10 minutes, after which time a degassed solution of **165** in triethylamine / acetonitrile was added, all still under a nitrogen atmosphere. The resultant solution was then heated under reflux for 8 hours in a nitrogen atmosphere. Unfortunately, even after several attempts no sign of cross-coupled product could be found, despite ensuring all solvents were dry and no oxygen was present, to prevent homo-coupling. The reaction was repeated using propargyl alcohol instead of **165**, however, the result remained unchanged. In order to ensure the reactivity of the palladium catalyst previously successful Sonogashira coupling was conducted. However, these reactions proved successful, therefore, there was no problem with the catalyst. Therefore, it proved impossible to carry on with the synthesis of isoxazole **158** and **155**. One possible hypothesis for the failure of this reaction could be as a consequence of steric effect. Perhaps the 4-position of this isoxazole is too crowded by groups on the 3- and 5-positions of the ring to allow for cross-coupling.



Scheme 5.5 Synthetic route towards the preparation of **172** and **173**.

5.5 Synthesis of building block 156 and 159

The formation of isoxazole **156** and **159** involved a number of reactions, starting from 4-nitro benzaldehyde **172**. Aldehyde **172** was converted to the oxime through the addition of hydroxylamine hydrochloride to a stirred solution of 4-nitrobenzaldehyde, EtOH and Amberlyst A21 at room temperature. After 12 hours oxime **173** was formed in 58 % yield. Oxime **173** was transformed into **174** by mixing *N*-chlorosuccinimide (NCS) with a stirred solution of **173** in DMF at 45 °C. A small volume of HCl gas was then bubbled through the mixture to initiate the reaction. Intermediate chloro-oxime **174** was not isolated but instead dissolved in toluene and cooled to 5° C, triethylamine was then added and the reaction stirred aggressively for 3 minutes. The resulting nitrile oxide was filtered off and mixed with propargyl alcohol and left to stir at room temperature for 4 hours in the dark, affording isoxazole **175** in 25% yield over three steps. In order to brominate **175** in the 4 position of the isoxazole ring radical bromination was attempted. This reaction had been proven to be successful in bromination of the *tert*-butyl-isoxazole counterpart **167**. However, all attempts at adding bromine to isoxazole **175** failed, it was concluded the nitro-group was deactivating the isoxazole ring to bromine attack.

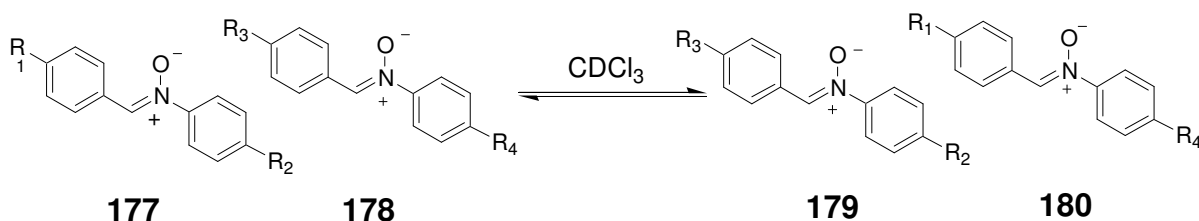


Scheme 5.6 Synthetic route towards the preparation of **156** and **159**.

In an attempt to solve this problem the nitro group was converted to an amine and protected by Boc_2O . However, attempts at brominating the isoxazole ring in this compound also proved unsuccessful, as now the phenyl ring was activated towards bromination, resulting in unwanted bromination. Therefore, using this route the synthesis of building blocks **156** and **159** was unattainable.

5.6 Conclusion and Future work

The synthesis of the six building blocks in **Figure 5.3** proved to be more difficult than had initially been anticipated. Several synthetic problems arose that meant formation of the desired products using the illustrated routes was impossible. Our initial network was perhaps too optimistic, with overly complicated molecules and long synthetic routes. While this project was underway, other researchers in our laboratory noticed that in some 1,3-dipolar cycloaddition reactions, conducted in CDCl_3 at 0°C at mM concentrations, containing two nitrones an exchange process was occurring (**Scheme 5.7**) with the formation of two new nitrones **179** and **180**, starting from nitrones **177** and **178**.



Scheme 5.7 Nitrones **177** and **178** were observed to exchange R groups to form two new nitrones, **179** and **180**.

These new nitrones contained the same R groups, but arranged in a different combination from the starting nitrones. The implication of this result, was that nitrone formation was in fact reversible and that they could revert back to their aldehyde and hydroxylamine starting materials and then react with other aldehydes or hydroxylamines. This discovery opened up the possibility of investigating a dynamic combinatorial library of nitrones utilizing a new reversible bond forming reaction not previously studied.

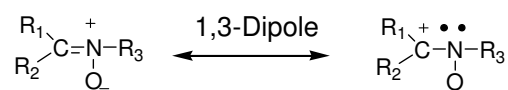
Therefore, instead of redesigning the building blocks in **Figure 5.3**, it was decided to abort this network altogether and instead focus on the design, synthesis and study of a simpler system utilizing the newly discovered reversible nature of nitrones.

5.7 Dynamic replicating templates, *via* reversible nitron exchange

As discussed at the beginning of the Chapter reversibility is a necessity of a dynamic combinatorial system. There are only a few reversible covalent bond forming reactions which are suitable, like imine formation, transacylation, Michael additions, Diels Alder etc. However, none so far have utilized nitron formation. As discussed in Section 5.1, a suitable exchange reaction for DCC must meet certain parameters. The nitron reaction should be reversible over a suitable timescale and the reversible reaction must be compatible with the experimental conditions of the selection process. Additionally nitron exchange occurs under mild conditions, products are usually soluble and it is possible to freeze the library. The fact nitron exchange fits these parameters means it is the ideal candidate for use in dynamic combinatorial chemistry.

Therefore, the goal of this project is to investigate a replicating network composed of a dynamic combinatorial library of replicating templates formed from the reversible formation of nitron molecules. The nitron moiety has an additional advantage over other reversible functional groups mentioned previously. Nitrones themselves are very reactive and readily undergo 1,3-dipolar cycloadditions. This fact creates the possibility of a thermodynamically favored nitron reacting with a dipole to form a cycloadduct, which in turn pushes the equilibrium more in favor of the thermodynamically favored product. The reactivity of the nitrones also makes it easier to trap products from the DCL, in order to trap products from imine DCL's harsh reductive conditions are used in order to reduce down to an amine.

Although the reversibility of nitron formation has not been analyzed extensively the structure of these 1,3-dipoles reveal clues as to why exchange of groups between different nitrones is possible. Nitrones contain a carbon nitrogen dipole double bond, with a 1,3-dipole resonance structure (**Scheme 5.8**).



Scheme 5.8 Resonance forms of the 1,3-dipole nitron.

The charge makes the nitrones look like a 1,2-dipole but nucleophilic attack on the nitrogen is impossible. Examination of the dipole structure implies that the nitron

structure should be vulnerable to nucleophilic attack at the carbon, whereas the oxygen atom has the potential to act as a nucleophile itself.

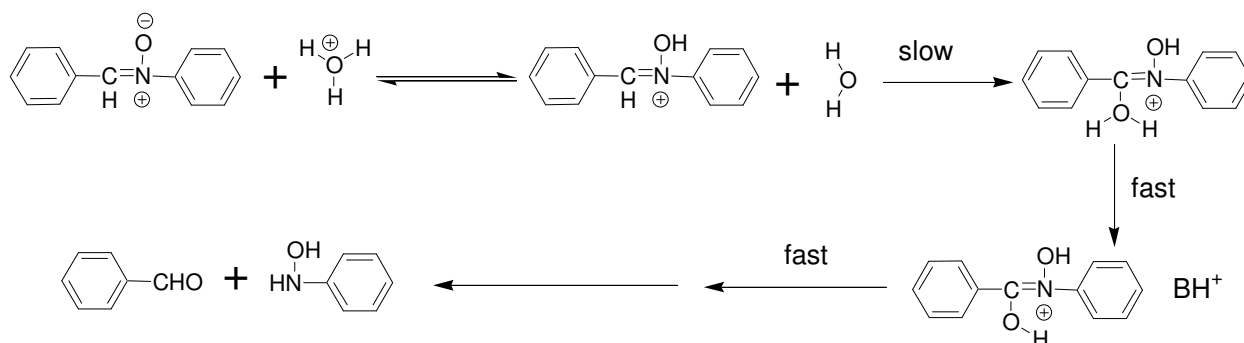
Although there has been no investigation of the use of nitroner reversibility in DCI or the mechanism of exchange, a bulletin was published^[200] in 1991 by Kim and Kwang on the “Kinetics and Mechanism of the Hydrolysis of α , *N*-diphenylnitroner”.

In the kinetic analysis of the mechanism of hydrolysis of α , *N*-diphenylnitroner Kim and Lee demonstrated that the rate of nitroner hydrolysis could be expressed by a combination of pH independent, k_0 and hydronium, k_H and hydroxide, k_{OH} , ion dependent parts. This resulted in the rate equation illustrated in (Figure 5.3).

$$\begin{aligned} \text{Rate} &= k_t [\text{Nitroner}] \\ &= (k_0 + k_H[\text{H}_3\text{O}^+] + k_{OH}[\text{OH}^-]) [\text{Nitroner}] \end{aligned}$$

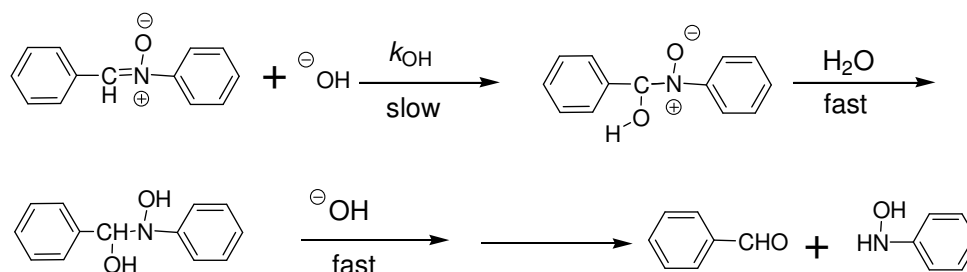
Figure 5.3 Rate equation for hydrolysis of α , *N*-diphenylnitroner.

At acidic pH, the hydrolysis of the nitrones is not subject to general base catalysis and the rate of hydrolysis is proportional to the concentration of hydronium ion. Therefore, the pH dependency is reliant on the very rapid equilibrium of the nitroner with its conjugate acid. The conjugate acid then undergoes the rate determining step through attack of water. Although no intermediate could be observed experimentally, Jencks suggested^[202] that a diol is involved in the formation of a nitroner. Through combining all these facts a general mechanism for nitroner hydrolysis at low pH was determined (Scheme 5.9)



Scheme 5.9 Mechanism of α , *N*-diphenylnitroner hydrolysis under acidic conditions. Adapted from reference 200.

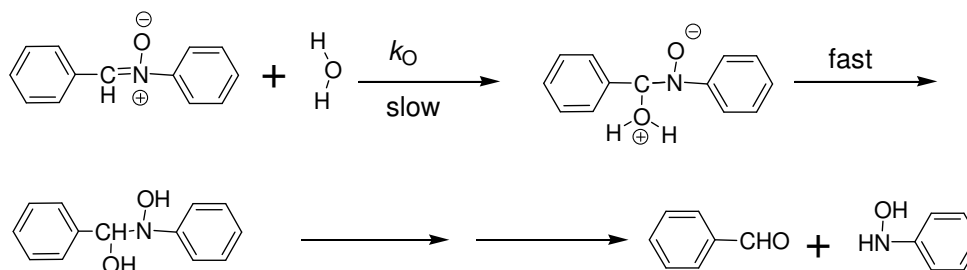
Under alkaline pH, the rate constant is directly proportional to the concentration of hydroxide ion. Therefore, the mechanism in **Scheme 5.10** was proposed for hydrolysis at high pH.



Scheme 5.10 Mechanism of α , *N*-diphenylnitron hydrolysis under basic conditions. Adapted from reference 200.

The rate limiting step is the nucleophilic attack of the hydroxide anion on the carbon of the nitron double bond. This product is then surmised to undergo rapid conversion to the diol intermediate before reverting back to the constitutional aldehyde and hydroxylamine.

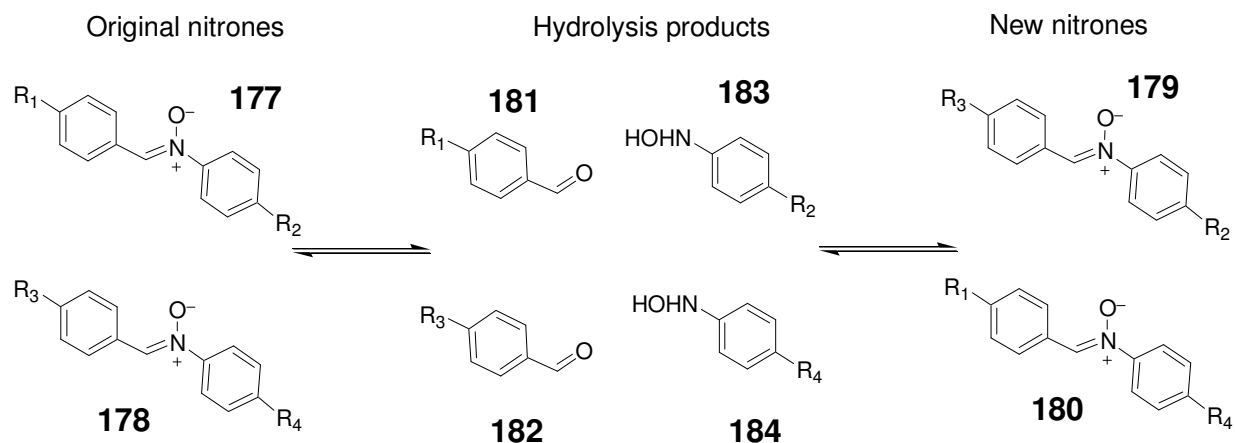
At close to neutral pH, the rate constant of nitron hydrolysis is independent of pH change. It therefore, is reasonable to assume (**Scheme 5.11**) that addition of water to the carbon atom of the nitron double bond is the limiting step, with the product undergoing rapid conversion to the diol before converting back to the aldehyde and hydroxylamine.



Scheme 5.11 Mechanism of α , *N*-diphenylnitron hydrolysis under neutral conditions. Adapted from reference 200.

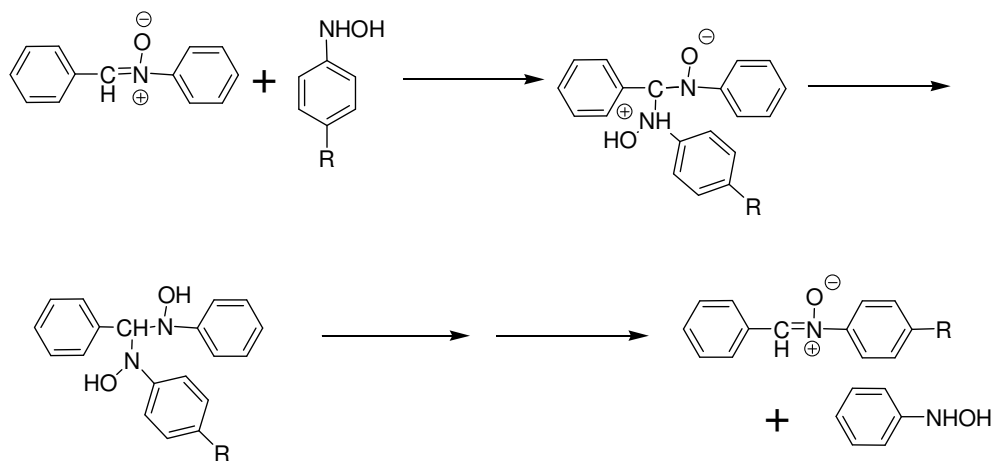
The work by Kim and Lee indicates the mechanism of nitron hydrolysis and helps to demonstrate how we observed the formation of new nitrones in some of our experiments. In an experiment containing two nitrones, hydrolysis will result in the formation of two aldehydes and hydroxylamines (**Scheme 5.12**). If the aldehydes then

react with the different hydroxylamine from the original hydrolysis two new nitrones can be formed. This mechanism explains how two nitrones can become four nitrones.



Scheme 5.12 Recombination of hydrolysis products from original nitrones can result in the formation of two new nitrones molecules.

Although **Scheme 5.12** implies both nitrones have to be hydrolyzed to their starting aldehydes and hydroxylamines before they can be recombined, there is another potential mechanism (**Scheme 5.12**) for nitrone exchange.



Scheme 5.13 Potential additional mechanism for nitrone recombination.

The basis of nitrone hydrolysis relies on the nucleophilic attack on the carbon atom of the 1,3-dipole. Depending on conditions this attack is by H₂O or ⁻OH. However, if more than one type of nitrone is present, the hydroxylamine from the hydrolysis of one nitrone could attack the carbon on the 1,3-dipole of the other, as illustrated in **Scheme 5.13**. The result of this nucleophilic attack is the formation of a new type of nitrone and the release of a new molecule of hydroxylamine. This process could occur if only one type of

nitron was present, but would result in the formation of the same nitron. We will be investigating nitron exchange in CDCl_3 which is slightly acidic. Examination of the mechanisms for nitron hydrolysis at acid and neutral pH (**Scheme 5.9** And **5.11**), reveals the rate determining step to be the nucleophilic attack of a water molecule. However, if hydroxylamine is present as in **Scheme 5.13**, as a consequence of its increased nucleophilicity compared to water it will attack the carbon atom of the $\text{C}=\text{N}$ nitron double bond faster. The result of this increased nucleophilicity is more rapid nitron exchange.

The following four building blocks were designed to form our dynamic combinatorial replicating network.

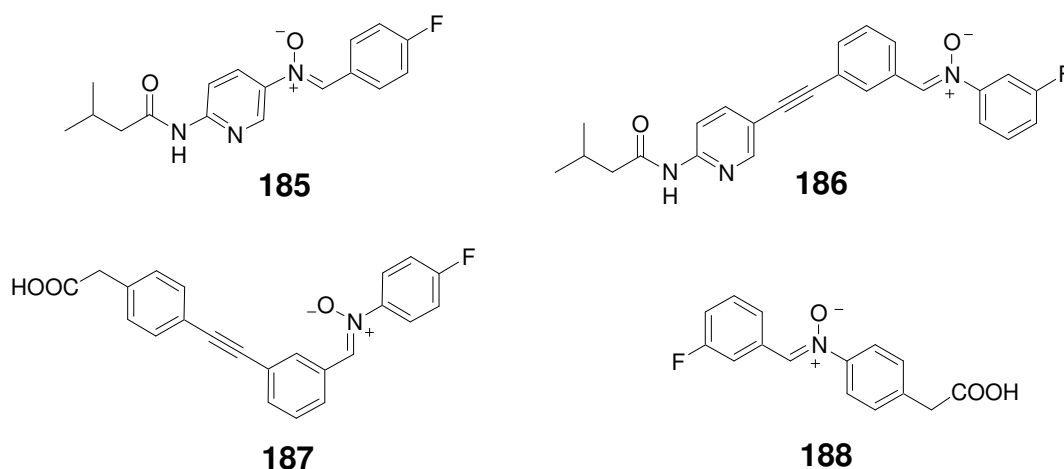
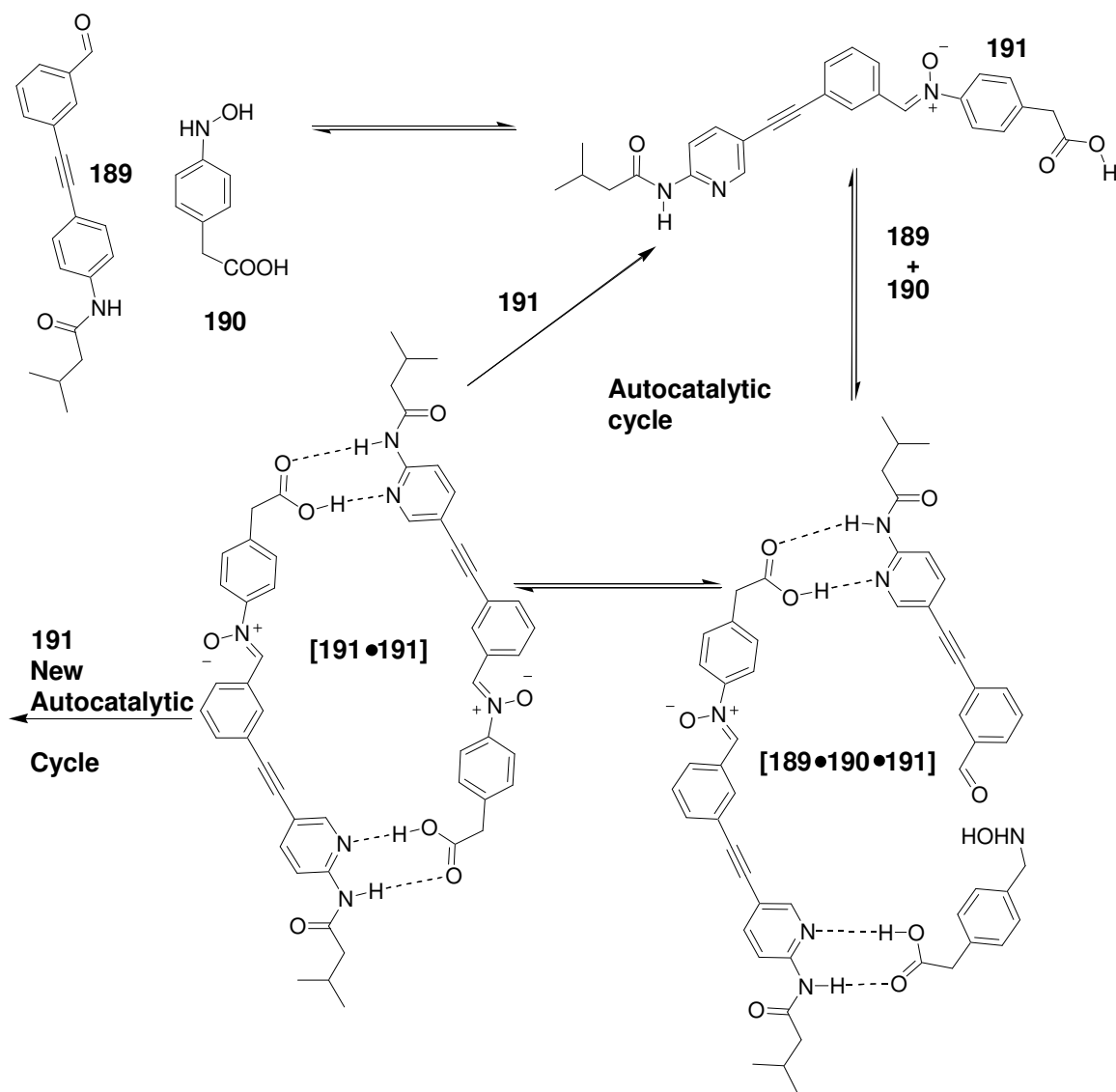


Figure 5.4 Four building blocks designed to form a series of dynamic replicating templates.

There are several important features in these four building blocks. The most important is the recognition motif, again we have utilized amidopyridine carboxylic acid association. It is this recognition which will hopefully help favor the more thermodynamically stable templates formed in our potential replicating network. Each building block also has a rigid backbone structure, which should hopefully avoid the formation of unwanted $[\text{A}\bullet\text{B}]$ complexes, which could result in closed template structures. The final feature of note in these building blocks is the fluorine tag present on each molecule. A fluorine atom has been attached to each building block to allow analysis of the network by ^{19}F NMR spectroscopy. Analysis of this network by ^1H NMR spectroscopy could prove difficult with the formation of complex proton spectra, with vital peaks obscured. However, ^{19}F NMR spectra usually show wide signal dispersion. Aryl fluorides have chemical shifts which are spread over a 50 ppm range centered at -120 ppm relative to CCl_3F and can be

more easily deconvoluted to determine concentrations. Unfortunately, though the resultant exchange reactions produce nitrones with no fluorine tag, therefore, other forms of analysis such as mass spectrometry and ^1H NMR spectroscopy will have to be used in the analysis of the dynamic combinatorial library.

These four building block molecules can form potentially two minimal and reciprocal replicating templates. An example of one of these potential minimal replicators is demonstrated in **Figure 5.14**, which illustrates the self-replication of nitronne template **191**.

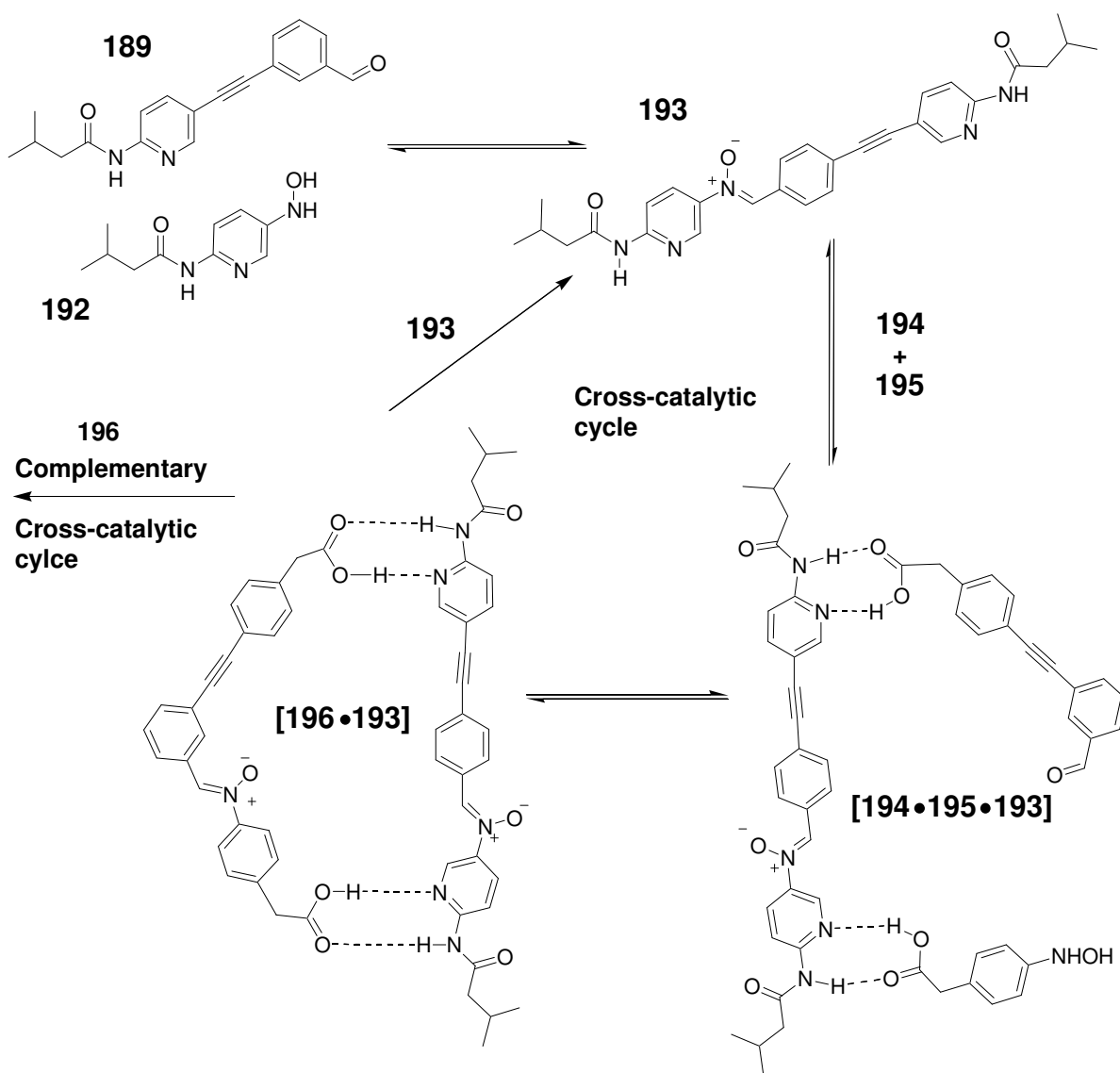


Scheme 5.14 Example of a potential minimal replicating template, formed from aldehydes **189** and **190**.

Aldehyde **189** and **190**, formed from the hydrolysis of **187** and **188** can react to form nitronne template **191**. Template **191** can associate the hydrolyzed products of nitronne

189 and **190** in a ternary complex structure [**189•190•191**]. This complex can render the reaction between aldehyde **189** and hydroxylamine **190** *pseudo*-unimolecular resulting in the formation of a duplex structure [**191•191**]. If the association between the two strands in the duplex is not too strong, then it can dissociate releasing two molecules of **191** the original parent and the new daughter, which can go on to compete in new self-replicating cycles.

The four building blocks as mentioned already can form two reciprocal replicating templates. An example of one of the two cross-catalytic cycles is examined in **Scheme 5.15**, where the formation of dicarboxylic acid **196** is cross-catalyzed by the bis(amidopyridine) nitron template **193**. Aldehyde **189** and **192**, hydrolyzed products of **186** and **185**, can react to form nitrones template **193**. Template **193** can associate **194** and **195**, hydrolyzed products of **187** and **188**, in a ternary complex structure. As with the minimal model this complex renders the reaction between aldehyde **195** and **194** *pseudo*-unimolecular, resulting in the formation of dicarboxylic acid **196** in a duplex structure with bis(amidopyridine) **193**. This duplex structure can then dissociate returning the bis(amidopyridine) nitrones **193** to the start of the cross-catalytic cycle. Leaving the dicarboxylic acid template, **196**, free to enter a complementary cross-catalytic cycle for the production of bis(amidopyridine) **193**.



Scheme 5.15 Example of potential cross-catalytic replicating templates, formed from aldehydes **189**, **192**, **194** and **195**.

5.8 Conclusions and future work

In this Chapter we have developed a new type of reversible reaction, with applications in the field of dynamic combinatorial chemistry. The discovery of the reversible nature of the C=N nitron double bond in chloroform at low temperatures, has allowed us to design a number of building blocks with the potential to form a series of replicating templates. Since these templates are formed *via* a reversible bond it gives us the opportunity to investigate replication where template formation depends on the relative thermodynamic stability and not the kinetic control highlighted in this thesis.

Unfortunately, as a result of time constraints we could not complete the synthesis and examination of this potential dynamic replicating network. However, the synthetic route towards the building blocks **185**, **186**, **187** and **188** utilizes reactions we have previously conducted on similar compounds and, therefore, their formation should be relatively straight forward. Therefore, it should be possible to investigate the resultant potential replicating network which these building blocks can create. The first series of experiments will involve the investigation of the individual minimal or reciprocal replicating templates. As before bimolecular, native and templated experiments will be used to determine the systems nature. Once these potential replicating systems have been studied in isolation, the building blocks can be combined in one experiment to observe how the different system's coexist under the competitive reaction conditions of a replication network. Investigation of the replicating network should provide pivotal information on whether the potential more thermodynamically stable cross-catalytic templates are favored over the more simplistic autocatalytic self-replicators.

The development of replicating systems which are under thermodynamic control as apposed to kinetic gives us the potential to analyze more complicated systems, with increased applications.

6. General Conclusions

This thesis has highlighted the complexity involved in the design, synthesis and kinetic analysis of replicating systems. However, at each stage we have demonstrated that important lessons can be learned for the design of subsequent replicating systems.

The relative weakness of the system examined in Chapter Two provided pivotal information about the key requirements for an efficient reciprocal replicating system. These failings include low selectivity and rate enhancements, which were as a consequence of the high reaction temperature (50 °C) utilized in the experiments. The reason for this temperature was a result of the low reactive nature of the maleimide/furan Diels- Alder and 1,3-dipolar azide/maleimide reactions utilized, to link individual units together into replicating templates. This high temperature had the effect of weakening recognition in the catalytic ternary complex, which lowered the efficiency of the replicator. The analysis of Chapter Two also revealed an addition problem with our design, the two templates were formed *via* different reaction types. If we were able to exam the catalytic effects of the two systems the results would be inherently unfair as we would be comparing two entirely different reaction types.

Although the end result of Chapter Two was a pair of weak cross-catalytic replicators the implementations of the lessons learned from this system allowed us to design a pair of very efficient reciprocal replicators, exhibiting high selectivity and rate accelerations. However, the aim of Chapter Three had shifted from analyzing a pair of simple cross-catalytic templates to the development of a complex replicating network comprising of two minimal and two reciprocal templates. Unfortunately however, only one of the two potential minimal replicators actually operates by a self-replicating pathway with the other proceeding through a binary [A•B] complex. The binary complex structure illustrated the importance of rigidity to minimal replicators. Despite only have a few freely rotatable bonds there was still enough flexibility in this complex to fold over into the closed template structure. This binary complex prevented us from analyzing a potential complex hypercyclic network composed of two minimal and two reciprocal templates, where the two forms of replication compete for common building blocks in a survival of the fittest environment.

In Chapter Four the goal was to create a successful replicating network comprising of two minimal and two reciprocal replicating templates. This feat was achieved by

redesigning the binary complex in Chapter Two by removing flexibility from the template building blocks. The self-replicating nature of this template allowed for the investigation of a potential hypercyclic network. A series of experiments were conducted into the behavior of each template when it is forced to compete for common starting materials. The replicating network was found not to exhibit mutually beneficial behavior (complex hypercycle); instead a Darwinian survival of the fittest situation arose, where the most efficient replicator dominated. Interestingly, this turned out to be the reciprocal replicating templates and not, as one might expect, the autocatalytic minimal replicators, demonstrating mutually beneficial reciprocal replicating systems can out-compete efficient selfish self-replicating templates under competitive evolutionary conditions. The work in Chapters Two to Four indicates the structural features which can limit efficiency of replicating systems.

In the final Chapter, the future direction of replication is examined. The systems discussed in this research project are under kinetic control ideally we would like to now examine replicating networks under thermodynamic control, where binding to the replicating template stabilizes product ground state as opposed to the transition state. Initially we attempted to use imine exchange reactions to design an artificial replicating template system with DNA like characteristics, unfortunately difficulties in synthesis halted our progress. However, work in the Philp laboratory opened up the possibility to investigate an entirely new exchange reaction with possible applications in dynamic combinatorial chemistry (DCC). The nitron exchange reaction meets all the requirements for a reversible exchange reaction making it ideal for DCC. Unfortunately, time constraints prevented analysis of a dynamic nitron exchange replicating network. However, the future of synthetic small molecule replication looks exceptionally bright with the development of systems under thermodynamic control opening up exciting new avenues of research.

Chapter 7. Experimental

7.1 General procedures

Chemical and solvents were purchased from, Acros, Aldrich, Avocado and Fluka or and were used as received unless otherwise stated. CH_2Cl_2 , MeCN and hexane were distilled over calcium hydride under an N_2 atmosphere. Et_2O and tetrahydrofuran were dried by heating under reflux with sodium-benzophenone ketyl under an N_2 atmosphere and collected by distillation. Thin-layer chromatography (TLC) was performed on aluminum plates coated with Merck Kieselgel 60 F₂₅₄. Developed plates were dried and scrutinized under a UV lamp (366 nm), where necessary stained with iodine, KMnO_4 , DNP and Ninhydrin solution to aid visualization and identification. Melting points were recorded using an Electrothermal 9200 melting point apparatus and are uncorrected. Column chromatography was performed on ICN EcoChrom Silica 32-63 μm , 60Å. Microanalysis (CHN) was carried out at the University of St. Andrews. Chemicals and samples used prior to kinetic experiments were weighed using a Sartorius balance (MC1 Analytic AC 120S) with an accuracy of ± 0.1 mg.

7.2 NMR spectroscopy

^1H Nuclear magnetic resonance (NMR), spectra were recorded on a Bruker Avance 300 (300 MHz) or a Varian UNITYplus (500 MHz) spectrometer using the deuterated solvent as the lock and the residual solvent as the internal reference in all cases. ^{13}C NMR spectra were acquired using the PENDANT sequence on Bruker Avance 300 (75.5 MHz) spectrometer. ^{19}F NMR spectra were recorded using a Bruker Avance (282.3 MHz) spectrometer, referenced to $\text{CCl}_3\text{F} = 0$ ppm. All ^1H and ^{19}F coupling constants are quoted in Hz and all spectra were recorded at 298 K, unless otherwise stated. The symbols s, d, t, q are used in the assignment of ^1H , ^{13}C and ^{19}F spectra denote singlet, doublet, triplet and quartet respectively. The abbreviations quat, Py (Pyr in ^1H NMR) and Ar in the assignment of both ^1H and ^{13}C are used to denote quaternary, aromatic and pyridine respectively. All ^1H , ^{13}C and ^{19}F spectra were analyzed using Bruker Topspin (Version 2.0 Bruker Biospin, 2006), and 1D WIN-NMR (Version 6.2.0.0 Bruker Daltonik GmbH 2000) software. Where stated, as a result of the diastereoisomeric ratio, only the

major stereoisomer of a product could be successfully characterized using ^1H and ^{13}C NMR spectroscopy.

7.3 Mass spectrometry

Electron impact mass spectrometry (EI), chemical ionization mass spectrometry (CI) and high-resolution mass spectrometry (HRMS) were carried out using a Micromass GCT spectrometer. Electrospray mass spectrometry (ES) was carried out using a Micromass LCT spectrometer at the University of St Andrews.

7.4 Kinetic measurements

All stock solutions were prepared by dissolving the appropriate quantity of a given reagent in 2 ml of dry CDCl_3 in a volumetric flask ($2 \text{ ml} \pm 0.02 \text{ ml}$). CDCl_3 was dried over calcium chloride for 4 hours and then filtered through Aluminum oxide to remove trace of acid and stored over molecular sieves. Masses of reagents were measured using a Sartorius BP 211D balance ($\pm 0.01 \text{ mg}$). The stock solutions were equilibrated at the appropriate temperature for at least one hour prior to use. Experimental samples were prepared by mixing equal volumes of the appropriate stock solutions using a Hamilton 1 ml gas-tight syringe into a clean dry Wilmad 528PP NMR tube. A polyethylene pressure cap was then applied to the top of the tube to prevent solvent evaporation. Once mixed, the samples were immediately analyzed over a fixed period of time. In every case the probe had been pre-equilibrated at the appropriate temperature at least 1 hour before use. The kinetic data were extracted using the deconvolution tool available in 1D WIN-NMR (Version 6.2.0.0 Bruker Daltonik GmbH 2000). Errors in calculated concentration values were estimated to be $\pm 4\%$.

7.5 Deconvolution of kinetic data

Kinetic experiments were monitored by 500 MHz ^1H NMR spectroscopy, with spectra of the reaction recorded every 30 minutes. The spectrum were then transformed and phased identically. The percentage completion of the reaction was monitored through the disappearance of the maleimide proton and the reappearance of the cycloadduct

protons. A simplified example is shown in **Figure 7.1**, between a maleimide and a nitrene, which can accurately ($\approx \pm 2\%$) be measured through the deconvolution of each spectrum using 1D WIN-NMR (Version 6.2.0.0 Bruker Daltonik GmbH 2000) software. Examples of actual spectrum deconvoluted from Chapters 2-4 can be examined in the appendices. In order to extract product concentrations from the ^1H NMR spectrum in **Figure 7.1** the area under the maleimide protons and one of the cycloadduct protons is calculated through deconvolution of the spectrum. This calculation results in the area of the maleimide protons and the cycloadduct proton being given as a percentage, with the total area of both peaks equaling a 100%. However, the maleimide peaks has an integration of 2 protons compared to 1 for the cycloadduct peak. Therefore, the percentage area for the maleimide peak is halved and added to the percentage area of the cycloadduct peak to give a new total percentage. Therefore, by dividing the cycloadduct area over the new total percentage and multiplying by the initial concentration of maleimide, the concentration of the product cycloadduct can be calculated.

The time at which each spectrum is recorded can be extracted from the log file which accompanies the proton NMR data. Using the percentage completion for each spectrum against the time we can plot a reaction profile for this reaction using graphing software KaleidoGraph (Synergy Software, Reading, PA, USA, version 3.51, 2000)

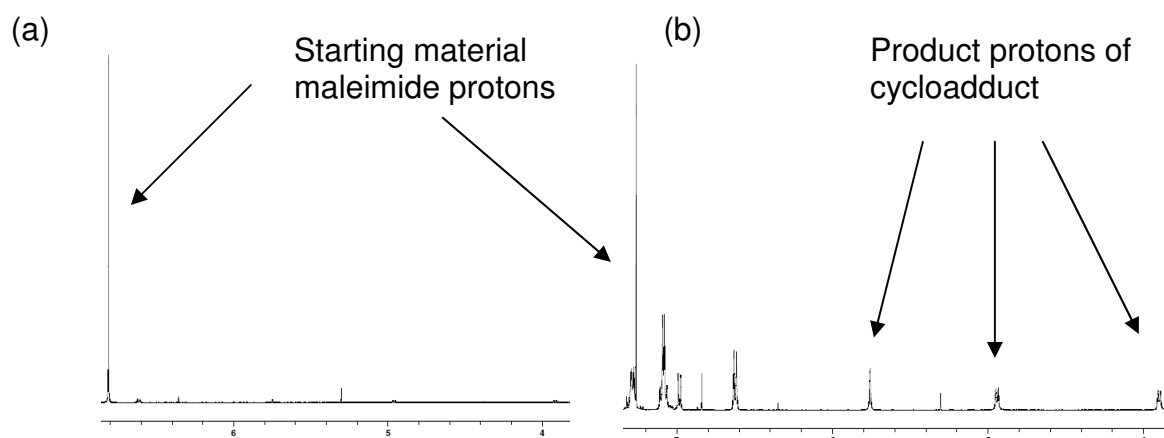


Figure 7.1 Partial 500 MHz ^1H NMR spectra (a) showing the resonance arising from the maleimide protons (b) the gradual disappearance of the signal corresponding to the maleimide protons and the appearance of the signal corresponding to the cycloadduct protons.

7.6 Determination of binding constants

Experimental values for the association constant K_a were determined using the NMR dilution method,^[203] using 500 MHz ^1H NMR spectroscopy at 273 K. All stock solutions and samples were made up using volumetric flasks (accuracy ± 0.02 ml) using CDCl_3 and equilibrating at 273 K in a water/ethylene glycol bath for at least 45 minutes. Solutions of the desired compounds or complex were prepared at concentration of 100 mM which was gradually diluted down to 1 mM and the chemical shift changes were recorded. The variation of the appropriate chemical shift with respect to concentration was observed and the dissociation constant, K_d , was calculated from this information by fitting the equation in **Figure 7.2** using a non-linear curve-fitting program.

$$\delta_{obs} = \delta_G + \Delta\delta \left[1 + \frac{K_d}{2C_0} - \sqrt{\left(\frac{K_d}{2C_0}\right)^2 + \left(\frac{K_d}{C_0}\right)} \right]$$

Figure 7.2 Equation for the calculation of dissociation constant, K_d , where δ_{obs} is the chemical shift at concentration C_0 of the molecule, and $\Delta\delta$ is the maximum change in chemical shift.

The association constant, K_a , was then determined using the equation in **Figure 7.3**.

$$K_a = \frac{1}{K_d}$$

Figure 7.3 Equation for association constant, K_a , using the dissociation constant, K_d .

This method for calculating K_a , was utilized in Chapter Four Section 4.1, to calculate the association constant between an amidopyridine nitron **115** and benzoic acid **137**, in CDCl_3 at 0 °C. The chemical shift change of the nitron amide proton was monitored as the reaction was diluted down from 100 mM to 1 mM. The change in this proton's chemical shift can be observed in the ^1H NMR spectra in **Figure 7.4**. Spectrum (a) in **Figure 7.4** shows the chemical shift of the amide proton of the nitron when uncomplexed to benzoic acid. Spectrum (b) shows the chemical shift of nitron bound to benzoic acid at 100 mM in a 1:1 solution.

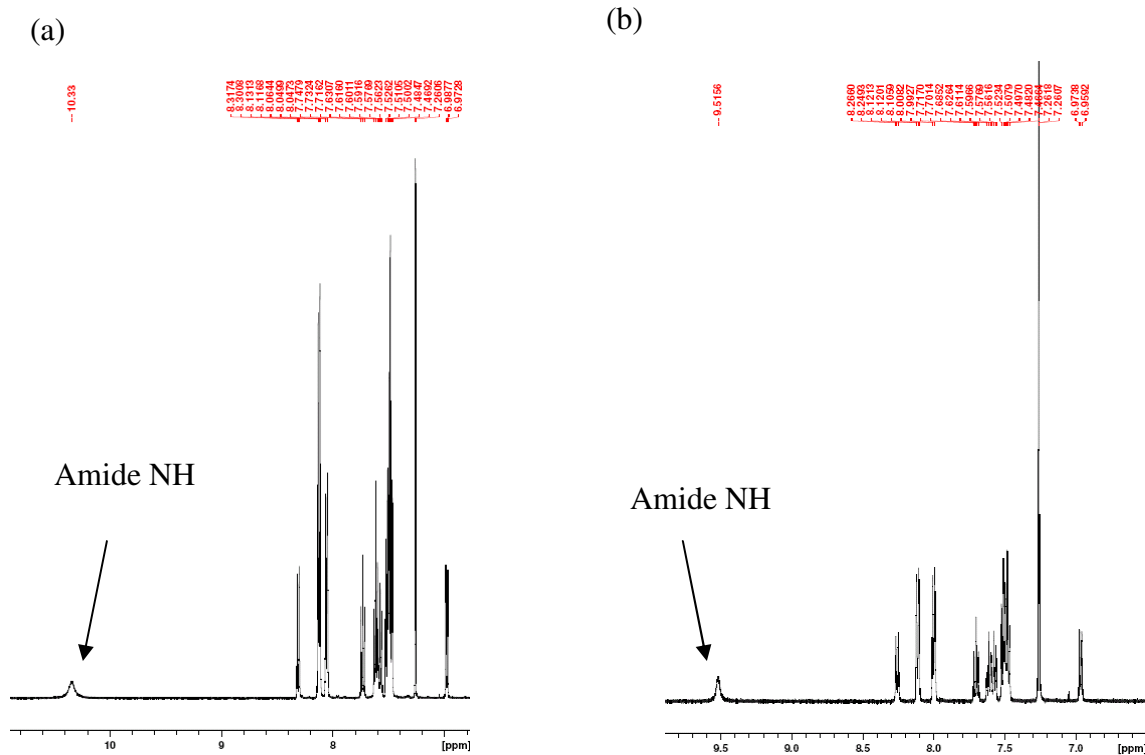


Figure 7.4 Spectra highlighting the chemical shift of the amide proton of nitrone **115** associated to benzoic acid in (a) 100 mM, 1:1 solution and (b) 1 mM, 1:1 solution in CDCl_3 .

The chemical shift change was recorded as the 1:1 solution of **115** and **137** was diluted down from 100 mM (0.1 M) to 1 mM (0.001 M) and plotted against solution concentration giving the graph in **Figure 7.5**.

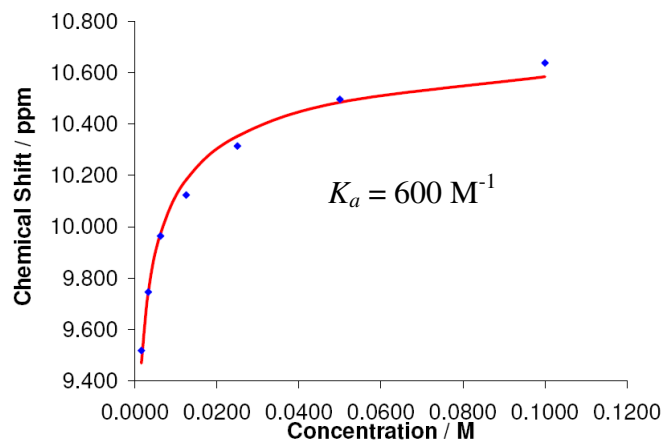


Figure 7.5 Graph of chemical shift vs concentration. The diamonds are the measured chemical shift of amide NH recorded from ^1H NMR spectra. The solid line represent the best fit of the equation in **Figure 7.2**, which is obtained when $K_a = 600 \text{ M}^{-1}$.

The graph in **Figure 7.5** contains a solid line which indicates the optimal fit of the equation given in **Figure 7.2**. From this equation a K_d of $1.66 \pm 0.17 \times 10^{-3}$ M was calculated which corresponds to a $K_a = 600 \pm 60$ M⁻¹.

7.7 Molecular Mechanics calculations

All molecular mechanics were carried out using the MMFFs* forcefield as implemented in the Maestro program together with the GB/SA salvation model for chloroform. Initially each molecule was energy minimized using a conjugated gradient (PRCG). Conformational searching was conducted using depending on the size of the molecule a 1000 to 2000 step Monte Carlo simulation and all conformations generated within 50 kJmol⁻¹ of the global minimum were minimized. Examples of Cartesian coordinates for a selected number of molecules is given in the appendices at the end of the thesis.

7.8 Kinetic Simulation and Fitting

All kinetic fitting and simulations were done using the software package SimFit (version 32 2003) and the isosim program incorporated within the SimFit package. A detailed kinetic model of all the possible interactions involved in the studied system was constructed. The first experiment analyzed was always the bimolecular reactions in order to determine rate constants for the bimolecular processes. An example of a bimolecular reaction model is shown in **Figure 7.6**.

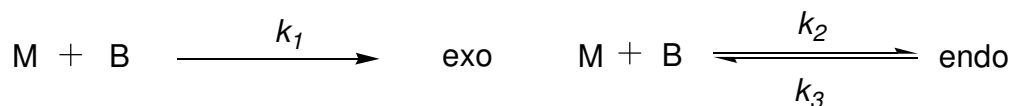


Figure 7.6 Example of a kinetic model for a simple bimolecular reaction where M can react with B to form *exo* with a rate constant k_1 or reversibly form *endo* with forward rate constant k_2 and reverse rate constant k_3 .

This model is entered into the SimFit program, a simplified example of this can be examined in **Figure 7.7**. The arrows in **Figure 7.7** give a brief explanation of what each part of the model means. The Simfit model converts this model into a series of rate equations which it integrates to determine the concentration of reactant and product species as a function of time. The program varies the unknown values until the

theoretical concentration matches the experimental. The quality of the fit is measured *via* an R value. The R value is the mean absolute difference between the experimental and theoretical concentrations with respect to the mean of the experimental concentration. A R value equal to or below 3% is considered a good fit, 3-5% is OK and 5-10% is considered a poor fit.

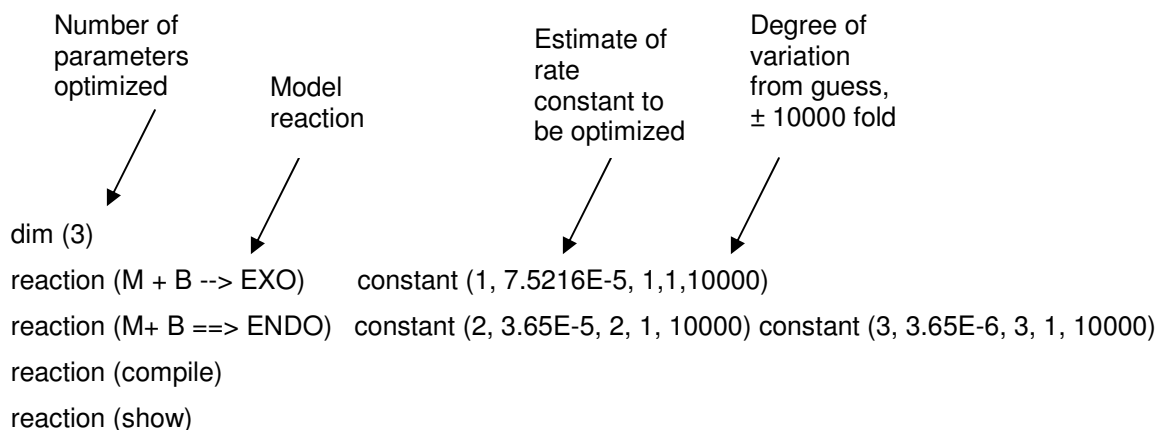


Figure 7.7 Example of how kinetic model appears in SimFit program.

The templated kinetic models are a lot more complicated and take up too much space to be shown here, an example of an input file, like the one shown above for the bimolecular reaction can be examined in appendix.

Once these values were determined the templated experiments could be analyzed. The calculated bimolecular rate constants and the experimentally determined individual association constants can now be entered into the model for the templated experiment. Unknown parameters such as the ternary complex rate constant and product duplex stability constants can then be optimized until the best fit is observed to the experimental data. Additional data on how all the different species concentrations vary with time over the experimental timecourse can also be calculated using the SimFit software package.

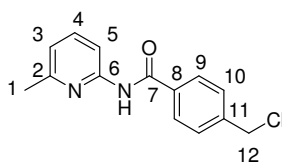
The templated model incorporates all the possible interactions in the system. This includes the bimolecular, template and binary complex reactions and the formation of productive and nonproductive complexes formed by molecular recognition.

The simulation package in SimFit, *isosim*, allowed us to take the data from the fitted kinetic models and simulate the experiment under a range of different conditions. This allowed us to investigate how our systems might react under concentrations of added

template not possible to be achieved experimentally, as a consequence of their insolubility. An example of an isosim input file can be seen in appendix.

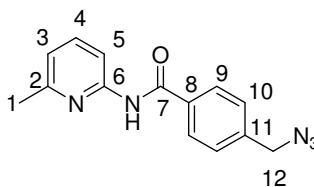
7.9. Synthetic Procedures

4-Chloromethyl-*N*-(6-methylpyridin-2-yl)benzamide (**108**)



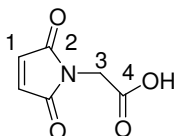
4-(Chloromethyl)benzoyl chloride (5.00 g, 27.0 mmol) **107** was dissolved in dry CH_2Cl_2 (50 ml) and added drop-wise to solid 6-methyl-2-aminopyridine (8.60 g, 80.0 mmol) under an atmosphere of nitrogen and this solution was stirred overnight. The resultant precipitate was filtered and the solvent removed under reduced pressure. The crude product was purified by column chromatography (SiO_2 , 3:1 hexane:EtOAc), to afford **108** as colorless solid (5.50 g, 80%); mp 126-127 °C. ^1H NMR (300.1 MHz, CDCl_3): δ_{H} 8.65 (1H, br s, NH), 8.18 (1H, d, $J_{\text{HH}} = 8.0$ Hz, Pyr CH, H3), 7.91 (2H, d, $J_{\text{HH}} = 8.5$ Hz, Ar CH, H9), 7.64 (1H, dd, $J_{\text{HH}} = 8.0$ Hz and 7.5 Hz, Pyr CH, H4), 7.50 (2H, d, $J_{\text{HH}} = 8.5$ Hz, Ar CH, H10), 6.93 (1H, d, $J_{\text{HH}} = 7.5$ Hz, Pyr CH, H5), 4.62 (2H, s, CH_2), 2.45 (3H, s, CH_3). ^{13}C NMR (75.5 MHz, CDCl_3): δ_{C} 165.0 (quat. C, C7), 157.4 (quat. C, C6), 151.1 (quat. C, C2), 141.9 (quat. C, C11), 139.2 (CH, PyH, C3), 134.7 (quat. C, C8), 129.3 (CH, 2 x Ar CH, C9), 128.1 (CH, 2 x Ar CH, C10), 120.0 (CH, PyH, C4), 111.4 (CH, PyH, C5), 45.7 (CH_2 , C12), 24.3 (CH_3 , C1). IR (KBr plates) 3440, 1676, 1598 cm^{-1} . MS (EI+) m/z 260 (18%, $[\text{M}^+]$), 153 (100). Found C 64.49 H 5.03 N 10.74 $\text{C}_{14}\text{H}_{13}\text{N}_2\text{OCl}$ requires C 64.43 H 5.15 N 10.67

4-Azidomethyl-*N*-(6-methylpyridin-2-yl)benzamide (azide **103**)



Sodium azide (12.30 g, 250.0 mmol) was added to a solution of 4-chloromethyl-*N*-(6-methyl pyridin-2-yl)benzamide **108** (5.50 g, 21.0 mmol) dissolved in acetone (100 ml) and this mixture was heated under reflux for 12 hours. The resultant suspension was filtered to remove the precipitate and the solvent removed *in vacuo*. The resulting yellow solid was dissolved in CH₂Cl₂ (100 ml) washed with brine (2 x 50 ml) and the organic fraction dried over MgSO₄. The resulting suspension was filtered before being concentrated *in vacuo* to afford **103** as a yellow solid (5.64 g, 72%); mp 65-67 °C. ¹H NMR (300.1 MHz, CDCl₃): δ_H 8.89 (1H, s, NHCO, H7), 8.09 (1H, d, J_{HH} = 8.5 Hz, Pyr H, H3), 7.80 (2H, d, J_{HH} = 8.5 Hz, Ar H, H9), 7.53 (1H, dd, J_{HH} = 8.5 Hz and 7.5 Hz, Pyr H, H4), 7.29 (2H, d, J_{HH} = 8.5 Hz, Ar H, H10), 6.81 (1H, d, J_{HH} = 7.5 Hz, Pyr H, H5), 4.30 (2H, s, CH₂), 2.28 (3H, s, CH₃). ¹³C NMR (75.5 MHz, CDCl₃): δ_C 165.6 (quat. C, C8), 157.3 (quat. C, C6), 151.2 (quat. C, C2), 140.2 (quat. C, C12), 139.2 (CH, PyH, C3), 134.7(quat. C, C10), 128.7 (CH, 2 x ArH, C10), 128.2 (CH, 2 x ArH, C11), 119.9 (CH, PyH, C4), 111.5 (CH, PyH, C5), 54.5 (CH₂, C13), 24.3 (CH₃, C1). MS (EI+) *m/z* 267 (8%, [M+]).132 (100). Found C 62.71 H 4.80 N 26.20 C₁₄H₁₃N₅O requires C 62.91 H 4.90 N 26.20

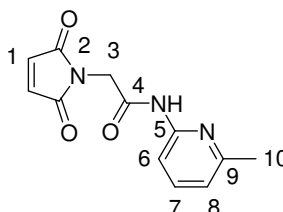
(2,5-Dioxo-2, 5-dihydro-pyrrol-1-yl)acetic acid (maleimide **63b**)



Glycine (10.00 g, 132.0 mmol) **109** was mixed with maleic anhydride (13.10 g, 132.0 mmol) and then dissolved in glacial acetic acid (200 ml). This solution was stirred at room temperature under a nitrogen atmosphere for 12 hours. After this time, the resulting suspension was heated under reflux until the reaction mixture was a clear solution (typically 2.5 hours). The solvent was then removed *in vacuo* and the resulting yellow solid purified by column chromatography (SiO₂; CH₂Cl₂:AcOH 20:1). Fractions containing the product were combined and the solvent removed under reduced pressure. Recrystallization of the cream residue afforded **63b** as a colorless solid (7.87 g, 40%); mp 113.0-114.0 °C (lit^[124]. 112-113 °C). ¹H NMR (300.1 MHz, CDCl₃): δ_H 9.73 (1H, s, CO₂H, H4), 6.73 (2H, s, CH=CH, H1), 4.26 (2H, s, CH₂, H3). ¹³C NMR (75.5 MHz, CDCl₃): δ_C 172.9 (quat. C, C4), 170.1 (quat. C, C2), 134.9 (2 x CH, CH=CH), 38.7

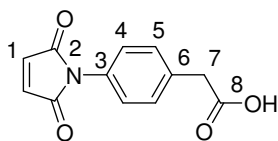
(CH₂, C3). IR (KBr plates) 1755 cm⁻¹. MS (EI+) *m/z* 155 (8%, [M+]), 110 (100). Found C 46.61 H 3.34 N 9.01 C₆H₅O₄N requires C 46.46 H 3.25 N 9.03.

2-(2,5-Dioxo-2,5-dihydropyrrol-1-yl)-*N*-(6-methylpyridin-3-yl)acetamide
(maleimide **73a**)^[207]



(2,5-Dioxo-2,5-dihydropyrrol-1-yl)acetic acid **63b** (0.60 g, 3.80 mmol) was dissolved in MeCN (8 ml) and the solution left to cool to -3 °C for a few minutes in a salt ice bath. Cyanuric fluoride (0.2 ml, 2.30 mmol) and pyridine (0.34 ml, 4.30 mmol) were then added to the reaction mixture. After 2 minutes, the solution was removed from the ice bath diluted in CH₂Cl₂ (10 ml) and left at room temperature for a further minute. The solution was then washed with brine (2 x 20 ml), the organic fraction was dried over MgSO₄ and filtered, before being concentrated to a volume of approximately 5 ml. The acid fluoride was assayed by ¹⁹F NMR (282.3 MHz, CDCl₃): δ_F + 31.6 (t, ³J_{HF} = 4.0 Hz, COF). 6-Methyl-2-aminopyridine (0.42 g, 3.80 mmol) was added to the solution stirred under nitrogen overnight. The reaction mixture was then washed with brine (2 x 30 ml), the organic layer dried over MgSO₄, filtered before being concentrated under reduced pressure. The crude product was purified using column chromatography (SiO₂, 1:1 Et₂O:CH₂Cl₂) to afford **73a** as a colorless solid (0.40 g, 42%); mp 136-137 °C (lit^[127] 126-127 °C). ¹H NMR (300.1 MHz, CDCl₃): δ_H 8.47 (1H, s, CONH), 7.90 (1H, d, J_{HH} = 7.5 Hz, Pyr H, H6), 7.57 (1H, dd, J_{HH} = 8.0 Hz and 7.5 Hz, Pyr H, H7), 6.87 (1H, d, J_{HH} = 8.0 Hz, Pyr H, H8), 6.75 (2H, s, CH=CH, H1), 4.36 (2H, s, CH₂), 2.43 (3H, s, CH₃). ¹³C NMR (75.5 MHz, CDCl₃): δ_C 170.5 (quat. C, C2), 164.1 (quat. C, C4), 157.3 (quat. C, C5), 150.4 (quat. C, C9), 139.2 (CH, Py CH, C6), 134.9 (2 x CH, CH=CH, C1), 120.2 (CH, Py CH, C7), 111.6 (CH, Py CH, C8), 41.4 (CH₂, C3) 24.3 (CH₃, C11). MS (EI+) *m/z* 245 (40%, [M+]). Found C 58.23 H 4.26 N 16.91 C₁₂H₁₁N₃O₃ requires C 58.77 H.4.52 N 17.13.

[4-(2,5-Dioxo-2,5-dihydro-pyrrol-1-yl)phenyl]acetic acid (maleimide 86)

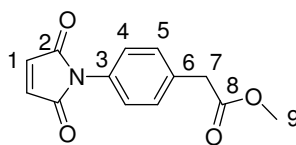


4-Aminophenylacetic acid (5.00 g, 33.0 mmol) **112** was mixed with maleic anhydride (3.20 g, 33.0 mmol) and then dissolved in glacial acetic acid (200 ml). This solution was stirred at room temperature under a nitrogen atmosphere for 12 hours. After this time, the resulting suspension was heated under reflux until the reaction mixture was a clear solution (typically 2.5 hours). The solvent was then removed *in vacuo* and the resulting yellow solid purified by column chromatography (SiO₂; CH₂Cl₂: AcOH 20:1). Fractions containing the product were combined and the solvent removed under reduced pressure. Recrystallization of the yellow residue afforded **86** as a yellow solid (3.53 g, 46%); mp 151-154 °C (lit^[144]. 151-153 °C). ¹H NMR (300.1 MHz, CDCl₃): δ_H 7.41 (2H, d, J_{HH} = 9.0 Hz, Ar H, H5), 7.32 (2H, d, J_{HH} = 9.0 Hz, Ar H, H4), 6.85 (2H, s, CH=CH, H1), 3.60 (2H, s, CH₂). ¹³C NMR (75.5 MHz, CDCl₃): δ_C 177.8 (C=O, C8), 169.9 (C=O, C2), 134.6 (2 x CH, CH=CH, C1), 133.5 (quat. C, C6), 130.8 (2x Ar CH, C5), 130.6 (quat. C, C3) 126.5 (2 x Ar CH, C4), 41.1 (CH₂, C7). MS (EI) *m/z* 231 (10%, [M⁺]); 186 (100) HRMS (EI⁺) calculated for C₁₂H₉NO₄ [M⁺] 231.0532, found 231.0526.

NaHSO₄•SiO₂^[169]

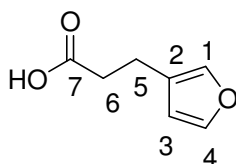
SiO₂ (10.00 g, 167.0 mmol) and NaHSO₄ (4.14 g, 35.0 mmol) were mixed in distilled H₂O (20 ml) and then left to stir for 15-20 minutes at 80 °C. The suspension was then left for a further 8 hours, with occasional stirring, until the water had evaporated off and a free flowing white solid was obtained. This was then dried at 120 °C for 48 hours to afford the catalyst NaHSO₄•SiO₂ (14.00 g, 99%) as a white solid.

Methyl 4-(2,5-Dioxo-2,5-dihydro-pyrrol-1-yl)phenylacetate^[169] (maleimide **86b**)



NaHSO₄•SiO₂ (0.65 g) was added to a solution of (3-bromophenyl) acetic acid (1.50 g, 6.45 mmol) **86** in MeOH (15 ml). After stirring for 1 days the resultant mixture was then filtered to remove the catalyst and concentrated *in vacuo* to afford **86b** as a pale yellow solid (0.78 g, 50%); mp 85-86 °C (lit^[128]. 87-88 °C). ¹H NMR (300.1 MHz, CDCl₃): δ_H 7.32 (2H, d, J_{HH} = 8.6 Hz, Ar CH, H5), 7.24 (2H, d, J_{HH} = 8.6 Hz, Ar CH, H4), 6.79 (2H, s, CH=CH, H1), 3.63 (3H, s, CH₃, H9), 3.59 (2H, s, CH₂, H7). ¹³C NMR (75.5 MHz, CDCl₃): δ_C 171.5 (ester), 169.9 (C=O), 134.6 (CH, CH=CH), 134.2 (quat. C, C3), 130.5 (CH, 2 x Ar CH, C5), 126.5 (CH, 2 x Ar CH, C4), 52.6 (CH₃, C9), 41.2 (CH₂, C7). MS (EI+) *m/z* 245 (40%, [M+]), 186 (100). Found C 63.19 H 4.22 N 5.60 C₁₃H₁₁NO₄ requires C 63.67 H 4.52 N 5.71.

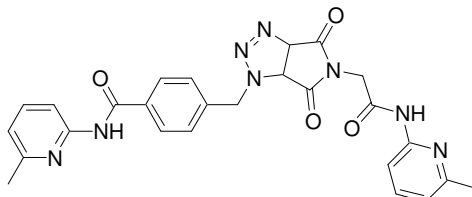
3-(Furan-3-yl) propionic acid (Furan **70**)



Furan acrylic acid (5.00 g, 36.0 mmol) **119** was mixed with 10% Pd/C (420 mg) and then flushed with nitrogen for 30 minutes. MeOH (30 ml) was then carefully syringed into the flask before being flushed with hydrogen and stirred under an atmosphere of hydrogen for 3.5 hours. The resulting mixture was then filtered through a pad of celite and concentrated *in vacuo*. The resulting brown solid was purified using Kugerlrohr distillation. The colorless solid obtained was recrystallized from hexane and stored in a freezer to afford **70**, as a colorless solid (1.02 g, 20% yield); mp 65-66 °C (lit^[127]. 65-66 °C). ¹H NMR (300.1 MHz, CDCl₃): δ_H 11.15 (1H, br s, CO₂H, 7H), 7.40-7.33 (1H, m, furyl-H, H4), 7.28-7.21 (1H, m, furyl-H, H1), 6.35-6.28 (1H, m, furyl-H, H3), 2.78 (2H, t, J_{HH} = 7.0 Hz, CH₂, H5), 2.64 (2H, t, J_{HH} = 7.0 Hz, CH₂, H6). ¹³C NMR (75.5 MHz, CDCl₃): δ_C 179.8 (quat. C, C7), 143.4 (CH, Furyl, C4), 139.5 (CH, Furyl, C1), 123.6

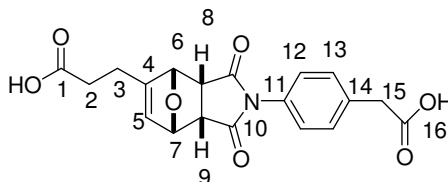
(quat. C, C2), 111.1 (CH, Furyl, C3), 35.0 (CH₂, C5), 20.9 (CH₂, C6). IR (KBr plates) 2550, 1694, 1499 cm⁻¹. MS (EI) *m/z* 140 (50%, [M+]). HRMS (EI+) calculated for C₇H₈O₃ [M+] 140.0478, found 140.0472.

***N*-(6-Methyl pyridin-2-yl)-4-{5-[6-methyl pyridin-2-ylcarbamoyl] methyl}-4,6,-dioxo-4,5,6,6 a-tetrahydro-3a*H*-pyrrolo[3,4-*d*][1,2,3]triazol-1-ylmethyl}benzamide (bis(amidopyridine) template 104).**



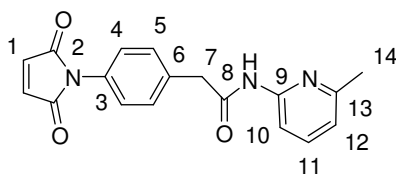
4-Azidomethyl-*N*-(6-methyl-pyridin-2-yl)benzamide (260 mg, 0.96 mmol) **103** and 2(2,5-dioxo-2,5 dihydro-pyrrol-1-yl)-*N*-(6-methyl-pyridin-3-yl)acetamide (240 mg, 0.96 mmol) **73b** were dissolved in CHCl₃ (10 ml) and this solution was left in the dark at 50 °C for 4 days. The solvent was then removed *in vacuo* and the resultant yellow solid purified through column chromatography (SiO₂, 3:1 CH₂Cl₂: Et₂O) to afford **104** as a yellow solid (0.40 g, 80%); mp 150-155 °C. ¹H NMR (300.1 MHz, CDCl₃): δ_H 8.66 (2H, br s, CONH), 8.09 (1H, d, J_{HH} = 8.0 Hz, Pyr H), 7.84 (2H, d, J_{HH} = 8.5 Hz, Ar H), 7.76 (1H, d, J_{HH} = 8.0 Hz, Pyr H), 7.58 (1H, dd, J_{HH} = 8.0 and 7.5 Hz, Pyr H), 7.44 (1H, dd J_{HH} = 8.0 Hz and 7.5 Hz, Pyr H), 7.39 (2H, d, J_{HH} = 8.5 Hz, Ar H), 6.87 (1H, d, J_{HH} = 7.5 Hz, Pyr H), 6.82 (1H, d, J_{HH} = 7.5 Hz, Pyr H), 5.52 (1H, d, J_{HH} = 11.0 Hz, CH), 5.31 (1H, d, J_{HH} = 13.0 Hz, CH₂), 4.76 (1H, d, J_{HH} = 13.0 Hz, CH₂) 4.25 (2H, br s, CH₂), 4.16 (1H, d, J_{HH} = 11.0 Hz, CH), 2.40 (3H, s, CH₃), 2.32 (3H, s, CH₃). ¹³C NMR (75.5 MHz, CDCl₃): δ_C 171.5 (C=O), 170.1 (C=O), 165.5 (quat C), 157.3 (2 x quat C) 151.1 (quat C) 150.2 (quat C) 139.3 (CH, 2 x Py CH), 138.9 (2 x quat C), 134.8 (quat C), 129.5 (CH, 2 x Ar CH), 128.4 (CH, 2 x Ar CH), 120.3 (CH, Py CH), 120.0 (CH, Py CH), 111.6 (CH, 2 x Py CH), 82.1 (CH), 57.2 (CH), 55.6 (CH₂), 43.4 (CH₂), 24.3 (CH₃), 24.2 (CH₃). MS (ES-) *m/z* 512 (10%, [M+]), 212 (100). HRMS (ES-) calculated for C₂₆H₂₄N₈O₈ (M-) 512.1921, Found 512.1103.

3-[4-(4-Carboxymethyl phenyl)-3,5-dioxo-10-oxa-4-aza tricyclo[5.2.1.0^{2,6}]dec-8-en-8-yl]propionic acid (dicarboxylic acid 105).



4-(2,5-dioxo-2,5-dihydro-pyrrol-1-yl)-phenylacetic acid **86** (310 mg, 1.35 mmol) and 3-furan-3-yl-acrylic acid (190 mg, 1.35 mmol) **70** were dissolved in CHCl_3 (10 ml) and this solution was left in the dark at 50 °C for 4 days. The resultant precipitate was filtered and washed with CHCl_3 before being dried under vacuum to afford **105** as a yellow solid (0.33 g, 66%); mp 174-175 °C (lit^[144] 174-175). ¹H NMR (300.1 MHz, CDCl_3): δ_{H} 12.35 (2H, br s, CO_2H , H1), 7.35 (2H, d, $J_{\text{HH}} = 8.0$ Hz, Ar CH, H12), 7.12 (2H, d, $J_{\text{HH}} = 8.0$ Hz, Ar H, H13), 6.13 (1H, d, $J_{\text{HH}} = 1.5$ Hz, $\text{CH}=\text{CH}$, H5), 5.16 (1H, s, CH, H6), 5.09 (1H, s, CH, H7), 3.62 (2H, s, CH_2 , H15), 3.16 (1H, d, $J_{\text{HH}} = 6.0$ Hz, CH, H8), 3.06 (1H, d, $J_{\text{HH}} = 6.0$ Hz, CH, H9), 2.50-2.40 (4H, m, CH_2 , H2-3). ¹³C NMR (75.5 MHz, CDCl_3): δ_{C} 176.3 (quat. C), 176.1 (quat. C), 174.1 (quat. C), 172.8 (quat. C), 150.7 (quat. C), 135.8 (quat. C), 131.0 (quat. C), 130.4 (2 x CH, Ar CH, C13), 129.2 (CH, $\text{CH}=\text{CH}$, C5), 127.0 (2 x CH, Ar CH, C12), 83.1 (CH, C6), 81.9 (CH, C7), 49.4 (CH, C8), 47.4 (CH, C9), 39.3 (CH_2), 31.8 (CH_2), 22.4 (CH_2). MS (ES-) m/z 371 (10%, $[\text{M}^+]$), 741 (100). HRMS (ES-) calculated for $\text{C}_{19}\text{H}_{17}\text{NO}_7$ $[\text{M}^+]$ requires 371.1005, found 371.1217.

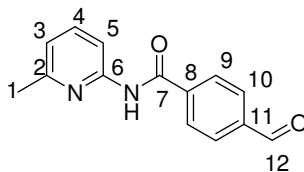
2-[4(2,5-dihydro-pyrrol-yl)-phenyl]-N-(6-methyl-pyridin-2-yl)acetamide (maleimide 116)^[207]



4-(2,5-Dioxo-2,5-dihydropyrrol-1-yl)phenylacetic acid (0.60 g, 2.60 mmol) was dissolved in MeCN (6 ml) and the solution left to cool to -3 °C for a few minutes in a salt ice bath. Cyanuric fluoride (0.14 ml, 1.60 mmol) and pyridine (0.30 ml, 3.80 mmol) were then added to the reaction mixture. After 2 minutes, the solution was removed from the ice

bath diluted in CH₂Cl₂ (20 ml) and left at room temperature for a further minute. The reaction mixture was then washed in brine (50 ml), the CH₂Cl₂ fraction was dried over MgSO₄ and filtered, before the filtrate was concentrated under reduced pressure to a volume of approximately 5 ml. The acid fluoride was assayed by ¹⁹F NMR (282.3 MHz, CDCl₃): δ_F + 44.8 (t, ³J_{HF} = 3.0 Hz, COF). 6-Methyl-2-aminopyridine (0.26 g, 2.4 mmol) was added to the solution and left to stir under nitrogen at room temperature overnight. The reaction mixture was then washed with brine (30 ml) and extracted using CH₂Cl₂ (2 x 50 ml). The organic fractions were combined, dried over MgSO₄, filtered, before the filtrate was concentrated *in vacuo* to afford a brown solid. The crude product was initially purified using column chromatography (SiO₂ 1:1 Et₂O: CH₂Cl₂) to afford a luminous green solid, which was recrystallised in EtOAc/hexane (1:1) to afford **116** as a colorless solid (0.40 g, 48%); mp 163-164 °C ; ¹H NMR (300.1 MHz, CDCl₃): δ_H 8.70 (1H, br s, NH), 7.95 (1H, d, J_{HH} = 8.5 Hz, Pyr H, H12), 7.58 (1H, dd, J_{HH} = 8.5 Hz and 7.4 Hz, Pyr H, H11), 7.40 (2H, d, J_{HH} = 8.4 Hz, Ar H, H5), 7.30 (2H, d, J_{HH} = 8.4 Hz, Ar H, H4) 6.80 (1H, d, J_{HH} = 7.5 Hz, Pyr H, H10), 6.70 (2H, s, CH=CH, H1), 3.67 (2H, s, CH₂), 2.33 (3H, s, CH₃). ¹³C NMR (75.5 MHz, CDCl₃): δ_C 169.4 (2 x C=O), 168.8 (C=O), 159.7 (quat. C, C9), 156.7 (quat. C, C13), 138.8 (CH, Py CH, C12), 134.3 (CH, CH=CH, C1), 133.9 (quat. C, C3) , 130.6 (quat. C, C6) 130.2 (CH, Ar CH, C5), 126.4 (CH, 2 x Ar CH, C4), 119.5 (CH, Py CH, C11), 110.8 (CH, Py CH, C10), 44.5 (CH₂), 23.8 (CH₃). IR (Nujol mull, NaCl plates) 3349, 2726, 1706, 1689 cm⁻¹. MS (ES+) *m/z* 344 (100%, [M⁺Na]). HRMS (ES+) calculated for C₁₈H₁₅N₃O₃ [M+Na] 344.1011, found 344.1016.

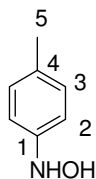
***N*-(6-methylpyridin-2-yl)-3-formylbenzamide^[168] 126**



Hexamethylene tetramine (1.90 g, 13.8 mmol) was added to a solution of 4-Chloromethyl-*N*-(6-methylpyridin-2-yl)benzamide **108** (1.20 g, 4.80 mmol) in EtOH/H₂O (1:1, 5 ml) and this mixture heated under reflux for 4 hours. While still heating under reflux, concentrated HCl (2 ml) was added to the solution. After 30 minutes, the solution was left to cool to room temperature and diluted in H₂O (20 ml). The reaction mixture

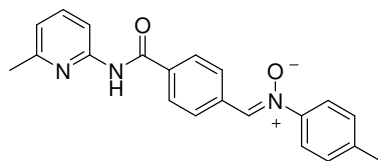
was then extracted using CH₂Cl₂ (2 x 100 ml). The CH₂Cl₂ fractions were combined and dried over MgSO₄, before the filtrate was concentrated *in vacuo* to afford **126** as a colorless solid (0.95 g, 85%); mp 106-107 °C (lit^[128] 108-110 °C). ¹H NMR (300.1 MHz, CDCl₃): δ_H 10.00 (1H, s, CHO, H12), 8.80 (1H, br s, NH), 8.14 (1H, d, J_{HH} = 8.2 Hz, Pyr H, H3), 8.03 (2H, d, J_{HH} = 8.3 Hz, 2 x Ar H, H10), 7.92 (2H, d, J_{HH} = 8.3 Hz, 2 x Ar H, H9), 7.62 (1H, dd, J_{HH} = 8.2 Hz and 7.4 Hz, Pyr H, H4) 6.89 (1H, d, J_{HH} = 7.4 Hz, Pyr H, H5), 2.45 (3H, s, CH₃). ¹³C NMR (75.5 MHz, CDCl₃) δ_C 191.8 (CHO, C12), 164.8 (Amide, C7), 156.3 (quat. C, C8), 150.6 (quat. C, C11) 140.6 (CH, Py CH, C3), 139.3 (quat. C), 139.1 (quat. C), 130.4 (CH, 2 x Ar CH, C10), 128.6 (CH, 2 x Ar CH, C9), 120.3 (CH, Py CH, C4), 112.1 (CH, Py CH, C5), 23.6 (CH₃). IR (solution CHCl₃, NaCl plates) 3326, 3256, 1682 cm⁻¹. MS (ES+) *m/z* 240 (7%, [M+]), 239 (100). HRMS (EI+) calculated for C₁₄H₁₂N₂O₂ [M+H] 241.0977, found 241.0977.

***p*-Methylphenylhydroxylamine 125**



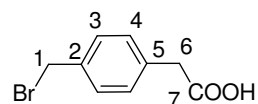
Ammonium chloride (1.90 g, 36.0 mmol) and 4-nitrotoluene (4.30 g, 31.1 mmol) were dispersed in H₂O/EtOH (2:5, 60 ml). While stirring rapidly at room temperature zinc dust (9.60 g, 146.0 mmol) was added portion-wise, this suspension was left to stir for 15 minutes. The slurry formed was then filtered through celite with warm water and left to cool to room temperature. The reaction mixture was then extracted using Et₂O (3 x 250 ml) and the organic fractions combined, before being dried over MgSO₄ and filtered. The solvent of the filtrate was then removed under reduced pressure to afford the crude product as a yellow solid, which was purified by recrystallisation from Et₂O/hexane (1:4) to afford **125** as a colorless solid (0.95 g, 25%): mp 71-72 °C. ¹H NMR (300.1 MHz, CDCl₃): δ_H 7.11 (2H, d, J_{HH} = 8.2 Hz, Ar H, H2), 6.95 (2H, d, J_{HH} = 8.2 Hz, Ar H, H3) 6.06 (2H, br s, NHOH), 2.32 (3H, s, CH₃). ¹³C NMR (75.5 MHz, CDCl₃): δ_C 147.4 (quat. C, C1), 132.5 (quat. C, C4), 129.9 (CH, 2 x Ar CH, C2), 115.9 (CH, 2x Ar CH, C3), 21.1 (CH₃). MS (CI+) *m/z* 124 (30%, [M+]).

**(Z)-4-methyl-N-(4-(6-methylpyridin-2-yl)carbamoyl)benzylidene)aniline oxide
(nitron 115).**



N-(6-methyl-pyridin-2-yl)-3-formylbenzamide (590 mg, 2.40 mmol) and *p*-methylphenylhydroxylamine (300 mg, 2.40 mmol) were dissolved in EtOH (10 ml). This solution was left to stand for 24 hours in the dark at room temperature. The resulting precipitate formed was then filtered, to remove the solvent and washed with hexane, affording **115** as a colorless solid (0.75 g, 90%); mp 195.3-196.5 °C. ¹H NMR (300.1 MHz, CDCl₃): δ_H 8.67 (1H, s, NH), 8.44 (2H, d, J_{HH} = 8.2 Hz, Ar H), 8.15 (1H, d, J_{HH} = 8.4 Hz, Pyr H) 7.98 (2H, d, J_{HH} = 8.7 Hz, Ar H), 7.93 (1H, s, CH=N), 7.62 (2H, d, J_{HH} = 8.7 Hz, Ar H), 7.61 (1H, dd, J_{HH} = 8.4 Hz and 7.5 Hz, Pyr H), 7.23 (2H, d, J_{HH} = 8.2 Hz, Ar H), 6.90 (1H, d, J_{HH} = 7.5 Hz, Pyr H), 2.44 (3H, s, CH₃), 2.37 (3H, s, CH₃). ¹³C NMR (75.5 MHz, CDCl₃): δ_C 165.1 (Amide), 157.2 (quat. C), 151.1 (quat. C), 147.1 (quat. C), 141.1 (quat. C), 139.3 (CH, Py CH), 135.8 (quat. C), 134.4 (quat. C), 133.5 (CH, CH=N), 130.1 (CH, 2 x Ar CH), 129.4 (CH, 2 x Ar CH), 128.0 (CH, 2 x Ar CH), 121.9 (CH, 2 x Ar CH), 120.0 (CH, Py CH), 111.6 (CH, Py CH), 24.3 (CH₃), 21.6 (CH₃). IR (CHCl₃ solution, NaCl plates) 1677 cm⁻¹. MS (ES⁺) *m/z* 368 (100%, [M+Na]). HRMS (ES⁺) calculated for C₂₁H₁₉N₃O₂ [M+Na] 368.1375 found, 368.1377.

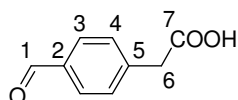
4-Bromomethylphenylacetic acid^[167] 128



Bromine (7.40 g, 46.0 mmol) was added to a solution of *p*-tolylacetic acid (6.30 g, 43.0 mmol) in chlorobenzene (50 ml). This solution was stirred at room temperature illuminated by a 60 watt tungsten lamp. After 15 minutes a precipitate had formed and the solid was filtered off. The filtrate was left to stir at room temperature under the light of the 60 watt lamp. This process was repeated until no more precipitate was formed.

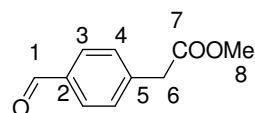
The resulting pale yellow solid was purified by recrystallization from acetone/hexane (1:3) to afford **128** as a colorless solid (5.20 g, 54%); mp 174-176 °C (lit^[167]. 179-180 °C). ¹H NMR (300.1 MHz, CDCl₃): δ_H 7.36 (2H, d, J_{HH} = 8.1 Hz, Ar H, H3), 7.25 (2H, d, J_{HH} = 8.1 Hz, Ar H, H4), 4.55 (2H, s, CH₂, H1), 3.65 (2H, s, CH₂, H6). ¹³C NMR (75.5 MHz, CDCl₃): δ_C 174.2 (C=O), 138.9 (quat. C, C2), 136.3 (quat. C, C5), 131.2 (CH, 2 x Ar CH, C3), 130.8 (CH, 2 x Ar CH, C4), 41.8 (CH₂, C1), 34.2 (CH₂, C6). IR (KBr plates) 2958, 2914, 2348, 1697 cm⁻¹. MS (EI+) *m/z* 229 (5%, [M+]), 227 (5%, [M+]), 149 (100). HRMS (ES+) calculated for C₉H₉O₂Br₈₁ [M+] 229.9765, found 229.9761, calculated for C₉H₉O₂Br₇₉ 227.9786, found 227.9793.

4-Formylphenylacetic acid **129**



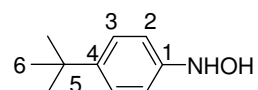
(4-Bromomethylphenyl) acetic acid (2.00 g, 8.80 mmol) and hexamethylene tetramine (1.90 g, 26.20 mmol) were dissolved in an EtOH/H₂O mixture (1:1, 10 ml) and heated under reflux for 4 hours. While still heating under reflux, concentrated HCl (4 ml) was then added to the solution. After 30 minutes the reaction mixture was left to cool to room temperature and diluted in water (30 ml). The reaction mixture was then extracted using CH₂Cl₂ (2 x 100 ml). The organic fractions were combined and dried over MgSO₄, before the filtrate is concentrated under reduced pressure to afford **129** as a colorless solid (0.80 g, 50%): mp 125-127 °C. ¹H NMR (300.1 MHz, CDCl₃): δ_H 9.93 (1H, s, CHO, H1), 7.79 (2H, d, J_{HH} = 8.2 Hz, 2 x Ar H, H3) 7.38 (2H, d, J_{HH} = 8.2 Hz, 2 x Ar H, H4), 3.68 (2H, s, CH₂). ¹³C NMR (75.5 MHz, CDCl₃): δ_C 192.4 (CHO), 176.9 (C=O), 140.5 (quat C, C2), 135.9 (quat C, C5), 130.6 (CH, 2 x Ar CH, C3), 130.5 (CH, 2 x Ar CH, C4), 41.5 (CH₂); IR (KBr plates) 2617, 1726, 1660. MS (ES+) *m/z* 164 (80%, [M+]).

Methyl 4-formylphenylacetate **129b**



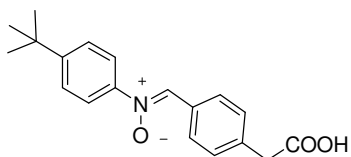
NaHSO₄•SiO₂ (0.39 g) was added to a solution of (4-formyl) acetic acid (0.65 g, 3.90 mmol) in MeOH (15 ml), and left to stir for 1 days at ambient temperature. This suspension was then filtered and the solvent was removed from the filtrate under reduced pressure, to afford **129b** as a colorless solid (0.42 g, 61%); mp 40-41 °C. ¹H NMR (300.1 MHz, CDCl₃): δ_H 10.00 (1H, s, CHO, H1), 7.85 (2H, d, J_{HH} = 8.3 Hz, 2 x Ar H, H3), 7.45 (2H, d, J_{HH} = 8.3 Hz, 2 x Ar H, H4), 3.72 (2H, CH₂), 3.71 (3H, CH₃). ¹³C NMR (75.5 MHz, CDCl₃): δ_C 192.3 (CHO), 171.5 (C=O), 141.2 (quat. C, C5), 135.8 (quat. C, C2), 130.5 (CH, 2 x Ar CH, C3), 130.4 (CH, 2 x Ar CH, C4), 52.7 (CH₃), 41.6 (CH₂). MS (EI+) *m/z* 178.06 (60%, [M⁺]), 119 (55), 91 (100).

N-(4-*tert*-Butylphenyl)hydroxylamine **131**



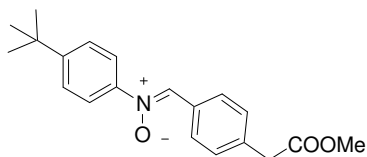
Ammonium chloride (3.40 g, 64.2 mmol) was added to a stirred dispersion of 1-*tert*-butyl-4-nitrobenzene (10.00 g, 55.8 mmol) in H₂O/EtOH (2:5, 14 ml), before heating to 65 °C. Zinc dust (7.30 g, 112.0 mmol) was carefully added to the solution, which was then left to cool to room temperature for 20 minutes. The suspension was then filtered through celite with warm water and the filtrate left to cool to ambient temperature. The reaction mixture was then extracted using Et₂O (3 x 250 ml), the organic fractions combined, dried over MgSO₄ and filtered, before the filtrate was concentrated *in vacuo* to afford a yellow solid. This solid was purified by recrystallization from Et₂O/hexane (1:3) to afford **131** as a colorless solid (1.85 g, 20%). ¹H NMR (300.1 MHz, CDCl₃): δ_H 7.32 (2H, d, J_{HH} = 8.4 Hz, Ar H, H2), 6.97 (2H, d, J_{HH} = 8.4 Hz, Ar H, H3), 5.77 (2H, br s, NHOH), 1.32 (9H, s, tBu). ¹³C NMR (75.5 MHz, CDCl₃): δ_C 147.0 (quat. C, C1), 145.5 (quat. C, C4), 125.8 (CH, 2 x Ar CH, C2), 114.8 (CH, 2 x Ar CH, C3), 34.2 (quat C) 31.5 (CH₃, tBu); MS (CI+) *m/z* 165 (60%, [M⁺]).

(Z)-4-tert-butyl-N-(4-(carboxymethyl)benzylidene)aniline N-oxide (nitron 117).



4-Formylphenylacetic acid (0.40 g, 2.40 mmol) and *N*-(4-*tert*-butylphenyl)-hydroxylamine (0.40 g, 2.40 mmol) were dissolved in ethanol (10 ml). This solution was left to stand for 24 hours in the dark. The resulting precipitate was filtered off and washed with hexane, to afford **117** as a colorless solid (0.60 g, 80%); mp 168-170 °C; ¹H NMR (300.1 MHz, CDCl₃): δ_H 8.19 (2H, d, J_{HH} = 8.2 Hz, Ar H), 7.85 (1H, s, CH=N), 7.60 (2H, d, J_{HH} = 8.7 Hz, Ar H) 7.40 (2H, d, J_{HH} = 8.7 Hz, Ar H), 7.25 (2H, d, J_{HH} = 8.2 Hz, Ar H), 3.54 (2H, s, CH₂), 1.27 (9H, s, tBu). ¹³C NMR (75.5 MHz, CDCl₃): δ_C 174.5 (C=O), 154.0 (quat. C), 146.3 (quat. C), 138.3 (quat. C), 137.0 (CH, CH=N), 130.2 (CH, 2 x Ar CH), 129.9 (CH, 2 x Ar CH), 129.3 (quat. C), 126.5 (CH, 2 x Ar CH), 121.8 (CH, 2 x Ar CH), 41.9 (CH₂), 35.3 (quat. C), 31.6 (CH₃, tBu). IR (Nujol mull, NaCl plates) 3388, 1698 cm⁻¹. MS (ES⁺) *m/z* 312 (50%, [M+H]), 334 (100). HRMS (ES⁺) calculated for C₁₉H₂₁NO₃ [M+H] 312.1600, found 312.1603.

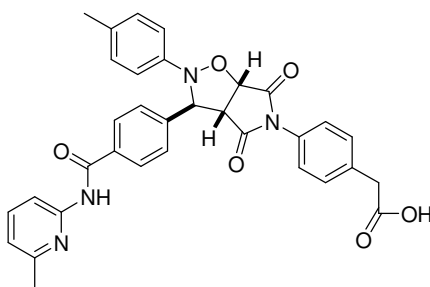
(Z)-4-tert-butyl-N-(4-(2-methoxy-2-oxoethyl)benzylidene)aniline N-oxide (nitron 117b).



4-Formylphenylacetic acid (0.40 g, 2.40 mmol) and *N*-(4-*tert*-butylphenyl)-hydroxylamine (0.40 g, 2.40 mmol) were dissolved in ethanol (10 ml). This solution was left to stand for 24 hours in the dark. The resulting precipitate was filtered off and washed with hexane, to affording **117b** as a colorless solid (0.63 g, 80%); mp 95-97 °C; ¹H NMR (300.1 MHz, CDCl₃): δ_H 8.36 (2H, d, J_{HH} = 8.1 Hz, Ar H), 7.91 (1H, s, CH=N), 7.69 (2H, d, J_{HH} = 8.7 Hz, Ar H) 7.48 (2H, d, J_{HH} = 8.7 Hz, Ar H), 7.39 (2H, d, J_{HH} = 8.1 Hz, Ar H), 3.71 (3H, s, CH₃), 3.69 (2H, s, CH₂), 1.36 (9H, s, tBu). ¹³C NMR (75.5 MHz,

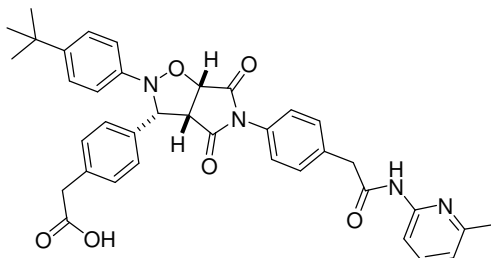
CDCl₃): δ_C 171.4 (ester), 153.4 (quat. C), 146.6 (quat. C), 136.7 (quat. C), 133.8 (CH, CH=N), 129.8 (quat. C), 129.6 (CH, 2 x Ar CH), 129.2 (CH, 2 x Ar CH), 126.1 (CH, 2 x Ar CH), 121.3 (CH, 2 x ArCH), 52.2 (CH₃), 41.3 (CH₂), 34.9 (quat. C), 31.3 (CH₃, tBu). IR (Nujol mull, NaCl plates) 1736 cm⁻¹. MS (ES⁺) *m/z* 348 (100%, [M+Na]). HRMS (ES⁺) calculated for C₂₀H₂₃NO₃ [M+Na] 348.1576, found 348.1568.

2-(4-(3-(4-(6-Methylpyridin-2-ylcarbonyl)phenyl)-4,6-dioxo-2-p-tolyldihydro-2H-pyrrolo[3,4-d]isoxazol-5(3H,6H,6aH)-yl)phenyl)acetic acid (Isoxazolidine-119).



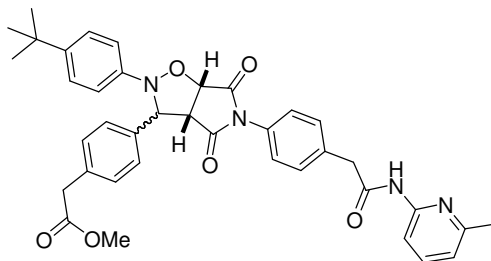
117 (8.6 mg, 0.025 mmol) and **116** (5.6 mg, 0.025 mmol) were dissolved in CHCl₃ (1 ml) and the solution left in the dark for 14 hours at 0 °C. The resultant precipitate formed was filtered off and washed with CHCl₃ to afford **119** as a colorless solid (13.4 mg, 95%); mp < 194 °C dec. ¹H NMR (300.1 MHz, CDCl₃): δ_H 11.09 (1H, s, NH), 8.38 (1H, d, J_{HH} = 8.4 Hz, Pyr H), 8.94 (2H, d, J_{HH} = 8.4 Hz, Ar H), 7.77 (1H, dd, J_{HH} = 8.4 Hz and 7.4 Hz, Pyr H), 7.44 (2H, d, J_{HH} = 8.4 Hz, Ar H), 7.32 (2H, d, J_{HH} = 8.4 Hz, Ar H), 7.14-7.07 (4H, m, Ar H), 6.99 (1H, d, J_{HH} = 7.4 Hz, Pyr H), 6.98 (2H, d, J_{HH} = 8.4 Hz, Ar H), 5.78 (1H, s, CH), 4.98 (1H, d, J_{HH} = 7.4 Hz, CH), 3.92 (1H, d, J_{HH} = 7.4 Hz, CH), 2.54 (2H, CH₂), 2.54 (3H, CH₃), 2.28 (3H, CH₃). ¹³C NMR (75.5 MHz, CDCl₃): δ_C 176.7 (C=O), 174.8 (2 x C=O), 173.4 (C=O), 166.5 (quat. C), 155.7 (quat. C), 151.7 (quat. C), 146.4 (quat. C), 142.6 (quat. C), 140.4 (CH, Py CH), 135.4 (quat. C), 133.6 (quat. C), 132.7 (quat. C), 130.5 (CH, 2 x Ar CH), 129.9 (CH, 2 x Ar CH), 128.8 (CH, 2 x Ar CH), 126.5 (CH, 2 x Ar CH), 126.1 (CH, 2 x Ar CH), 119.9 (CH, Py CH), 114.6 (CH, 2 x Ar CH), 113.24 (CH, Py CH), 77.0 (CH), 68.8 (CH), 57.1 (CH), 40.2 (CH₂), 22.0 (CH₃), 20.5 (CH₃). IR (Nujol mull, NaCl plates) 3333, 2726, 2363, 1710, 1682 cm⁻¹. MS (ES⁺) *m/z* 577 (5%, [M+H]), 599 (100). Found C 68.3 H 4.8 N 9.5, C₃₃H₂₈N₄O₆ requires C 68.7 H 4.9 N 9.7.

2-(4-(-2-(4-*tert*-Butylphenyl)-5-(4-(2-(6-methylpyridin-2-ylamino)-2-oxoethyl)phenyl)-4,6-dioxohexahydro-2H-pyrrolo[3,4-d]isoxazol-3-yl)phenyl)acetic acid (Isoxazolidine 119).



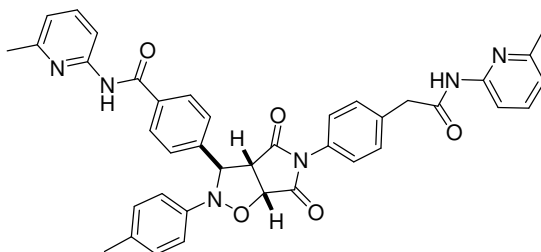
116 (0.19 g, 0.60 mmol) and **117** (0.19 g, 0.60 mmol) were dissolved CHCl₃ (1 ml) and the solution left in the dark for 14 hours at 0 °C. The resultant precipitate formed was filtered off and washed with CHCl₃ to afford **119** as a colorless solid (0.23 g, 60%); mp >195 °C dec. ¹H NMR (300.1 MHz, Acetone): δ_H 9.84 (1H, s, NH), 7.80 (1H, d, J_{HH} = 8.3 Hz, Pyr H), 7.44 (1H, dd, J_{HH} = 8.3 Hz and 7.3 Hz, Pyr H), 7.32 (2H, d, J_{HH} = 8.5 Hz, Ar H), 7.31 (2H, d, J_{HH} = 8.2 Hz, Ar H), 7.16 (2H, d, J_{HH} = 8.2 Hz, Ar H), 7.15 (2H, d, J_{HH} = 8.9 Hz, Ar H), 6.96 (2H, d, J_{HH} = 8.9 Hz, Ar H), 6.86 (2H, d, J_{HH} = 8.5 Hz, Ar H), 6.76 (1H, d, J_{HH} = 7.3 Hz, Pyr H), 5.29 (1H, d, J_{HH} = 7.8 Hz, CH), 4.94 (1H, d, J_{HH} = 9.1 Hz, CH), 4.05 (1H, dd, J_{HH} = 9.1 Hz and 7.8 Hz, CH), 3.66 (2H, s, CH₂), 3.42 (2H, s, CH₂), 2.23 (3H, s, CH₃), 1.09 (9H, s, tBu). ¹³C NMR (75.5 MHz, DMSO): δ_C 174.3 (C=O), 172.6 (C=O), 172.0 (C=O), 169.7 (C=O), 156.5 (quat. C), 151.1 (quat. C), 147.4 (quat. C), 144.7 (quat. C), 138.5 (CH, Py CH), 136.3 (quat. C), 134.8 (quat. C), 133.6 (quat. C), 130.1 (quat. C), 129.8 (CH, 2 x Ar CH), 129.5 (CH, 2 x Ar CH), 127.5 (CH, 2 x Ar CH), 126.5 (CH, 2 x Ar CH), 125.5 (CH, 2 x Ar CH), 119.3 (CH, 2 x Ar CH), 118.8 (CH, Py CH), 110.3 (CH, Py CH), 77.3 (CH), 70.0 (CH), 54.4 (CH), 42.5 (CH₂), 38.3 (CH₂), 34.0 (quat. C), 31.0 (CH₃), 23.5 (CH₃, tBu). IR (Nujol mull, NaCl plates) 3600, 1722cm⁻¹. MS (ES⁺) *m/z* 655 (100%, [M⁺Na]). HRMS (ES⁺) calculated for C₃₇H₃₆N₄O₆ [M+Na] 655.2533, found 655.2536.

Methyl 2-(4-(-2-(4-*tert*-butylphenyl)-5-(4-(2-(6-methylpyridin-2-ylamino)-2-oxoethyl)phenyl)-4,6-dioxohexahydro-2H-pyrrolo[3,4-d]isoxazol-3-yl)phenyl)acetate (Isoxazolidine 119b).



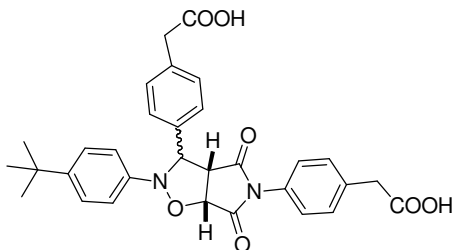
116 (200 mg, 0.62 mmol) and **117b** (200 mg, 0.62 mmol) were dissolved CHCl_3 (1 ml) and left in the dark for 3 days at room temperature. The solvent was then removed *in vacuo* to afford **119b** as a colorless solid (0.23 g, 60%); mp 107-108 °C. For *trans* isomer only; ^1H NMR (300.1 MHz, CDCl_3): δ_{H} 7.98 (1H, d, $J_{\text{HH}} = 8.2$ Hz, Pyr H), 7.88 (1H, s, NH), 7.57 (2H, d, $J_{\text{HH}} = 8.3$, Ar H), 7.41 (1H, dd, $J_{\text{HH}} = 8.2$ Hz and 7.5 Hz, Pyr H), 7.36 (2H, d, $J_{\text{HH}} = 8.3$ Hz, Ar H), 7.28 (2H, d, $J_{\text{HH}} = 8.9$ Hz, Ar H), 7.27 (2H, d, $J_{\text{HH}} = 8.4$ Hz, Ar H), 7.09 (2H, d, $J_{\text{HH}} = 8.9$ Hz, Ar H), 6.90 (1H, d, $J_{\text{HH}} = 7.5$ Hz, Pyr H), 6.54 (2H, d, $J_{\text{HH}} = 8.4$ Hz, Ar H), 5.81 (1H, s, CH), 5.08 (1H, d, $J_{\text{HH}} = 7.8$ Hz, CH), 4.02 (1H, d, $J_{\text{HH}} = 7.8$ Hz, CH), 3.76 (5H, s, CH_2 , CH_3), 3.68 (2H, s, CH_2), 2.43 (3H, s, CH_3), 1.27 (9H, s, 3 x tBu). ^{13}C NMR (75.5 MHz, CDCl_3): δ_{C} 174.1 (C=O), 172.6 (C=O), 171.9 (C=O), 168.5 (C=O), 156.8 (quat. C), 150.3 (quat. C), 146.5 (quat. C), 146.0 (quat. C), 138.7 (CH, Py CH), 137.8 (quat. C), 135.1 (quat. C), 133.9 (quat. C), 130.2 (quat. C), 130.1 (CH, 2 x Ar CH), 129.9 (CH, 2 x Ar CH), 126.7 (CH, 4 x Ar CH), 126.3 (CH, 2 x Ar CH), 121.3 (CH, Py CH), 113.9 (CH, 2 x Ar CH), 110.7 (CH, Py CH), 77.5 (CH), 69.5 (CH), 57.4 (CH), 52.1 (CH_3), 44.5 (CH_2), 40.7 (CH_2), 34.2 (quat. C), 31.4 (CH_3), 23.9 (CH_3 , tBu). IR (Nujol mull, NaCl plates) 3327, 1718 cm^{-1} . MS (ES+) m/z 669 (100%, $[\text{M}^+\text{Na}]$). HRMS (ES+) calculated for $\text{C}_{38}\text{H}_{38}\text{N}_4\text{O}_6$ $[\text{M}^+\text{Na}]$ 669.2689, found 669.2693.

***N*-(6-Methylpyridin-2-yl)-4-(-5-(4-(2-(6-methylpyridin-2-ylamino)-2-oxoethyl)phenyl)-4,6-dioxo-2-p-tolylhexahydro-2H-pyrrolo[3,4-d]isoxazol-3-yl)benzamide (Isoxazolidine-120).**



116 (200 mg, 0.60 mmol) and **115** (190 mg, 0.60 mmol) were dissolved CHCl₃ (1 ml) and the solution left in the dark for 3 days at room temperature. The solvent was removed under reduced pressure to afford the crude product as a green solid, which was purified using column chromatography (SiO₂ 3:1 EtOAc:hexane) to afford **120** as a colorless solid (0.27 g, 70%); mp 147-150 °C. ¹H NMR (300.1 MHz, CDCl₃): δ_H 8.43 (1H, s, NH), 8.11 (1H, d, J_{HH} = 8.3 Hz, Pyr H), 7.90 (4H, d, J_{HH} = 8.4 Hz, Ar H), 7.64 (2H, d, J_{HH} = 8.4 Hz, Ar H), 7.60 (1H, dd, J_{HH} = 8.3 Hz and 7.5 Hz, Pyr H), 7.50 (1H, dd, J_{HH} = 8.5 Hz and 7.5 Hz, Pyr H), 7.25 (1H, d, J_{HH} = 8.5 Hz, Pyr H), 6.99 (4H, s, Ar H), 6.88 (1H, d, J_{HH} = 7.5 Hz, Pyr H), 6.82 (1H, d, J_{HH} = 7.5 Hz, Pyr H), 6.58 (2H, d, J_{HH} = 8.4 Hz, Ar H), 5.73 (1H, d, J_{HH} = 0.9 Hz, CH), 5.04 (1H, d, J_{HH} = 7.6 Hz, CH), 3.95 (1H, dd, J_{HH} = 7.5 Hz and 0.9 Hz, CH), 3.63 (2H, s, CH₂), 2.49 (3H, s, CH₃), 2.42 (3H, s, CH₃) 2.20 (3H, s, CH₃). ¹³C NMR (300.1 MHz, CDCl₃): δ_C 173.8 (C=O), 172.4 (C=O), 168.5 (C=O), 164.9 (C=O), 157.0 (quat. C), 156.9 (quat. C), 150.7 (quat. C), 150.3 (quat. C), 146.1 (quat. C), 142.8 (quat. C), 138.8 (CH, Py CH), 138.7 (CH, Py CH), 135.1 (quat. C), 134.1 (quat. C), 133.0 (quat. C), 130.2 (quat. C), 130.0 (CH, 4 x Ar CH), 127.9 (CH, 2 x Ar CH), 127.2 (CH, 2 x Ar CH), 126.6 (CH, 2 x Ar CH), 119.6 (CH, Py CH), 119.5 (CH, Py CH), 114.6 (CH, 2 x Ar CH), 111.0 (CH, Py CH), 110.7 (CH, Py CH), 77.2 (CH), 69.6 (CH), 57.2 (CH), 44.5 (CH₂), 24.1 (CH₃), 24.0 (CH₃), 20.5 (CH₃). IR (solution CHCl₃, NaCl plates) 3350, 2923, 1718, 1675 cm⁻¹. MS (ES⁺) *m/z* 689 (100%, [M⁺Na]). HRMS (ES⁺) calculated for C₃₉H₃₅N₆O₅ [M+H] 667.2669, found 667.2666.

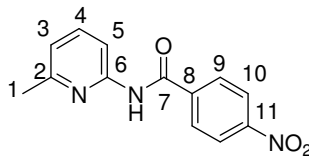
2-(4-(2-(4-*tert*-butylphenyl)-3-(4-(carboxymethyl)phenyl)-4,6-dioxodihydro-2H-pyrrolo[3,4-d]isoxazol-5(3H,6H,6aH)-yl)phenyl)acetic acid (Isoxazolidine 121).



86 (0.20 g, 0.60 mmol) and **117** (0.19 g, 0.60 mmol) were dissolved in CHCl_3 (1 ml) and the solution left in the dark for 3 days at room temperature. The solvent was removed under reduced pressure to afford the crude product as pale yellow solid, which was purified using column chromatography (SiO_2 4:1 EtOAc:hexane) to afford **121** as a colorless solid (0.23 g, 40%); mp > 188 °C dec. ^1H NMR (300.1 MHz, MeOH/ CDCl_3): δ_{H} 7.48 (2H, d, $J_{\text{HH}} = 8.1$ Hz, Ar H, *trans*), 7.33 (2H, d, $J_{\text{HH}} = 8.2$ Hz, Ar H, *cis*), 7.28 (2H, d, $J_{\text{HH}} = 8.2$ Hz, Ar H, *cis*), 7.27 (2H, d, $J_{\text{HH}} = 8.2$ Hz, Ar H, *trans*), 7.26 (2H, d, $J_{\text{HH}} = 8.5$ Hz, Ar H, *trans*), 7.20 (2H, d, $J_{\text{HH}} = 8.9$ Hz, Ar H, *cis*), 7.19 (2H, d, $J_{\text{HH}} = 8.7$ Hz, Ar H, *cis*), 7.14 (2H, d, $J_{\text{HH}} = 8.5$ Hz, Ar H, *trans*), 7.01 (2H, d, $J_{\text{HH}} = 8.9$ Hz, Ar H, *cis*), 6.98 (2H, d, $J_{\text{HH}} = 8.7$ Hz, Ar H, *cis*), 6.87 (2H, d, $J_{\text{HH}} = 8.5$ Hz, Ar H, *trans*), 6.39 (2H, d, $J_{\text{HH}} = 8.4$ Hz, Ar H, *trans*), 5.71 (1H, s, CH, *trans*), 5.23 (1H, d, $J_{\text{HH}} = 7.8$ Hz, CH, *cis*), 5.03 (1H, d, $J_{\text{HH}} = 7.6$ Hz, CH, *trans*), 4.88 (1H, d, $J_{\text{HH}} = 9.0$ Hz, CH, *cis*), 3.99 (1H, dd, $J_{\text{HH}} = 9.0$ Hz and 7.8 Hz, CH, *cis*), 3.98 (1H, d, $J_{\text{HH}} = 7.6$ Hz, CH, *trans*), 3.56 (2H, s, CH_2 , *cis*), 3.51 (4H, s, 2 x CH_2 , *cis* and *trans*), 3.49 (2H, s, CH_2 , *trans*), 1.21 (9H, tBu, *trans*), 1.18 (9H, tBu, *cis*). ^{13}C NMR (75.5 MHz, MeOH/ CDCl_3): δ_{C} 176.1 (C=O), 175.5 (C=O), 175.4 (C=O), 175.2 (C=O), 174.8 (C=O), 174.6 (2 x C=O), 173.2 (C=O), 149.4 (quat. C), 148.0 (2 x quat. C), 147.4 (quat. C), 146.1 (quat. C), 139.1 (quat. C), 136.9 (quat. C), 136.6 (quat. C), 136.4 (quat. C), 135.7 (quat. C), 134.7 (quat. C), 131.5 (CH, 2 x Ar CH), 131.3 (CH, 2 x Ar CH), 131.2 (CH, 4 x Ar CH), 131.1 (quat. C), 129.1 (CH, 2 x Ar CH), 128.0 (CH, 2 x Ar CH), 127.7 (CH, 2 x Ar CH), 127.5 (CH, 4 x Ar CH), 127.1 (CH, 2 x Ar CH), 120.5 (CH, 2 x Ar CH), 115.3 (CH, 2 x Ar CH), 78.6 (CH, 2 x CH), 72.5 (CH), 70.8 (CH), 58.7 (CH), 56.0 (CH), 42.3 (CH_2), 42.2 (2 x CH_2), 42.1 (CH_2), 35.5 (2 x quat. C), 32.6 (CH_3 , tBu), 32.5 (CH_3 , tBu). IR (solution CHCl_3 , NaCl plates) 3480, 2533,

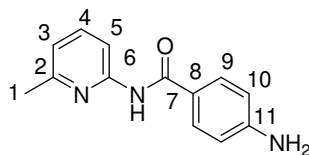
1716 cm^{-1} . MS (ES+) m/z 565.27 (5%, $[\text{M}^+\text{Na}]$). Found C 68.7 H 5.5 N 5.0, $\text{C}_{31}\text{H}_{30}\text{N}_2\text{O}_7$ requires C 68.6 H 5.6 N 5.2.

N*-(6-Methylpyridin-2-yl)-4-nitrobenzamide **139*



4-Nitrobenzoyl chloride (15.00 g, 80.0 mmol) was dissolved in dry CH_2Cl_2 (60 ml) and added drop-wise to a solution of 6-methyl-2-aminopyridine (8.80 g, 80.0 mmol) in triethylamine (15 ml) under an atmosphere of nitrogen and then stirred overnight. The resultant precipitate was filtered and the solvent removed from the filtrate under reduced pressure. The crude product was purified by column chromatography (SiO_2 2:1 Hexane: EtOAc), to afford **139** as a colorless solid (14.20 g, 70%); mp 130-132 $^\circ\text{C}$. ^1H NMR (CDCl_3 , 300.1 MHz): δ_{H} 8.70 (1H, br s, NH), 8.29 (2H, d, $J_{\text{HH}} = 8.8$ Hz, Ar H, H10), 8.12 (1H, d, $J_{\text{HH}} = 8.2$ Hz, Pyr H, H3), 8.06 (2H, d, $J_{\text{HH}} = 8.8$ Hz, Ar H, H9), 7.63 (1H, dd, $J_{\text{HH}} = 8.2$ Hz and 7.5 Hz, Pyr H, H4), 6.93 (1H, d, $J_{\text{HH}} = 7.5$ Hz, Pyr H, H5), 2.43 (3H, s, CH_3). ^{13}C NMR (CDCl_3 , 75.5 MHz): δ_{C} 164.0 (C=O), 156.7 (quat. C), 151.2 (quat. C), 150.2 (quat. C), 138.6 (CH, 2 x Ar CH, C9), 129.2 (CH, Py CH, C3), 123.6 (quat. C), 119.0 (CH, 2 x Ar CH, C10), 114.2 (CH, Py CH, C4), 110.8 (CH, Py CH, C5), 24.1 (CH_3). MS (ES+) m/z 256 (100%, $[\text{M}^+]$); HRMS (ES+) calculated for $\text{C}_{13}\text{H}_{11}\text{N}_3\text{O}_3$ $[\text{M}+\text{H}]$ 256.07222, found 256.0722.

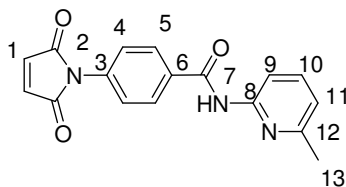
4-Amino-*N*-(6-methylpyridin-2-yl)benzamide^[170] **140**



A saturated solution of $\text{Cu}(\text{acac})_2$ in MeOH (13 ml) was added to a solution of **139** (1.25 g, 4.80 mmol), MeOH (170 ml). Sodium borohydride (1.85 g, 4.90 mmol) was added portion-wise and the resultant suspension was left to stir for 15 minutes at ambient temperature. The reaction mixture was carefully quenched into water (100 ml) and

extracted using CH₂Cl₂ (2 x 100 ml). The organic fractions were combined, washed with water (2 x 100 ml), dried over MgSO₄ and filtered, before removing the solvent *in vacuo* to afford the crude product as a brown solid. The crude product was recrystallized from EtOAc/hexane (1:3) to afford **140** as a colorless solid (0.90 g, 82%); mp 169-170 °C. ¹H NMR (CDCl₃, 300.1 MHz): δ_H 8.73 (1H, br s, NH), 8.19 (1H, d, J_{HH} = 8.3 Hz, Pyr H, H3), 7.74 (2H, d, J_{HH} = 9.1 Hz, Ar H, H9), 7.60 (1H, dd, J_{HH} = 8.3 Hz and 7.5 Hz, Pyr H, H4), 6.83 (1H, d, J_{HH} = 7.5 Hz, Pyr H, H5), 6.63 (2H, d, J_{HH} = 9.1 Hz, Ar H, H10), 4.01 (2H, s, NH₂), 2.42 (3H, s, CH₃). ¹³C NMR (CDCl₃, 75.5 MHz): δ_C 166.1 (C=O), 156.7 (quat. C), 151.2 (quat. C), 150.2 (quat. C), 138.6 (CH, Py CH, C3), 129.2 (CH, 2 x Ar CH, C9), 123.6 (quat. C), 119.0 (CH, Py CH, C4), 114.2 (CH, Py CH, C5), 110.8 (CH, 2 x Ar CH, C10), 24.1 (CH₃). MS (ES+) *m/z* 250 (100%, [M+Na]); HRMS (ES+) calculated for C₁₃H₁₃N₃O [M+H] 228.1142, found 228.1142.

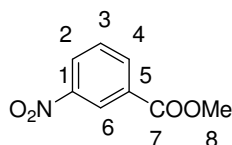
4-(2, 5-Dioxo-2, 5, dihydro pyrrol-1-yl)-N-(6-methyl pyridin-2-yl)benzamide (maleimide 132).



4-Amino-*N*-(6-methyl-pyridin-2-yl)benzamide (0.90 g, 3.75 mmol) was mixed with maleic anhydride (0.40 g, 3.75 mmol) and the resulting mixture was dissolved in glacial acetic acid (30 ml). This solution was stirred at room temperature under a nitrogen atmosphere for 4 hours. After this time the resulting suspension was heated under reflux for 4 hours. The solvent was then removed *in vacuo* and the resulting yellow solid purified by column chromatography (SiO₂, 3:1 EtOAc:Hexane). Fractions containing the product were combined and the solvent removed under reduced pressure to afford a maleimide **132** as a colorless solid (0.50 g, 43%); mp > 239 °C decomposed. ¹H NMR (CDCl₃, 300.1 MHz): δ_H 8.46 (1H, br s, NH), 8.12 (1H, d, J_{HH} = 8.3 Hz, Pyr H, H11), 7.97 (2H, d, J_{HH} = 8.8 Hz, Ar H, H5), 7.59 (1H, dd, J_{HH} = 8.3 Hz and 7.6 Hz, Pyr H, H10), 7.50 (2H, d, J_{HH} = 8.8 Hz, Ar H, H4), 6.88 (1H, d, J_{HH} = 7.6 Hz, Pyr H, H9), 6.83 (2H, s, CH=CH), 1.98 (3H, s, CH₃). ¹³C NMR (CDCl₃, 75.5 MHz): δ_C 169.0 (2 x C=O), 164.6 (amide), 156.9 (quat. C, C8), 150.1 (quat. C, C12), 138.9 (CH, PyCH, C11), 134.8 (quat. C, C3), 134.4 (CH,

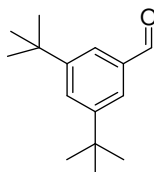
CH=CH, C1), 133.2 (quat. C, C6), 128.1 (CH, 2 x Ar CH, C5), 125.6 (CH, 2 x Ar CH, C4), 119.6 (CH, Py CH, C10), 111.0 (CH, Py CH, C9), 24.0 (CH₃). IR (NaCl plates). MS (ES+) *m/z* 308 (100%, [M+]). HRMS (ES+) calculated for C₁₇H₁₃N₃O₃ [M+Na] 330.0855, found 330.0865.

Methyl 3-nitrobenzoate 145



Concentrated sulfuric acid (0.08 ml) was added carefully to a solution of 3-nitrobenzoic acid (2.00 g, 12.0 mmol) in MeOH (3 ml), this mixture was then heated to reflux for 4 hours. The solvent was removed *in vacuo* to afford brown oil, which was re-dissolved in CH₂Cl₂, washed in saturated aqueous sodium bicarbonate until CO₂ evolution had ceased. The organic fraction was then collected, dried over MgSO₄, filtered and concentrated *in vacuo* to afford **145** as a colorless solid (1.90 g, 88%); mp 79-80 °C (lit^[205]. mp 78-79 °C). ¹H NMR (CDCl₃, 300.1 MHz): δ_H 8.77 (1H, dd, J_{HH} = 1.1 Hz and 1.3 Hz, Ar H, H6), 8.35 (1H, ddd, J_{HH} = 7.1 Hz, 2.4 Hz and 1.1 Hz, Ar H, H2), 8.31 (1H, ddd, J_{HH} = 7.8 Hz, 2.4 Hz and 1.3 Hz, Ar H, H4) 7.62 (1H, dd, J_{HH} = 7.8 Hz and 7.1 Hz, Ar H, H3) 3.94 (3H, s, CH₃). ¹³C NMR (CDCl₃, 75.5 MHz): δ_C 165.3 (ester), 148.2 (quat. C, C1), 135.6 (CH, Ar CH, C6), 132.2 (quat. C, C5), 130.1 (CH, Ar CH, C2), 127.7 (CH, Ar CH, C4), 124.9 (CH, Ar CH, C3), 53.2 (CH₃). IR (Nujol mull, NaCl plates) 1725, 1376, 1351 cm⁻¹. Found C 52.9 H 3.6 N 7.4 C₈H₇NO₄ Requires C 53.0 H 3.9 N 7.4.

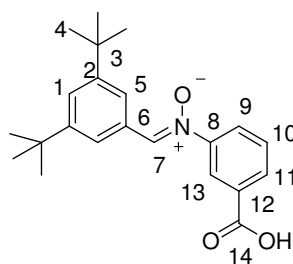
3, 5,-Di-*tert*-butylbenzaldehyde 149



AIBN (20 mg) was added to a solution of 3,5-di-*tert*-butyltoluene (5.00 g, 24.0 mmol) and *N*-bromosuccinimide (8.70 g, 48.0 mmol) in chlorobenzene (200 ml) and the resultant mixture heated under reflux for 15 hours. This solution was filtered through celite and

the solvent removed from the filtrate under reduced pressure to give an oil which was a mixture of 3,5-di-*tert*-butylbenzylbromide (33%) and 3,5-di-*tert*-butylbenzyl dibromide (66%). For 3,5-di-*tert*-butylbenzyl bromide ¹H NMR (CDCl₃, 300.1 MHz): δ_H 7.40-7.25 (3H, m, Ar H), 4.53 (2H, s, CH₂Br), 1.37 (18H, s, 2 x tBu). For 3,5-di-*tert*-butylbenzyl dibromide 7.40- 7.25 (3H, m, Ar H), 6.70 (1H, s, CHBr₂), 1.37 (18H, s, 2 x tBu)¹. The mixture of 3,5-di-*tert*-butylbenzyl bromide and 3,5-di-*tert*-butylbenzyl dibromide was added to a solution of hexamethylenetetramine (10.10 g, 72.0 mmol) dissolved in a 1:1 water/ethanol mixture (15 ml). This solution was heated to reflux for 4 hours after which concentrated HCl (7 ml) was added and the resultant solution was refluxed for a further 30 minutes. The reaction mixture was then extracted using CH₂Cl₂ (2 x 100 ml). The organic extracts were combined washed with brine, dried over MgSO₄, filtered and concentrated under reduced pressure. The resultant brown oil was initially purified using Kugerlrohr distillation. The resultant oil was then recrystallized from EtOH to afford **149** as a colorless solid (2.00 g, 38%); mp 86-87 °C. ¹H NMR (CDCl₃, 300.1 MHz): δ_H 10.02 (1H, s, CHO), 7.73 (3H, m, Ar H), 1.37 (18H, s, 2 x tBu). ¹³C NMR (CDCl₃, 75.5 MHz): δ_C 193.3 (CHO), 151.9 (2 x quat. C), 136.2 (quat. C), 128.9 (CH, Ar CH), 124.2 (CH, 2 x Ar CH), 35.0 (2 x quat. C), 31.3 (CH₃, 2 x tBu). IR (Nujol mull, NaCl plates) 1693, cm⁻¹. HRMS (EI) m/z 218 (100%, M⁺); HRMS (CI) calculated for C₁₅H₂₂O [M⁺] 218.1671, found 218.1675¹.

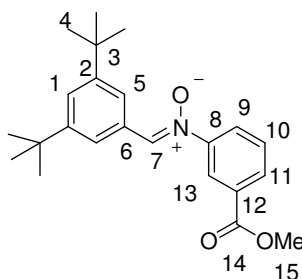
(Z)-3-Carboxy-N-(3,5-di-*tert*-butylbenzylidene)aniline oxide^[171] (nitrone 133)



BiCl₃ (0.45 g, 1.45 mmol) was suspended in a solution of 3-nitrobenzoic acid (1.00 g, 6.00 mmol) in an EtOH:H₂O mixture (4:1, 10 ml). Potassium borohydride (0.60 g, 12.00 mmol) was added portion-wise to this suspension and the resulting mixture was left to stir for 10 minutes. The reaction mixture was then quenched with water (2 ml) and aldehyde (1.30 g, 6.00 mmol) was then added in one portion. The resulting suspension

was stirred at room temperature for 12 hours before direct extraction using CH₂Cl₂ (2 x 50 ml). The CH₂Cl₂ extracts were combined and then washed with brine (2 x 10 ml). The organic fractions was separated, dried over MgSO₄ and filtered, before being concentrated under reduced pressure to afford a pale yellow solid. This solid was then recrystallized from EtOH to afford **133** as a colorless solid (0.65 g, 30%). mp > 170 °C decomposed. ¹H NMR (CDCl₃, 300.1 MHz): δ_H 8.37 (1H, br s, Ar H, H13), 8.23 (2H, d, J_{HH} = 1.6 Hz, Ar H, H5), 8.07 (1H, d, J_{HH} = 7.9 Hz, Ar H, H9), 8.02 (1H, d, J_{HH} = 7.4 Hz, Ar H, H11), 7.96 (1H, s, CH=N, H7), 7.54 (1H, dd, J_{HH} = 7.9 Hz and 7.4 Hz, Ar H, H10), 7.53-7.52 (1H, m, Ar H, H1), 1.29 (18H, s, 2 x tBu). ¹³C NMR (CDCl₃, 75.5 MHz): δ_C 169.0 (C=O), 151.3 (2 x quat. C), 149.0 (quat. C), 137.0 (CH=N), 131.4 (CH, Ar CH), 130.7 (quat. C), 130.1 (quat. C), 129.7 (CH, Ar CH), 127.1 (CH, Ar CH), 126.3 (CH, Ar CH), 124.1 (CH, 2 x Ar CH), 122.9 (CH, Ar CH), 35.0 (2 x quat. C), 31.4 (CH₃, 2 x tBu). IR (Nujol mull, NaCl plates) 1701 cm⁻¹. MS (ES-) *m/z* 352 (100%, [M-H]). HRMS (ES-) calculated for C₂₂H₂₇NO₃ [M-H] 352.1913, found 352.1917.

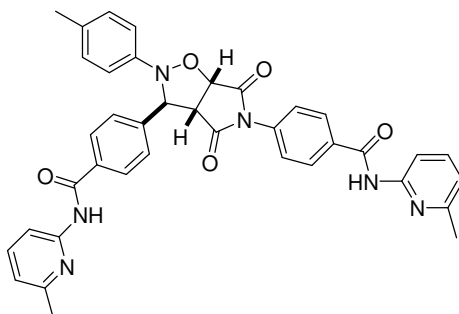
(Z)-N-(3,5-Di-*tert*-butylbenzylidene)-3-(methoxycarbonyl)aniline oxide
(nitrone 133b)



BiCl₃ (0.07 g, 0.20 mmol) was suspended in a solution of 3-nitrobenzyl methyl ester (0.20 g, 1.10 mmol) dissolved in an EtOH:H₂O mixture (4:1, 10 ml). Potassium borohydride (0.12 g, 2.20 mmol) was added portion-wise to this solution and the resulting mixture was left to stir for 10 minutes. The reaction mixture was then quenched with water (2 ml) and aldehyde (0.25 g, 1.10 mmol) was then added in one portion. This solution was left to stir at room temperature for 12 hours before the reaction mixture was extracted directly using CH₂Cl₂ (2 x 50 ml). The CH₂Cl₂ extracts were combined and washed with brine (2 x 10 ml). The CH₂Cl₂ fraction was then dried over MgSO₄ and filtered, before being concentrated under reduce pressure to afford a pale yellow solid.

This solid was then purified using column chromatography (SiO₂ 2:1 EtOAc:Hexane with 0.05% Et₃N) and then recrystallised from ethanol to afford **133b** as a colorless solid (0.26 g, 65%). mp 101-102 °C. ¹H NMR (CDCl₃, 300.1 MHz): δ_H 8.37 (1H, br s, Ar H, H13), 8.23 (2H, d, J_{HH} = 1.6 Hz, 2 x Ar H, H5), 8.07 (1H, d, J_{HH} = 7.9 Hz, Ar H, H9), 8.02 (1H, d, J_{HH} = 7.4 Hz, Ar H, H11), 7.96 (1H, s, CH=N), 7.53 (1H, d, J_{HH} = 7.9 Hz and 7.4 Hz, Ar H, H10), 7.52-7.50 (1H, m, Ar H, H1), 3.89 (CH₃), 1.29 (18H, s, 2 x tBu). ¹³C NMR (CDCl₃, 75.5 MHz): δ_C 165.5 (ester), 151.2 (2 x quat. C), 149.2 (quat. C), 135.8 (CH, CH=N), 131.2 (quat. C), 130.7 (CH, Ar CH), 129.9 (quat. C), 129.5 (CH, Ar CH), 126.3 (CH, Ar CH), 126.0 (CH, Ar CH), 123.7 (CH, 2 x Ar CH), 122.5 (CH, Ar CH), 52.6 (CH₃), 35.0 (2 x quat. C), 31.4 (CH₃, 2 x tBu).

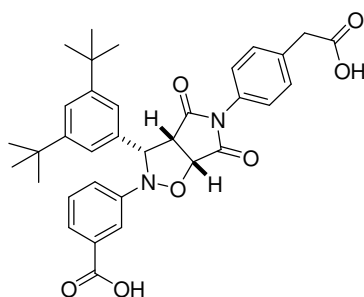
4,4'-(4,6-dioxo-2-p-tylyltetrahydro-2H-pyrrolo[3,4-d]isoxazole-3,5(3H)-diyl)bis(*N*-(6-methylpyridin-2-yl)benzamide) (*trans*-135).



Maleimide **132** (300 mg, 0.97 mmol) and nitrone **115** (330 mg, 0.97 mmol) were dissolved in CHCl₃ (5 ml) and this solution was left to react at ambient temperature for 3 days in the dark. The solvent was then removed *in vacuo* and the resultant yellow solid purified by column chromatography (SiO₂, 4:1 EtOAc:Hexane), to afford a colorless solid *trans*-**135** (345 mg, 55%); mp 198-199 °C. ¹H NMR (CDCl₃, 300.1 MHz): δ_H 8.56 (1H, br s, NH), 8.51 (1H, br s, NH), 8.12 (2H, dd, J_{HH} = 8.0 Hz and 7.6 Hz, Pyr H), 7.89 (2H, d, J_{HH} = 8.4 Hz, Ar H), 7.80 (2H, d, J_{HH} = 8.6 Hz, Ar H), 7.61 (2H, d, J_{HH} = 8.4 Hz, Ar H), 7.58 (1H, dd, J_{HH} = 8.0 Hz and 3.8 Hz, Pyr H), 7.57 (1H, dd, J_{HH} = 8.0 Hz and 3.8 Hz, Pyr H), 6.98 (4H, s, Ar H), 6.87 (2H, d, J_{HH} = 7.6 Hz and 3.8 Hz, Pyr H), 6.72 (2H, d, J_{HH} = 8.6 Hz, Ar H), 5.73 (1H, d, J_{HH} = 0.7 Hz, CH), 5.05 (1H, d, J_{HH} = 7.5 Hz, CH), 3.96 (1H, d, J_{HH} = 7.5 Hz and 0.7 Hz, CH), 2.39 (3H, s, CH₃), 2.38 (3H, s, CH₃), 2.20 (3H, s, CH₃). ¹³C NMR (CDCl₃, 75.5 MHz): δ_C 173.5 (C=O), 172.1 (C=O), 165.0 (C=O), 164.4 (C=O),

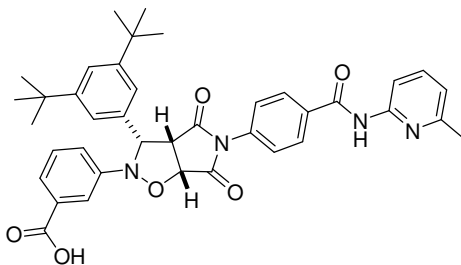
157.0 (2 x quat. C), 150.7 (quat. C), 150.6 (quat. C), 146.0 (quat. C), 142.6 (quat. C), 138.8 (CH, 2 x Py CH), 134.7 (quat. C), 134.2 (quat. C), 134.1 (quat. C), 133.1 (quat. C), 129.9 (CH, 2 x Ar CH), 127.9 (CH, 4 x Ar CH), 127.1 (CH, 2 x Ar CH), 126.4 (CH, 2 x Ar CH), 119.7 (CH, Py CH), 119.6 (CH, Py CH), 114.7 (CH, 2 x Py CH), 111.0 (CH, 2 x Ar CH), 77.2 (CH), 69.6 (CH), 57.3 (CH), 24.0 (2 x CH₃), 20.5 (CH₃). IR (CHCl₃ solution, NaCl plates) 3325, 2923, 1788, 1723, 1675 cm⁻¹. MS (ES⁺) *m/z* 653 (60%, [M+H]), 346 (100), 308 (90). HRMS (ES⁺) calculated for C₃₈H₃₂N₆O₅ [M+H] 653.2512 found, 653.2522.

3-[5-(4-Carboxymethylphenyl)-3-(3,5-di-*tert*-butylphenyl)-4,6-dioxo hexahydro pyrrolo[3,4-*d*]isoxazol-2-yl] benzoic acid (*cis*-136).



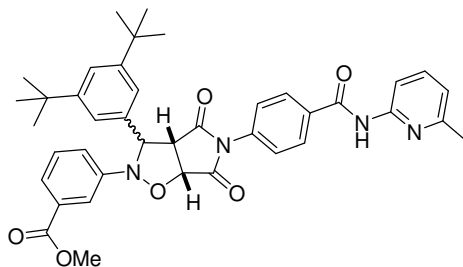
Maleimide **86** (300 mg, 1.30 mmol) and acid nitrone **133** (460 mg, 1.30 mmol) were dissolved in CHCl₃ (5 ml) and this solution was left to react at ambient temperature for 3 days in the dark. The solvent was then removed *in vacuo* and the resultant yellow solid purified by column chromatography (SiO₂, 4:1 EtOAc:Hexane), to afford a colorless solid *cis*-**136** (380 mg, 50%); mp > 185 °C decomposed. ¹H NMR (CDCl₃, 300.1 MHz): δ_H 7.75 (1H, br s, CH, Ar H), 7.61 (1H, d, J_{HH} = 7.3 Hz, Ar H), 7.33- 7.20 (5H, m, Ar H), 7.16 (2H, d, J_{HH} = 8.4 Hz, Ar H), 6.50 (2H, d, J_{HH} = 8.4 Hz, Ar H), 5.41 (1H, d, J_{HH} = 8.2 Hz, CH), 5.22 (1H, d, J_{HH} = 8.7 Hz, CH), 4.03 (1H, dd, J_{HH} = 8.2 Hz and 8.7 Hz, CH), 3.42 (2H, s, CH₂), 1.15 (18H, s, 2 x *t*Bu). ¹³C NMR (CDCl₃, 75.5 MHz): δ_C 175.1 (C=O), 173.4 (C=O), 152.2 (2 x C=O), 150.5 (2 x quat. C), 138.4 (quat. C), 136.5 (quat. C), 135.7 (quat. C), 131.1 (quat. C), 130.6 (CH, 2 x Ar CH), 129.8 (CH, Ar CH), 127.6 (CH, 2 x Ar CH), 127.3 (quat. C), 126.4 (CH, Ar CH), 123.7 (CH, 2 x Ar CH), 123.3 (CH, Ar CH), 121.8 (CH, Ar CH), 119.5 (CH, Ar CH), 79.6 (CH), 73.8 (CH), 55.8 (CH), 43.6 (2 x quat. C), 35.8 (CH₂), 31.9 (CH₃, 2 x *t*Bu). MS (ES⁻) *m/z* 583 (100%, [M-H]), 539 (40), 352 (40). HRMS (ES⁻) calculated for C₃₄H₃₆N₂O₇ [M-H] 583.2449, found 583.2444.

3-{3-(3,5-Di-*tert*-butylphenyl)-5-[4-(6-methylpyridin-2-ylcarbamoyl)phenyl]-4,6-dioxo hexahydro pyrrolo[3,4-*d*]isoxazol-2-yl} benzoic acid (*cis*-134).



Maleimide **132** (300 mg, 0.97 mmol) and acid nitrone **133** (345 mg, 0.97 mmol) were dissolved in CHCl_3 (5 ml) and this solution was left to react at ambient temperature for 2 days in the dark. The solvent was then removed *in vacuo* and the resultant yellow solid purified by column chromatography (SiO_2 , 3:1 EtOAc:Hexane), to afford a colorless solid *cis*-**134** (340 mg, 53%); mp 198-200 °C. ^1H NMR (CDCl_3 , 300.1 MHz): δ_{H} 11.33 (1H, br s, NH), 8.28 (1H, d, $J_{\text{HH}} = 8.3$ Hz, Pyr H), 8.04 (1H, dd, $J_{\text{HH}} = 1.7$ Hz and 2.0 Hz, Ar H), 7.96 (2H, d, $J_{\text{HH}} = 8.6$ Hz, Ar H), 7.78 (1H, d, $J_{\text{HH}} = 7.9$ Hz and 1.7 Hz, Ar H), 7.71 (1H, dd, $J_{\text{HH}} = 8.3$ Hz and 7.5 Hz, Pyr H), 7.38-7.37 (1H, m, Ar H), 7.33 (2H, d, $J_{\text{HH}} = 2.0$ Hz, Ar H), 7.32 (1H, dd, $J_{\text{HH}} = 7.9$ Hz and 7.6 Hz, Ar H), 7.08 (1H, dd, $J_{\text{HH}} = 7.6$ Hz and 2.0 Hz, Ar H), 6.94 (1H, d, $J_{\text{HH}} = 7.5$ Hz, Pyr H), 6.55 (2H, d, $J_{\text{HH}} = 8.6$ Hz, Ar H), 5.52 (1H, d, $J_{\text{HH}} = 8.5$ Hz, CH), 5.31 (1H, d, $J_{\text{HH}} = 8.4$ Hz, CH), 4.00 (1H, dd, $J_{\text{HH}} = 8.5$ Hz and 8.4 Hz, CH), 2.54 (3H, s, CH_3), 1.19 (18H, s, 2 x tBu). ^{13}C NMR (CDCl_3 , 75.5 MHz): δ_{C} 171.8 (C=O), 171.0 (C=O), 170.7 (C=O), 166.1 (C=O), 155.9 (quat. C), 151.6 (2 x quat. C), 151.5 (quat. C), 150.3 (quat. C), 140.4 (CH, Ar CH), 134.3 (quat. C), 134.2 (quat. C), 133.8 (quat. C), 131.8 (quat. C), 129.2 (CH, Ar CH), 129.0 (CH, 2 x Ar CH), 126.2 (CH, 2 x Ar CH), 125.2 (CH, Ar CH), 122.7 (CH, Ar CH), 122.4 (CH, 2 x Ar CH), 121.3 (CH, Ar CH), 120.0 (CH, Ar CH), 116.2 (CH, Ar CH), 113.3 (CH, Ar CH), 78.7 (CH), 73.2 (CH), 54.3 (CH), 35.0 (2 x quat. C), 31.4 (CH_3 , 2 x tBu), 22.2 (CH_3). IR (CHCl_3 solution, NaCl plates) 3310, 1800, 1725 cm^{-1} . MS (ES⁺) m/z 661 (100%, [M+H]), 662.3 (10). HRMS (ES⁺) calculated for $\text{C}_{39}\text{H}_{40}\text{N}_4\text{O}_6$ [M+H] 661.3026, found 661.3041.

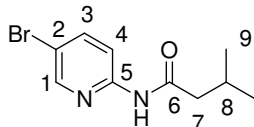
3-{3-(3,5-Di-*tert*-butyl phenyl)-5-[4-(6-methyl pyridin-2-ylcarbamoyl) phenyl]-4,6-dioxo hexahydro pyrrolo[3,4-*d*]isoxazol-2-yl] benzoic acid methyl ester (Isoxazolidine 134b).



Maleimide **132** (300 mg, 0.97 mmol) and acid nitron ester **133b** (345 mg, 0.97 mmol) were dissolved in CHCl₃ (5 ml) and this solution was left to react at ambient temperature for 2 days in the dark, before removal of solvent under reduced pressure, to afford a colorless solid containing a mixture of *trans*- and *cis*-**134** (640 mg, 99%); mp 112-114 °C. ¹H NMR (CDCl₃, 300.1 MHz): δ_H 8.37 (1H, s, NH, *trans*) 8.35 (1H, s, NH, *cis*) 8.10 (1H, s, Ar H, *trans*) 8.07 (1H, s, Ar H, *cis*) 7.84 (2H, d, J_{HH} = 8.6 Hz, Ar H, *cis*), 7.80 (2H, d, J_{HH} = 6.8 Hz, Ar H, *trans*), 7.78 (2H, s, Ar H, *cis*), 7.72-7.69 (1H, m, Ar H, *cis*), 7.66-7.65 (1H, m, Ar H, *trans*), 7.61-7.56 (3H, m, 2 x Ar H, *cis* and Ar H, *trans*), 7.35-7.22 (10H, m, 3 x Ar H, *cis* and 7 x Ar H *trans*), 6.89-6.87 (3H, m, Ar H, *cis* and 2 x Ar H, *trans*), 6.78 (2H, d, J_{HH} = 8.6 Hz, Ar H, *cis*), 5.68 (1H, s, CH, *trans*), 5.37 (1H, d, J_{HH} = 8.3 Hz, CH, *cis*) 5.18 (1H, d, J_{HH} = 8.4 Hz, CH, *cis*), 5.13 (1H, d, J_{HH} = 7.5 Hz, *trans*), 4.04 (1H, d, J_{HH} = 7.5 Hz, *trans*) 4.01 (1H, dd, J_{HH} = 8.5 Hz and, CH, *cis*), 3.83 (3H, s, CH₃, *cis*), 3.82 (3H, s, CH₃, *trans*) 2.41 (3H, s, CH₃, *cis* and *trans*), 1.26 (18H, s, 2 x tBu, *trans*) 1.19 (18H, s, 2 x tBu, *cis*). ¹³C NMR (CDCl₃, 75.5 MHz): δ_C 173.7 (C=O), 172.2 (C=O), 171.9 (C=O), 170.4 (C=O), 166.6 (C=O), 166.4 (C=O), 164.3 (2 x C=O), 157.0 (quat. C), 151.7 (2 x quat. C, *trans*), 151.5 (2 x quat. C, *cis*), 150.5 (quat. C), 149.0 (quat. C), 148.9 (quat. C), 138.8 (CH, 2 x Ar CH, *cis* and *trans*), 136.8 (quat. C), 134.6 (quat. C), 134.4 (quat. C), 134.3 (quat. C), 134.2 (2 x quat. C), 133.1 (2 x quat. C), 131.2 (2 x quat. C), 129.4 (CH, Ar CH), 129.2 (CH, Ar CH), 128.0 (CH, 2 x Ar CH, *trans*), 127.8 (CH, 2 x Ar CH, *cis*), 126.4 (CH, 2 x Ar CH, *cis*), 126.2 (CH, 2 x Ar CH, *trans*), 125.5 (CH, Ar CH), 124.0 (CH, Ar CH), 123.7 (CH, Ar CH), 122.7 (CH, Ar CH), 122.3 (CH, 2 x Ar CH), 122.2 (CH, Ar CH), 121.3 (CH, 2 x Ar CH), 120.8 (CH, Ar CH), 119.7 (CH, Ar CH), 119.2 (CH, Ar CH), 117.9 (CH, Ar CH), 115.7 (CH, Ar CH), 111.0 (CH, Ar CH),

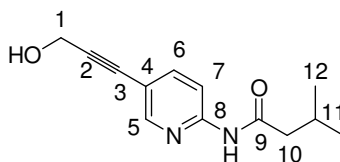
110.9 (CH, Ar CH), 77.7 (CH, *cis*), 77.2 (CH, *trans*), 72.8 (CH, *cis*), 71.1 (CH, *trans*), 57.4 (CH, *trans*), 54.4 (CH, *cis*), 52.3 (2 x CH₃, *cis* and *trans*), 35.0 (2 x quat. C) 34.9 (2 x quat. C), 31.4 (CH₃, 4 x tBu, *cis* and *trans*), 29.7 (CH₃, *trans*), 24.0 (CH₃, *cis*). IR (CHCl₃ solution, NaCl plates) 3336, 1786, 1724, 1673 cm⁻¹. MS (ES+) *m/z* 675 ([M+H], 15%), 707 (100).

***N*-(5-Bromo pyridin-2-yl)-3-methyl butyramide 162**



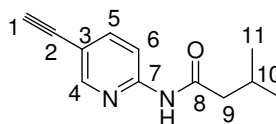
Isovaleryl chloride (2.50 g, 20.80 mmol) was added to a solution of 2,6-aminobromopyridine (3.58 g, 20.80 mmol) in CH₂Cl₂ (100 ml) and pyridine (1 ml). The reaction mixture was left to stir at room temperature under a nitrogen atmosphere for 8 hours. This suspension was then filtered and the solvent removed from the filtrate under reduced pressure. The crude product was then purified by column chromatography (SiO₂, 1:1 EtOAc:Hexane) and the product fractions combined and concentrated *in vacuo* to afford **162** as a colorless solid (5.12 g, 96%); mp 95-96 °C. ¹H NMR (300.1 MHz, CDCl₃): δ_H 8.72 (1H, s, NH), 8.21 (1H, d, J_{HH} = 2.3 Hz, 1 x Pyr H, H1), 8.15 (1H, d, J_{HH} = 8.9 Hz, Pyr H, H4), 7.73 (1H, dd, J_{HH} = 8.9 Hz and 2.3 Hz, Pyr H, H3), 2.21 (2H, d, J_{HH} = 1.6 Hz, CH₂), 2.18-2.10 (1H, m, CH), 0.92 (6H, d, J_{HH} = 6.3 Hz, 2 x CH₃). ¹³C NMR (75.5 MHz, CDCl₃): δ_C 171.9 (amide), 150.7 (quat. C), 148.6 (CH, Py CH, H1), 141.4 (CH, Py CH, H4), 115.9 (CH, Py CH, H3), 114.7 (quat. C), 47.2 (CH₂), 26.5 (CH), 22.8 (2 x CH₃). IR (Nujol mull, NaCl plates) 3235, 1662 cm⁻¹. MS (CI+) *m/z* 257 (100%, [M+H]), 259 (100%, [M+H]). HRMS (CI+) calculated for C₁₀H₁₃N₂OBr⁷⁹ [M+H] 257.0289, found 257.0288, calculated for C₁₀H₁₃N₂OBr⁸¹ [M+H] 259.0269, found 259.0276.

***N*-[5-(3-Hydroxy prop-1-ynyl) pyridine-2-yl]-3-methyl butyramide 164**



A degassed solution of **162** (1.00 g, 3.89 mmol) in dry Et₃N/MeCN (1:1, 10 ml) was added to PPh₃ (0.10 g, 0.38 mmol), Pd[(PPh₃)(Cl)]₂ (0.14 g, 0.19 mmol) and CuI (0.04 g, 0.19 mmol). The reaction mixture was then stirred under a nitrogen atmosphere and heated until reflux. The solution was then left to cool to room temperature for 10 minutes, before a degassed solution of propargyl alcohol (0.45 ml, 7.78 mmol) in Et₃N/MeCN (1:1, 10 ml) was added to the reaction mixture. The solution was then stirred and heated under reflux, while still under a nitrogen atmosphere for 8 hours. The solvent was then removed from the reaction mixture *in vacuo* to afford a brown oil. This was redissolved in Et₂O (50 ml) and washed in brine (2 x 50 ml), before the organic fraction was dried over MgSO₄, filtered and concentrated under reduced pressure. The crude product was then purified by column chromatography (SiO₂, 2:3 Hexane: EtOAc), to afford **164** as a colorless solid (0.53 g, 60%); mp 148-149 °C. ¹H NMR (300.1 MHz, CDCl₃): δ_H 8.26 (1H, d, J_{HH} = 2.2 Hz, Pyr H, H5), 8.14 (1H, d, J_{HH} = 8.6 Hz, Pyr H, H7), 7.86 (1H, s, NH), 7.66 (1H, dd, J_{HH} = 8.6 Hz and 2.2 Hz, Pyr H, H6), 4.44 (2H, s, CH₂, H1), 2.20 (2H, d, J_{HH} = 1.6 Hz, CH₂, H10), 2.19-2.11 (1H, m, CH), 0.95 (6H, d, J_{HH} = 6.4 Hz, 2 x CH₃). ¹³C NMR (75.5 MHz, CDCl₃): δ_C 171.25 (amide), 150.5 (quat. C), 150.4 (CH, Py CH, H5), 141.3 (CH, Py CH, H7), 115.2 (quat. C), 113.3 (CH, Py CH, H6), 89.8 (quat. C, H3), 82.2 (quat. C, H2), 51.5 (CH₂, H1), 47.1 (CH₂, H10), 26.1 (CH), 22.5 (2 x CH₃). IR (Nujol mull, NaCl plates) 3357, 2115, 1685 cm⁻¹. MS (ES+) *m/z* 233 (100%, [M+H]). HRMS (ES+) calculated for C₁₃H₁₆N₂O₂ [M+H] 233.1296, found 233.1282.

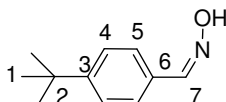
N*-(5-Ethynyl pyridine-2-yl)-3-methyl butyramide **165*



Activated MnO₂ (1.13 g, 12.97 mmol) was added to a solution of **164** (0.30 g, 1.29 mmol), KOH (0.36g, 6.45 mmol) in CH₂Cl₂ (50 ml) and the reaction mixture was left to stir overnight at room temperature. The suspension was then filtered, and the solvent removed from the filtrate *in vacuo* to afford **165** as a pale yellow solid (0.25 g, 95%); mp 97-98 °C. ¹H NMR (300.1 MHz, CDCl₃): δ_H 8.31 (1H, d, J_{HH} = 2.2 Hz, Pyr H, H4), 8.15 (1H, d, J_{HH} = 8.7 Hz, Pyr H, H6), 8.04 (1H, s, NH), 7.71 (1H, dd, J_{HH} = 8.7 Hz and 2.2 Hz, Pyr H, H5), 3.09 (1H, s, CH, H1), 2.21 (2H, d, J_{HH} = 2.1 Hz, CH₂), 2.20-2.09 (1H, m,

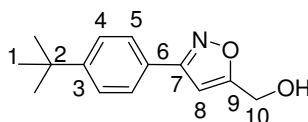
CH, H10), 0.96 (6H, d, $J_{\text{HH}} = 6.3$ Hz, 2 x CH₃). ¹³C NMR (75.5 MHz, CDCl₃): δ_{c} 171.17 (amide), 151.1 (CH, Py CH, C4), 150.8 (quat. C), 141.6 (CH, Py CH, C6), 114.9 (quat. C), 113.2 (CH, Py CH, C5), 80.3 (quat. C, C2), 79.6 (CH, C≡CH, C1), 47.1 (CH₂), 26.1 (CH, C10), 22.5 (2 x CH₃). IR (Nujol mull, NaCl) 3278, 3223, 1660 cm⁻¹. MS (CI⁺) m/z (100%, [M+H]), 119 (45), 118 (30). HRMS (CI⁺) calculated for C₁₂H₁₄N₂O [M+H] 203.1184, found 203.1180.

4-*tert*-Butylbenzaldehyde oxime^[185] **167**



Hydroxylamine hydrochloride (1.72 g, 24.8 mmol) was added to a mixture of 4-*tert*-butyl benzaldehyde (2.00 g, 12.33 mmol) and Amberlyst A21 (6.00 g) in ethanol (20 ml). The reaction mixture was stirred for 12 hours at room temperature under a nitrogen atmosphere. This suspension was then filtered through celite and the solvent removed from the filtrate under reduced pressure to afford **167** as a colorless solid (1.82 g, 83%); mp 99-102 °C. ¹H NMR (300.1 MHz, CDCl₃): δ_{H} 8.93 (1H, s, NOH), 8.19 (1H, s, CHN), 7.55 (2H, d, $J_{\text{HH}} = 8.4$ Hz, 2 x Ar H, H5), 7.44 (2H, d, $J_{\text{HH}} = 8.4$ Hz, 2 x Ar H, H4), 1.36 (9H, s, tBu). ¹³C NMR (75.5 MHz, CDCl₃): δ_{c} 153.6 (quat. C, C3), 152.2 (CH, CHN), 128.9 (quat. C, C6), 125.9 (CH, 2 x Ar CH, C5), 125.8 (CH, 2 x Ar CH, C4), 34.9 (quat. C), 31.1 (CH₃, tBu). IR (solution CHCl₃, NaCl plates) 3282, 1607, 1509 cm⁻¹. MS (ES⁺) m/z 178.1 (100%, [M+H]). HRMS (ES⁺) calculated for C₁₁H₁₅NO [M+H] 178.1232, found 178.1284.

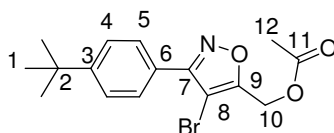
[3-(4-*tert*-Butylphenyl) isoxazol-5-yl] methanol^[186] **169**



N-Chlorosuccinimide (0.07 g, 0.56 mmol) was added to a stirred solution of 4-*tert*-Butyl benzaldehyde oxime (0.50 g, 2.82 mmol) **167** in DMF (2.5 ml) at 30 °C, resulting in a slight decrease in temperature. HCl gas (0.2 ml) was then bubbled through the solution,

resulting in a slight increase in temperature, and more *N*-Chlorosuccinimide (0.30 g, 2.26 mmol) was added carefully keeping the temperature of reaction mixture below 35 °C. When the temperature had stabilized the solution was diluted in Et₂O (100 ml) and washed with brine (2 x 100 ml). The organic fraction was then dried over MgSO₄ and filtered, before the solvent was removed from the filtrate *in vacuo* to give the chloro-oxime, which was diluted in toluene (10 ml). This solution was then cooled to 5 °C in an ice water bath, before adding Et₃N (0.35 ml, mmol) and stirring for 3 minutes. The resultant suspension was filtered and the filtrate was added to propargyl alcohol (0.15 ml, 2.82 mmol). The reaction mixture was then left to stir at room temperature for 4 hours in the dark. The solvent was then removed from the reaction mixture to afford **169** as a colorless solid (0.39 g, 60%); mp 53-54 °C. ¹H NMR (300.1 MHz, CDCl₃): δ_H 7.68 (2H, d, J_{HH} = 8.6 Hz, 2 x Ar H, H4), 7.45 (2H, d, J_{HH} = 8.6 Hz, 2 x Ar H, H5), 6.54 (1H, s, Ar H, H8), 4.78 (2H, s, CH₂), 4.05 (1H, br s, OH), 1.33 (9H, s, tBu). ¹³C NMR (75.5 MHz, CDCl₃): δ_C 172.6 (quat. C, C9), 162.8 (quat. C, C7), 153.9 (quat. C, C6), 127.0 (CH, 2 x Ar CH, C4), 126.3 (CH, 2 x Ar CH, C5), 126.2 (quat. C, C3), 100.4 (CH, Ar CH, C8), 56.7 (CH₂), 35.2 (quat. C), 31.6 (CH₃, tBu). IR (Nujol mull, NaCl plates) 3378, 1718, 1613 cm⁻¹. MS (ES⁺) *m/z* 254 (100%, [M+Na]). HRMS (ES⁺) calculated for C₁₄H₁₇N₂O₂ [M+Na] 254.1157, found 252.1158.

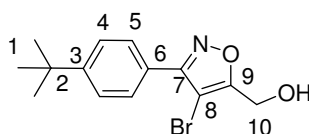
Acetic acid 4-bromo-3-(4-*tert*-butylphenyl) isoxazol-5-ylmethyl ester **170b**



Bromine (1.13 ml, 22.05 mmol) was added to a solution of **169** (1.70 g, 7.35 mmol) in acetic acid (6 ml) and left to stir at room temperature for 6 hours. The reaction mixture was washed with saturated aqueous sodium thiosulphate (2 x 25 ml) and then extracted into Et₂O (2 x 100 ml). The Et₂O fractions were combined, dried over MgSO₄ and filtered, before the solvent was removed from the filtrate *in vacuo*. The resultant oil was then purified by column chromatography (SiO₂ 1:1 EtOAc:hexane). The fractions containing the product were combined and the solvent was removed under reduced pressure to afford **170b** as a colorless oil (1.90 g, 75%); bp > 180 °C dec. ¹H NMR (300.1 MHz, CDCl₃): δ_H 7.81 (2H, d, J_{HH} = 8.6 Hz, 2 x Ar H, H4), 7.54 (2H, d, J_{HH} = 8.6

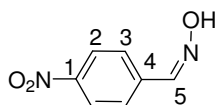
Hz, 2 x Ar H, H5), 5.27 (2H, s, CH₂), 2.18 (3H, s, CH₃), 1.44 (9H, s, tBu). ¹³C NMR (75.5 MHz, CDCl₃): δ_c 170.14 (C=O), 164.3 (quat. C, C9), 160.7 (quat. C, C7), 153.7 (quat. C, C6), 127.9 (CH, 2 x Ar CH, C4), 125.7 (CH, 2 x Ar CH, C5), 124.4 (quat. C, C3), 93.9 (quat. C, C8), 55.1 (CH₂) 34.9 (quat. C), 31.2 (CH₃, tBu), 20.6 (CH₃). IR (Nujol mull, NaCl plates) 1753, 1614 cm⁻¹. MS (ES+) *m/z* 374 (100%, [M+Na]), 376 (90% [M+Na]). HRMS (ES+) calculated for C₁₆H₁₈N₃O₃Br⁷⁹ [M+Na] 374.0368, found 374.0367, calculated for C₁₆H₁₈N₃O₃Br⁸¹ [M+Na] 376.0347, found 376.0357.

[4-Bromo-3-(4-*tert*-butylphenyl)-isoxazol-5-yl]-methanol **170**



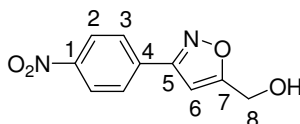
A saturated aqueous solution of K₂CO₃ (15 ml) was added to a solution of **170b** (1.80 g, 5.11 mmol) in MeOH (5 ml). The reaction mixture was then stirred at room temperature overnight, before diluting in CH₂Cl₂ (50 ml). The reaction mixture was then washed with brine (2 x 30 ml) and the organic fraction dried over MgSO₄ and filtered. The solvent was then removed from the filtrate under reduced pressure to afford **170** as a colorless solid (1.30 g, 83%); mp 77-78 °C. ¹H NMR (300.1 MHz, CDCl₃): δ_H 7.82 (2H, d, J_{HH} = 8.5 Hz, 2 x Ar H, H4), 7.45 (2H, d, J_{HH} = 8.5 Hz, 2 x Ar H, H5), 4.78 (2H, s, CH₂), 1.28 (9H, s, tBu). ¹³C NMR (75.5 MHz, CDCl₃): δ_c 168.9 (quat. C, C9), 160.9 (quat. C, C7), 154.1 (quat. C, C6), 128.3 (CH, 2 x Ar CH, C4), 126.2 (CH, 2 x Ar CH, C5), 124.9 (quat. C, C3), 92.15 (quat. C, C8), 55.2 (CH₂), 35.3 (quat. C), 31.6 (CH₃, tBu). IR (Nujol mull, NaCl plates) 3397, 1614 cm⁻¹. MS (ES+) *m/z* 332 (100%, [M+Na]), 334 (80%, [M+Na]). HRMS (ES+) calculated for C₁₄H₁₆NO₂Br⁷⁹ [M+Na] 332.0262, found 332.0261, calculated for C₁₄H₁₆NO₂Br⁸¹ [M+Na] 334.0242, found 334.0249.

4-Nitrobenzaldehyde oxime **173**



Hydroxylamine hydrochloride (1.72 g, 24.8 mmol) was added to a mixture of 4-nitro benzaldehyde (1.86 g, 12.33 mmol) and Amberlyst A21 (6.00 g) in ethanol (20 ml). The reaction mixture was stirred for 12 hours at room temperature under a nitrogen atmosphere. This suspension was then filtered through celite and the solvent removed from the filtrate under reduced pressure to afford **173** as a colorless solid (1.18 g, 58%); mp 116-118 °C (lit^[206]. 120-121 °C). ¹H NMR (300.1 MHz, CDCl₃): δ_H 8.16 (2H, d, J_{HH} = 8.8 Hz, 2 x Ar H, H2), 8.12 (1H, s, CHN, H5), 7.67 (2H, d, J_{HH} = 8.8 Hz, 2 x Ar H, H3). ¹³C NMR (75.5 MHz, CDCl₃): δ_C 148.3 (quat. C, C1), 147.8 (CH, CHN, C5), 138.7 (quat. C, C4), 127.5 (CH, 2 x Ar CH, C2), 123.6 (CH, 2 x Ar CH, C3). IR (Nujol mull, NaCl plates) 3299, 1604, 1537 cm⁻¹. MS (ES+) *m/z* 167.13 (100%, [M+H]).

[3-(4-Nitrophenyl) isoxazol-5-yl]-methanol **175**



N-Chlorosuccinimide (0.07 g, 0.56 mmol) was added to a stirred solution of 4-nitro-benzaldehyde oxime (0.50 g, 3.00 mmol) **173** in DMF (2.5 ml) at 45 °C, resulting in a slight decrease in temperature. HCl gas (0.2 ml) was then bubbled through the solution, resulting in a slight increase in temperature, and more *N*-chlorosuccinimide (0.32 g, 2.44 mmol) was added carefully keeping the temperature of reaction mixture below 55 °C. When the temperature had stabilized the solution was diluted in Et₂O (100 ml) and washed with brine (2 x 100 ml). The organic fraction was then dried over MgSO₄ and filtered, before the solvent was removed from the filtrate *in vacuo* to give the oxime chloride, which was diluted in toluene (15 ml). This solution was then cooled to 5 °C in an ice water bath, before adding Et₃N (0.37 ml, mmol) and stirring for 3 minutes. The resultant suspension was filtered and the filtrate was added to propargyl alcohol (0.16 ml, 3.00 mmol). The reaction mixture was then left to stir at room temperature for 4 hours in the dark. The solvent was then removed from the reaction mixture under reduced pressure and the crude product purified by column chromatography (SiO₂ 2:1 EtOAc:Hexane). Fractions containing the product were combined and the solvent removed under reduced pressure, to afford **175** as a colorless solid (0.16 g, 25%); mp 155 -156 °C. ¹H NMR (300.1 MHz, CDCl₃): δ_H 8.27 (2H, d, J_{HH} = 9.2 Hz, 2 x Ar H, H2),

7.92 (2H, d, $J_{\text{HH}} = 9.2$ Hz, 2 x Ar H, H3), 6.59 (1H, s, Ar H, H6), 4.80 (2H, s, CH_2). ^{13}C NMR (75.5 MHz, CDCl_3): δ_{c} 172.9 (quat. C, C7), 160.7 (quat. C, C5), 148.7 (quat. C, C1), 135.0 (quat. C, C4), 127.7 (CH, 2 x Ar CH, C2), 124.3 (CH, 2 x Ar CH, C3), 100.2 (CH, Ar CH, C6), 56.6 (CH_2). IR (solution CHCl_3 , NaCl plates) 3630, 1620, 1515 cm^{-1} . MS (Cl+) m/z 221 (100%, [M+H]). HRMS (Cl+) calculated for $\text{C}_{10}\text{H}_8\text{N}_2\text{O}_4$ [M+H] 221.0562, found 221.0556.

8. References

- [1] Kay, E. R., Leigh, D. A., Zerbetto, F., *Angew. Chem. Int. Ed.*, **2007**, 46, 72.
- [2] Stoddart, J. F., *Acc. Chem. Res.*, **2001**, 34, 410.
- [3] Anelli, L. P., Ashton, R. P., Ballardini, R., Balzani, V., Delgado, M., Gandolfi, M.T., Goodnow, T. T., Kaifer, A. E., Philp, D., Pietraszkiewicz, L. P., Reddington, M. V., Slawin, M. Z. A, Spencer, N., Stoddart, J. F., Vicent, C., and Williams, J. D., *J. Am. Chem. Soc.*, **1992**, 114, 193.
- [4] Breault, G. A., Hunter, C. A., Mayers, P. C., *Tetrahedron*, **1999**, 55., 5265.
- [5] Nguyen, T. D., Liu, Y., Saha, S., Leung, K. C. -F., Stoddart, J. F., Zink, J. I., *J. Am. Chem. Soc.*, **2006**, 114, 193.
- [6] Green, J. E., Choi, J. W., Boukai, A., Bunimovich, Y., Johnston-Halperin, E., Delonno, E., Luo, Y., Sheriff, B. A., Xu, K., Shin, Y. S., Tseng, H- .R., Stoddart, J. F., Heath, J. R., *Nature*, **2007**, 445, 414.
- [7] Leigh, D. A., Thomson, A. R., *J. Org. Chem.*, **2006**, 8, 5377.
- [8] Cooke, G., Woisel, P., Bria, M., Delattre, F., Garety, J. F., Hewage, S. G., Rabani, G., Rosair, G. M., *Org. Lett.*, **2006**, 8, 1423.
- [9] Cooke, G., Garety, J. F., Mabruk, S., Rabani G., Rotello, V. M, Suprateanu W. P. *Tetrahedron Lett.*, **2006**, 47, 783-786.
- [10] Zeng, F., Zimmerman, S. C., *Chem. Rev.*, **1997**, 97, 1681.
- [11] Smith, D. K., *Chem. Commun.*, **2006**, 34.
- [12] Smith, D. K., *Tetrahedron*, **2003**, 59, 3797.
- [13] Hardy, J. G., *Org. Biomol.Chem.*, **2007**, 5, 900.
- [14] Dykes, G. M., Smith, D. K., Seeley, G. J., *Angew.Chem. Int. Ed.*, **2002**, 41, 3254.
- [15] Dykes, G. M., Smith, D. K., *Tetrahedron*, **2003**, 59, 3999.
- [16] Pedersen, C. J., *J. Am. Chem. Soc.*, **1967**, 89, 2495.
- [17] Pedersen, C. J., *J. Am. Chem. Soc.*, **1967**, 89, 7017.
- [18] Cram, D. J., *Angew.Chem. Int. Ed. Engl.*, **1988**, 27, 3254
- [19] Dietrich, B., Lehn, J. M., Sauvage, P., *Tetrahedron Lett.*, **1969**, 2885.
- [20] Dietrich, B., Lehn, J. M., Sauvage, P., *Tetrahedron Lett.*, **1969**, 2889.
- [21] Anslyn, E. V., Dougherty, D.A., *Modern Physical Organic Chemistry*, University Science Books, Sausalito, California, **2006**, 224.

- [22] Takahashi, K., *Chem. Rev.*, **1998**, 98, 2013.
- [23] Adams, H., Harris, K. D. M., Hembury, G. A., Hunter, C. A., Livingstone, D., McCabe, J. F., *Chem. Commun.*, **1996**, 2531.
- [24] Adams, H., Blanco, J. -L. J., Chessari, G., Hunter, C. A., Low, C. M. R., Sanderson, J. M., Vinter, J. G., *Chem. Eur. J.*, **2001**, 7, 3494.
- [25] Prins, L. J., Reinhoudt, D. N., Timmerman, P., *Angew. Chem. Int. Ed.*, **2001**, 40, 2382.
- [26] Kyogoku, Y., Lord, R. C., Rich, A., *Proc. Natl. Acad. Sci. USA.*, **1967**, 57, 250
- [27] Hamilton, A. D., Van Engen, D., *J. Am. Chem. Soc.*, **1987**, 109, 5035.
- [28] Jørgensen, W. L., Pranata, J., *J. Am. Chem. Soc.*, **1990**, 112, 2008.
- [29] Pranata, J., Wierschke, S. G., Jørgensen, W. L., *J. Am. Chem. Soc.*, **1991**, 113, 2810.
- [30] Murray, T.J., Zimmerman, S. C., *J. Am. Chem. Soc.*, **1992**, 114, 4010.
- [31] Sartorius, J., Schneider, H. -J., *Chem. Eur. J.*, **1996**, 2, 1446.
- [32] Jencks, W. P., *Proc. Natl. Acad. Sci. USA.*, **1981**, 78, 4046.
- [33] Williams, D., Westwell, M. S., *Chem. Soc. Rev.*, **1998**, 27, 57.
- [34] Badjic, D. J., Nelson, A., Cantrill, S. J., Turnbull, W. B., Stoddart, J. F., *Acc. Chem. Res.*, **2005**, 38, 723.
- [35] Hunter, C. A., Tomas, S., *Chem. Biol.*, **2003**, 10, 1023.
- [36] Bisson, A. P., Hunter, C. A., Morales, J. C., Young, K., *Chem. Eur. J.*, **1998**, 4, 845.
- [37] Murray, T. J., Zimmerman, S. C., *Tetrahedron. Lett.*, **1994**, 35, 4077.
- [38] Taylor, R., Kennard, O., Versichel, *J. Am. Chem. Soc.*, **1984**, 106, 244.
- [39] Zimmerman, S. C., Wang, Y., Bharathi, P., Moore, J. S., *J. Am. Chem. Soc.*, **1998**, 120, 2172.
- [40] Fenlon, E. E., Murray, T. J., Baloga, M. H., Zimmerman, S. C., *J. Am. Chem. Soc.*, **1992**, 114, 4010.
- [41] Djurdjevic, S., Leigh, D. A., McNab, H., Parsons, S., Teobaldi, G., Zerbetto, F., *J. Am. Chem. Soc.*, **2007**, 129, 476.
- [42] Sijbesma, P. R., Meijer, E. W., *Chem. Commun.*, **2003**, 5.
- [43] Gallant, M., Viet, M. T. P, Wuest, J. D., *J. Am. Chem. Soc.*, **1991**, 113, 721.
- [44] Boucher, E., Simard, M., Wuest, J. D., *J. Org. Chem.*, **1995**, 60, 1408.

- [45] Prabhakaran, P., Puranim, V. G., Sanjayan, G. J., *J. Org. Chem.*, **2005**, 70, 100067.
- [46] Schmuck, C., Wienand, W., *Angew. Chem. Int. Ed.*, **2001**, 40, 4363.
- [47] Corbin, P. S., Zimmerman, S. C., *J. Am. Chem. Soc.*, **2000**, 122, 3779.
- [48] Park, T., Zimmerman, S. C., Nakashima, S., *J. Am. Chem. Soc.*, **2005**, 127, 6520.
- [49] Park, T., Todd, E. M., Nakashima, S., Zimmerman, S. C., *J. Am. Chem. Soc.*, **2005**, 127, 18133.
- [50] Park, T., Zimmerman, S. C., *J. Am. Chem. Soc.*, **2006**, 128, 14236.
- [51] Kirby, A. J., *Angew. Chem. Int. Ed. Engl.*, **1996**, 35, 707.
- [52] Motherwell, W. B., Bingham, M. J., Six, Y., *Tetrahedron*, **2001**, 57, 4663.
- [53] Kirby, A. J., *Adv Phys. Org. Chem.*, **1980**, 17, 183.
- [54] Bruice, T. C., Pandit, U. K., *J. Am. Chem. Soc.*, **1960**, 82, 5858.
- [55] Bruice, T. C., Pandit, U. K., *J. Am. Chem. Soc.*, **1960**, 82, 3386.
- [56] Lightstone, F. C., Bruice, T. C., *J. Am. Chem. Soc.*, **1996**, 118, 2595.
- [57] Lightstone, F. C., Bruice, T. C., *Bioorg. Chem.*, **1998**, 26, 193.
- [58] Storm, D. R., Koshland, D. E., *J. Am. Chem. Soc.*, **1972**, 94, 5805.
- [59] Storm, D. R., Koshland, D. E., *J. Am. Chem. Soc.*, **1972**, 94, 5815.
- [60] Page, M. I., Jencks, W. P., *Proc. Nat'l. Acad. Sci, USA.*, **1971**, 68, 1678.
- [61] Page, M. I., *Chem. Soc. Rev.*, **1973**, 2, 295.
- [62] Hoare, D. G., *Nature*, **1972**, 236, 437.
- [63] Menger, F. M., *Acc. Chem. Res.*, **1985**, 18, 128.
- [64] Menger, F. M., *Acc. Chem. Res.*, **1993**, 26, 200.
- [65] Bruice, T. C., Lightstone, F. C., *Acc. Chem. Res.*, **1999**, 32, 127.
- [66] Koshland, D. E., Stoddard, B. L., Mesecar, A., *Science*, **1997**, 277, 202.
- [67] Beesley, R. M., Ingold, C. K., *J. Am. Chem. Soc.*, **1915**, 107, 1080.
- [68] Schowen, R. L., *Proc. Natl. Acad. Sci. USA.*, **2003**, 100, 11931.
- [69] Ranaghan, K. E., Mulholland, A. J., *Chem. Comm.*, **2004**, 1238.
- [70] Garcia-Viloca, M., Gao, J., Karplus, M., Truhlar, D.G., *Science*, **2004**, 303, 186.
- [71] Anderson, S., Anderson, H. L., Sanders, J. K. M., *Acc. Chem. Res.*, **1993**, 26, 469.
- [72] Li, X., Liu., D. R., *Angew. Chem. Int. Ed.*, **2004**, 43, 4848.
- [73] Anderson, S., Anderson. H. C., *Templated Organic Synthesis*, Eds. F. Diederich and P. J. Stang, Wiley-VCH, Weinheim, **2000**.

- [74] Kelly, R. T, Zhao, C., Bridger, G. J., *J. Am. Chem. Soc.*, **1989**, 111, 3744.
- [75] Kelly, R. T, Zhao, C., Bridger, G. J., *J. Am. Chem. Soc.*, **1990**, 112, 8024.
- [76] Nakash, M., Clyde-Watson, Z., Feeder, N., Davies, J. E., Teat, S. J., Sanders, J. K. M., *J. Am. Chem. Soc.*, **2000**, 122, 5286.
- [77] Mock, W. L, Irra, T. A., Wepsiec, J.P., Adhya, M., *J. Org. Chem.*, **1989**, 54, 5302.
- [78] Ohshima, S., Tamura, N., Naeshima, T., Yano, Y., *J. Chem. Soc.*, **1993**, 712.
- [79] Cram, D. J., *Angew. Chem. Int. Ed. Engl.*, **1988**, 27, 1009.
- [80] Wolfe, J., Nemeth, D., Costero, A., Rebek, J., *J. Am. Chem. Soc.*, **1998**, 110, 112, 983.
- [81] Cram, D. J., Katz, H. E., *J. Am. Chem. Soc.*, **1983**, 105, 135.
- [82] Cram, D. J., Lam, P. Y. S., *Tetrahedron*, **1986**, 42, 1607.
- [83] Trainor G.L., Breslow, R., *J. Am. Chem. Soc.*, **1981**, 103, 154.
- [84] Breslow, R., Trainor G. L., Veno, A., *J. Am. Chem. Soc.*, **1983**, 105, 2739.
- [85] Allen, V. C., PhD Thesis, University of Birmingham, **2000**.
- [86] Quayle, J. M., PhD Thesis, University of St Andrews, **2002**.
- [87] Kassianidis, E., PhD Thesis, University of St Andrews, **2005**.
- [88] Minto, M. J., PhD Thesis, University of St Andrews, **2005**, Chapter 4.
- [89] von Kiedrowski, G., Bag, B. G., *Pure Appl. Chem.*, **1996**, 68, 2145.
- [90] Robertson, A., Sinclair, A. J., Philp, D., *Chem. Soc. Rev.*, **2000**, 29, 141
- [91] Paul, N., Joyce, G. F., *Curr. Opin. Chem. Biol.*, **2004**, 8, 634.
- [92] von Kiedrowski, G., *Bioorganic Chemistry Frontiers*, Vol 3, Springer-Verlag, Berlin Heidelberg, **1993**, 113.
- [93] Kim, D. –E., Joyce, G. F., *Chem. Biol.*, **2004**, 11, 1505.
- [94] von Kiedrowski, G., Wlotzka, B., Helbing, *Angew. Chem. Int. Ed. Engl.*, **1986**, 25, 932.
- [95] von Kiedrowski, G., Wlotzka, B., Helbing, *Angew. Chem. Int. Ed. Engl.*, **1989**, 28, 1235.
- [96] von Kiedrowski, G., Wlotzka, B., Helbing, *Angew. Chem. Int. Ed. Engl.*, **1991**, 30, 423.
- [97] Severin, K., Lee, D. H., Martinez, J. A., Ghardiri, M. R., *Chem. Eur. J.*, **1997**, 3, 1017.
- [98] Xiangqun, L., Chmielewski, J., *Org. Biomol. Chem.*, **2003**, 1, 901.
- [99] Natasha, P., Joyce, G. F., *Proc. Natl. Acad. Sci. USA.*, **2002**, 99, 12733.

- [100] McGinness, K. E., Joyce, G. F, *Chem. Biol.*, **2003**, 10, 5.
- [101] McGinness, K. E., Joyce, G. F, *Chem. Biol.*, **2002**, 9, 297.
- [102] Kemp, D.S., Petrakis, K.S., *J. Org. Chem.*, **1981**, 46, 5140.
- [103] Wintner, E. A., Rebek, J. Jr, *Acta. Chem. Scand.*, **1996**, 50, 469.
- [104] Rebek, J. Jr, Nemeth, D., Ballester, P., Lin, F. T., *J. Am. Chem. Soc.*, **1987**, 109, 3474.
- [105] Park, T. K., Schroeder, J., Rebek, J. Jr., *Tetrahedron*, **1991**, 47, 2507.
- [106] Norwich, J. S, Feng, Q., Tjivikua, T., Ballester, P., Rebek, J. Jr., *J. Am. Chem. Soc.*, **1996**, 113, 8831.
- [107] Famulok, M., Nowick, J. S., Rebek, J. Jr., *Acta. Chem. Scand.*, **1992**, 46, 315.
- [108] Tjivikua, T., Ballester, P., Rebek, J. Jr., *J. Am. Chem. Soc.*, **1990**, 112, 1249.
- [109] Winter, E. A., Conn, M. M, Rebek, J. Jr., *J. Am. Chem. Soc.*, **1994**, 116, 8877
- [110] Reinhoudt, D. N., Rudkevich, D. M., de Jong, F., *J. Am. Chem. Soc.*, **1996**, 118, 6880.
- [111] Menger, F. M., Eliseev, A. U., Khanjin, N. A., *J. Am. Chem. Soc.*, **1994**, 116, 3613.
- [112] Menger, F. M., Eliseev, A. U., Khanjin, N. A., Sherrod, M.J., *J. Org. Chem.*, **1995**, 60, 2870.
- [113] Conn, M. M., Wintner, E. A., Rebek, J. Jr., *J. Am. Chem. Soc.*, **1994**, 116, 8823.
- [114] Wintner, E. A., Tsao, B., Rebek, J. Jr., *J. Org. Chem.*, **1995**, 60, 7997.
- [115] Norwick, J.S., Feng, Q., Tjivikua, T., Ballester, P., Rebek, J. Jr., *J. Am. Chem. Soc.*, **1991**, 113, 8831.
- [116] Rotello, V., Hong, J-. I., Rebek, J. Jr., *J. Am. Chem. Soc.*, **1991**, 113, 9422.
- [117] Park, T. K., Feng, Q., Rebek, J. Jr., *J. Am. Chem. Soc.*, **1992**, 114, 4529.
- [118] Hong, J-. I., Feng, Q., Rotello, V., Rebek, J. Jr., *Science*, **1992**, 255, 849.
- [119] Huc, I., Pieters, R. J., Rebek, J. Jr., *J. Am. Chem. Soc.*, **1994**, 116, 10296.
- [120] Wang, B., Sutherland, I. O., *Chem. Commun.*, **1997**, 1495.
- [121] Allen. C. V. Philp, D., Spencer, N., *Org. Lett.*, **2001**, 3, 777.
- [122] Quayle, J. M., Slawin, A. M. Z., Philp, D., *Tetrahedron Lett.*, **2002**, 43, 7229.
- [123] Pearson, R. J., Kassianidis, E., Philp, D., *Tetrahedron Lett.*, **2004**, 45, 4777.
- [124] Pearson, R. J., Kassianidis, E., Slawin, A. M. Z., Philp, D., *Org. Biomol. Chem.*, **2004**, 2, 3434.

- [125] Pearson, R. J., Kassianidis, E., Slawin, A. M. Z., Philp, D., *Chem. Eur. J.*, **2006**, 12, 6829.
- [126] Kassianidis, E., Pearson, R. J., Philp, D., *Org. Lett.*, **2005**, 7, 3833.
- [127] Kassianidis, E., Pearson, R. J., Philp, D., *Chem. Eur. J.*, **2006**, 12, 8798.
- [128] Kassianidis, E., Philp, D., *Angew. Chem. Int. Ed.*, **2006**, 45, 6344.
- [129] von Kiedrowski, G., Bag, B. G., *Angew. Chem. Int. Ed.*, **1999**, 38, 3713.
- [130] Thordarson, P., Marquis, A., Crossley, M.J., *Org. Biomol. Chem.*, **2003**, 1, 1216.
- [131] Schramm, G., Grotsch, H., Pollman, W., *Angew. Chem. Int. Ed. Engl.*, **1962**, 1, 1.
- [132] Naylor, R., Gilham, P. T., *Biochemistry.*, **1966**, 5, 2722.
- [133] Orgel, L. E., Lohrmann, R., *Acc. Chem. Res.*, **1974**, 7, 368.
- [134] Orgel, L. E., Inoue, T., Joyce, G. F., Grzeskowiak, K., Brown, J. M., *J. Mol. Biol.*, **1984**, 178.
- [135] Zielinski, W., Orgel, L. E., *Nature*, **1987**, 327, 346.
- [136] Wu, T., Orgel, L. E., *J. Am. Chem. Soc.*, **1992**, 114, 317.
- [137] Orgel, L. E., *Nature*, **1992**, 358, 203.
- [138] Nicolaou, K. C., Li, T., *Nature*, **1994**, 369, 218.
- [139] Sievers, D., von Kiedrowski, G., *Nature*, **1994**, 369, 221.
- [140] Sievers, D., von Kiedrowski, G., *Chem. Eur. J.*, **1998**, 4, 629.
- [141] Luther, A., Brandsch, R., von Kiedrowski, G., *Nature*, **1998**, 396, 245.
- [142] Pieters, R. J., Huc, I., Rebek, J. Jr., *Angew. Chem. Int. Ed. Engl.*, **1994**, 33, 1579.
- [143] Pieters, R. J., Huc, I., Rebek, J. Jr., *Tetrahedron*, **1995**, 51, 485.
- [144] Kassianidis, E., Philp, D., *Chem. Commun.*, **2006**, 39, 4072.
- [145] Yao, S., Ghosh, I., Zutshi, R., Chmielewski, J., *Nature*, **1998**, 396, 447.
- [146] Ashkensay, G., Jagasia, R., Yadav, M., Ghadiri, M. R., *Proc. Natl. Acad. Sci. USA.*, **2004**, 101, 10872.
- [147] Ashkensay, G., Ghadiri, M. R., *J. Am. Chem. Soc.*, **2004**, 126, 11140.
- [148] Kindermann, M., Stahl, I., Reimold, M., Pankau, W. M., von Kiedrowski, G., *Angew. Chem. Int. Ed.*, **2005**, 44, 6750.
- [149] Stahl, I., von Kiedrowski, G., *J. Am. Chem. Soc.*, **2006**, 128, 14014.
- [150] Hosseini, M. W., Lehn, J. M., *J. Am. Chem. Soc.*, **1982**, 104, 3525.
- [151] Watson, J. D., Crick, F. H. C., *Nature*, **1953**, 171, 964.
- [152] Fan, E., van Arman, S., S. A., Kincaid, S., Hamilton, A. D., *J. Am. Chem. Soc.*, **1993**, 115, 369.

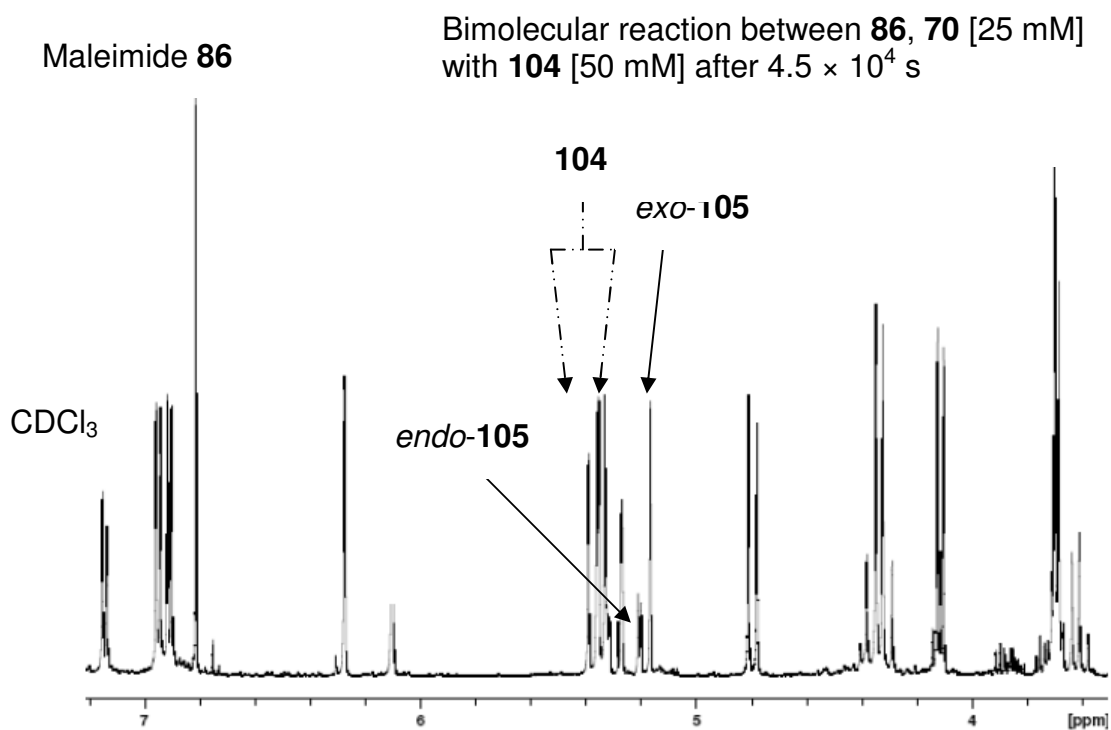
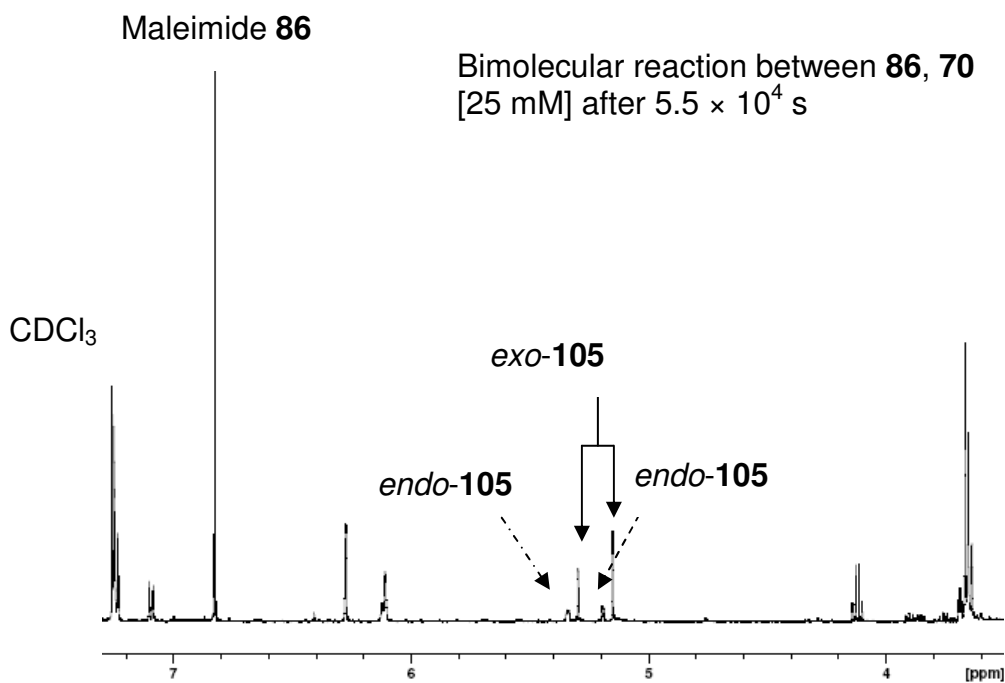
- [153] Gracia-Tellado, F., Goswami, S., Chang, S. K., Geib, S., Hamilton, A. D., *J. Am. Chem. Soc.*, **1990**, 112, 7393.
- [154] Hirst, S. C., Hamilton, A. D., *J. Am. Chem. Soc.*, **1991**, 113, 382.
- [155] Yang, J., Fan, E., Geib, S., Hamilton, A. D., *J. Am. Chem. Soc.*, **1993**, 115, 5314.
- [156] Goswami, S., Ghosh, S., Dasgupta, S., *J. Org. Chem.*, **2000**, 65, 1907.
- [157] Clayden, J., Greeves, N., Warren, S., Wothers, P., *Organic Chemistry*, Oxford University Press, Oxford, **2001**. 912.
- [158] Mustafa, A., Abdel., S. M., Zayed, D., Khattab, S., *J. Am. Chem. Soc.*, **1956**, 78, 145.
- [159] Scriven, E., Turnbull, K., *Chem. Rev.*, **1988**, 88, 351.
- [160] Huisgen, R., *Angew. Chem., Int. Ed. Engl.*, **1963**, 2, 633.
- [161] Huisgen, R., *Angew. Chem., Int. Ed. Engl.*, **1963**, 2, 565.
- [162] Huisgen, R., *J. Org. Chem.*, **1976**, 41, 403.
- [163] Houk, K. N., Sims, J., Duke, R. E., Strozier, R. W., George, J. K., *J. Am. Chem. Soc.*, **1973**, 95, 7287.
- [164] Fleming, I., *Frontier Orbitals and Organic Chemical Reactions*, John Wiley and Sons, Bristol, **1976**.
- [165] Stauffer, D. A., Barrens, R. E., Jr, Dougherty, D.A., *J. Org. Chem.*, **1990**, 55, 2762.
- [166] Iwakura, Y., Keikichi, U., Hong, S.- J., Tatsuhiko, H., *Bull. Chem. Soc, Jpn.*, **1971**, 192.
- [167] Takahashi, S., Takeshi, H., Sawada, S., *Bull. Chem. Soc, Jpn.*, **1988**, 61, 2467.
- [168] Blazevic, N., Kolbah, D., Berlin, B., Sunjic., V., Kajifez, F., *Synthesis*, **1979**, 161.
- [169] Breton, G. W., *J. Org. Chem.*, **1997**, 62, 8952.
- [170] Hanaya, K., Muramatsu, T., Kudo, H., Chow, Y. L., *J. Chem. Soc., Perkin Trans I*, **1979**, 2409.
- [171] Ren, P.- D., Pan, X.- W., Jin, Q.- H., Yao, P. Z., *Synth. Commun*, **1997**, 27, 3497.
- [172] Watts, D. S., Strogatz, S. H., *Nature*, **1998**, 393, 440.
- [173] Jeong, H, Tombor, B., Albert, R., Oltaval, Z. N., Barabasi, A. L., *Nature*, **2000**, 407, 651.
- [174] Ravasz, E, Somera, D. A., Mongru, Oltvai, Z. N., Barabasi, L., *Science*, **2002**, 297, 1551.
- [175] Girvan, M., Newman, M. E. J., *Proc. Natl. Acad. Sci. USA.*, **2002**, 99, 7821.

- [176] Guimera, R., Amaral, L. A. N., *Nature.*, **2005**, 433, 614.
- [177] Perez, J. J., *Chem. Soc. Rev.*, **2005**, 34, 143.
- [178] Ding, K., Yaun, D. Y., Long, J., *Chem. Eur. J.*, **2001**, 10, 2872.
- [179] Breaker, R. R., *Nature.*, **2004**, 432, 838.
- [180] Dobson, C. M., *Nature.*, **2004**, 432, 824.
- [181] Lavinge, J. J., Anslyn, E. V., *Angew. Chem. Int. Ed.*, **2001**, 40, 3118.
- [182] Xu, J., Deng, Q., Chen, J., Houk, K. N., Bartek, J., Hilvert, D., Wilson, I. A., *Science*, **1999**, 286, 2345.
- [183] Wright, M. C., Joyce, G. F., *Science*, **1997**, 276, 614.
- [184] Siemsen, P., Livingston, R. C., Diederich, F., *Angew. Chem. Int. Ed.*, **2000**, 39, 2632.
- [185] Ballini, R., Barboni, L., Filippone, P., *Chem. Lett.*, **1997**, 475.
- [186] Rajagopalan, S., Advani, B., Talaty, C. N., *Org. Syn. Coll.* 5, 787.
- [187] Corbett, P.T., Leclaire, J., Vial, L., West, K.R., Wietor, J.- L., Sanders, J. K. M., Otto, S., *Chem. Rev.*, **2006**, 9, 3652.
- [188] Rowan, S. J., Cantrill, S. J., Cousins, G. R. L., Sanders, J. K. M., Stoddart, J. F., *Angew. Chem. Int. Ed.*, **2002**, 41, 898.
- [189] Hasenknopf, B., Lehn, J.- M., Baum, G., Kneisel, B. O., Fenske, D., *Angew. Chem. Int. Ed. Engl.*, **1996**, 35, 1838.
- [190] Hasenknopf, B., Lehn, J.- M., Boumediene, N., Dupont-Gervais, A., Van Drosselaer, A., Kneisel, B. O., Fenske, D., *J. Am. Chem. Soc.*, **1997**, 119, 10956.
- [191] Lehn, J.- M., *Chem. Eur. J.*, **1999**, 5, 2455.
- [192] Schiff, H., *Ann. Chem. Pharm.*, **1864**, 131, 118.
- [193] Nitschke, J. R., *Acc. Chem. Res.*, **2007**, 40, 103.
- [194] Iwasawa, T., Mann, E., Rebek, J. Jr., *J. Am. Chem. Soc.*, **2006**, 128, 9308.
- [195] Hidetoshi, K., Umehara, T., Fujiwara, K., Tsuji, T., Suzuki, T., *Angew. Chem. Int. Ed.*, **2006**, 4281.
- [196] Nguyen, R., Huc, I., *Chem. Commun.*, **2003**, 942.
- [197] Bornaghi, L. F., Wilkinson, B. L., Kiefel, M. J., Poulsen, S. A., *Tetrahedron Lett.*, **2004**, 45, 9281.
- [198] Boul, P. J., Reutenauer, P., Lehn, J. M., *Org. Lett.*, **2005**, 7, 15.
- [199] Bennes, R.M., Philp, D., *Org. Lett.*, **2006**, 8, 3651.
- [200] Kim, T. R., Kwang-Il, L., *Bull. Korean. Chem. Soc.*, **1991**, 12, 273.

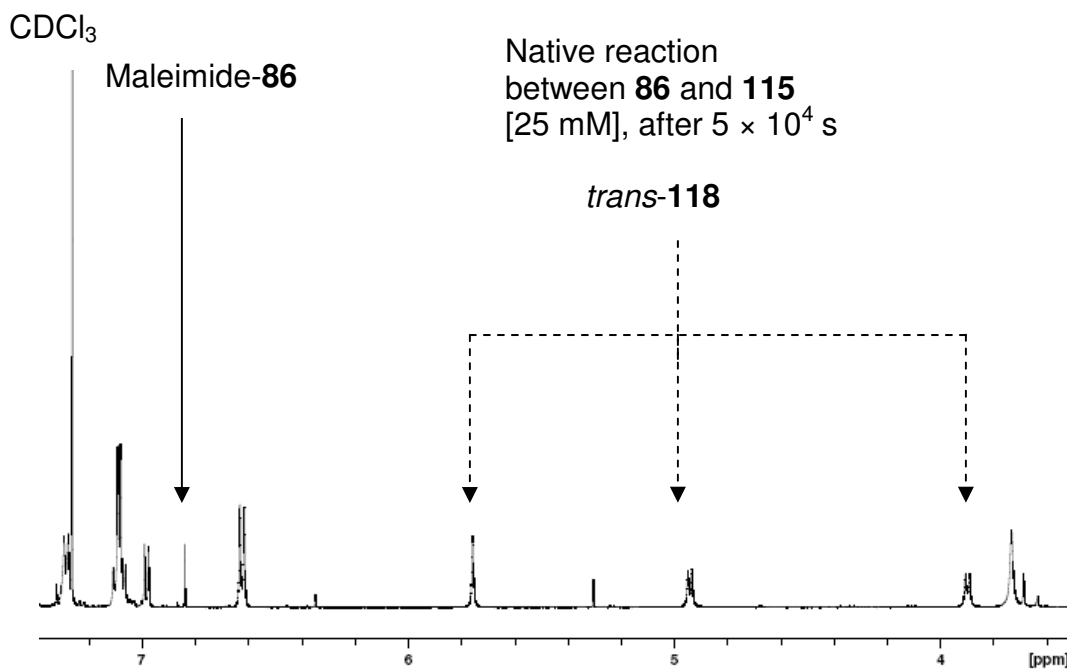
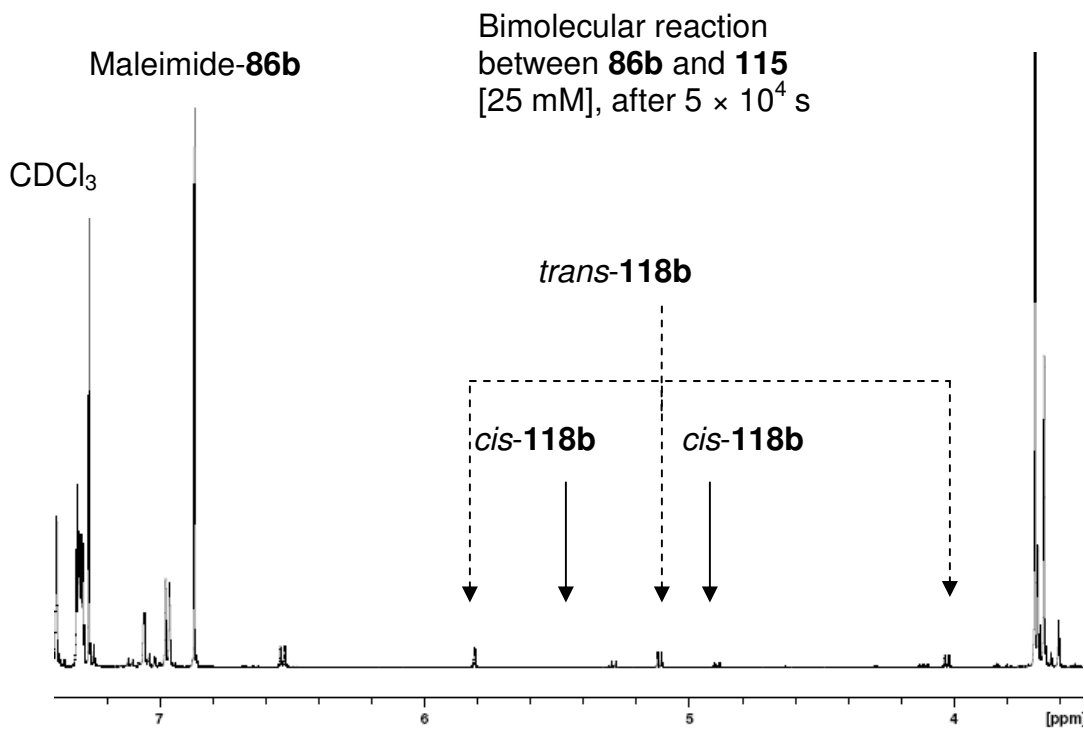
- [201] Allen, V. C., Ph.D. Thesis, University of Birmingham, **2000**, p. 43
- [202] Reimann, J. E., Jencks, W. P., *J. Am. Chem. Soc.*, **1966**, 88, 3975.
- [203] Schneider, H., Durr, H., *Frontiers in Supramolecular Organic Chemistry.*, VCH Publishers, Ltd., London, **1991**.
- [204] Mandolini, L., *Adv. Phys. Org. Chem.*, **1986**, 22, 1-111.
- [205] Ramana, M. M. V., Malik, S. S., Parihar, J. A., *Tetrahedron. Lett.*, **2004**, 45, 8681.
- [206] Sharghi, H., Sarvari, M. H., *Synlett.*, **2001**, 1, 99.
- [207] Olah, G. A., *Synthesis*, **1973**, 8, 487.
- [208] Amstrong, A. A., Amzel, L. M., *J. Am. Chem. Soc.*, **2003**, 125, 14596.
- [209] Fenlon, E. E., Murray, T. J., Baloga, M. H., Zimmerman, S. C., *J. Org. Chem.*, **1993**, 58, 6625.
- [210] Wang, X- Z., Li, X- O., Shao, X- B., Zhao, X., Deng, P., Jiang, X- K., Li, Z- T., Chen, Y- Q., *Chem. Eur. J.*, **2003**, 9, 2904.
- [211] Sijbesma, R. P., Beijer, F. H., Brunsveld, L., Folmer, B. J. B., Folmer., Hirschberg, J. H. K., Lange., R. F. M., Lowe., J. K. L., Meijer., E. W., *Science*, **1997**, 278, 1601.
- [212] Sanders, J. K. M., *Pure Appl. Chem.*, **2000**, 72, 2265.
- [213] Bag, B. G., Kiedrowski, G. V., *Pure Appl. Chem.*, **1996**, 68, 2145.
- [214] Allen, V. C., Philp, D., Spencer, N., *Org. Lett.*, **2001**, 3, 777.

9. Appendix

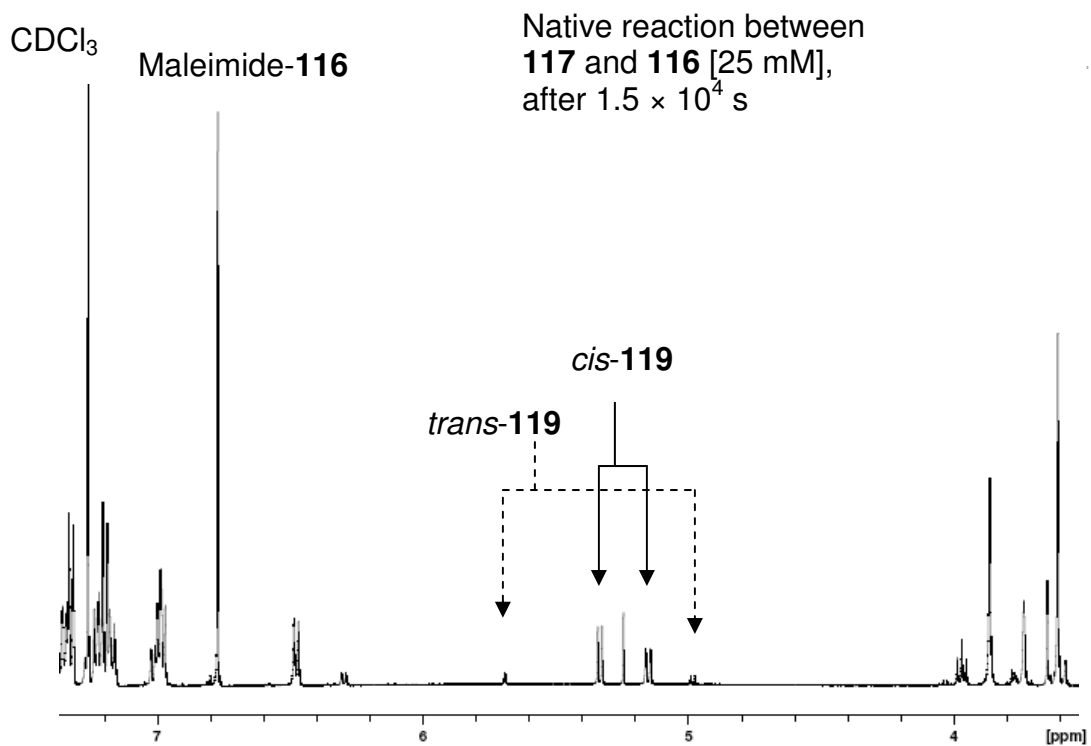
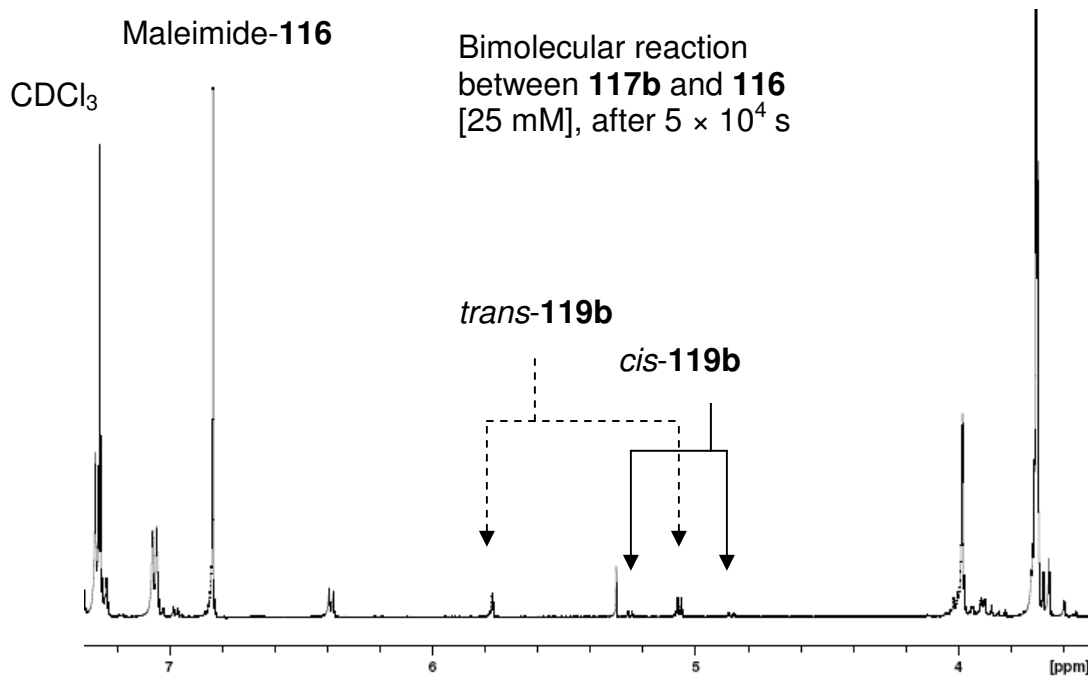
Appendix One



Appendix Two



Appendix Three

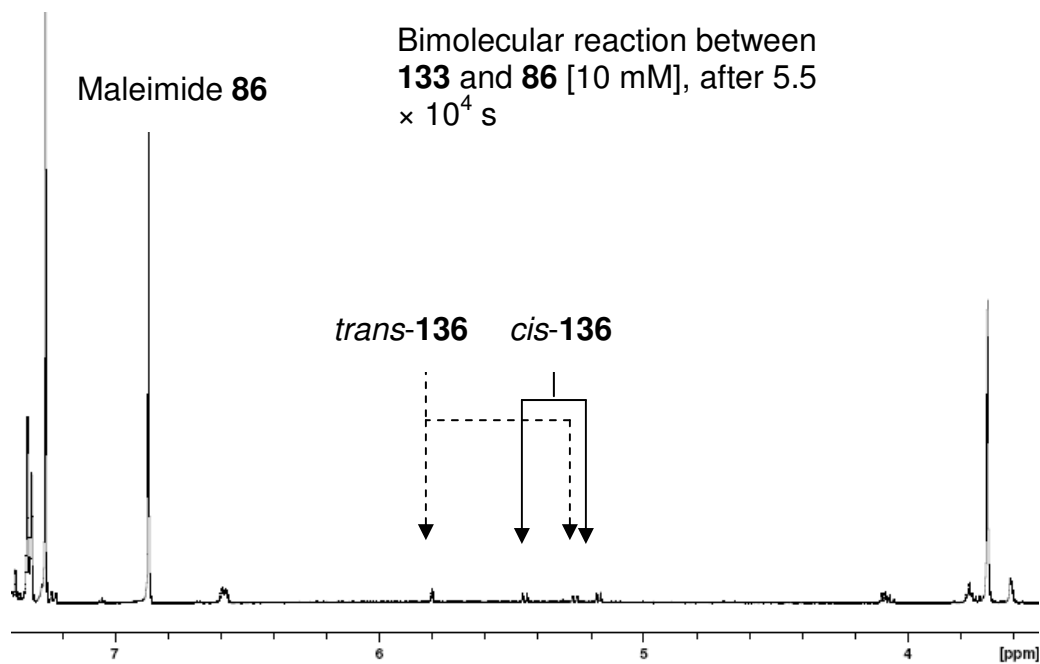


Appendix Four

CDCl_3

Maleimide **86**

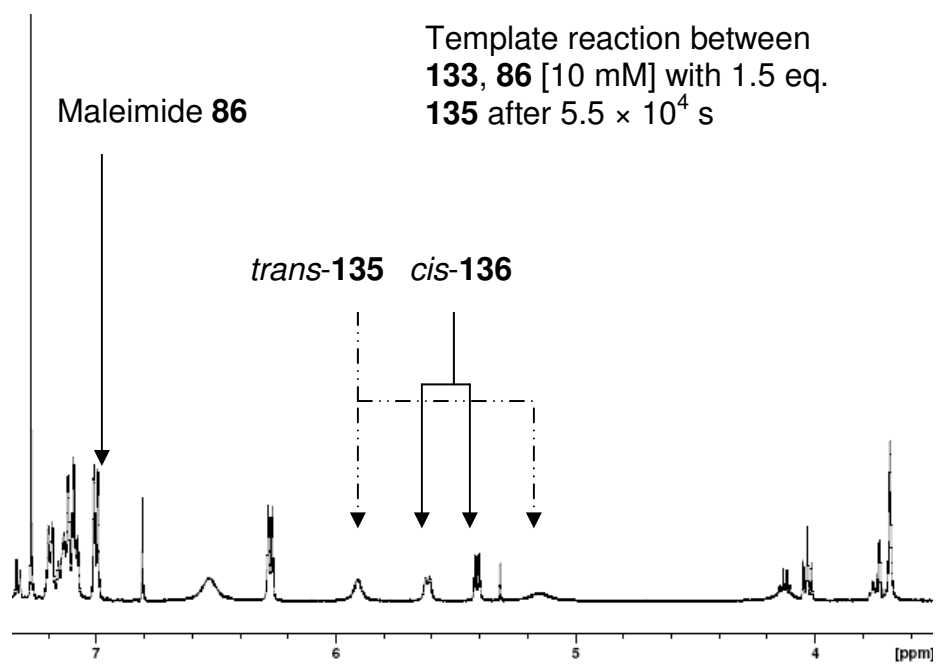
Bimolecular reaction between
133 and **86** [10 mM], after 5.5×10^4 s



CDCl_3

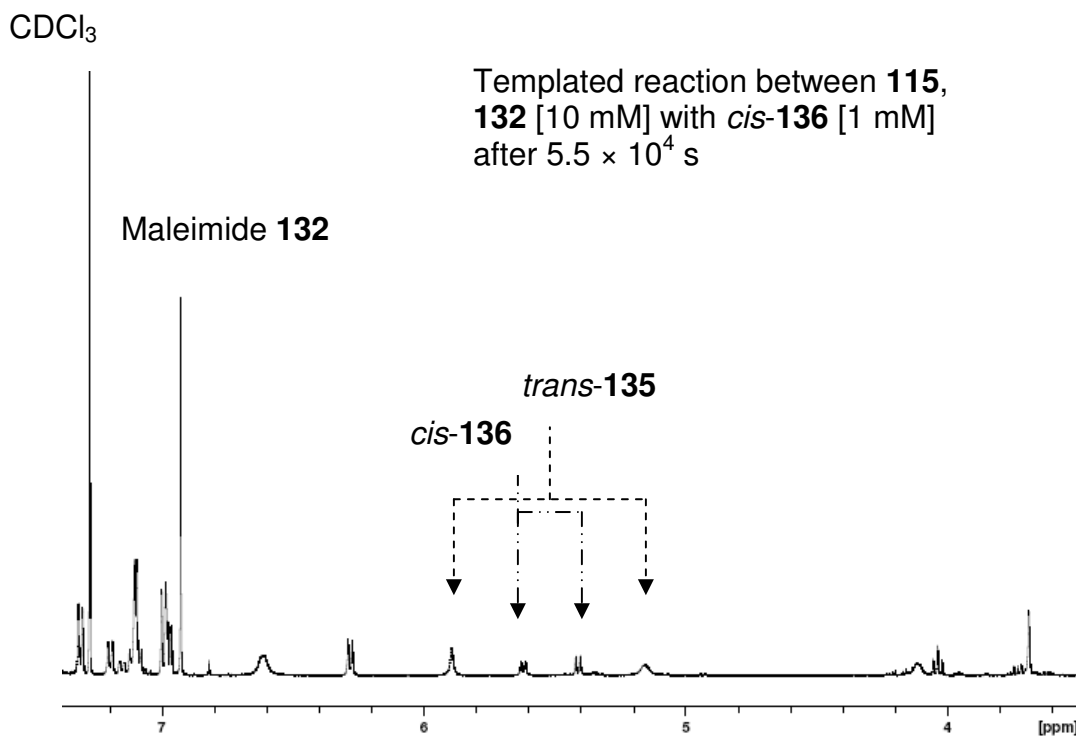
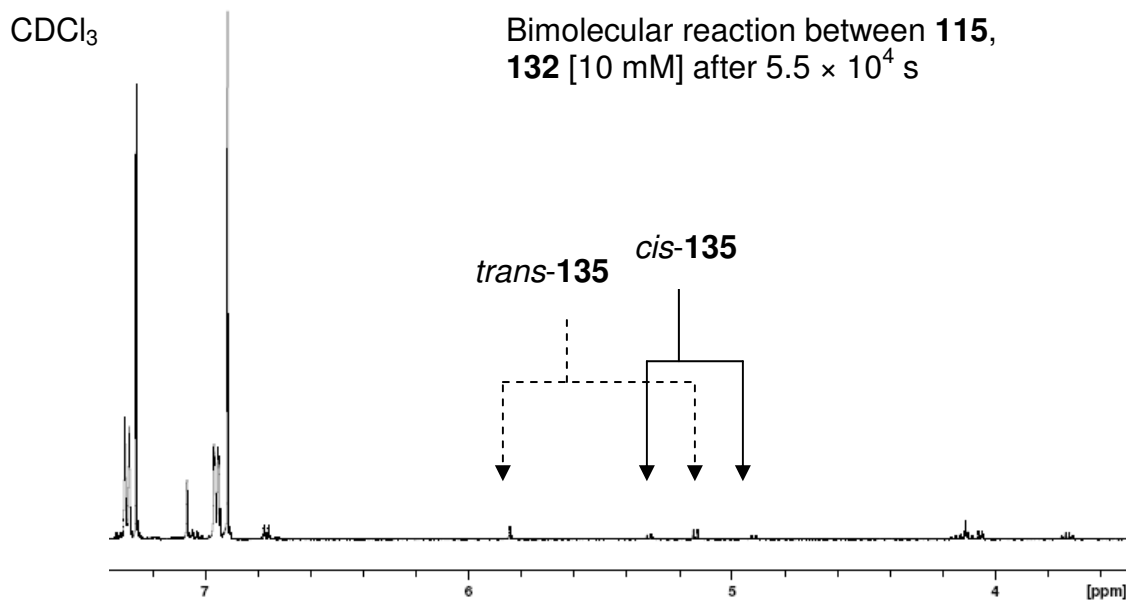
Maleimide **86**

Template reaction between
133, **86** [10 mM] with 1.5 eq.
135 after 5.5×10^4 s



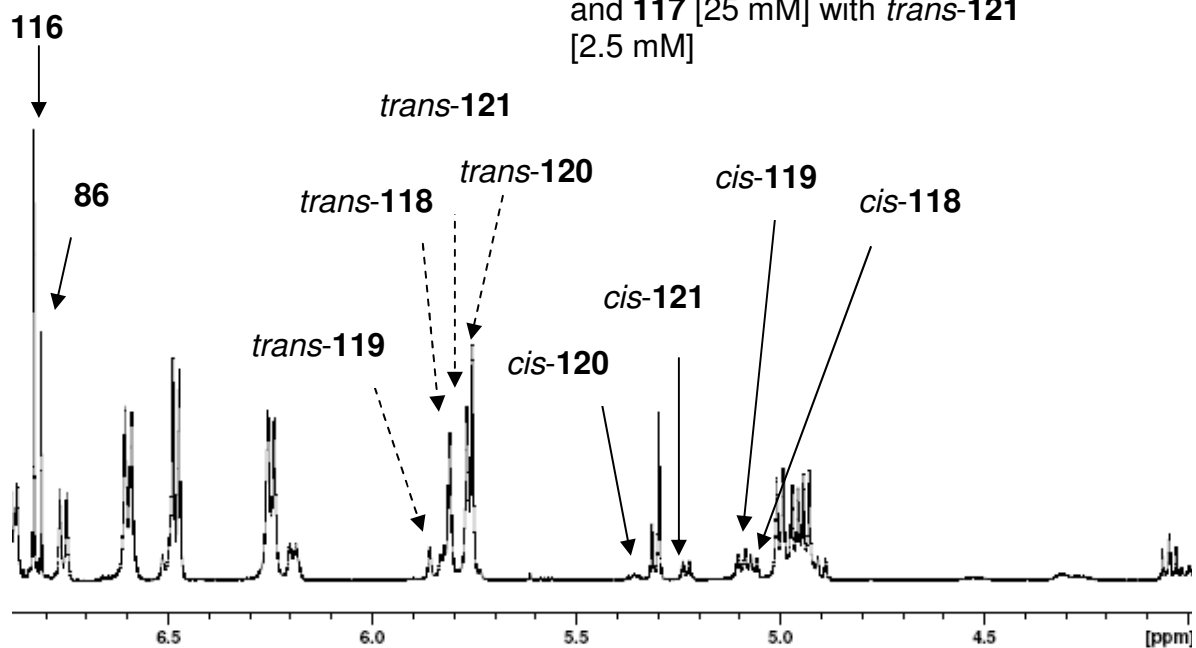
Appendix Five

Maleimide **132**

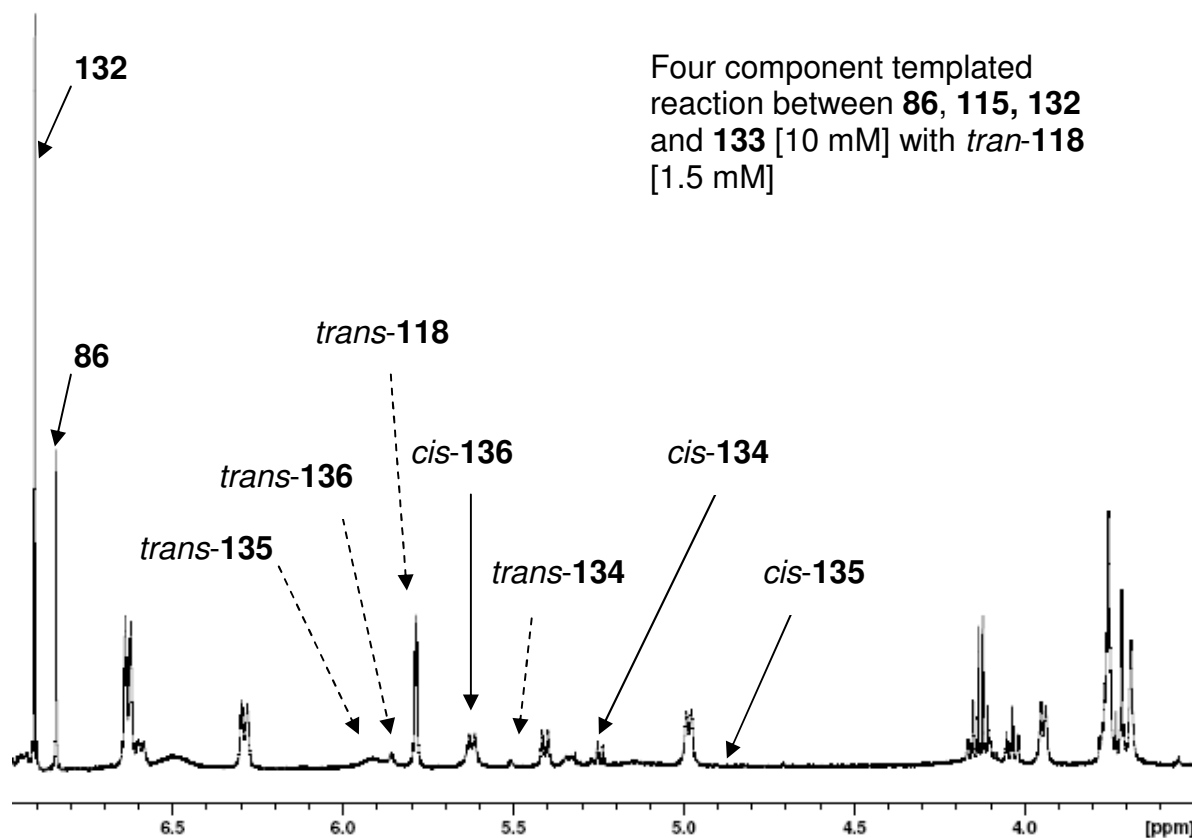


Appendix Six

Four component templated reaction between **86**, **115**, **116** and **117** [25 mM] with *trans*-**121** [2.5 mM]



Four component templated reaction between **86**, **115**, **132** and **133** [10 mM] with *trans*-**118** [1.5 mM]



Appendix Seven

```
*=====
* FURAN 70 + MALEIMIDE 86 at 25 mM templated with
* Bis(amidopyridine) template 104 at 50 mM.
*=====
* RECIPROCAL REPLICATION KINETIC MODEL
*=====
* This model allows the dimerisation constant
* and the rate constant in the ternary complex
* to vary.
*
* M = 86; B = 70 ENDO = endo-105; EXO = exo-105
* T = 104
*
* Bimolecular rates from experiments
* Ka = 120 M-1
*
* Final R % = 1.6 %
*=====

DIM (4)

* Bimolecular routes to TRANS
REACTION (M + B --> EXO) CONSTANT (1, 3.33E-4, 0)

* Bimolecular routes to CIS
REACTION (M + B ==> ENDO) CONSTANT (2, 2.45E-4, 0) CONSTANT (3, 2.41E-5, 0)

* ROUTES FOR Formation of binary AND TERNERY WHERE T IS RECIPROCAL TEMPLATE

REACTION (M + T ==> MT) CONSTANT (4, 1E9, 0) CONSTANT (5, 8.3E6, 0)
REACTION (T + M ==> TM) CONSTANT (6, 1E9, 0) CONSTANT (7, 8.3E6, 0)
REACTION (B + T ==> BT) CONSTANT (8, 1E9, 0) CONSTANT (9, 8.3E6, 0)
REACTION (T + B ==> TB) CONSTANT (10, 1E9, 0) CONSTANT (11, 8.3E6, 0)
REACTION (M + BT ==> MBT) CONSTANT (12, 1E9, 0) CONSTANT (13, 8.3E6, 0)
REACTION (M + TB ==> BMT) CONSTANT (14, 1E9, 0) CONSTANT (15, 8.3E6, 0)
REACTION (B + MT ==> BMT) CONSTANT (16, 1E9, 0) CONSTANT (17, 8.3E6, 0)
REACTION (B + TM ==> MBT) CONSTANT (18, 1E9, 0) CONSTANT (19, 8.3E6, 0)

* DUPLEX ASSOCIATION

REACTION (EXO + T ==> TEXO) CONSTANT (20, 1E9, 0) CONSTANT (21, 1.6E5, 1, 1, 100000)
REACTION (T + EXO ==> EXOT) CONSTANT (22, 1E9, 0) CONSTANT (23, 1.6E5, 1, 1, 100000)
REACTION (T + ENDO ==> ENDOT) CONSTANT (24, 1E9, 0) CONSTANT (25, 1.6E5, 2, 1, 100000)
REACTION (ENDO + T ==> TENDO) CONSTANT (26, 1E9, 0) CONSTANT (27, 1.6E5, 2, 1, 100000)

* TERNARY COMPLEX REACTION

REACTION (MBT --> TEXO) CONSTANT (28, 5.15E-3, 2, 1, 1000)
REACTION (BMT --> EXOT) CONSTANT (29, 5.15E-3, 2, 1, 1000)
REACTION (MBT ==> ENDOT) CONSTANT (30, 4.15E-3, 3, 1, 1000) CONSTANT (31, 2.41E-5, 4, 1, 1000)
REACTION (BMT ==> TENDO) CONSTANT (32, 4.15E-3, 3, 1, 1000) CONSTANT (33, 2.41E-5, 4, 1, 1000)

*Bimolecular Reactions of Complexes

REACTION (MT + B --> TEXO) CONSTANT (34, 3.33E-4, 0)
REACTION (TM + B --> EXOT) CONSTANT (35, 3.33E-4, 0)
REACTION (MT + B ==> ENDOT) CONSTANT (36, 2.45E-4, 0) CONSTANT (37, 2.41E-5, 0)
REACTION (TM + B ==> TENDO) CONSTANT (38, 2.45E-4, 0) CONSTANT (39, 2.41E-5, 0)
REACTION (BT + M --> TEXO) CONSTANT (40, 3.33E-4, 0)
REACTION (TB + M --> EXOT) CONSTANT (41, 3.33E-4, 0)
```

REACTION (BT + M ==> ENDOT) CONSTANT (42, 2.45E-4, 0) CONSTANT (43, 2.41E-5, 0)
REACTION (TB + M ==> TENDO) CONSTANT (44, 2.45E-4, 0) CONSTANT (45, 2.41E-5, 0)

*UNPRODUCTIVE COMPLEXES

REACTION (M + MT ==> MMT) CONSTANT (46, 1E9, 0) CONSTANT (47, 8.3E6, 0)
REACTION (M + TM ==> MTM) CONSTANT (48, 1E9, 0) CONSTANT (49, 8.3E6, 0)
REACTION (B + BT ==> BBT) CONSTANT (50, 1E9, 0) CONSTANT (51, 8.3E6, 0)
REACTION (B + TB ==> BTB) CONSTANT (52, 1E9, 0) CONSTANT (53, 8.3E6, 0)

REACTION (COMPILE)

REACTION (SHOW)
CONSTANT (SHOW)

DEFINE (1, EXO, P, 1) SCALE (3,1)
DEFINE (2, ENDO, P, 4) SCALE (3,1)

SELECT (EXO, ENDO)

READ (C+Dtemplated50)
REACTION (DOC)
CONSTANT (DOC)

TIME (SEC)
WIN (0, 60000, 30000, 200, 0, 25e-3, 5e-3, 3e-4)

ASSIGN (OBS, EXO = EXO + TEXO + EXOT)
ASSIGN (OBS, ENDO = ENDO + TENDO + ENDOT)
ASSIGN (SPEC, M = #25e-3)
ASSIGN (SPEC, B = #25e-3)
ASSIGN (SPEC, T = #50e-3)

CHOOSE (EXP1)

INTEG (STIFF, 1E-9, 1, 0.08, 50, 50)

PLOT (FILE, SPEC)

* 10 rounds of Simplex optimizer without screen
* update

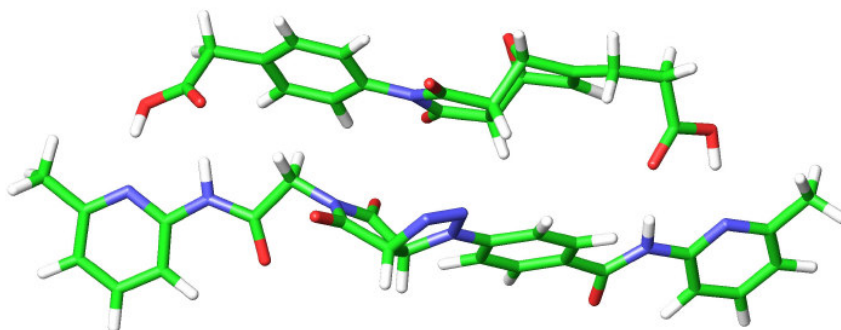
SIMPLEX (PLOT)
SIMPLEX (PLOT)
SIMPLEX (PLOT)

NEWTON (PLOT)

PLOT (FILE, SPEC)

MAKE

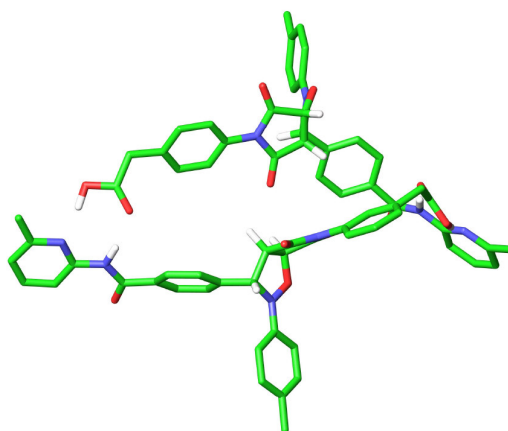
Appendix Eight



[exo-105•104]

C	-4.136	-0.2056	2.3877	C	-1.1569	-4.3339	-1.9984	H	5.3455	0.403	-5.1645
N	-3.7936	0.5981	0.2048	C	-0.8903	-3.5317	-0.7594	N	-2.9297	-4.6709	-0.6278
C	-4.8784	-1.1092	1.4055	N	-1.0608	-2.0838	-2.5852	C	-2.1017	-3.7878	4.3036
H	-3.4038	-0.7275	3.0097	H	-0.4414	-5.1439	-2.1628	C	-1.1771	-3.0251	3.583
C	-5.2854	0.4367	3.1669	N	-2.5236	-4.8381	-1.8072	C	-1.1446	-3.0745	2.1819
H	-4.583	-2.1596	1.4573	H	0.1016	-3.7348	-0.343	C	-2.03	-3.8832	1.4536
C	-6.3419	-0.854	1.7641	N	-1.9962	-3.9594	0.0641	C	-2.9558	-4.6361	2.1975
C	-3.4652	0.8218	1.5277	C	-0.9306	-0.8886	-3.3928	H	-0.4656	-2.3885	4.1072
O	-2.7956	1.721	2.0234	H	-5.1105	1.4004	3.6478	H	-0.4053	-2.4544	1.6802
C	-4.5621	-0.54	0.0578	H	-7.0992	-1.0274	0.9974	H	-3.6608	-5.2924	1.6892
O	-4.9529	-1.0822	-0.97	H	-2.8979	4.1995	-4.8734	H	-3.6915	-5.2553	4.1101
C	-2.5696	3.0753	-3.0597	H	-1.5386	4.7548	-3.8997	C	-2.0588	-3.7322	5.7968
C	-1.8971	3.1256	-1.8366	H	-5.9248	-0.6751	5.0743	N	-3.2301	-4.0385	6.4533
C	-2.3066	2.3221	-0.7641	H	-8.4291	-2.4381	2.7917	O	-1.0024	-3.4009	6.3268
C	-3.3884	1.4358	-0.8808	H	-7.0059	-3.4706	2.8739	H	-4.0806	-4.1807	5.9121
C	-4.0614	1.4088	-2.1134	H	-8.2504	-2.0338	5.287	C	-4.0269	-4.4993	10.4998
C	-3.6623	2.2153	-3.1863	H	-8.6497	-3.6934	4.8004	C	-4.9901	-4.6213	9.5067
C	-2.0651	3.8586	-4.2486	C	-1.0048	-2.0975	-1.2211	N	-4.7187	-4.4275	8.1853
H	-1.032	3.7739	-1.7061	O	-1.0182	-1.1162	-0.4887	C	-3.4334	-4.1567	7.8349
H	-1.7168	2.3834	0.1466	C	-1.1371	-3.3371	-3.1162	C	-2.4209	-4.0325	8.7764
H	-4.9297	0.7756	-2.2754	O	-1.1847	-3.6109	-4.3077	C	-2.7254	-4.1986	10.1254
H	-4.2042	2.1461	-4.1282	C	0.5601	-0.7004	-3.7178	H	-4.2782	-4.6421	11.5463
C	-1.1387	3.0201	-5.0947	N	0.7717	0.2445	-4.6953	C	-6.4054	-4.9533	9.8858
O	-0.0358	3.6847	-5.4884	O	1.435	-1.3252	-3.1186	H	-1.3955	-3.8179	8.5024
O	-1.3029	1.8439	-5.3931	H	-0.0422	0.6879	-5.1184	H	-1.9453	-4.103	10.876
H	0.5619	3	-5.8876	C	4.2248	1.7718	-6.391	H	-1.4983	-1.0032	-4.3213
C	-5.9772	-0.6035	3.9995	C	2.9475	2.2116	-6.7156	H	-1.2761	-0.0151	-2.8353
C	-6.6302	-1.4036	3.1391	N	1.8254	1.7158	-6.1261	H	3.277	3.0119	-8.6768
O	-6.2799	0.5604	2.1092	C	1.9784	0.7183	-5.2148	H	1.7134	3.447	-7.9703
C	-7.4936	-2.6058	3.3403	C	3.2225	0.2312	-4.8432	H	3.1902	4.2324	-7.3774
C	-7.8638	-2.9298	4.7877	C	4.36	0.7703	-5.4388	H	-6.8829	-4.0833	10.3464
C	-6.7029	-3.4751	5.5722	H	5.102	2.1954	-6.8705	H	-6.9862	-5.2443	9.0051
O	-6.8941	-3.3492	6.8987	C	2.7732	3.2902	-7.7459	H	-6.4272	-5.7913	10.5898
O	-5.6937	-3.9978	5.1261	H	3.3429	-0.5585	-4.1121				
H	-6.0919	-3.7452	7.3278								

Appendix Nine

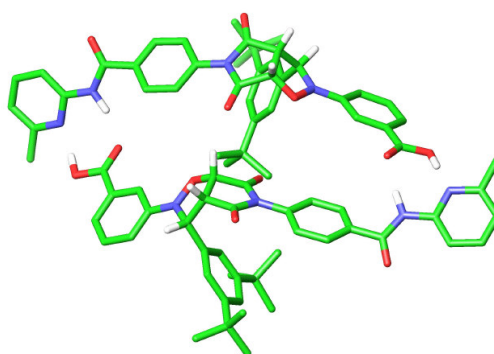


[*trans*-118•*trans*-118]

C	0.7679	4.7024	7.0528	C	9.9426	6.9635	4.2998	H	-4.9925	10.9703	7.8808
N	3.0449	4.2082	6.7163	C	9.6569	8.0673	5.1127	H	-1.7088	9.4196	5.2945
C	1.6038	5.658	7.8487	C	8.4099	8.6953	5.0415	H	0.3189	8.2776	4.6542
C	-0.1633	4.0943	8.0732	C	7.4267	8.2398	4.1467	H	2.5927	10.906	7.2439
C	4.3113	7.373	4.3523	C	7.7259	7.1356	3.3321	H	0.5586	12.0516	7.8454
N	2.8656	8.8275	5.473	C	8.974	6.5081	3.3999	H	5.3432	0.9915	4.3255
C	5.1439	8.3355	5.1432	C	11.3018	6.3522	4.3811	H	3.3113	2.1346	4.9384
H	4.6296	6.3322	4.4563	N	11.3765	5.0105	4.0794	H	5.5944	4.7545	7.5284
O	4.3446	7.7599	2.9787	O	12.2369	7.0712	4.7195	H	7.6198	3.6156	6.8765
H	5.6244	7.8859	6.0185	H	10.5111	4.486	3.9607	H	8.2096	0.9134	6.1254
C	6.0737	8.9411	4.1202	C	14.667	2.5387	3.5523	H	7.6723	0.6732	4.4524
C	1.7712	3.7005	6.5586	C	13.3524	2.1048	3.4399	H	4.2904	9.626	-1.4916
O	1.4233	2.625	6.0849	N	12.2825	2.9213	3.6562	H	3.9633	8.438	0.6206
C	2.9972	5.4449	7.3245	C	12.5292	4.2272	3.9407	H	7.2466	10.6301	2.3513
O	3.8804	6.2937	7.4056	C	13.8189	4.7285	4.0539	H	7.5641	11.8111	0.2525
C	2.916	7.5882	4.8705	C	14.8993	3.8699	3.8653	H	5.221	11.644	-2.6277
O	2.0332	6.7389	4.7898	C	13.0747	0.6692	3.0946	H	6.5592	12.541	-1.9111
C	4.138	9.3378	5.6311	N	0.5643	4.2899	9.326	H	6.8683	10.9698	-2.6909
O	4.4834	10.416	6.1003	H	-0.3157	3.0237	7.8888	H	10.4078	8.4452	5.8044
H	0.288	5.1582	6.1804	C	-0.0496	2.196	12.9614	H	8.2157	9.5491	5.6896
H	1.2866	6.7	7.7539	C	0.9592	3.1528	12.8416	H	6.9947	6.7561	2.6195
O	1.574	5.2595	9.2192	C	1.1494	3.8337	11.6329	H	9.1719	5.6786	2.7258
C	-0.7427	10.8192	6.6316	C	0.3408	3.5923	10.5108	H	15.4983	1.859	3.3923
C	-0.7695	9.7446	5.7393	C	-0.6786	2.641	10.6561	H	14.0202	5.7685	4.2786
C	0.4125	9.0801	5.3816	C	-0.8767	1.9552	11.8624	H	15.9154	4.2451	3.9535
C	1.6616	9.4741	5.8889	C	-0.2818	1.4881	14.2631	H	12.0317	0.5369	2.7914
C	1.6726	10.5493	6.7891	C	-4.0289	6.0802	7.9122	H	13.7059	0.3459	2.2606
C	0.4922	11.2117	7.1555	C	-3.7521	4.9709	7.1035	H	13.2701	0.0319	3.9621
C	6.6492	2.2207	5.5375	C	-2.5058	4.341	7.1674	H	1.6077	3.3795	13.685
C	5.4121	1.8293	5.0177	C	-1.5145	4.7995	8.0514	H	1.9484	4.5697	11.5761
C	4.233	2.4902	5.3908	C	-1.8042	5.9097	8.8614	H	-1.3558	2.4153	9.8375
C	4.2472	3.5625	6.2943	C	-3.0514	6.5394	8.8006	H	-1.6867	1.2322	11.9329
C	5.4982	3.9547	6.7984	C	-5.388	6.6928	7.8402	H	0.6565	1.3669	14.8144
C	6.679	3.2918	6.4338	N	-5.4588	8.0358	8.1369	H	-0.9834	2.0587	14.8793
C	7.8972	1.4325	5.211	O	-6.3269	5.9733	7.5131	H	-0.6913	0.4865	14.0951
C	9.066	2.2355	4.6921	H	-4.592	8.5602	8.2452	H	-4.5099	4.5903	6.4208

O	10.1921	1.4899	4.678	C	-8.7423	10.5115	8.6884	H	-2.319	3.4829	6.5229
O	9.0793	3.3922	4.3003	C	-7.4264	10.9452	8.7851	H	-1.0663	6.2914	9.566
H	10.9068	2.0736	4.3135	N	-6.3594	10.1272	8.5607	H	-3.2419	7.3732	9.4715
N	5.3462	8.7374	2.8687	C	-6.6097	8.8203	8.284	H	-9.5715	11.1922	8.8548
H	6.2236	10.0129	4.2996	C	-7.9007	8.3194	8.1862	H	-8.1049	7.2786	7.9677
C	5.9363	10.828	-0.7724	C	-8.9786	9.1793	8.3828	H	-9.9958	8.8044	8.3069
C	4.9371	9.8615	-0.6494	C	-7.1441	12.3818	9.122	H	-7.7648	12.7082	9.9626
C	4.7546	9.1819	0.5613	C	-1.9922	11.6077	6.9508	H	-6.0973	12.515	9.4117
C	5.5618	9.4343	1.6822	C	-3.155	10.8074	7.4871	H	-7.3501	13.0163	8.2548
C	6.571	10.3956	1.5339	O	-4.2821	11.5515	7.5044	H	-1.7671	12.3797	7.6963
C	6.7615	11.0801	0.3255	O	-3.1631	9.654	7.8884	H	-2.3109	12.1113	6.0299
C	6.1607	11.5345	-2.0762								

Appendix Ten



[*cis*-134•*cis*-134]

C	-0.0269	3.4815	0.942	C	-5.697	4.3403	-0.3761	C	-4.1339	-5.955	1.4094
N	-1.9403	4.5671	0.0791	H	-5.1414	7.422	-1.6749	C	-4.6045	-4.7383	1.9339
C	0.4043	4.6224	0.0708	H	-2.8757	6.8688	-1.1142	C	-4.5667	-3.5439	1.1972
H	0.1572	3.6911	2.002	H	-4.2226	3.0371	0.4215	C	-4.0533	-3.5836	-0.1071
O	0.7065	2.3219	0.565	H	-6.4886	3.6307	-0.1502	C	-3.5658	-4.771	-0.6815
H	1.1377	5.2438	0.5975	C	-7.3617	5.9933	-1.3381	H	-3.2412	-6.8659	-0.3223
C	1.016	3.9445	-1.1402	N	-8.1588	5.0464	-1.9423	C	-4.1758	-7.2308	2.2729
C	-3.4278	-0.4981	1.6816	O	-7.6581	7.1636	-1.1164	H	-4.9894	-4.7114	2.953
N	-1.7498	-2.0891	2.0697	H	-7.7787	4.1171	-2.1235	H	-4.0159	-2.6624	-0.6882
C	-3.9487	-1.5129	2.6556	C	-11.9526	5.4414	-3.5988	C	-2.9762	-4.747	-2.1053
H	-3.192	0.4474	2.1776	C	-11.1776	4.2959	-3.718	C	-4.0171	-4.1882	-3.1007
O	-4.4079	-0.2859	0.6801	N	-9.9557	4.1634	-3.1275	C	-2.5478	-6.1353	-2.6334
H	-4.3739	-1.0107	3.5321	C	-9.4551	5.2315	-2.4515	C	-1.7227	-3.8462	-2.1206
C	-5.0156	-2.2541	1.8694	C	-10.1793	6.4071	-2.2993	C	-5.6312	-7.5245	2.6996
C	-1.5333	3.4152	0.7355	C	-11.4447	6.5084	-2.8735	C	-3.3067	-7.028	3.5336
O	-2.2079	2.4883	1.167	H	-12.9311	5.5089	-4.064	C	-3.6499	-8.4956	1.5561
C	-0.8524	5.3792	-0.1788	C	-11.701	3.1274	-4.5044	H	-2.1144	-1.0607	-3.7479
O	-0.806	6.5446	-0.5532	H	-9.7994	7.2566	-1.7457	H	-0.7951	-0.0989	-4.4316
C	-2.1437	-1.1144	1.1663	H	-12.0225	7.4218	-2.7608	H	-0.9769	-0.2486	-2.6799
O	-1.6194	-0.7835	0.111	C	1.9855	-4.1702	1.9446	H	-4.0142	0.1299	-2.4507
C	-2.7274	-2.2855	3.0256	C	1.7276	-3.1265	1.0596	H	-2.8739	1.0524	-1.4702
O	-2.6967	-2.9527	4.0527	C	0.5033	-2.4454	1.1054	H	-4.0916	1.8983	-2.4262
N	1.4905	2.7018	-0.54	C	-0.51	-2.8034	2.0104	H	-4.0415	1.8227	-4.9625
H	1.8634	4.5568	-1.4752	C	-0.2452	-3.8965	2.8546	H	-2.6869	1.052	-5.8146

C	4.9568	0.5878	-1.716	C	0.9839	-4.5721	2.8259	H	-3.8673	0.0709	-4.9417
C	4.2944	0.2536	-0.5313	H	2.4632	-2.824	0.3196	H	-1.7481	7.8825	-5.3037
C	3.1313	0.9496	-0.1604	H	0.393	-1.6187	0.409	H	-2.576	6.8448	-4.1317
C	2.6225	1.9979	-0.9452	H	-0.9821	-4.2735	3.5577	H	-0.918	7.3771	-3.8334
C	3.3061	2.2993	-2.1353	H	1.1513	-5.4084	3.5019	H	0.1954	6.9036	-6.7362
C	4.4581	1.6066	-2.5199	C	3.2908	-4.8838	1.9593	H	1.0141	6.4356	-5.2499
H	5.8544	0.0578	-2.0251	N	4.3969	-4.0835	1.7768	H	0.6912	5.221	-6.4928
H	2.6225	0.68	0.7633	O	3.2843	-6.0931	2.1609	H	-2.127	6.3635	-7.2049
H	2.9469	3.0759	-2.8056	H	4.2708	-3.0723	1.7308	H	-1.7651	4.6394	-7.106
H	4.9611	1.8636	-3.4491	C	8.4309	-5.0344	1.6115	H	-3.094	5.3325	-6.1527
C	-1.7096	3.4424	-4.4584	C	7.9417	-3.7369	1.5347	H	-10.9047	2.4029	-4.7011
C	-0.9548	4.6255	-4.3562	N	6.6114	-3.4473	1.5589	H	-12.4972	2.627	-3.9451
C	-0.0613	4.7323	-3.2758	C	5.7392	-4.4773	1.716	H	-12.0935	3.4607	-5.4704
C	0.0846	3.7114	-2.3226	C	6.1605	-5.7969	1.7986	H	9.3697	-2.6109	0.4072
C	-0.6848	2.5479	-2.4728	C	7.5239	-6.0766	1.7414	H	8.382	-1.6322	1.5113
C	-1.5954	2.3876	-3.5333	H	9.4971	-5.2352	1.5746	H	9.6767	-2.645	2.1649
H	-2.4139	3.3421	-5.2771	C	8.9003	-2.5892	1.3953	H	-3.6322	-4.2071	-4.1271
C	-1.0945	5.7901	-5.3556	H	5.4674	-6.6217	1.9084	H	-4.94	-4.7797	-3.079
H	0.5211	5.6457	-3.156	H	7.8724	-7.104	1.8055	H	-4.2864	-3.1488	-2.8833
H	-0.5862	1.7473	-1.7393	N	-5.4241	-1.2263	0.9161	H	-3.3927	-6.8333	-2.6615
C	-2.4433	1.1032	-3.6297	H	-5.846	-2.4834	2.5501	H	-2.152	-6.0649	-3.6537
C	4.7893	-0.8337	0.3488	C	-9.1893	-0.7854	-0.9397	H	-1.758	-6.5777	-2.0151
O	5.9571	-1.3448	-0.0767	C	-8.2049	0.1945	-1.0797	H	-1.2634	-3.823	-3.1157
O	4.2254	-1.2658	1.3391	C	-6.9561	0.0164	-0.4718	H	-1.9558	-2.8113	-1.8497
H	6.1835	-2.0709	0.5601	C	-6.6665	-1.1166	0.3043	H	-0.9678	-4.2081	-1.4126
C	-1.5299	-0.1424	-3.6189	C	-7.6704	-2.0874	0.4245	H	-5.6925	-8.4498	3.2843
C	-3.4067	1.0422	-2.4262	C	-8.9178	-1.9288	-0.1917	H	-6.0516	-6.7264	3.3211
C	-3.3052	1.0122	-4.9102	H	-10.1648	-0.6679	-1.4047	H	-6.2826	-7.6386	1.8249
C	-1.6108	7.0422	-4.6133	H	-6.1959	0.7865	-0.592	H	-2.2703	-6.7924	3.2638
C	0.2785	6.1041	-5.9906	H	-7.5008	-2.9987	0.9918	H	-3.6748	-6.212	4.165
C	-2.0756	5.5106	-6.5174	H	-9.6767	-2.7002	-0.0832	H	-3.2927	-7.9319	4.1537
C	-5.9841	5.5625	-0.9779	C	-8.4343	1.4505	-1.8284	H	-3.7099	-9.374	2.2099
C	-4.9408	6.455	-1.2162	O	-9.7118	1.5924	-2.2141	H	-4.2353	-8.7223	0.6573
C	-3.623	6.1192	-0.8757	O	-7.5983	2.3117	-2.0429	H	-2.5994	-8.3863	1.2624
C	-3.2977	4.8954	-0.2645	H	-9.753	2.5025	-2.6061				
C	-4.3703	4.0148	-0.0285	C	-3.6189	-5.9408	0.0997				